Aston University

If you have discovered material in AURA which is unlawful e.g. breaches copyright, (either yours or that of a third party) or any other law, including but not limited to those relating to patent, trademark, confidentiality, data protection, obscenity, defamation, libel, then please read our Takedown Policy and contact the service immediately

The use of lubricants in iron powder metallurgy

by

MELVYN WARD, B.Sc.

A Thesis submitted for the degree of

Doctor of Philosophy of the

University of Aston in Birmingham

April 1977

SUMMARY

This investigation has been concerned with the behaviour of solid internal lubricant during mixing, compaction, ejection, dewaxing and sintering of iron powder compacts.

Zinc stearate (0.01%-4.0%) was added to irregular iron powder by admixing or precipitation from solution. Pressure/density relationships, determined by continuous compaction, and loose packed densities were used to show that small additions of zinc stearate reduced interparticle friction during loose packing and at low compaction pressures. Large additions decreased particle/die-wall friction during compaction and ejection but also caused compaction inhibition.

Transverse rupture strengths were determined on compacts containing various stearate based lubricants and it was found that green strength was reduced by the interposition of a thin lubricant layer within interparticle contacts. Only materials much finer than the iron powder ($<5\mu m$ and $<180\mu m$ respectively) were able to form such layers.

Investigations were undertaken to determine the effect of the decomposition of these lubricants on the development of mechanical properties in dewaxed or sintered compacts. Physical and chemical influences on tensile strength were observed. Decomposition of lubricants was associated with reductions of strength caused by the physical effects of pressure increases and removal of lubricant from interparticle contacts. There were also chemical effects associated with the influence of gaseous decomposition products and solid residues on sintering mechanisms.

Thermogravimetry was used to study the decomposition behaviour of various lubricants as free compounds and within compacts. The influence of process variables such as atmosphere type, flow-rate and compact density were investigated. In a reducing atmosphere the decomposition of these

lubricants was characterised by two stages. The first involved the rapid decomposition of the hydrocarbon radical. The second, higher temperature, reactions depended on lubricant type and involved solid residues. The removal of lubricant could also markedly affect dimensional change.

INDEX

1 Introduction

It is now an established procedure in industry to use admixed solid lubricants in metal powder mixes. Metallic soaps (zinc and lithium stearate) or some petroleum derivatives are commonly used.

The purposes of a lubricant in metal powder compacts have been listed as follows[1]:-

(1) To reduce friction between die/core walls and boundary grains of powder, resulting in more transmitted force within the compact.

(2) To reduce friction between powder grains to give more even density distribution during early stages.

(3) To reduce ejection force and prolong die life.

(4) To prevent seizure and galling. This is a more pronounced fault with high compressibility powders.

(5) To prevent subsieve fractions of powder falling into tool clearances.

Work by Bockstiegel and Svensson[2] concerned with the prolongation of die life has suggested that most types of lubricant, such as metallic soaps, are so-called surface active agents. They may have certain chemical and physical effects on the die bore surface such as lowering fatigue resistance by reducing the yield strength according to the 'Rehbinder effect'.

The main purpose of admixed lubricant is die-wall lubrication for ejection. Many high density, high compressibility powder compacts could not be removed from their forming tools without the presence of a lubricant. In most cases its absence would mean excessive die-wear, galling or seizing, poor frictional surface finish and possibly breakage of compacts. It has been shown that lubricant applied directly to the die wall is more efficient than admixed lubricant[24]. In the latter a very important mechanism appears to be extrusion of lubricant onto the die wall[2,4,24] and this means that a considerable proportion of the added lubricant is not

utilised during the ejection of compacts.

Subsequent difficulties have also been experienced with removal of admixed lubricants during or prior to sintering[5]. Unfortunately the application of lubricants directly to forming tool faces has proved to be a considerable practical engineering problem. There is also very little information available, concerning the decomposition characteristics of lubricants, to assist in understanding their behaviour during sintering.

2 The use of lubricants in powder metallurgy, literature survey

2-1 Stearates used as admixed lubricants

Metallic stearates have been established as lubricants in the powder metallurgy field because of their ability to withstand considerable amounts of frictional heat and adhere to tool surfaces[6]. Metallic stearates or soaps are reaction products of metallic radicals and fatty acids. General properties stemming from the fatty acid component include lubricity, water repellency and solubility. Characteristics influenced by the metal or cation portion of the stearate include relative toxicity, melting point (table 2-1), solubility and additional effects on lubricity[6].

The particle size of a stearate also affects lubricity in that small particles have greater surface area to impart lubricity, whilst large particles, combined with high stearate bulk density, improve mix flow and apparent density. To prevent segregation particle size should be smaller than the metal powder grains[6]. Carr and Kearns[6] recommend zinc stearate for iron and lithium stearate for copper and bronze powders.

It has been suggested that the presence of residual chlorides in lubricants may cause corrosion problems[7] if they are not completely removed, especially from sintered compacts.

Table 2-1

Some thermal properties of stearates

	Chemical composition	Melting point °C				Boiling point °C	Flash point °C
Source of data	8	8	9	10	11	8	10
Stearic acid	$CH_3(CH_2)_{16}.CO_2H$	69.6			53	291	
Zinc stearate	$Zn(C_{36}H_{70}O_4)$		120	77	130	Decomposes	304
Lithium "			209	99			275
Sodium "	$NaO_2C_{18}H_{35}$					Decomposes	
Ammonium "	$C_{17}H_{35}CO_2NH_4$	74			110	Decomposes	

2-2 The application of solid lubricants

Normal commercial practice of applying solid lubricants is to admix as powder simultaneously with the metal powders during blending. Abrasion is relied upon to cause lubricant to adhere to metal particles.

There is a maximum apparent density achieved after a specific mix-time for any given mix composition. Beyond this maximum the apparent density usually falls, possibly due to agglomeration of powder particles by cold working to form larger particles with poorer packing qualities. S-Å. Kvist et al[7] have also shown that different lubricants react differently with the mix-time required to achieve a given density, agglomeration tendencies are also a function of lubricant type and grade.

Some workers[3,12,13] have used hot evaporation techniques, using solvents such as benzene, to obtain idealised uniform lubricant layers enabling film thicknesses to be estimated.

2-3 Friction in the loose packing of powders

In the unlubricated condition, friction in a powder mass is not only affected by the particle characteristics but also by the type of metal involved. Generally, friction rises with the ratio of surface energy to hardness[14]. Hausner[14] has also shown that the presence of an oxide film substantially changes the friction conditions. The medium surrounding a powder, gaseous or liquid, also substantially changes friction conditions and the coefficient of friction.

Friction in loose metal powders may be characterised by flow properties, apparent density, the ratio D_t/D_a (where D_t and D_a are tapped and apparent densities respectively), or an arbitrary die-fill capability. All of these have been used by various workers to determine the effects of variables, such as particle morphology and the presence of lubricants, on frictional properties of loose powders.

The variables affecting loose powder density have been listed as follows;[14]

(1) Material density.

(2) Particle density.

(3) Average particle size.

(4) Particle size distribution.

(5) Average particle shape.

(6) Particle shape distribution.

(7) Specific surface area of the powder.

(8) Oxide films.

(9) Additions, such as lubricants.

(10) The atmosphere surrounding the particles.

R.E.Riley and H.H.Hausner[15] have demonstrated that predictions of powder behaviour based on average particle size can be entirely misleading. They suggest that the friction behaviour of a powder is less dependent on average size than on size distribution or specific surface area. Particle size affects the friction in a powder mass in several ways,[14] it determines the number of contact points where friction occurs (particularly for regular spheres), the specific surface area and the surface energy of the particles (also important during sintering). Hausner[14] has found that with increasing particle size apparent density and tapped density both increase whereas D_t/D_a decreases. This indicates reduced friction between large particles. He has also shown that increasing proportions of fines (-400 mesh) in particle size distributions and decreasing mean particle size increases friction in a powder mass (increasing D_t/D_a).

Friction in a loose powder is independently affected by particle shape. The greater the deviation of particle shape from a sphere, the larger is the specific surface area, the number of contact points and the surface energy. By using copper powder of varying particle shape and size

fractions it has been shown[14] that apparent density (D_a) is highest with spherical powders and increases only slightly by tapping. Apparent density is lowest for flake powder but increases markedly with tapping. This demonstrated that friction in a loose powder mass is lowest for spheres and highest for flakes.

Loose powder density and its consistency is particularly important in the die fill stage. As the apparent density of a given material increases a smaller die cavity and compaction stroke is required for a given compact weight. For a given particle shape apparent density decreases as particle size decreases, markedly so for irregularly shaped powders. However it is evident that care must be taken in the choice of measured parameter. Particle size, size distribution and shape can only be considered separately with difficulty.

2-4 The reduction of friction in loose powders.

Friction between powder particles may be reduced in several ways[14];

(a) The addition of lubricant to the powder.

(b) Oxidation of particle surfaces, reducing the coefficient of friction.

(c) Handling the powder in a friction reducing medium.

The addition of a small amount of lubricant to a powder lowers the interparticle friction and increases the apparent density[13,14]. The lubricating action depends on the type of lubricant. Flow (the ability of a powder to fall freely through an orifice) is greatly affected by the presence of lubricants which may form agglomerates and thus cause defects in sintered components. Kvist et al[7] have found no apparent relationship between percentage agglomeration and flow rate for various lubricants but do not state whether this was before or after agglomerates were screened off. They have also found that a lubricant of high apparent density (zinc stearate) improves mix flow rate.

Yarnton and Davies[13] have found that the packing density (D_a) of a powder in free fall can be increased by up to 20%, relative to the unlubricated condition, by the introduction of a thin layer of solid lubricant (stearic acid). Optimum conditions were found to correspond to boundary lubrication by a monomolecular layer, perhaps maintained by adsorption. Below this optimum addition only partial coverage was observed. Above it, the formation of free lubricant particles occurred, reducing the apparent density.

Findings were expressed in terms of a slip factor, F, and a size factor. F is the maximum true density obtained under lubricated conditions divided by the true density of the original powder (for Cu and Fe powders approximately 1.2). At less than 100% coverage with a monomolecular layer equation 2-1 was employed;

$$D_L = D_U \left[1 + x (F - 1) \right] \qquad ..(2-1)$$

where, D_L is lubricated true density,

D_U is unlubricated true density,

x is the proportion of powder surface covered with a monolayer.

At 100% coverage x = 1 and $D_L = FD_U$.

In size factor terms Yarnton and Davies[13] have suggested that as lubricant content increases film thickness increases and particles are thrust apart so that apparent density is reduced. For ideal conditions of uniform sphere sizes and coating thickness the resultant decrease in density was found to be proportional to the cube of the diameters of the coated and uncoated particles.

$$D_L = FD_U \left(\frac{d_1}{d_2} \right)^3 \qquad ..(2-2)$$

where d_1 is the diameter of uncoated particles

and d_2 that of coated particles.

According to equation 2-2 a practically constant value of packing density should be obtained under ideal conditions until complete coverage is produced. Further increases in film thickness should then cause a progressive fall in D_a proportional to $\left(\frac{d_1}{d_2}\right)^3$.

The limitations of this size factor approach when applied to more typical non-ideal systems have been stated[13]. Deviations from ideal conditions include;

(a) particle shape changes as lubricant is deposited,

(b) the presence of free lubricant,

(c) agglomeration between particles,

(d) the formation of metal stearates by reaction with stearic acid,

(e) the progressive filling of internal porosity within metal powder particles.

Growth of the lubricant layer is also unlikely to conform to the uniform layering assumed in the calculations.

Experimental results[13] suggested that fractional coverage of particles minimises friction between particles to a fractional degree and that this effect is cumulative until a full monomolecular layer is achieved. This is not a straight line relationship as suggested by consideration of the slip factor. Above 0.052% by weight lubricant, with the materials studied, variations between calculated and actual results were high, possibly due to agglomeration or segregation.

Ljungberg and Arbstedt[1] have also investigated the effects of lubricants on filling characteristics. They found that filling characteristics of electrolytic powders are more sensitive to lubricant additions, due to their smooth surface creating a thick lubricant film, compared to absorbent sponge iron powders. A small addition of zinc stearate was found to reduce flow rate but initially increase apparent density, in agreement with Hausner[14] and Yarnton and Davies[13].

Following this initial increase the apparent density decreases, the rate of decrease being greatest for electrolytic iron powder. This again indicates the importance of particle morphology on sensitivity to solid lubricant additions. Ljungberg and Arbstedt[1] also assessed flowability and die-fill capacity with die-cavity models using apparent density as criterion. Overall findings were that as lubricant content increases die-fill capacity and apparent density decrease. Apparent density decreases with die-cavity cross-sectional area. Atomised and sponge iron powders were found able to fill narrow sections whilst electrolytic were not.

Metal powders are generally oxidised and the coefficient of friction between oxidised surfaces is considerably lower than that between clean metallic surfaces[14]. Reduction of an oxide film produces a clean metallic surface which increases friction between particles and hence decreases apparent density. However the improved plastic deformability of powders without an oxide skin allows greater formed densities to be achieved for a given compaction pressure. The presence of an oxide film is often detrimental to sintering particularly in the presence of a liquid phase[16].

Hausner[14] has shown that the effect of gaseous atmospheres on loose powder packing is small. If the surrounding medium is a liquid considerable reduction of friction occurs due to interposition of that liquid between particles. This is illustrated by the metal powder slip casting process where cast densities are appreciably higher than those obtained by free flow in air.

2-5 Compaction in the absence of admixed lubricant

Hausner[14] has drawn attention to the correlation between compression ratio and the ratio D_t/D_a. He has suggested that the compression of a plastic, deformable metal powder consists of two partly overlapping parts. The initial low pressure part results in rearrangement of loose

particles and the applied pressure has only to overcome the frictional forces between particles. The second, high pressure part, results in plastic deformation of particles. Data quoted by Hausner[14] shows that the compression ratio divided by D_t/D_a for various size fractions of electrolytic iron powder compacted at constant pressure remained practically constant at 2.2.

Heckel[17] has also regarded the compaction process as being multi-stage as follows:

1- Densification during filling of the die.

2- Densification by individual particle movement and rearrangement at low pressures before interparticle bonding becomes appreciable.

3- Densification by compact deformation after interparticle bonding becomes appreciable.

Stages 2 and 3 correspond to those suggested by Hausner[14].

Heckel[17] has discussed attempts to apply straight line empirical relationships to powder compaction data and found equation 2-3 to be valid over the widest pressure range.

$$\ln\ [1/(1-D)] \propto P \qquad ..(2-3)$$

where D is the fractional relative true metal density and P the applied pressure. Investigations[17] using various materials (Fe, Ni, Cu, W) have indicated that the proportionality suggested by equation 2-3 occurred typically at compaction pressures in excess of 103-172Nmm^{-2}.

Equation 2-3 has been justified[17,18] by considering the rate of change of density with applied pressure (P) to be proportional to the void fraction (1-D).

$$dD/dP \propto (1-D) \quad \text{or} \quad dD/(1-D) = k\,dP \qquad ..(2-4)$$

integrating equation 2-4,

$$\int_{D_o}^{D} dD/(1-D) = k\int_{0}^{P} dP \qquad ..(2-5)$$

FIGURE 2-1. ln[1/(1-D)] versus applied pressure P.
(after Heckel[17])

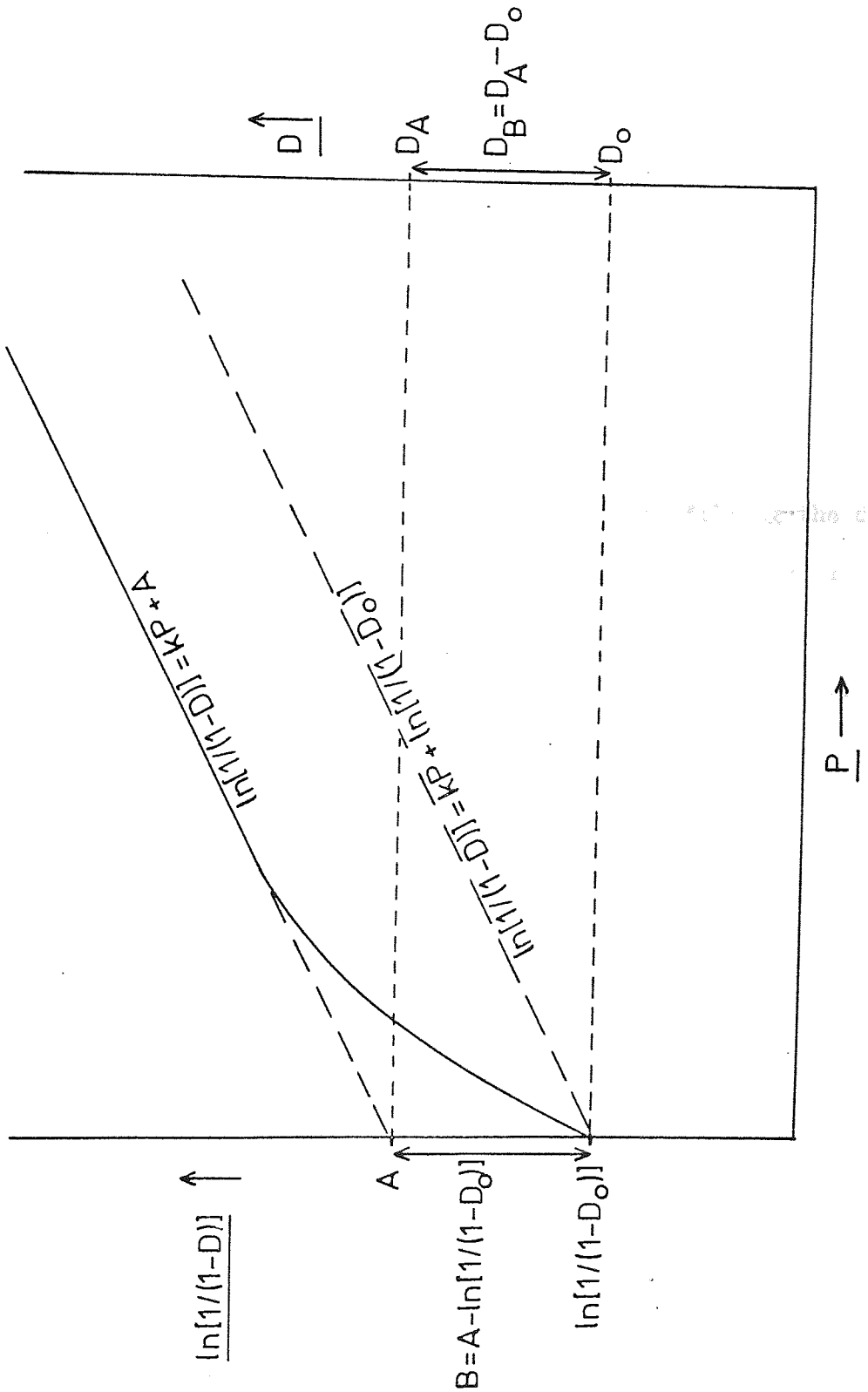

gives equation 2-6.

$$\ln \left[1/(1-D) \right] = k P + \ln \left[1/(1-D_o) \right] \quad ..(2-6)$$

where D_o is the relative apparent density of the powder.
The replacement of $\ln [1/(1-D_o)]$ with constant A gives equation 2-7 which has been found to be more valid at low pressures[17, 18].

$$\ln \left[1/(1-D) \right] = kP + A \quad ..(2-7)$$

A schematic representation of the results of Heckel is shown in figure 2-1[17]. The curved region of the plot of $\ln [1/(1-D)]$ versus P represents particle movement and rearrangement processes before interparticle bonding becomes appreciable. The linear region shows the stage where densification is proportional to void fraction, corresponding to both plastic deformation and cold working. As can be seen from figure 2-1, A in equation 2-7 combines the effects of densification by individual particle motion and densification brought about by filling the die. Thus equation 2-7 represents a three stage process[17, 18] as described above.

'A' may be considered [17, 18] as the sum of two terms related to the apparent density of the powder, $\ln(1/1-D_o)$, and densification by individual particle motion B before interparticle bonding becomes appreciable.

$$A = \ln(1/1-D_o) + B \quad \text{or} \quad D_A = D_o + D_B \quad ..(2-8)$$

From figure 2-1, $\ln(1/1-D_A) = A$ or $D_A = 1-e^{-A}$. Thus Heckel[17] was able to calculate D_B the density contribution from individual particle movement and rearrangement. The apparent density of a powder D_o may be determined experimentally.

Double end compression and die wall lubrication, with compaction data taken continuously over the pressure range, were used to quantitatively evaluate the extent of the various mechanisms involved in compaction [17, 18]. It was found that D_o increased and D_B decreased as particle size

decreased, due to the increase of interparticle contacts and hence more rigid structure produced. D_B for spherical powders tended to zero, further supporting the hypothesis that D_B is the densification which occurs by individual particle movement. D_B was found to be sensitive to variation of particle shape[17], but later[18] it was stated that particle size, shape, size distribution and surface preparation seemed to have only minor effects in terms of A, k, D_B and D_o. The sensitivity of spherical powders to size distribution was an exception.

Powder material variation gave the greatest variation in k, which is defined as a measure of the ability of a compact to deform and which Heckel[17,18] regarded as a material constant. k increases with particle softness or ductility and decreases for powders with a high discrete oxide content or high oxide surface film. It approximates to $1/(3\sigma_o)$[17], where σ_o is the material yield strength.

Equation 2-7 has been applied to the isostatic compaction of iron and nickel-based alloy powders[19] to determine the role of plastic deformation in metal powder compaction. Hewitt et al[19] were able to relate X-ray line broadening from compacted samples to strain and with increasing pressure believed the following stages to occur;

(1) Compression and consolidation of fines, leading to point contact between larger particles.

(2) Plastic distortion in the surface regions of the larger particles at contact points, producing convoluted and interlocking interparticle boundaries.

(3) Bulk plastic flow, causing a gradual decrease in pore size.

Results of microhardness and X-ray line broadening both suggested that extensive plastic deformation occurs early in compaction. It was concluded that during stage 1 the flow stress of the powder is greater than the compressive pressure and hence local deformation results. The transition

from stage 1 to stage 2 occurs when the applied pressure exceeds the bulk yield stress of the material, hence plastic flow becomes homogeneous instead of local.

A two stage process for the compaction of metal powders has been suggested by Brackpool[20];

1- Initial packing.

2- Particle deformation.

The importance of plastic deformation and strain hardening were emphasised by the adoption of a general stress-strain relationship of the form given in equation 2-9 [20];

$$P = k\varepsilon^n \qquad \ldots(2\text{-}9)$$

where P is the applied pressure,

k and n material constants,

and ε the volume strain given by equation 2-10.

$$\varepsilon = \ln\left[(D-D_t) / D(1-D_t)\right] \qquad \ldots(2\text{-}10)$$

D_t, the tapped density, being chosen as close to the density where particle deformation commences. Strong relationships were obtained between k and n and material properties.

Brackpool[20] suggested that during initial packing particle contact area must be exceedingly small so that deformation may occur at very low applied pressures. Surface topography could therefore influence the extent of stage 1. D_t was found to be incorrect as a measure of the extent of stage 1 for irregular particles. The second stage is controlled by deformation of particles, quantitatively measured in terms of material properties (yield strength and work-hardening properties).

Beddow[21] has also confirmed that D_t rarely corresponds with the end of the initial stage of compaction. He has also shown that attrition

and plastic deformation must start early during compaction. It appears that compaction effected by the direct application of a force probably causes local deformation even during initial particle rearrangement stages. Compaction by the indirect application of energy, such as vibration during the determination of tapped density D_t, does not seem to cause appreciable deformation.

Donachie and Burr[22] and Morgan and Sands[23] have also used empirical straight line relationships to reveal compaction stages. Morgan and Sands[23] used the Heckel type of equation (2-7) whilst Donachie and Burr[22] used a more generalised relationship of which equation 2-7 is a simplified version. The more generalised relationship was found[22] to be more applicable at very high pressures and it was concluded that the following stages occur during the compaction of a metal powder.

1- Initial die-fill,

2- transitional restacking,

3- plastic deformation (local deformation in commercial powders),

4- isostatic compression.

It is apparent that several discrete stages occur during the compaction of a metal powder containing no admixed lubricant. These stages must obviously overlap but empirical straight line relationships have been found useful in indicating the transition from one stage to another. An equation, such as 2-7, may also be of value in determining the influence of lubricants on these various compaction stages.

2-6 The role of lubricants during compaction

Sajdak et al[12] have listed the types and contribution of friction to compaction as follows;

(a) Friction between moving punches and die walls - generally negligible, but may become significant with no lubricant and the presence of fines[1].

(b) Friction between powder particles and die wall - the primary cause of pressure losses during compaction. The magnitude depends on powder

material, particle size and size distribution, morphology and surface condition.

(c) Friction between particles - this was found to play only a small part in compaction.

(d) Internal friction within the particles during deformation - this is a material constant.

The compaction behaviour of powders containing lubricants were studied in terms of pressure transfer characteristics using single end compression. Conclusions may be summarised as follows[12].

(a) In the majority of tests no advantage was found in adding lubricant greatly in excess of 3% by weight. Below 3%, admixing was inferior to 1% by weight in benzene applied directly to the die-wall. There is therefore an optimum admixed lubricant addition for maximum efficiency in terms of the ratio of transmitted/applied load. Admixed lubricant is less efficient in reducing die-wall friction than application directly to the wall.

(b) The ratio transmitted/applied load reduced as the thickness/diameter ratio of compacts increased, but was increased by increasing additions of lubricant up to the optimum. This illustrates the effect of compact length on pressure transfer. Lubrication reduces interparticle friction and particle/wall friction thus improving pressure transmission.

(c) For a given compact thickness/diameter ratio transmitted load was found to improve in the following order for iron powders, flake, sponge, atomised, electrolytic. This is probably the result of dependence on several material variables including particle size and distribution, particle shape, purity, level of oxidation and hardness.

It is interesting to note from this work the relative importance of particle/die-wall friction during compaction. Application of lubricant directly to the die-wall was found to be more efficient at reducing this friction than admixed lubricant. The extrusion of lubricant from within

pores onto the die-wall during compaction has been suggested or observed by other workers[2,4,24,25]. It seems that the interposition of lubricant between particles and the die-wall, to prevent direct contact, is more desirable than extruding lubricant between surfaces during compaction. This becomes more significant when the ejection of compacts is considered (section 2-7).

Yarnton and Davies[24,25] have worked extensively in this area and have also concluded that there is an optimum proportion of admixed lubricant for minimising the various forms of friction. However, it is not necessarily the same level for all types of friction. Stearic acid was applied in the same manner as their work on loose powder packing[13]. At low compaction pressures it was shown that the lubrication effect was apparently constant whatever the film thickness once molecular coverage was achieved. It was found that there is an optimum lubricant addition (0.1-0.2% by weight) which allows lubrication rather than inhibition to be the dominant factor over the widest range of pressures.

The lubrication effect was detected by improved compact densities [24,25] and it is interesting to note that an optimum addition was observed again. However, it seems that the optimum lubricant addition suggested by this method differs considerably from that required for maximum transmitted/applied load ratios[12]. Beyond this optimum addition Yarnton and Davies [24,25] note that the opposing effect of inhibition (reduced compacted density relative to the unlubricated condition) seemed to be present over the whole range of pressure and content. This increased with an increase in both factors.

Transition pressure has been defined[24,25] as the compaction pressure where a state of lubrication changes to a state of inhibition in terms of true compact density. (True compact density = green density x $\frac{\%\ \text{metal}}{100}$ (24)). This has been used[24] to determine optimum lubricant additions for improved

FIGURE 2-2. Schematic representation of the Lubricant Effect and Transition Pressure.[24,25]

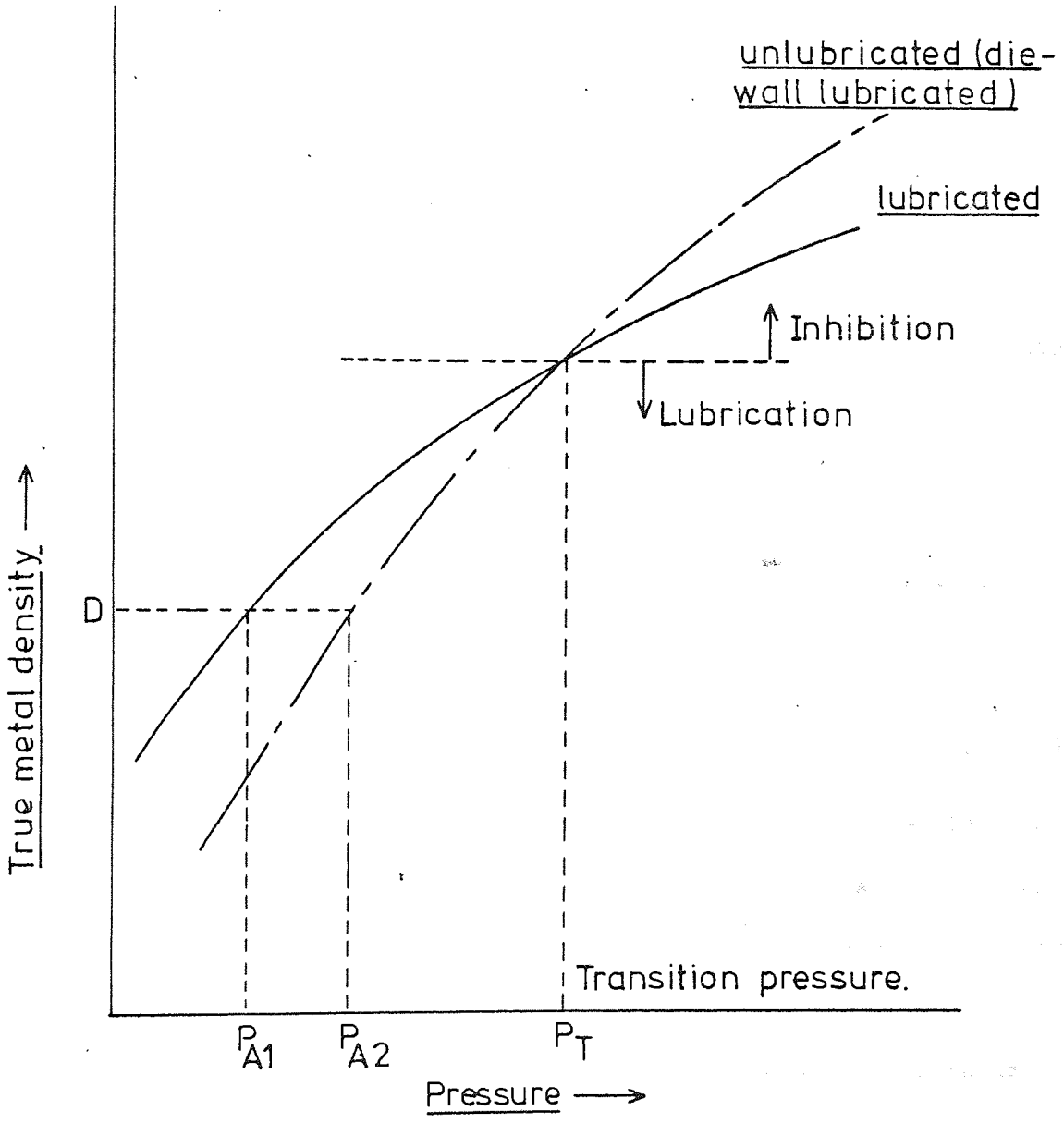

densification. Yarnton and Davies[25] have also used the 'Lubricant Effect' to indicate the positive, or negative, contribution of lubricant additions to compaction. The relation between the applied compaction pressure P_A the effective densification pressure P_E and the frictional pressure losses L can be expressed as equation 2-11[25].

$$P_E = P_A - L \qquad \ldots(2\text{-}11)$$

If a metal powder compacted in the absence and presence of lubricant (admixed or die-wall) is considered then identical true densities will be achieved when corresponding effective pressures are equal[25]. It can be seen from figure 2-2, which also schematically illustrates transition pressure, that at a given density D the applied pressures for lubricated and unlubricated compacts are P_{A1} and P_{A2} respectively. At D the effective pressures must be equal, therefore,

$$P_{E1} = P_{E2}$$

$$P_{E1} = P_{A1} - L_1 = P_{A2} - L_2$$

$$P_{A1} - P_{A2} = L_1 - L_2$$

or $P_{A1} = P_{A2} = \Delta P = \Delta L$, the Lubricant Effect[25] $\qquad \ldots(2\text{-}12)$

It should be stressed here that all this work is evaluated in terms of true compact density or true metal density which reflects the spacing or deformation of metal powder particles only. Lubricant is eliminated by considering only the weight of metal in a compact.

Transition pressure[24,25] was found to increase with increasing additions of lubricants up to an optimum level. Beyond this level transition pressure decreased indicating inhibition of compaction by admixed lubricants. Die-wall lubrication was found[24] to be more efficient in achieving a given density than admixed lubricant over the whole of the pressure range used. This would seem to indicate the importance of metal particle/die-wall friction during compaction, as noted previously[12].

Yarnton and Davies[24] have suggested that during early compaction stages inhibitive effects are minimal. There is sufficient voidage to allow both metal particles and lubricant to flow into voids with little interference. As pressure increases lubricant is preferentially extruded into pores containing neither metal nor lubricant at the expense of metal. Therefore in the early stages the gain in densification due to lubrication is lost. The inhibitive effect increases with lubricant content[24] and obviously densification must effectively cease when the volume percentage of lubricant and porosity are equal. The Lubricant Effect, which is positive when lubrication predominates and negative when inhibition is operating, is a particularly effective measure of the degree of lubrication or inhibition operating in a particular system[25].

The importance of extrusion of lubricant from pores is indicated by work by Yarnton and Davies[24] using die-wall and admixed lubrication simultaneously. This was found to yield low transition pressures due to the presence of die-wall lubricant preventing exudation of lubricant from within compacts.

The existence of an optimum level of admixed lubricant for maximum density has been confirmed by Leopold and Nelson[4], Ljungberg and Arbstedt [1], Mallender et al[27] and El Wakil and Davies[28]. Leopold and Nelson[4] have used the ratio of transmitted to applied load to study the influence of admixed lubricant on compaction. Their conclusions may be summarised as follows:

(a) A linear relationship was found to exist between the applied force and the transmitted force for all conditions investigated. The slope of this relationship was termed the k-factor.

(b) Only a small amount of either die-wall or admixed lubricant is necessary to give a high k-factor. Increasing amounts of lubricant have little effect. Die-wall lubrication was considered more effective than admixed

lubricant for increasing k, since admixed lubricant must be forced from the powder onto the die-wall during pressing to effectively increase transmitted pressure.

(c) There was found to be an optimum amount of stearic acid which gave maximum true density for a given combination of powder weight and compaction pressure. This optimum lubricant addition increases with decreasing compaction pressure presumably due to less lubricant being forced onto the die-wall. It decreases with increasing compact weight at higher compaction pressures.

(d) For small compacts admixed lubricant had little effect on true density, whereas a small amount markedly increased the true density of large compacts.

(e) There was no apparent optimum amount of die-wall lubrication which gave a maximum density. For all weights and pressures investigated the true density was found to increase with the amount of die-wall lubrication.

(f) Die-wall lubrication resulted in a higher density at high pressures compared to admixed lubricant. This is probably due to inhibition.

(g) There was found to be a weight of compact for which maximum density occurred and which was not necessarily the lowest. This was assumed to be due to restricted particle movement with decreasing compact size which did not allow satisfactory particle repacking and deformational bonding.

The work of Yarnton and Davies[24] has indicated the insignificance of interparticle friction relative to particle/die-wall friction during compaction. Investigations using measurement of transmitted/applied load ratios[4,12] seem to indicate that both interparticle and particle/wall friction may be important. For example, the conclusions of Leopold and Nelson[4] given above (b) and (e) would seem to indicate the importance of particle/wall friction, whilst (d) and (g) seem to stress the significance of interparticle friction. The relative importance of each, for a

given powder type, may well depend on compact geometry.

Ljungberg and Arbstedt[1] have shown that at low pressures lubricant additions improve compacted densities relative to die-wall lubrication contrary to the findings of Yarnton and Davies[24]. This effect was found to diminish with increasing pressure due to the controlling influence of interparticle friction being superseded by competitive flow of metal and lubricant. Due to the short movement of powder particles relative to die-walls during forming, die surface finish was found to have little effect on compacted densities[1]. Even small amounts of lubricant were able to diminish the friction effect.

El Wakil and Davies[28] agree with Leopold and Nelson[4] that the ratio transmitted/applied load is not affected much by lubricants at low compaction speeds. However, at high speeds this ratio is markedly affected by the presence of lubricants.

Compaction in the absence of admixed lubricants[17,20] has shown that early stages, involving rearrangement, are sensitive to particle morphology such as shape and size distribution. The apparent influence of lubricants on interparticle friction will therefore depend on the extent of particle rearrangement and particle morphology. Spherical particles, undergoing little rearrangement after initial packing[17], would not be expected to benefit greatly from admixed lubricants at this stage. Improvements in particle rearrangement processes during early compaction stages, before interparticle bonding becomes appreciable, could be beneficial in reducing density variations in complex shaped components.

Compaction inhibition[24,25] could possibly improve density distributions within compacts by preventing further densification in regions of high density and hence increasing the ratio of transmitted/applied load. However, large amounts of lubricant, above a certain optimum,[4,12] have been found to have little or deleterious effects on pressure transmission.

2-7 The role of lubricants during compact ejection

The main purpose of admixed lubricant is the reduction of ejection forces during the manufacture of powder metal compacts. This decreases the energy expenditure and die-wear rate, and improves component surface finish. The object is to interpose a lubricant film between particles in the surface of the compact and any tool surfaces against which they slide during ejection. In terms of material usage maximum efficiency would be expected with lubricant applied directly to the tool surfaces. However, engineering difficulties generally prevent this method being adopted. Stearate lubricants must be dissolved in environmentally undesirable solvents such as benzene and ether. The extra process may also adversely affect production rates.

The usual and most convenient method of applying lubrication is the admixing of lubricant with the metal powder. Lubricant is then extruded[2, 4,24] out of the compact onto the tool surfaces during compaction. Unfortunately this utilises only that lubricant near the compact surface.

2-7-1 Friction during ejection

Much work has been carried out on the determination of friction coefficients between iron powder compacts and die-walls during ejection by Mallender et al[27,29]. The interface between a compact and die-wall is not a continuous smooth surface, contact is therefore only made at asperities[27]. For such a system the frictional force to shear metal/metal contacts (F) during a process such as ejection may be expressed as equation 2-13[27].

$$F = \sigma_{Av.} A_r \qquad \ldots(2\text{-}13)$$

where $\sigma_{Av.}$ is the average shear stress over the areas of contact,

and A_r is the real area of contact.

Lubricant may fill the valleys between metal/metal contacts and interpose itself between contacts when sliding commences. The total frictional force is now the sum of the forces required to slide lubricated interfaces, F_2, and the forces required to overcome the sticking effect of unlubricated interfaces, F_1. The coefficient of friction for such conditions is given by equation 2-14[27].

$$\frac{F_1 + F_2}{P} = \mu \qquad \ldots(2\text{-}14)$$

where μ is the coefficient of friction

and P the load forcing the two surfaces together.

Mallender et al[27] consider that for a given load the highest and sharpest asperities are more lightly loaded when lubricant is present, with a consequently smaller contribution from F_1. The hardness of a lubricant film is normally lower than that of the metal such that the contribution from F_2 tends to be dependent on film thickness. High applied loads should lead to appreciable film perforation, increasing the proportion of metal/metal contact with a resultant increase in the friction coefficient with increasing F_1.

The sliding behaviour of a compact/die-wall interface system will be dependent on the metal/metal contact area, lubricant film area, lubricant type and content, and the density of the metal surface[27].

2-7-2 Ejection-stress

The ejection-stress is the stress required to overcome the frictional forces described above. Ejection-stress has been found to be inversely proportional to lubricant content[2,4,12,24,27,28]. The relationship between ejection pressure and lubricant content is generally hyperbolic[24] in form with little advantage in additions above a certain optimum. Mallender et al[27] quote 2% by weight for maximum lubricity. At high levels

lubricant is extruded[2] from pores in sufficient quantity to supply a thick film between metal/metal contacts, although resistivity measurements [29] have indicated that direct metal/metal contacts still exist at lubricant levels as high as 2%.

At low lubricant additions (less than 0.2%)[24] lubricant exudation onto die-walls is insufficient for complete lubrication. F_1 (equation 2-14) increases and the ejection pressure increases to overcome the resistance to shear of the greater number of cold pressure welds[24]. In this region of fractional coverage ejection-stress decreases rapidly with small increases in lubricant content.

Leopold and Nelson[4] have shown that for unlubricated conditions ejection pressure is directly proportional to the area over which friction is acting. The coefficient of friction along the compact length is constant. When lubricant is admixed the friction coefficient is found to be non-linear with respect to contact surface area. Leopold and Nelson[4] plotted ejection pressure against the distance compacts move in a die during ejection. Low lubricant levels caused an increase in ejection-stress towards the end of the ejection cycle due to their inability to maintain a lubricant film. Large additions produced maximum ejection pressure towards the start of the cycle, as did die-wall lubrication, reflecting the thick film supplied. Yarnton and Davies[24] have reported that admixed lubricant in excess of 0.2% by weight is required to provide the full lubrication provided by die-wall lubrication in terms of ejection pressure/compaction pressure relationships.

When compared to low admixed lubricant additions die-wall lubrication would seem to be advantageous in that lubricant is deliberately interposed between particle/die-wall contacts discouraging cold pressure welds. However, if perforation of a die-wall lubricant film occurs then there is no admixed lubricant to replenish it. High admixed lubricant

additions would therefore be expected to be advantageous at high densities, but obviously only where compaction inhibition did not occur.

Mallender et al[27] have obtained detailed ejection-stress/compact movement curves for compacts containing various proportions of lubricant. The three main types of relationships are shown in figure 2-3, obtained at low ejection rates. All are characterised by an initial sharp peak(A), termed the break stress, the stress required to overcome initial sticking friction. The break stress is followed by a slightly lower stress, the initial slip stress(B). Beyond this point the form of the curve differs with varying lubricant content. At low contents, curve (1), the stress rises to a maximum slip stress(C) and then, as the lubricant film is incomplete, ejection proceeds by a series of stick/slip conditions. The maximum stress occurs during this stage(D), the maximum stick stress.

As lubricant content increases, curves (2) and (3) in order of increasing content, the maximum slip stress and maximum stick stress become coincident and conditions of slipping friction are attained. This occurred at lubricant levels in excess of 0.5% (zinc stearate) in the work of Mallender et al[27]. It can be seen from figure 2-3 that the maximum recorded ejection-stress depends on the lubricant level. At high levels the maximum occurs at the initial break stress. The conditions of slipping friction indicated by curves (2) and (3) in figure 2-3 were those investigated by Mallender et al[27,29].

Fast ejection rates have been found to reduce[27,28] ejection stresses, at least at low lubricant levels (less than 1%)[27]. The ejection-stress/compact movement relationship also changes at high speeds as shown by curve (4) in figure 2-3[27].

2-7-3 Coefficients of sliding friction and lubrication

Mallender et al[27] have shown that coefficients of sliding friction at high lubricant levels (in excess of 2.0% by weight) are nearly constant

FIGURE 2-3. Typical ejection stress/compact movement relationships (after Mallender et al[27])

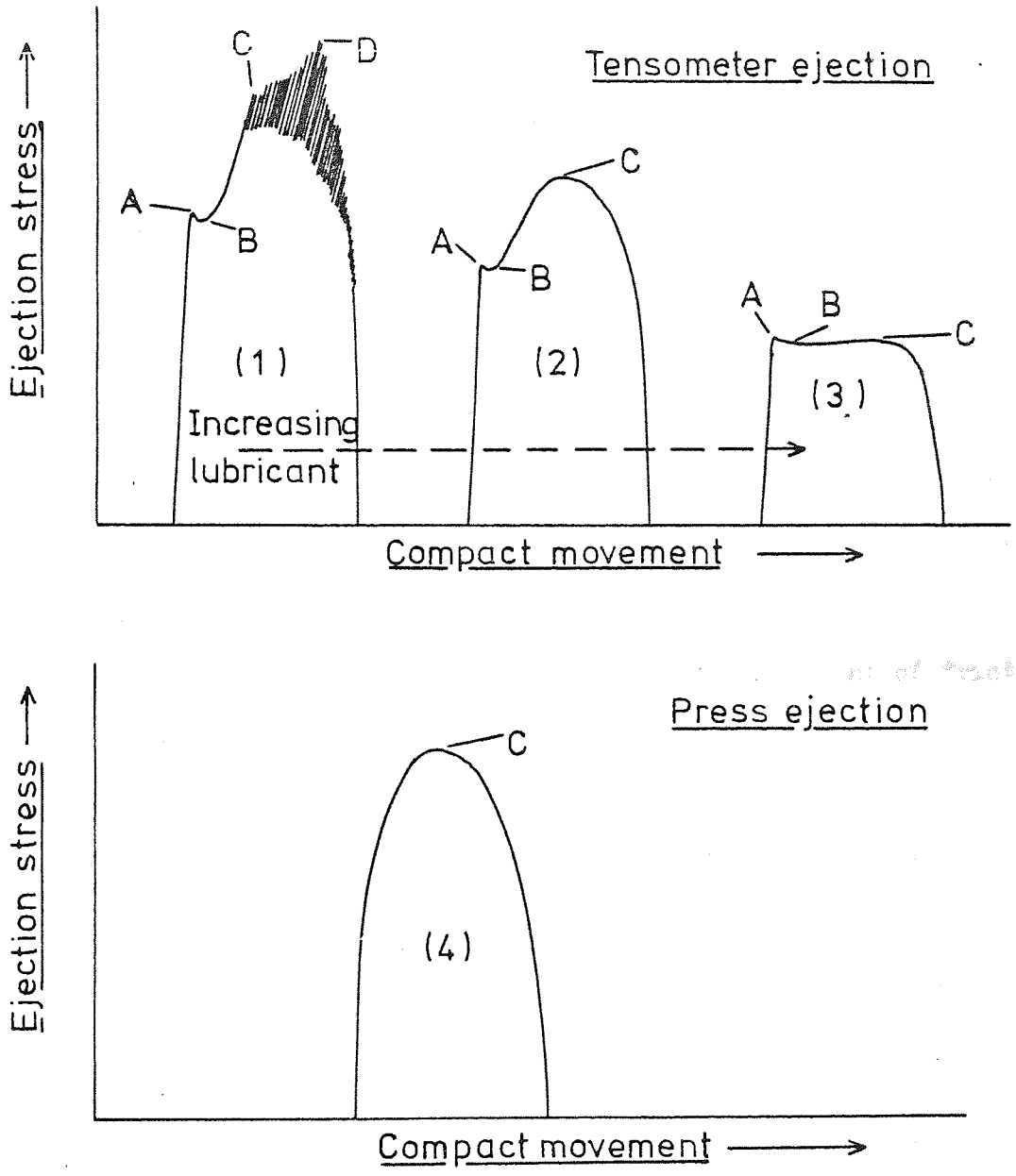

A — Break stress.
B — Initial slip stress.
C — Maximum slip stress.
D — Maximum stick stress.

and independent of compact density. This is attributed to a thick coherent film which provides almost complete compact coverage. Low lubricant levels produce incomplete films, as discussed previously, so that for a constant load P and density, F_1 in equation 2-14 increases with a corresponding increase in the coefficient of friction. Coefficients of sliding friction measured during ejection of iron powder compacts containing zinc stearate [27] fell rapidly from approximately 1.1 for unlubricated compacts to less than 0.2 for additions of 0.5% and then to approximately 0.1 at 2% lubricant.

Values of the coefficient of sliding friction of zinc stearate obtained by the 'pin and disc' method[29] were found to be insensitive to the velocity of sliding and inversely proportional to load, but only to a slight degree. This seems to indicate that high ejection-stresses obtained at low lubricant levels are due to an increase in the number of unlubricated metal/metal contacts rather than a change in the coefficient of friction of lubricated contacts.

Increasing lubricant particle size tends to reduce the coefficient of sliding friction[27], a constant minimum being obtained above an optimum median particle size. This effect is also most marked as density increases. This was attributed to the ability of larger zinc stearate particles to produce an extensive coherent film.

2-8 The effect of admixed lubricants on green strength and ability to handle.

The most important parameters governing the strength of cold-pressed metal powder compacts[30] are freedom from oxidation and the plastic properties of the powder particles. These determine the roles played by surface energy and powder geometry in powder compaction. Therefore lubricants such as stearates, described as surface-active agents[2], could reasonably be expected to influence compacted properties by affecting surface properties.

An interparticle contact in a pressed compact may perhaps be regarded as two surfaces in mutual contact, at least at low densities. The presence of lubricants in such surfaces could possibly reduce their strength.

The presence of admixed lubricant in a compact does reduce green strength relative to the unlubricated condition. This effect increases with increasing lubricant additions[1,28] and is attributed to a rapid reduction of interparticle contact area[24]. At high lubricant contents and/or high densities it is possible to envisage the inhibitive influence of lubricants encouraging interposition of lubricant. However, at very low densities the possibility of high lubricant contents acting as a binder cannot be entirely discounted although the high contents and low densities involved probably have no practical significance in iron powder metallurgy.

2-9 The removal of lubricants from compacts during sintering.

The initial stages of commercial sintering are concerned with the removal of solid admixed lubricants prior to attaining maximum sintering temperatures. Sintering furnaces are generally arranged such that the atmosphere flow carries lubricant decomposition products away from the sintering zone. These products can often be seen condensed around the entrance of furnaces, particularly zinc oxide from zinc stearate decomposition. However, little work has been carried out to determine the decomposition characteristics of lubricants and the influence of decomposing lubricants on sintered compacts.

Some investigations have been undertaken by Meyer et al[11] to examine the dewaxing process and products and decomposition characteristics of various lubricants. Various lubricants, including several stearates, were studied as free compounds not within compacts, using thermogravimetry. Atmospheres employed were air, nitrogen, hydrogen and vacuum, with a linear temperature rise of $125^{o}C.hr.^{-1}$ From this work Meyer et al[11] have

indicated the temperature limits above which decomposition may be considered as total. These temperatures for the stearates are shown in figure 2-4. It can be seen that generally decomposition in air required the highest temperature whilst in vacuum a temperature some 100°C lower than the gaseous atmospheres was required. The thermogravimetric curves may be used to determine the temperature zone in which the compacts are subject to dewaxing. It has been noted[11] that within this zone the temperature should be raised gradually to avoid defects caused by over-rapid expulsion of lubricant.

Of the lubricants studied zinc stearate appeared to be the most stable and was the only material which left a considerable solid residue (approximately 18% by weight) after burn-off at 750°C. This solid residue was reduced in quantity after sintering at 1125°C in a reducing atmosphere. The reduction product condensed in cooler parts of the furnace giving zinc oxide and zinc metal. As zinc stearate is the most widely employed powder metallurgy lubricant it can be envisaged that such residues could be a source of practical problems in sintering, particularly with inclusion sensitive high strength materials[11]. If complete elimination of zinc is not achieved there may also be a problem in reactions between zinc vapour and furnace elements or furnace muffles.

The thermogravimetric data of Meyer et al[11] were confirmed by studies of isothermal decomposition. All the materials investigated were generally eliminated after one hour at 450°C, atmosphere having little effect. Solid residues were always negligible after complete burn-off but there were considerable proportions of residues condensing by 20°C (70%-90% of initial weight), a high percentage condensed at 60°C-80°C. Volatilisation rather than decomposition was observed to be the predominant mechanism. None of the lubricants studied decomposed into gases exclusively. A condensed residue always formed in cooler parts of the furnace, tending

FIGURE 2-4. Temperature for complete decomposition of lubricants in different atmospheres (after Meyer et al[11])

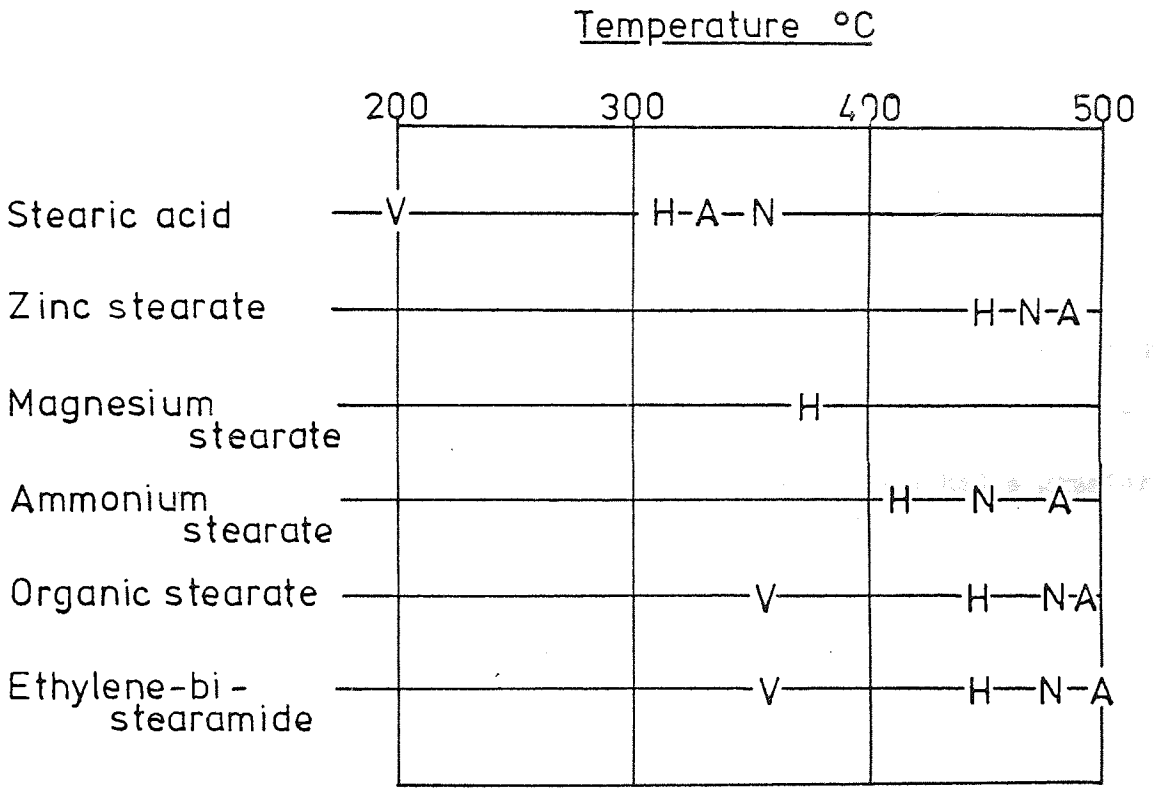

ATMOSPHERE
V—Vacuum (approx. 0·1 torr)
A—Air
N—Nitrogen
H—Hydrogen

to block gas exits. The formation of a saturated, volatilised lubricant 'fog' in sintering furnaces has been suggested elsewhere[5].

The burn-off characteristics of common lubricants in 316L stainless steel powder compacts have been considered by Moyer[10]. The burn-off, or dewaxing, temperature for complete removal of various lubricants has been found to be proportional to the amount of lubricant, to some extent, and also dependent on the type of atmosphere employed. Air was more efficient than dissociated ammonia. In this work residual carbon was found to be a major problem when using stearates. It was noted that a burn-off in air prior to sintering tended to reduce strength after sintering but also reduced residues from stearates by a factor of two or three.

Oxygen contents were found to increase[10] after sintering whether a burn-off period was employed or not. It was thought that stable chromium oxides may be formed by reaction with oxygen in the lubricant. Lithium stearate behaved sluggishly compared to zinc stearate and had a greater affinity for oxygen pick-up.

2-10 The effect of lubricant decomposition on mechanical properties of sintered compacts.

There is evidence to suggest[1] that as the proportion of admixed lubricant increases the sintered strength of a compact decreases. This is particularly so at high lubricant contents due to the lack of good contact between particles. It has also been suggested that elongation of sintered compacts is reduced[1] not only because of increased porosity but also by poorer sintering activity. However, the presence of a carbon deposit from decomposition of stearic acid additions is thought to be responsible for increased sintering activity in Fe/Cu/Sn compacts by reducing SnO_2[31]. Yarnton and Davies[25] have also obtained improvements in sintered mechanical properties relative to the unlubricated condition for iron compacts containing purified paraffin wax. It was thought that solution of carbon

during wax burn-off was responsible for this improvement.

Elwakil and Davies[28] have shown that as the zinc stearate content of sponge iron powder mixes increases sintered strength decreases relative to the unlubricated condition. This is particularly so at high densities. Elongation was observed[28] to decrease linearly with increasing lubricant addition. These phenomena have been attributed to the fact that zinc stearate is extruded between particle boundaries preventing true metallic contact. Zinc stearate may also become entrapped by the deforming particles during compaction, resulting in isolated enclaves which become interconnected on release of the burnt lubricant during sintering.

Comparative testing by Meyer et al[11] using 1% zinc stearate and 1% ethylene-bi-stearamide, which leaves no solid residue, has suggested that the solid residue of zinc oxide remaining after decomposition of the stearate has adverse effects on the properties of sintered components. This adverse effect varied in direct proportion to the proportion of lubricant added so that small additions such as 0.25% were considered to have negligible effect on properties.

It seems by no means clear whether lubricants adversely or beneficially effect sintered properties of compacts. The dependence of any influence of process variables such as lubricant type and thermal conditions is also virtually unknown.

3 Project outline

The proposed practical work was seen as consisting of two separate but interrelated sections. One part, probably the most important, was concerned with the decomposition behaviour of the solid admixed stearates which are used in the powder metallurgy industry. The final object was not necessarily recommendations for alternative dewaxing practice or lubricants. However, it was aimed at providing basic information on lubricant decomposition behaviour which seemed to be lacking.

Particular emphasis was placed on the nature of decomposition reactions within compacts and their influence on the development of properties in such compacts. Iron powder was used throughout as this was the highest commercial tonnage material and allowed a wide range of temperatures to be used.

The first section of work was concerned with the influence of lubricant on loose powder properties, compaction, ejection and as-pressed properties. The main object was the further understanding of the behaviour of lubricant during the stages in the production of a powder metal compact prior to sintering. It was intended to use the same materials throughout to facilitate determination of the interrelationship between successive stages. Previous investigations have been made difficult to understand due to the use of different materials at each stage.

Mixing and green strength were investigated in some detail since there did seem to be a lack of information relating to these. However, ejection was studied superficially only. It was thought that without the availability of equipment such as an instrumented press ejection studies could not be advanced further than those carried out elsewhere[27,29].

3-1 Part 1 - Loose powder and compact properties

The majority of this investigation was carried out with one lubricant only (zinc stearate). However, green strength was studied using all of the

lubricants investigated in part II (Heat treatment). This was seen as a necessary precursor to the study of the influence of decomposing lubricant on the development of mechanical properties.

(a) Mixing. Simple tumble mixing was used with various additions of lubricant. Loose powder properties (apparent density) were determined at various mixing stages. Results were compared with those of iron powder with lubricant coatings prepared by the more controlled method of precipitation from a solvent[13].

(b) Compaction. The loose packing of powder in a die cavity may be regarded as the initial stage of compaction. Therefore, the determination of apparent density in the previous stage linked it with this section.

The various overlapping stages of compaction and the mechanisms operating in them have been identified by using empirical straight line relationships between density and compaction. It was proposed to take one of these relationships, that used by Heckel[17], and apply it to the compaction of iron powder containing admixed lubricant. It was hoped that by assuming that such a relationship existed it would be possible to determine the influence of lubricants on each stage of compaction.

The influence of lubricants on compaction was investigated also with the aid of such phenomena as compaction inhibition and the lubricant effect[24,25]. The effect of lubricant dispersion (admixed or precipitated) was restudied. Results obtained from compacts containing lubricant with and without die-wall lubrication were used to isolate the effect of particle/die-wall friction during compaction.

(c) Ejection. The ejection-stress of compacts was measured during the preceding stage. As stated previously ejection was not studied in great detail but it was hoped to relate particle/die-wall friction during ejection with that occurring during compaction. The lubricating properties of admixed and precipitated additions were studied again.

(d) Green strength. The effect of lubricant content and dispersion on green strength were determined by using the same materials as in the previous stages. In addition the effects of lubricant type and particle size were investigated by employing the various lubricants used in part II. It was hoped finally to be able to state whether lubricant type, morphology, dispersion or content had the most important influence on as-pressed strength.

3-2 Part II - Heat treatment.

This section of work was concerned initially with the decomposition behaviour of several free lubricants. The influence of process variables such as atmosphere type or flow rate were investigated also. When the decomposition reactions of these lubricants were known it was possible to study their occurrence within iron powder compacts and show the influence of compacts on them. Process variables investigated included;

(a) atmosphere type and flow rate,

(b) lubricant content,

(c) compact density and pore size,

(d) heating rate.

It was proposed to use thermogravimetry to detect, identify and study reactions of free lubricants and those within compacts. The actual mode of decomposition, especially within compacts, was studied by using direct observation.

It has been stated previously that it was by no means clear whether decomposing lubricants adversely or beneficially affect the development of mechanical properties of sintering compacts (2-10). It was envisaged that both physical (such as pressure build-up) and chemical (effects on sintering mechanisms) effects may be involved. The significance of physical effects were determined by using tensile specimens containing lubricants, treated at high and low heating rates.

Chemical influences were investigated by using tensile specimens containing lubricants heat treated isochronally or isothermally at various temperatures and in several atmospheres. The parameters measured were tensile strength and dimensional change.

4 Materials

Several different iron powders were used during the study of compaction although most of the investigation in part 1 was carried out using only one powder, MP32, and one lubricant, zinc stearate. In part II (Heat Treatment) only one iron powder was used (MP32) but the decomposition characteristics of five lubricants were studied. This section provides a brief description of each material.

4-1 Metal powders

The iron powders and any treatment they were given such as sieving are listed in table 4-1. Total oxygen contents, obtained by analysis in a Balzer Exhalograph, are also recorded in this table. Particle morphology is illustrated by the scanning electron photomicrographs of plates 4-1(a-j).

Table 4-1

The metal powders used during this investigation

Identification	Type and origin	Treatment	Total oxygen %
A	ROSPOL MP32	sieved 104-180μm	---
B	ROSPOL MP32	sieved 53-104μm	---
C	ROSPOL MP32	sieved -53μm	---
D	ROSPOL MP32	As received -180μm	0.25-0.30
E	ROSPOL MP32	53-104μm. Carburised	---
F	ROSPOL MP32	53-104μm. Annealed	---
G	MANNESMANN WP150	As received -147μm	0.18
H	" " HOGANAS NC100	As received	0.49
I	" " HOGANAS ASC100	As received	0.10
J	CARBONYL IRON	sieved -53μm	0.25

All of these powders were used in the initial investigation of compaction carried out with no admixed lubricant. They were all iron powders,

PLATE 4-1. Scanning electron micrographs of metal powders

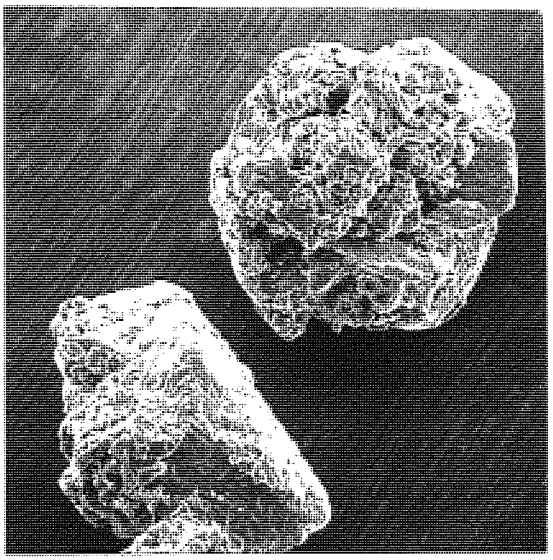

100 μm

(a) MP32 (104 - 180 μm)

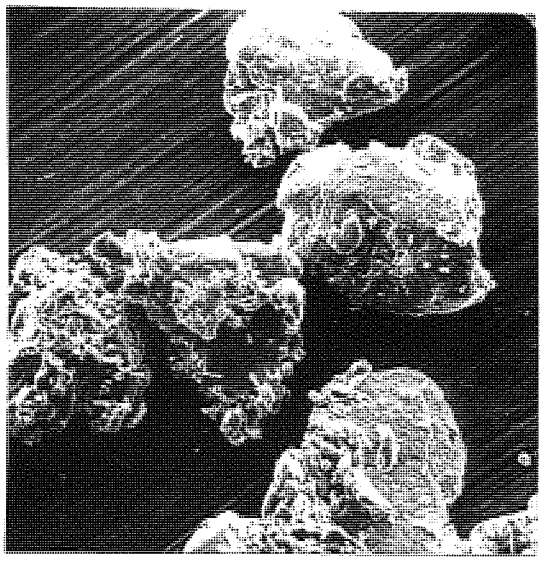

100 μm

(b) MP32 (53-104 μm)

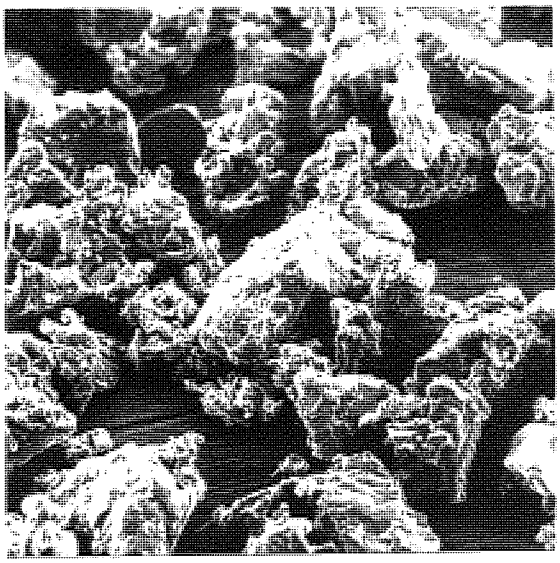

100 μm

(c) MP32 (-53 μm)

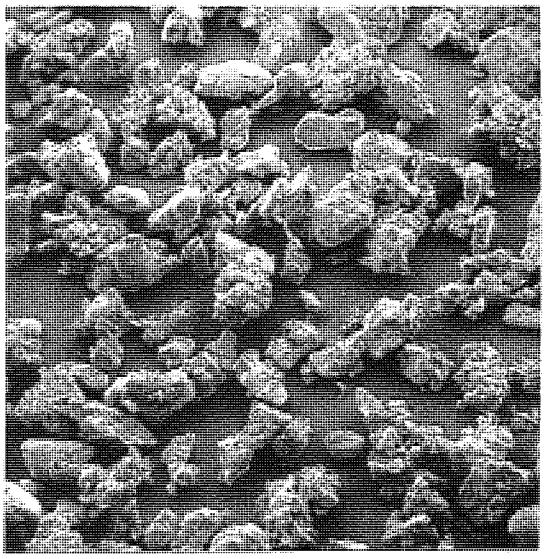

100 μm

(d) MP32 (as received)

PLATE 4-1 continued.

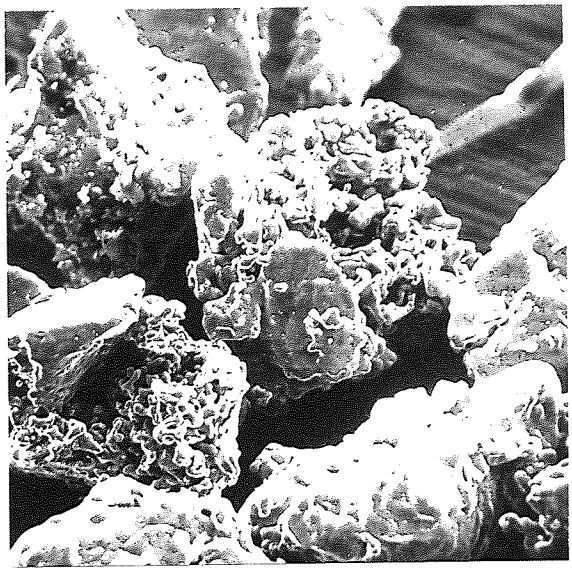

100 μm

(e) Material B carburised.

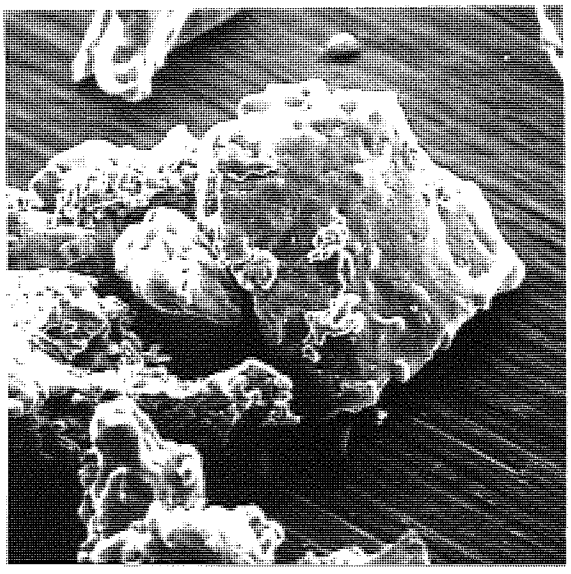

100 μm

(f) Material B annealed

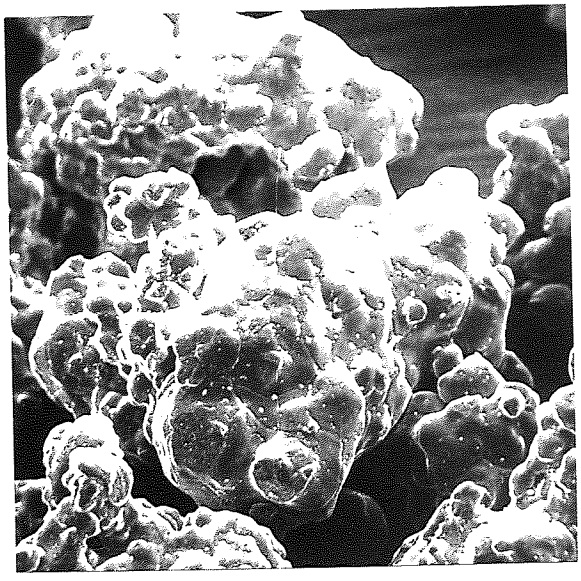

100 μm

(g) WP 150

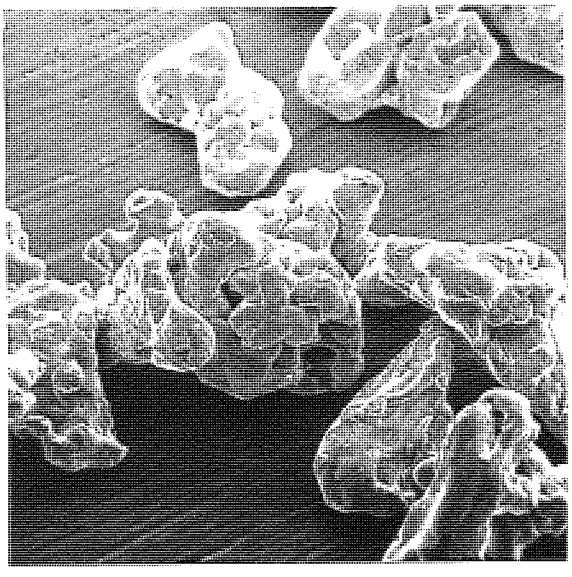

100 μm

(h) NC 100

PLATE 4-1 continued

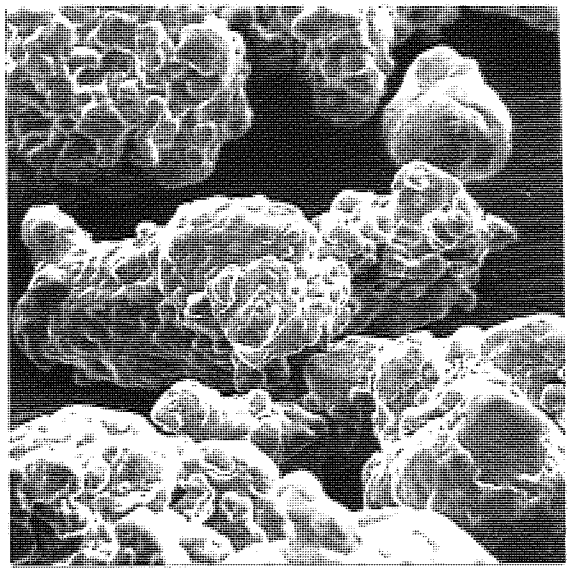

(i) ASC 100

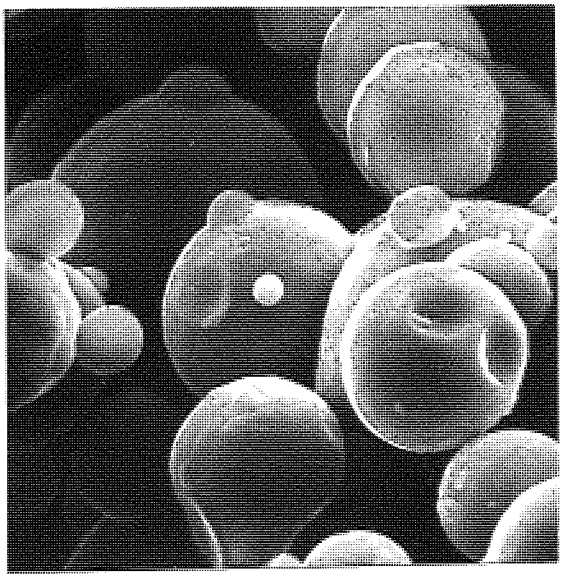

(j) Carbonyl iron.

at least initially, and were chosen to fall into the broad category of irregular particle shape (plate 4-1). The exception was the carbonyl iron (J) which was a spherical powder (plate 4-1,j). The general irregular shape was chosen as this covers a wide range of available iron powders. It was also hoped that high green strengths would be developed, compared to other particle shapes, so that it was possible to handle low density compacts for density distribution determinations.

Material D (MP32 as received) was found to sieve to three similar weight fractions in the particle size ranges indicated for A, B and C, (table 4-1). These fractions were used to investigate the role of particle size during compaction. The range of deformation properties was increased by heat-treating two samples of material B (MP32, 53-104μm). One sample (material E) was carburised by admixing 0.4% by weight graphite and heating at 950°C for 1 hour in an atmosphere of $N_2/10\%H_2$ plus approximately 10% CO in a horizontal tube furnace. Material F was annealed at 950°C for 1 hour in $N_2/10\%H_2$. Both powders were furnace cooled in $N_2/10\%H_2$ and required light hand grinding to reduce the resultant cakes to powder. The photomicrographs of plates 4-1(b)(e) and (f) were used to check for any gross changes of particle morphology due to heat-treatment or grinding. The microstructures of materials B, E and F are shown in plate 4-2, all were etched in 2% Nital.

Material D (MP32, as received) was used throughout part I wherever the influence of lubricants on the process stages was studied (mixing, loose powder properties, compaction, ejection and green strength). The sieve analysis of this powder is given in table 4-2.

Material D was also used for the majority of the work in part II. However, A, B and C were used for some studies and this is indicated in the appropriate sections of work.

PLATE 4-2. Microstructures of heat-treated iron powders
(Etched 2% Nital, x350)

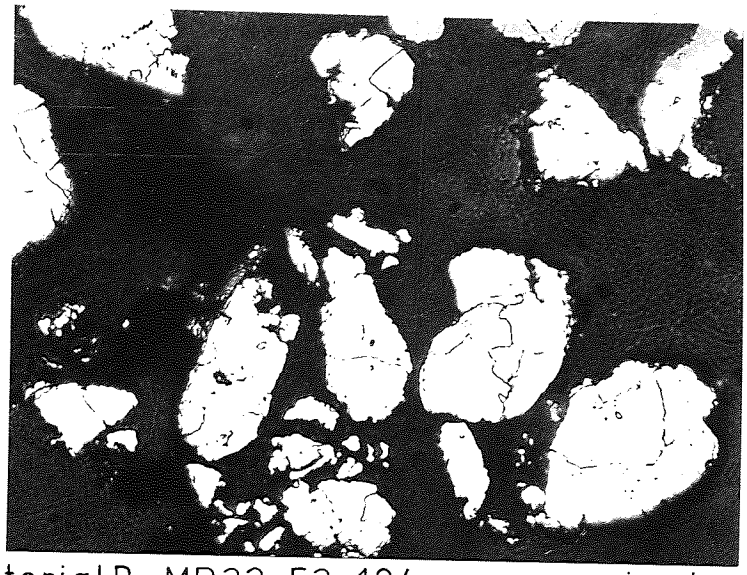

Material B. MP32 53-104μm, as received.

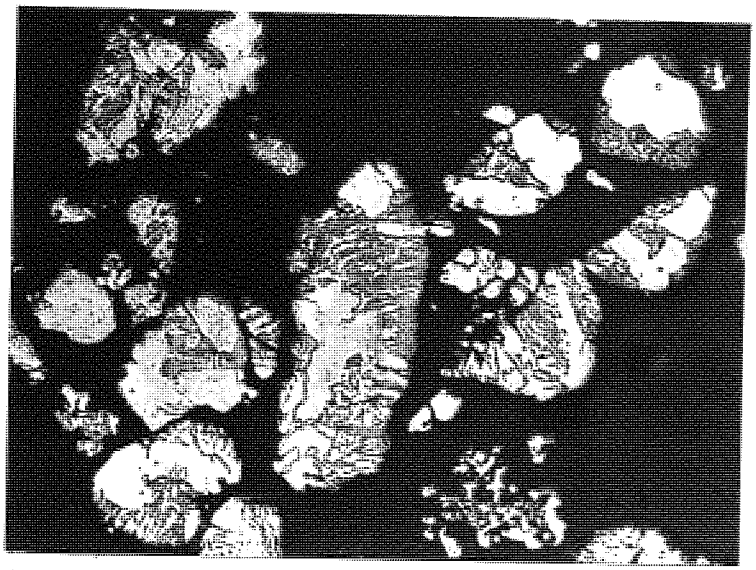

Material E. MP32 53-104μm, carburised

Material F. MP32 53-104μm, annealed.

Table 4-2

Sieve analysis of MP32 powder (as-received)

particle size μm	% by weight
+ 180	0.2
149 - 180	3.0
104 - 149	21.6
74 - 104	32.5
53 - 74	25.4
- 83	17.0

4-2 Lubricants

The particle morphology of the lubricants used in this study are illustrated by the scanning electron photomicrographs of plate 4-3. It was found necessary to coat all these materials with carbon to prevent them charging up and decomposing within the microscope. Melting points are recorded in table 4-3. These were determined on a Reichart hot stage microscope and represent the temperature where melting was observed to begin.

Table 4-3

Melting points of lubricants used in this investigation

Material	Melting point. ^{o}C.
Stearic acid - fine	67
medium	64
coarse	69
Zinc stearate	122
Lithium stearate	205
Stearamide	90
Cosmic 64 wax	138

PLATE 4-3. Scanning electron photomicrographs of lubricant powders

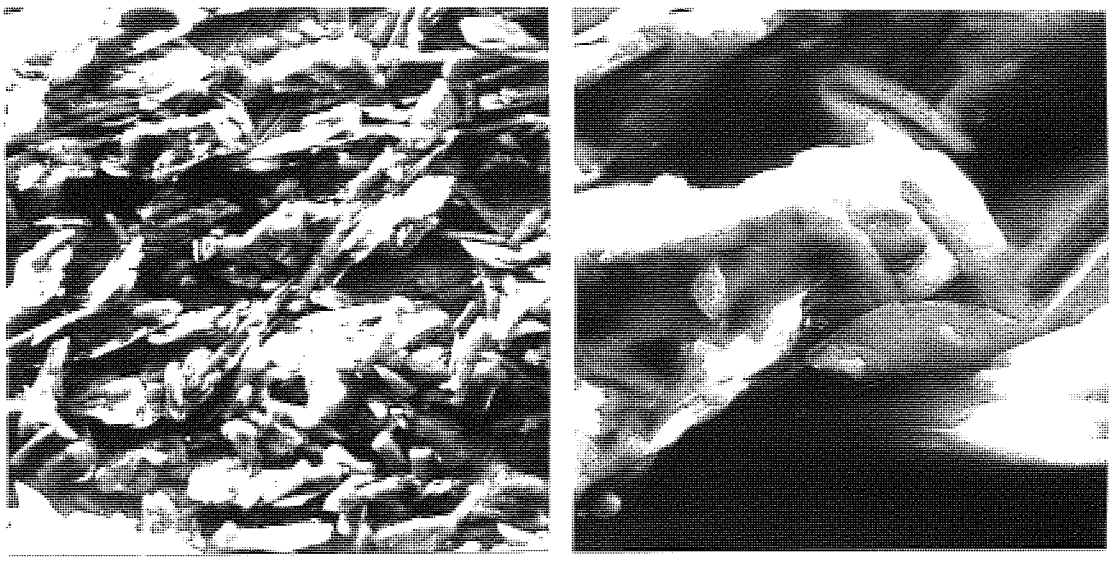

(a) Fine stearic acid

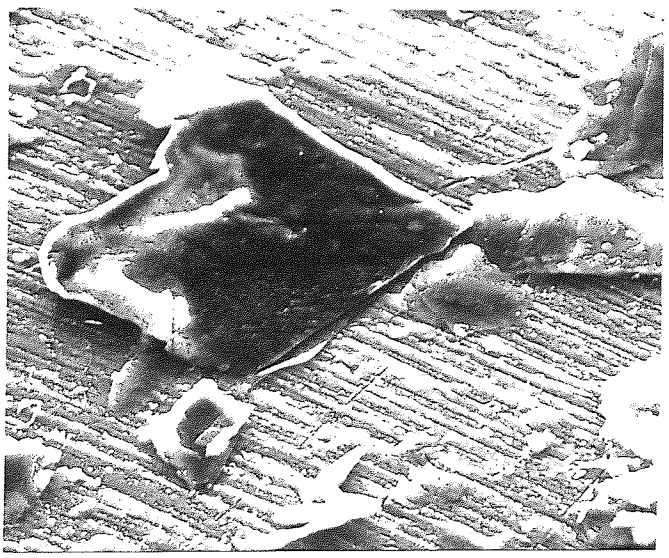

(b) Medium stearic acid

PLATE 4-3 continued.

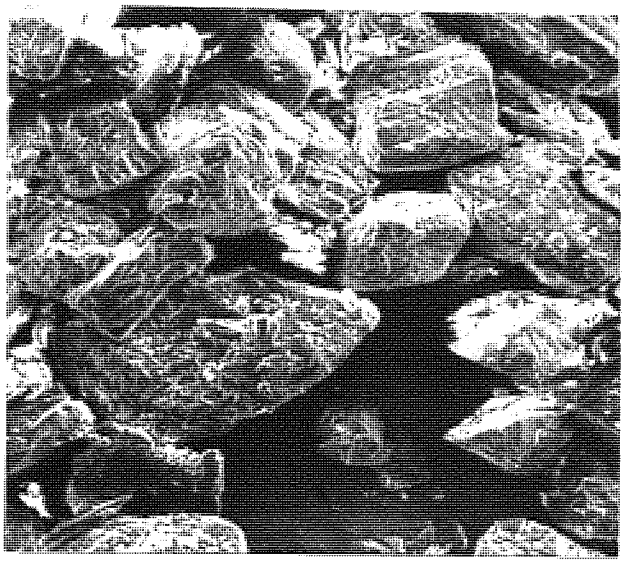

200μm

(c) Coarse stearic acid.

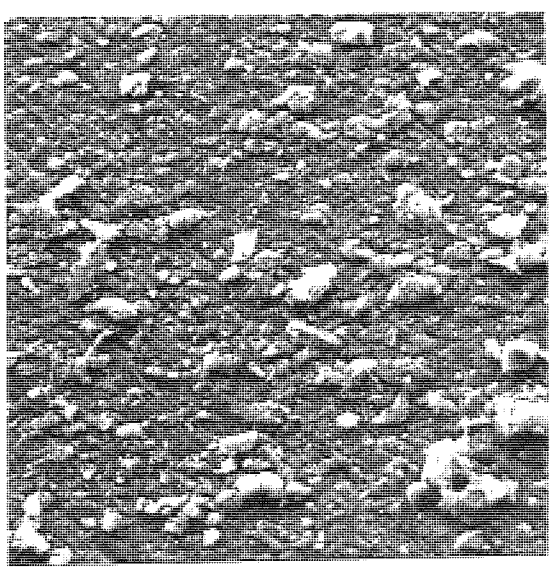

100μm

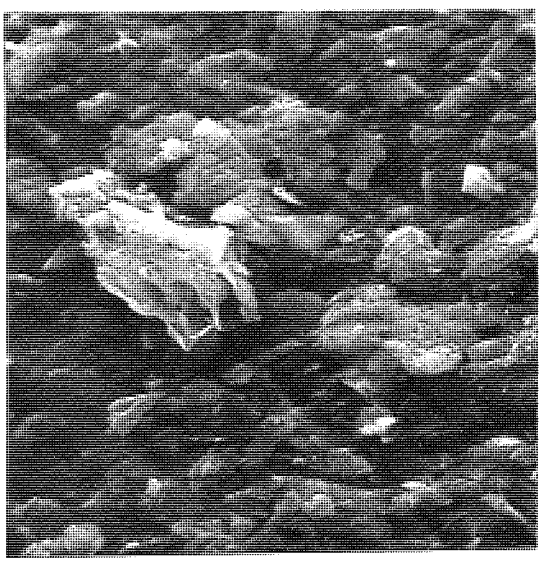

10μm

(d) Zinc stearate

PLATE 4-3 continued

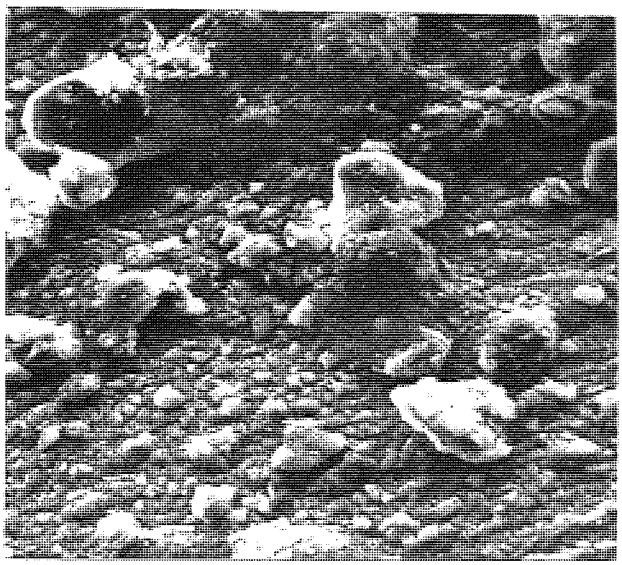

100μm

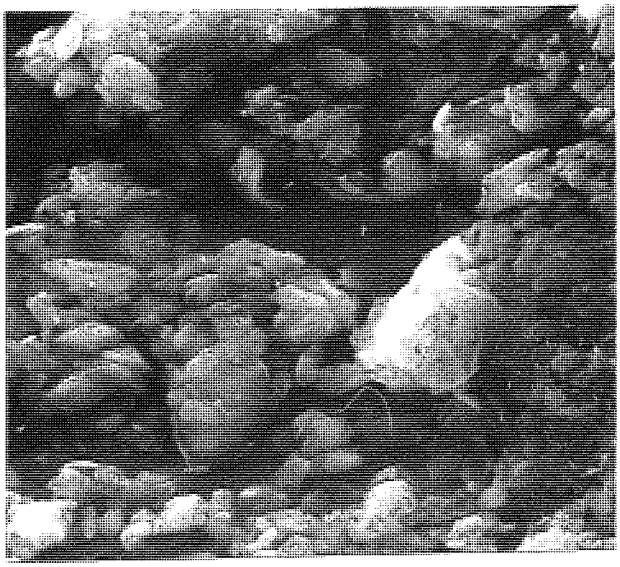

10μm

(e) Lithium stearate

PLATE 4-3 continued

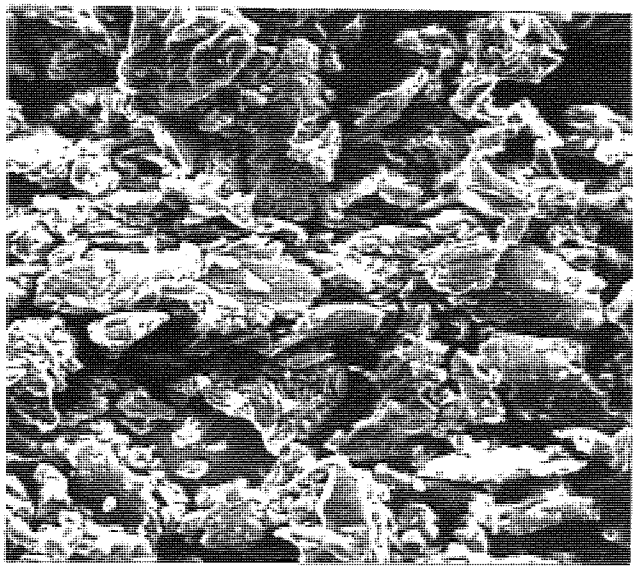

(f) Stearamide

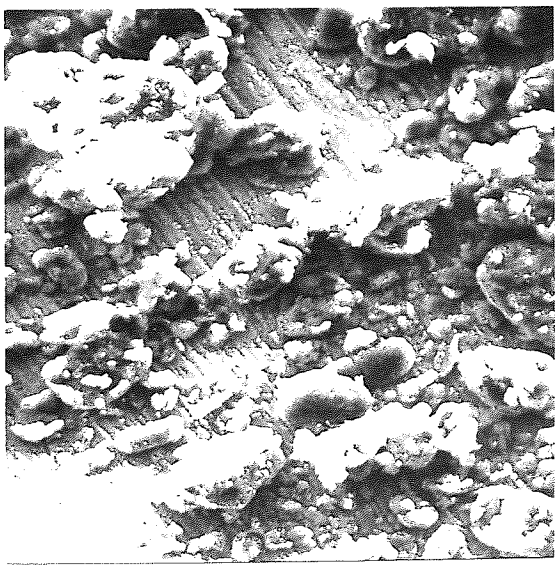

100µm

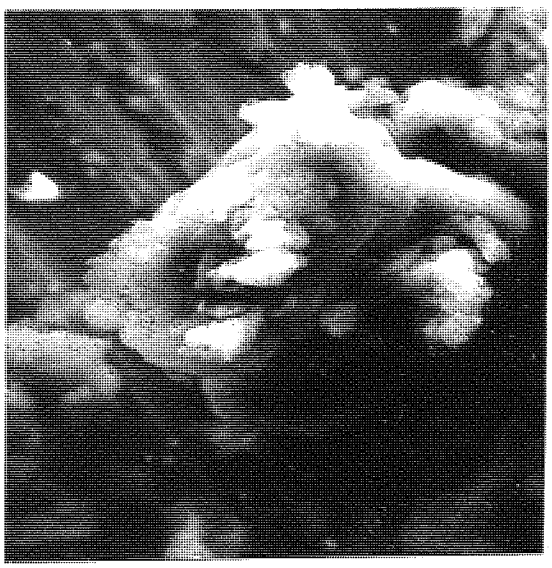

10µm

(g) Cosmic 64 wax

(a) Stearic acid. Stearic acid is formed by the combination of an aliphatic chain ($C_{17}H_{35}$) and the carboxylic acid radical (-COOH);

$$CH_3.(CH_2)_{16}.C \begin{matrix} = O \\ \diagdown OH \end{matrix}$$

This was obtained as a laboratory reagent (Hopkins and Williams) and as such was too coarse for use as an admixed lubricant. Therefore, it was decided to prepare some powders with smaller particle sizes than the original. This would also allow the influence of lubricant particle size on decomposition characteristics to be studied.

Three size fractions were prepared, fine and coarse by ball-milling and sieving, and medium by precipitation from a solvent. The solvent was diethyl ether and stearic acid was dissolved in this, almost to saturation, then the solvent was allowed to evaporate at room temperature (within a fume cupboard) leaving the medium particle sized stearic acid as the precipitate. The shapes of the particles produced may be seen in plate 4-3. The fine and medium (4-3,a,b) materials were flake or plate like, whilst the coarse powder (4-3,c) was markedly angular. Particle size measurement on such materials is difficult and in this case not absolutely necessary. However, the sieve sizes for the fine and coarse powders were (-53μm and 104-420μm, respectively). It was also possible to estimate typical particle sizes from plate 4-3 and these were of the order of 10, 50 and 250μm for the three size fractions.

(b) Zinc stearate. It is possible to replace the hydrogen ion associated with the carboxyl group of stearic acid with a metal ion to produce a metal stearate. Divalent zinc combines with two stearate groups to form zinc stearate, the most common commercial lubricant.

$$CH_3.(CH_2)_{16}.C \begin{matrix} = O \\ \diagdown O - Zn - O \end{matrix} \begin{matrix} O = \\ \diagup \end{matrix} C.(CH_2)_{16}.CH_3$$

The morphology of this powder can be seen from plate 4-3(d). It was difficult to separate the particles of this material or the lithium stearate so that individual particles could be discerned. Some separation was obtained by floating a sample on water but it can be seen from plates 4-3(d)and(e)that this was not totally successful. However, the particle size appeared to be generally less than 5μm. This lubricant was obtained as a general laboratory reagent (Hopkins and Williams).

(c) Lithium stearate. Monovalent lithium is able to replace the hydrogen ion of the carboxyl group to form lithium stearate.

$$CH_3.(CH_2)_{16}.C \begin{matrix} = O \\ \diagdown O - Li \end{matrix}$$

This material was provided by Durham Raw Materials Ltd(9) and is a commercial powder metallurgy lubricant. The particle morphology of this powder is shown by plate 4-3(e). The problems with agglomeration have been outlined above, however the particle size did seem to be less than 5μm.

(d) Stearamide. This was chosen as a stearate based compound which did not involve a metal ion. It was obtained as a general laboratory reagent (Koch-Light).

Stearamide is produced by replacement of the hydroxyl group of the carboxylic acid radical (-COOH) with an amide group.

$$CH_3.(CH_2)_{16}.C \begin{matrix} = O \\ \diagdown NH_2 \end{matrix}$$

It can be seen from plate 4-3(f)that the particle size of this material was of the order of 100μm.

(e) Cosmic 64 wax. This was a commercial wire-drawing lubricant conveniently available as a fine powder (plate 4-3,g). It had been used as a powder metallurgy lubricant in a project concerned with the preheating

of sinter forging blanks[41]. No stoichiometric structure was available, but the following analysis was obtained:

C - 74 %, H - 11%, N - 4%, Balance - unknown.

The single melting point obtained for this material (table 4-3) suggested that it was not a mixture of compounds.

Zinc stearate was the lubricant used mainly in part I. All five lubricants were used during heat-treatment studies (part II).

Stearates contain considerable carbon as can be seen from their chemical formulae. For example zinc stearate is 67% by weight carbon and a 1% by weight addition to a compact could represent a maximum addition of 0.6-0.7% carbon. This fact may be of significance when the decomposition of lubricants during dewaxing is considered.

Lubricant contents from 0.01 to 4.0% by weight are discussed in this work. However, it should be noted that actual additions were made as extra additions to the iron powder, not as a percentage of the total. The difference would be largest for the highest content, 4%, and this will serve as an example. A 100g mix of nominally 4% lubricant would be produced by adding 4g of lubricant to 100g of iron powder. The actual content would be 3.8%, however the actual and theoretical figures equate if the former are rounded to one significant figure.

4-2-1 Specific gravity

It was necessary to determine the specific gravity of the zinc stearate to enable the volume percentage of lubricant to be calculated during compaction studies. There was one value available for zinc stearate (1.1[11]) and several for stearic acid (0.85[8], 0.97[11] and 0.94[46]).

The specific gravities of stearic acid and zinc stearate were determined by pressing compacts of each material in the manner described in

section 2-2-1, part 1. The forming tools were lubricated with petroleum jelly to prevent adhesion. The compaction pressure was increased until the ram movement/unit load was equal to that expected from elastic distortion of the tools only. It was assumed now that each compact was fully dense and there was no entrapped air.

The compacts were ejected, weighed, measured and their specific gravities calculated as 0.98 for stearic acid and 1.05 for zinc stearate (the latter did just sink in water). These values compare favourably with those quoted above.

PART 1

LOOSE POWDER AND COMPACT PROPERTIES

1 Introduction

The investigations in this part were concerned with the behaviour of lubricant during the production of green or as-pressed compacts and its effect on their properties and those of loose powders. The areas studied are listed below.

(a) Mixing.

(b) Compaction.

(c) Ejection.

(d) Green strength.

The same combination of materials (MP32 iron powder and zinc stearate) were used in most of the stages in order to maintain continuity. Two methods of applying the lubricant to the iron powder were studied, admixing and precipitation from a solution.

1-1 Glossary

Some of the terms relating to density and used most frequently in this investigation are defined below.

D^* - (Actual density). The overall density of a sample including additions such as lubricant. This was determined as (total weight)/(volume of sample) and may be recorded in terms of g cm^{-3}, relative density % or fractional relative density.

D - (True metal density). The density of the metal in a sample. Calculated as (weight of metal in sample)/(volume of sample) or D^* x (% of metal in sample)/100. The units are the same as those for D^*, depending on usage.

D_a - The apparent density of a loose powder sample in terms of true metal density. Calculated as (weight of metal in sample)/(loose packed volume).

D_t - The tapped density of a powder sample in terms of true metal density. Calculated as (weight of metal in sample)/(tapped volume).

Pore space - The volume of space in a compact not occupied by metal. Determined from true metal density as a percentage of the total volume (100 - D%) or as a fraction (1 - D).

Relative density - The density of a sample expressed as a proportion of the theoretical solid density of the material and hence indicating the degree of densification. It may be determined in terms of actual density or true metal density.

Voidage - The proportion of a compact occupied by air only and determined as (100 - D^*%) or (1 - D^*) fractional.

2 Experimental Procedure

2-1 Loose powder properties

Loose powder packing properties were determined by measuring apparent density (D_a) and maximum tapped density (D_t). The majority of the investigation was carried out using D_a only. However, D_t was determined for the iron powders used in section 2-3 and for mixes containing precipitated/evaporated zinc stearate. D_a was felt to be the most important parameter since this has been shown to be a better indication than D_t of loose packing in a die cavity[17,18,20,21].

2-1-1 Tapped density (D_t).

No proprietary apparatus was available for the determination of D_t. However, it was found that reproducible tapped densities could be determined by placing powder in a narrow, glass, $25cm^3$ measuring cylinder and tapping the barrel with a rubber coated striker. Density was calculated from the weight and volume of the powder.

Tapping was continued until settling was complete. It was thought that it would be difficult to regulate the force of each tap, as would be required for a fixed time or number. Settling took longer as the lubricant content increased.

The density measured in this way was termed 'maximum tapped density' (D_t) and was found to be sensitive to sample weight, shown in figure 2-1. Sample weight was maintained between 60g and 80g (approximately $20cm^3$), within the plateau of figure 2-1.

At least two determinations were obtained for each material and maximum variation was $\overline{D_t}$ % $\pm$ 0.3% for both unlubricated and lubricated powder.

2-1-2 Apparent density (D_a)

Values of D_a were determined using glass apparatus constructed to

FIGURE 2-1. The effect of sample weight on D_t.

MP32 53-104 μm, no lubricant.

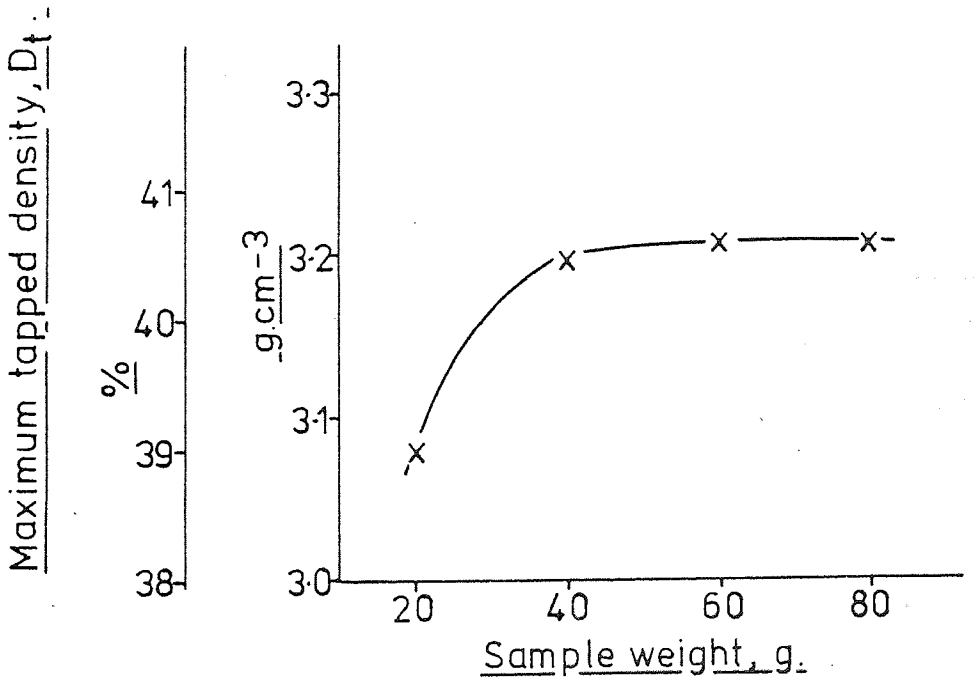

ASTM standard B213 and shown in plate 2-1. At least two determinations were used for each material maximum variation being $\overline{D_a}$ % ± 0.1% for unlubricated and $\overline{D_a}$ ± 0.5% for lubricated powder.

2-1-3 Lubricant precipitation/evaporation

Zinc stearate was precipitated onto MP32 iron powder (material D) using a method similar to that of Yarnton and Davies[13]. Weighed amounts of zinc stearate were completely dissolved in benzene. The iron powder (again preweighed) was then added to the solutions and the benzene slowly evaporated over a hot plate. The mixture was stirred continuously during evaporation. All operations involving benzene were carried out in protective conditions.

Additions of 0.01, 0.02, 0.05, 0.10, 0.20, 0.50, 1.0, 2.0, 3.0 and 4.0% by weight were obtained in this way. MP32 with no lubricant addition was also washed in benzene to eliminate the solvent as a variable. Free lubricant was apparent for additions greater than 0.5%.

All mixes were sieved after evaporation through a 60 mesh (246μm) screen to break up any agglomerates of free lubricant which may have formed.

The results of D_a and D_t for these materials are shown in figure 3-1.

2-1-4 Admixing

The same proportions of zinc stearate in MP32 iron powder as used in section 2-1-3 (excluding 3.0%) were tumble mixed by rotation in polythene containers. Total mix weight was maintained constant at 400g. The rotary mixer with a container was operated at 38r.p.m. and is shown in plate 2-2.

The powders were sieved together (60 mesh, 246μm) prior to mixing, which prevented agglomeration of the lubricant. Mixing was interrupted at various stages between the start (0 cycles) and approximately 60 minutes

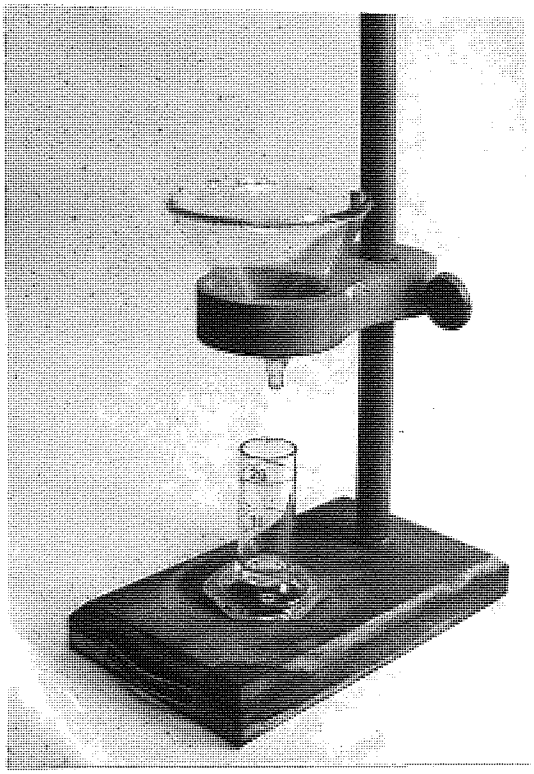

PLATE 2-1 Apparent density apparatus

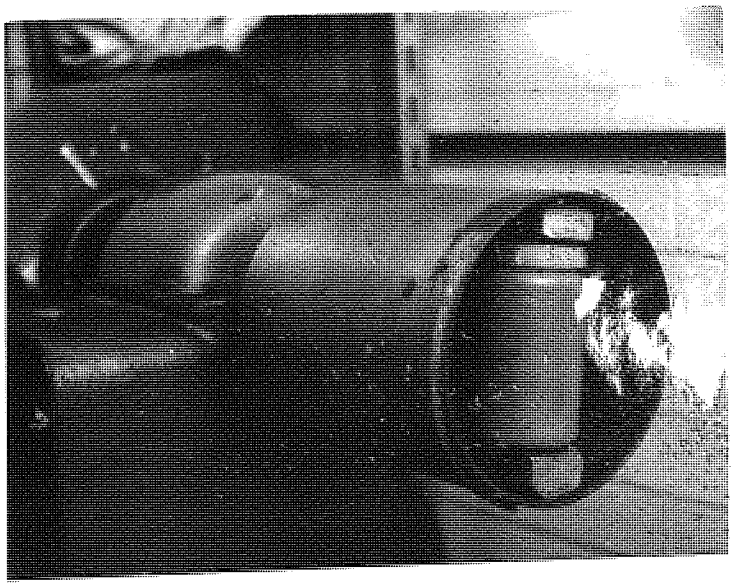

PLATE 2-2 Mixer and container

(2290 cycles) to check the development of apparent density.

Reproducibility is illustrated by figure 2-2 each curve in this figure was obtained by interrupting a single mix containing 1% zinc stearate. A similar mix was taken to 50 cycles in a single stage to determine the influence of interruption. The apparent density of this mix was 2.50g cm^{-3} which corresponded to those of figure 2-2.

The results of D_a versus mix duration for the various lubricant additions are shown in figures 3-2 to 3-4. These have been separated into three groups on the basis of mixing behaviour.

2-1-5 Observation of lubricant coatings.

Direct observation of lubricant dispersion and coatings on particles was found to be difficult. Optical metallography was unrewarding due to the irregularity of the iron powder.

Plates 3-1(a) and (b) are scanning electron micrographs obtained from a 1% zinc stearate mix. These provide some indication of the general dispersion of lubricant after 10 cycles and 1152 cycles admixing. However, the sample size of the scanning electron microscope (S.E.M) was too small to provide a truly representative indication of lubricant dispersion within mixes.

The S.E.M was found to be useful in providing illustrations of lubricant pickup on individual iron powder particles during mixing. Plates 3-2(a) to 3-2(d) are typical micrographs and corresponding zinc X-ray maps obtained from MP32 plus 1% zinc stearate admixed to various degrees.

It was hoped that the S.E.M would enable the coatings produced by precipitation and mixing to be compared. There were no major differences evident. However, it was found that it was easier generally to detect zinc X-rays from the surface of iron powder particles coated by precipitation. It was correspondingly more difficult to detect free lubricant in

FIGURE 2-2. Reproducibility of D_a versus mix duration (MP32 +1% zinc stearate)

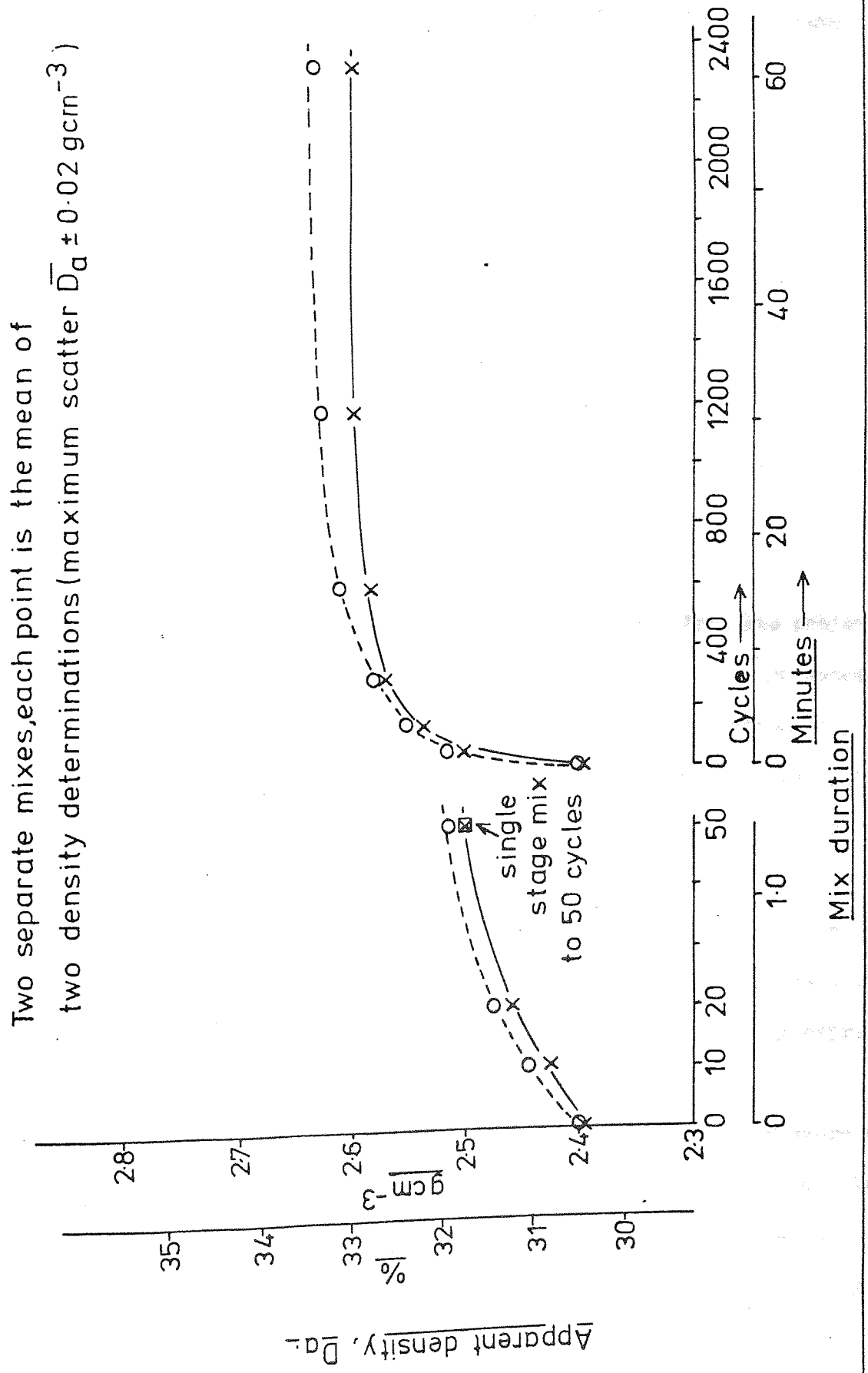

these materials.

Examples have been reproduced in plates 3-3(a) and (b). These would seem to indicate that precipitation/evaporation provided a more even, thicker coating than admixing.

2-2 Compaction

2-2-1 The compaction method

Compaction was carried out using a single action hydraulic press (Denison, 300 tons) with the floating die tool arrangement shown in figure 2-3. Cylindrical compacts of 28.6mm diameter were formed. This arrangement (fig.2-3) enabled pressure/density data to be obtained for a wide pressure range including low pressures where coherent compacts were not normally formed.

Each pressure/density relationship was determined continuously using a single specimen over the entire pressure range. This was achieved by using the dial gauge (fig.2-3) to measure ram displacement and hence, change in compact length. The applied force was increased continuously with displacement readings being taken at $5x10^{3}$N increments initially and $2x10^{4}$N increments finally. The gauge was zeroed at $5x10^{3}$N applied force and the maximum was $3x10^{5}$N (pressure range, 8-470 Nmm^{-2}).

A pressure/displacement relationship was obtained with no compact in the die to correct actual displacement readings for elastic strain in the tools and press. This was found to be linear and conveniently expressed as 0.025mm/10KN applied force.

The final compact length, corresponding to a compaction pressure of 470 Nmm^{-2}, was measured on the ejected compact. This length was added to the total corrected displacement to find the length at $5x10^{3}$N applied force (8 Nmm^{-2}). It was possible to calculate the density corresponding to each force increment in this manner.

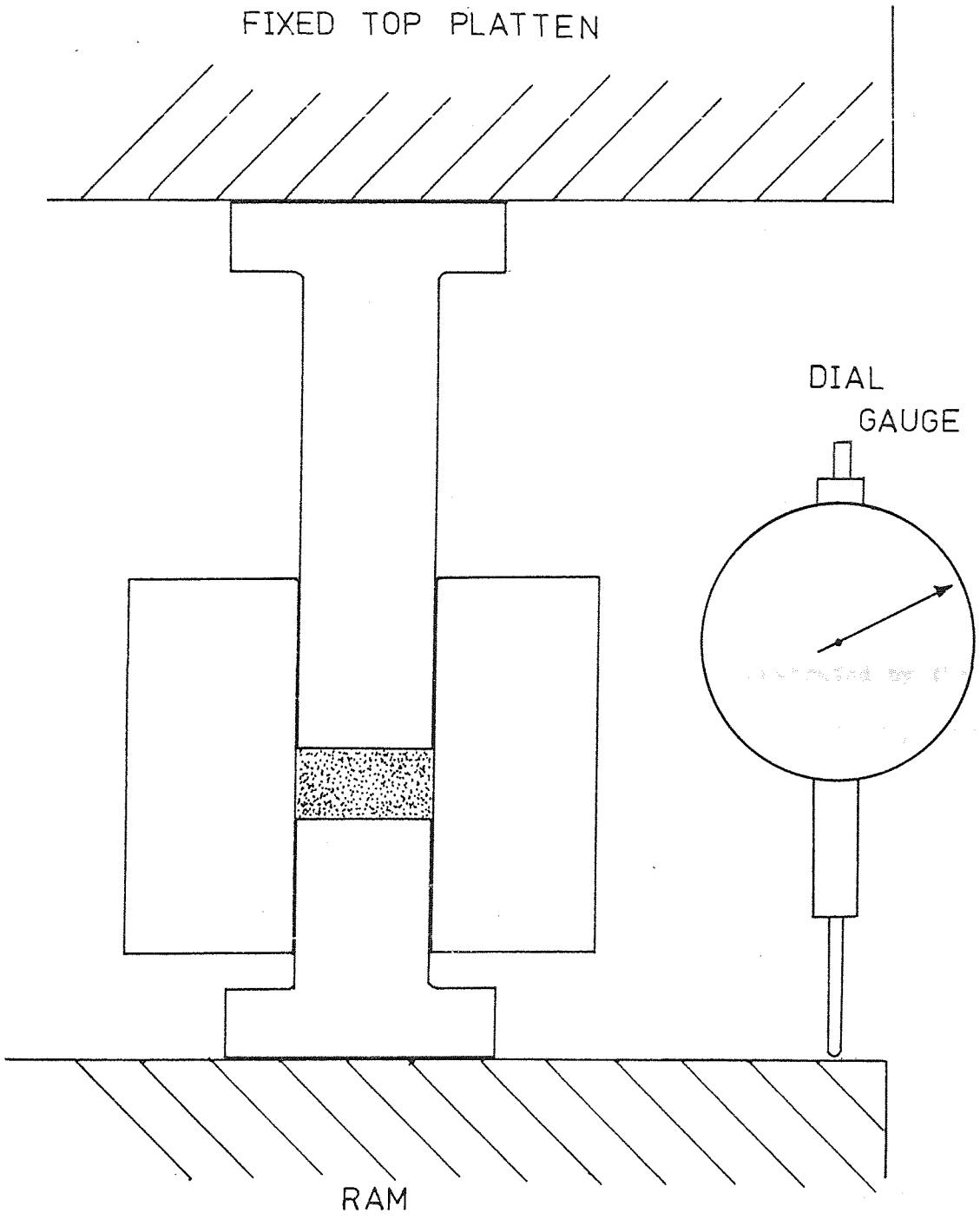

FIG.2-3 Floating die compaction tool arrangement.

2-2-1-1 Die-wall lubrication

Die-wall lubrication was applied where necessary by placing a small amount of a saturated solution of stearic acid in diethyl ether into the die cavity with the bottom punch raised. The punch was slowly withdrawn allowing the ether to evaporate and leave a film of stearic acid on the die-wall. Excess lubricant was removed from the die faces and punch by wiping.

Thick, visible films were produced in this way. These were required to minimise particle/die-wall friction during compaction and reduce the ejection stress of unlubricated powders. The reproducibility of these films will be indirectly assessed with the aid of pressure/density data (section 2-2-1-2) and ejection studies (section 2-3-2).

2-2-1-2 Compaction reproducibility

The reproducibility of the compaction method is illustrated by the compaction curve of figure 2-4. The results shown in this figure represent the mean of three separate density determinations. Scatter bars are also included in figure 2-4 showing that there was little variation from the mean.

Die-wall lubrication, as described in the previous section, was used for these samples. The reproducibility of compaction obtained was therefore some indication that the die-wall lubricant films were also reproducible.

The results of density determinations from ejected compacts pressed to various pressures are also shown in figure 2-4. It can be seen from these that there was little difference between pressure/density data obtained from one compact pressed continuously and that from individually pressed and ejected compacts.

FIGURE 2-4. Compaction reproducibility and comparison of continuously compacted with ejected densities (MP 32 53-104 μm die-wall lubricated)

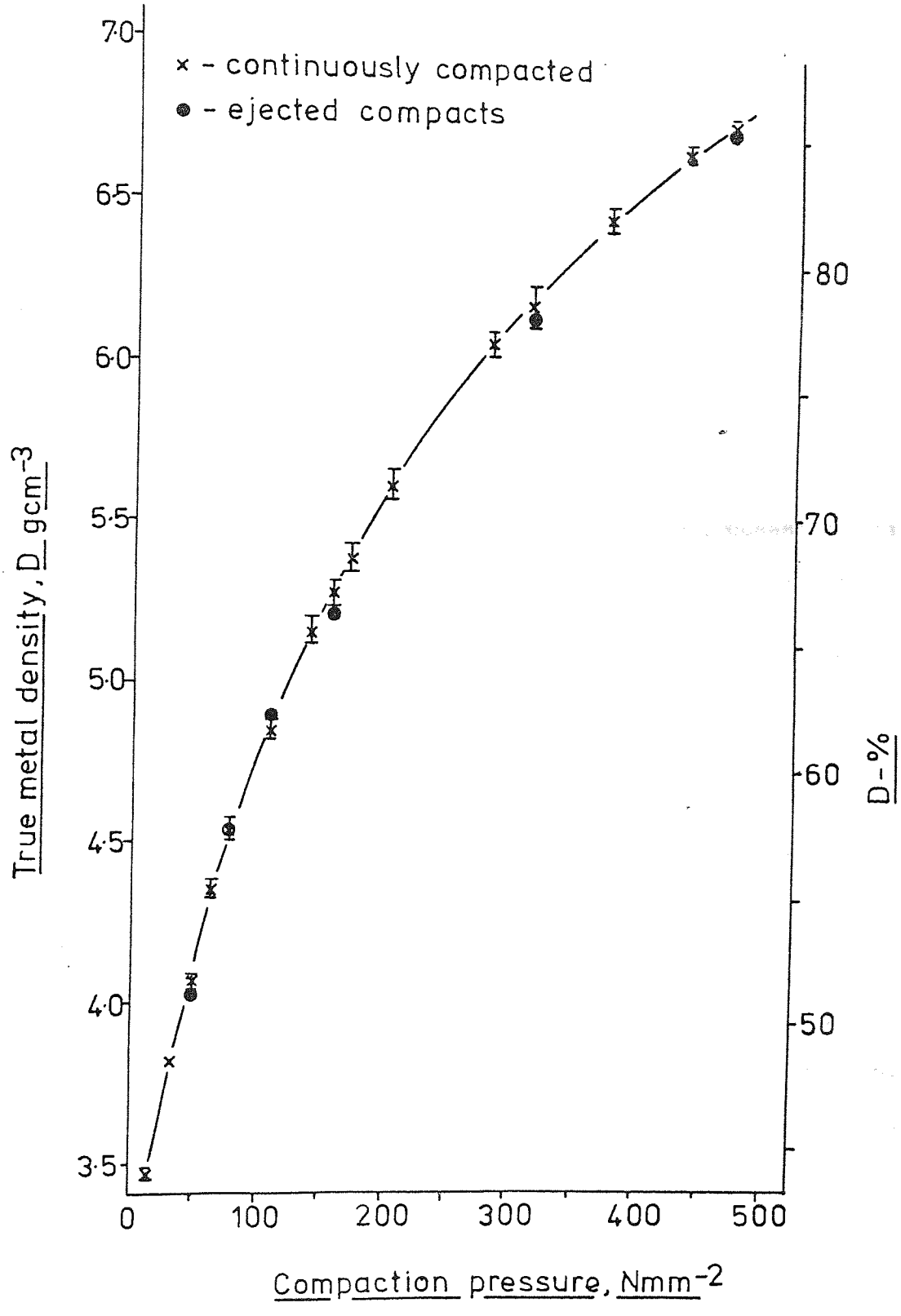

2-2-1-3 The effect of compact weight on compaction

Pressure/density relationships were found to be dependent on compact weight, as shown in figure 2-5. These results were obtained from continuous compaction of 20g and 80g compacts of powder B with die-wall lubrication. It was obviously necessary to standardise compact weight and this was fixed at 60g after consideration of sizes suitable for density distribution determinations.

2-2-2 Analysis of the linear compaction relationship

The linear relationship chosen for application to the compaction of powders containing lubricants was that of Heckel[17,18], equation 2-1, as discussed in the literature survey (2-5).

$$\ln\left(\frac{1}{(1-D)}\right) = kP + A \qquad \ldots(2\text{-}1)$$

This presents powder compaction as a three stage process[17,18]:

Stage 1, filling of the die. The amount of densification is indicated by the apparent density, D_a.

Stage 2, individual particle movement and rearrangement at low pressures before interparticle bonding becomes appreciable.

Stage 3, bulk deformation of particles. Characterised by proportionality between the rate of change of density with pressure $\left(\frac{dD}{dP}\right)$ and the void fraction of the compact $(1-D)$.

It was not assumed that this linear relationship perfectly described the compaction data obtained in this investigation, or that any such relationship existed. However, it was assumed that it could be applied to compaction data to isolate the stages outlined above and determine the effect of process variables such as the presence of lubricant on them.

Prior to studying the influence of lubricants on the various stages of compaction it was necessary to establish the characteristics of each

FIGURE 2-5. The effect of sample weight on compaction (MP32 53-104 μm die-wall lubricated)

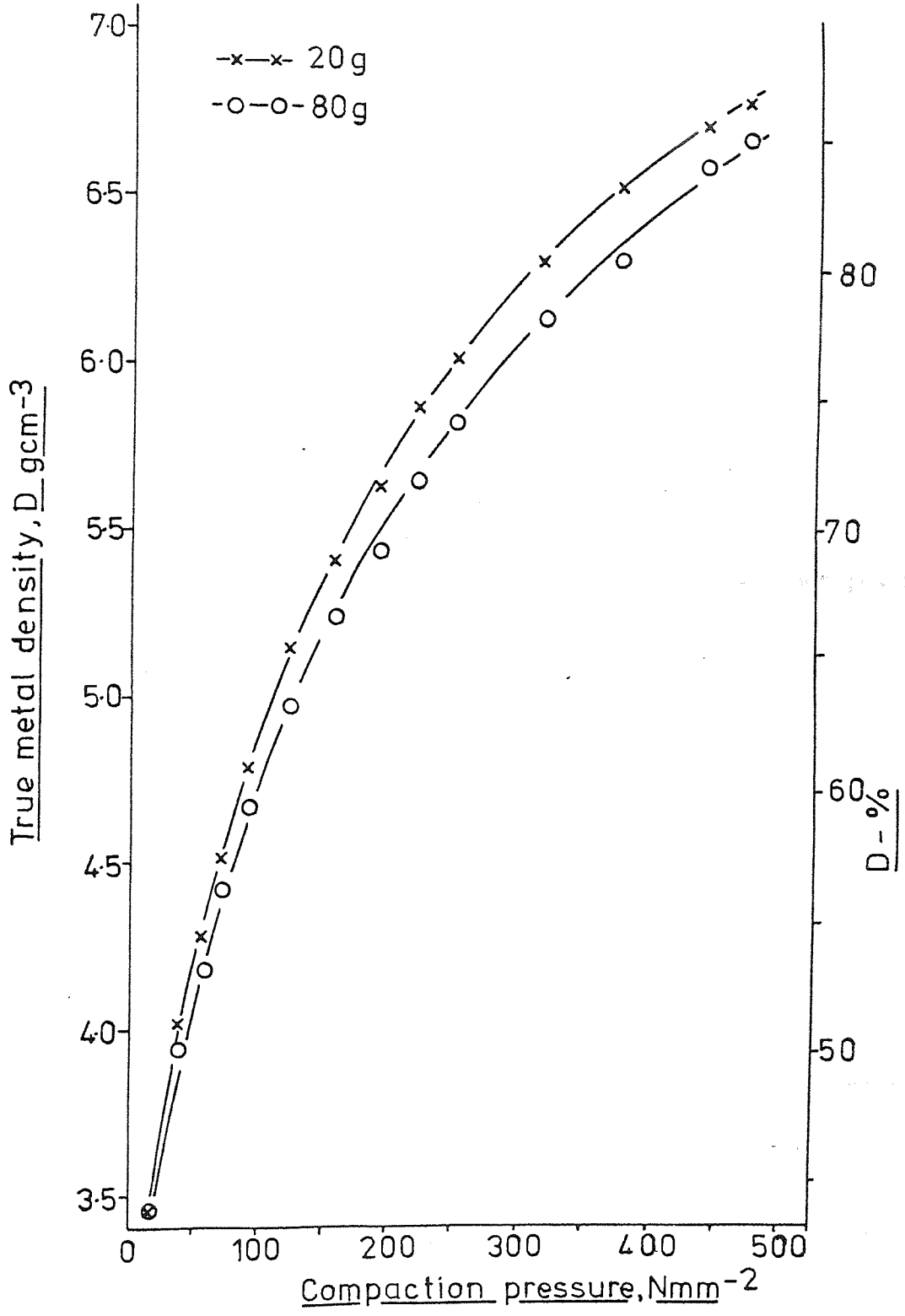

stage. This was achieved by using the various iron powders described in the materials section (4).

It was possible with these powders to vary particle morphology (A, B, C, D, J) and deformation properties (B, E, F). In the carburised material (E) it was hoped that the pearlite would restrain the ferrite and alter its deformation characteristics causing work hardening (stage 3) to occur sooner.

2-2-2-1 Powder properties

Tapped (D_t) and apparent (D_a) densities of the iron powders were determined as described in sections 2-1-1 and 2-1-2. The results are recorded in table 3-1.

Initial particle microhardness was determined on each material to provide an indication of its deformation properties. A Leitz microhardness tester was used with polished and etched (2% Nital) microspecimens. The lowest load (25g) of this apparatus was used but it was not possible to obtain reliable results from the two fine powders, C and J. Hardness values are recorded in table 3-1.

Seven random determinations were made on each material. The two extremes were discarded and the results in table 3-1 are the means of the five remaining determinations. Hardness ranges are also recorded in table 3-1.

The two phase material E (MP32 53-104μm, carburised) was checked in both the etched and unetched conditions. In the etched condition hardness determinations were carried out separately on ferrite and pearlite areas. The mean hardness of the separate determinations was equal to that of those obtained randomly.

2-2-2-2 Compaction

All materials were continuously compacted with die-wall lubrication.

The significance of particle/die-wall friction during compaction was assessed by also pressing material B with no die-wall lubrication (K).

Density results are recorded in tables 3-2(A) to (K) as true metal density D (gcm^{-3} and relative fractional) and $\ln(\frac{1}{(1-D)})$. They have also been plotted as $\ln(\frac{1}{(1-D)})$ versus compaction pressure in figures 3-5 to 3-8. Not all points have been plotted in these figures to avoid confusion. The densities plotted at zero compaction pressure are apparent densities, D_a, recorded in table 3-1.

2-2-2-3 Density distributions and microhardness relationships

Density distributions were determined on vertical radial sections of compacts pressed to various densities from materials B, E, F (i.e varying particle deformation properties) and also K (material B, no die-wall lubrication). The method, results and discussion are given in Appendix A.

These density distributions were used primarily for the detection of bulk deformation of particles within compacts. It was hoped that by measuring individual particle microhardnesses and relating them to density it would be possible to detect the onset of stage 3 (section 2-2-2) directly.

Particle microhardness tests were carried out on the etched density distribution microspecimens using the Leitz microhardness tester (25g load). The individual particle microhardness results are plotted versus density in figures 3-9 to 3-11. Wherever possible areas were chosen for hardness determinations on each specimen such that their densities overlapped those of neighbouring compacts. This was possible with material K as can be seen from figure 3-9. The correlation between different compacts shown in figure 3-9 helps to confirm the validity of the microhardness/density relationships.

Microhardness determinations corresponding to zero compaction

pressure were taken from loose powder microspecimens and have been plotted against apparent density (D_a). Determinations on compacts have been taken towards the centre of each area (Appendix A) and plotted against the average density of that area.

Microhardness determinations for the carburised material, E (fig. 3-11), were obtained from ferritic areas only. Random determinations were also carried out and the results are shown in figure 3-12. It can be seen that the apparent rate of work hardening ($\frac{dHv}{dD}$) in figure 3-12 was lower than that of ferrite alone (fig.3-11). Deformation was therefore largely confined to ferritic areas in this material.

2-2-3 The compaction of powders containing lubricants

The materials used in this section were those prepared during the study of loose powder properties, sections 2-1-3 and 2-1-4. These provided zinc stearate additions between 0 and 4.0% by weight applied to MP32 iron powder by precipitation/evaporation or admixing.

Mixes containing precipitated lubricant were continuously compacted with simultaneous die-wall lubrication (tables 3-3(A) to 3-3(K)) and with no die-wall lubrication (tables 3-4(A) to 3-4(K)). Powders containing admixed lubricant were only pressed with no die-wall lubrication (tables 3-5(A) to 3-5(J)). When no die-wall lubrication was applied powders with small lubricant contents (0.01% to 0.1%, excluding 0%) were pressed to low densities only to protect the forming tools.

Densities are recorded in tables 3-3 to 3-5 as actual density D* (g cm^{-3}), true metal density D ($g.cm^{-3}$ and relative), and $\ln(\frac{1}{(1-D)})$.

2-2-3-1 The effect of lubricants on compaction behaviour.

The influence of lubricants on compaction behaviour was studied by comparing results of powder containing no lubricant (table 3-3(A)) with those of powders containing precipitated/evaporated zinc stearate (tables

3-3(B)) to 3-3(K)). It was assumed that the simultaneous use of die-wall lubrication would almost eliminate particle/die-wall friction during compaction. This would leave only phenomena such as compaction inhibition [24] and the influence of lubricant on particle packing to be considered.

Examples of linear plots are shown in figure 3-13. To avoid confusion not all points are shown. It had become clear at this stage that plots of $\ln(\frac{1}{(1-D)})$ versus P for powders containing lubricants were not as linear as those containing no lubricant (section 2-2-2-2). The amount of information yielded by such treatment was also disappointingly low. This is given further consideration in the discussion (section 4).

Examples of more conventional plots of true metal density (D) versus compaction pressure (P) are shown in figure 3-14. These relationships were used to determine the lubricant effect, ΔL [25].

ΔL is the difference between the compaction pressures required to achieve a given density in a lubricated compact and a compact containing no lubricant. This is illustrated in figure 2-2 in the literature survey. ΔL has been plotted as a function of D for the data of tables 3-3(A) to 3-3(K) in figure 3-15. Positive values for ΔL indicate beneficial influences whilst negative values indicate compaction inhibition.

The transition pressure, P_T, has been defined [24] as the pressure where conditions within a forming compact containing lubricant change from lubrication to conditions of inhibition. P_T is the pressure where the lubricant effect (ΔL) is zero. Therefore, it was possible to calculate values of P_T for various lubricant contents by noting the pressures where ΔL was zero in figure 3-15. P_T is shown as a function of lubricant content in figure 3-16.

2-2-3-2 The significance of particle/die-wall friction.

Two of the important factors which influence the development of density during the compaction of powders containing lubricant are;

(a) particle/die-wall friction,

(b) interparticle friction and inhibitive effects.

In the previous section (b) was studied by assuming that (a) was eliminated by applying die-wall lubrication.

Particle/die-wall friction would be expected to decrease the densification effect of the applied compaction pressure P due to the necessity to shear particle/die-wall contacts. As P increases the force required to shear these contacts will increase since both the real contact area and the force on that area will increase[32]. The applied compaction pressure (P) will, therefore, be reduced to an effective pressure (P_E) by an amount proportional to P (equation 2-2).

$$P_E = P - f(P) \qquad \ldots(2\text{-}2)$$

Values of $f(P)$ may be calculated by comparing compaction data from material with (table 3-3) and without (table 3-4) die-wall lubrication. Lubricant content would be eliminated as a variable by only comparing curves of equal content.

The data of tables 3-3 and 3-4 are plotted as D versus P in figures 3-17 to 3-22, for lubricant contents of 0, 0.2, 0.5, 1.0, 2.0, 3.0 and 4.0%. True metal density (D) has been used rather than actual density (D*) because the densification mechanism concerned is the movement of the metal powder particles relative to the die-wall.

The difference between the pressures required to achieve given densities with and without die-wall lubrication is f(P). Values of f(P) have been determined from the results of figures 3-17 to 3-22 and are plotted versus P in the same figures.

2-2-3-3 The effect of mixing on compaction behaviour

The effect of admixing on the compaction behaviour of MP32 with no added lubricant is illustrated by the compaction curves of figure 3-23.

It can also be seen from this figure that the solvent used for precipitation (benzene) had no significant effect on compaction behaviour.

The reproducibility of compaction of powders containing admixed lubricant is shown in figure 2-6. These results were obtained from three separate mixes containing 1% zinc stearate admixed for 1 hour. It can be seen that the variation was not significantly different to that obtained for the as-received material (fig.2-4).

The effect of mix duration on compaction behaviour was studied by mixing 1% zinc stearate with MP32 iron powder for 50, 2290 and 9120 cycles. Compaction results are recorded in full in tables 3-5(H)and 3-6. They are also shown as true metal density (D) versus compaction pressure (P) in figure 3-24.

2-2-3-4 The effect of lubricant coating type on compaction behaviour

Lubricant coatings were applied to the iron powder in two ways; (a) by precipitation/evaporation, and (b) by admixing. Compaction results from these two materials are recorded in tables 3-4 and 3-5. It was possible to compare the compaction behaviour of these two types of coating by using the data of these tables. Examples of comparative pressure/density relationships are plotted in figures 3-25 to 3-27.

2-3 Ejection.

Ejection stresses were determined on the same type of compact and by using the same hydraulic press as used during compaction (2-2-1). The bottom punch of the forming tools was removed, a cylindrical ejection block placed beneath the die and the compact was ejected by the top punch. The maximum ejection force was noted.

Maximum ejection stress was calculated as (ejection force)/(total compact/die-wall contact area). This may correspond to the break stress[27] (sticking friction) or sliding friction. This would depend at least part-

FIGURE 2-6. The compaction reproducibility of admixed powder (MP 32 +1% zinc stearate, admixed 1 hour)

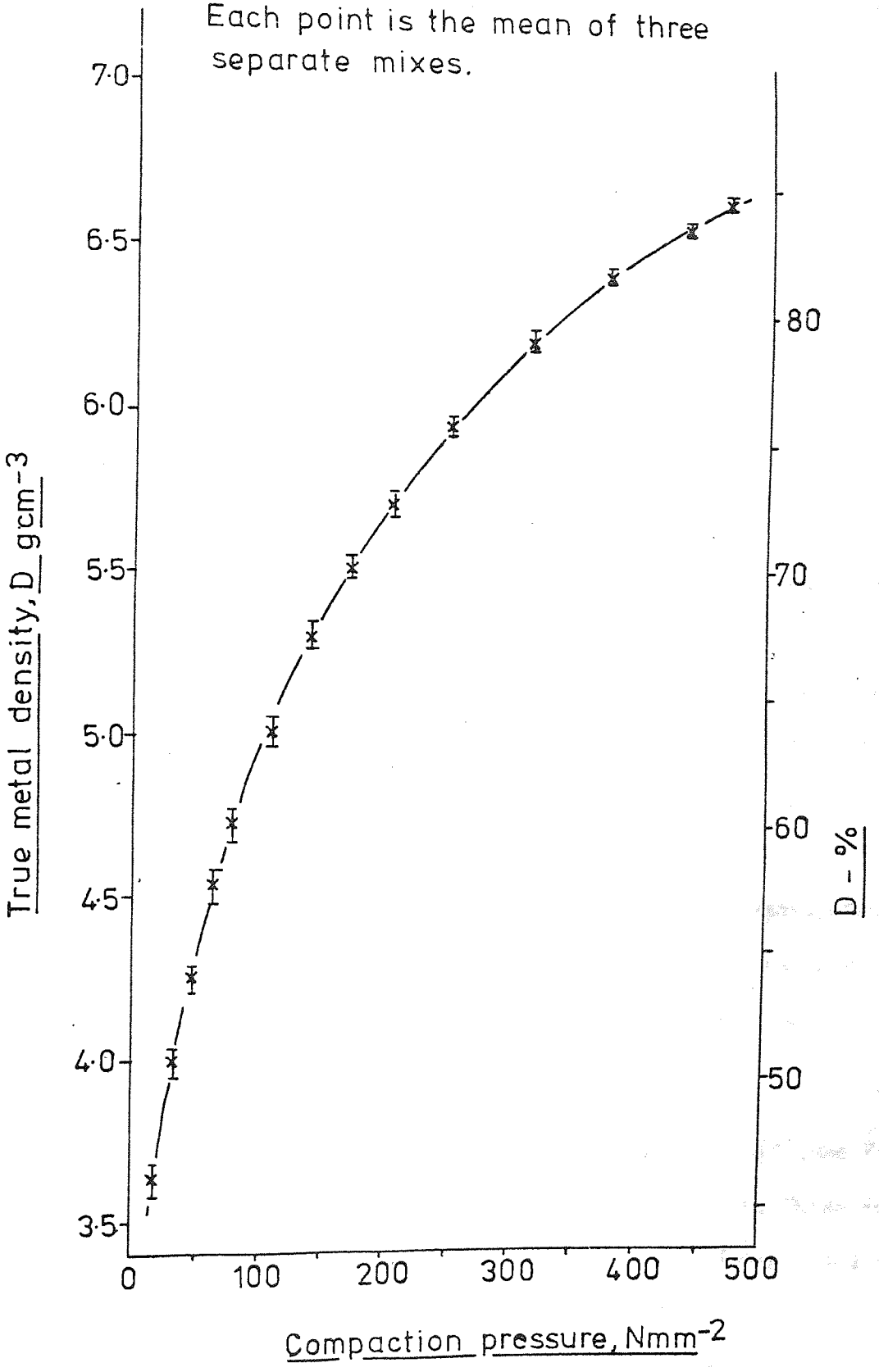

ially on the lubricant level[27].

The recorded ejection forces were low compared to the press capacity. It was also difficult to gauge strain rate which is probably best described as slow, consequently no emphasis has been placed on absolute values of ejection stress. However, differences obtained with varying lubricant contents were greater than reproducibility variation. Values of stress obtained in this way were therefore quite adequate for comparative purposes.

Compacts weighing 60g were formed from MP32 iron powder with the appropriate lubricating conditions. Three determinations were carried out for each material using compacts pressed to 3, 10 and 30×10^4N(47, 156 and 470Nmm^{-2}), each compact being pressed specifically for measurement of ejection stress. Results have been recorded as maximum ejection stress versus true metal density.

2-3-1 Ejection without die-wall lubrication.

The lubricating properties of precipitated/evaporated and admixed zinc stearate were studied by using the same materials as used in section 2-2-3-4. The results are shown in figures 3-28 and 3-29 as maximum ejection stress versus compaction pressure.

The effect of mix duration on ejection stress was investigated by using compacts pressed from MP32 plus 1% zinc stearate admixed for 50, 2290 and 9120 cycles. The results are presented in figure 3-30.

2-3-1-1 Reproducibility

The reproducibility of ejection stress measurements obtained from compacts containing lubricant is illustrated in figure 2-7. These results were obtained from three separate batches of MP32 plus 1% zinc stearate admixed for 1 hour.

Comparison of figure 2-7 with figures 3-28 and 3-29 shows that

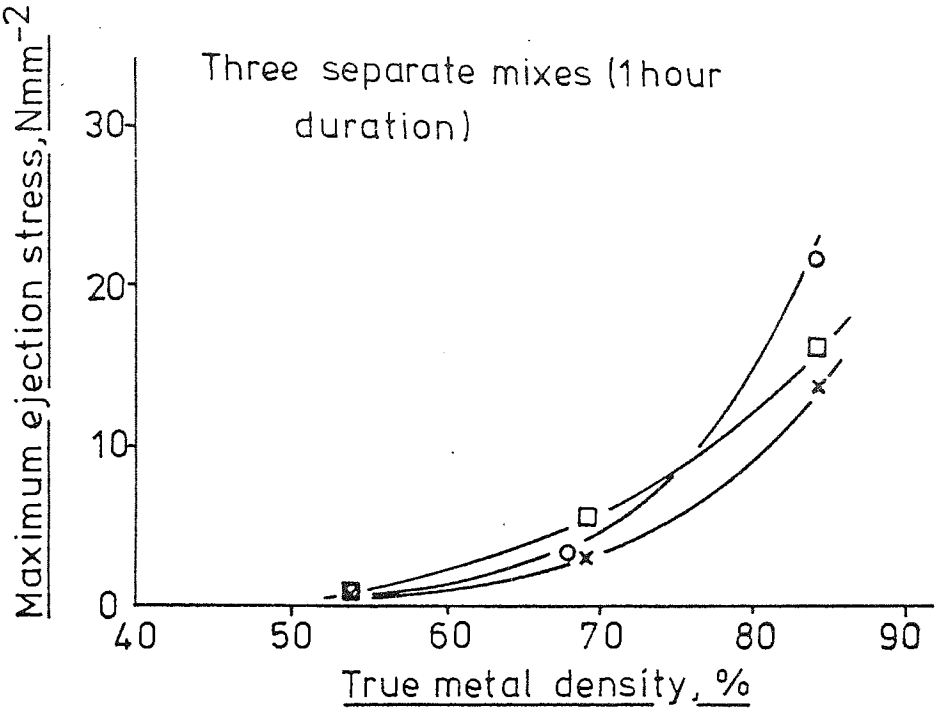

FIGURE 2-7. Reproducibility of ejection stress for MP32 plus 1% zinc stearate

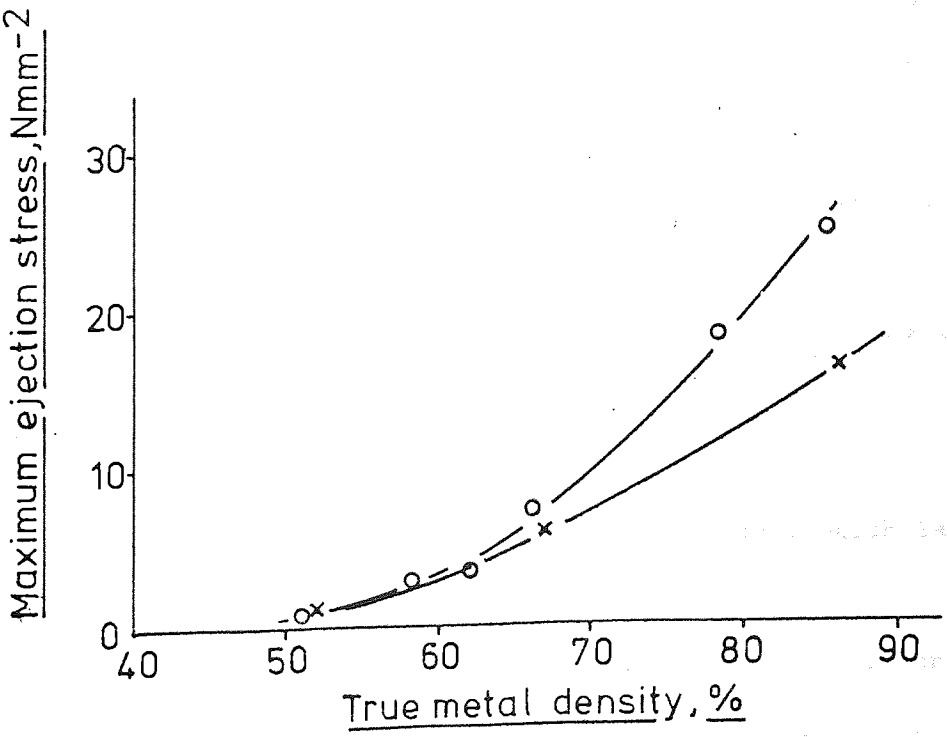

FIGURE 2-8. Reproducibity of the die-wall lubricant film.

variation of ejection stress caused by differing lubricant content was much greater than the experimental scatter.

2-3-2 Ejection with die-wall lubrication

Ejection stresses were determined for compacts pressed from powders containing precipitated zinc stearate with die-wall lubrication. The results are presented in figure 3-31 and will be used to assess the effect of simultansous die-wall and internal lubrication.

2-3-2-1 Reproducibility

The results shown in figure 2-8 have been obtained from compacts of MP32, 53-104μm (material B), pressed with die-wall but with no admixed lubricant. They are a good indication of the reproducibility of the die-wall lubricant film (see section 2-2-1-1).

2-3-3 Examination of ejected compact surfaces.

The surfaces of selected compacts were examined after ejection using scanning electron microscopy. It was thought that comparison of the external surfaces of unlubricated and lubricated compacts may assist the studies of ejection behaviour. Features of particular interest would be the extent of pore closure or smearing during ejection and the extrusion of lubricant from pores.

Two surfaces were available for examination on each compact;

(a) the surface in contact with the die, which is the area of shear during ejection,

(b) the surface in contact with the punches, which is not sheared during ejection.

The punch contact surfaces were considered to be representative of the friction surfaces before deformation by shear occurred during ejection. However, this was not strictly correct since some degree of particle/die-wall sliding also occurs during compaction.

Compacts were examined at two density levels corresponding to 3 and 30 x 10^4N applied force (47 and 470Nmm^{-2}). Sections were taken from the corner of each compact so that the two surfaces could be examined on one specimen and density variation between the surfaces was minimised (see appendix A).

Conditions studied were MP32 iron powder compacted with:

(a) no lubricant, plate 3-4

(b) die-wall lubrication only, plate 3-5

(c) 0.5% and 2.0% admixed zinc stearate (no die-wall lubrication), plates 3-6 and 3-7.

The parallel markings seen on the punch contact surfaces reflect the surface finish of the punches which were as-ground.

White featureless areas in the plates are the lubricant which characteristically charges up in the electron beam of the S.E.M.

2-4 Green strength.

As-pressed strengths were determined as transverse rupture strengths. The inherently low strengths of as-pressed compacts precluded the use of uniaxial tensile testing. Unfortunately the testing axis of either method was that least sensitive to the presence of lubricants, the axis perpendicular to the pressing axis.

Rectangular compacts, 76.5mm by 12.5mm, were pressed from MP32 with the appropriate lubricant content. Die-wall lubrication was used only when no other lubrication was present. Applied compaction forces were 15, 25, 35 and 45 x 10^4N, giving a compact thickness range of 4 to 6mm at 25g weight. True metal densities were calculated from physical dimensions and were in the range 5.3 to 6.7g cm^{-3}.

Each compact was carefully divided into two transverse rupture specimens. These were tested using a three point bend jig in a Hounsfield tensometer, motor driven at a strain rate of 3.2mm.min^{-1}. The transverse

rupture strength S is given by equation 2-3, from ASTM standard B312-64,

$$S = \frac{3PL}{2t^2w} \qquad \ldots(2\text{-}3)$$

where, P is the load,

L span (19.5mm),

w width, and

t thickness.

Results have been presented as transverse rupture strength (S) versus true metal density (D) to eliminate density as a variable.

2-4-1 The effect of lubricant content and dispersion.

Compacts were pressed from MP32 containing 0, 0.5 and 2.0% zinc stearate, either precipitated or admixed for 2292 cycles (sections 2-1-3, 2-1-4). It was hoped that the variation of content and dispersion would provide information on the mechanisms through which lubricants influence green strength. Results are shown in figure 3-32.

2-4-2 The effect of lubricant type.

It was essential to determine the influence of the lubricants studied in part II on as-pressed properties to fully understand their effect on the development of the mechanical properties of compacts during their decomposition.

1% by weight of each lubricant was admixed (except precipitated stearic acid) with MP32 iron powder for 45 minutes after sieving. The same mixes were used for the thermogravimetric specimens of part II. Compacts were pressed to 15, 25 and 45 x 10^4N applied force and the green strength results are shown in figure 3-33.

3 RESULTS.

FIGURE 3-1. Apparent (D_a) and tapped (D_t) densities for zinc stearate precipitated onto MP 32 Fe powder.

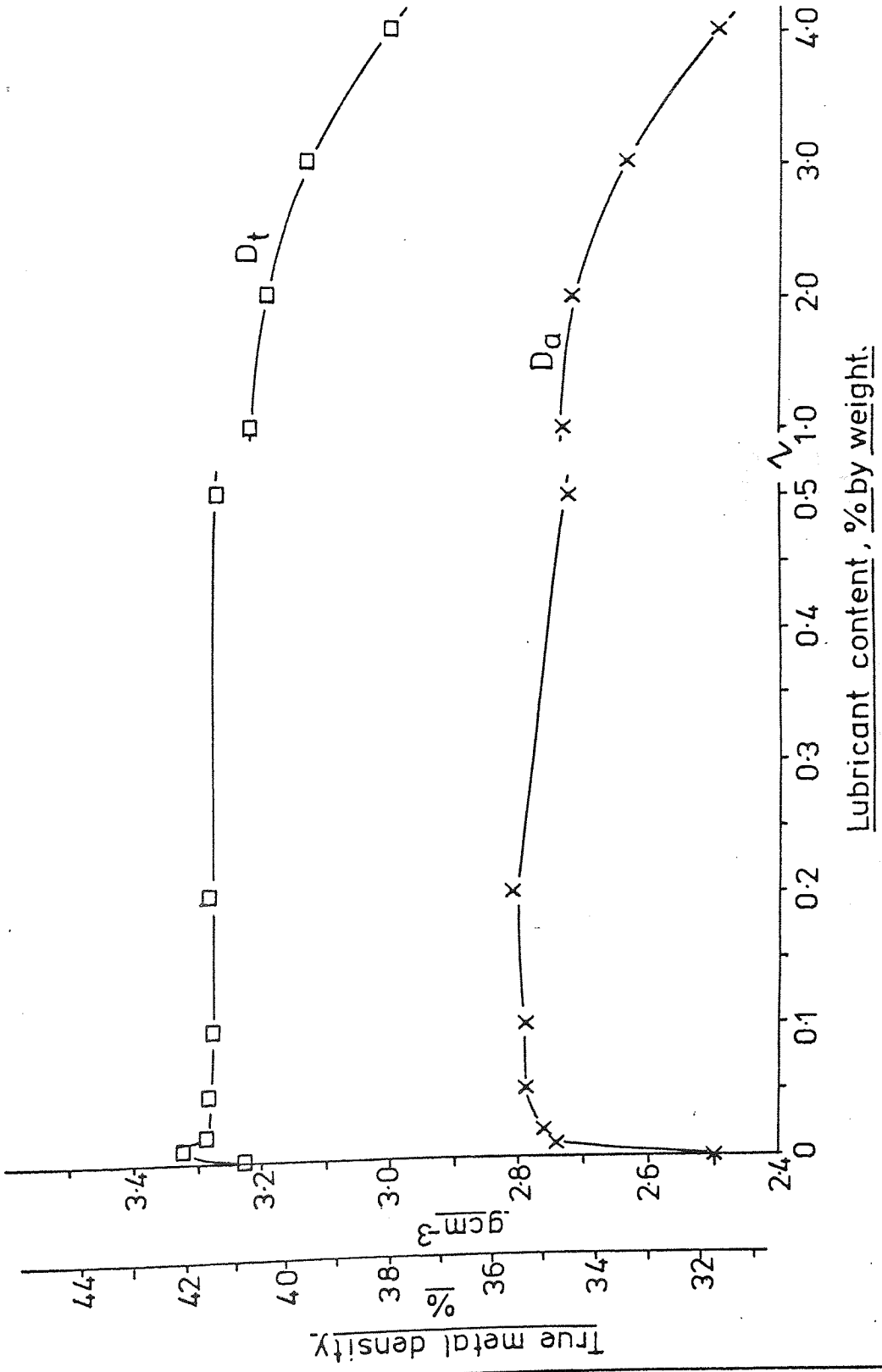

FIGURE 3-2. Apparent density versus mix duration for MP 32 plus zinc stearate.

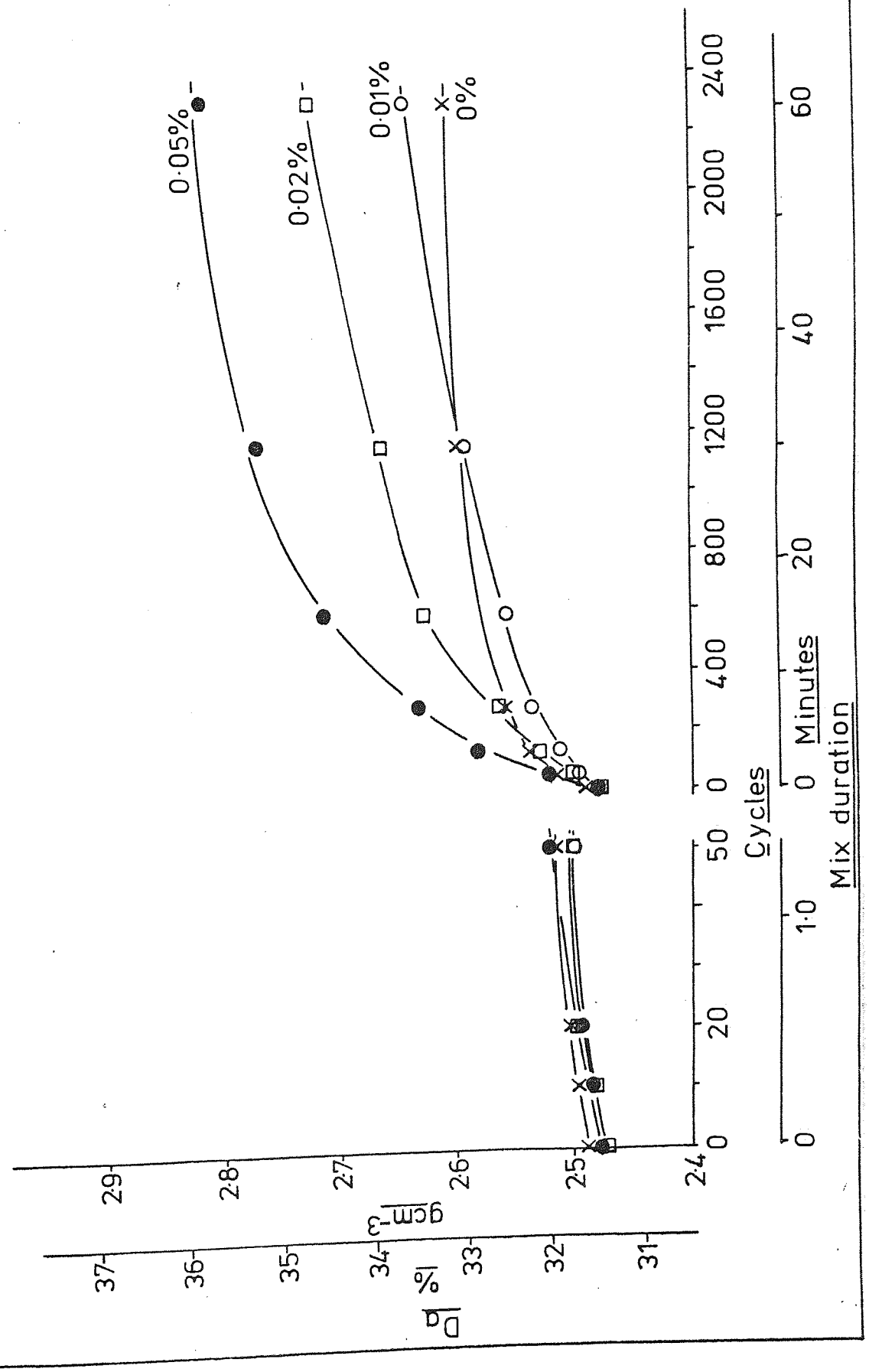

FIGURE 3-3. Apparent density versus mix duration for MP32 plus zinc stearate.

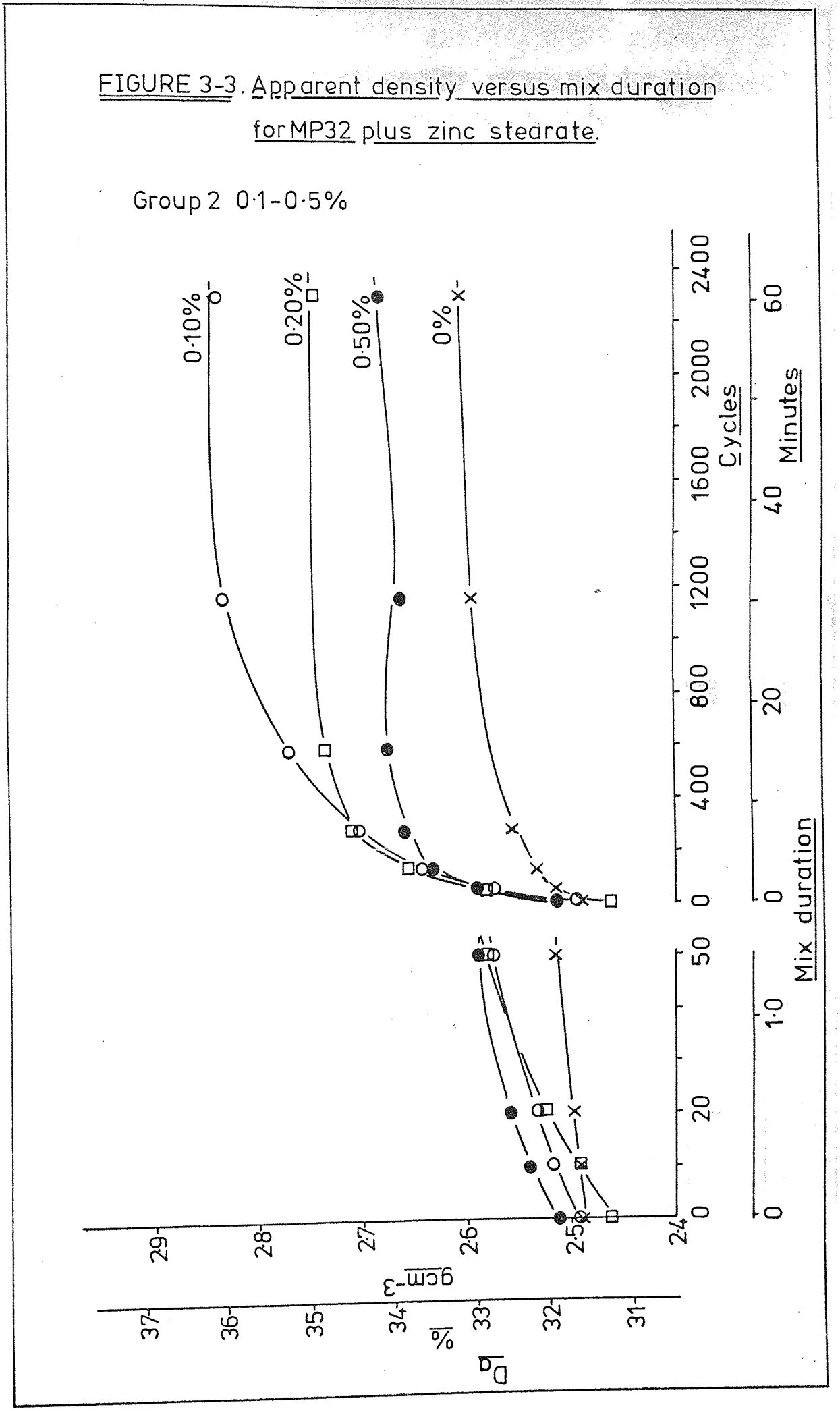

FIGURE 3-4. Apparent density versus mix duration for MP32 plus zinc stearate.

Group 3 1·0 – 4·0 %

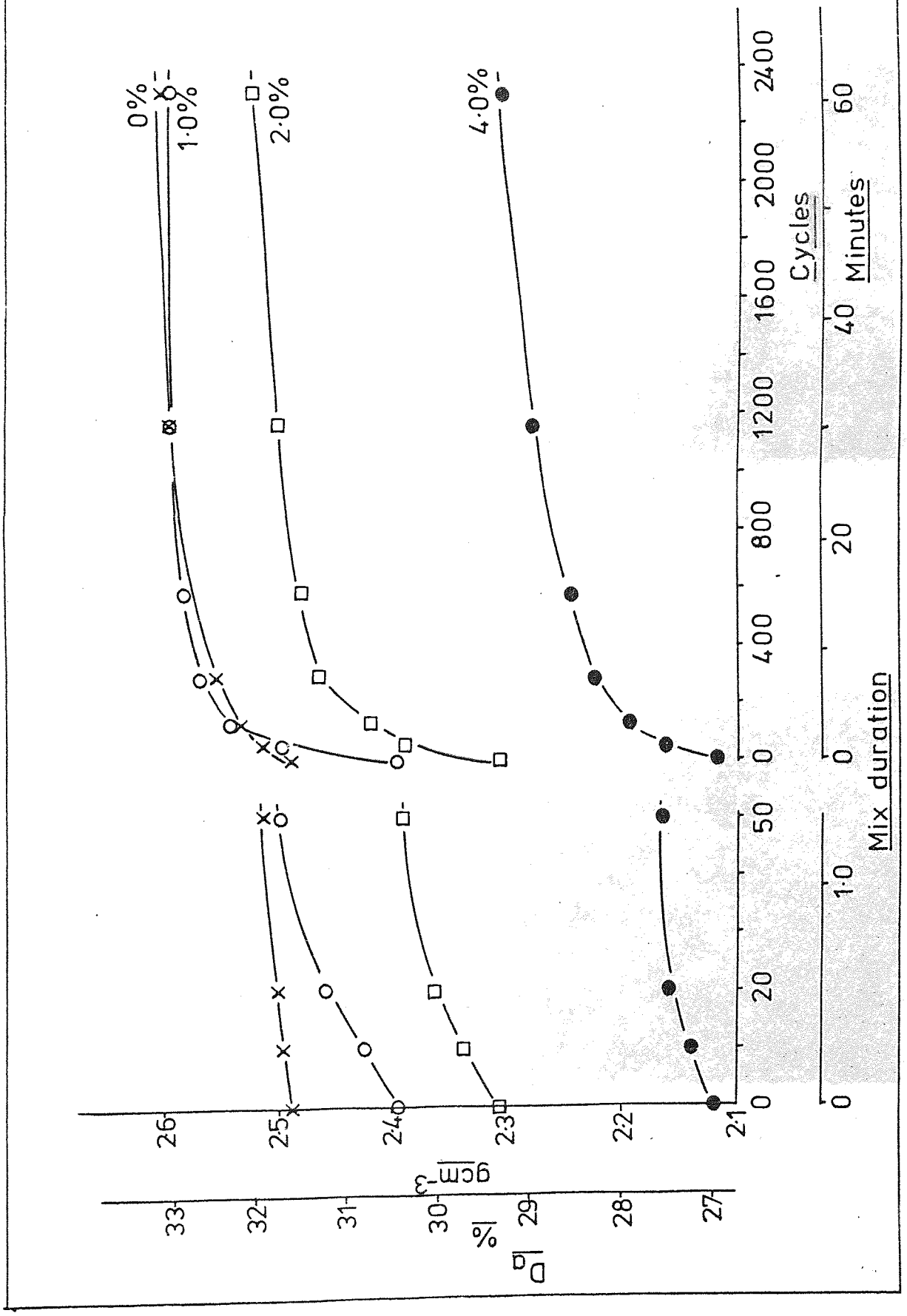

PLATE 3-1 The effect of mix duration on the general dispersion of 1% zinc stearate

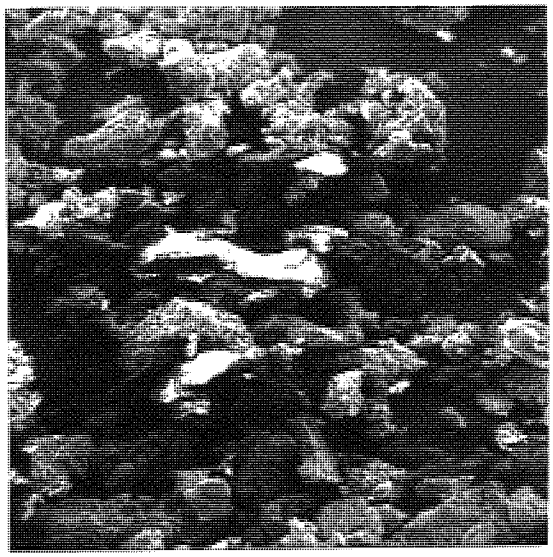

100μm

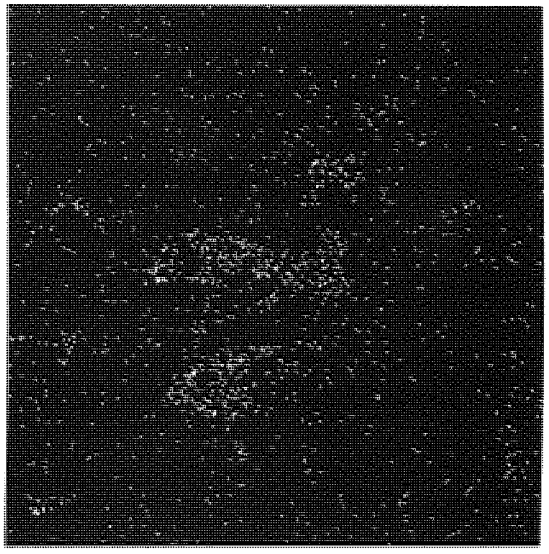

Zn X-ray map

10 Cycles

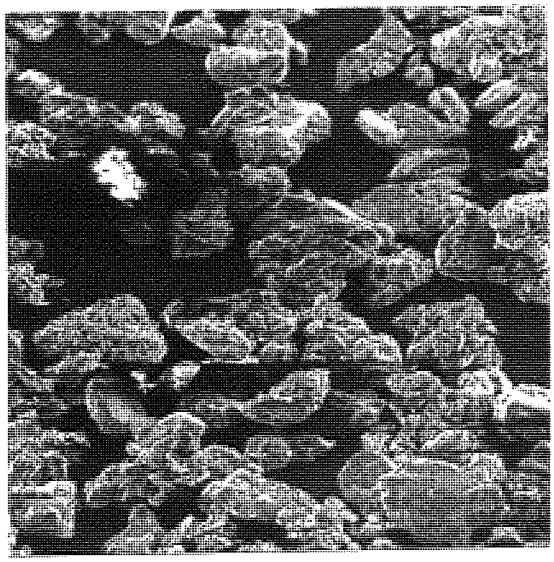

100μm

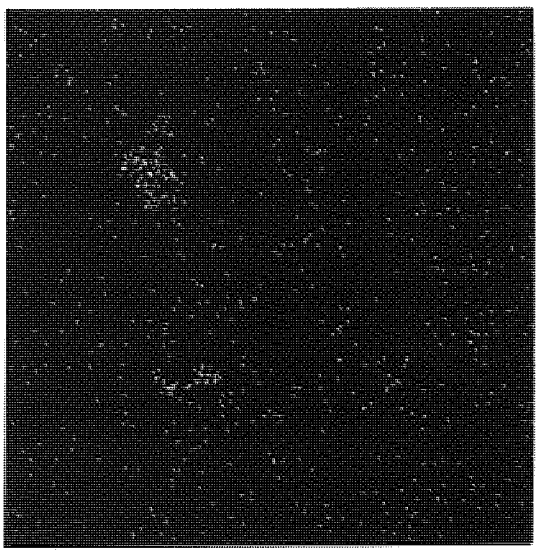

Zn X-ray map

1152 Cycles

PLATE 3-2 Lubricant pickup on iron particles during admixing (1% zinc stearate)

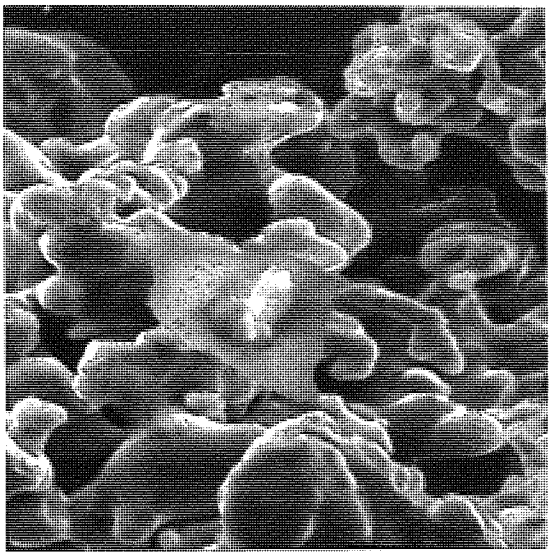

10μm

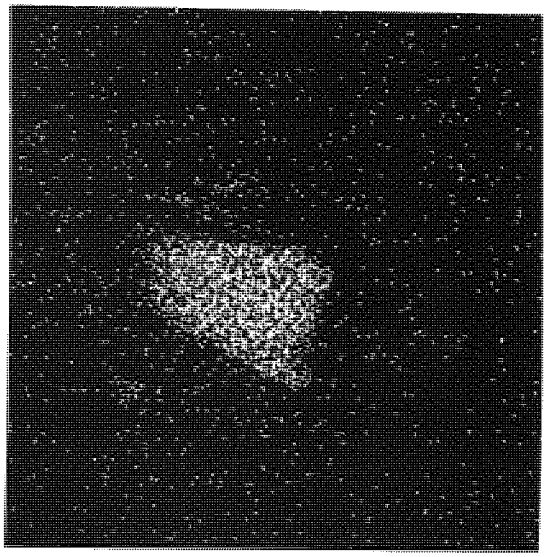

Zn X-ray map

(a)10 Cycles

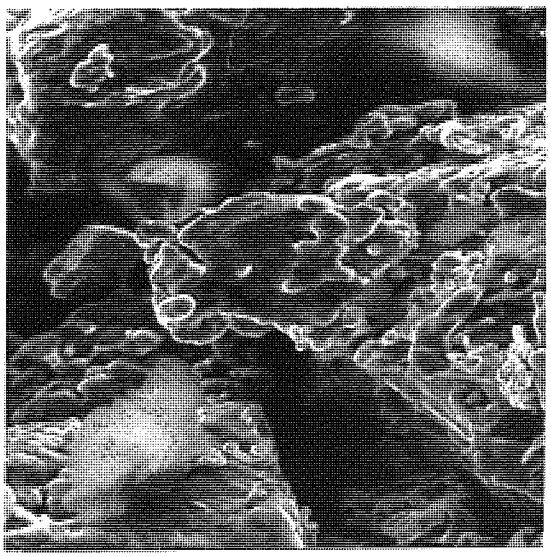

10μm

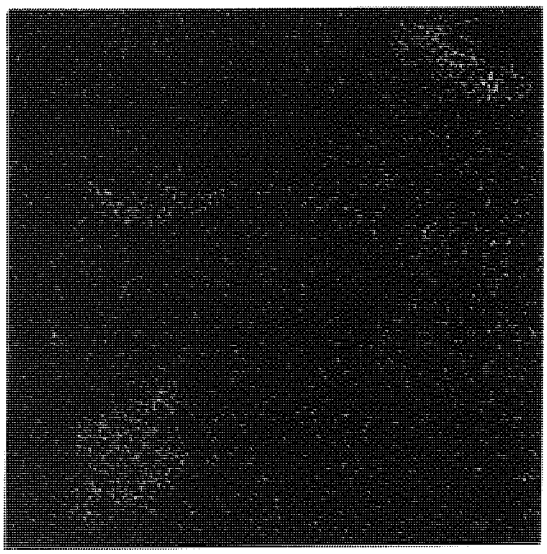

Zn X-ray map

(b)50 Cycles

PLATE 3-2 continued

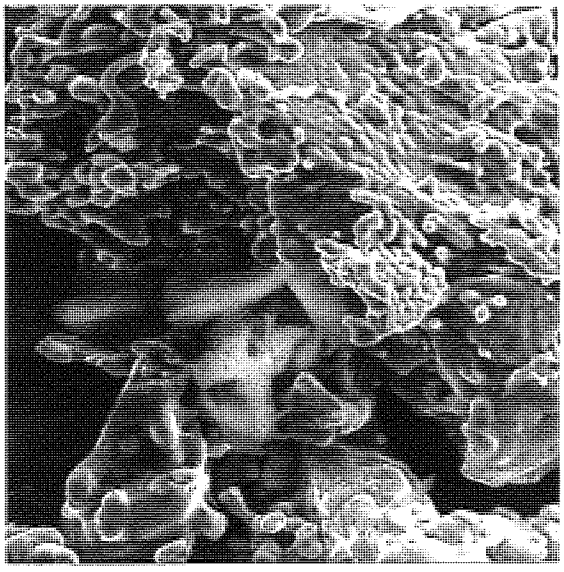

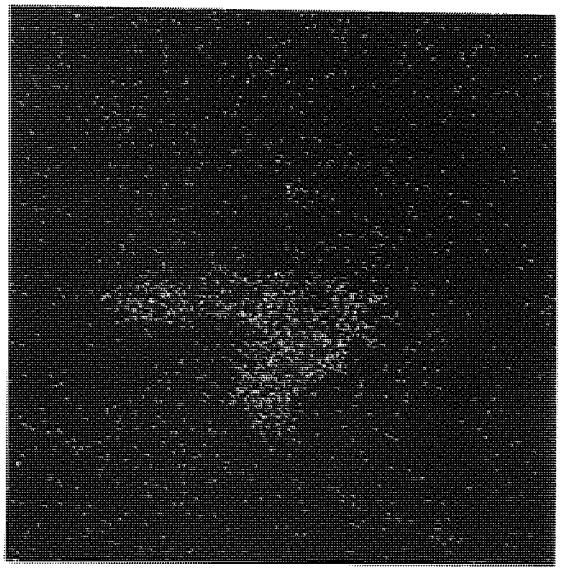

10μm

Zn X-ray map

(c) 278 Cycles

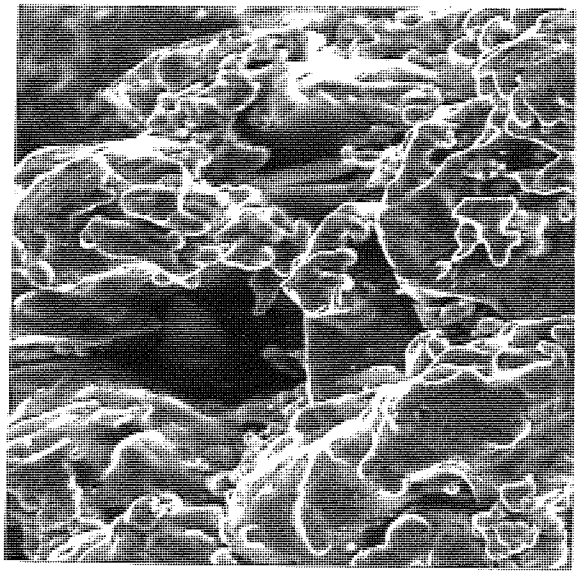

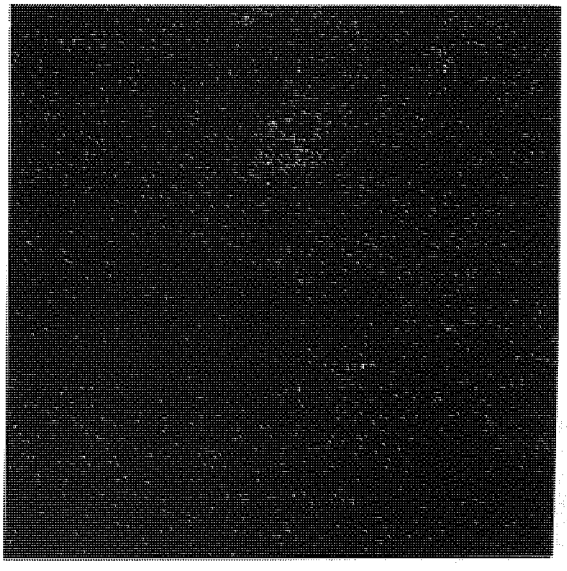

10μm

Zn X-ray map

(d) 1152 Cycles

PLATE 3-3 The effect of precipitation or admixing on the dispersion of 2% zinc stearate

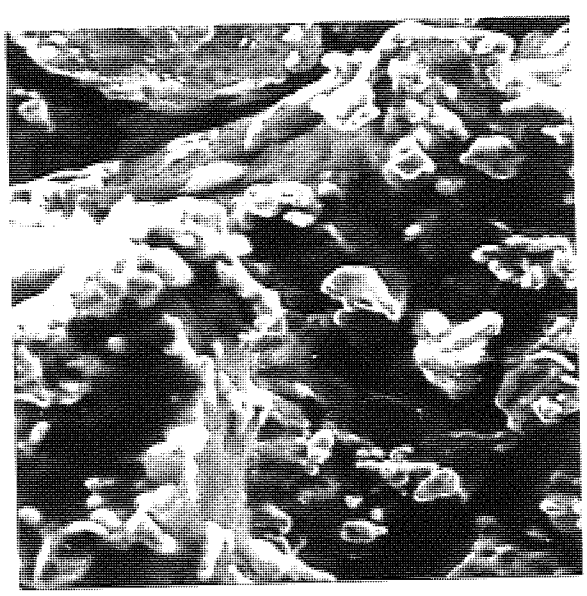

10 μm

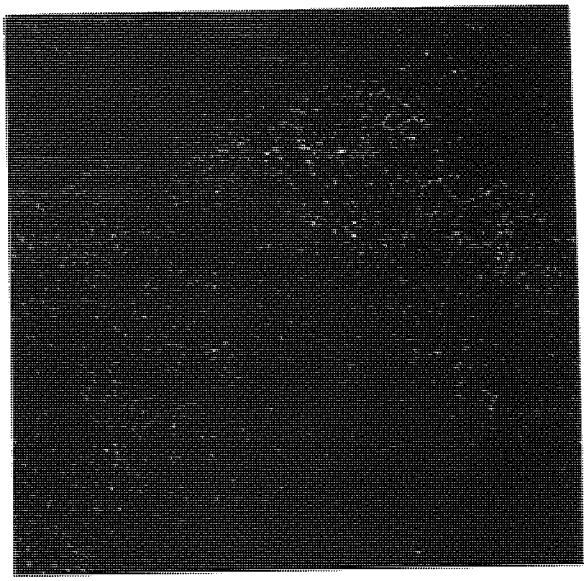

Zn X-ray map

(a) Precipitated

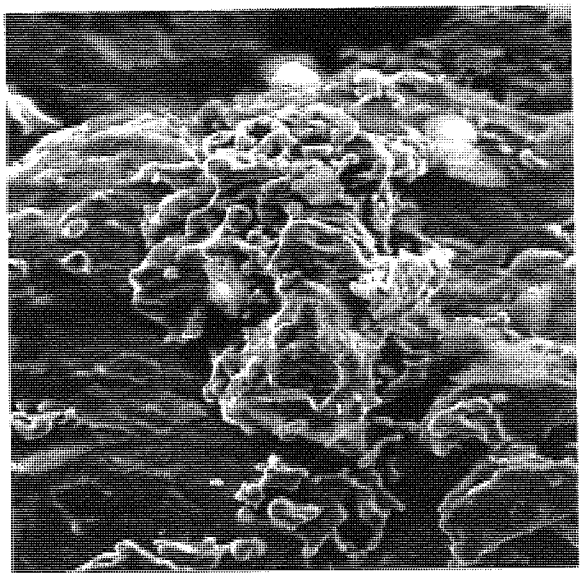

10 μm

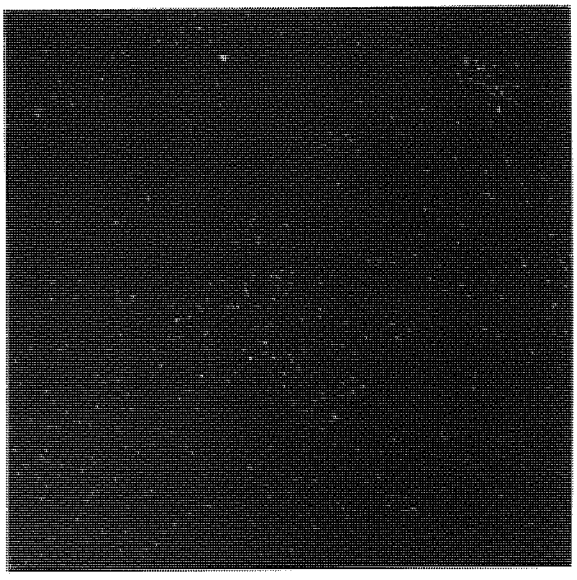

Zn X-ray map

(b) Admixed (2290 cycles)

TABLE 3 - 1

Iron powder properties (apparent density D_a , tapped density D_t, initial particle microhardness Hv0.025)

Material.	D_a	D_t	Microhardness Hv0.025	
			Mean	Range
A - MP32 104-180 um	0.31	0.39	122	112-134
B - MP32 53-104 um	0.32	0.40	122	110-126
C - MP32 -53 um	0.28	0.38	N/D	N/D
D - MP32 as-received	0.32	0.41	122	108-150
E - (B) carburised	0.34	0.42	178	148-247
F - (B) annealed	0.34	0.42	109	98-119
G - Mannesmann WP150	0.38	0.48	135	116-145
H - Höganäs NC100	0.32	0.42	110	103-119
I - Höganäs ASC100	0.38	0.50	107	103-112
J - Carbonyl iron	N/D*	0.50	N/D	N/D

* N/D - not determinable

D_a and D_t are fractional relative true metal densities, assuming solid density as 7.87 $g.cm^{-3}$.

TABLE 3-2. Analysis of the linear relationship - compaction results.

(All materials, except K, die-wall lubricated.)

3-2(A). Material A. MP 32 104-180 μm.

Compaction pressure $N.mm^{-2}$	True metal density		ln(1/(1-D))
	$g.cm^{-3}$	D fractional	
8	3.07	0.390	0.494
16	3.40	0.431	0.564
23	3.59	0.456	0.609
31	3.78	0.481	0.656
39	3.94	0.501	0.695
47	4.05	0.515	0.724
54	4.22	0.536	0.768
62	4.35	0.553	0.805
70	4.46	0.567	0.837
78	4.56	0.580	0.868
93	4.73	0.602	0.922
109	4.87	0.619	0.965
124	5.05	0.641	1.025
140	5.18	0.658	1.073
156	5.30	0.674	1.121
171	5.41	0.688	1.165
187	5.52	0.701	1.207
202	5.64	0.716	1.259
218	5.73	0.729	1.306
249	5.90	0.750	1.386
280	6.07	0.772	1.478
311	6.22	0.790	1.561
342	6.35	0.807	1.645
373	6.45	0.820	1.715
404	6.55	0.833	1.790
436	6.66	0.847	1.877
467	6.74	0.857	1.945

TABLE 3-2, continued.

3-2(B). Material B. MP 32 53-104 μm.

Compaction pressure $N.mm^{-2}$	True metal density		ln(1/(1-D))
	$g.cm^{-3}$	D fractional	
8	3.17	0.403	0.516
16	3.46	0.440	0.580
23	3.65	0.464	0.624
31	3.82	0.485	0.664
39	3.98	0.506	0.705
47	4.08	0.518	0.730
54	4.24	0.539	0.774
62	4.38	0.557	0.814
70	4.47	0.568	0.839
78	4.58	0.582	0.872
93	4.76	0.605	0.929
109	4.88	0.620	0.968
124	5.06	0.643	1.030
140	5.20	0.661	1.082
156	5.31	0.675	1.124
171	5.43	0.690	1.171
187	5.54	0.704	1.217
202	5.66	0.719	1.269
218	5.75	0.731	1.313
233	5.85	0.743	1.359
249	5.93	0.754	1.402
280	6.09	0.774	1.487
311	6.23	0.792	1.570
342	6.35	0.807	1.645
373	6.47	0.822	1.726
404	6.58	0.836	1.808
436	6.66	0.846	1.871
467	6.74	0.857	1.945

TABLE 3-2, continued.

3-2(C). Material C. MP32 -53 μm.

Compaction pressure $N.mm^{-2}$	True metal density		ln(1/(1-D))
	$g.cm^{-3}$	D fractional	
8	2.94	0.374	0.468
16	3.27	0.416	0.538
23	3.46	0.440	0.580
31	3.65	0.464	0.624
39	3.80	0.483	0.660
47	3.92	0.498	0.689
54	4.07	0.517	0.728
62	4.20	0.534	0.764
70	4.32	0.549	0.796
78	4.41	0.561	0.823
93	4.58	0.582	0.872
109	4.72	0.599	0.914
124	4.88	0.620	0.968
140	5.03	0.639	1.019
156	5.13	0.652	1.056
171	5.25	0.667	1.100
187	5.35	0.680	1.139
202	5.48	0.696	1.191
218	5.58	0.709	1.234
249	5.75	0.731	1.313
280	5.92	0.752	1.394
311	6.05	0.769	1.465
342	6.18	0.786	1.542
373	6.31	0.802	1.620
404	6.41	0.814	1.682
436	6.51	0.827	1.754
467	6.59	0.838	1.820

TABLE 3-2, continued.

3-2(D). Material D. MP32 as-received.

Compaction pressure $N.mm^{-2}$	True metal density		ln(1/(1-D))
	$g.cm^{-3}$	D fractional	
8	3.19	0.405	0.519
16	3.49	0.443	0.585
23	3.67	0.466	0.628
31	3.85	0.489	0.671
39	4.01	0.510	0.713
47	4.12	0.523	0.740
54	4.27	0.543	0.783
62	4.41	0.560	0.821
70	4.49	0.571	0.846
78	4.59	0.583	0.875
93	4.76	0.604	0.926
109	4.90	0.623	0.976
124	5.06	0.643	1.030
140	5.20	0.661	1.082
156	5.31	0.675	1.124
171	5.43	0.690	1.171
187	5.53	0.703	1.214
202	5.65	0.717	1.264
218	5.74	0.729	1.306
249	5.89	0.749	1.382
280	6.07	0.771	1.474
311	6.21	0.789	1.556
342	6.34	0.806	1.640
373	6.44	0.818	1.704
404	6.55	0.833	1.790
436	6.64	0.843	1.851
467	6.73	0.856	1.938

TABLE 3-2, continued.

3-2(E). Material E. MP32 53-104 μm, carburised.

Compaction pressure $N.mm^{-2}$	True metal density		ln(1/(1-D))
	$g.cm^{-3}$	D fractional	
8	3.16	0.402	0.514
16	3.39	0.431	0.564
23	3.53	0.450	0.598
31	3.66	0.466	0.628
39	3.79	0.483	0.660
47	3.88	0.494	0.681
54	4.00	0.509	0.711
62	4.10	0.522	0.738
70	4.18	0.532	0.759
78	4.26	0.543	0.783
93	4.40	0.561	0.823
109	4.51	0.575	0.855
124	4.66	0.594	0.901
140	4.79	0.610	0.942
156	4.90	0.624	0.978
171	4.99	0.636	1.011
187	5.08	0.647	1.041
202	—	—	—
218	5.28	0.672	1.115
249	5.43	0.692	1.178
280	5.60	0.713	1.248
311	5.73	0.730	1.309
342	5.85	0.745	1.367
373	5.94	0.757	1.415
404	6.06	0.771	1.474
436	6.17	0.786	1.542
467	6.26	0.798	1.599

TABLE 3-2, continued.

3-2(F). Material F. MP32 53-104 μm, annealed.

Compaction pressure $N.mm^{-2}$	True metal density		ln(1/(1-D))
	$g.cm^{-3}$	D fractional	
8	3.29	0.418	0.541
16	3.56	0.453	0.603
23	3.75	0.476	0.646
31	3.92	0.498	0.689
43	4.14	0.526	0.747
47	4.19	0.533	0.761
54	4.34	0.551	0.801
62	4.48	0.570	0.844
70	4.60	0.584	0.877
78	4.70	0.597	0.909
93	4.87	0.619	0.965
109	5.00	0.636	1.011
124	5.19	0.659	1.076
140	5.33	0.677	1.130
156	5.43	0.690	1.171
171	5.56	0.706	1.224
187	5.66	0.719	1.269
202	5.80	0.736	1.332
218	5.89	0.748	1.378
249	6.05	0.769	1.465
280	6.22	0.791	1.566
311	6.36	0.808	1.650
342	6.48	0.823	1.732
373	6.59	0.837	1.814
404	6.69	0.851	1.904
436	6.79	0.863	1.988
467	6.87	0.873	2.064

TABLE 3-2, continued.

3-2(G). Material G. Mannesmann WP150.

Compaction pressure $N.mm^{-2}$	True metal density		ln(1/(1-D))
	$g.cm^{-3}$	D fractional	
8	3.61	0.459	0.614
16	3.77	0.479	0.652
23	3.89	0.494	0.680
31	4.04	0.513	0.719
39	4.14	0.526	0.747
47	4.22	0.536	0.768
54	4.35	0.552	0.803
62	4.46	0.566	0.835
70	4.55	0.578	0.863
78	4.63	0.589	0.889
93	4.78	0.607	0.934
109	4.91	0.624	0.978
124	5.07	0.645	1.036
140	5.20	0.660	1.079
156	5.30	0.674	1.121
171	5.40	0.687	1.162
187	5.51	0.700	1.204
202	5.62	0.714	1.252
218	5.72	0.726	1.295
249	5.88	0.747	1.375
280	6.05	0.768	1.461
311	6.18	0.785	1.537
342	6.31	0.801	1.614
373	6.43	0.817	1.698
404	6.53	0.830	1.772
436	6.63	0.842	1.845
467	6.72	0.854	1.924

TABLE 3-2, continued.

3-2(H). Material H. Höganäs NC100.

Compaction pressure $N.mm^{-2}$	True metal density		ln(1/(1-D))
	$g.cm^{-3}$	D fractional	
8	3.01	0.383	0.483
16	3.24	0.412	0.531
23	3.38	0.430	0.562
31	3.55	0.451	0.599
39	3.69	0.470	0.635
47	3.80	0.483	0.660
54	3.95	0.502	0.697
62	4.08	0.519	0.732
70	4.19	0.532	0.759
78	4.28	0.544	0.785
93	4.47	0.568	0.839
109	4.61	0.585	0.880
124	4.79	0.608	0.937
140	4.93	0.627	0.986
156	5.06	0.642	1.027
171	5.18	0.658	1.073
187	5.29	0.672	1.114
202	5.42	0.688	1.165
218	5.52	0.701	1.207
233	5.61	0.713	1.248
280	5.89	0.749	1.382
311	6.02	0.765	1.448
342	6.15	0.781	1.519
373	6.38	0.811	1.666
404	6.49	0.825	1.743
436	6.59	0.837	1.814
467			

TABLE 3-2, continued.

3-2(I). Material I. Höganäs ASC100.

Compaction pressure $N.mm^{-2}$	True metal density		ln(1/(1-D))
	$g.cm^{-3}$	D fractional	
8	3.51	0.446	0.591
16	3.77	0.478	0.650
23	3.91	0.497	0.687
31	4.07	0.518	0.730
39	4.24	0.538	0.772
47	4.34	0.551	0.801
54	4.48	0.570	0.844
62	4.61	0.586	0.882
70	4.72	0.600	0.916
78	4.82	0.612	0.947
93	5.00	0.635	1.008
109	5.12	0.651	1.054
124	5.30	0.673	1.118
140	5.44	0.691	1.174
156	5.57	0.707	1.228
171	5.68	0.721	1.277
187	5.78	0.735	1.328
202	5.90	0.749	1.382
218	6.00	0.763	1.440
249	6.17	0.784	1.533
280	6.34	0.806	1.640
311	6.48	0.823	1.732
342	6.61	0.839	1.826
373	6.72	0.853	1.917
404	6.81	0.866	2.010
436	6.90	0.877	2.096
467	6.98	0.887	2.180

TABLE 3-2, continued.

3-2(J). Material J. Carbonyl iron -53 μm.

Compaction pressure $N.mm^{-2}$	True metal density		ln(1/(1-D))
	$g.cm^{-3}$	D fractional	
8	3.80	0.483	0.660
16	3.92	0.498	0.689
23	3.98	0.506	0.705
31	4.05	0.515	0.724
39	4.11	0.523	0.740
47	4.16	0.529	0.753
54	4.23	0.538	0.772
62	4.30	0.546	0.790
70	4.35	0.553	0.805
78	4.39	0.558	0.816
93	4.48	0.569	0.842
109	4.55	0.579	0.865
124	4.65	0.591	0.894
140	4.74	0.602	0.922
156	4.81	0.611	0.944
171	4.89	0.621	0.970
187	4.95	0.629	0.991
202	5.03	0.639	1.019
218	5.10	0.648	1.044
249	5.23	0.665	1.094
280	5.38	0.684	1.152
311	5.50	0.699	1.201
342	5.61	0.713	1.248
373	5.72	0.727	1.298
404	5.82	0.739	1.343
436	5.92	0.752	1.394
467	6.02	0.765	1.448

TABLE 3-2, continued.

3-2(K). Material K. MP32 53-104 μm, no die-wall lubrication.

Compaction pressure $N.mm^{-2}$	True metal density		ln(1/(1-D))
	$g.cm^{-3}$	D fractional	
8	3.19	0.405	0.519
16	3.45	0.438	0.576
23	3.62	0.460	0.616
31	3.79	0.482	0.658
39	3.95	0.502	0.697
47	4.04	0.513	0.719
54	4.18	0.531	0.757
62	4.30	0.546	0.790
70	4.43	0.563	0.828
78	4.51	0.573	0.851
93	4.67	0.593	0.899
109	4.81	0.611	0.944
124	4.96	0.630	0.994
140	5.08	0.645	1.036
156	5.16	0.656	1.067
171	5.26	0.668	1.103
187	5.36	0.681	1.143
202	5.48	0.696	1.191
233	5.65	0.718	1.266
249	5.72	0.727	1.298
280	5.90	0.750	1.386
311	6.02	0.765	1.448
351	6.17	0.784	1.533
373	6.26	0.795	1.585
404	6.35	0.807	1.645
436	6.43	0.817	1.698
467	6.52	0.828	1.760

FIGURE.3-5. Linear compaction relationships, the effect of material work hardening properties.

(only alternate points plotted)

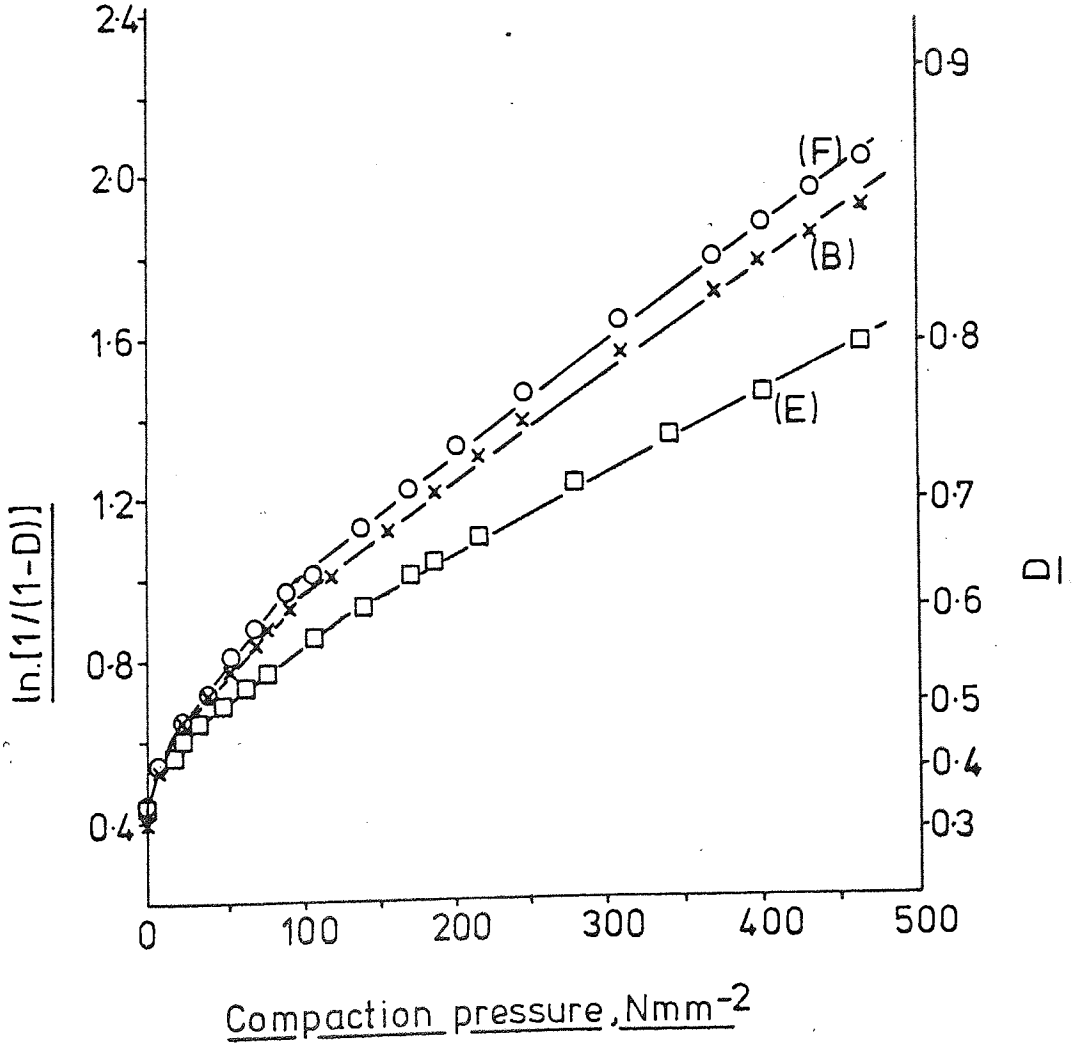

FIGURE 3-6. Linear compaction relationships, the effect of particle morphology.

(only alternate points plotted)

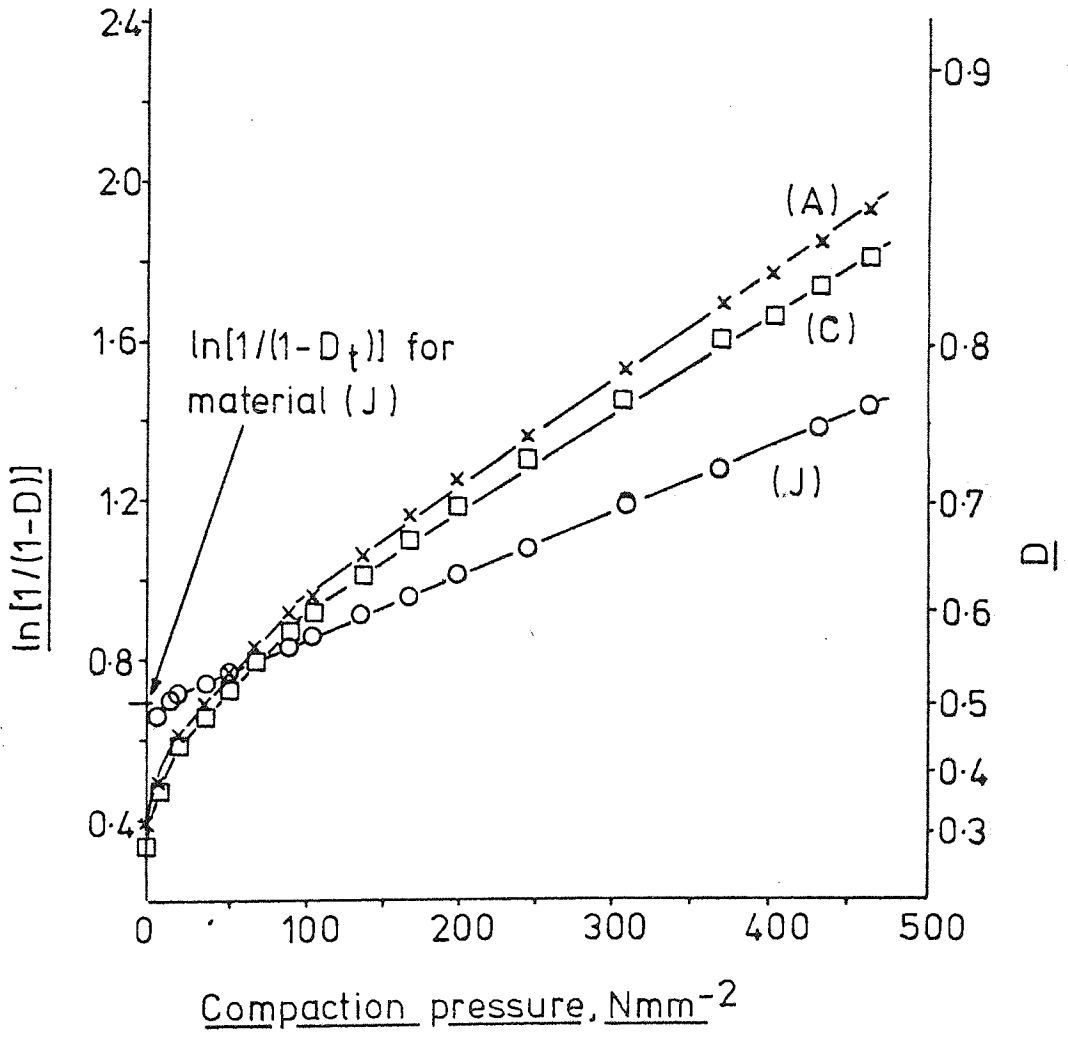

FIGURE 3-7. Linear compaction relationships, the compaction of as-received powders.

(only alternate points plotted)

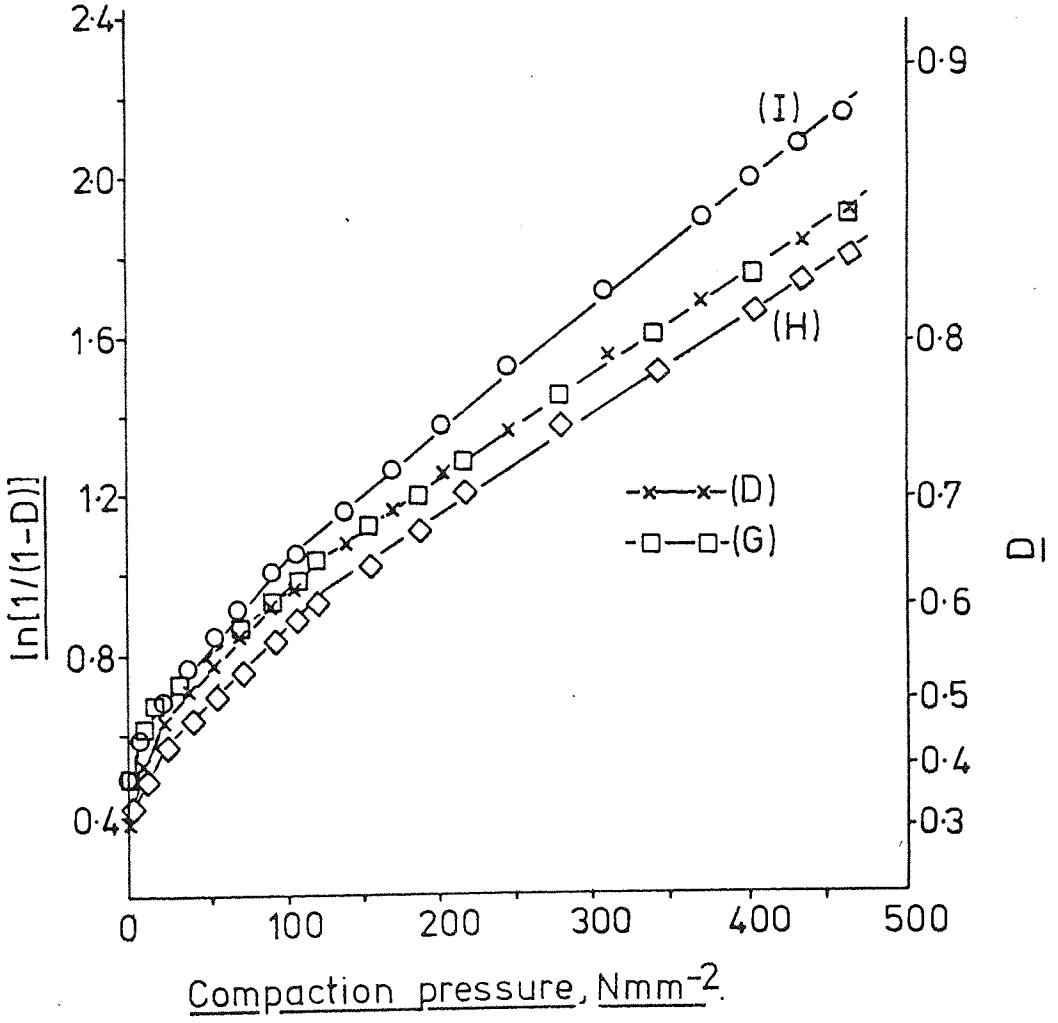

FIGURE 3-8. Linear compaction relationships, the effect of particle/die-wall friction

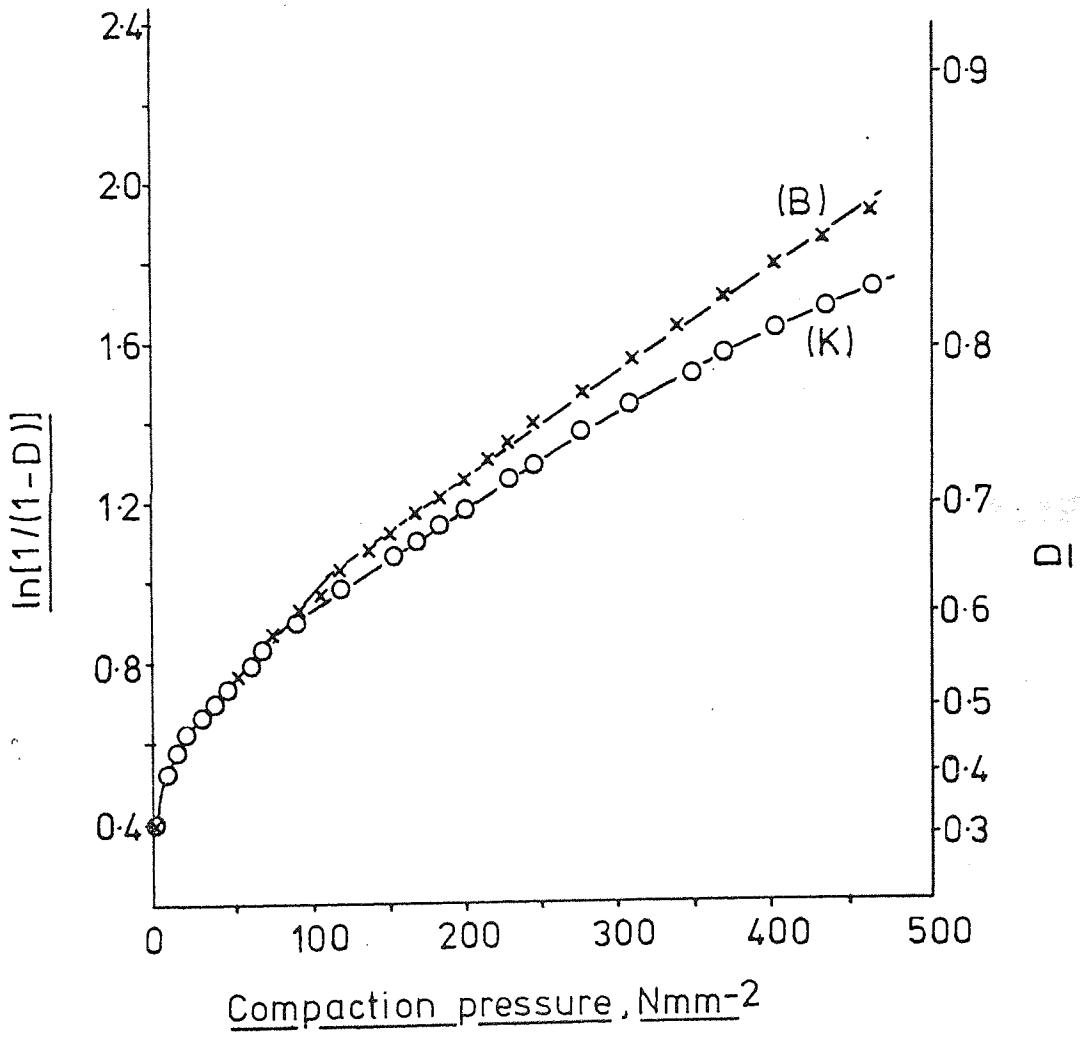

FIGURES 3-9 and 3-10 Individual particle microhardness versus density.

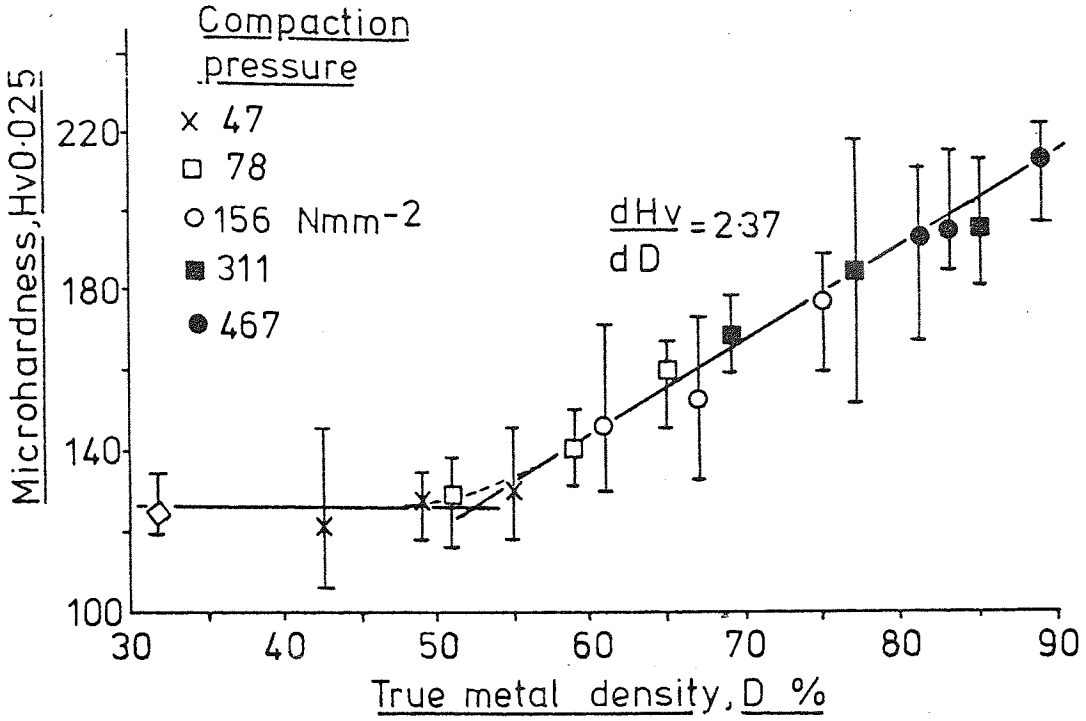

FIGURE 3-9 Material K (MP32 53-104 μm, no die-wall lubrication)

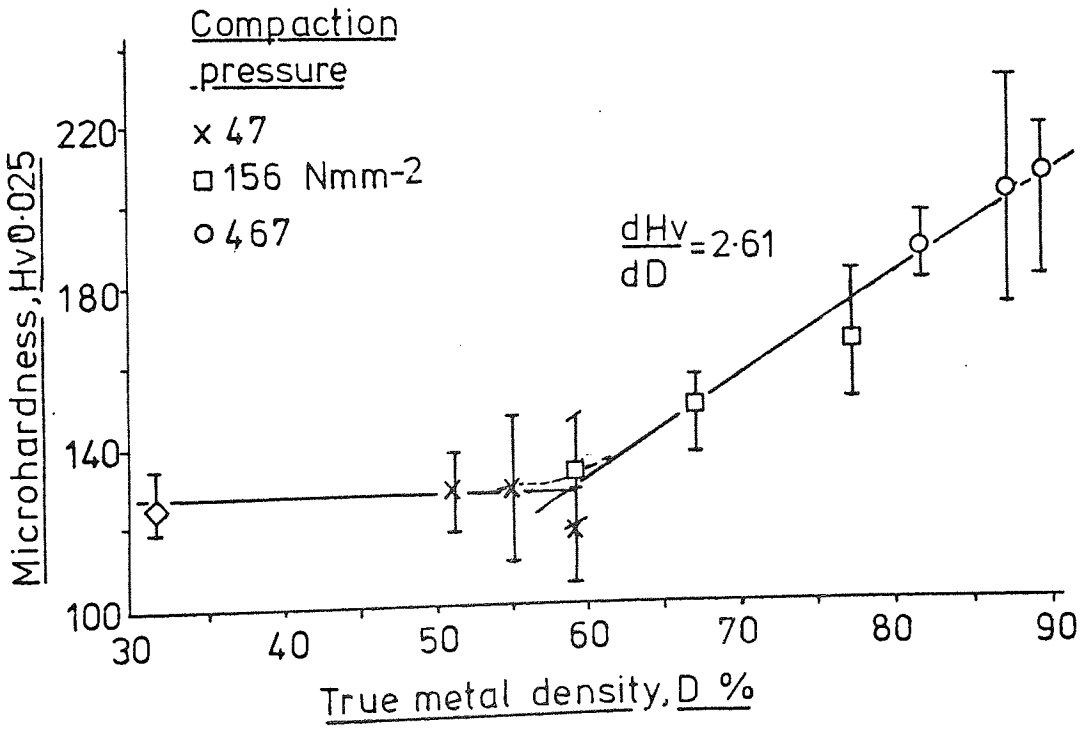

FIGURE 3-10. Material B (MP32 53-104 μm, die-wall lubricated)

FIGURES 3-11 and 3-12. Individual particle microhardness versus density

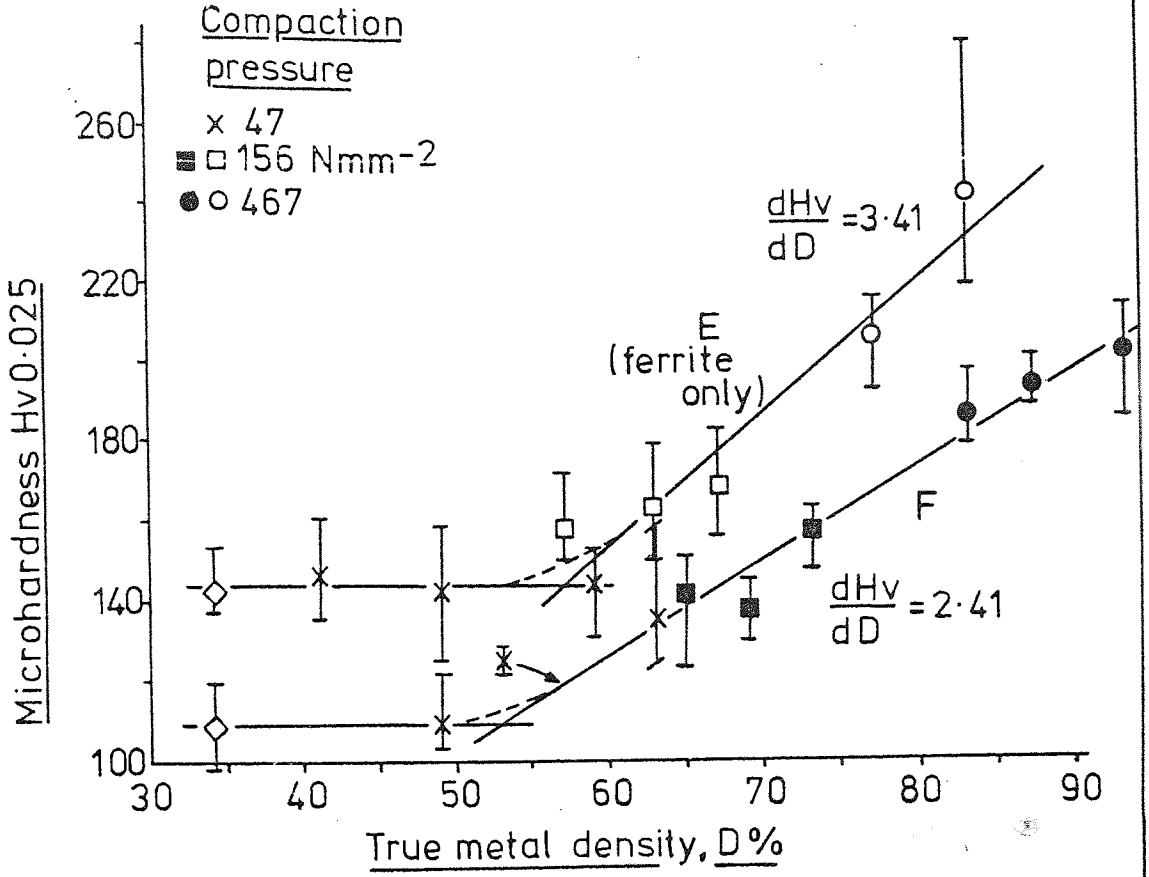

FIGURE 3-11. Materials E and F (MP32 53-104 μm carburised and annealed respectively)

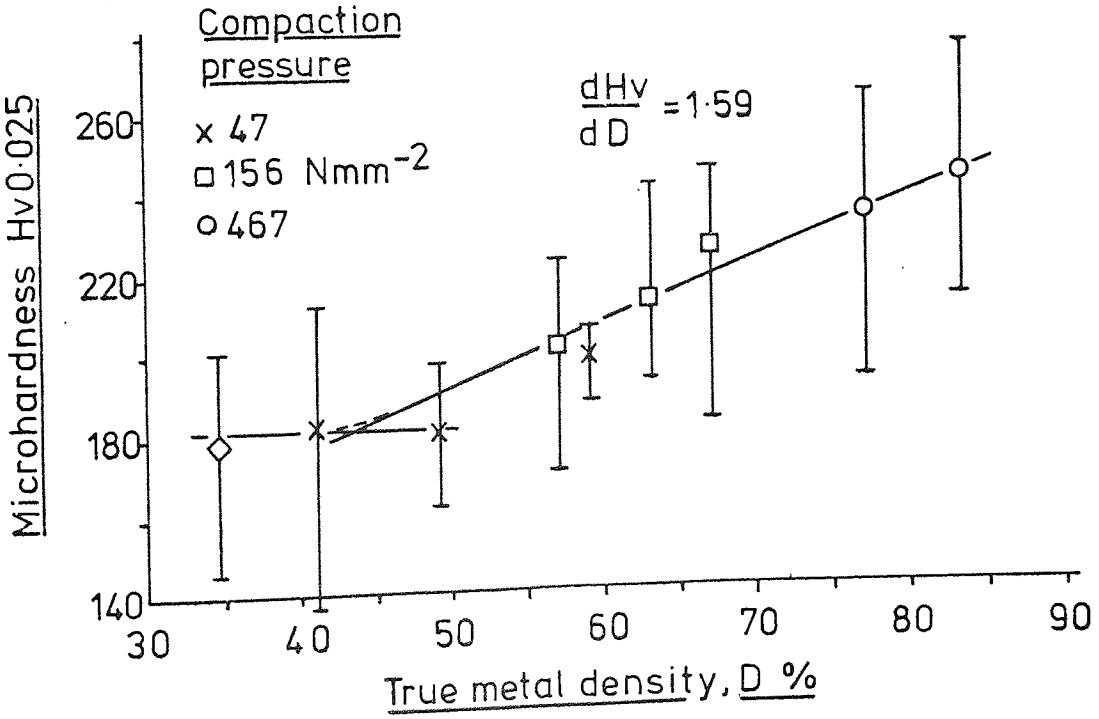

FIGURE 3-12. Material E, random determinations (ferrite and pearlite)

TABLE 3-3. Compaction results - MP32 plus precipitated/evaporated zinc stearate, die-wall lubricated.

3-3(A). No lubricant, MP32 washed in benzene.

Compaction pressure $N.mm^{-2}$	Actual density D* $g.cm^{-3}$	True metal density		ln(1/(1-D))
		$g.cm^{-3}$	D fractional	
8	As true metal density	3.30	0.420	0.544
16		3.50	0.445	0.588
23		3.69	0.469	0.634
31		3.90	0.495	0.683
39		4.06	0.516	0.725
47		4.16	0.528	0.751
54		4.32	0.549	0.796
62		4.45	0.565	0.832
70		4.55	0.578	0.863
78		4.65	0.591	0.893
93		4.82	0.612	0.946
109		4.95	0.628	0.990
124		5.11	0.650	1.048
140		5.24	0.666	1.098
156		5.35	0.680	1.140
171		5.46	0.694	1.185
187		5.56	0.707	1.228
202		5.68	0.721	1.278
218		5.77	0.733	1.319
249		5.93	0.753	1.398
280		6.08	0.773	1.483
311		6.22	0.790	1.561
342		6.35	0.807	1.643
373		6.45	0.820	1.712
404		6.55	0.833	1.788
436		6.65	0.845	1.864
467		6.72	0.854	1.926

Actual density, D*, has been recorded to 3 decimal places in tables 3-3, 3-4 and 3-5. This was to show the small differences between D* and true metal density at low lubricant levels. This small variation may produce a more noticeable difference between ln(1/(1-D*)) and ln(1/(1-D)).

TABLE 3-3, continued.

3-3(B). 0.01 % precipitated zinc stearate.

Compaction pressure $N.mm^{-2}$	Actual density D* $g.cm^{-3}$	True metal density		ln(1/(1-D))
		$g.cm^{-3}$	D fractional	
8		3.38	0.429	0.561
16		3.66	0.465	0.626
23		3.85	0.489	0.671
31		4.02	0.510	0.714
39		4.18	0.531	0.757
47		4.27	0.542	0.782
54		4.41	0.561	0.822
62		4.55	0.578	0.862
70		4.66	0.592	0.898
78		4.75	0.603	0.924
93	As	4.90	0.623	0.976
109	true	5.05	0.641	1.025
124	metal	5.20	0.661	1.082
140	density	5.33	0.677	1.131
156		5.45	0.692	1.178
171		5.55	0.705	1.220
187		5.63	0.715	1.257
202		5.75	0.731	1.313
218		5.84	0.742	1.353
249		6.00	0.762	1.436
280		6.17	0.784	1.531
311		6.28	0.798	1.601
342		6.39	0.812	1.673
373		6.49	0.825	1.744
404		6.60	0.838	1.823
436		6.69	0.851	1.901
467		6.77	0.860	1.966

TABLE 3-3, continued.

3-3(C). 0.02 % precipitated zinc stearate .

Compaction pressure $N.mm^{-2}$	Actual density D* $g.cm^{-3}$	True metal density		ln(1/(1-D))
		$g.cm^{-3}$	D fractional	
8	As true metal density	3.37	0.428	0.558
16		3.63	0.461	0.618
23		3.81	0.484	0.661
31		3.99	0.507	0.707
39		4.16	0.528	0.751
47		4.26	0.541	0.779
54		4.41	0.561	0.823
62		4.55	0.578	0.863
70		4.65	0.591	0.895
78		4.74	0.602	0.922
93		4.90	0.623	0.976
109		5.03	0.639	1.020
124		5.20	0.660	1.080
140		5.33	0.677	1.129
156		5.44	0.691	1.173
171		5.54	0.704	1.218
187		5.64	0.716	1.259
202		5.75	0.731	1.312
218		5.84	0.742	1.357
249		6.00	0.762	1.435
280		6.15	0.781	1.519
311		6.29	0.799	1.602
342		6.41	0.814	1.682
373		6.51	0.827	1.754
404		6.59	0.837	1.816
436		6.69	0.850	1.895
467		6.76	0.859	1.959

TABLE 3-3, continued.

3-3(D). 0.05 % precipitated zinc stearate.

Compaction pressure $N.mm^{-2}$	Actual density D* $g.cm^{-3}$	True metal density		ln(1/(1-D))
		$g.cm^{-3}$	D fractional	
8	3.422	3.42	0.434	0.569
16	3.692	3.69	0.469	0.633
23	3.872	3.87	0.492	0.676
31	4.042	4.04	0.514	0.721
39	4.192	4.19	0.532	0.760
47	4.292	4.29	0.545	0.787
54	4.432	4.43	0.563	0.829
62	4.562	4.56	0.579	0.866
70	4.672	4.67	0.593	0.900
78	4.762	4.76	0.604	0.927
93	4.912	4.91	0.624	0.977
109	5.043	5.04	0.640	1.021
124	5.203	5.20	0.661	1.081
140	5.333	5.33	0.677	1.130
156	5.433	5.43	0.690	1.171
171	5.543	5.54	0.703	1.215
187	5.633	5.63	0.715	1.256
202	5.743	5.74	0.730	1.309
218	5.843	5.84	0.741	1.352
249	5.993	5.99	0.761	1.430
280	6.153	6.15	0.781	1.519
311	6.273	6.27	0.797	1.595
342	6.393	6.39	0.812	1.673
373	6.503	6.50	0.825	1.745
404	6.593	6.59	0.837	1.815
436	6.673	6.67	0.848	1.882
467	6.773	6.77	0.860	1.968

TABLE 3-3, continued.

3-3(E). 0.10 % precipitated zinc stearate.

Compaction pressure $N.mm^{-2}$	Actual density D* $g.cm^{-3}$	True metal density		$\ln(1/(1-D))$
		$g.cm^{-3}$	D fractional	
8	3.443	3.44	0.436	0.573
16	3.704	3.70	0.470	0.635
23	3.894	3.89	0.494	0.681
31	4.074	4.07	0.517	0.728
39	4.214	4.21	0.535	0.766
47	4.314	4.31	0.548	0.793
54	4.454	4.45	0.566	0.834
62	4.595	4.59	0.583	0.874
70	4.695	4.69	0.596	0.906
78	4.775	4.77	0.607	0.933
93	4.935	4.93	0.626	0.985
109	5.075	5.07	0.644	1.032
124	5.235	5.23	0.664	1.091
140	5.355	5.35	0.680	1.139
156	5.465	5.46	0.694	1.185
171	5.576	5.57	0.708	1.231
187	5.676	5.67	0.720	1.273
202	5.786	5.78	0.734	1.324
218	5.876	5.87	0.746	1.369
249	6.016	6.01	0.763	1.440
280	6.176	6.17	0.784	1.531
311	6.316	6.31	0.801	1.616
342	6.426	6.42	0.816	1.690
373	6.537	6.53	0.830	1.773
404	6.627	6.62	0.841	1.837
436	6.697	6.69	0.850	1.897
467	6.767	6.76	0.860	1.963

TABLE 3-3, continued.

3-3(F). 0.20 % precipitated zinc stearate.

Compaction pressure $N.mm^{-2}$	Actual density D* $g.cm^{-3}$	True metal density		ln(1/(1-D))
		$g.cm^{-3}$	D fractional	
8	3.377	3.37	0.428	0.558
16	3.687	3.68	0.467	0.630
23	3.878	3.87	0.491	0.676
31	4.058	4.05	0.514	0.722
39	4.218	4.21	0.535	0.766
47	4.309	4.30	0.547	0.792
54	4.469	4.46	0.567	0.837
62	4.589	4.58	0.582	0.873
70	4.699	4.69	0.596	0.906
78	4.790	4.78	0.608	0.936
93	4.950	4.94	0.628	0.989
109	5.080	5.07	0.645	1.035
124	5.250	5.24	0.666	1.096
140	5.381	5.37	0.683	1.147
156	5.491	5.48	0.696	1.190
171	5.591	5.58	0.709	1.233
187	5.681	5.67	0.721	1.275
202	5.792	5.78	0.734	1.325
218	5.882	5.87	0.746	1.371
249	6.042	6.03	0.766	1.451
280	6.192	6.18	0.785	1.538
311	6.323	6.31	0.801	1.616
342	6.443	6.43	0.817	1.697
373	6.533	6.52	0.828	1.763
404	6.633	6.62	0.840	1.836
436	6.723	6.71	0.853	1.916
467	6.784	6.77	0.861	1.971

TABLE 3-3, continued.

3-3(G). 0.50 % precipitated zinc stearate .

Compaction pressure $N.mm^{-2}$	Actual density D* $g.cm^{-3}$	True metal density		ln(1/(1-D))
		$g.cm^{-3}$	D fractional	
8	3.397	3.38	0.430	0.562
16	3.688	3.67	0.466	0.627
23	3.869	3.85	0.489	0.672
31	4.060	4.04	0.513	0.720
39	4.211	4.19	0.533	0.761
47	4.311	4.29	0.545	0.787
54	4.462	4.44	0.565	0.832
62	4.603	4.58	0.582	0.872
70	4.703	4.68	0.595	0.904
78	4.784	4.76	0.605	0.930
93	4.955	4.93	0.627	0.985
109	5.085	5.06	0.642	1.028
124	5.246	5.22	0.663	1.089
140	5.377	5.35	0.680	1.140
156	5.497	5.47	0.694	1.185
171	5.598	5.57	0.707	1.228
187	5.688	5.66	0.719	1.270
202	5.799	5.77	0.733	1.320
218	5.889	5.86	0.745	1.365
249	6.050	6.02	0.764	1.446
280	6.191	6.16	0.782	1.526
311	6.321	6.29	0.799	1.603
342	6.432	6.40	0.813	1.675
373	6.533	6.50	0.826	1.748
404	6.623	6.59	0.838	1.819
436	6.703	6.67	0.847	1.877
467	6.784	6.75	0.858	1.952

TABLE 3-3, continued.

3-3(H). 1.0% precipitated zinc stearate.

Compaction pressure $N.mm^{-2}$	Actual density D* $g.cm^{-3}$	True metal density		ln(1/(1-D))
		$g.cm^{-3}$	D fractional	
8	3.505	3.47	0.441	0.581
16	3.747	3.71	0.472	0.638
23	3.929	3.89	0.495	0.683
31	4.111	4.07	0.517	0.728
39	4.262	4.22	0.537	0.769
47	4.363	4.32	0.549	0.796
54	4.505	4.46	0.567	0.837
62	4.626	4.58	0.582	0.873
70	4.747	4.70	0.597	0.908
78	4.838	4.79	0.608	0.938
93	5.00	4.95	0.628	0.990
109	5.131	5.08	0.645	1.035
124	5.292	5.24	0.665	1.094
140	5.424	5.37	0.682	1.145
156	5.525	5.47	0.695	1.188
171	5.626	5.57	0.708	1.231
187	5.727	5.67	0.720	1.273
202	5.828	5.77	0.734	1.323
218	5.919	5.86	0.744	1.364
249	6.060	6.00	0.763	1.438
280	6.212	6.15	0.782	1.523
311	6.343	6.28	0.798	1.600
342	6.454	6.39	0.812	1.672
373	6.545	6.48	0.824	1.736
404	6.626	6.56	0.834	1.796
436	6.706	6.64	0.843	1.853
467	6.777	6.71	0.852	1.914

TABLE 3-3, continued.

3-3(I). 2.0 % precipitated zinc stearate.

Compaction pressure $N.mm^{-2}$	Actual density D* $g.cm^{-3}$	True metal density		ln(1/(1-D))
		$g.cm^{-3}$	D fractional	
8	3.590	3.52	0.447	0.593
16	3.835	3.76	0.477	0.649
23	4.009	3.93	0.499	0.691
31	4.192	4.11	0.522	0.737
39	4.345	4.26	0.541	0.780
47	4.468	4.38	0.556	0.812
54	4.610	4.52	0.574	0.854
62	4.723	4.63	0.588	0.888
70	4.835	4.74	0.602	0.922
78	4.937	4.84	0.615	0.953
93	5.090	4.99	0.634	1.006
109	5.212	5.11	0.650	1.049
124	5.375	5.27	0.670	1.108
140	5.498	5.39	0.685	1.154
156	5.600	5.49	0.697	1.195
171	5.702	5.59	0.710	1.239
187	5.804	5.69	0.723	1.283
202	5.896	5.78	0.734	1.326
218	5.987	5.87	0.745	1.368
249	6.100	5.98	0.760	1.428
280	6.242	6.12	0.777	1.501
311	6.344	6.22	0.791	1.563
342	6.436	6.31	0.802	1.618
373	6.518	6.39	0.812	1.670
404	6.589	6.46	0.820	1.717
436	6.630	6.50	0.826	1.751
467	6.671	6.54	0.831	1.777

TABLE 3-3, continued.

3-3(J). 3.0 % precipitated zinc stearate.

Compaction pressure $N.mm^{-2}$	Actual density D* $g.cm^{-3}$	True metal density		ln(1/(1-D))
		$g.cm^{-3}$	D fractional	
8	3.533	3.43	0.436	0.572
16	3.780	3.67	0.467	0.629
23	3.986	3.87	0.492	0.677
31	4.172	4.05	0.515	0.723
39	4.326	4.20	0.533	0.762
47	4.429	4.30	0.547	0.791
54	4.584	4.45	0.566	0.834
62	4.717	4.58	0.582	0.873
70	4.820	4.68	0.594	0.902
78	4.913	4.77	0.606	0.932
93	5.078	4.93	0.626	0.984
109	5.202	5.05	0.641	1.025
124	5.346	5.19	0.660	1.078
140	5.469	5.31	0.675	1.124
156	5.572	5.41	0.687	1.163
171	5.665	5.50	0.699	1.200
187	5.758	5.59	0.710	1.237
202	5.850	5.68	0.722	1.281
218	5.923	5.75	0.730	1.310
249	6.036	5.86	0.744	1.364
280	6.149	5.97	0.758	1.419
311	6.232	6.05	0.768	1.462
342	6.293	6.11	0.776	1.496
373	6.355	6.17	0.784	1.533
404	6.386	6.20	0.788	1.552
436	6.427	6.24	0.792	1.571
467	6.448	6.26	0.795	1.585

TABLE 3-3, continued.

3-3(K). 4.0 % precipitated zinc stearate .

Compaction pressure $N.mm^{-2}$	Actual density D* $g.cm^{-3}$	True metal density		ln(1/(1-D))
		$g.cm^{-3}$	D fractional	
8	3.526	3.39	0.431	0.564
16	3.796	3.65	0.464	0.624
23	4.004	3.85	0.489	0.671
31	4.191	4.03	0.512	0.717
39	4.353	4.19	0.532	0.760
47	4.462	4.29	0.545	0.788
54	4.618	4.44	0.564	0.830
62	4.732	4.55	0.579	0.864
70	4.846	4.66	0.592	0.897
78	4.930	4.74	0.602	0.922
93	5.086	4.89	0.621	0.971
109	5.200	5.00	0.636	1.011
124	5.356	5.15	0.654	1.060
140	5.470	5.26	0.668	1.103
156	5.564	5.35	0.679	1.137
171	5.637	5.42	0.688	1.166
187	5.710	5.49	0.697	1.194
202	5.782	5.56	0.707	1.227
218	5.845	5.62	0.713	1.250
249	5.928	5.70	0.724	1.286
280	6.011	5.78	0.734	1.325
311	6.074	5.84	0.741	1.353
342	6.094	5.86	0.745	1.367
373	6.136	5.90	0.750	1.386
404	6.157	5.92	0.753	1.396
436	6.178	5.94	0.755	1.407
467	6.188	5.95	0.756	1.412

TABLE 3-4. Compaction results - MP32 plus precipitated/ evaporated zinc stearate, no die-wall lubrication.

3-4(A). No lubricant , MP32 washed in benzene.
NO DIE-WALL LUBRICATION.

Compaction pressure $N.mm^{-2}$	Actual density D* $g.cm^{-3}$	True metal density		ln(1/(1-D))
		$g.cm^{-3}$	D fractional	
8		3.18	0.404	0.518
16		3.43	0.436	0.573
23		3.60	0.458	0.612
31		3.78	0.480	0.654
39		3.92	0.498	0.689
47		4.02	0.510	0.714
54		4.16	0.528	0.752
62		4.29	0.545	0.787
70		4.39	0.558	0.816
78		4.47	0.568	0.840
93	As	4.63	0.588	0.887
109	true	4.76	0.605	0.928
124	metal	4.92	0.625	0.982
140	density	5.04	0.641	1.023
156		5.15	0.655	1.064
171		5.26	0.669	1.105
187		5.36	0.681	1.143
202		5.48	0.696	1.191
218		5.56	0.707	1.226
249		5.72	0.727	1.299
280		5.88	0.747	1.373
311		6.03	0.766	1.453
342		6.17	0.784	1.531
373		6.28	0.798	1.601
404				
436		6.46	0.820	1.717
467		6.54	0.832	1.784

TABLE 3-4, continued.

3-4(B). 0.01 % precipitated zinc stearate.
NO DIE-WALL LUBRICATION.

Compaction pressure $N.mm^{-2}$	Actual density D* $g.cm^{-3}$	True metal density		ln(1/(1-D))
		$g.cm^{-3}$	D fractional	
8	As true metal density	3.44	0.438	0.576
16		3.63	0.461	0.618
23		3.78	0.480	0.654
31		3.94	0.501	0.695
39		4.10	0.521	0.737
47		4.21	0.535	0.766
54		4.35	0.552	0.804
62		4.45	0.565	0.832
70		4.54	0.576	0.859
78		4.62	0.586	0.883
93		4.78	0.607	0.934

3-4(C). 0.02 % precipitated zinc stearate.
NO DIE-WALL LUBRICATION.

Compaction pressure $N.mm^{-2}$	Actual density D* $g.cm^{-3}$	True metal density		ln(1/(1-D))
		$g.cm^{-3}$	D fractional	
8	As true metal density	3.43	0.435	0.571
16		3.61	0.459	0.615
23		3.79	0.481	0.656
31		3.97	0.504	0.701
39		4.11	0.522	0.738
47		4.20	0.533	0.762
54		4.33	0.551	0.800
62		4.45	0.565	0.832
70		4.54	0.577	0.859
78		4.62	0.588	0.886
93		4.79	0.608	0.937

TABLE 3-4, continued.

3-4(D). 0.05 % precipitated zinc stearate.
NO DIE-WALL LUBRICATION.

Compaction pressure $N.mm^{-2}$	Actual density D* $g.cm^{-3}$	True metal density		ln(1/(1-D))
		$g.cm^{-3}$	D fractional	
8	3.392	3.39	0.431	0.564
16	3.652	3.65	0.464	0.624
23	3.832	3.83	0.486	0.666
31	3.982	3.98	0.506	0.705
39	4.132	4.13	0.524	0.743
47	4.222	4.22	0.536	0.769
54	4.362	4.36	0.554	0.808
62	4.472	4.47	0.568	0.840
70	4.572	4.57	0.580	0.868
78	4.652	4.65	0.591	0.894
93	4.802	4.80	0.610	0.942

3-4(E). 0.10 % precipitated zinc stearate.
NO DIE-WALL LUBRICATION.

Compaction pressure $N.mm^{-2}$	Actual density D* $g.cm^{-3}$	True metal density		ln(1/(1-D))
		$g.cm^{-3}$	D fractional	
8	3.393	3.39	0.431	0.563
16	3.634	3.63	0.462	0.619
23	3.804	3.80	0.483	0.659
31	3.984	3.98	0.506	0.706
39	4.124	4.12	0.524	0.742
47	4.214	4.21	0.535	0.766
54	4.354	4.35	0.553	0.805
62	4.474	4.47	0.568	0.840
70	4.575	4.57	0.580	0.868
78	4.655	4.65	0.591	0.893
93	4.805	4.80	0.610	0.941

TABLE 3-4, continued.

3-4(F). 0.20 % precipitated zinc stearate.
NO DIE-WALL LUBRICATION.

Compaction pressure $N.mm^{-2}$	Actual density D* $g.cm^{-3}$	True metal density		ln(1/(1-D))
		$g.cm^{-3}$	D fractional	
8	3.447	3.44	0.437	0.574
16	3.637	3.63	0.462	0.619
23	3.798	3.79	0.482	0.658
31	3.958	3.95	0.502	0.686
39	4.108	4.10	0.521	0.737
47	4.198	4.19	0.533	0.760
54	4.339	4.33	0.551	0.800
62	4.459	4.45	0.565	0.833
70	4.559	4.55	0.578	0.863
78	4.649	4.64	0.590	0.891
93	4.830	4.82	0.612	0.947
109	4.920	4.91	0.624	0.979
124	5.080	5.07	0.644	1.033
140	5.200	5.19	0.660	1.077
156	5.311	5.30	0.674	1.120
171	5.411	5.40	0.687	1.160
187	5.501	5.49	0.698	1.197
202	5.611	5.60	0.712	1.244
218	5.701	5.69	0.723	1.283
249	5.852	5.84	0.742	1.356
280	5.992	5.98	0.760	1.429
311	6.142	6.13	0.779	1.511
342	6.263	6.25	0.794	1.580
373	6.373	6.36	0.808	1.648
404	6.473	6.46	0.820	1.717
436	6.553	6.54	0.831	1.776
467	6.643	6.63	0.843	1.849

TABLE 3-4, continued.

3-4(G). 0.50 % precipitated zinc stearate.
NO DIE-WALL LUBRICATION.

Compaction pressure $N.mm^{-2}$	Actual density D* $g.cm^{-3}$	True metal density		ln(1/(1-D))
		$g.cm^{-3}$	D fractional	
8	3.407	3.39	0.431	0.564
16	3.698	3.68	0.467	0.629
23	3.879	3.86	0.490	0.673
31	4.030	4.01	0.510	0.713
39	4.191	4.17	0.529	0.753
47	4.281	4.26	0.541	0.780
54	4.422	4.40	0.560	0.820
62	4.543	4.52	0.575	0.855
70	4.643	4.62	0.587	0.884
78	4.734	4.71	0.599	0.913
93	4.894	4.87	0.619	0.964
109	5.015	4.99	0.634	1.004
124	5.176	5.15	0.655	1.064
140	5.306	5.28	0.671	1.111
156	5.397	5.37	0.682	1.147
171	5.497	5.47	0.696	1.189
187	5.588	5.56	0.707	1.228
202	5.698	5.67	0.720	1.273
218	5.779	5.75	0.730	1.310
249	5.919	5.89	0.749	1.381
280	6.090	6.06	0.770	1.468
311	6.211	6.18	0.785	1.538
342	6.321	6.29	0.800	1.608
373	6.422	6.39	0.812	1.673
404	6.522	6.49	0.825	1.744
436	6.603	6.57	0.835	1.804
467	6.683	6.65	0.844	1.860

TABLE 3-4, continued.

3-4(H). 1.0 % precipitated zinc stearate.
NO DIE-WALL LUBRICATION.

Compaction pressure $N.mm^{-2}$	Actual density D* $g.cm^{-3}$	True metal density		ln(1/(1-D))
		$g.cm^{-3}$	D fractional	
8	3.424	3.39	0.431	0.564
16	3.727	3.69	0.469	0.632
23	3.909	3.87	0.492	0.677
31	4.101	4.06	0.516	0.726
39	4.252	4.21	0.535	0.766
47	4.353	4.31	0.547	0.793
54	4.505	4.46	0.567	0.837
62	4.626	4.58	0.581	0.871
70	4.727	4.68	0.594	0.902
78	4.798	4.75	0.604	0.925
93	4.959	4.91	0.624	0.978
109	5.090	5.04	0.641	1.023
124	5.242	5.19	0.660	1.078
140	5.373	5.32	0.675	1.125
156	5.474	5.42	0.688	1.166
171	5.565	5.51	0.700	1.204
187	5.656	5.60	0.712	1.245
202	5.757	5.70	0.724	1.288
218	5.848	5.79	0.736	1.331
249	5.989	5.93	0.754	1.402
280	6.141	6.08	0.773	1.483
311	6.262	6.20	0.788	1.549
342	6.383	6.32	0.803	1.623
373	6.474	6.41	0.814	1.683
404	6.565	6.50	0.826	1.748
436	6.363	6.57	0.835	1.801
467	6.706	6.64	0.844	1.858

TABLE 3-4, continued.

3-4(I). 2.0 % precipitated zinc stearate.
NO DIE-WALL LUBRICATION.

Compaction pressure $N.mm^{-2}$	Actual density D* $g.cm^{-3}$	True metal density		ln(1/(1-D))
		$g.cm^{-3}$	D fractional	
8	3.529	3.46	0.440	0.579
16	3.784	3.71	0.472	0.638
23	3.978	3.90	0.496	0.685
31	4.141	4.06	0.516	0.726
39	4.304	4.22	0.536	0.769
47	4.406	4.32	0.549	0.796
54	4.559	4.47	0.568	0.839
62	4.692	4.60	0.584	0.877
70	4.794	4.70	0.597	0.909
78	4.876	4.78	0.607	0.935
93	5.049	4.95	0.628	0.990
109	5.171	5.07	0.644	1.032
124	5.324	5.22	0.663	1.089
140	5.447	5.34	0.678	1.134
156	5.549	5.44	0.691	1.173
171	5.661	5.55	0.705	1.219
187	5.743	5.63	0.716	1.258
202	5.855	5.74	0.729	1.307
218	5.936	5.82	0.739	1.343
249	6.049	5.93	0.754	1.401
280	6.171	6.05	0.769	1.465
311	6.304	6.18	0.785	1.537
342	6.395	6.27	0.796	1.590
373	6.467	6.34	0.806	1.639
404	6.548	6.42	0.816	1.693
436	6.599	6.47	0.822	1.726
467	6.650	6.52	0.828	1.760

TABLE 3-4, continued.

3-4(J). 3.0 % precipitated zinc stearate.
NO DIE-WALL LUBRICATION.

Compaction pressure $N.mm^{-2}$	Actual density D* $g.cm^{-3}$	True metal density		ln(1/(1-D))
		$g.cm^{-3}$	D fractional	
8	3.533	3.43	0.436	0.573
16	3.801	3.69	0.468	0.631
23	3.996	3.88	0.492	0.678
31	4.182	4.06	0.515	0.724
39	4.336	4.21	0.535	0.766
47	4.439	4.31	0.548	0.795
54	4.594	4.46	0.567	0.836
62	4.717	4.58	0.582	0.872
70	4.831	4.69	0.596	0.905
78	4.913	4.77	0.607	0.933
93	5.078	4.93	0.627	0.985
109	5.212	5.06	0.643	1.029
124	5.356	5.20	0.661	1.082
140	5.490	5.22	0.677	1.130
156	5.583	5.42	0.688	1.165
171	5.675	5.51	0.700	1.204
187	5.758	5.59	0.710	1.237
202	5.840	5.67	0.721	1.276
218	5.923	5.75	0.730	1.310
249	6.036	5.86	0.744	1.364
280	6.139	5.96	0.757	1.414
311	6.221	6.04	0.767	1.457
342	6.293	6.11	0.776	1.497
373	6.345	6.16	0.783	1.527
404	6.407	6.22	0.790	1.559
436	6.427	6.24	0.792	1.572
467	6.458	6.27	0.797	1.592

TABLE 3-4, continued.

3-4(K). 4.0 % precipated zinc stearate.
NO DIE-WALL LUBRICATION.

Compaction pressure $N.mm^{-2}$	Actual density D* $g.cm^{-3}$	True metal density		ln(1/(1-D))
		$g.cm^{-3}$	D fractional	
8	3.494	3.36	0.426	0.556
16	3.796	3.65	0.463	0.623
23	4.014	3.86	0.490	0.673
31	4.181	4.02	0.511	0.716
39	4.347	4.18	0.531	0.757
47	4.441	4.27	0.543	0.783
54	4.597	4.42	0.561	0.824
62	4.711	4.53	0.576	0.858
70	4.826	4.64	0.590	0.891
78	4.909	4.72	0.600	0.916
93	5.054	4.86	0.617	0.961
109	5.179	4.98	0.633	1.003
124	5.325	5.12	0.651	1.052
140	5.450	5.24	0.665	1.094
156	5.533	5.32	0.676	1.128
171	5.616	5.40	0.686	1.157
187	5.689	5.47	0.695	1.188
202	5.762	5.54	0.704	1.218
218	5.814	5.59	0.711	1.241
249	5.907	5.68	0.722	1.281
280	6.001	5.77	0.733	1.320
311	6.053	5.82	0.739	1.343
342	6.105	5.87	0.745	1.367
373	6.136	5.90	0.750	1.387
404	6.167	5.93	0.754	1.402
436	6.188	5.95	0.757	1.413
467	6.209	5.97	0.759	1.424

TABLE 3-5. Compaction results - MP32 plus admixed zinc stearate, no die-wall lubrication.

TABLE 3-5(A). No lubricant, MP32 mixed for 1 hour. NO DIE-WALL LUBRICATION.

Compaction pressure $N.mm^{-2}$	Actual density D* $g.cm^{-3}$	True metal density		ln(1/(1-D))
		$g.cm^{-3}$	D fractional	
8		3.21	0.407	0.523
16		3.47	0.441	0.581
23		3.61	0.459	0.614
31		3.77	0.478	0.651
39		3.88	0.493	0.679
47		3.96	0.504	0.700
54		4.09	0.520	0.734
62		4.21	0.535	0.765
70	As	4.31	0.547	0.792
78	true	4.38	0.557	0.814
93	metal	4.55	0.578	0.862
109	density	4.67	0.594	0.901
124		4.84	0.615	0.954
140		4.97	0.631	0.998
156		5.08	0.645	1.037
171		5.19	0.660	1.078
187		5.29	0.672	1.115
202		5.42	0.688	1.165
218		5.50	0.699	1.202
249		5.67	0.721	1.276
280		5.84	0.741	1.353
311		5.97	0.758	1.420
342		6.11	0.776	1.495
373		6.22	0.790	1.562
404		6.33	0.804	1.629
436		6.41	0.815	1.688
467		6.51	0.827	1.752

TABLE 3-5, continued.

TABLE 3-5(B). 0.01 % admixed zinc stearate.
NO DIE-WALL LUBRICATION.

Compaction pressure $N.mm^{-2}$	Actual density D* $g.cm^{-3}$	True metal density		ln(1/(1-D))
		$g.cm^{-3}$	D fractional	
8		3.21	0.408	0.525
16		3.42	0.435	0.571
23		3.57	0.454	0.605
31		3.71	0.471	0.637
39	As	3.84	0.488	0.669
47	true	3.92	0.499	0.690
54	metal	4.06	0.516	0.725
62	density	4.18	0.531	0.758
70		4.28	0.544	0.785
78		4.35	0.553	0.806
93		4.53	0.575	0.856

TABLE 3-5(C). 0.02 % admixed zinc stearate.
NO DIE-WALL LUBRICATION.

Compaction pressure $N.mm^{-2}$	Actual density D* $g.cm^{-3}$	True metal density		ln(1/(1-D))
		$g.cm^{-3}$	D fractional	
8		3.29	0.418	0.542
16		3.54	0.450	0.598
23		3.69	0.469	0.633
31		3.85	0.489	0.672
39	As	4.00	0.508	0.709
47	true	4.09	0.520	0.734
54	metal	4.24	0.538	0.773
62	density	4.34	0.552	0.803
70		4.44	0.564	0.830
78		4.52	0.574	0.854
93		4.69	0.596	0.906

TABLE 3-5, continued.

TABLE 3-5(D). 0.05 % admixed zinc stearate.
NO DIE-WALL LUBRICATION.

Compaction pressure $N.mm^{-2}$	Actual density D* $g.cm^{-3}$	True metal density		ln(1/(1-D))
		$g.cm^{-3}$	D fractional	
8	3.332	3.33	0.423	0.550
16	3.602	3.60	0.458	0.612
23	3.732	3.73	0.474	0.642
31	3.872	3.87	0.492	0.677
39	4.012	4.01	0.510	0.713
47	4.122	4.12	0.523	0.740
54	4.242	4.24	0.539	0.774
62	4.362	4.36	0.554	0.808
70	4.462	4.46	0.566	0.835
78	4.542	4.54	0.576	0.859
93	4.692	4.69	0.596	0.907

TABLE 3-5(E). 0.10 % admixed zinc stearate.
NO DIE-WALL LUBRICATION.

Compaction pressure $N.mm^{-2}$	Actual density D* $g.cm^{-3}$	True metal density		ln(1/(1-D))
		$g.cm^{-3}$	D fractional	
8	3.383	3.38	0.430	0.562
16	3.634	3.63	0.461	0.617
23	3.784	3.78	0.481	0.655
31	3.924	3.92	0.499	0.690
39	4.054	4.05	0.515	0.723
47	4.154	4.15	0.527	0.749
54	4.284	4.28	0.544	0.785
62	4.394	4.39	0.558	0.817
70	4.484	4.48	0.569	0.841
78	4.555	4.55	0.578	0.864
93	4.715	4.71	0.599	0.913

TABLE 3-5, continued.

TABLE 3-5(F). 0.20 % admixed zinc stearate.
NO DIE-WALL LUBRICATION.

Compaction pressure $N.mm^{-2}$	Actual density D* $g.cm^{-3}$	True metal density		ln(1/(1-D))
		$g.cm^{-3}$	D fractional	
8	3.427	3.42	0.434	0.570
16	3.687	3.68	0.468	0.631
23	3.858	3.85	0.489	0.671
31	4.018	4.01	0.510	0.713
39	4.168	4.16	0.528	0.751
47	4.269	4.26	0.541	0.778
54	4.399	4.39	0.558	0.817
62	4.519	4.51	0.573	0.851
70	4.619	4.61	0.585	0.880
78	4.689	4.68	0.595	0.903
93	4.860	4.85	0.616	0.957
109	4.970	4.96	0.631	0.996
124	5.120	5.11	0.650	1.049
140	5.250	5.24	0.666	1.098
156	5.361	5.35	0.680	1.139
171	5.461	5.45	0.692	1.177
187	5.551	5.54	0.704	1.218
202	5.651	5.64	0.717	1.263
218	5.731	5.72	0.727	1.299
249	5.902	5.89	0.748	1.378
280	6.042	6.03	0.766	1.454
311	6.172	6.16	0.783	1.527
342	6.303	6.29	0.799	1.604
373	6.423	6.41	0.814	1.682
404	6.503	6.49	0.824	1.737
436	6.563	6.55	0.833	1.788
467	6.663	6.65	0.845	1.863

TABLE 3-5, continued.

TABLE 3-5(G). 0.50 % admixed zinc stearate.
NO DIE-WALL LUBRICATION.

Compaction pressure $N.mm^{-2}$	Actual density D* $g.cm^{-3}$	True metal density		ln(1/(1-D))
		$g.cm^{-3}$	D fractional	
8	3.407	3.39	0.430	0.563
16	3.678	3.66	0.465	0.626
23	3.859	3.84	0.488	0.670
31	4.050	4.03	0.512	0.717
39	4.201	4.18	0.531	0.757
47	4.291	4.27	0.543	0.783
54	4.442	4.42	0.562	0.825
62	4.583	4.56	0.579	0.865
70	4.673	4.65	0.591	0.894
78	4.764	4.74	0.602	0.922
93	4.914	4.89	0.621	0.971
109	5.054	5.02	0.638	1.016
124	5.216	5.19	0.659	1.077
140	5.327	5.30	0.674	1.119
156	5.437	5.41	0.687	1.162
171	5.528	5.50	0.699	1.202
187	5.628	5.60	0.711	1.241
202	5.729	5.70	0.724	1.288
218	5.819	5.79	0.735	1.329
249	5.960	5.93	0.754	1.403
280	6.110	6.08	0.773	1.481
311	6.231	6.20	0.788	1.551
342	6.352	6.32	0.803	1.623
373	6.432	6.40	0.814	1.681
404	6.543	6.51	0.827	1.752
436	6.623	6.59	0.837	1.813
467	6.703	6.67	0.847	1.879

TABLE 3-5, continued.

TABLE 3-5(H). 1.0 % admixed zinc stearate.
NO DIE-WALL LUBRICATION.

Compaction pressure $N.mm^{-2}$	Actual density D* $g.cm^{-3}$	True metal density		ln(1/(1-D))
		$g.cm^{-3}$	D fractional	
8	3.373	3.34	0.425	0.553
16	3.687	3.65	0.464	0.623
23	3.868	3.83	0.487	0.667
31	4.060	4.02	0.511	0.716
39	4.232	4.19	0.532	0.760
47	4.333	4.29	0.546	0.789
54	4.495	4.45	0.566	0.834
62	4.636	4.59	0.583	0.874
70	4.737	4.69	0.596	0.906
78	4.818	4.77	0.606	0.932
93	4.969	4.92	0.626	0.983
109	5.111	5.06	0.643	1.030
124	5.282	5.23	0.664	1.091
140	5.404	5.35	0.680	1.139
156	5.505	5.45	0.693	1.181
171	5.606	5.55	0.706	1.223
187	5.696	5.64	0.716	1.260
202	5.808	5.75	0.731	1.313
218	5.898	5.84	0.742	1.353
249	6.040	5.98	0.760	1.426
280	6.181	6.12	0.778	1.503
311	6.302	6.24	0.792	1.571
342	6.393	6.33	0.805	1.633
373	6.494	6.43	0.817	1.700
404	6.575	6.51	0.828	1.757
436	6.646	6.58	0.836	1.811
467	6.727	6.66	0.846	1.868

TABLE 3-5, continued.

TABLE 3-5(I). 2.0 % admixed zinc stearate.
NO DIE-WALL LUBRICATION.

Compaction pressure $N.mm^{-2}$	Actual density D* $g.cm^{-3}$	True metal density		ln(1/(1-D))
		$g.cm^{-3}$	D fractional	
8	3.376	3.31	0.420	0.546
16	3.682	3.61	0.459	0.614
23	3.876	3.80	0.483	0.660
31	4.070	3.99	0.508	0.708
39	4.233	4.15	0.527	0.748
47	4.335	4.25	0.540	0.776
54	4.498	4.41	0.560	0.821
62	4.631	4.54	0.577	0.860
70	4.743	4.65	0.590	0.892
78	4.825	4.73	0.601	0.919
93	4.988	4.89	0.622	0.972
109	5.120	5.02	0.638	1.017
124	5.273	5.17	0.657	1.071
140	5.406	5.30	0.673	1.118
156	5.508	5.40	0.686	1.159
171	5.600	5.49	0.698	1.196
187	5.692	5.58	0.709	1.233
202	5.794	5.68	0.722	1.280
218	5.875	5.76	0.732	1.318
249	6.018	5.90	0.749	1.383
280	6.151	6.03	0.766	1.451
311	6.253	6.13	0.779	1.508
342	6.324	6.20	0.788	1.552
373	6.416	6.29	0.799	1.605
404	6.487	6.36	0.808	1.648
436	6.538	6.41	0.815	1.687
467	6.599	6.47	0.822	1.727

TABLE 3-5, continued.

TABLE 3-5(J). 4.0 % admixed zinc stearate.
NO DIE-WALL LUBRICATION.

Compaction pressure $N.mm^{-2}$	Actual density D* $g.cm^{-3}$	True metal density		ln(1/(1-D))
		$g.cm^{-3}$	D fractional	
8	3.390	3.26	0.415	0.536
16	3.723	3.58	0.455	0.607
23	3.921	3.77	0.479	0.652
31	4.108	3.95	0.502	0.696
39	4.264	4.10	0.521	0.735
47	4.368	4.20	0.534	0.764
54	4.543	4.36	0.554	0.807
62	4.649	4.47	0.568	0.840
70	4.753	4.57	0.581	0.869
78	4.846	4.66	0.591	0.895
93	4.992	4.80	0.610	0.941
109	5.106	4.91	0.624	0.978
124	5.262	5.06	0.643	1.029
140	5.366	5.16	0.656	1.066
156	5.460	5.25	0.666	1.098
171	5.533	5.32	0.676	1.128
187	5.606	5.39	0.685	1.154
202	5.678	5.46	0.694	1.184
218	5.741	5.52	0.702	1.209
249	5.845	5.62	0.714	1.251
280	5.928	5.70	0.724	1.287
311	5.990	5.76	0.732	1.318
342	6.042	5.81	0.738	1.340
373	6.084	5.85	0.743	1.359
404	6.126	5.89	0.748	1.378
436	6.157	5.92	0.752	1.393
467	6.178	5.94	0.754	1.403

FIGURE 3-13. Examples of ln[1/(1-D)] versus compaction pressure for MP32 plus precipitated/evaporated zinc stearate, die-wall lubricated

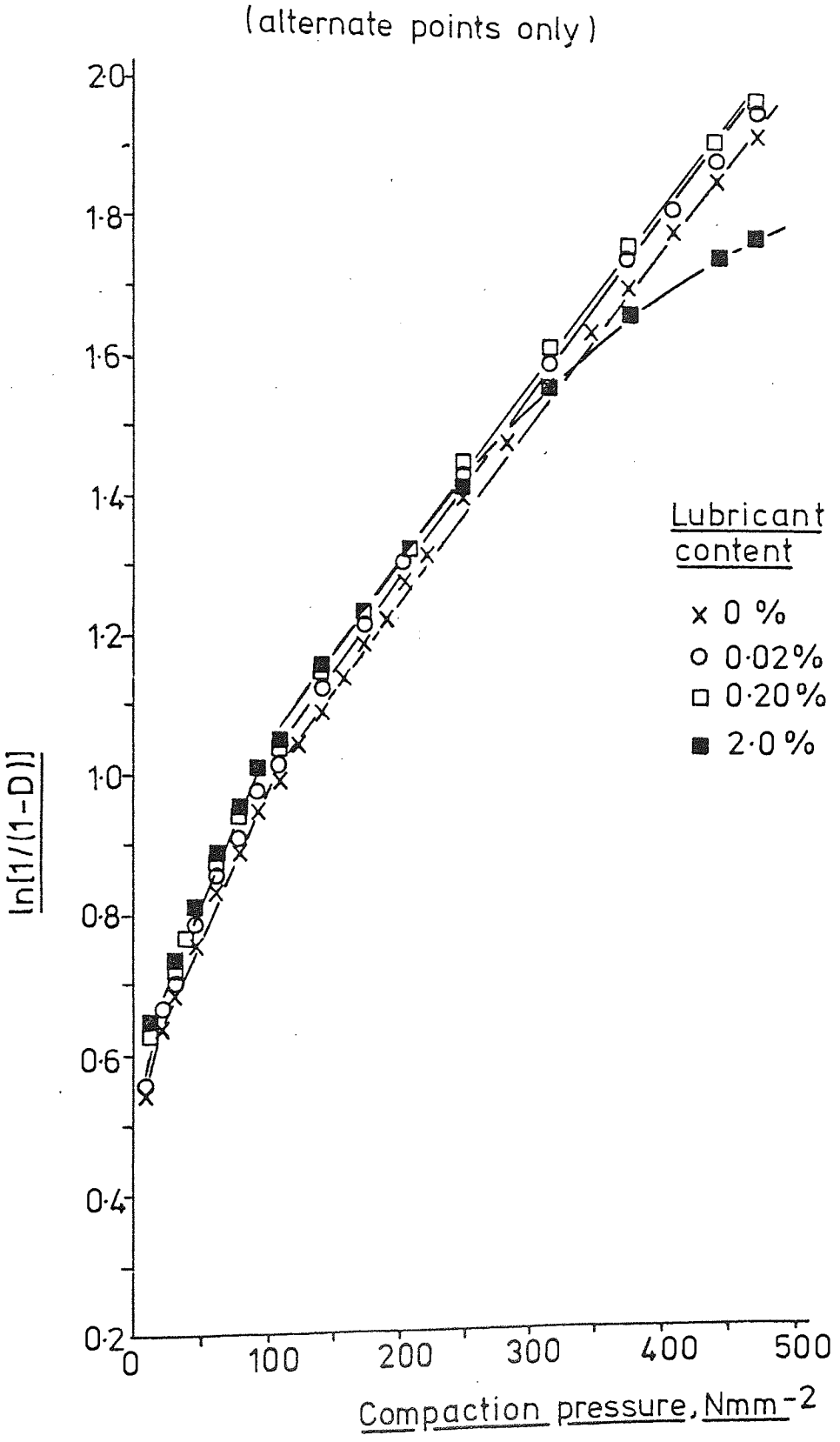

FIGURE 3-14. Examples of pressure/density relationships for MP32 plus precipitated/evaporated zinc stearate, die-wall lubricated.

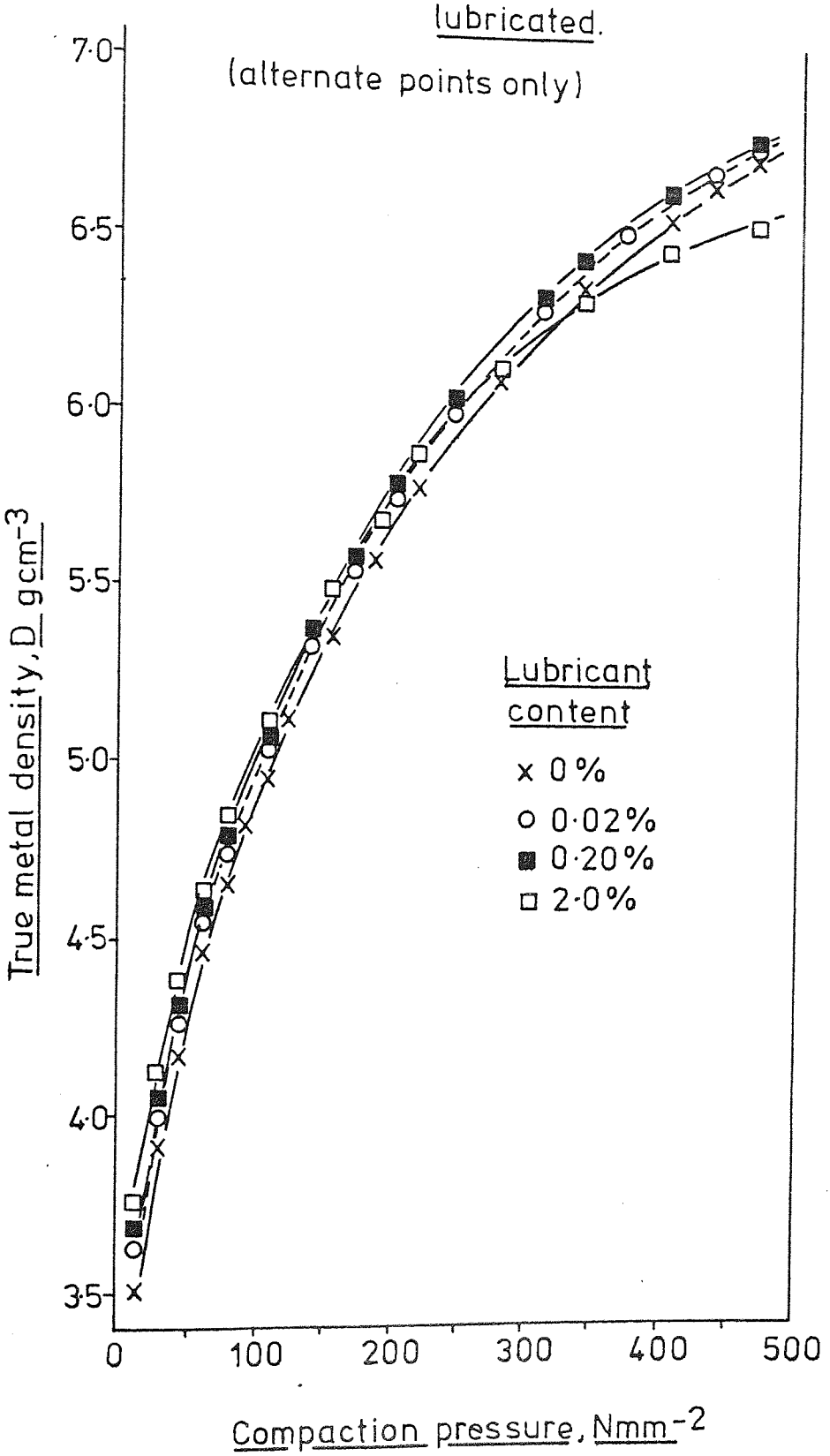

FIGURE 3-15. The lubricant effect ΔL versus compaction pressure (unlubricated) for MP 32 plus precipitated zinc stearate, die-wall lubricated.

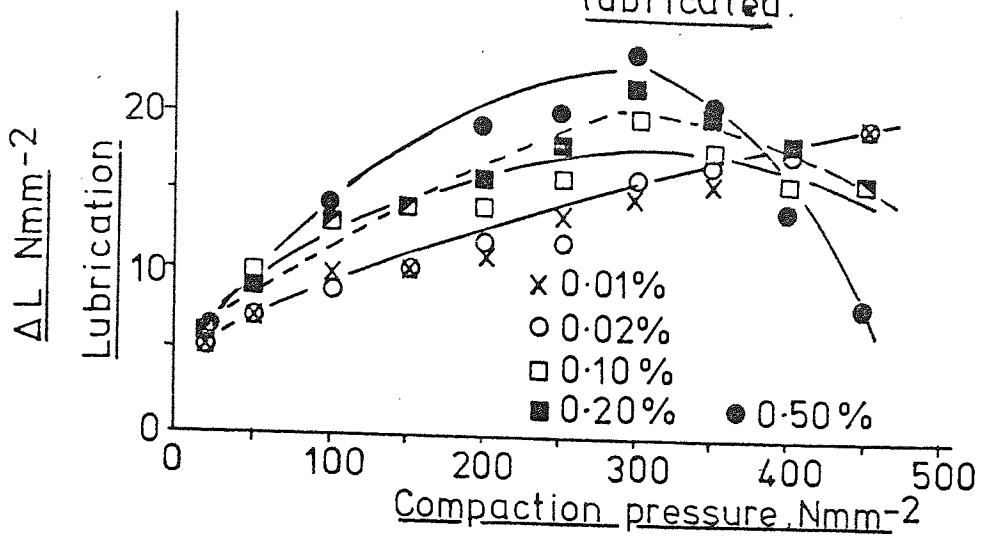

(a) Additions up to 0-5% by weight

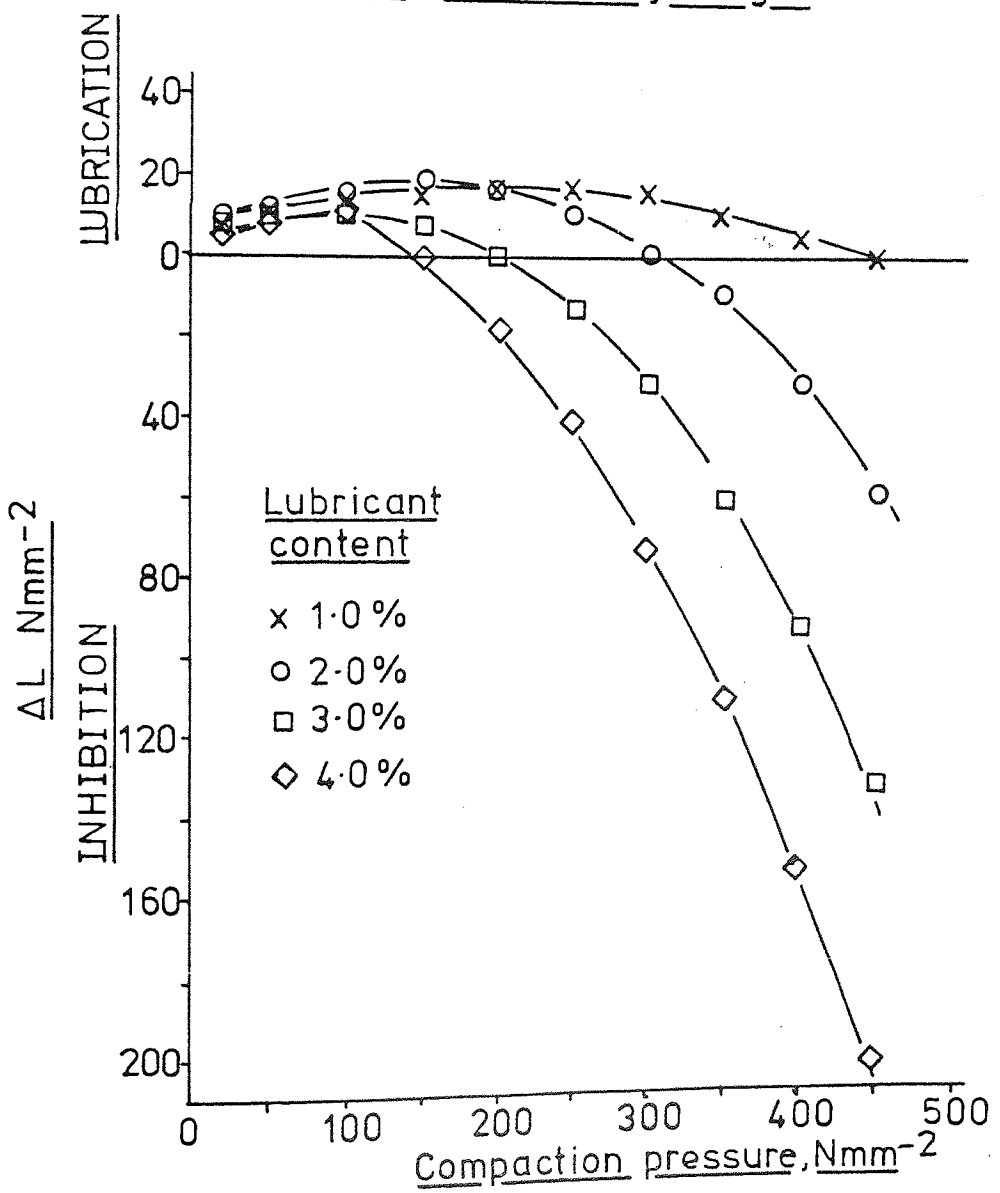

(b) Additions above 0·5% by weight.

FIGURE 3-16. Transition pressure P_T as a function of lubricant content for MP32 plus precipitated/evaporated zinc stearate, die-wall lubricated.

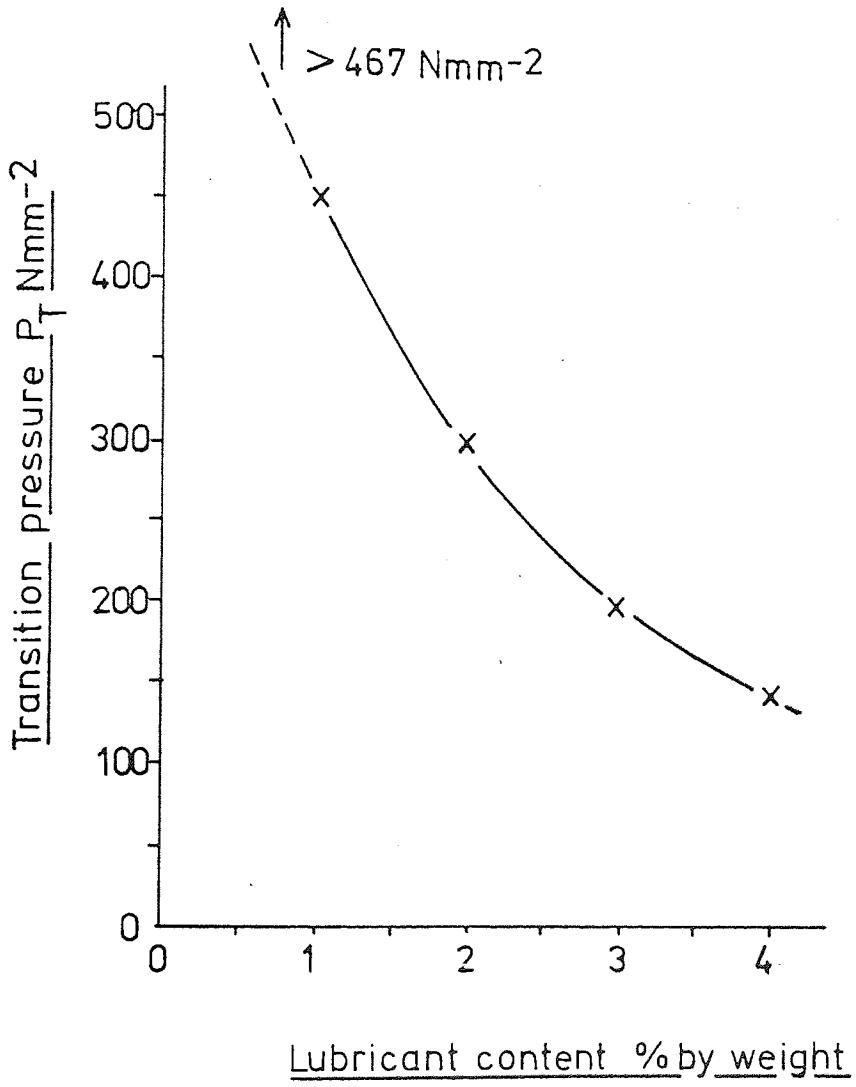

FIGURE 3-17. The effect of particle/die-wall friction during compaction.

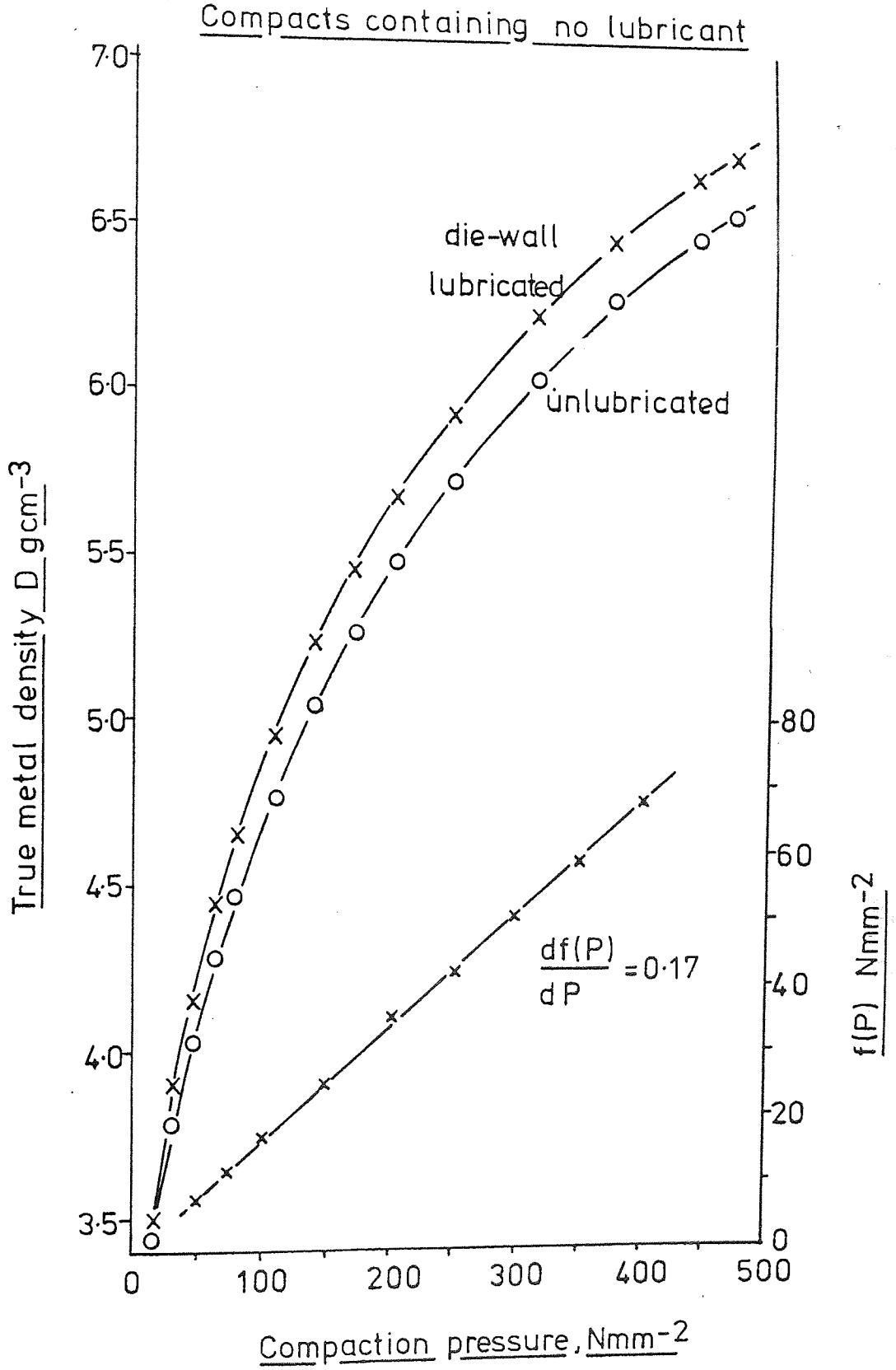

FIGURE 3-18. The effect of particle / die-wall friction during compaction.

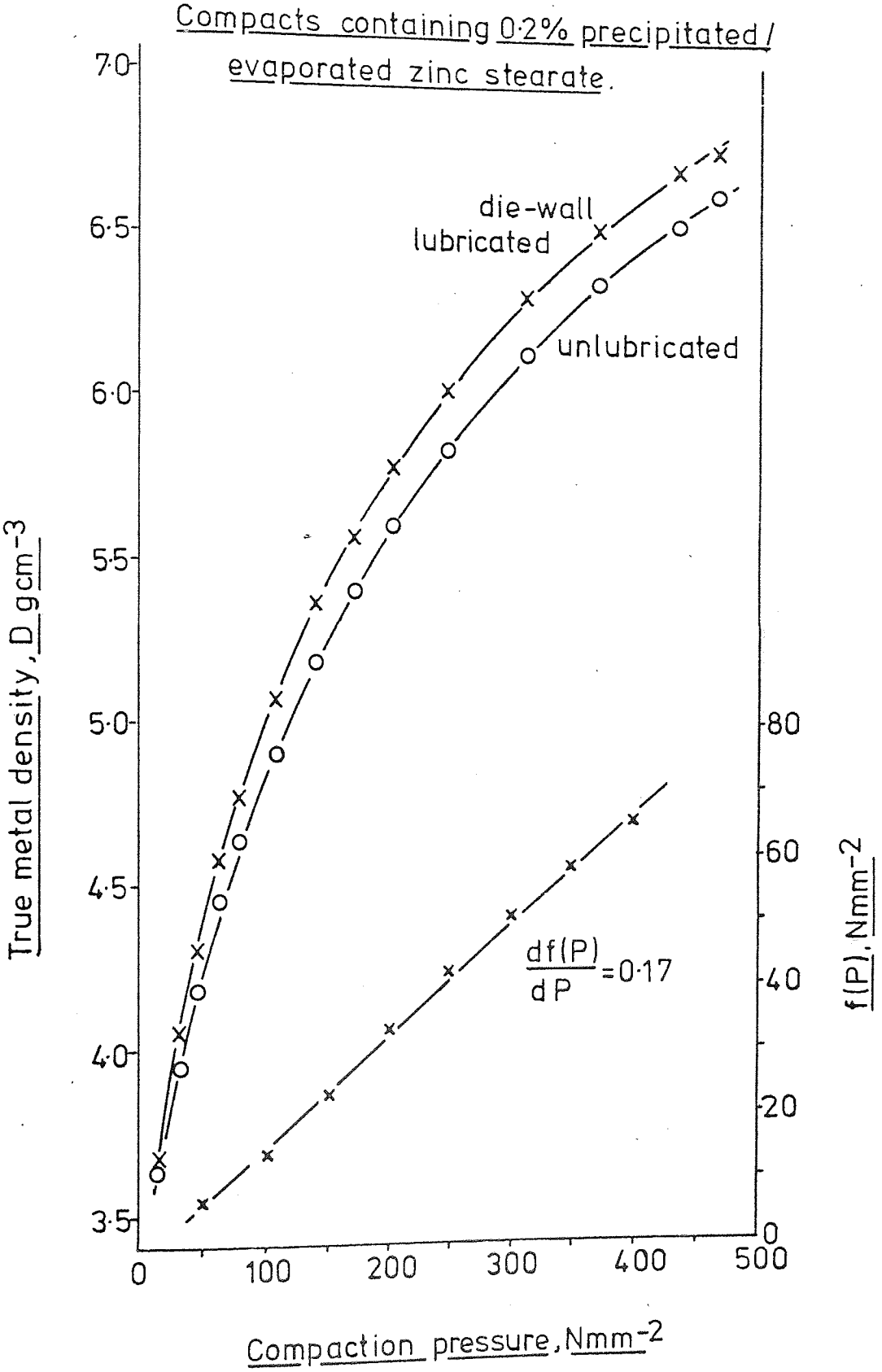

FIGURE 3-19. The effect of particle/die-wall friction during compaction

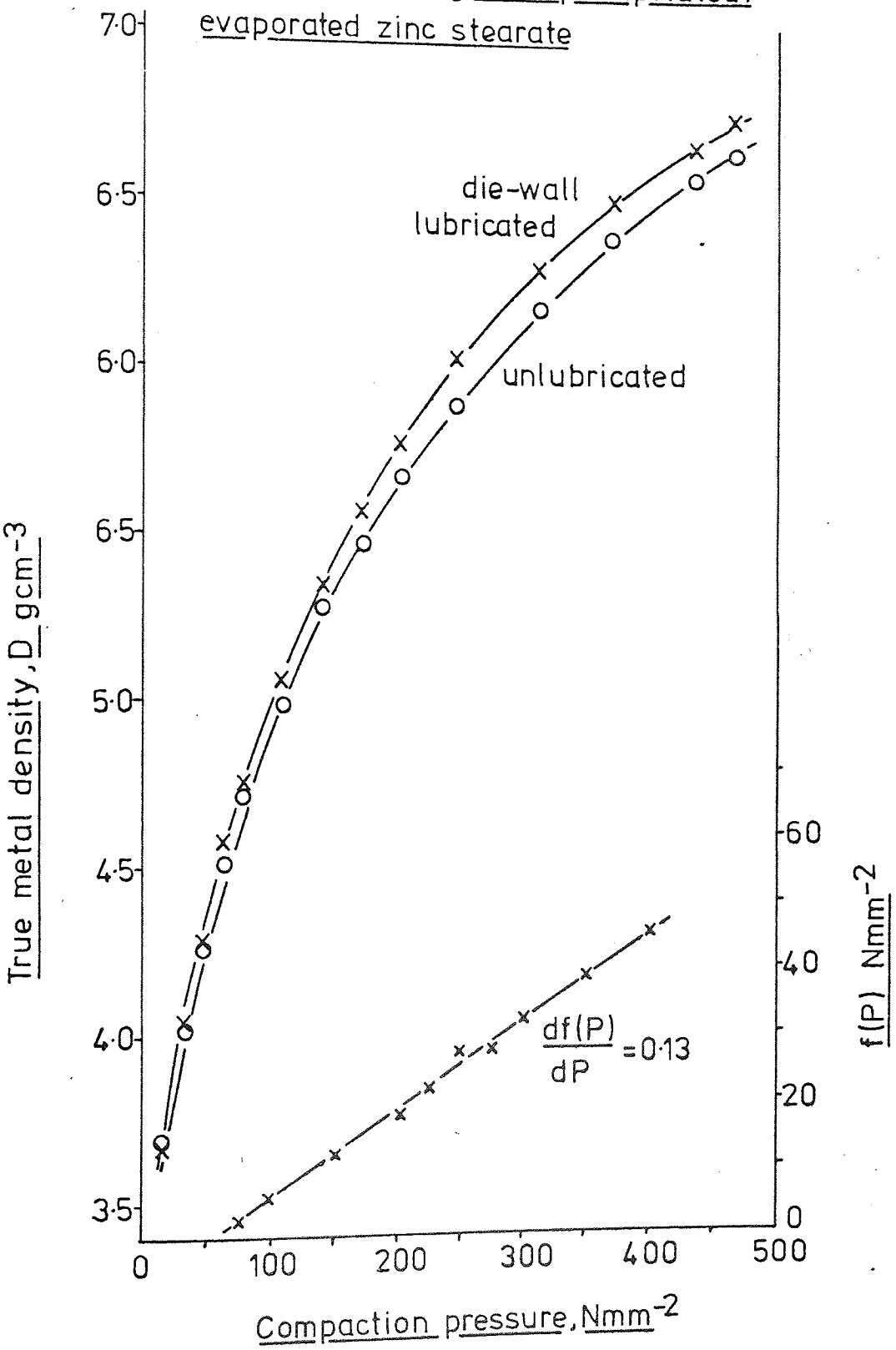

FIGURE 3-20. The effect of particle/die-wall friction during compaction

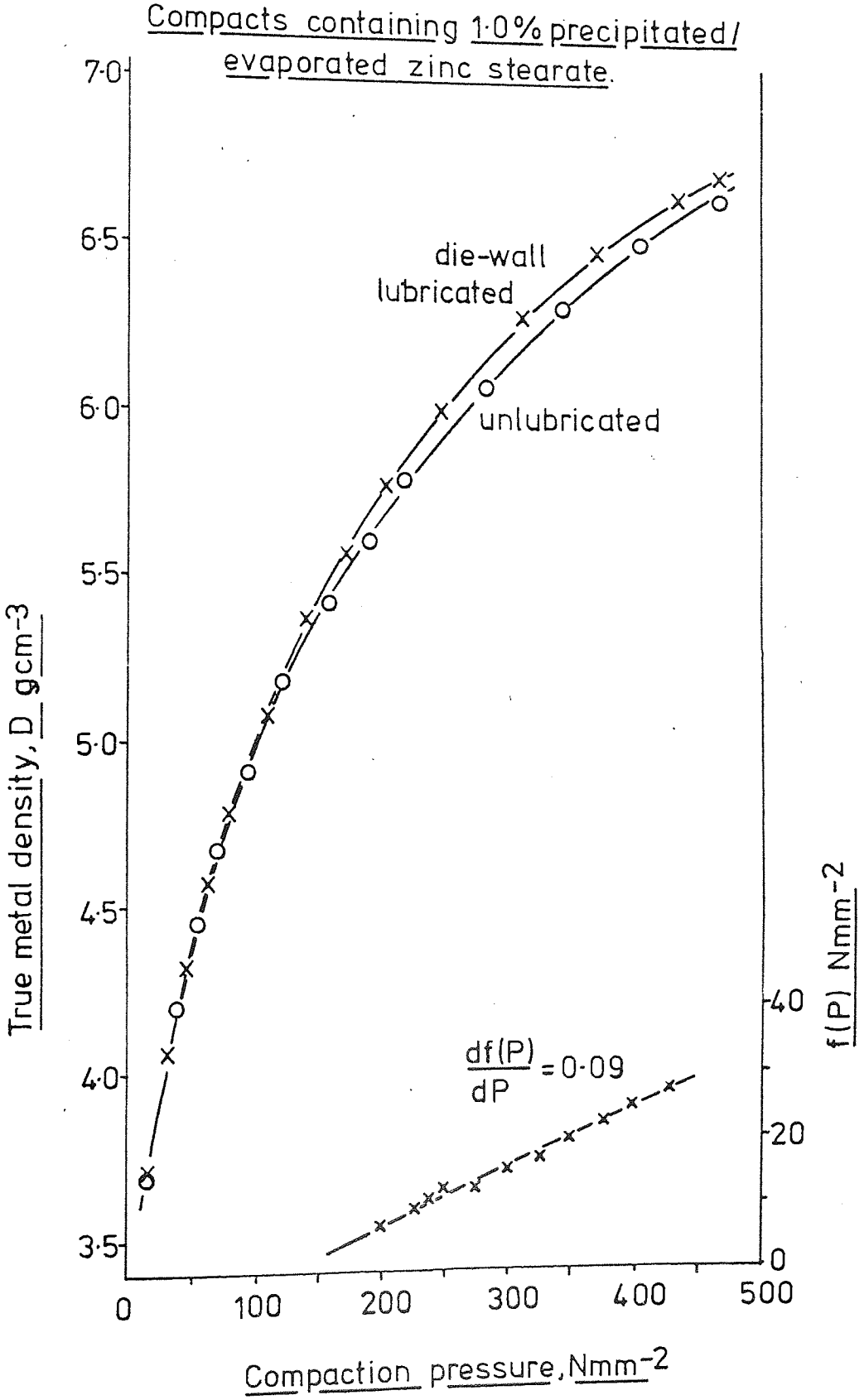

FIGURE 3-21 The effect of particle/die-wall friction during compaction.

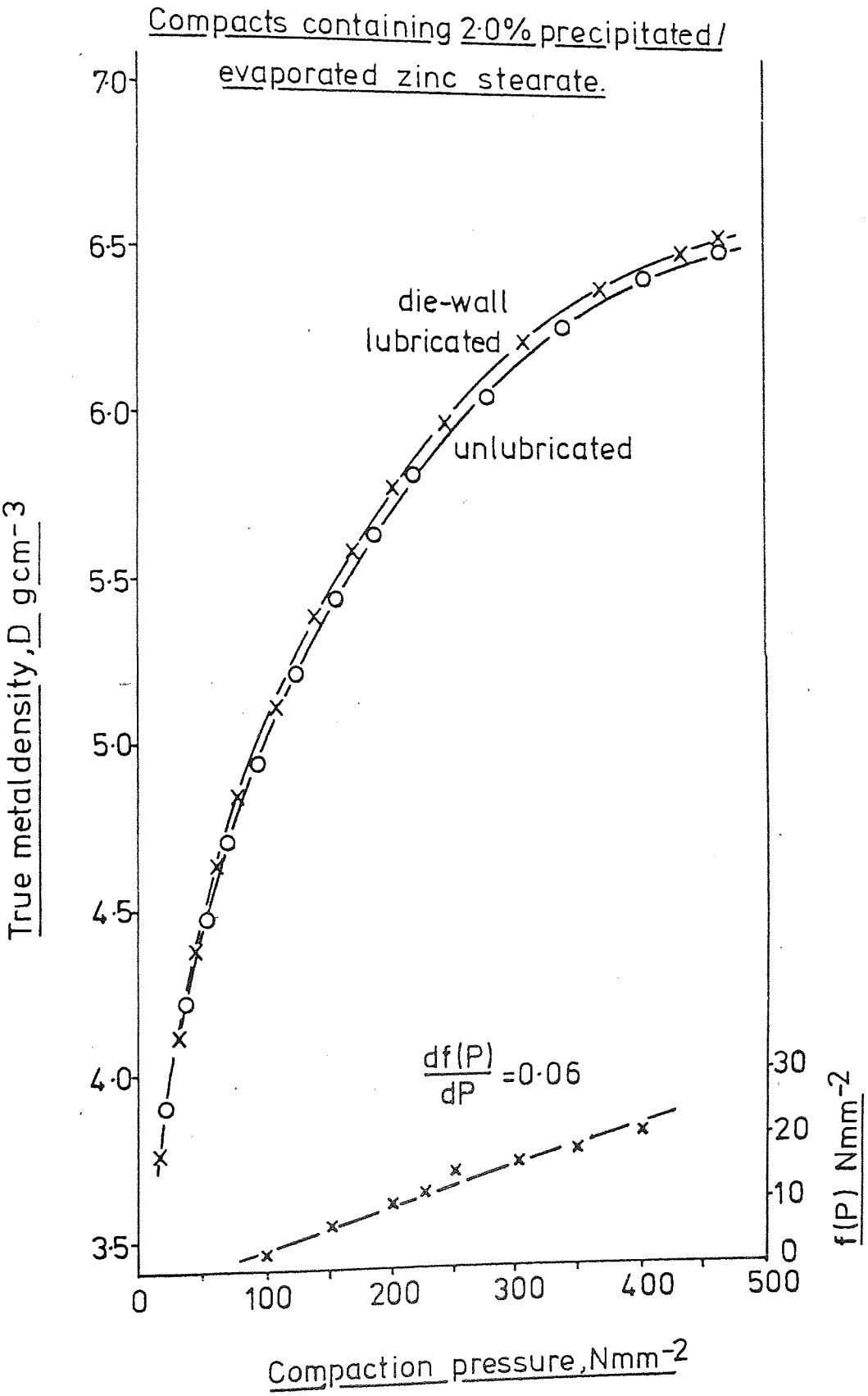

FIGURE 3-22. The effect of particle/die-wall friction during compaction.

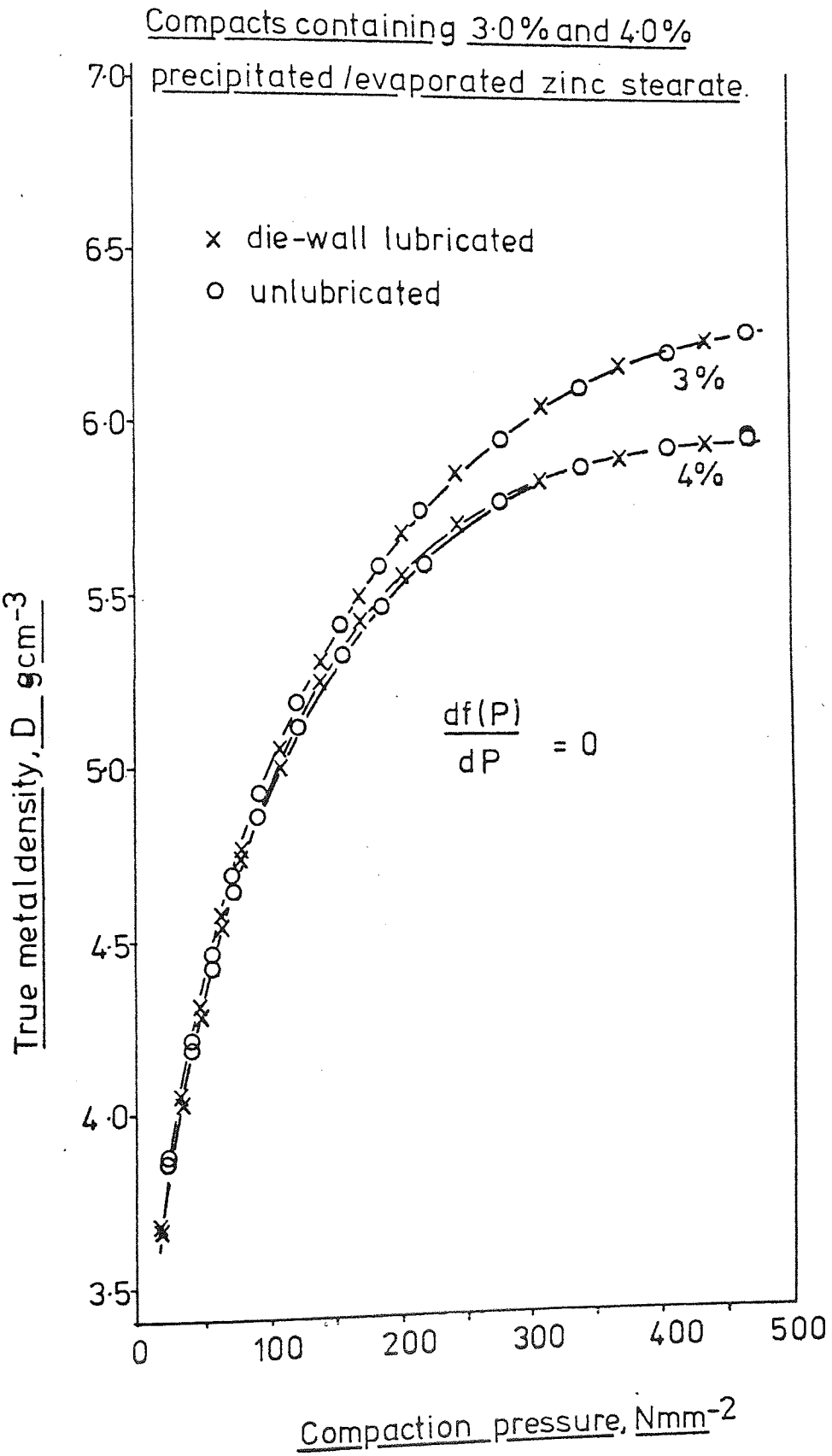

FIGURE 3-23. The effect of pretreatment on the compaction behaviour of MP 32 Fe powder.

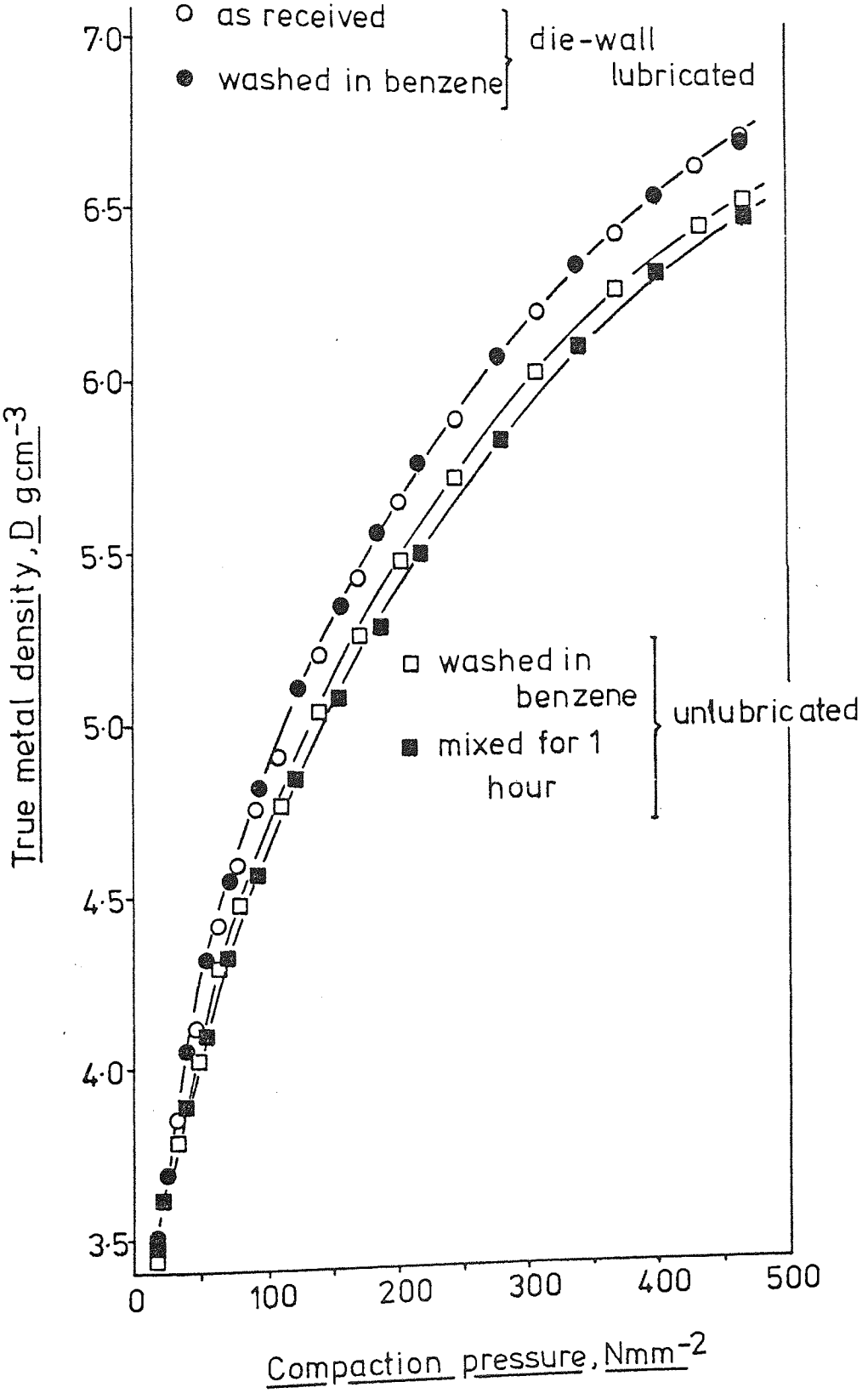

TABLE 3-6. Compaction results - the effect of mix duration on the compaction behaviour of MP32 plus 1.0 % zinc stearate, no die-wall lubrication.

Compaction pressure $N.mm^{-2}$	True metal density $g.cm^{-3}$	
	50 cycles	9120 cycles
8	3.27	3.42
16	3.58	3.72
23	3.75	3.93
31	3.94	4.10
39	4.10	4.24
47	4.20	4.36
54	4.36	4.52
62	4.50	4.65
70	4.59	4.75
78	4.68	4.83
93	4.85	4.99
109	4.98	5.12
124	5.15	5.28
140	5.28	5.41
156	5.39	5.50
171	5.48	5.61
187	5.57	5.69
202	5.70	5.79
218	5.78	5.87
249	5.92	6.02
280	6.07	6.17
311	6.18	6.27
342	6.29	6.38
373	6.39	6.47
404	6.48	6.55
436	6.55	6.61
467	6.62	6.68

FIGURE 3-24. The effect of mix duration on the compaction behaviour of powder containing 1% zinc stearate.

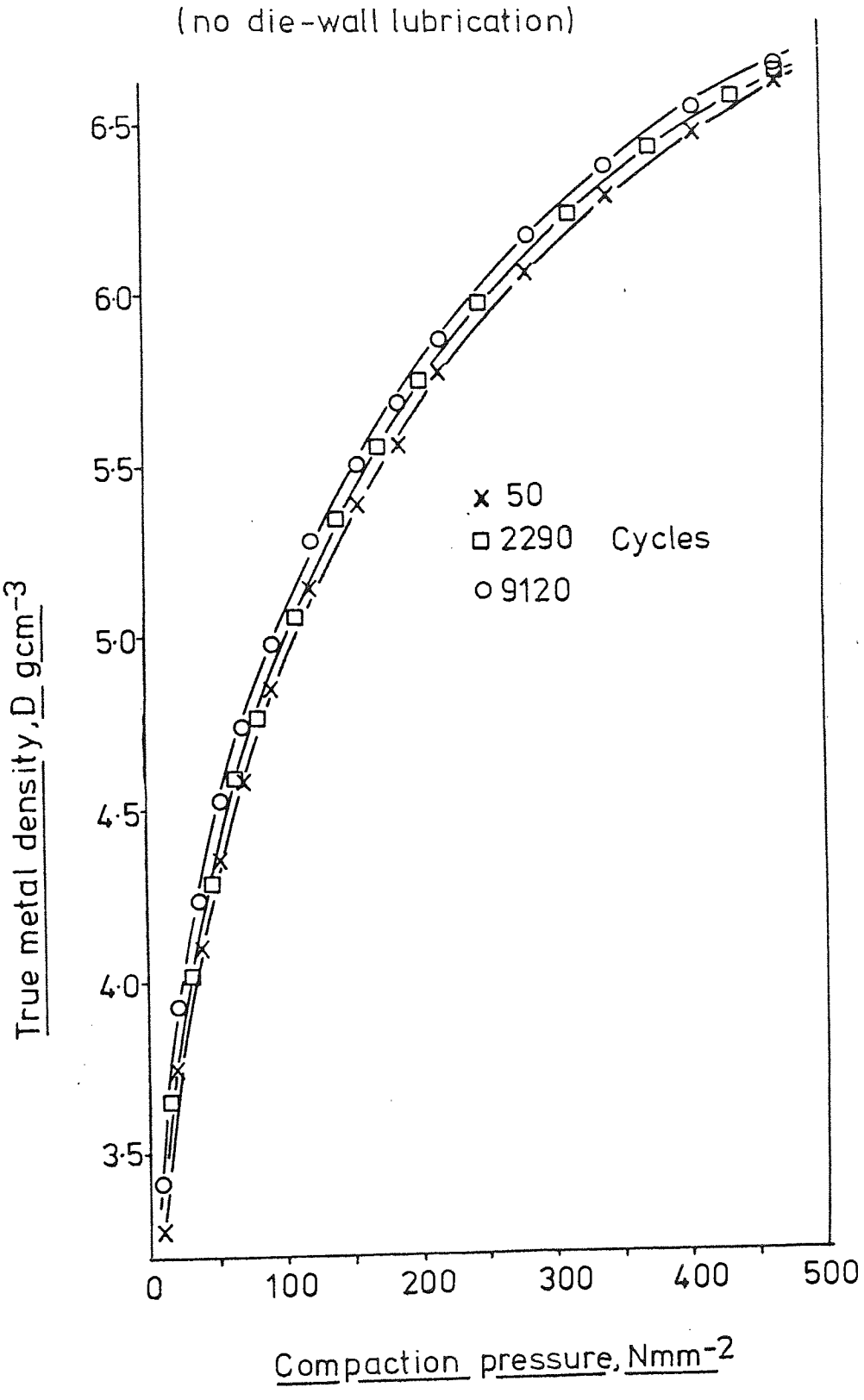

FIGURE 3-25 The effect of zinc stearate dispersion on compaction behaviour.

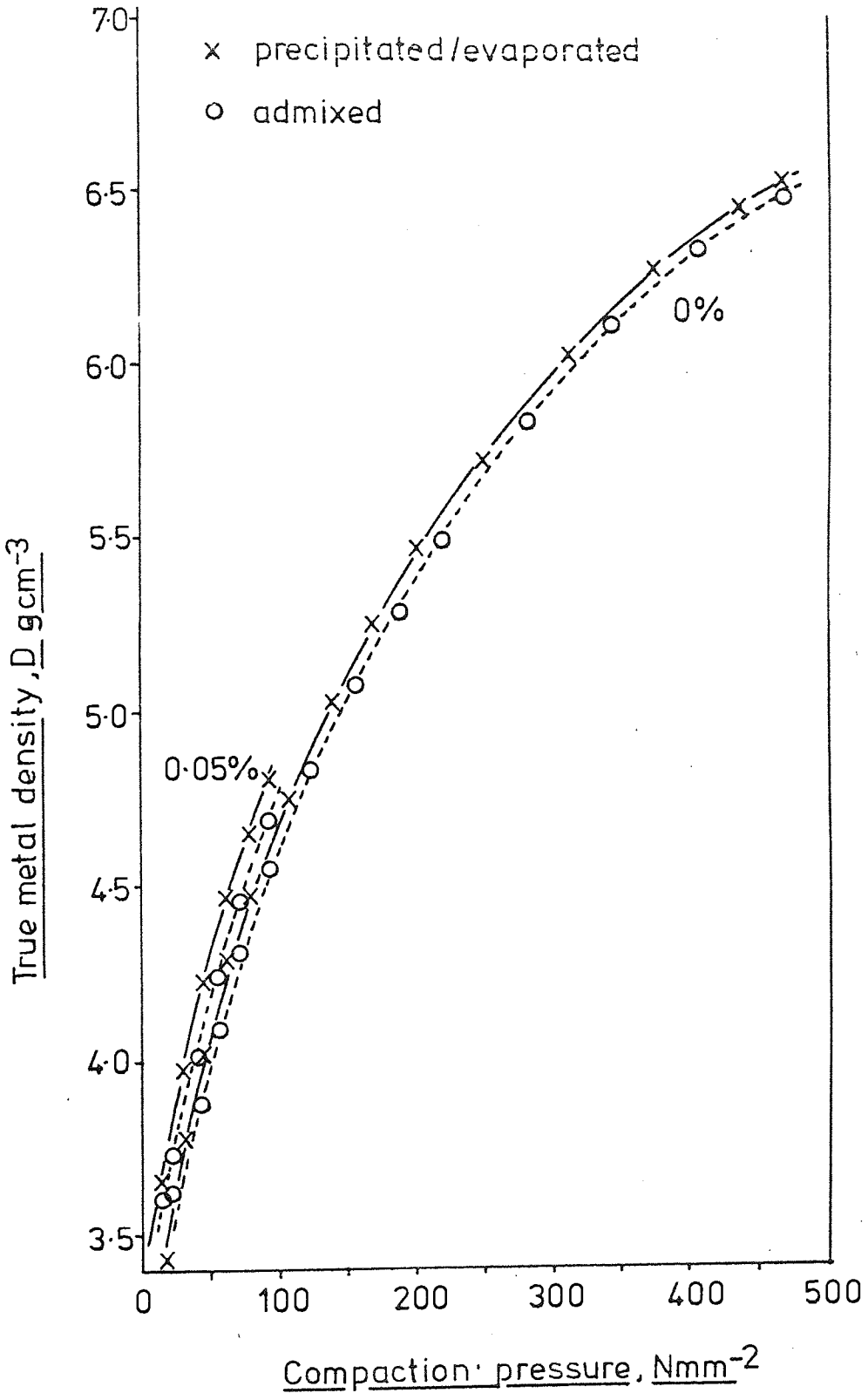

FIGURE 3-26. The effect of zinc stearate dispersion on compaction behaviour.

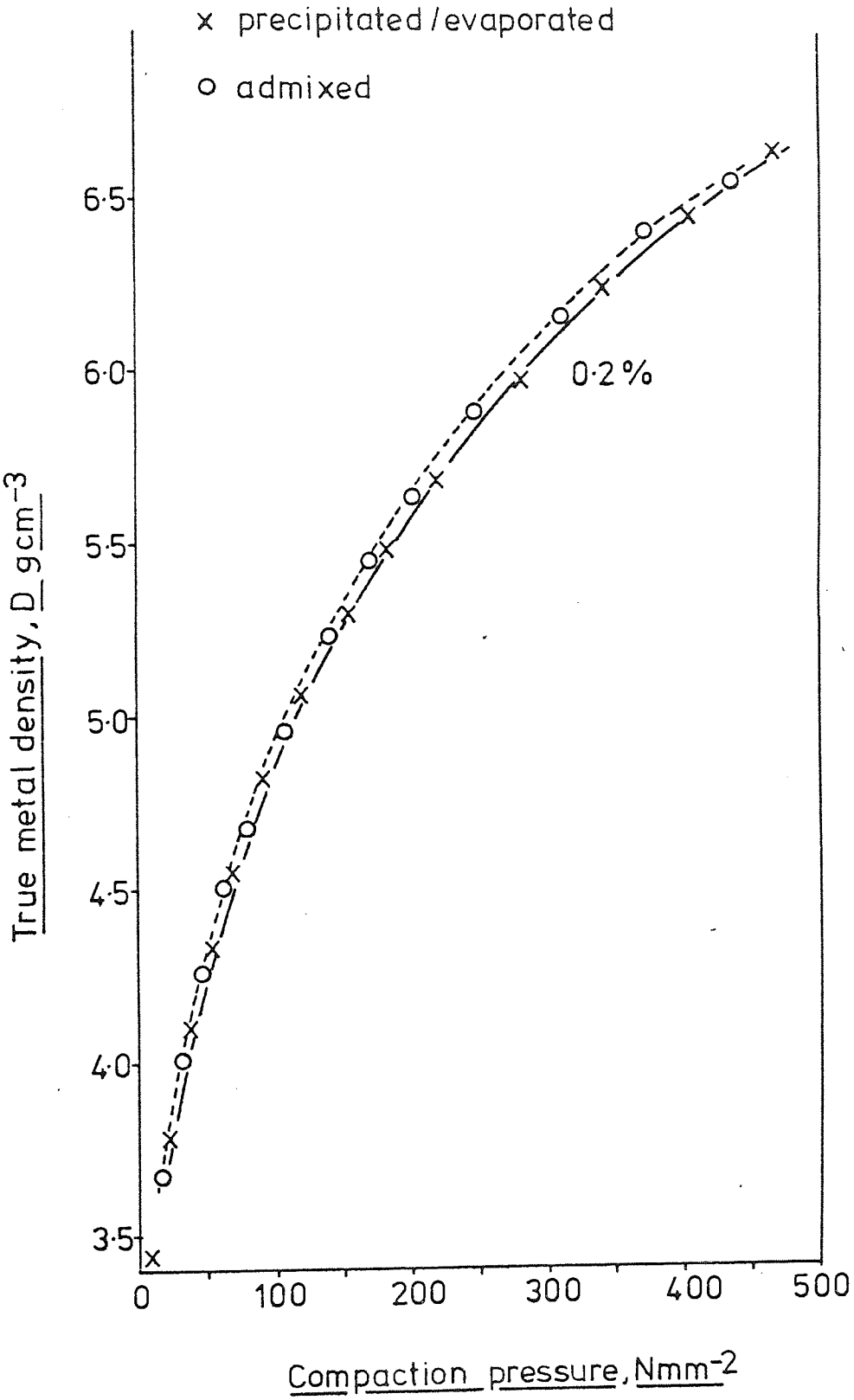

FIGURE 3-27. The effect of zinc stearate dispersion on compaction behaviour.

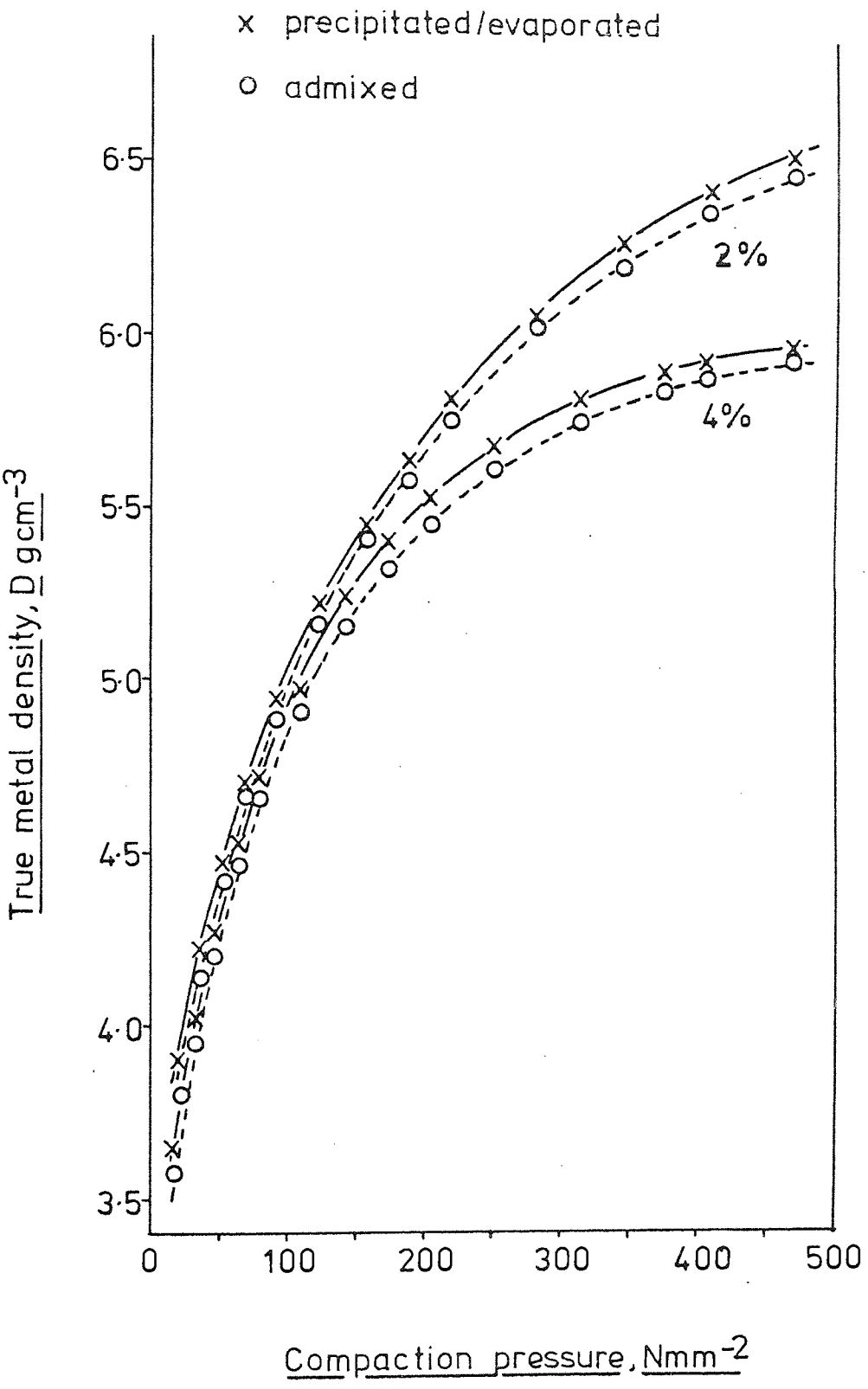

FIGURES 3-28 and 3-29. Maximum ejection stress versus true metal density.

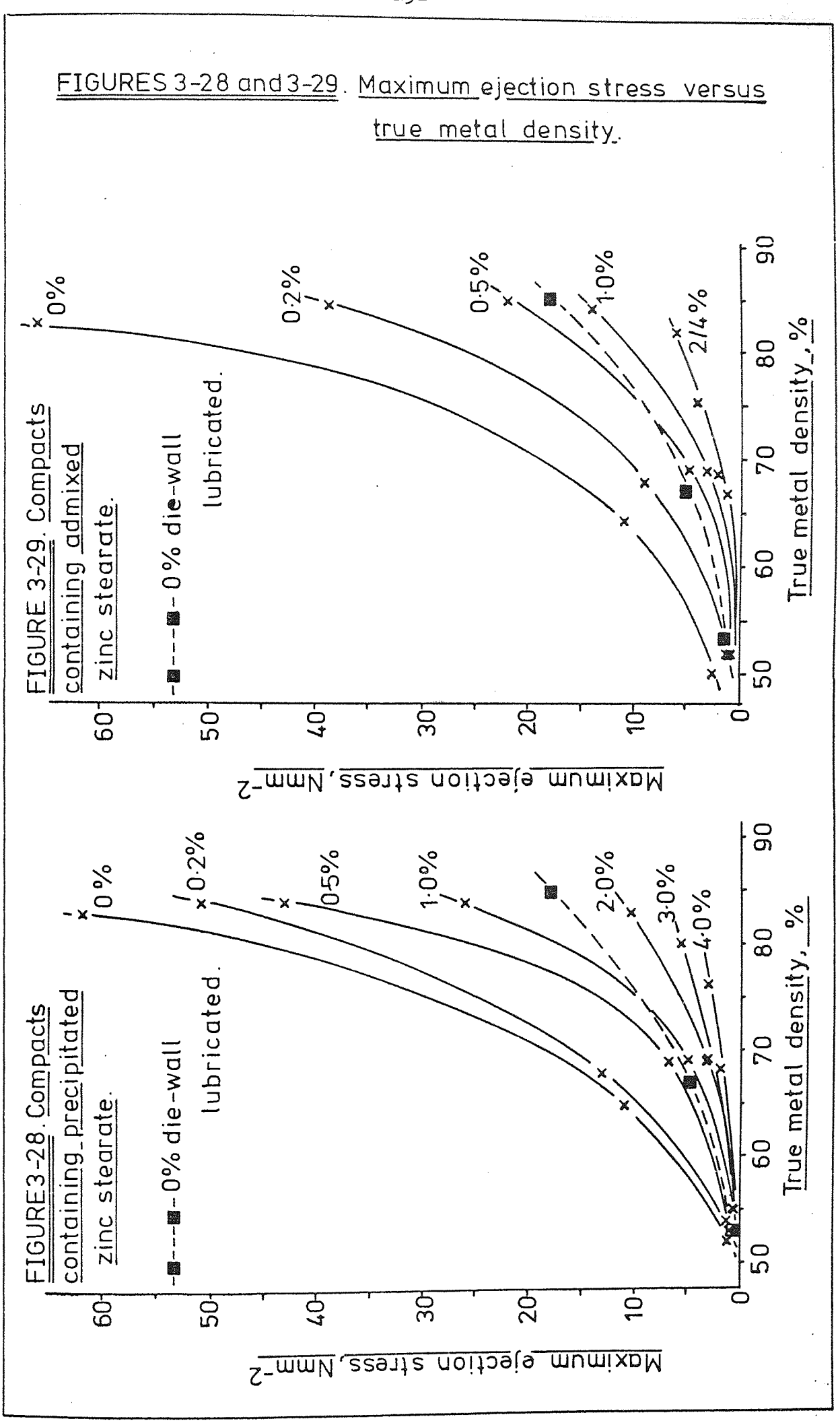

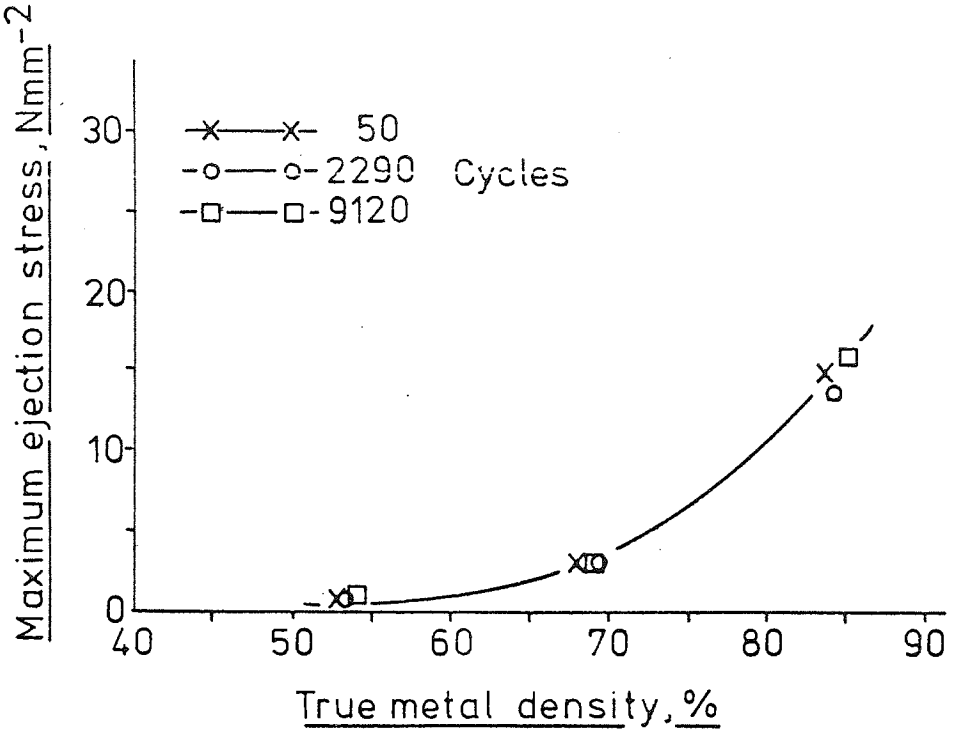

FIGURE 3-30. The effect of mix duration, MP32 plus 1% zinc stearate.

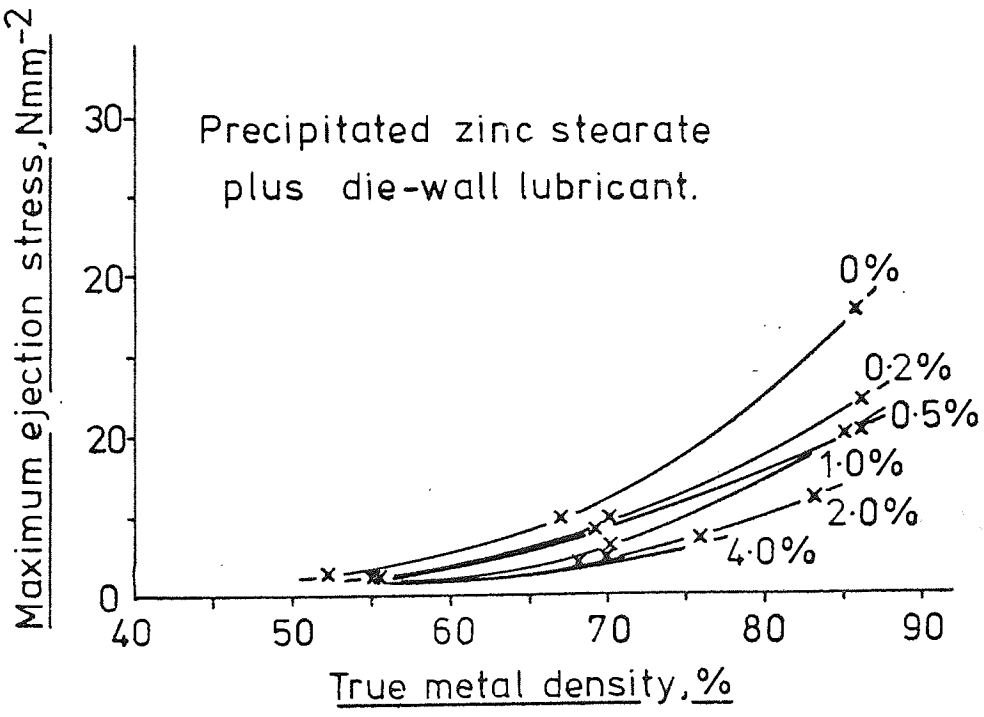

FIGURE 3-31. The effect of simultaneous die-wall lubrication.

PLATE 3-4 Scanning electron photomicrographs of the surface of compacts pressed and ejected with no lubrication.

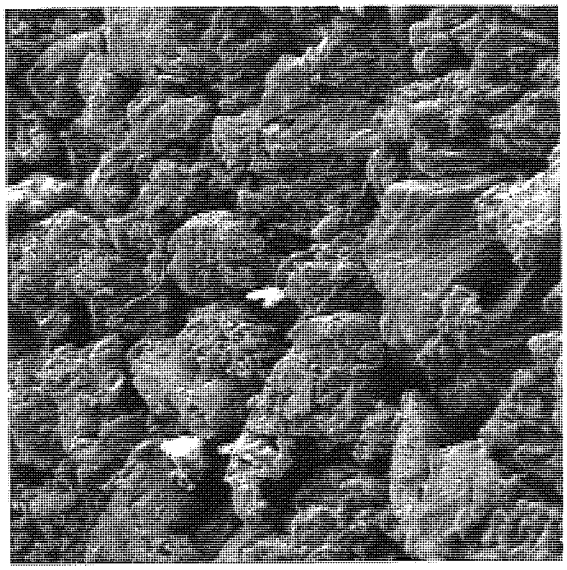

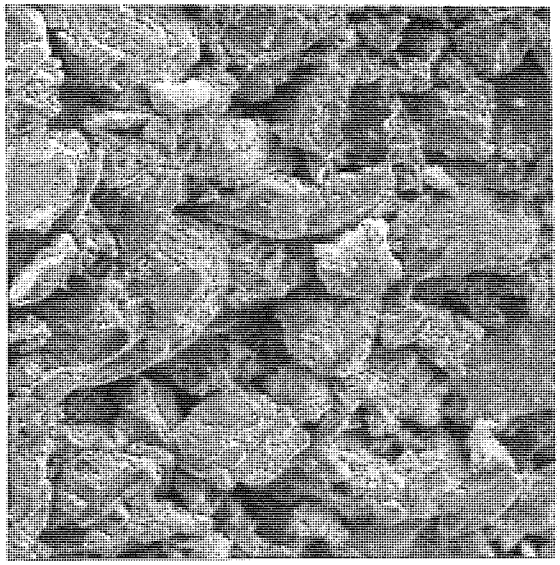

100 μm

P = 47 Nmm^{-2}

(a) Punch contact

(b) Friction surface

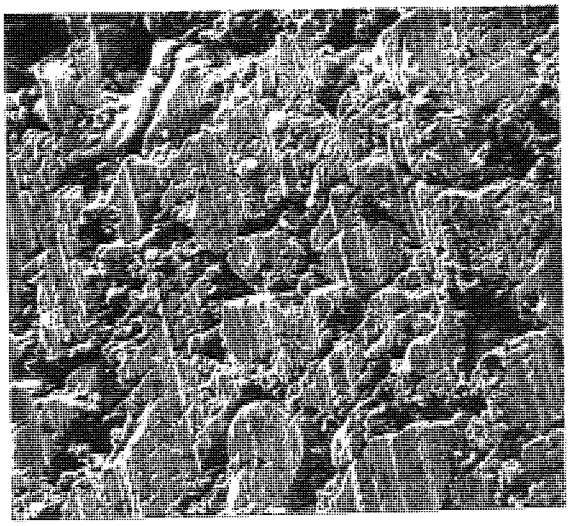

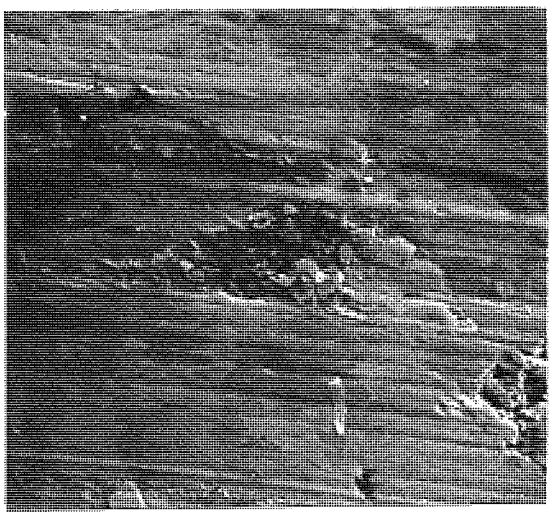

100 μm

P = 467 Nmm^{-2}

(c) Punch contact

(d) Friction surface

PLATE 3-5 Scanning electron photomicrographs of the surface of ejected, die-wall lubricated compacts.

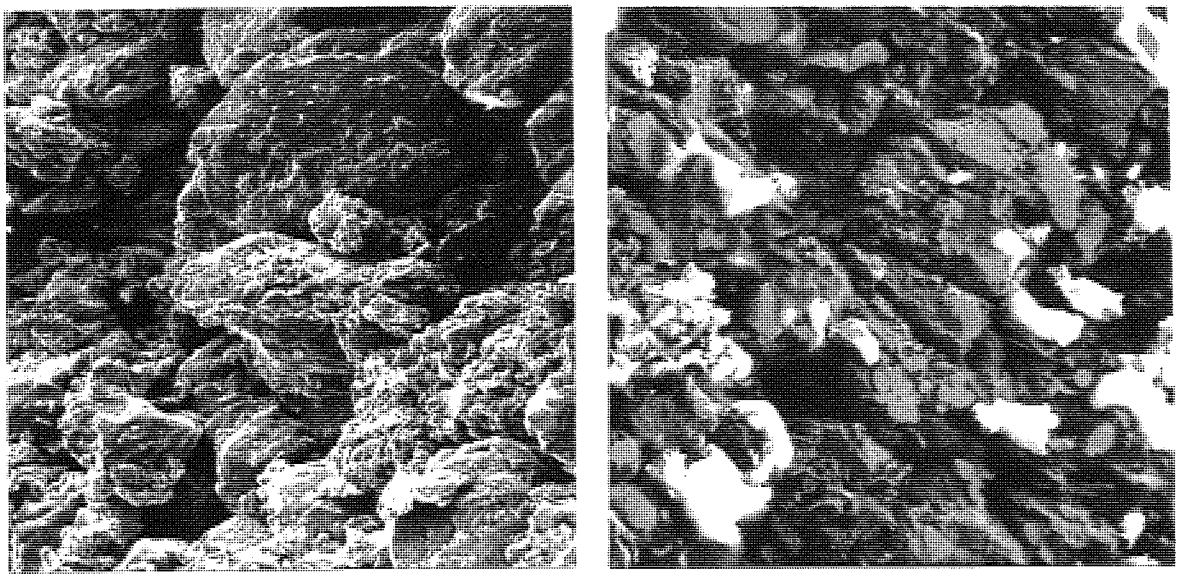

100 μm

P = 47 Nmm^{-2}

(a) Punch contact

(b) Friction surface

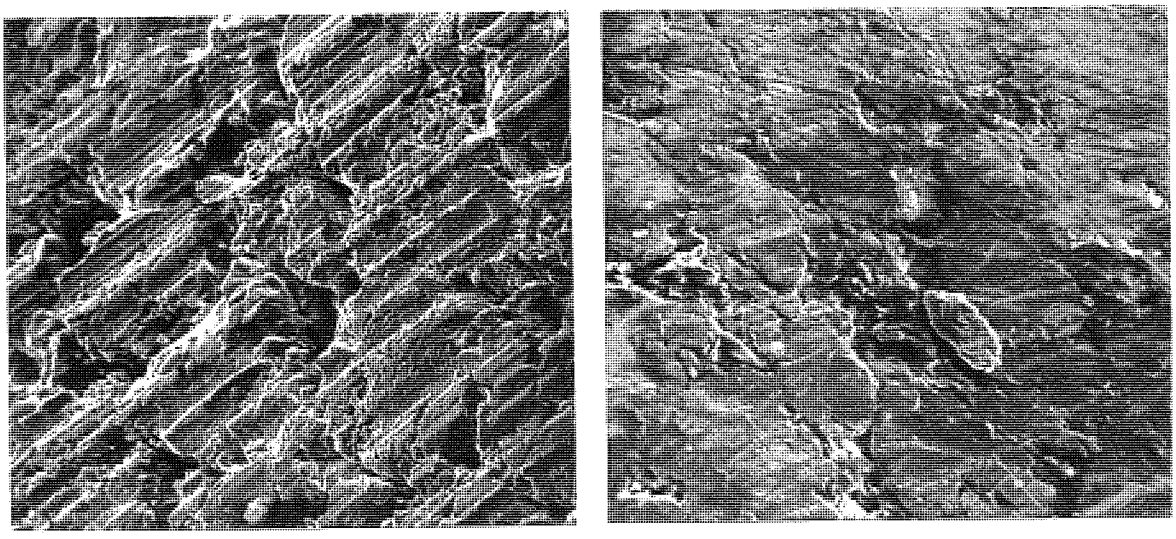

100 μm

P = 467Nmm^{-2}

(c) Punch contact

(d) Friction surface

PLATE 3-6 Scanning electron photomicrographs of the surface of ejected compacts - 0·5 % admixed zinc stearate

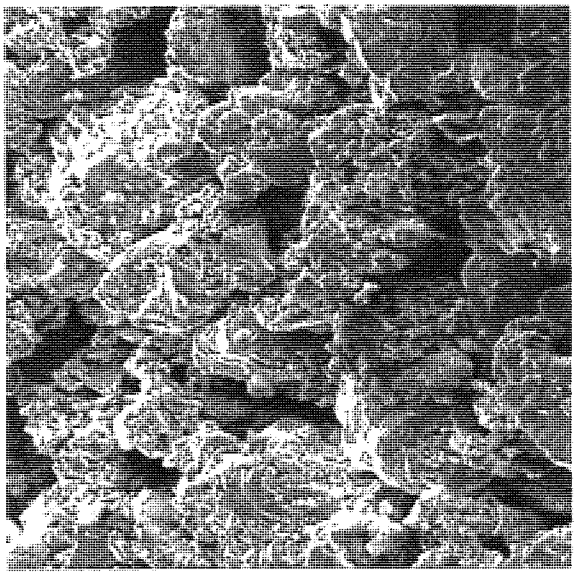

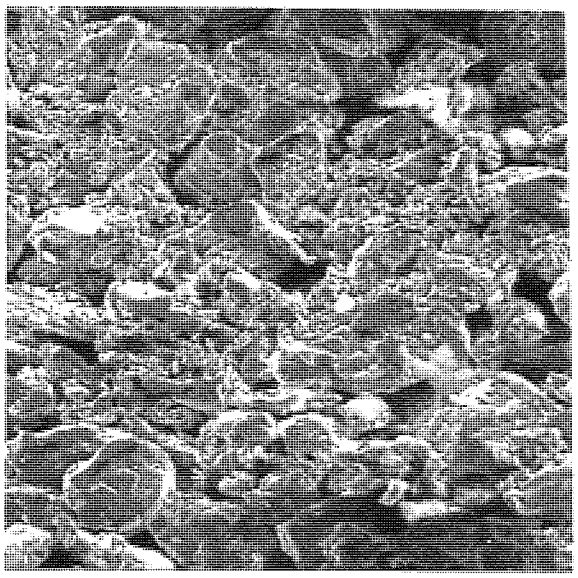

100 μm

P = 47 Nmm^{-2}

(a) Punch contact

(b) Friction surface

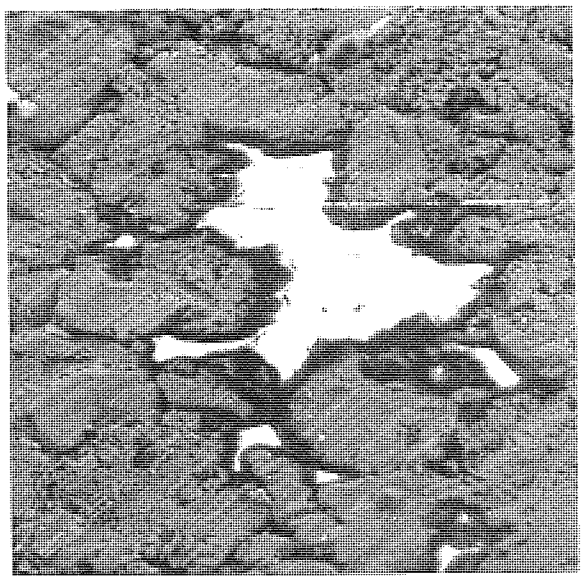

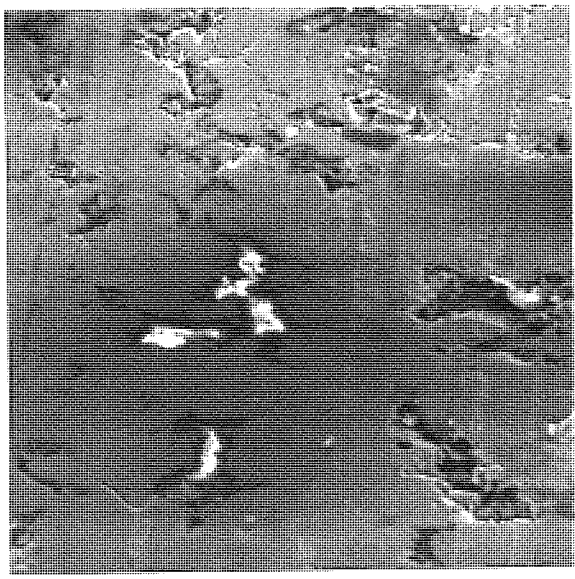

100 μm

P = 467 Nmm^{-2}

(c) Punch contact

(d) Friction surface

PLATE 3-7 Scanning electron photomicrographs of the surface of ejected compacts - 2% admixed zinc stearate.

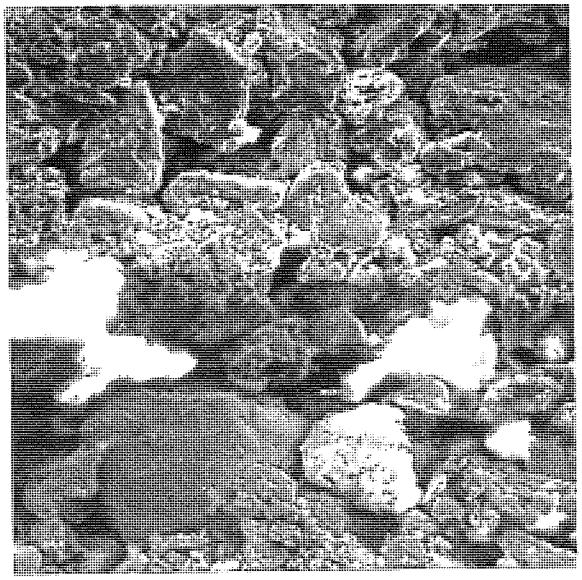

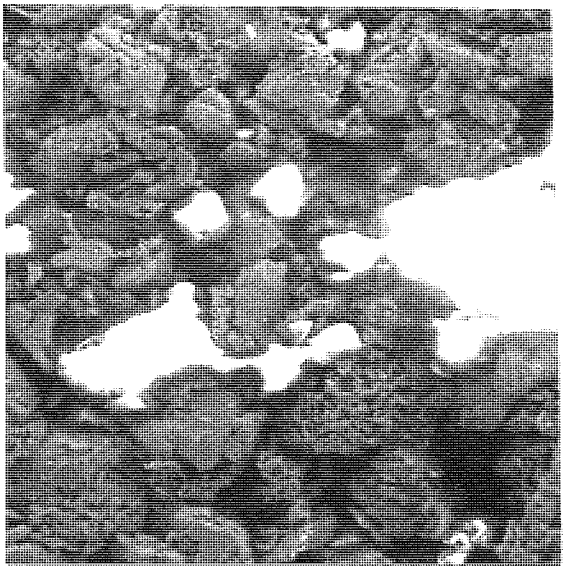

100 μm

P = 47 Nmm^{-2}

(a) Punch contact

(b) Friction surface

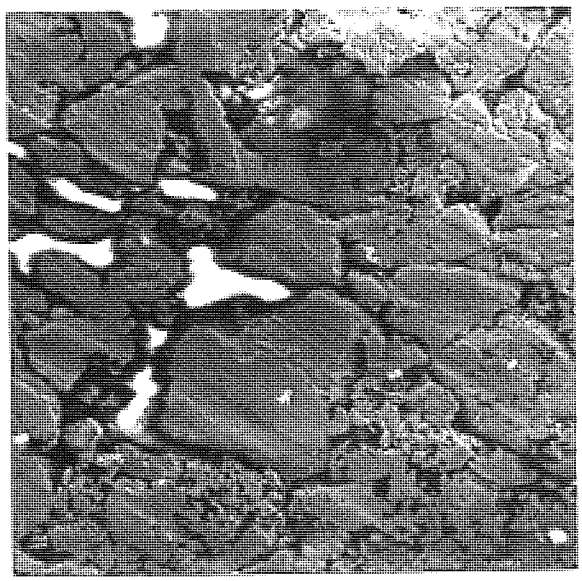

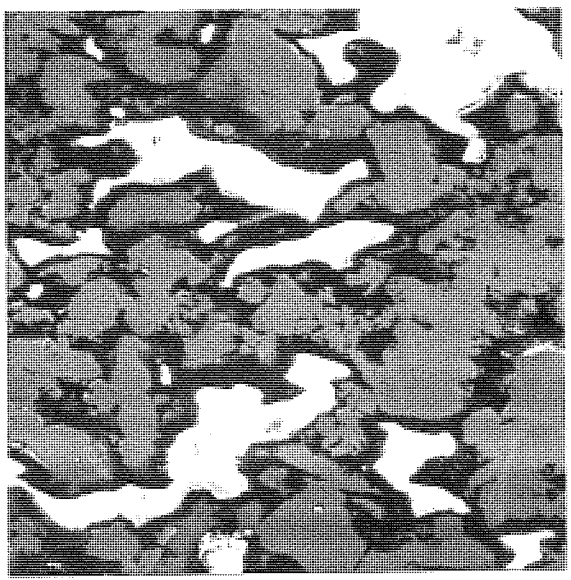

100 μm

P = 467 Nmm^{-2}

(c) Punch contact

(d) Friction surface

FIGURE 3-32. The effect of zinc stearate content and dispersion on green strength.

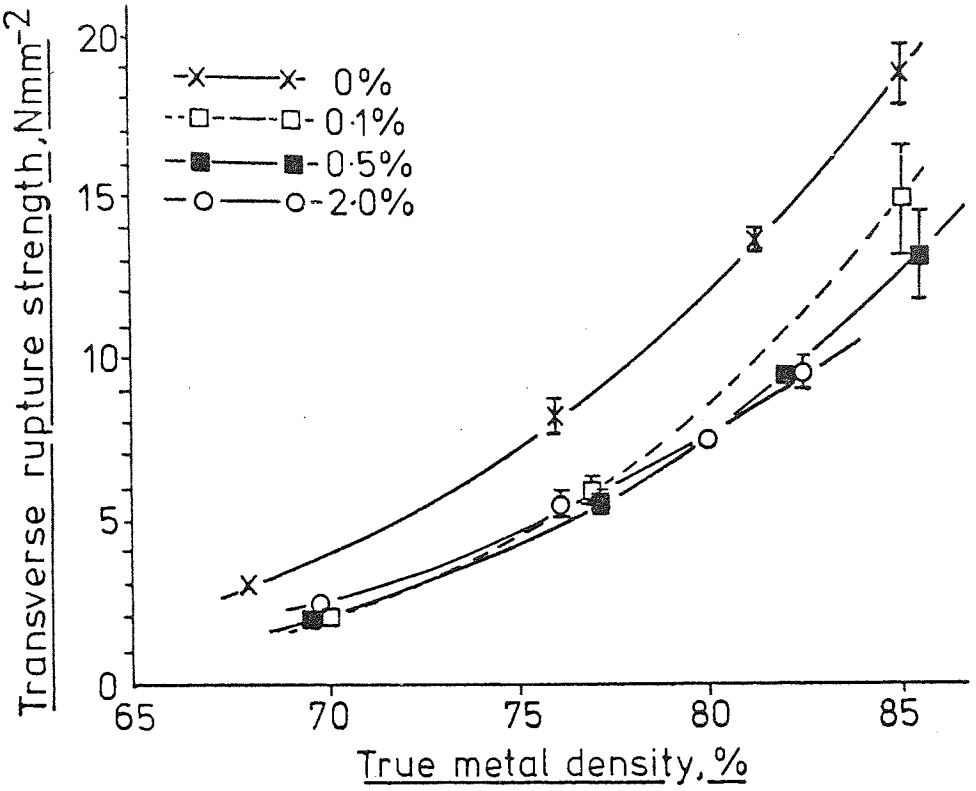

(a) Admixed lubricant.

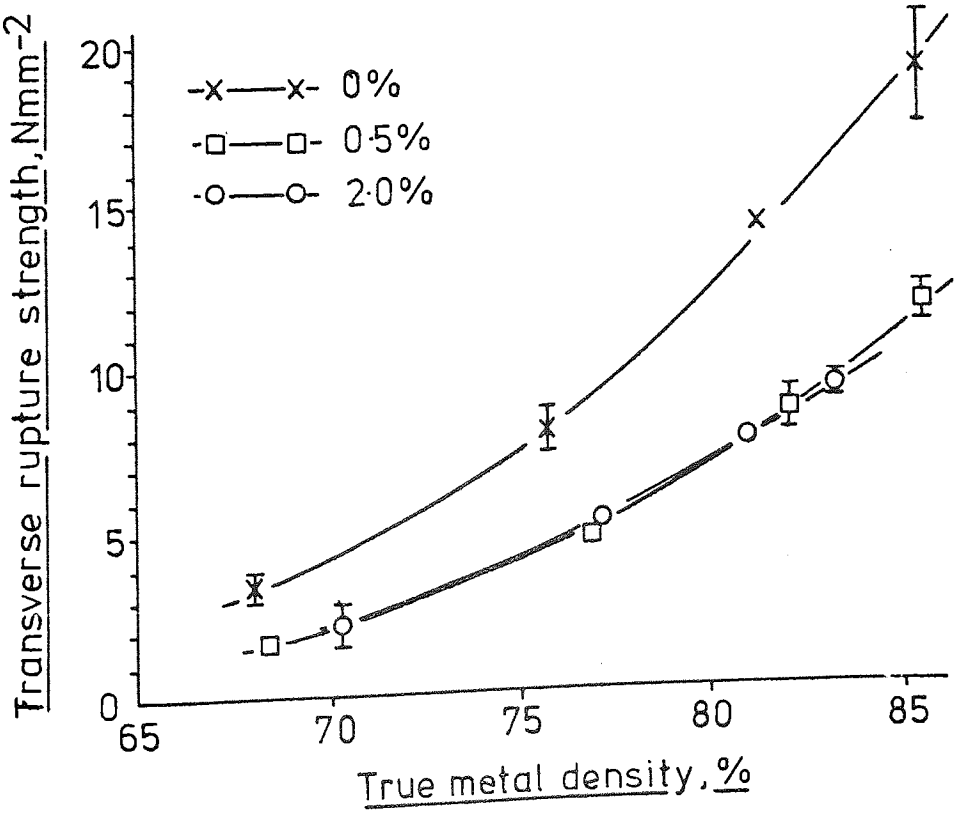

(b) Precipitated lubricant.

FIGURE 3-33. The effect of lubricant type on green strength.

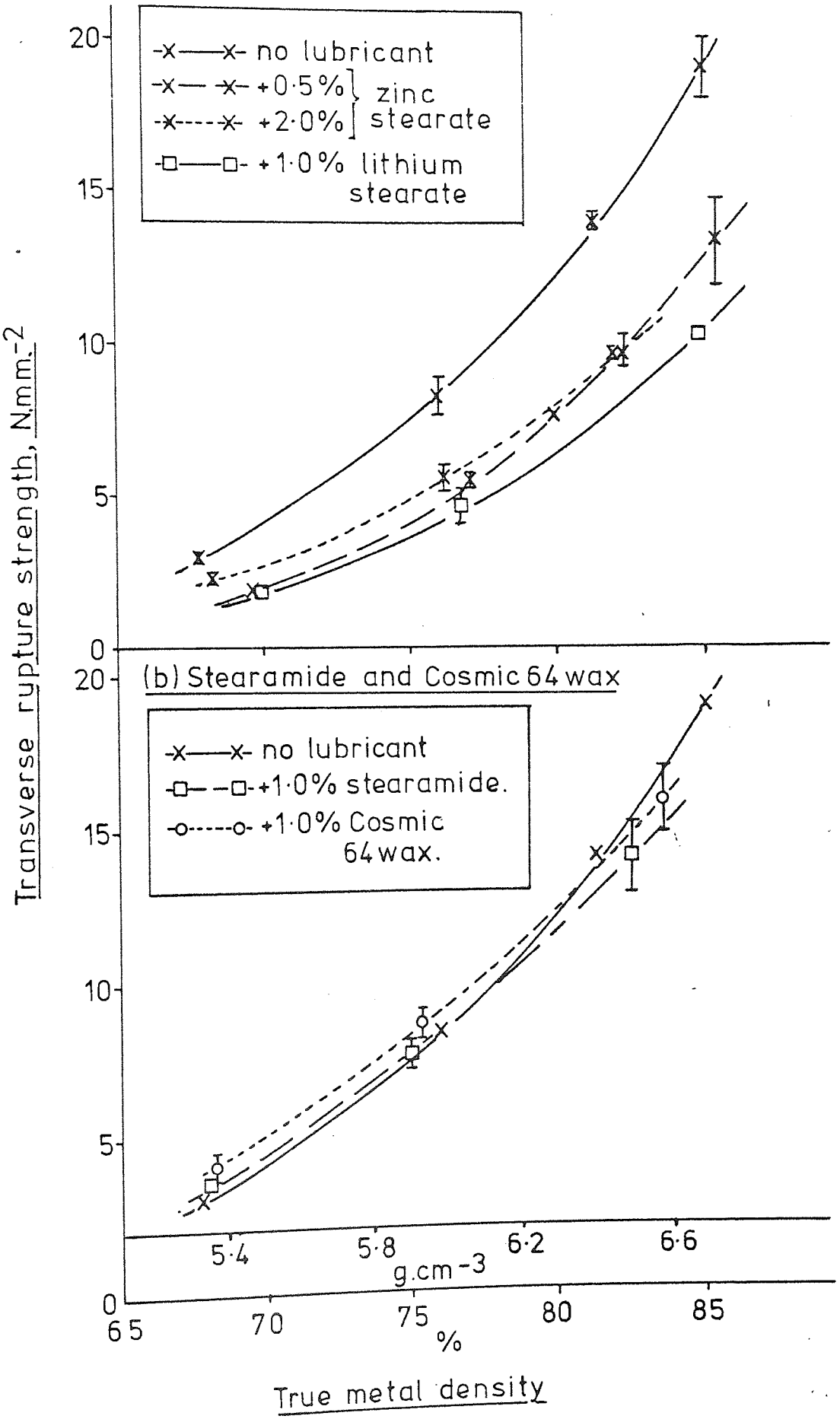

FIGURE 3-33, continued.

(c) Stearic acid.

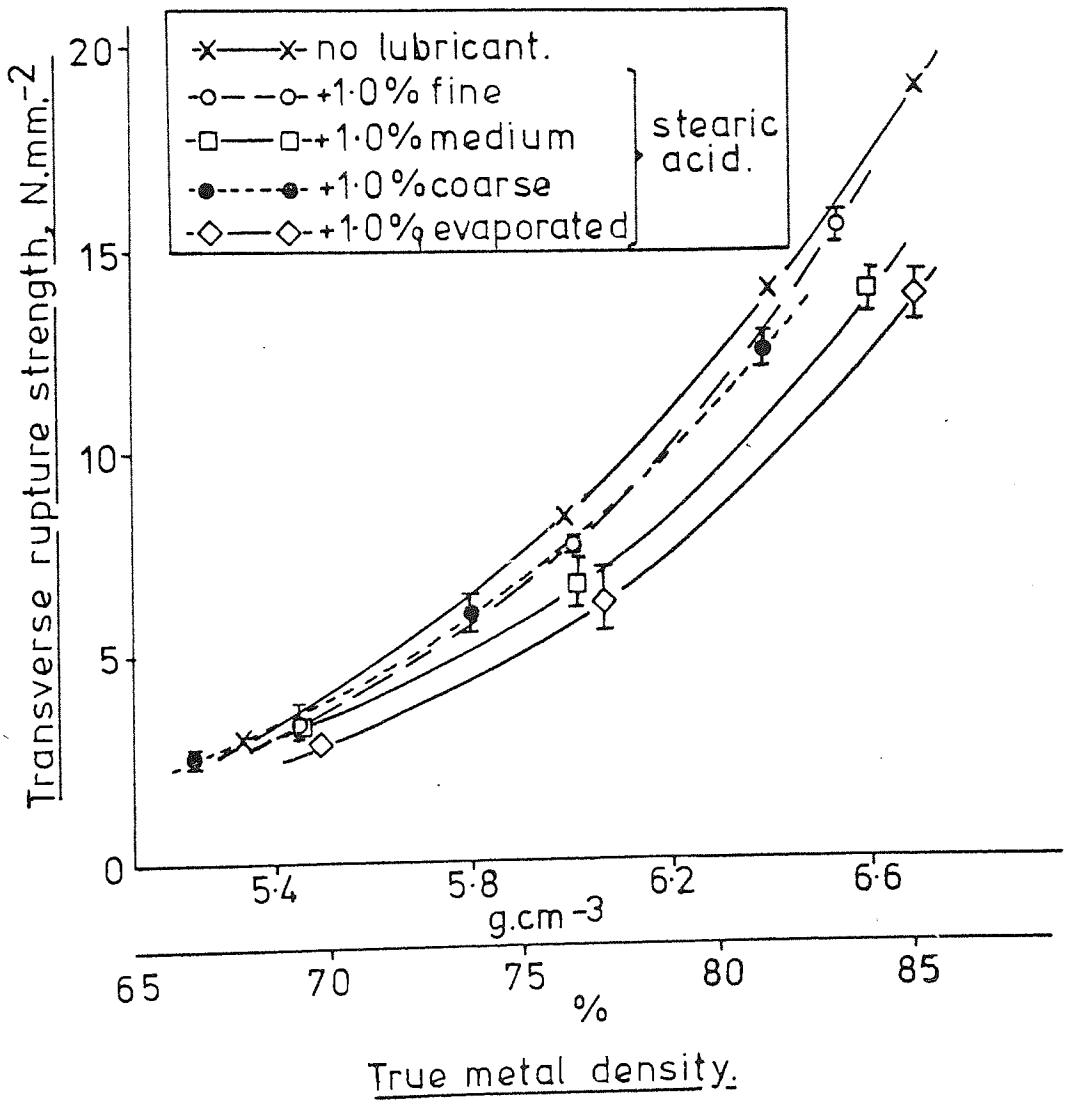

4 Discussion.

4-1 Loose powder properties

4-1-1 Precipitated lubricant

The results of D_a and D_t for zinc stearate precipitated onto MP32 iron powder are shown in figure 3-1. These reflect behaviour observed elsewhere[1,3,13] in that only small lubricant additions were required to improve density relative to the unlubricated condition. D_a for unlubricated powder was equal to that of as-received powder (2.49 g cm^{-3}) therefore the solvent itself had no effect on packing properties.

Yarnton and Davies[13] have attributed the initial rapid increase in density at low lubricant contents to progressive coverage of the metal powder surface with lubricant. The optimum density corresponds to boundary lubrication between particles by a complete layer of monomolecular thickness. Yarnton and Davies[13] have described the lubrication effect for additions up to this optimum in terms of a slip factor F, defined in equation 4-1.

$$F = \frac{D_a(\text{lubricated powder})}{D_a(\text{unlubricated powder})} \qquad \ldots.(4\text{-}1)$$

where D_a is the apparent true metal density of the powder.

For copper and iron powders with stearic acid F was found to be approximately 1.2[13]. In the present work (fig.3-1) F was 1.14 for apparent density, D_a.

Beyond the optimum conditions of 100% coverage with a monomolecular layer, density decreases due to an increase in lubricant coating thickness [13] and the formation of free lubricant. Both factors prevent close packing of the metal particles so that density decreases with increasing lubricant content. It can be seen from figure 3-1 that this did occur for both D_a and D_t in the present work.

Yarnton and Davies[13] assumed that free lubricant was not present and described this stage with a size factor approach, equation 4-2.

$$\frac{D_L}{D_U} \propto \left(\frac{d_1}{d_2}\right)^3 \qquad \ldots.(4\text{-}2)$$

where D_U and D_L are the apparent true metal densities of unlubricated and lubricated powder and,

d_1 and d_2 are the diameters of uncoated and coated particles respectively.

The problems they encountered with this approach have been outlined in the literature review (2-4).

In figure 3-1 it can be seen that a sharply defined optimum was obtained for D_t only. D_a achieved a maximum value over a range of lubricant contents (0.05%-0.2%). If 100% coverage with a monomolecular layer was obtained at the lower limit of this range (0.05%) then a decrease in D_a caused by the size factor would be expected at the higher contents.

The iron powder used in this investigation did not consist of regular, smooth solid particles which would conform with the slip and size factor approach. MP32 is an irregular, sponge type of powder (Materials section 4). Contact between such particles during loose packing would be largely at asperities and so boundary lubrication of these points would be more important than lubrication of the entire surface. Therefore the lower limit of the optimum range for D_a (fig.3-1) may have corresponded to monomolecular coverage of asperities only. The range could then represent progressive covering of the remainder of the surface.

If a complete monomolecular layer was produced by an addition of 0.05% then the range may have represented the progressive filling of cavities and open internal porosity within the iron powder particles. The absorption of lubricant into sponge powder particles has been suggested elsewhere[1].

High lubricant contents were associated with reductions from the optimum value of D_a (fig.3-1). Increasing lubricant coating thickness and the presence of free lubricant reduced D_a for 4% zinc stearate to the level of the unlubricated powder. D_t for 4% lubricant was considerably lower than for unlubricated powder.

The densities recorded in figure 3-1 were true metal densities and therefore were a measure of the packing of the iron particles only, not overall density. The formation of free lubricant, clearly visible at contents above 0.5%, would seem to have had a significant effect in inhibiting packing of the metal particles at high additions. This is given further consideration during discussion of admixing (section 4-1-2).

4-1-1-1 Tapped density, D_t

The apparent density (D_a) of a powder represents loose packing under the influence of the force of gravity only. Improvements in loose packing may be made by encouraging slip by providing a boundary layer of lubricant as discussed in 4-1-1 particularly on asperities, or by providing vibrational energy as in tapping.

It can be seen from figure 3-1 that tapping was more efficient than adding lubricant, probably causing more actual rearrangement of particles rather than aiding short range slip between particles. Consequently the further improvement in packing produced by a boundary lubricant layer was small for D_t (fig.3-1). The optimum was more definite and occurred at a lower lubricant content (0.01%) than for D_a.

The effect of free lubricant with large additions was more marked for D_t where it prevented iron particles rearranging to the same degree as in unlubricated powder (fig.3-1).

4-1-1-2 Lubricant coating thickness

It had been hoped to calculate lubricant coating thickness by

measuring the specific surface area of the iron powder. Other work was to be undertaken also on the use of specific surface area to characterise metal powder morphology. Apparatus was constructed for determining surface area by monitoring the adsorption of gas gravimetrically, but delivery delays and consequent time restrictions prevented the establishment of a reproducible method. The principle, construction and operation of this equipment is outlined in appendix B.

The arbitrary assumption of a specific surface area of $0.07 m^2 g^{-1}$ for the iron powder (see appendix B) enabled a coating thickness range to be calculated for the optimum lubricant additions for D_a (fig.3-1). The specific gravity of the zinc stearate had been calculated as 1.05 (section 4) and it was assumed that each lubricant content corresponded to 100% coverage of metal particles, with no free lubricant formation.

Coating thickness was calculated as 7×10^{-9}m and 3×10^{-8}m for additions of 0.05% and 0.2% respectively. These compared favourably with a value of 2.7×10^{-7}m for a 1% addition of stearic acid to an iron powder obtained by Yarnton and Davies[13] by measuring particle diameters. Lubricant coatings corresponding to optimum packing conditions were certainly very thin.

4-1-2 Admixed lubricant

The results of admixing zinc stearate with MP32 iron powder have been presented as D_a versus mix duration in figures 3-2 to 3-4. These have been divided into three groups on the basis of mix behaviour relative to the unlubricated powder.

4-1-2-1 General mixing behaviour

It was found generally that loose packing properties improved with increasing mix duration as shown by D_a in figures 3-2 to 3-4. Ljungberg and Arbstedt[1] also observed that die-fill capability improved with increasing mix time. Direct observation of lubricant coatings and dispersion

was found to be very difficult (see section 2-1-5). However results obtained from scanning electron metallography (plates 3-1 to 3-3) were used to support interpretation of the density data but were never used alone to explain lubricant behaviour.

The photomicrographs of plate 3-1 were obtained to illustrate the influence of mix duration on the general dispersion of 1% zinc stearate. It can be seen that the progression of mixing appeared to be associated with a reduction in the proportion of free lubricant which could be detected by zinc X-ray mapping.

Lubricant pickup on individual iron powder particles is illustrated by plate 3-2 which is typical of photomicrographs obtained from a mix containing 1% zinc stearate. Particles of zinc stearate can be seen adhering to metal particles and there was a tendency for them to enter cavities or convolutions as mixing proceeded.

It was not possible to detect surface coatings produced by smearing or disintegration of lubricant particles, even by zinc X-ray mapping at high magnifications. This was attributed to the relatively low proportion of zinc in the stearate (approximately 10% of the total addition) and the extremely thin films produced (section 4-1-1-2). Detection was difficult even with a coating precipitated from a 2% addition of zinc stearate (plate 3-3).

4-1-2-2 Loose packing properties of admixed powders

It can be seen from either of figures 3-2 to 3-4 that there was a small, gradual increase in D_a for the unlubricated powder as mix duration increased. This may have been caused by attrition, particularly smoothing of asperities, and possibly agglomeration of fines with large particles. Both factors could improve loose packing properties.

The initial (0 cycles) packing behaviour of lubricated powders was largely unaffected by lubricant until the total addition was between 0.5%

and 1.0% (figs.3-3 and 3-4). There was no deliberate mixing at this stage and so it may be assumed that the majority of the lubricant was present in the free state. Therefore, during this work it appeared that the presence of free lubricant would have no deleterious effect on packing until the total addition and mixing/dispersion conditions provided between 0.5% and 1.0% of it. This does assume the absence of complicating factors such as the formation of lubricant surface coatings on the metal powder.

The characteristics of the three groups corresponding to figures 3-2 to 3-4 and mentioned previously may be outlined as follows;

Group 1. (fig.3-2) 0.01%-0.05%. D_a was initially similar to that of unlubricated powder but increased gradually as mixing proceeded and showed no optimum mix time (no plateau). Final densities were all higher than unlubricated powder.

Group 2. (fig.3-3) 0.1%-0.5%. Initial values of D_a differed little from unlubricated powder but there was a rapid increase during the early stages of mixing. There was a definite optimum mix duration for each addition as shown by the plateaux in the D_a versus duration curves. Final densities were higher than the unlubricated powder.

Group 3. (fig.3-4) 1.0%-4.0%. Initial values of D_a were lower than the unlubricated powder. They increased rapidly as mixing proceeded but there was no indication of an optimum mix time. Final values of D_a were lower than in the unlubricated condition.

The 1% zinc stearate addition had a low value of D_a initally but did have an optimum mix time, exhibiting characteristics of both group 2 and 3.

The influence of admixed lubricant on loose packing properties may also be illustrated by figure 4-1. This is D_a as a function of lubricant

FIGURE 4-1. D_a versus lubricant content for various mix durations.

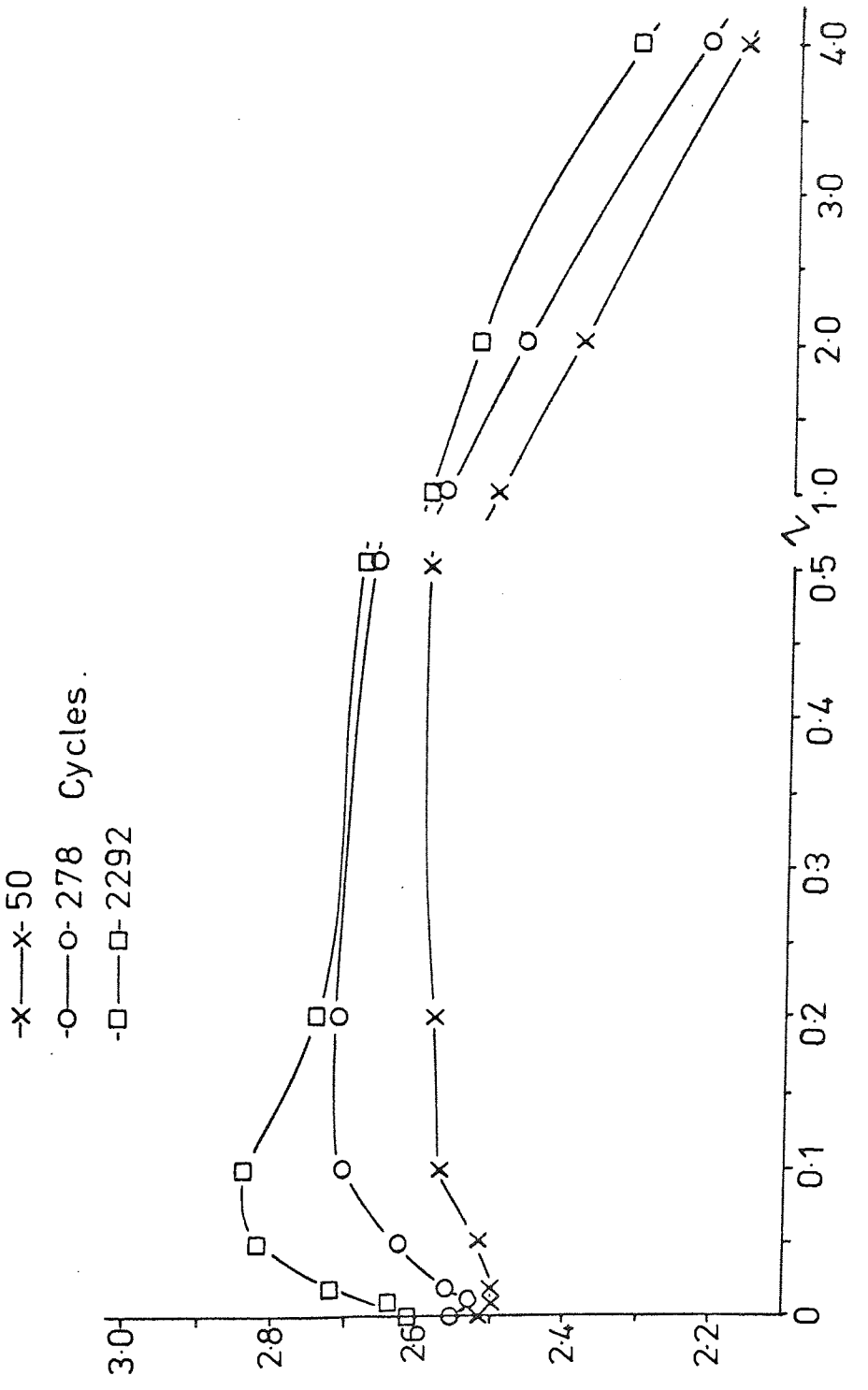

content, points being taken from figures 3-2 to 3-4 at various mix times. Certain similarities between this and the results of D_t for precipitated lubricant (fig.3-1) were evident.

There was a definite optimum addition (0.05%-0.1%) which was strongly dependent on mix duration. The value of F for the final mix duration (fig. 4-1,2292 cycles) was 1.09, approaching the value of 1.14 obtained for precipitated lubricant (fig.3-1). This was followed by a range of contents (0.2%-1.0%) where the addition of lubricant had little apparent effect on D_a. Beyond 1.0% D_a decreased to values below those for unlubricated powder. D_a increased with mix duration for all additions as would be expected from the form of the mixing curves (figs.3-2 to 3-4).

Loose packing behaviour during the mixing of low lubricant contents (group 1,fig.3-2) was attributed to the gradual pickup of lubricant onto metal particles to form thin coatings, particularly on asperities. At such low additions size factor effects and the presence of free lubricant were not significant and optimum packing conditions (fig.4-1) corresponded to boundary lubrication by thin films of lubricant.

Lubricant contents lower than the optimum (less than 0.1%) provided only fractional coverage and hence D_a became directly proportional to content (figs.3-2 and 4-1). Fractional coverage may indicate incomplete coverage of each iron powder particle. Alternatively it may indicate that the small quantities of lubricant present adhered to only some particles which then had complete coverage at the expense of others. Consequently the gradual increase of D_a with mix time (fig.3-2) would reflect lubricant transfer between iron powder particles rather than between free lubricant and the metal powder.

The marked relationship between the development of the optimum density and mix duration (fig.4-1) reflected the sluggish mixing behaviour of small additions (fig.3-2). The initial dispersion would have been

uneven and long times were required to disperse such small quantities throughout the mix, particularly if the transfer between metal particles suggested above is considered.

Intermediate lubricant contents (0.2% to 1.0%, fig.4-1) were characterised by values of D_a which decreased only slightly with increasing lubricant. In this range there was insufficient free lubricant to influence loose packing but there was sufficient to ensure rapid mixing by transfer from free lubricant to the iron powder particles (fig.3-3).

The optimum mix durations shown by this group (fig.3-3) may have been the result of the rapid build up of thick surface layers which were then maintained constant by a process of attrition and rebuilding during mixing. The inverse relationship between final density and lubricant content reflected the increase in coating thickness with increasing lubricant (size factor effect[13]).

Sufficient free lubricant remained after the admixing of high lubricant contents (1.0%-4.0%, fig.4-1) to reduce D_a values below those of the unlubricated powder. Large additions ensured that mixing was rapid during early stages (fig.3-4) as surface coatings developed. Lubricant build up appears to have continued even after extensive mixing as shown by the absence of optimum durations (fig.3-4). There would have been a corresponding decrease in the proportion of free lubricant as more adhered to metal particles which would have produced further improvements in D_a. The reductions in D_a relative to the unlubricated powder were strongly dependent on lubricant content at all mix durations (figs.3-4 and 4-1) emphasising the influence of free lubricant on loose packing properties.

During mixing the proportion of free lubricant in the 1% mix was reduced to a level where it did not depress D_a below the unlubricated values. It has been suggested previously that 0.5% free lubricant would not significantly affect D_a. Therefore, during the final stages of mixing

the 1% addition may have consisted of approximately 0.5% free lubricant with the remainder adhered to the metal particles.

4-1-3 Summary

The absolute values of D_a recorded in figure 4-1 did not allow for the increase in D_a of the unlubricated powder during admixing (see figs. 3-2 to 3-4). A better indication of the influence of lubricant on loose powder packing properties was provided by considering ΔD_a, the change in apparent density relative to the unlubricated condition (equation 4-3).

$$\Delta D_a = D_a(\text{lubricated}) - D_a(\text{unlubricated}) \quad \ldots.(4\text{-}3)$$

This is shown as a function of lubricant content in figure 4-2 for both precipitated and admixed zinc stearate additions. It has been assumed that even with lubricant present the iron powder still underwent attrition during mixing although this was not necessarily true.

As mixing proceeded ΔD_a for low admixed additions (0.01%-0.1%) approached that of precipitated lubricant. This was the region where fractional coverage of metal particles progressed towards complete coverage with a thin lubricant layer as lubricant content or mix duration increased. The formation of a complete thin layer, which may have been monomolecular [13], produced an optimum loose packed density. It was not apparent whether the thin lubricant layer was a general coating over the entire particle surface or on the external surface or asperities only.

Over the intermediate lubricant range (0.1%-0.5%) ΔD_a decreased rapidly with increasing lubricant content at the maximum mix duration (2292 cycles). This was the region where loose packing properties were mainly affected by the formation of thick coatings on particle surfaces. At short mix times (50 cycles) these were thin and hence ΔD_a was not dependent on lubricant content.

FIGURE 4-2. ΔD_a as a function of lubricant content for MP32 iron powder plus zinc stearate.

$\Delta D_a = D_a$ (lubricated) $- D_a$ (unlubricated)

(D_a = apparent true metal density)

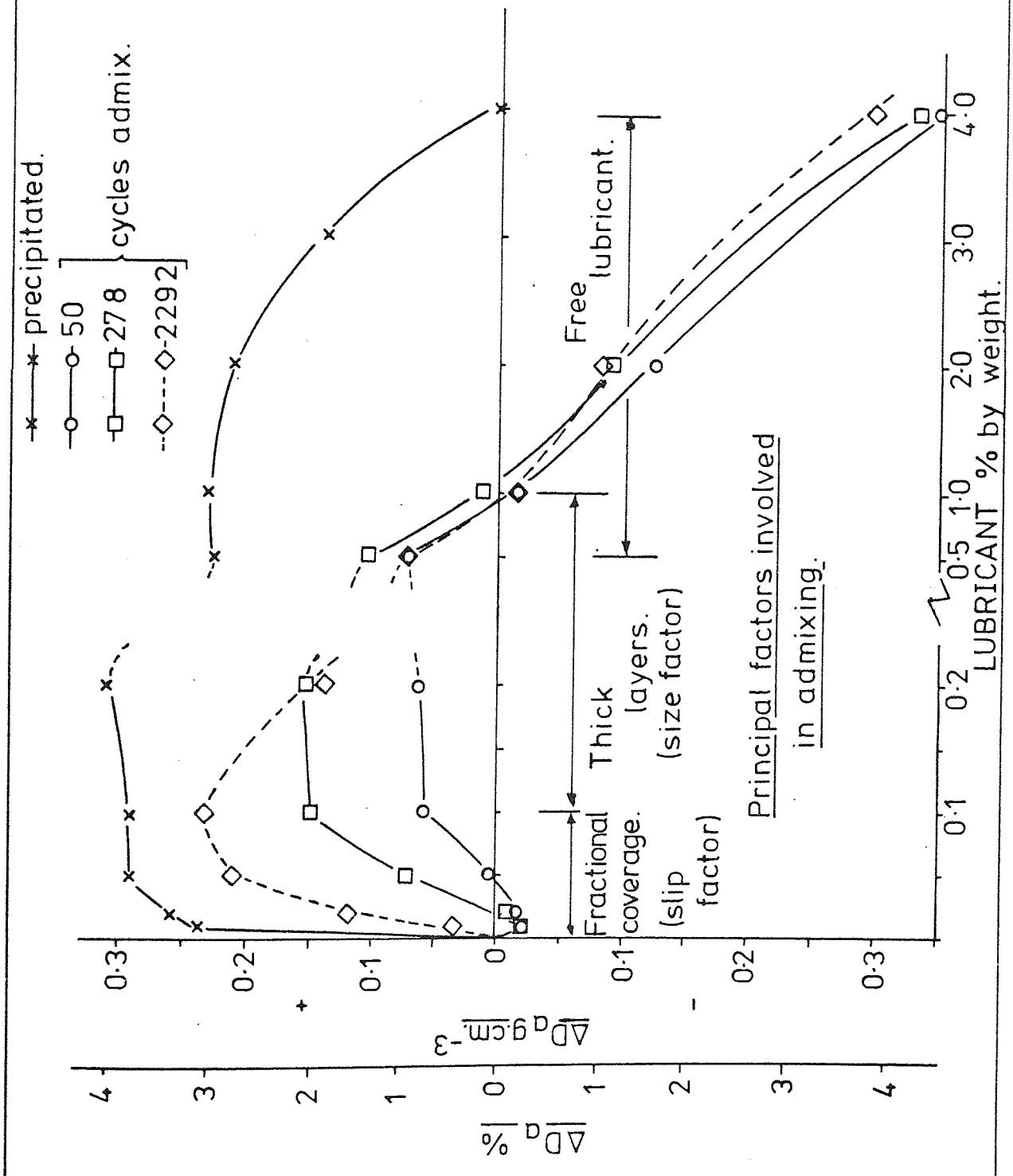

ΔD_a for precipitated additions remained constant at the maximum value over a similar range of contents (0.05%-0.2%). It is possible that lubricant was precipitated in cavities, open internal porosity and over the general surface such that the exposed surface coating did not increase sufficiently to decrease ΔD_a. Comparison of this with the relative sensitivity of admixed additions as discussed above suggested that lubricant pickup during admixing may have been mainly on the exposed surface or asperities of metal particles.

The effect of the presence of large quantities (in excess of 0.5%) of free lubricant can be seen clearly for additions of admixed lubricant larger than 0.5%-1.0%. ΔD_a rapidly became negative as the particles of free lubricant prevented close packing of the iron particles.

ΔD_a for precipitated lubricant did not become negative but reduced to zero at the maximum addition (4%). It seems that the overall level of free lubricant was reduced by internal precipitation in the iron particles as discussed previously. The build up of thick surface coatings may have been of more significance at the lower lubricant contents (0.5%-2.0%) of this range.

The factors which are believed to control the influence of admixed lubricant on loose packing properties have also been indicated on figure 4-2.

4-2 Compaction

4-2-1 The linear relationship

Linear relationships obtained from continuous compaction of the ferrous-based powders are shown in figures 3-5 to 3-8. The materials involved are listed in table 4-1 of the Materials Section and have been recorded with some properties in table 3-1 also. The corresponding compaction results are recorded in full in tables 3-2(A) to 3-2(K). Die-wall lubrication was employed in each case except material K (fig.3-8).

The results shown in figures 3-5 to 3-8 were based on equation 4-3 which was used by Heckel[17,18].

$$\ln(1/(1-D)) = kP + A \qquad \ldots.(4-3)$$

where D is the fractional relative true metal density of the compact,

P is the compaction pressure,

k is the slope or rate of densification,

and A is the intercept on the $\ln(1/(1-D))$ axis.

By using this relationship Heckel[17,18] and Morgan and Sands[23] were able to show that the closed die compaction of metal powders could be considered as a three stage process with a different predominant densification mechanism in each. These stages have been outlined in section 2-5 of the literature review and in the experimental procedure (section 2-2). A schematic representation of the type of relationship obtained by Heckel[17,18] has been reproduced in figure 2-1 of the literature review. The present investigation was aimed at determining the suitability of this relationship (equation 4-3) for assessing the influence of lubricant on the various mechanisms which operate during densification.

Stages similar to those observed previously[17,18] were obtained but with the inclusion of a short linear region at the higher pressures

of stage 2 (figs.3-5 to 3-8). This is shown more clearly in figure 4-3 which is a schematic representation of these results. The main derived parameters (D_2, D_3, k_2 and k_3) have been indicated in this diagram also. The straight lines of best fit (figs.3-5 to 3-8) and values of D and k were determined by the use of linear regression (least squares method). Values of D and k are recorded in table 4-1 and the statistical significance of the regression results is discussed in section 4-2-1-4 . k_2 and k_3 were the slopes of the linear portions of stages 2 and 3 respectively (fig.4-3) and indicated the rate of densification with pressure. D_2 and D_3 were the intercepts of these linear regions and were expressed as fractional true metal density at zero compaction pressure. They did not define the limits of either stage but were an indication of the general level of densification achieved.

The results of the work-hardening studies described in section 2-2-2-3 are shown in figures 3-9 to 3-12 as individual particle microhardness versus true metal density. Microhardness measurements on individual sectioned particles (see appendix A) were used to detect work hardening and hence bulk plastic deformation of the material. Normal hardness determinations would probably have been dependent on the level of porosity as well as the degree of hardening. In figures 3-9 to 3-12 density has been used as an indication of strain.

Certain degrees of densification were obtained before work-hardening was detected as was shown by the initial portions of figures 3-9 to 3-12. When hardening, and hence bulk deformation, was detected the hardness/density relationships appeared to be linear within the limits of the present work. The best straight lines were determined by regression and the correlation is discussed further in section 4-2-1-4. The work-hardening rate has been expressed as d Hv/dD and these results are included on the appropriate figures.

FIGURE 4-3. Schematic representation of the linear compaction relationships.

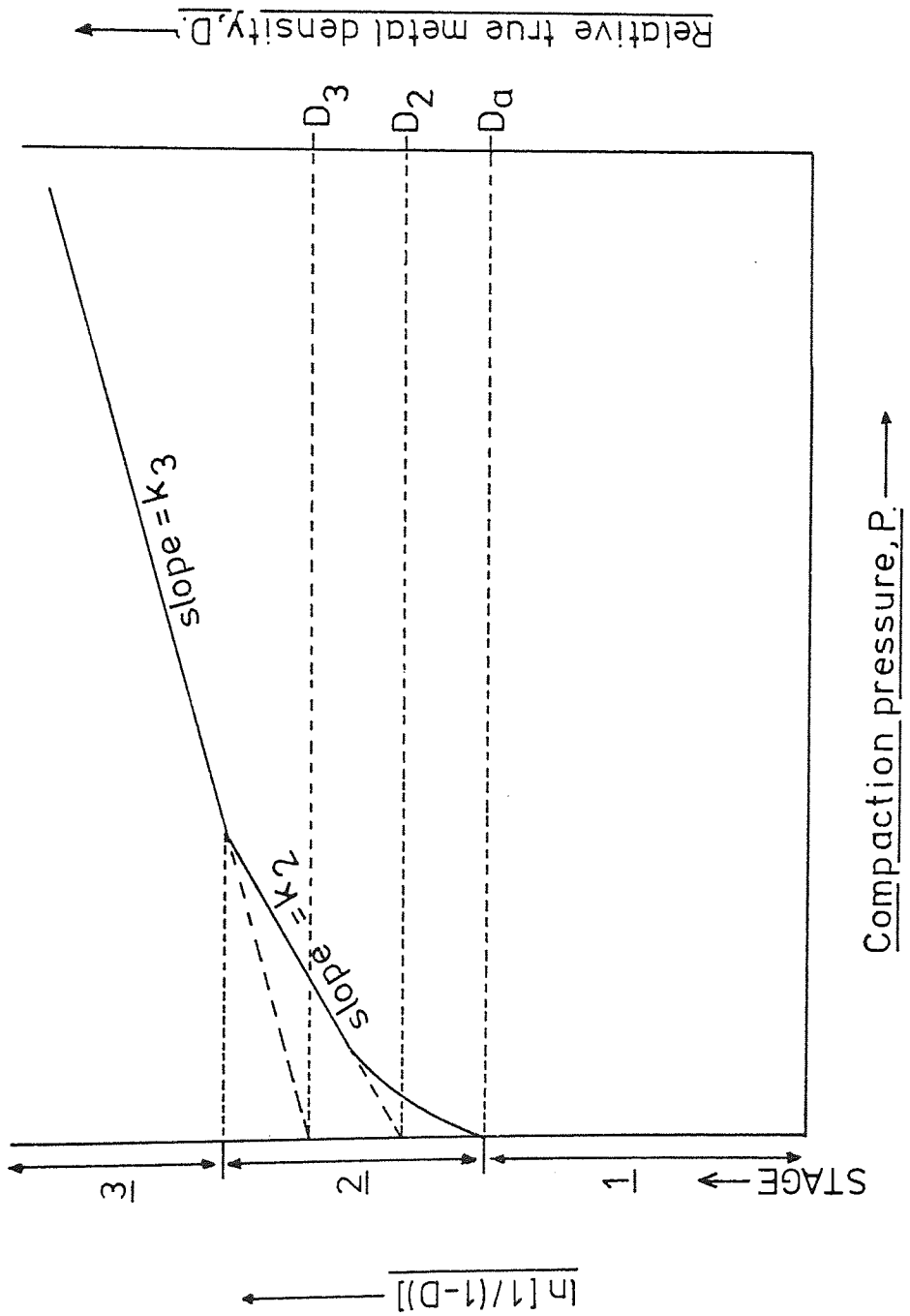

TABLE 4-1.

Densification rates (k_2 and k_3) and intercepts (D_2 and D_3) for the linear compaction relationships of figures 3-5 to 3-8.

Material	k_2 $(N.mm^{-2})^{-1} \times 10^{-3}$	D_2	k_3 $(N.mm^{-2})^{-1} \times 10^{-3}$	D_3
A	5.0	0.39	2.8	0.50
B	4.6	0.41	2.7	0.50
C	4.7	0.38	2.5	0.48
D	4.9	0.40	2.7	0.51
E	3.6	0.40	2.1	0.48
F	4.9	0.42	2.9	0.52
G	3.9	0.44	2.7	0.51
H	4.2	0.37	2.7	0.46
I	4.9	0.44	3.2	0.52
J	N/D	N/D	1.6	0.50

N/D - not determinable

Bulk plastic deformation may have occurred at lower densities than those indicated by the intersection of the lines in figures 3-9 to 3-12, or even by the more realistic curves (dashed lines). A certain degree of hardening may have been required to come within the limits of detectability of the microhardness test. However, the high rates of hardening obtained in these results would seem to suggest that the microhardness test was quite sensitive and bulk plastic deformation did initiate close to the indicated densities.

It was possible to identify the main densification mechanisms responsible for the stages observed in this work on a limited range of materials, by relating derived parameters (D and k, table 4-1) to powder properties (table 3-1) and work-hardening studies (figs.3-9 to 3-12).

4-2-1-1 Stage 1

This stage was initial die-fill, under the force of gravity only, with limits defined by D_a the apparent density of the powder. Comparison with previous investigations was difficult because other workers[19,20] often include die-fill with subsequent stages under the general description of initial packing. However Heckel[17,18] and Donachie and Burr[22] did consider die-fill to be the first stage of compaction.

In figures 3-5 to 3-8 D_a (table 3-1) has been plotted as $\ln(1/(1-D_a))$ at zero compaction pressure. This seemed to match the compaction results well when the curved regions of stage 2 were extrapolated to zero. In all cases the tapped density D_t (table 3-1) was found to exceed the first density obtained under pressure ($8 Nmm^{-2}$). Previous work[20,21] has also shown that D_t is rarely a good indication of the extent of either die-fill or initial packing except for spherical particles[20] whose shape allowed good loose packing.

4-2-1-2 Stage 2

This stage was dominated by densification by particle rearrangement

under the influence of the applied compaction pressure. The curved region of a plot of $\ln(1/(1-D))$ versus P (fig.4-3) has been attributed to particle rearrangement[17,18] and Donachie and Burr[22] also considered the second stage of compaction to be transitional restacking.

The linear portion of this stage (fig.4-3) conformed to the relationship,

$$\ln(1/(1-D)) = k_2P + \ln(1/(1-D_2)) \qquad \ldots.(4-4)$$

where k_2 is the slope or rate of densification
and D_2 is the intercept (fractional relative true metal density).

There was found to be a correlation between D_2 and loose powder packing properties (D_a and D_t) as shown in figure 4-4. As discussed in the previous section, D_t was not usually a good indication of the limit of rearrangement except for spherical powder[20]. It can be seen from figure 3-6 that D_t was a good indication of the limit of the small curved portion of the relationship obtained for material J (spherical carbonyl iron). D_t does reflect densification produced by a rearrangement process although encouraged by vibration not by the application of a unidirectional force during compaction. Therefore a relationship between D_2 and D_t would suggest that particle rearrangement did have some significance during the linear portion of stage 2.

The total densification produced in stage 2 (see figs.3-5 to 3-8) was greater than that achieved by particle rearrangement alone (D_t, table 3-1) except again for spherical powder (J). This would seem to suggest that other densification mechanisms were also operating. The close packing produced by rearrangement leads to irregular particles interlocking and forming a more rigid structure[19], interparticle contacts being mainly at asperities with correspondingly small contact areas. Therefore large

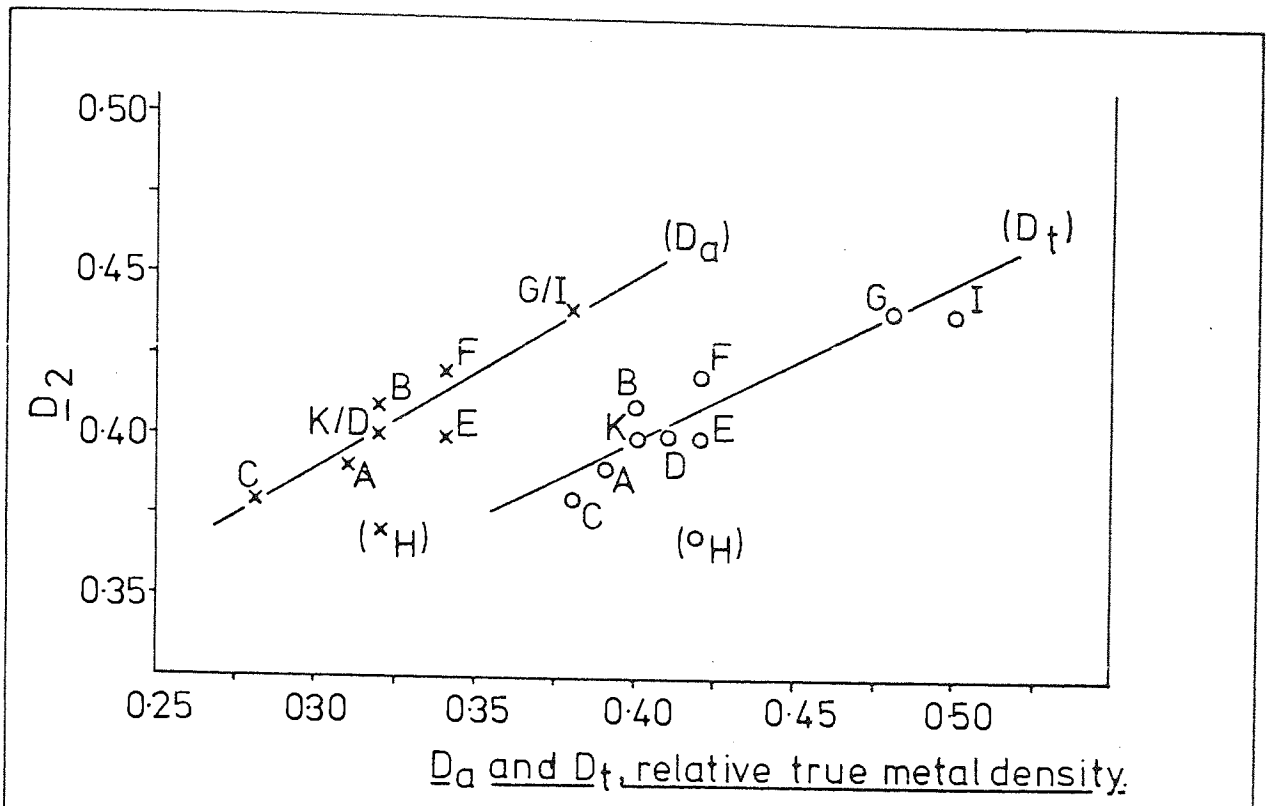

FIGURE 4-4. The relationship between D_2 and D_a and D_t.

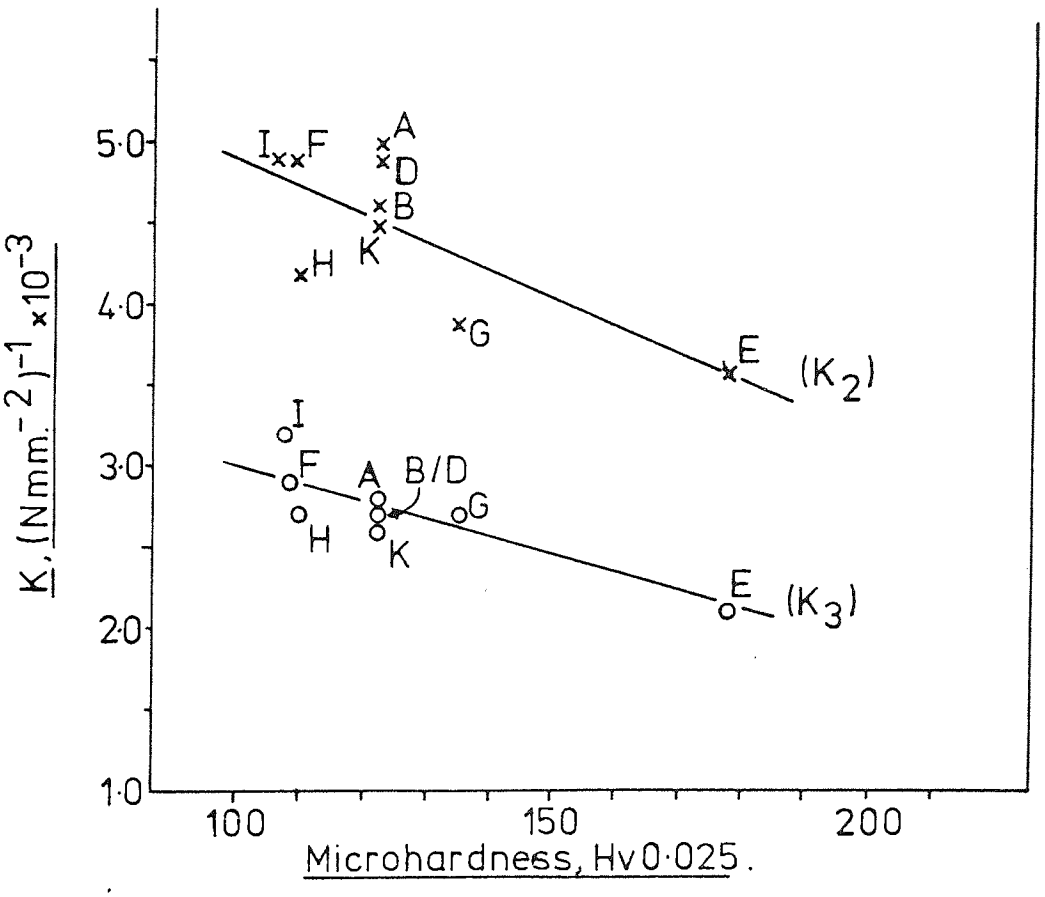

FIGURE 4-5. The relationship between initial particle microhardness and K_2 and K_3.

effective stresses may be produced at low applied pressures and cause local plastic deformation[19,20,22] in surface regions. Beddow[21] has observed also that attrition and plastic deformation during compaction must occur at an early stage.

There was an inverse relationship, shown in figure 4-5, between the rate of densification in this region (k_2, table 4-1) and the work-hardening properties of the material as indicated by initial microhardness (table 3-1). This suggested that some degree of plastic deformation did occur at this stage, and following the preceeding discussion it seems probable that this was local surface rather than bulk deformation.

The change from stage 2 to stage 3 did not correspond with the density at the onset of work-hardening. This may be illustrated by comparison of the compaction relationships for materials B, E and F (fig.3-5) and the appropriate work-hardening results (figs.3-10 and 3-11). It can be seen that the onset of work-hardening, indicated by an increase of microhardness with density, occurred at densities within the linear portion of stage 2. Therefore bulk plastic deformation apparently initiated towards the end of stage 2 but a certain degree of deformation was required before the onset of stage 3.

Overall, stage 2 appears as a complex transitional stage where densification mechanisms changed from pure rearrangement via local deformation to bulk plastic deformation. The mechanisms occurring in this stage with increasing pressure may be summarised as follows:

(a) Particle rearrangement leading to a more rigid close-packed structure.

(b) Rearrangement with attrition and local surface deformation caused by high stresses at interparticle contact points.

(c) A decrease in the role of rearrangement as particle interlocking and plastic deformation become more extensive, leading to bulk plastic deformation and eventually the onset of stage 3.

It is interesting to note that in the present work (figs.3-5 to 3-8) this stage accounted for more than 50% of the total densification of irregular powders following initial die-fill (stage 1).

The absence of the linear portion in the results of Heckel[17,18] may be related to compact geometry. He used a tensile bar die, 645mm^2 cross-sectional area and 12.5mm fill depth. The depth of fill for the cylindrical compacts used in the present work must have exceeded 30mm and hence particle rearrangement processes may have been more significant.

4-2-1-3 Stage 3

The final stage identified in this work corresponded to that observed by Heckel[17,18] where densification by bulk plastic deformation of the metal powder predominated. The rate of densification dD/dP was directly proportional to the pore volume (1-D) [17,18] and it conformed to the relationship,

$$\ln(1/(1-D)) = k_3P + \ln(1/(1-D_3)) \qquad \ldots.(4-5)$$

Brackpool[20] stressed the importance of plastic deformation by adopting a general stress-strain relationship and other workers[19,22] have accepted bulk plastic deformation as the final stage of compaction.

There was an inverse linear relationship between the rate of densification (k_3, table 4-1) and material work hardening properties (initial microhardness, table 3-1) which is shown in figure 4-5. It can be seen from figures 3-9 to 3-12 also that work hardening occurred throughout this stage. In fact there was a direct inverse relationship between the apparent work hardening rate (d Hv/dD) and the rate of densification (k_3), shown in figure 4-6. However results were limited to three points only since the microhardness/density data was difficult to determine (appendix A).

FIGURE 4-6 . The relationship between K_3 and the rate of work hardening in stage 3.

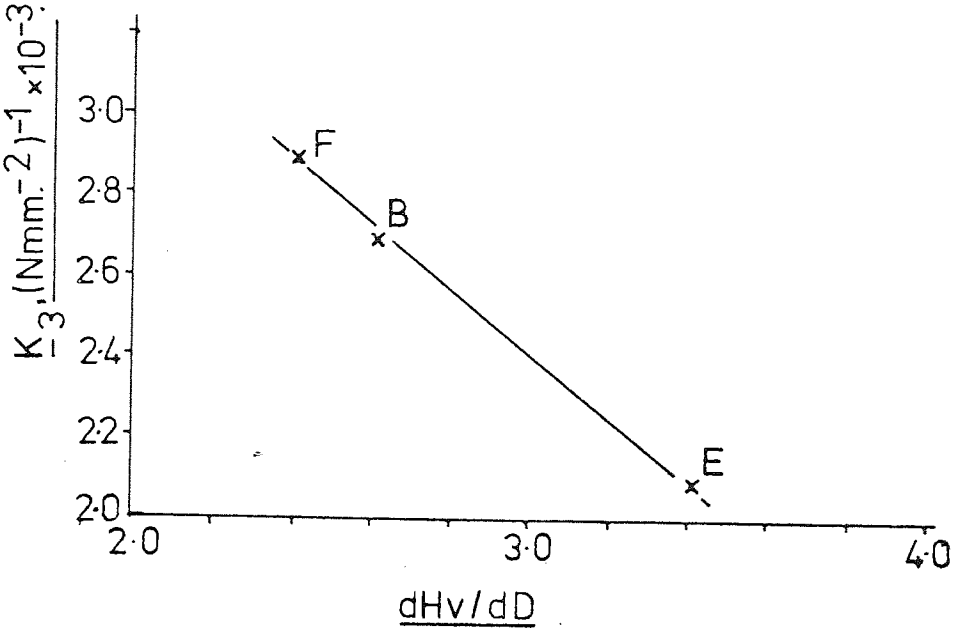

4-2-1-4 Regression analysis

Linear regression was used to determine the straight lines of best fit for the results of compaction (figs.3-5 to 3-8), work hardening (figs. 3-9 to 3-12) and the relationships between D, k and powder properties (figs.4-4 and 4-5). Correlation coefficients obtained from the experimental results were compared with tabulated values[53] to assess the significance of these relationships.

Coefficients obtained for both stages 2 and 3 of the linear compaction relationships (figs.3-5 to 3-8) were all greater than 0.996, indicating significance levels of at least 99.9%. Regression was carried out on the mean values of microhardness shown in figures 3-9 to 3-12 and the correlation coefficients indicated minimum significance levels of 99.5%.

Significance levels of 99.9% were obtained for the relationship between the intercept D_2 and loose packing properties (fig.4-4). However material H was omitted from analysis of these results, which is a point given further consideration in the following section (4-2-1-5). A significance of only 98% was obtained for the relationship between k_2 and initial microhardness (fig.4-5) compared to 99.9% for k_3 versus microhardness. This may be a further indication that densification was only partially dependent on plastic deformation during the later portion of stage 2 (4-2-1-2).

4-2-1-5 Deviations

Several deviations from the linear relationships established during the course of this work were noted. Two concerned deviations from linearity during the third stage of compaction (figs.3-5 to 3-8) and a third was concerned with the relationship between D_2 and the loose packing properties of material H (fig.4-4).

To avoid confusion only alternate points were plotted in the linear relationships, full results are recorded in tables 3-2(A) to (K). Good

correlations were obtained (4-2-1-4) but it can be seen that the points did generally follow very shallow curves during stage 3, particularly at low pressures. It was noted also that at high pressures points tended to return to linearity.

The overall true metal density of each compact was used in these relationships but it was obvious from the density distributions obtained in appendix A that there was always a density range within compacts and the compaction results only represented the mean of these. This may be illustrated by considering material B compacted to $156 Nmm^{-2}$. The average or overall density was 67.5% (table 3-2(B)) but the density within such a compact ranged from 58% to 78% (fig.A-3). The appropriate compaction relationship for material B is shown in figure 3-5 and by referring to the relative density axis (D) it can be seen that in this compact low density regions were still within stage 2 whilst denser regions were undergoing deformation corresponding to stage 3. The rate of densification in stage 2 (k_2) was higher than that of stage 3 (k_3, table 4-1) so that, even without considering pressure transmission throughout compacts, different regions would be experiencing varying densification rates as the compact moved from stage 2 to stage 3. When the region of lowest density was within the third stage the whole compact would experience the same densification rate and the pressure/density relationship would return to normal linearity.

It is also extremely unlikely that there was a sudden change from one densification mechanism to another within a particular region. It has been shown that several mechanisms were involved in stage 2 and it is possible that several occurred during the third stage even though bulk plastic deformation predominated. Bulk deformation may have allowed some further rearrangement particularly at lower densities and pressures and thus produced a temporarily higher densification rate. Where particle

rearrangement was not a significant densification mechanism, as with spherical particles[17,18], an excellent linear relationship was obtained during stage 3 (material J, fig.3-6).

Particle/die-wall friction caused considerable deviation from linearity as can be seen in figure 3-8. During stage 2 the results obtained with no die-wall lubrication (K) were equivalent to those obtained with lubrication (B). When bulk plastic deformation was established during the later part of stage 2 friction inhibited densification by preventing slip at the die-wall. The effect obviously worsened as density or pressure increased.

The results of D_2 versus D_a and D_t shown for material H (NC100) in figure 4-4 were deliberately omitted from regression because they deviated markedly from the other results. Determinations of D_a and D_t were repeated and another compact formed to check D_2. All were similar to the original results.

This material was notable in having the highest total oxygen content at 0.49% (materials section, table 4-1). Heckel[17] has observed that the presence of oxides may reduce the rate of densification of metal powders. The values of k_2 and k_3 obtained for this material were slightly low (fig. 4-5) but this did not explain the anomalous loose packing behaviour (fig. 4-4).

Hausner[14] has observed that the presence of a surface oxide film reduces interparticle friction and improves densification during loose packing. If material H did have a thick surface oxide film then it is possible that this may have improved D_a and D_t resulting in the deviations of figure 4-4.

The behaviour of material H did serve to emphasise the limited applicability of the linear relationship applied to this compaction procedure.

4-2-1-6 The effect of material variation

Variation of powder material, or more precisely work hardening properties, markedly influenced the rate of densification (fig.3-5) which was observed by Heckel[17,18] also. As initial particle microhardness increased the values of both k_2 and k_3 decreased (fig.4-5).

The ease with which deformation could occur in the annealed material (F) increased the extent of densification by rearrangement during stage 2 by allowing considerable local deformation to occur. During stage 3 the low work hardening rate (fig.3-11) resulted in more bulk plastic deformation for a given applied pressure. Consequently this material had the highest overall densification rate (fig.3-5).

4-2-1-7 The effect of particle morphology

For constant particle shape the degree of densification in terms of both D and k decreased with decreasing particle size, which is illustrated by comparison of materials A and C (MP32 104-180μm and -53μm respectively) in figure 3-6. The values of D_a in table 3-1 indicate that loose packing was marginally poorer for the fine powder. Densification in both stages 2 and 3 reduced as particle size decreased and this may be attributable to the relatively high number of interparticle contact points,which produced a more rigid structure. However,the change in densification rate produced by varying particle size was small compared to that produced by material variation (fig.3-5). In addition the possibility of effects caused by varying particle size distribution was not considered, although Heckel[17,18] did observe that this had little effect on either D or k.

The results obtained from compaction of material J (carbonyl powder) illustrate the effect of a change from irregular to spherical particle shape. Spherical powders pack well initially (D_t, table 3-1), there were few asperities on the particles (plate 4-1j, materials section) and con-

sequently there was very little opportunity for densification by rearrangement under pressure[17,18]. Stage 2 was almost completely absent for this material (fig.3-6) and after initial die-fill further densification was mainly by bulk plastic deformation.

The good linearity obtained with this material supported the suggestion that particle rearrangement was one of the causes of deviation from linearity during stage 3 (4-2-1-5).

4-2-1-8 The effect of lubricant

Examples of linear pressure/density relationships for compacts containing lubricant are shown in figure 3-13. There was little obvious influence on parameters such as D and k attributable to the presence of lubricant and this has also been observed elsewhere[18]. Other variables discussed in previous sections (4-2-1-6 and 4-2-1-7) had greater effects. During stage 3 high lubricant additions (2% fig.3-13) caused marked deviations from linearity due to inhibition (4-2-2-2) and consequently there was a lower overall degree of densification of the metal.

Equation 4-3 indicates the degree of densification of the metal within a compact by utilising true metal density D. When no internal lubricant is present the overall density of a compact and its true metal density are equal. When lubricant is added to the system, other than to the die-wall, its compaction must be considered also.

The origins of equation 4-3 lie in the assumption that during the bulk plastic deformation of particles the rate of change of density with pressure (dD/dP) is proportional to the void fraction of the compact (1-D) [17,18], equation 4-6.

$$dD/dP \propto (1-D) \qquad \ldots.(4-6)$$

Voidage is the volume of a compact not occupied by metal, when lubricant is present it is the volume occupied by neither metal nor

lubricant[24,25]. Therefore the void fraction of compacts containing lubricant is not given by (1-D) but by ($1-D^*$) where D^* is the overall fractional relative density of the compact. Equation 4-3 becomes,

$$\ln(1/(1-D^*)) = kP + A \qquad \ldots.(4-7)$$

Values of $\ln(1/(1-D^*))$ are recorded in table 4-2 for die-wall lubricated compacts containing various additions of precipitated zinc stearate. Actual compact densities (D^* g cm^{-3}) have been taken from tables 3-3(A) to (K).

The determination of relative densities was made possible by first calculating the theoretical solid densities of compacts containing lubricants. This was achieved by assuming densities of 7.87 and 1.05 g cm^{-3} (materials section) for iron and zinc stearate respectively and by using the simple calculation shown in equation 4-8.

$$\text{Theoretical solid density (g cm}^{-3}) = (V_M x D_M) + (V_L x D_L) \qquad \ldots.(4-8)$$

where V_M and V_L are the volume fractions of metal and lubricant, and D_M and D_L are the densities of metal and lubricant respectively.

True volume percentages of lubricant have been used (see materials section) and the resultant theoretical solid densities are recorded in table 4-3.

The data of table 4-2 have been plotted in figure 4-7 and it can be seen that when overall compact densities were considered there was greater variation in rates of densification. Good linear relationships were obtained for additions up to 1% with the densification rate in each stage increasing with increasing lubricant content.

Additions in excess of 1% were characterised by non-linear relationships where the rate of densification (k) increased with applied

TABLE 4-2.

Values of $\ln(1/(1-D^*))$ for compacts containing precipitated zinc stearate, die-wall lubricated.

Compaction pressure Nmm^{-2}	$\ln(1/(1-D^*))$					
	0%	0.02%	0.20%	1.0%	2.0%	4.0%
8	0.544	0.560	0.570	0.648	0.743	0.900
16	0.588	0.620	0.644	0.713	0.821	1.019
23	0.634	0.663	0.691	0.765	0.880	1.121
31	0.683	0.709	0.739	0.819	0.947	1.221
39	0.725	0.754	0.783	0.867	1.006	1.324
47	0.751	0.781	0.809	0.900	1.056	1.386
54	0.796	0.824	0.856	0.949	1.118	1.500
62	0.832	0.865	0.893	0.993	1.169	1.593
70	0.863	0.896	0.928	1.038	1.224	1.688
78	0.893	0.924	0.958	1.074	1.275	1.772
93	0.946	0.977	1.013	1.140	1.359	1.937
109	0.990	1.022	1.061	1.198	1.431	2.079
124	1.048	1.084	1.126	1.273	1.536	2.322
140	1.098	1.134	1.179	1.339	1.623	2.525
156	1.140	1.178	1.227	1.393	1.701	2.748
171	1.185	1.221	1.271	1.450	1.786	2.956
187	1.228	1.265	1.314	1.510	1.879	3.244
202	1.278	1.316	1.368	1.574	1.971	3.650
218	1.319	1.359	1.415	1.636	2.072	4.200
249	1.398	1.442	1.503	1.740	2.211	5.521
280	1.483	1.526	1.594	1.865	2.422	-
311	1.561	1.612	1.681	1.988	2.606	-
342	1.643	1.691	1.767	2.104	2.807	-
373	1.712	1.763	1.838	2.211	3.026	-
404	1.788	1.824	1.922	2.317	3.268	-
436	1.864	1.906	2.005	2.435	3.438	-
467	1.926	1.968	2.064	2.552	3.644	-

FIGURE 4-7. ln[1/(1-D*)] for compacts containing precipitated zinc stearate.
(die-wall lubricated)
(Alternate points plotted only)

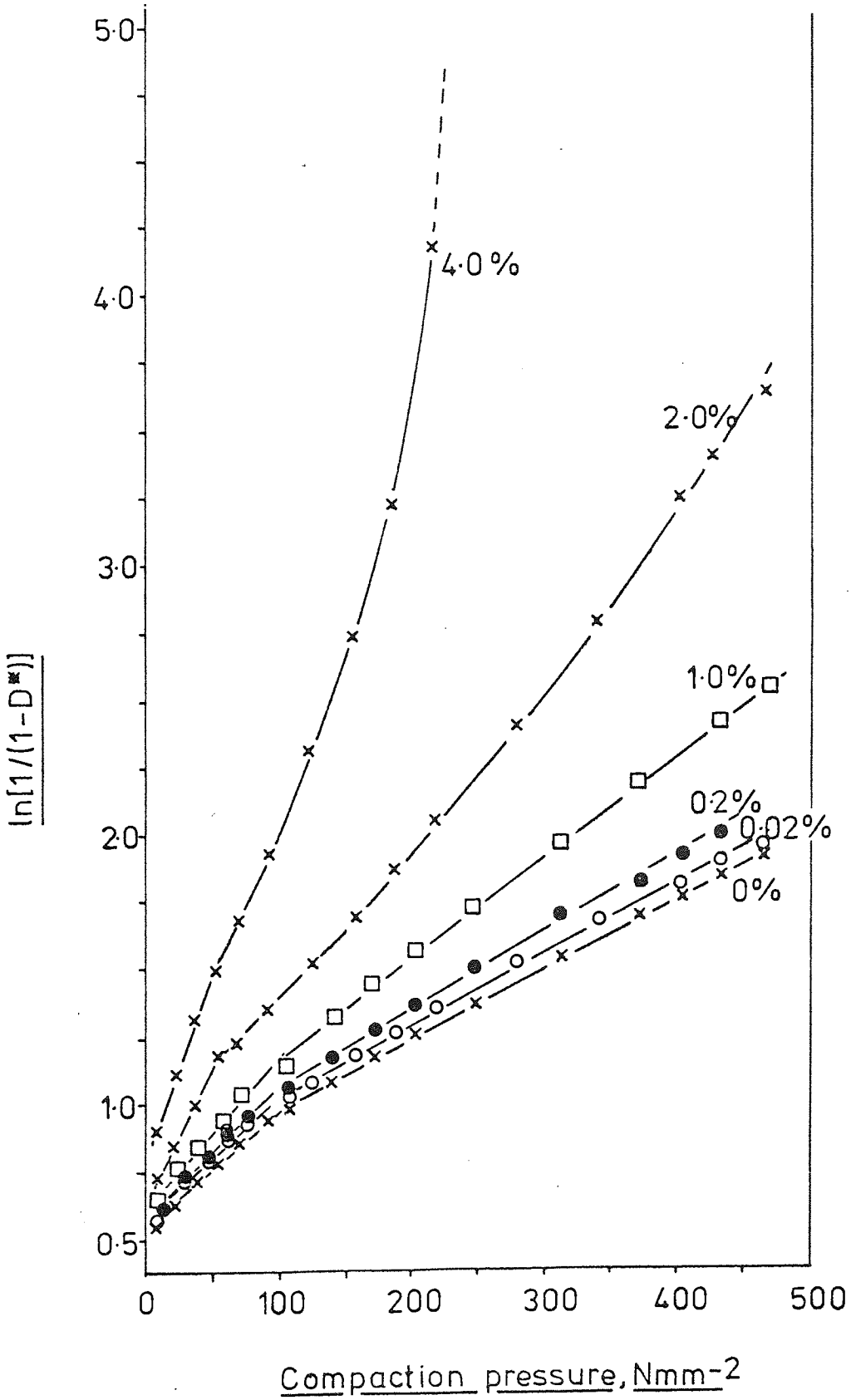

Table 4-3

Theoretical solid densities for compacts containing precipitated zinc stearate

Nominal lubricant content % by weight	Actual lubricant content		Theoretical solid density g cm^{-3}
	% by weight	% by volume	
0.2	0.2	1.5	7.77
0.5	0.5	3.8	7.61
1.0	1.0	7.5	7.35
2.0	2.0	15.0	6.85
3.0	2.9	21.8	6.38
4.0	3.8	28.4	5.94

pressure (P) (fig.4-7). This was attributed to compaction inhibition by the lubricant (section 4-2-2). Preferential extrusion of lubricant into pores inhibited densification of the metal powder, as illustrated by considering true metal density (fig.3-13), but the rapid filling of pores with lubricant produced a rapid increase in the actual or overall density of the compact (fig.4-7).

No values of $\ln(1/(1-D^*))$ were recorded for the 4% addition beyond an applied pressure of 249 Nmm^{-2} (table 4-2). Comparison of the actual densities (D^* g cm^{-3}) given in table 3-3(K) with the theoretical solid density of a compact containing 4% lubricant (table 4-3) shows that at high pressures actual densities apparently exceeded theoretical solid. The final relative density was 1.04 or 104% and as relative density (D^*) approached unity, $\ln(1/(1-D^*))$ approached infinity, beyond this the values had no meaning.

If a higher density was used for the zinc stearate, such as 1.10g

cm^{-3} (11), the theoretical solid density increased to 6.03g cm^{-3} but the final relative density of a compact containing 4% lubricant was still 102%. The solid density could be exceeded if lubricant was removed from the compact, perhaps by exuding zinc stearate onto the external surface of a compact and into the compact/forming tool interface. This is given further consideration in section 4-2-3.

The relationships between $\ln(1/(1-D^*))$ and compaction pressure (fig. 4-7) have provided some indication of the effect of lubricant on the overall density of compacts. Unfortunately this did not illustrate their effect on the compaction behaviour of the metal within those compacts. The more conventional approaches discussed in the following sections were found to be of greater value.

The true metal density compaction relationships of figure 3-13 did show that the densification mechanisms experienced by the metal powder (discussed in section 4-2-1) still occurred in the presence of lubricant. However they also illustrated the limited applicability of the linear relationship (equation 4-3).

4-2-2 Interparticle friction and compaction inhibition

Two of the forms of friction which occur during the closed die compaction (2-2-3) of a metal powder are,

(a) friction between metal particles,

(b) friction between metal particles and the die-wall.

In this investigation die-wall friction was eliminated by considering only compacts pressed with die-wall lubrication (table 3-3).

The lubricant effect ΔL was the parameter employed to study interparticle friction and inhibition. This has been defined (2-2-3-1) as the difference between the compaction pressures required to achieve a given density in unlubricated and lubricated powders. It has been based on relationships between true metal density and pressure (fig.3-14) and

hence reflects the influence of lubricant on densification of the metal, not on the overall density of compacts. A positive value of ΔL indicated that beneficial lubrication effects occurred, the presence of internal lubricant improving densification relative to the unlubricated state. A negative value indicated inhibition by preferential extrusion into pores at the expense of metal.

ΔL is shown as a function of compaction pressure (unlubricated) in figure 3-15 for die-wall lubricated compacts containing precipitated zinc stearate.

4-2-2-1 Interparticle friction

ΔL was positive at low compaction pressures and lubricant contents less than 1.0% (fig.3-15). It also increased with increasing lubricant content up to a maximum for an addition of 0.5%. Additions above 0.1% were characterised by an optimum ΔL at an intermediate pressure beyond which ΔL decreased as the applied pressure increased.

As the precipitated lubricant content increased, the coverage, lubricant film thickness and proportion of free lubricant increased (section 4-1-2) such that interparticle friction was reduced. The opposing effect of compaction inhibition (4-2-2-2) became more noticeable as lubricant content increased and the presence of free lubricant became more significant (4-1-1). The maximum positive ΔL was approximately $23 Nmm^{-2}$ for a compact containing 0.5% lubricant pressed to $300 Nmm^{-2}$, beyond this pressure ΔL decreased due to compaction inhibition as discussed above. It is interesting to note that the optimum addition for reducing interparticle friction during compaction was greater than those observed for loose packing (fig.3-1). The presence of a small proportion of free lubricant in addition to the increased thickness of coatings may have played a beneficial role. This probably reflected the more arduous service conditions experienced by the lubricant as interparticle contact

area increased with increasing pressure and density.

The conditions of lubrication within compacts containing increasing proportions of lubricant were determined by a compromise between reduction of interparticle friction, due to increasing coating thickness and the presence of free lubricant, and the opposing effect of inhibition caused by the presence of increasing proportions of free lubricant which became more significant as pore space diminished with increasing density. It can be seen from figure 3-15 that the lubrication effects (positive ΔL) were small compared with the influence of compaction inhibition (negative ΔL).

4-2-2-2 Compaction inhibition

Compaction inhibition is caused by the preferential extrusion of lubricant into pores at the expense of metal[24,25]. The overall density of a compact increases as lubricant fills more of the available pore space but the presence of lubricant restricts densification of the metal, consequently true metal density does not increase as rapidly as overall density. Compaction would be expected to cease effectively when the volume of space was equal to the volume of lubricant present. Obviously this consideration does not take into account elastic deformation, entrapped air or the removal of lubricant from within the compact, perhaps by exudation into the compact/forming tool interface (4-2-3).

The degree of inhibition can be estimated by calculating the transition pressure P_T [24,25], which is the compaction pressure where conditions change from lubrication to inhibition and ΔL is zero (fig.3-15). The principles have been outlined in section 2-2-3-1. Values of P_T for die-wall lubricated compacts containing precipitated zinc stearate are presented as a function of lubricant content in figure 3-16.

In terms of the lubricant effect ΔL (fig.3-15b) inhibition increased markedly with lubricant content, which was also observed elsewhere

(24,25). This was reflected by decreasing transition pressures as the lubricant content increased (fig.3-16).

It was possible to calculate the volume of pore space within compacts at the transition pressure by simply finding the true metal density corresponding to P_T from the compaction curves of figure 3-14 or the data of table 3-3. True volumes of lubricant have been recorded in table 4-3 and the relationship between the volumes of pore space at P_T and of lubricant is shown in figure 4-8. It was assumed that when no lubricant was present (other than die-wall) there would be no inhibition and so the curve must pass through the origin. It can be seen from figure 4-8 that the pore space was not completely filled with lubricant at P_T but the difference between the pore and lubricant volumes decreased as the lubricant content increased. This difference may have been caused by air entrapped within pores by lubricant, densification proceeding by plastic deformation of the iron powder and zinc stearate and by compression of this air.

Densification did not cease with the onset of inhibition and it has been noted previously that final overall densities apparently exceeded 100% at the highest lubricant contents of 3% and 4% (4-2-1-8). This is shown more clearly in figure 4-9 which is the relationship between compaction pressure and the overall relative density (not true metal density) of die-wall lubricated compacts containing 2%, 3% and 4% precipitated zinc stearate. Values of overall density D^* g cm^{-3} are recorded in table 3-3 and theoretical solid densities in table 4-3. Overall relative densities could exceed 100% only if lubricant were removed from within compacts. It was suggested previously (4-2-1-8) that lubricant could be exuded into the compact/tool interface and this would be further encouraged by entrapped air reducing the available pore space. The formation of a lubricant film in the compact/tool interface will be discussed in greater detail in the following section (4-2-3).

FIGURE 4-8. Lubricant volume versus pore volume at the transition pressure, P_T.

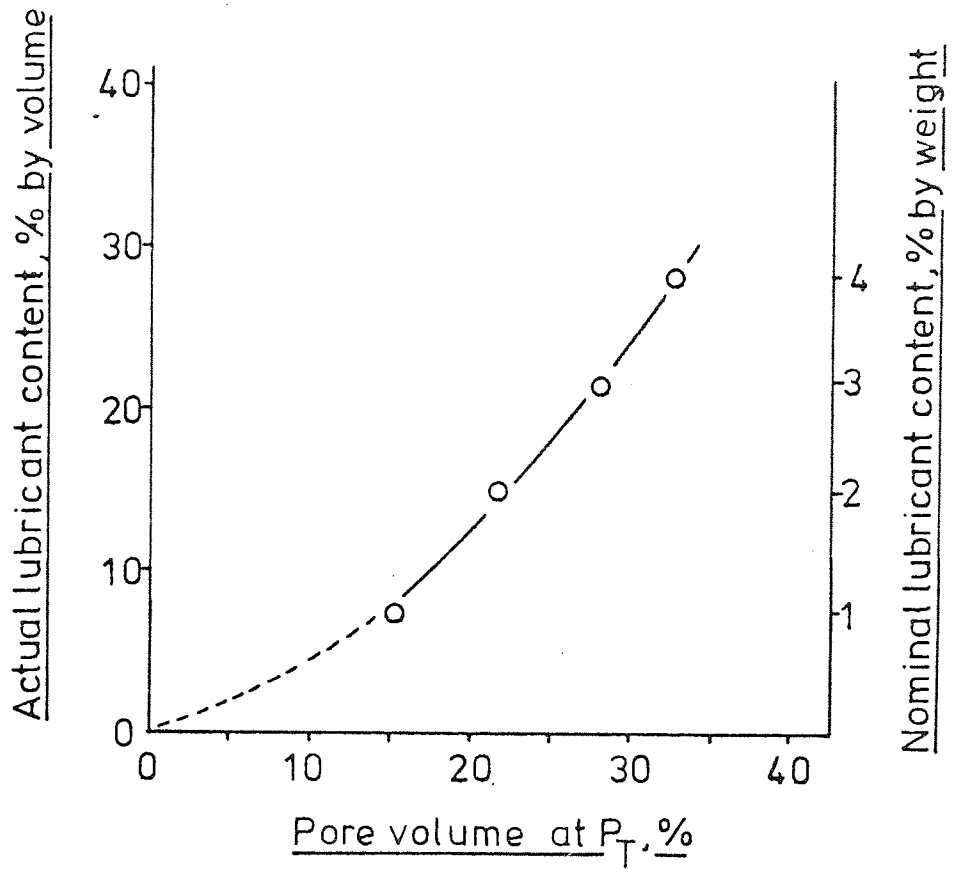

FIGURE 4-9. Overall relative density versus compaction pressure for compacts containing precipitated zinc stearate – die-wall lubricated.

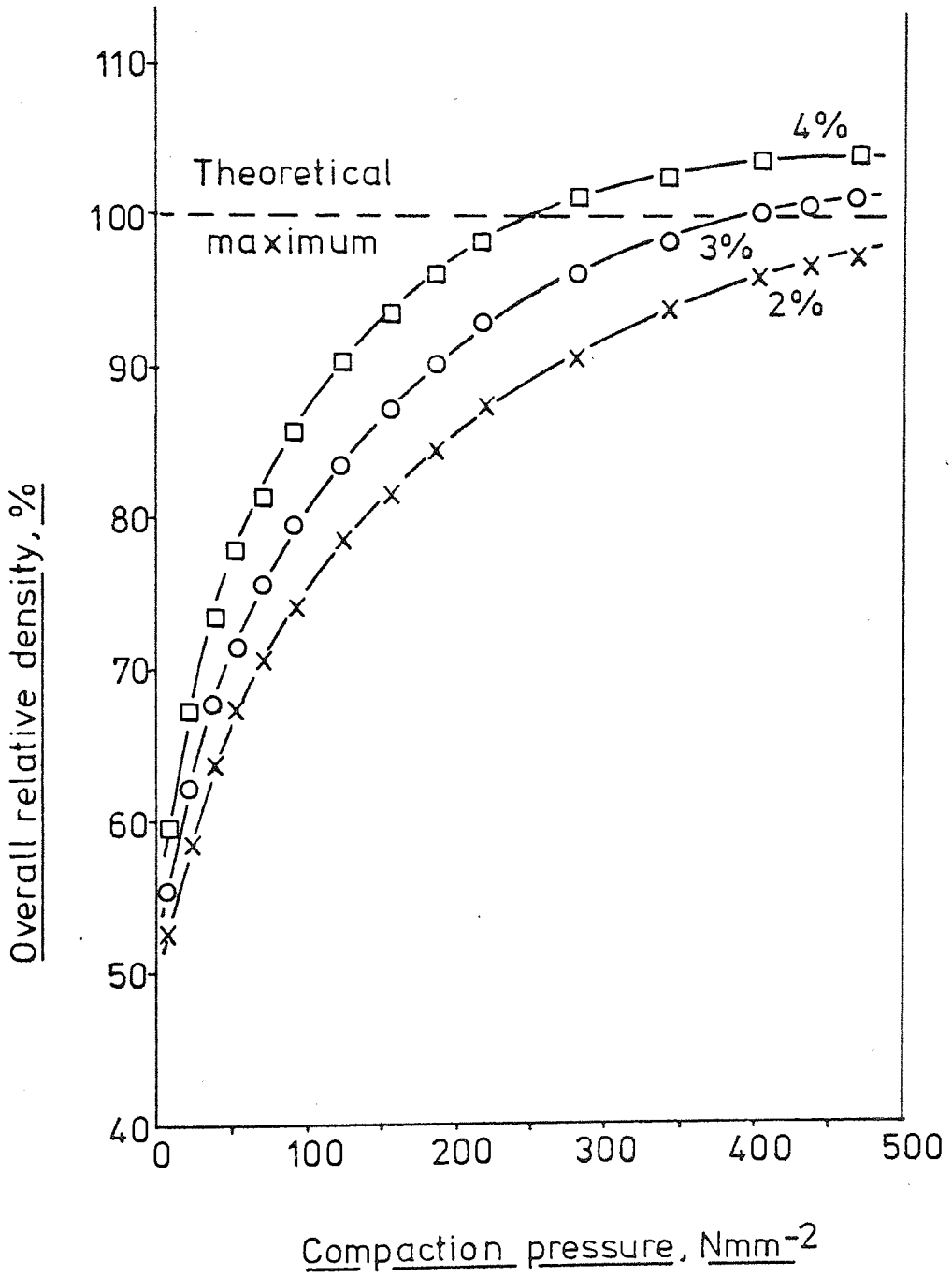

A further consideration in the removal of lubricant could be the density distribution within compacts. It has been shown in appendix A that with die-wall lubrication densification was greatest on the circumference of compacts, particularly at corners, and lowest in the centre. The result is a density gradient decreasing or a porosity gradient increasing from the corners to the centre and this may have encouraged lubricant to move from outer regions of a compact towards the centre as densification proceeded. This would discourage exudation onto the external surface, especially during the later stages of compaction when pore size was restricted also. However it is not clear whether exudation occurred during later stages, or perhaps at pressures lower than P_T since the force exerted by the die on the compact must be overcome in order to form a film.

The density is not uniform throughout a uniaxially pressed compact and P_T will be merely an indication of the pressure or density where more than 50% of a compact is experiencing inhibition. Corner regions which densify rapidly probably would have undergone inhibition at an early stage and much of the exuded lubricant may have come from these areas at compaction pressures lower than the mean values of P_T (fig.3-16).

In this work the presence of a film of die-wall lubricant could have restricted the removal of internal lubricant and this is given further consideration in the next section also.

4-2-3 Particle/die-wall friction

Opinions on the relative significance of particle/die-wall friction are divided. It has been cited[12] as a primary cause of pressure losses during compaction, but Ljungberg and Arbstedt[1] regarded die-wall friction as insignificant due to the extremely short movement of particles relative to the die.

The cylindrical compacts used in this investigation typically changed

length from approximately 29mm to 14mm during compaction. Floating die compaction (2-2-1) should effectively produce double end compression so that particles at the extremities of compacts would move furthest, approximately 7mm. Particles lying midway between compact ends would not be expected to move significantly. These differences in relative movement could be at least partly responsible for variations in true metal density along the compact/die contact area, particularly in the absence of lubricant.

In appendix A it was shown that in the absence of lubrication the formation of low density areas around the circumference of compacts, due to particle/die-wall friction, were entirely responsible for reducing density relative to the lubricated condition. It is possible that the relative significance of particle/die-wall friction depends largely upon compact geometry, interparticle friction being more significant in compacts with a low surface area to volume ratio.

In the present work pressure losses due to particle/die-wall friction were isolated by comparing compacts with and without die-wall lubrication but of equal lubricant contents. The procedure has been outlined in section 2-2-3-2. Pressure losses were recorded as a function of the applied pressure, f(P). Comparative pressure/density curves for compacts containing precipitated zinc stearate are shown in figures 3-17 to 3-22. Values of f(P) determined from these curves have been plotted against applied pressure P in the same figures. Linear relationships between f(P) and P were obtained and the slopes (df(P)/dP) of these are recorded as a function of lubricant content in figure 4-10. Absolute values of f(P) were generally larger than those of ΔL for lubrication shown in figure 3-15. This suggests that particle/die-wall friction had more significance than interparticle friction with this compact geometry.

It can be seen from figure 4-10 that large proportions of internal

FIGURE 4-10. df(P)/dP as a function of lubricant content for compacts containing precipitated zinc stearate.

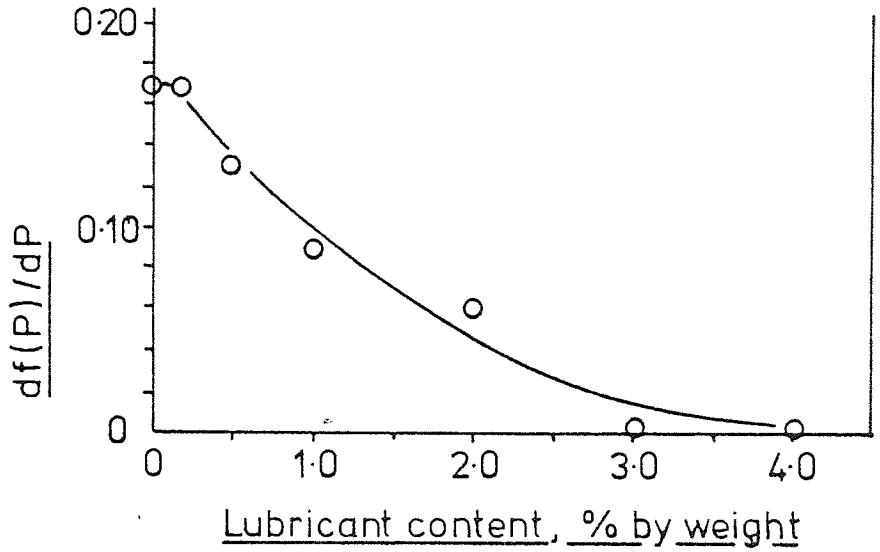

lubricant were required to reduce die-wall friction to the same level as with die-wall lubrication. Compacts become shorter as compaction proceeds, the total compact/die-wall contact area decreases and consequently the concentration of die-wall lubricant within the interface would increase. As the applied force increases the force transmitted to particles in contact with the die increases and attempts to remove lubricant from within the contact points. However, die-wall lubricant can probably only easily enter pores in the surface of compacts during the early stages of compaction since densification proceeds from the surface towards the compact centre (appendix A). In the surface, pore size will become restricted rapidly, limiting the removal of lubricant from the compact/die-wall interface. Lubricant picked up from the die onto a compact surface can be seen in plate 3-5 (compact pressed to $47 Nmm^{-2}$).

It has been suggested (4-1-1) that during the precipitation of up to 0.5% zinc stearate onto the iron powder, lubricant was deposited in cavities and internal porosity such that over a wide range of additions coating thickness did not alter appreciably. Thick surface films and significant quantities of free lubricant formed only at high contents. In the absence of die-wall lubrication, the majority of lubricant trapped between particles and the die-wall for small additions would be the coating adhered to the particles, and these have been shown to be thin (4-1-1-2).

To reduce friction in the absence of die-wall lubricant free lubricant and lubricant adhered to particles not at the interface must be moved through pores and forced into particle/die-wall contacts. Unfortunately the density distribution in such compacts (appendix A) did not favour movement of internal lubricant towards the die, except perhaps from areas in close proximity to the surface. The results shown in figure 4-10 did seem to suggest that there was a connection between compaction

inhibition (4-2-2-2) and the reduction of f(P). It would seem that densification encourages the retention of die-wall lubricant in the compact/die interface to reduce friction,but discourages the formation of an external film from internal lubricant.

Final overall densities in excess of 100% were obtained for compacts containing more than 2% zinc stearate (fig.4-9) and it was suggested in previous sections that this was made possible by forcing lubricant from within compacts into the compact/forming tool interface. With the method used (2-2-1) such a surface film would not have caused a detectable volume change during compaction since it would remain trapped within the die-cavity. However densities were determined by relating compact lengths at intermediate pressures to that of the final ejected compact. This final length was measured directly with a micrometer and it is quite possible that this penetrated the thin lubricant film,or perhaps the film was already penetrated by asperities. The following calculation will show that such a film could be thin even at a high lubricant content.

The final overall density for a compact containing 4% lubricant was apparently 104% (fig.4-9). It was possible to calculate the theoretical coating thickness by assuming that the excess 4% was accounted for by an external lubricant film and entrapped air did not force more lubricant out of the compact. An ejected compact of 60g weight pressed to $467 Nmm^{-2}$ was approximately 14mm long and 28.6mm in diameter giving a total surface area of $2.55 \times 10^{3} mm^{2}$. 4% of zinc stearate by volume in such a compact would have a total volume of $340 mm^{3}$ and therefore would produce an external film approximately 130μm (1.3×10^{-1}mm) thick. This would represent an average thickness since the presence of pores has been ignored. Electrical resistivity measurements made by Mallender et al[29] have shown that there are also considerable metal/metal contacts between forming tools and metal powders even with high lubricant contents.

There was also no indication of when such a film would be produced. It could form at an early stage of compaction when movement through pores was still relatively easy, during later stages when inhibition became significant or perhaps progressively as densification proceeded.

It is tempting to consider the values obtained for $df(P)/dP$ as coefficients of friction for the iron particles in contact with the steel die. They were obtained under the dynamic conditions of continuous compaction (2-2-1) and hence would be representative of sliding friction. The compaction pressure P was calculated as the applied load divided by A_p, the cross-sectional area perpendicular to the pressing direction. If it was assumed that there was 100% transmission of force through compacts then the force W acting on the sliding area was $P \times A_p$. $f(P)$ was the proportion of the applied pressure required to slide particle/die-wall contacts. As a function of the applied pressure this was also determined on the pressing area, hence the force F required to slide particle/die-wall contacts was $f(P) \times A_p$. The coefficient of friction μ is given by F/W [32] which was equal to $(f(P) \times A_p)/(P \times A_p)$, or $f(P)/P$ in this work. Therefore the slope $df(P)/dP$ satisfied the requirements for a coefficient of friction.

In dry friction (no lubricant) the force to slide or shear contact points is determined by equation 4-9 [32]

$$F = As \qquad \ldots.(4\text{-}9)$$

where A is the real contact area

and s is the shear strength of the junctions

Surfaces are generally rough, touching at asperities only [27,32] and with metals where contact regions flow plastically the real contact area A is defined by equation 4-10 [32].

$$A = W/p \qquad \ldots.(4\text{-}10)$$

where W is the load and p the yield stress or hardness.

The contact area increases with the applied load W (equation 4-10) and consequently the frictional force F increases proportionately (equation 4-9). Therefore the coefficient of dry friction should show no dependence on load. This was obtained for df(P)/dP when no lubricant was present (fig.3-17).

When lubricant is present there are two components to the total frictional force[27]. F_1 is the force required to shear the metal/metal contacts which exist even with high levels of lubricant[29]. F_2 is the force required to slide contacts which have a film of lubricant between. The coefficient of friction is now given by equation 4-11 [27].

$$\mu = (F_1 + F_2)/W \qquad \ldots.(4\text{-}11)$$

Increasing the lubricant content decreases the proportion of the load carried by metal/metal contacts, the contribution of F_1 is reduced and consequently μ decreases. df(P)/dP also decreased with increasing lubricant content (fig.4-10).

Increasing the load should increase the contribution of F_1, due to greater perforation of the lubricant film and the consequent increase in metal/metal contacts[27], therefore μ should increase with increasing load. When internal lubricant was present df(P)/dP did not vary with the applied load (figs.3-18 to 3-22). This may be explained by considering the movement of lubricant out of compacts and into the compact/die interface. As the applied load increased the true contact area increased but more lubricant would have been forced from the compact producing a balance between the total areas of lubricated and unlubricated contacts. Consequently df(P)/dP was not dependent on P.

Unfortunately the values of df(P)/dP obtained in this work were much lower than coefficients of friction observed elsewhere. Mallender et al[27] obtained coefficients of sliding friction ranging from 1.14 with

no lubrication to 0.045 for fully lubricated conditions (>2.0%) by ejecting reduced iron powder compacts from steel dies. In the present work it was assumed that the application of lubricant directly to the die-wall eliminated particle/die-wall friction during compaction. This assumption was probably false since even the presence of large quantities of lubricant do not prevent considerable metal/metal contacts occurring either between the die and particles[29] or between the metal particles themselves[25]. Complete elimination of friction by die-wall lubrication would have increased f(P) particularly at high applied pressures.

It was also assumed that the force acting on the friction interface was equal to the applied force, no consideration being given to pressure transmission through compacts. It is unlikely that 100% transmission occurred and therefore P should be replaced by smaller values of effective pressure, increasing values of df(P)/dP.

These results (fig.4-10) have shown that with this compaction method and compact geometry particle/die-wall friction was significant. For commercial lubricant contents of 0.5% to 1.0% the effective compaction pressure was reduced to 87% and 91% of the applied pressure due to this form of friction alone. More complex commercial shapes of similar pressing areas ($645mm^2$) would have much higher compact/die contact areas than the simple cylinders used in this investigation. df(P)/dP would increase and effective compaction pressures decrease proportionately and consequently there would be an increase in energy expenditure during forming. The high levels of internal lubricant required to reduce die-wall friction to the same level as lubricant applied directly to the tools are associated with problems of inhibition (4-2-2-2) therefore die-wall lubrication seems the most promising for optimising energy expenditure during compaction.

4-2-4 The compaction of powders containing admixed lubricant

4-2-4-1 The effect of mixing

It has been noted previously (2-2-3-3) that benzene, the solvent used during precipitation of zinc stearate, had no effect on the compaction behaviour of the iron powder (fig.3-23).

There was a slight reduction in the compressibility of the unlubricated iron powder attributable to mixing. This is illustrated by comparing the pressure/density curves shown in figure 3-23 for powder washed in benzene and powder mixed for 1 hour at 38r.p.m (no die-wall lubrication). There was an improvement in the loose packing of unlubricated powder as mixing proceeded (4-1-2-2) and this was attributed to some degree of attrition during mixing. However, under pressure (fig.3-23) densification was marginally lower than unmixed powder. During mixing attrition may result in a slight reduction in particle size,and densification rate has been shown to reduce with decreasing particle size (4-2-1-7). However, a considerable size difference was necessary to produce a significant change in compaction behaviour.

The influence of mix duration on the compaction behaviour of powders containing lubricant is illustrated by the results shown in figure 3-24, complete results are recorded in tables 3-5(H) and 3-6. The effect of mixing was slight again but compacted densities did improve with increasing mix duration. This may have been caused by the improved loose packing properties associated with mixing or by the decrease of free lubricant as mixing proceeded (4-1-2-2).

4-2-4-2 Comparison of powders containing admixed and precipitated zinc stearate.

Examples of comparative pressure/density relationships are shown in figures 3-25 to 3-27 and complete results are recorded in tables 3-4 and

3-5, no die-wall lubrication was used. The difference in compaction behaviour obtained with the two types of coating was very small, barely greater than that expected from experimental scatter (fig.2-6). However some interesting points arose from consideration of the density differences at given compaction pressures. These have been expressed as ΔD which is defined in equation 4-12.

$$\Delta D = D(\text{precipitated}) - D(\text{admixed}) \qquad \ldots.(4\text{-}12)$$

where D is the fractional relative true metal density at a given applied pressure.

Effects related to the densification of metal within compacts were considered by using true metal density rather than overall compact density.

The results of ΔD are shown as a function of compaction pressure in figures 4-11 to 4-13. The results for unlubricated compacts have been plotted in each figure to provide a reference point. For a given pressure a positive ΔD indicates that compacts containing precipitated zinc stearate attained the higher density. A negative value indicated that densification was greater in compacts containing admixed lubricant. The results were divided into three groups on the basis of their behaviour and these were similar to those observed during the work on loose packing properties (4-1-2-2).

Results for unlubricated compacts reflected the pressure/density curves of figure 3-23 which were discussed in the previous section (4-2-4-1). Initially ΔD was negative due to the superior packing of admixed powder. During compaction ΔD became positive because of the poorer densification properties of powder which had undergone attrition during mixing.

The first group (fig.4-11) corresponded to low lubricant additions, 0.01% to 0.1%. During initial packing at zero compaction pressure ΔD became more negative with increasing lubricant content but increased to

FIGURE 4-11. ΔD as a function of compaction pressure for compacts containing zinc stearate.

ΔD = D(precipitated) - D(admixed)

D - fractional relative true metal density

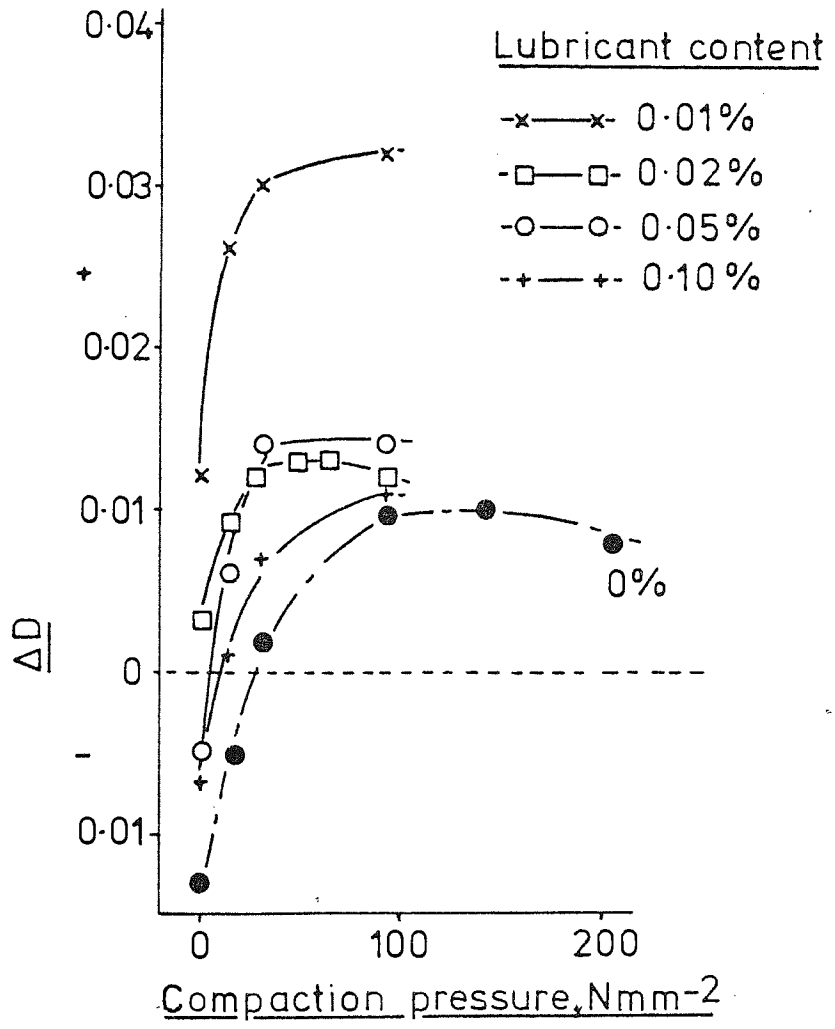

FIGURE 4-12. ΔD as a function of compaction pressure for compacts containing zinc stearate.

ΔD = D(precipitated) - D(admixed)

D - fractional relative true metal density.

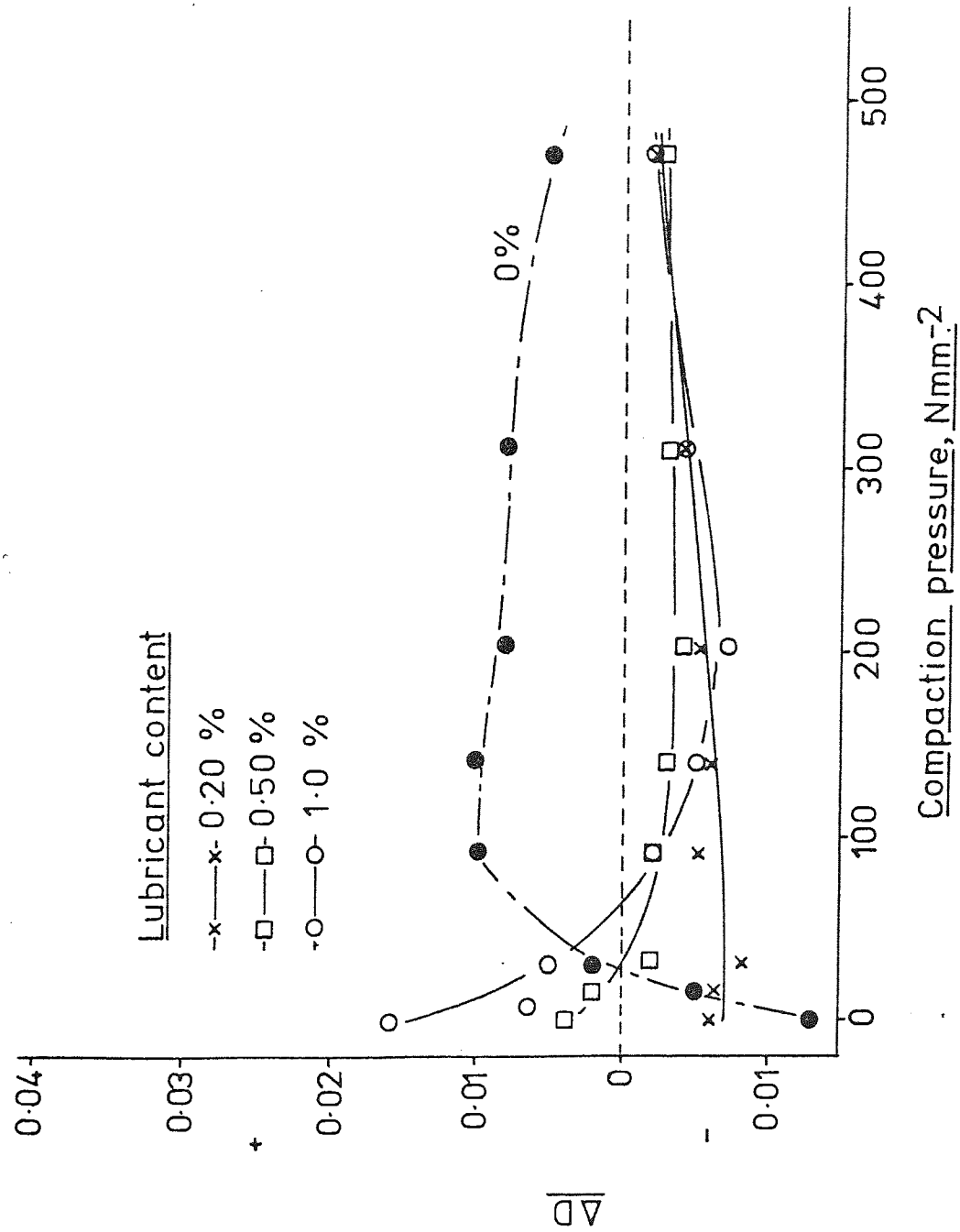

FIGURE 4-13. ΔD as a function of compaction pressure for compacts containing zinc stearate

ΔD = D(precipitated) - D(admixed)

D - fractional relative true metal density.

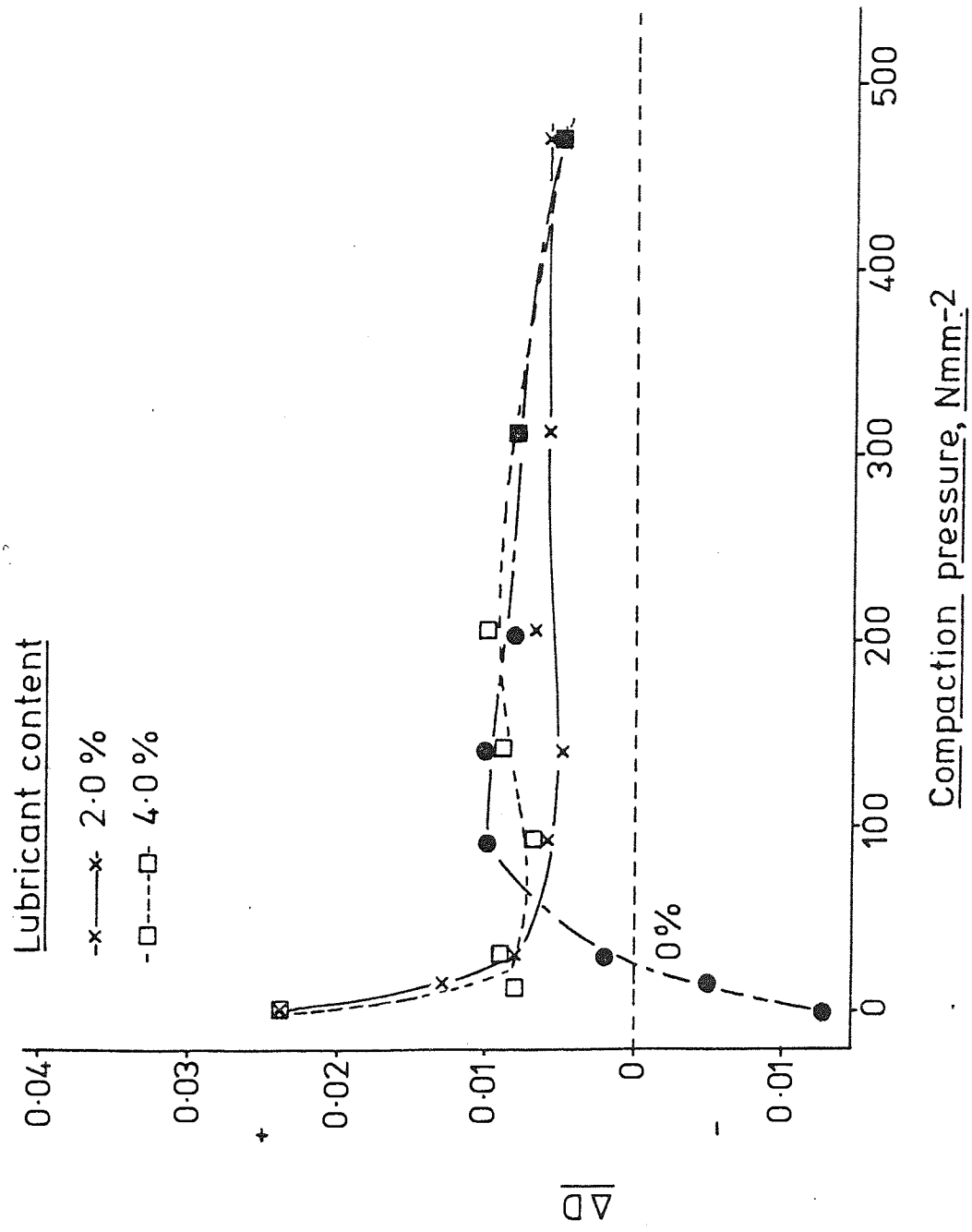

of figure 4-11 corresponded to stage 2 of compaction (4-2-1-2) where particle rearrangement played a significant role.

In this lubricant content range the coverage on admixed particles (4-1-2-2) progressed from fractional (0.01%) to full (0.1%) and the loose packing behaviour improved correspondingly. Powders with precipitated coatings (4-1-1) achieved complete coverage at lower additions (0.05%) but then showed little change over a wide range,due to deposition of lubricant in cavities and internal porosity.

The second group (fig.4-12) 0.2% to 1.0% corresponded to optimum coating conditions for admixed lubricant, where thick films were formed on particles without the presence of large proportions of free lubricant. The formation of such films had deleterious effects on initial packing compared to powders containing precipitated lubricant. Consequently at zero pressure ΔD increased to positive values as lubricant content increased. However these thick films aided rearrangement under pressure so that ΔD became negative with increasing applied pressure,indicating improved densification for admixed powders.

The presence of greater proportions of free lubricant than were obtained by precipitation (4-1-3) may have also reduced the deleterious effects of particle/die-wall friction. It will be shown in the next section (4-3) that admixed lubricant was more effective than precipitated for reducing friction during ejection.

The third group (fig.4-13) corresponded to the highest lubricant contents. It has been suggested (4-1-3) that less free lubricant resulted from precipitation than admixing and the presence of large proportions in admixed powders reduced loose packed densities relative to precipitated powders. This was reflected by positive values of ΔD at zero pressure (fig.4-13). As densification proceeded the difference (ΔD) decreased as this free lubricant helped to reduce the effect of die-wall friction.

However it also produced the adverse effect of inhibition and consequently final values of ΔD were still positive, indicating greater densification for powders containing precipitated lubricant.

4-3 Ejection

Ejection stresses were determined as the maximum force recorded during ejection divided by the total apparent compact/die-wall contact area (section 2-3). Relationships between ejection stress and true metal density are shown in figures 3-28 and 3-29 for compacts containing zinc stearate, pressed without additional die-wall lubrication. Relationships between ejection stress and compaction pressure were similar to these since density is proportional to applied pressure. However, pressure/density relationships varied with lubricant content and coating type (4-2) and so density was considered to be a more suitable parameter for comparative purposes. The results obtained from die-wall lubricated compacts containing no internal lubricant have been reproduced in figures 3-28 and 3-29 also.

These results concurred with previous work[4] in showing that at low lubricant levels ejection stress increased rapidly with density (or applied pressure), but high additions were characterised by low stresses which increased only slightly with density. The influence lubricant content had on ejection stress is more effectively illustrated by figure 4-14 where ejection stresses at specific densities, taken from figures 3-28 and 3-29, have been plotted as a function of lubricant content. The form of these relationships follows previous work[1,11,12,24,27] and shows that ejection stress decreased rapidly with increasing lubricant content, the effect being most pronounced at high densities and low additions. Minimum ejection stresses were obtained with optimum lubricant additions which increased with density. Further additions beyond each optimum had little effect on reducing stress.

During compaction the applied force presses particles into contact with the die-wall and deforms them at these contact points. The die imposes restraint on radial movement of particles and elastically deforms as the applied force increases. When the compaction force is removed radial

FIGURE 4-14. Ejection stress versus lubricant content at selected true metal densities (data taken from figures 3-28 and 3-29)

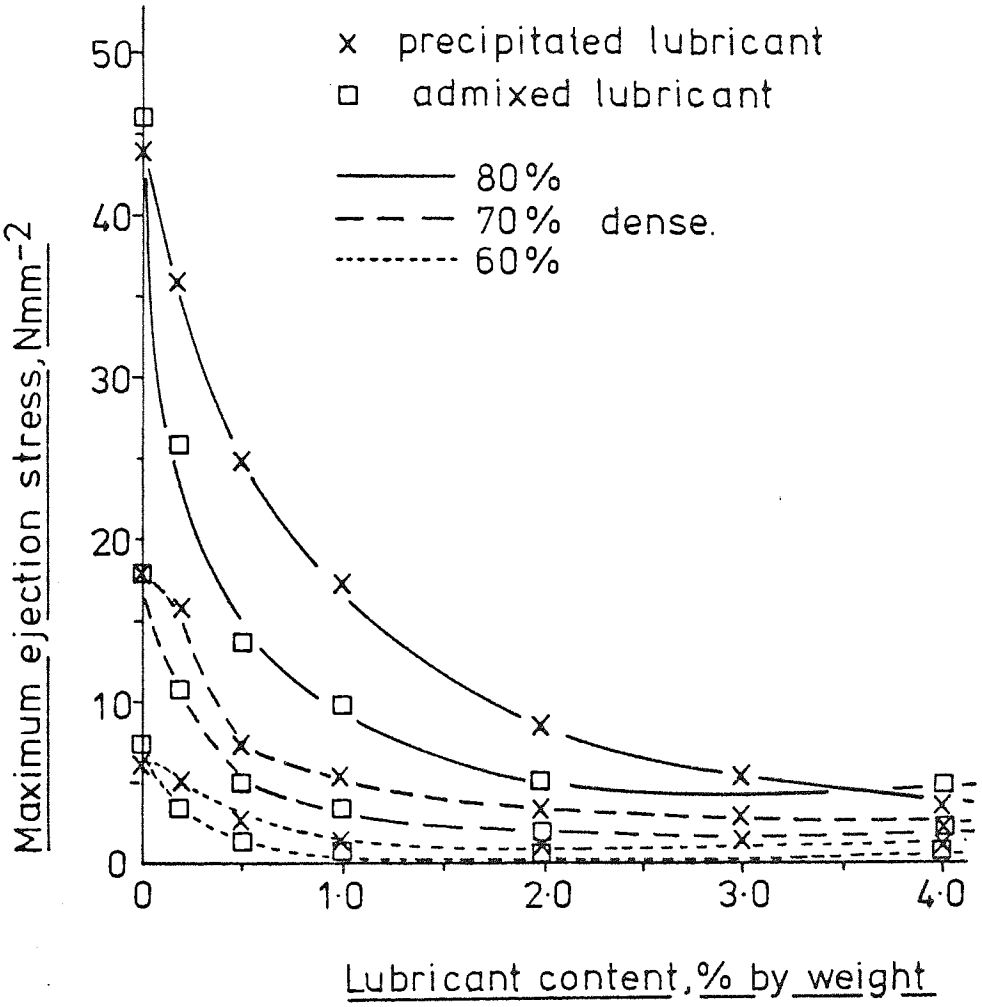

stresses resulting from this elastic deformation force the die onto the compact. There are also residual radial stresses within the compact[27,28] resulting from compaction and these cause it to attempt to expand when the applied force is removed and when it is ejected. The overall result is a force W perpendicular to the compact/die interface which acts on the particle/die-wall contacts. The ejection force of a compact is the force required to overcome friction between the metal particles and the die-wall at the contact points.

The considerations given to particle/die-wall friction during compaction (4-2-3) also apply to ejection. In dry friction (no lubrication) the coefficient of friction μ equals F/W[32] where F is the force required to shear metal/metal contacts and W is the force acting perpendicular to the sliding area. μ remains constant as the applied load or pressure (P) increases (4-2-3) but W, the reaction by the tools when the load is removed, must also increase. Therefore the frictional force increases with applied pressure or density ($F = \mu.W$). F is equal to A.s. also[32], where A is the real contact area and s is the shear strength of metal/metal contacts. A increases with applied pressure due to plastic deformation of particle/die-wall contacts (plates 3-4 to 3-7), consequently F increases and the ejection stress of unlubricated compacts increases rapidly with increasing density.

When lubricant is present there are two components to the frictional force, F_1 and F_2[27] (see equation 4-11, section 4-2-3). F_1 is the force required to slide dry contact areas and F_2 that required to slide lubricated areas. An increase in the applied compaction pressure causes greater penetration of the lubricant film, an increase in the dry contact areas and consequently increases the contribution of F_1 during ejection. F_1 is larger then F_2, therefore ejection stress increases with density (figs. 3-28 and 3-29) or compaction pressure. The thickness of the lubricant film

in the compact/die-interface increases with content (4-2-3) particularly when compaction inhibition (4-2-2-2) is significant. Perforation by asperities is more difficult during compaction and so the ejection force or stress decreases with increasing lubricant content (fig.4-14).

Plates 3-4 to 3-7 are scanning electron photomicrographs of the surfaces of typical ejected compacts. These compacts were formed at the same pressures as the compacts of lowest and highest density used to determine ejection stress (47 and 467Nmm^{-2}). Photomicrographs (a) and (c) are of punch contact surfaces, representing the morphology of the die-wall contact area before ejection. Friction surfaces after ejection are shown in (b) and (d).

The ejection stresses used in this investigation were determined from the maximum forces required to eject compacts. However, ejection stress/compact movement behaviour during ejection has been shown to depend on lubricant content[27], illustrated in figure 2-3 of the literature review. The maximum measured ejection stress will correspond to different stages of ejection or types of friction depending on the level of lubrication.

In the absence of lubricant or at low levels (0, 0.2% fig.3-28) the maximum stress occurs during a period of stick/slip sliding (literature review, fig.2-3* curve 1) and has been called the maximum stick stress[27]. At intermediate lubricant contents (curve 2) the maximum force corresponds with the maximum slip stress. This is higher than the break stress required to initiate sliding because such additions (0.5-1.0% fig.3-28) produce an incomplete film. Sliding plastically deforms particle/die-wall contacts and increases the true area of dry contacts and there is also little possibility of replenishing the film by lubricant from surface pores (plate 3-6). At high contents (curve 3) a thick film is formed, which may be replenished from surface pores during sliding. Therefore the

* p 27

maximum force or stress becomes that required to initiate sliding, the break stress[27].

Typical surface finishes produced by the three modes of ejection behaviour can be seen in plates 3-4, 3-6 and 3-7 and comparison of the photomicrographs of punch (c) and friction (d) surfaces for high density compacts illustrates the effect of sliding. Stick/slip behaviour produced extensive smearing of the surface and pore closure (plate 3-4). This would have been progressive as ejection proceeded (literature review, fig. 2-3 curve 1) and the maximum ejection stress probably coincided with maximum contact area resulting from almost complete pore closure. Partial lubrication (plate 3-6) causes polishing of the surface and closure of fine porosity within particles but large interparticle pores remained open. Lubrication by a thick boundary film (plate 3-7) produced a degree of polishing but some fine intraparticle porosity remained open and there was no closure of interparticle pores.

4-3-1 Die-wall versus internal lubrication

The ejection stress/density relationships for compacts formed with die-wall lubrication only are shown in figures 3-28 and 3-29. As compaction proceeded compact length decreased and so the effective concentration of die-wall lubricant in the compact/die interface increased (section 4-2-3). The density distribution in such compacts was also unfavourable for the removal of lubricant from the interface and into surface pores (appendix A). Consequently a thick boundary film was interposed between particles and the die-wall at the beginning of compaction and remained there up to the highest applied pressure. Therefore the ejection stress did not increase rapidly with density or pressure.

When the level of internal lubricant was too low to provide a thick coherent film, 0.2%-1.0% for precipitated and 0.2%-0.5% admixed, there was only fractional coverage of the surface where lubricant adhering to

particles during precipitation or admixing was trapped between particles and the die-wall. The resultant ejection stress was generally higher than obtained with die-wall lubrication, markedly so at high densities, due to a significant contribution from F_1.

At high levels of lubricant, 2%-4% precipitated and 1%-4% admixed, inhibition forced lubricant into the interface to balance perforation of the film by asperities during compaction. In addition some of the high proportion of free lubricant (4-1) may have been trapped between particles and the die during die-fill. A thick coherent boundary film was produced, as with die-wall lubrication, but there was also the possibility of replenishing this film with lubricant exuding from surface pores during ejection (plate 3-7). Such conditions decreased ejection stress to a level below that produced by die-wall lubrication (figs.3-28 and 3-29). The residual radial stress within compacts also depends on green strength[28] and this may be reduced by internal lubricant, however it will be shown in section 4-4 that green strength was relatively insensitive to zinc stearate content in the range 0.1% to 2.0%

4-3-2 Precipitated versus admixed lubricant

Admixed lubricant was generally more effective than precipitated at reducing ejection stress (fig.4-14). The ejection stresses of compacts containing 0.2% precipitated lubricant were similar to those of unlubricated compacts (figs.3-28 and 4-14) and they ejected with the same slip/stick behaviour. This probably reflected the precipitation of lubricant into cavities and internal porosity of particles (4-1-1) leaving less external lubricant to reduce friction.

Admixing formed thicker superficial coatings on particles (4-1-3), there was generally more free lubricant present and consequently there was more lubricant available to reduce friction. A similar effect to free lubricant may be obtained with large lubricant particle sizes which are

able to form more coherent films [27]. Compaction inhibition tended to occur at lower densities or applied pressures in admixed powders (4-2-2-2) also causing thick films to be formed in the compact/die interface.

4-3-3 True shear stress at particle/die-wall contacts.

The true area of contact between particles and the die was not considered during calculation of the ejection stresses used in this investigation. If the true contact area is considered the actual shear stress of contacts in a compact of 50% average relative density would be twice the measured ejection stress. At a density of 80% the factor reduces to 1.25 and at 100% dense the ejection and true contact shear stresses will be equal. However if true shear stresses obtained in this way replaced the measured ejection stress in figures 3-28 and 3-29 there would be little change in the form of the stress/density curves.

The total apparent compact/die contact area decreased with increasing density or applied pressure as the compact length decreased. Therefore the measured ejection stress increased arithmetically with density, even without considering the real change caused by increasing W, the compressive force on the contact area. True contact shear stress was more dependent on the increase of W which was associated with increasing the applied pressure or density. True contact area was only a function of density in so far as an increase in the applied pressure caused more deformation of particle/die-contacts, shown by the photomicrographs of punch contact surfaces (plates 3-4 to 3-7). If there was no deformation then an increase in density would merely increase the concentration of contacts and not the true contact area.

Conditions at the compact/die-wall interface were more complex than indicated by considering the average density only. The density along the interface was not simply the average compact density but was generally higher, varied along the length and further-more varied with the lubric-

ating conditions (appendix A).

The particle/die-wall contacts changed their form as ejection proceeded as was shown by the results of scanning electron metallography (plates 3-4 to 3-7). If punch contact surfaces are representative of contact morphology prior to sliding then it can be seen that at low applied pressures ($47 Nmm^{-2}$) contact was at asperities only and did not change appreciably for either condition during ejection. The morphology of high pressure contacts has been discussed previously (4-3) when it was observed that the degree of change was dependent on the conditions of lubrication. With no lubricant present (plate 3-4) pore closure was almost complete and true contact shear stress and the measured ejection stress would have equated. At high lubricant levels there was little change other than the closure of some fine intraparticle porosity and hence the contact shear stress would have exceeded the ejection stress.

The punch contact surface was not necessarily truly representative of the condition of contacts before ejection since there was relative sliding along the die-wall even during compaction (4-2-3). Furthermore, the degree of sliding varied with position along the compact length and only particles lying midway could be considered to remain stationary until ejection.

The relationship between true contact shear stresses and the measured ejection stresses generally depended on the density, or more precisely applied pressure, the lubricant level and the stage reached in the ejection cycle.

4-3-4 The effect of mix duration

It can be seen from figure 3-30 that there was no variation in ejection stress which could be attributed to mix duration. This was surprising initially since it has been suggested that the proportion of free lubricant reduces with increasing mix time (4-1-2-2) and the presence

of free lubricant reduces ejection stress (4-3-2). An increase in ejection stress would be expected with longer mix duration.

It was observed that the influence of mix duration became less pronounced as the service conditions of the lubricant became more arduous. Mix duration had the greatest influence on loose powder properties (4-1-2-2), less effect on compaction behaviour (4-2-4-1) and apparently none on ejection stress.

4-3-5 Simultaneous internal and die-wall lubrication

The effect of using die-wall lubrication together with internal precipitated zinc stearate can be seen in the results of figure 3-31. The general level of ejection stress was low, being lowest when internal lubricant was present, however there seemed little advantage in using the two forms of lubrication simultaneously. The ejection stresses for additions of 3% and 4% were similar to those obtained with no die-wall lubrication (fig.3-28) and it seems that once a coherent boundary film was produced there was no advantage in increasing its thickness. This was also illustrated by the existence of optimum lubricant additions which minimised ejection stress in the absence of die-wall lubricant (fig.4-14). The presence of a film of lubricant in the compact/die interface may have restricted exudation of internal lubricant and actually worsened inhibition during compaction (4-2-2-2).

One possible advantage in applying simultaneous die-wall lubrication could be with a low addition (0.1% to 0.2%). The die-wall lubricant would reduce particle/die-wall friction during compaction and ejection, whilst the low internal addition would optimise the loose packed density but would not cause compaction inhibition. This does presuppose that a high packed density at the die-fill stage is advantageous. In complex parts it may be more advantageous to have a low initial density with a high degree of rearrangement under pressure so that narrow sections are properly filled. However, small lubricant additions may aid rearrangement also (4-2-2-1).

4-4 Green strength

The green, or as-pressed, strength of compacts were determined on three point bend specimens as transverse rupture strength (section 2-4). The results are shown as a function of true metal density in figures 3-32 and 3-33, each point represents the mean of two determinations and duplicates were coincident where no scatter bars are shown. The results obtained from admixed powders are shown in figure 3-32(a) and those for precipitated in figure 3-32(b). It can be seen from the relationships for unlubricated compacts in these figures that pretreatment (mixing or solvent) had no effect on the green strength of the matrix.

4-4-1 The effect of lubricant content and dispersion.

It can be seen from figures 3-32(a) and (b) that, irrespective of dispersion, additions of zinc stearate reduced green strength relative to the unlubricated condition. Precipitation did generally lower strength slightly more than admixing, but this difference was small compared to the effect due to content observed with the initial additions (0.5% and 2.0%) and so the range was extended by using compacts pressed from material containing 0.1% admixed zinc stearate. The results are presented in figure 3-32(a). At densities below approximately 75% this material did not differ from the higher additions. Above 75% dense the strength improved relative to additions of 0.5% and 2.0%, but the major change was still simply due to the presence of lubricant. Ljungberg and Arbstedt[1] have also noted that small additions of lubricant reduce green strength.

When unlubricated powders are compacted, initially particles rearrange, interparticle friction helps clean contacts and some friction bonding may occur. As the density or applied pressure increases irregular particles interlock and deformational bonding occurs at contact points, consequently green strength increases with increasing density (fig.3-32).

Within a compact, lubricant reduces green strength by becoming interposed in interparticle contacts. However a degree of strength is still provided by interlocking and metallic (metal-metal) contacts, which have been shown to exist even with lubricant contents as high as 2.0%[25]. The overall green strength in a lubricated system will be determined by the ratio of metallic to lubricated interparticle contacts.

It has been suggested that lubricant is forced into particle/particle contacts during compaction[28], but this would seem unlikely while interconnected pore space was still readily available. It may be possible to force lubricant from contacts lying perpendicular to the pressing axis and into contacts lying on axes parallel to the pressing direction. However, the testing axis was also perpendicular to the pressing direction and so a stronger relationship would have been expected between green strength and content. In part II (section 4-3-2-9) it will be shown also that during dewaxing there were no pronounced shrinkage effects which could be attributed to lubricant on this axis. It may be forced into contacts when inhibition occurs (4-2-2-2) but this also reduces the degree of densification and so would not necessarily be revealed by strength/density relationships such as those in figure 3-32.

It seems more probable that lubricant is forced out of contacts and into pores during compaction, to leave only a thin layer, perhaps monomolecular, which would be difficult to remove due to its inherent lubricating properties. Since the reduction in strength would be related to a thin film it should be relatively insensitive to lubricant content (fig.3-32a). The major requirement would be that lubricant initially adhered to particles so that it could be trapped. Large particles of free lubricant may be moved away from interparticle contacts during rearrangement at low applied pressures.

Within the range of admixed additions the lubricant dispersion (4-1-

2-2) changed from coverage of metal particle asperities with a thin layer (0.1%) to coverage with a thick layer plus considerable free lubricant (2.0%). A coating on asperities was common to each addition and so at low densities green strength was not dependent on lubricant content (fig.3-32a). The coating produced by 0.1% zinc stearate was perforated at high densities, perhaps by interparticle penetration into the cavities which admixed lubricant did not fill (4-1-3). Consequently the proportion of metallic contacts increased and strength improved relative to the higher additions (fig.3-32a).

Precipitation produced more extensive coverage of particles than admixing (4-1-1 and 4-1-3) so that at a given density the proportion of lubricated contacts was higher, even when interparticle penetration occurred, and the green strength was slightly lower (figs.3-32a and b). Admixed lubricant did not produce such extensive coverage and so it was possible for the proportion of metallic contacts to increase with density, particularly when the asperities of some particles penetrated the cavities of others (interparticle penetration). The ratio of the green strength of unlubricated compacts to that of compacts containing 0.5% and 2.0% admixed zinc stearate was effectively constant over the whole density range. This suggested that there was a constant lubricated/metallic contact area ratio even as density varied.

It seems that the important factor in the development of the green strength of compacts containing lubricant is the proportion of the total interparticle contact area which contains a thin layer of lubricant and not the thickness of the lubricant in these contacts.

4-4-2 The effect of lubricant type

Strength/density relationships obtained from compacts containing lubricants of varying types are shown in figure 3-33. It can be seen from these that when type was considered the influence of lubricant on as-

pressed strength became more complex. Initially it was tempting to consider the effects on strength to be caused by varying chemical composition. The metal stearates reduced green strength (fig.3-33a) whilst stearamide and Cosmic 64 wax did not (fig.3-33b). However, the behaviour of the various forms of stearic acid (fig.3-33c) suggested that morphology may have had a significant influence.

During mixing it was observed that particles of zinc stearate adhered to the metal powder (4-1-2-1) and Mallender et al[27] also noted that zinc stearate pickup was generally particulate and not by smearing. If this behaviour applies to all stearates then the formation of a coating on metal powders would be associated with small lubricant particle sizes. Coarse particles, particularly those approaching the metal particle size, would not be picked up easily by the metal powder. The reduction of green strength by lubricant is associated with the formation of coatings, as discussed above (4-4-1), and so fine lubricants would be expected to produce the greatest changes in strength.

The morphology of the lubricants has been discussed previously in the materials section (4) and typical scanning electron photomicrographs are shown in plate 4-3*of that section. The metal stearates (plate 4-3d,e) were the only truly fine lubricants ($<5\mu m$), fine stearic acid (plate 4-3 a) was only fine relative to the medium and coarse powders (plate 4-3b,c). The metal stearates were able to form coatings on the iron powder and hence reduce green strength (fig.3-33a), as did precipitated/evaporated stearic acid (fig.3-33c) where extensive coverage was deliberately produced by the method of application.

The medium stearic acid seemed anomalous, it had a relatively large particle size (plate 4-3) but also reduced green strength (fig.3-33c). The particle shape of this material was notably plate-like (plate 4-3b) and consequently may have been trapped easily between particles to form

* p 45

interparticle films during compaction. This lubricant was not produced by ball-milling, like the fine and coarse stearic acid (materials section), but by precipitation from solution. It is possible that such material was able to disintegrate to a fine particle size during mixing and consequently coat the iron powder particles.

Particle morphology seems to be the most important factor in deciding the effect any given lubricant will have on the development of strength in as-pressed compacts. However this morphology may be determined by chemical composition or the method of application.

PART II. - HEAT TREATMENT

1 - Introduction

The main function of a solid admixed lubricant is the reduction of frictional forces during ejection of a pressed compact. It has been shown in section 4-3* that ejection stresses may be markedly reduced by the addition of a lubricant, implying a corresponding decrease in tool wear. The beneficial effect of lubricants during ejection far outweighs any deleterious effects they may have upon as-pressed compacts, such as the reduction of green strength, a high lubricant content may even act as a binder in low density compacts (section 4-4)*.

After ejection, its prime function being fulfilled, a lubricant is regarded as a necessary evil and its removal during sintering is often associated with problems. Deleterious effects on the mechanical and physical properties of sintered compacts containing lubricants[1,11,28] have been reported, but otherwise there is little information available on lubricant decomposition characteristics within compacts and the effect of sintering process variables on its breakdown. Some information[1] is available on pure lubricant decomposition.

The stearate radical present in the most commonly used lubricants, such as zinc stearate, contains approximately 67% by weight carbon. A 1% lubricant addition may therefore be equivalent to a possible addition of 0.6% to 0.7% carbon. There is also a considerable quantity of hydrogen, a little oxygen, and metal radicals in the metal stearates. These elements are in a combined form initially. However, breakdown during pyrolysis may provide an atmosphere around and within a sintering compact completely different to the externally imposed atmosphere.

It has been shown[11] that the breakdown characteristics of pure lubricants, in the absence of a compact, are similar to volatilisation rather than complete chemical decomposition, with condensation in cooler parts of the furnace. If breakdown occurs in this manner in the presence of a compact

(* Part I)

the risk of chemical reaction of decomposition products with the matrix is lessened. However, a small volume of solid lubricant is transformed to a large volume of vapour over a short temperature range[11]. The possible physical effect of such a change upon a compact cannot be discounted.

The aims of this part of work may be summarised as follows:-

[a] The identification of and effect of process variables on reactions occurring during the decomposition of a limited range of pure lubricants. (In this context the word pure is used to indicate the absence of a compact, not chemical purity).

[b] A study of the decomposition characteristics of lubricants within compacts and the influence of process variables on them.

[c] The effect of lubricants and their removal on the mechanical and physical properties of dewaxed and sintered compacts.

Much of the work involved in sections [a] and [b] has utilised a modified Stanton thermobalance with a maximum heating rate of 6°C per minute. To make results more compatible with industrial practice some dewaxing experiments and all of section [c] were carried out using a sintering furnace with heating rates of the order of 100°C per minute.

It is not intended that this work should lead to suggestions for alternative lubricants or lubricating practice. However, it should provide a clearer understanding of lubricant behaviour during compact heat treatment.

2 - Experimental Procedure

2-1 Thermogravimetry

The measurement of weight change under controlled thermal conditions, thermogravimetry, has been successfully used by Meyer et al[11] to study the breakdown of several lubricants. The use of a thermobalance, rather than isothermal specimens, enables reactions to be studied over wide temperature ranges with single specimens by monitoring the attendant weight changes.

In a thermobalance weight changes are automatically recorded by following beam movement with a capacitor plate. At the limit of beam movement the balance is automatically re-tared to allow further weight changes to be recorded. At regular intervals the beam is lifted from its knife edges and then lowered to ensure that the system is not sticking. The result is a continuous trace of weight change with time, with a parallel trace of temperature with time.

2-1-1 Modification of thermobalance

A Stanton HT-M thermobalance was available for this investigation. This had a vertical bi-filar Pt-Rh wound tube furnace capable of a maximum temperature of 1350 deg.C and a maximum heating rate of 6^{o}C per minute. In its normal condition such a thermobalance would be used for oxidation studies since the furnace was open and there were no facilities for providing a protective atmosphere.

The provision of a protective atmosphere was made possible by a modification similar to those described by Smith[33] and Bassett and Betts[34]. The equipment necessary for this modification was supplied by Stanton Ltd. and is shown in plate 2-1(a)and(b), and diagrammatically in figure 2-1(a). The Stanton conversion relies on deliberate leakage of the atmosphere, plus a shield gas directed downwards by a baffle plate, to prevent ingress of atmospheric oxygen with the upflowing protective atmosphere.

PLATE 2-1 Modified thermobalance

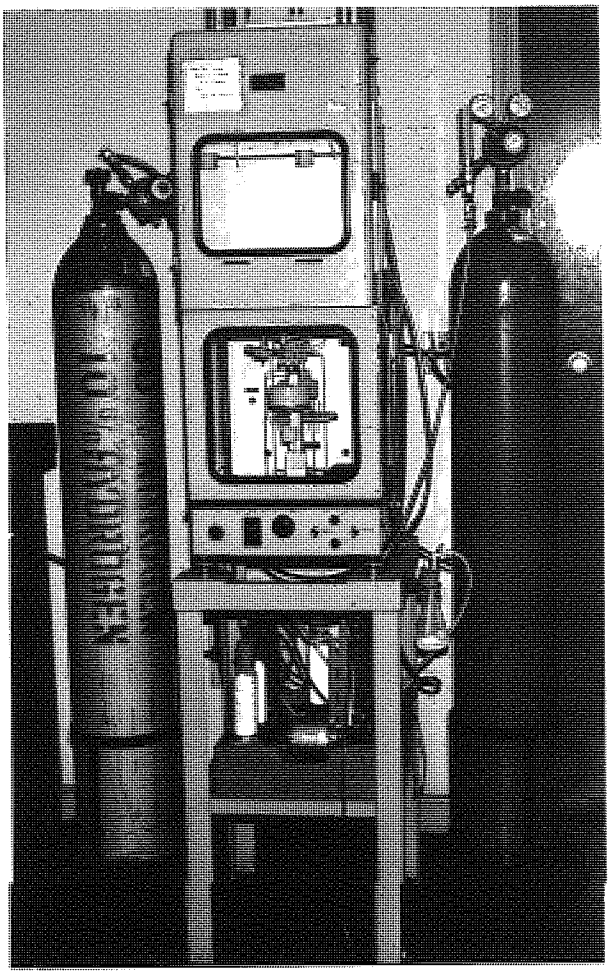

(a) General view

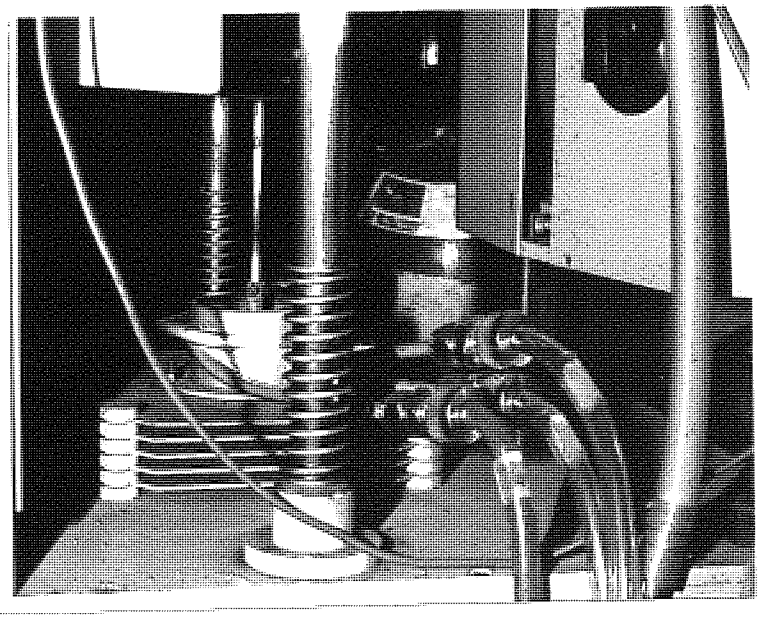

(b) Gas flange with water and gas inlets

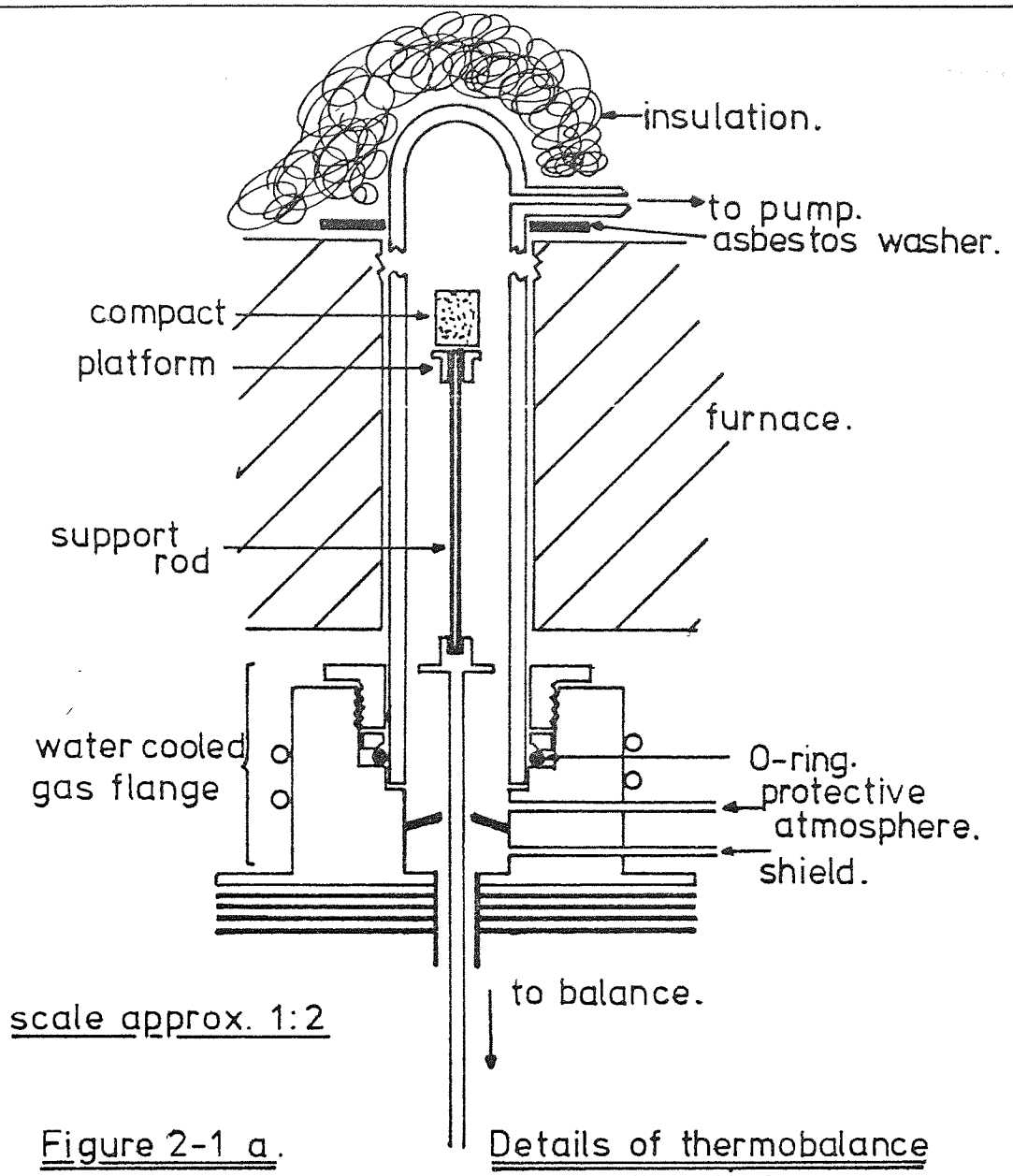

scale approx. 1:2

Figure 2-1 a. Details of thermobalance conversion

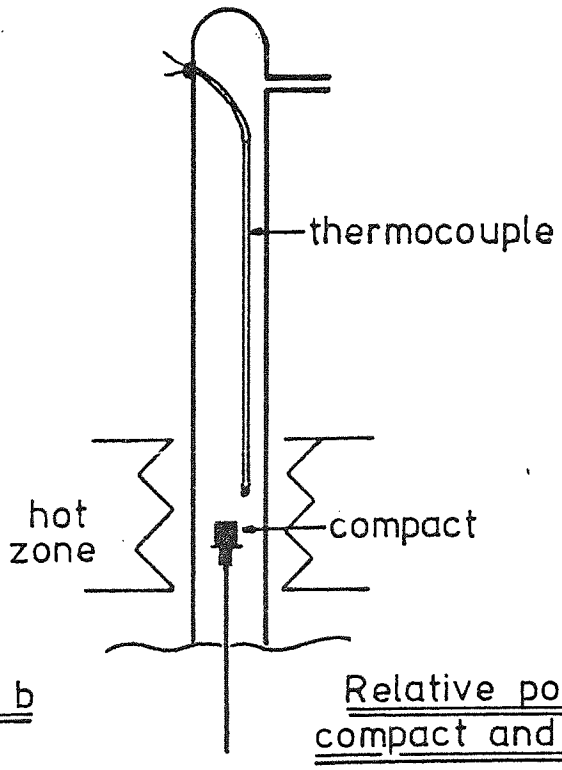

Figure 2-1 b Relative position of compact and thermocouple

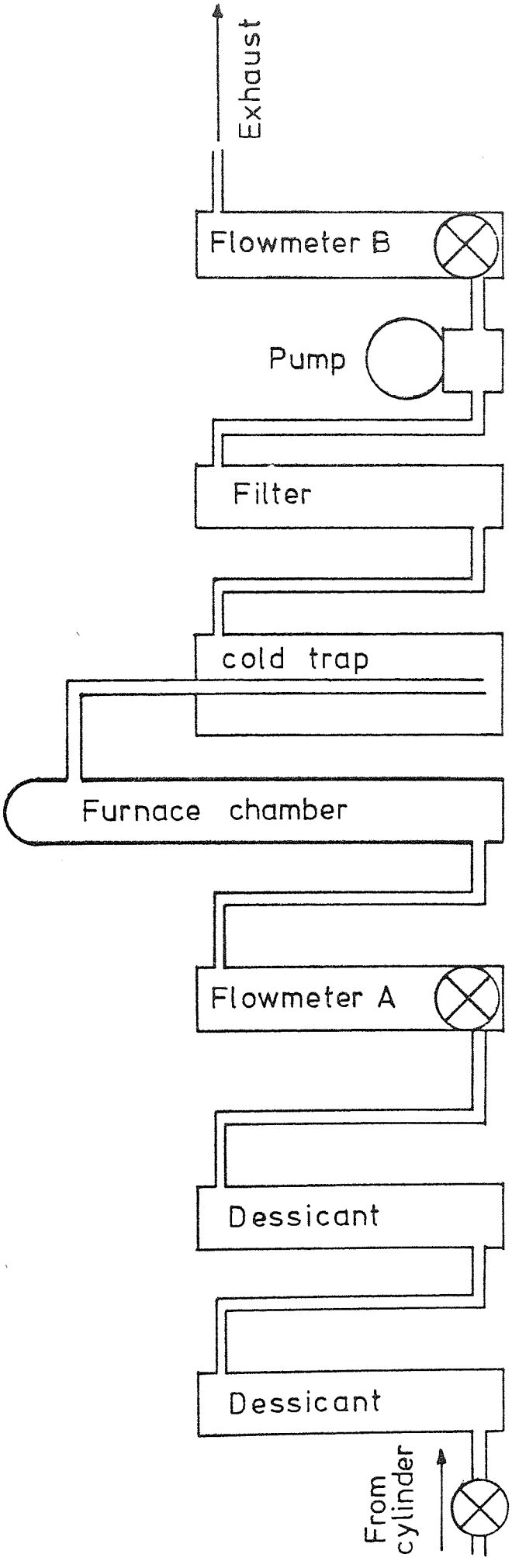

Figure 2-1 c. Schematic representation of Thermobalance gas control apparatus.

The protective atmosphere and the shield gas were dried by passing through silica gel followed by magnesium perchlorate. Dewpoints were not determined but oxygen analyses were carried out on suitable presintered compacts to determine the oxidation potential of the dried gas during thermogravimetric treatment. These results are discussed later (section 2-1-3). After the protective gas had passed through the dessicating towers, the flowrate controlled by meter A (figure 2-1 c), it was allowed into the alumina furnace sheath via the water cooled gas flange (figure 2-1 a). If this atmosphere was then allowed to flow up the furnace chamber under its own momentum it was probable that the following problems would be encountered;

(a) Atmospheric oxygen would enter the chamber by being drawn in past the sample support rod and, at low input rates, by back diffusion through the outlet.

(b) Decomposition products, often seen caking the entrance of industrial furnaces, might have blocked the restricted outlet. This would interrupt gas flow causing erroneous weight changes due to variation of buoyancy.

(c) Buoyancy effects would probably have become seriously temperature dependent despite the imposed input flow rate.

These potential problems were overcome by using a pump to draw the atmosphere and decomposition products through the outlet. Flowmeter B (figure 2-1c), on the outlet side of the system, was used to control the pump rate and was always set 100 $ml.min^{-1}$ less than the input to induce leakage outwards rather than inwards. Argon, dried as described above, was used as the shield gas. This was introduced into the gas flange beneath the baffle plate (figure 2-1a). This ensured that if gas was drawn in past the support rod it would be dry argon. The downward flow of argon against the support rod would also help to cancel the buoyancy effect of the upflowing protective atmosphere.

Decomposition products were collected in a cold trap and a filter, both at ambient temperature.The function of the latter being mainly pump protection.

This furnace arrangement still limited the choice of atmosphere to non-toxic, non-combustible and non-corrosive types. It was decided to restrict atmosphere usage to reducing ($N_2/10\%H_2$), inert (argon) and, for pure lubricants only, oxidising (air). $N_2/10\%H_2$ was regarded as the principal atmosphere throughout this investigation, being the only one of this selection equating to a commercial atmosphere.

The mid-range flow on the meters was 500 $ml.min^{-1}$ and this was chosen as the general purpose flow-rate. Low and high rates of 200 $ml.min^{-1}$ and 1100 $ml.min^{-1}$ respectively were used for varying flow studies. The ability of a flowing atmosphere to remove decomposition products does not only depend on overall flow-rate but also on actual velocity. Where the furnace tube is restricted for a given flow-rate the local velocity of the atmosphere will change.

Two types of sample were used in this investigation, a crucible containing free lubricant (21mm diameter) and a compact (12.7mm diameter). Since both input and output were controlled, constant and handling gas at ambient temperature, the velocity must increase past each type of sample as their cross-sectional areas changed. The theoretical velocities past each type of sample are recorded in table 2-1 with the input and output flow-rates.

TABLE 2-1

INPUT $ml.min^{-1}$	OUTPUT $ml.min^{-1}$	VELOCITY $mm.S^{-1}$		
		OPEN TUBE	CRUCIBLE	COMPACT
300	200	5.2	11.4	6.5
600	500	13.1	28.5	16.3
1200	1100	28.8	62.8	35.9

Furnace tube internal diameter - 28.5mm.

Any increased buoyancy effect due to increasing local velocity when cold gas entered the furnace hot zone would probably be eliminated by the corresponding decrease in gas density. The total flow-through of gas was controlled by the pump and outlet meter.

2-1-2 Specimens

Pure lubricant investigations were carried out using loose lubricant powder placed in silica crucibles of 21mm. outside diameter. A sample weight of 200mg was generally used as a compromise between crucible overfill and ensuring detectability of reactions.

Cylindrical compacts were pressed in a 12.7mm internal diameter die by floating die compaction, in a similar manner to that used during compaction in part I. Rospol MP32 iron powder sieved to a restricted particle size range (53μm to 104μm) was used initially. However, the majority of the work was performed using as-received MP32 powder containing 1% by weight admixed lubricant pressed to a density of 80% of theoretical solid (assumed as 7.87g cm^{-3}), except where variations are stated. Mixing was carried out for 45 minutes using the same method as described in part I. Apparent densities (true metal density) of the mixes are given in table 2-2.

Table 2-2

Apparent densities of mixes used for thermogravimetric specimens

Lubricant	Apparent density	
	g cm^{-3}	Relative
Fine stearic acid	2.61	0.33
Medium stearic acid	2.53	0.32
Coarse stearic acid	2.76	0.35
Evaporated stearic acid	2.55	0.32
Zinc stearate	2.60	0.33
Lithium stearate	2.72	0.35
Stearamide	2.42	0.31
Cosmic 64 wax	2.50	0.32

Compact weight was maintained at 10g total, the balance limit was 20g but a 10g compact with a 1% lubricant addition had a potential weight loss of 100mg, considered as most convenient for calculations. Such a compact, 80% dense, had a length/diameter ratio of approximately one, the length being well within the quoted 38mm long hot zone of this furnace. The use of a 20g compact would increase density variation and increase the risk of a vertical temperature gradient. Examples of typical compacts are shown in plate 4-2. Considerations of the difference in thermal properties of crucibles and compacts are discussed later.

2-1-3 Temperature calibration, bucyancy and oxidation.

As can be seen in figure 2-1(b)it was necessary to place the thermocouple away from specimens to ensure that there was no mutual interference and hence no interference with beam movement. It could not be positioned between the specimens and the furnace wall due to insufficient clearance particularly when using a crucible. It was necessary therefore to calibrate temperature measurement and correlate indicated temperature with actual specimen temperature. This was achieved by removing the specimen support rod and replacing it with a calibrated thermocouple inserted from the balance chamber and fixed with the bead in the normal sample position. A normal run was then made to 1200°C in $N_2/10\%H_2$ at a flow rate of 500 ml.min^{-1} with the thermocouple connected to a separate recorder. A calibration graph was plotted, as shown in figure 2-2.

Reaction zones or fronts in cylindrical compacts would be expected to start at the surface, when heated in this manner, and follow the thermal gradient moving into the specimen. The use of an exposed reference thermocouple during calibration would indicate the temperature at the external surface of the compact. The temperature indicated at the onset of any characteristic weight change should therefore correspond to the actual temperature at the surface where reactions are initiated.

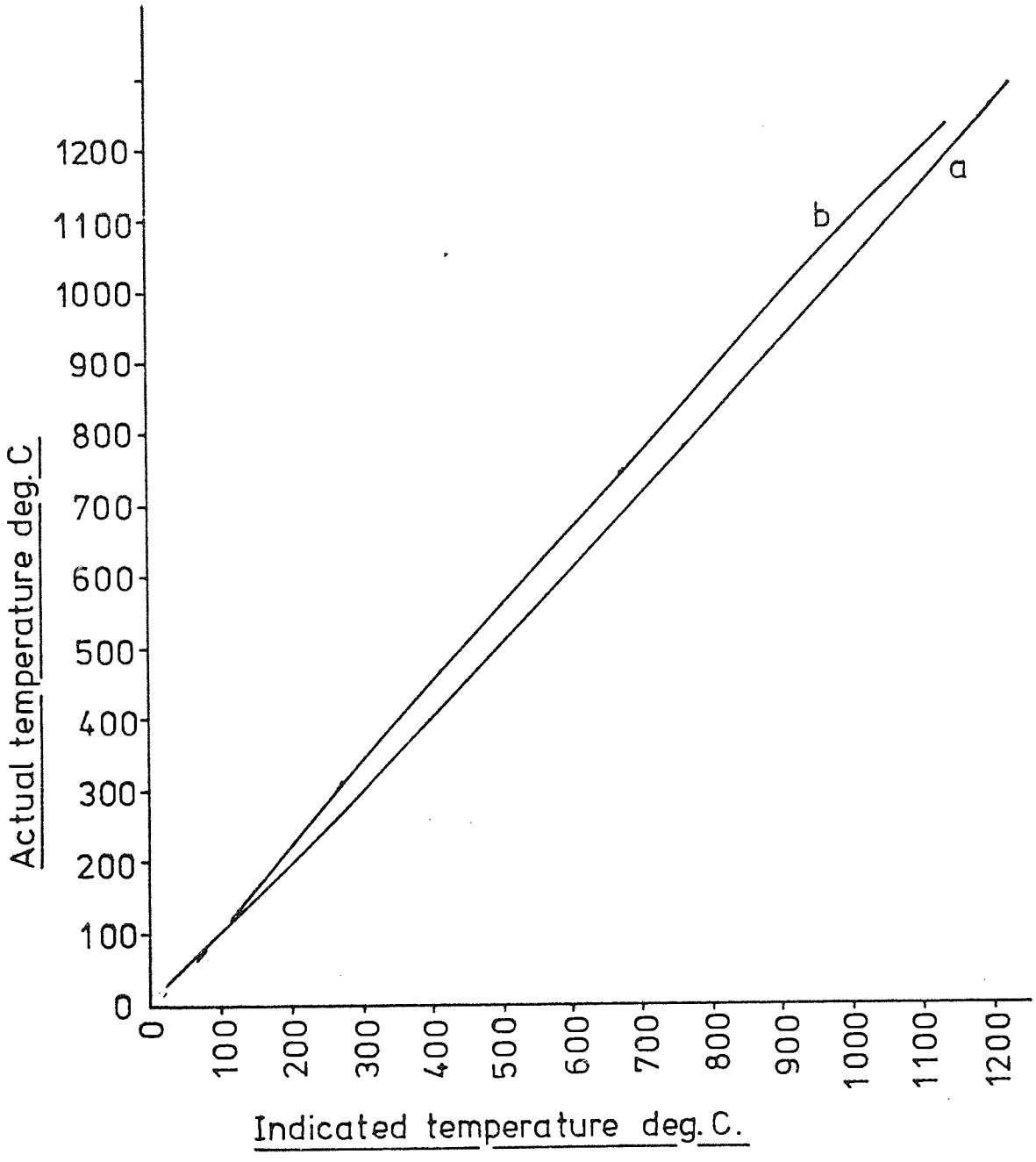

Figure 2-2 Thermobalance temperature calibration.

The proportion of specimen involved in a reaction at any given moment will depend on the temperature range of the particular reaction and the thermal gradient within the specimen[35]. If the temperature range is narrow and the thermal gradient is high then the reaction front or zone will be restricted. The low heating rate conditions in the thermobalance ($6^{\circ}C\ min^{-1}$) probably produce a shallow thermal gradient in a compact and hence a large proportion of material would be expected to participate in a reaction at a given temperature.

Temperature calibration was also carried out at atmosphere flow rates of 200 and 1100 $ml.min^{-1}$ to assess the effect of flow rate on heat transfer. It was also repeated for argon at a flow rate of 500 $ml.min^{-1}$. The maximum difference* was $\pm$ 10°C and maximum recorder detectability was 10°C. This difference was therefore discarded with the provision that only indicated temperature differences in excess of 20°C would be taken as significant. It seems probable that the slow heating rate and narrow tube enabled thermal equilibrium to be established irrespective of gas flow.

Two calibration curves are shown in figure 2-2, curve (a) is the initial calibration, (b) is the calibration made at a later stage after the furnace sheath had been stripped and overhauled. The difference between (a) and (b) was probably caused by a change in thermocouple position. Thermograms obtained prior to the refit have been plotted using calibration (a) and subsequent thermograms plotted using (b).

Compacts of 10g weight, pressed to a density of 80% and containing no lubricant were presintered for 1 hour at 1100°C in $N_2/10\%H_2$ to remove volatile materials and reducible oxides. These were used for buoyancy determinations in the principal atmosphere $N_2/10\%H_2$ during thermogravimetric analysis. Figure 3-1 shows the result of this buoyancy effect. Buoyancy effects for a crucible were determined in both $N_2/10\%H_2$ and argon and results are shown in figure 3-2.

(* relative to the calibration curve for $N_2/10\%H_2$)

Oxygen contents were determined, using a Balzer Exhalograph, on a presintered blank thermogravimetrically treated in $N_2/10\%H_2$ to 1300°C (the specimen used for buoyancy trials) and also on compacts pressed from as-received MP32 and treated in $N_2/10\%H_2$ and argon to 1200°C. These results are shown in table 3-1 with analyses on as-received iron powder and an as-sintered blank. Each analysis is the mean of two determinations. It was possible therefore to assess the oxidation potential of both atmospheres relative to the initial oxygen content.

2-1-4 Thermobalance operation and pure lubricant reactions.

The first section of practical work following calibration of the system was concerned with the pyrolysis of pure lubricants, in the absence of a compact. A weighed sample of each lubricant (usually 200mg) was placed in an open silica crucible on the platform of the support rod. Total sample/crucible weight was only approximately 2g and it was found unnecessary to counterbalance by placing weights on the balance sample pan.

The system was tared to midscale on the weight change recorder with the atmosphere flowing and metered so that this zero point included the initial buoyancy contribution of upflowing gas. The equilibrium time allowed before starting the furnace was taken as the time necessary for the weight and temperature recorders to stabilise. This time varied slightly between samples.

When stabilisation had been achieved the temperature recorder was zeroed and the furnace switched on. There was no heating rate control between ambient and 140°C. To avoid damage to the furnace element power input was maintained low and the furnace allowed to proceed at its natural heating rate. The overall heating rate at this stage was $2^{\circ}C\ min^{-1}$. Beyond 140°C it was possible to control the heating rate normally, linearly at $6^{\circ}C\ min^{-1}$.

Pure lubricant samples were heated until weight loss was complete, or up to a maximum temperature of 1200°C if it was incomplete. Cooling to

ambient temperature was generally carried out in the protective atmosphere, particularly if a residue was suspected.

The ultimate aim was the determination of the characteristics of decomposition reactions due to lubricants and their environment only, independent of physical dispersion. The identification of these reactions and the effect of process variables on them was a necessary precursor to the detection of these same reactions within a compact. This knowledge was also a necessity for the identification of other possible reactions caused by the introduction of the physical and chemical restraints of a compact.

The process variables investigated were:

(a) Lubricant type. These were limited to zinc stearate, lithium stearate, stearic acid, stearamide and Cosmic 64 wax as described in section 4 (Materials).

(b) Lubricant particle size. It was not intended to investigate the effect of lubricant particle size fully during either mixing, compaction or sintering. This was partly due to the difficulty of characterising the particle morphology of such material. However, it was thought desirable that any significant particle size effects should be identified since the lubricants were known to have different particle sizes. The materials used were coarse, medium and fine stearic acid, as described in section 4 (Materials).

(c) Atmosphere composition. Atmosphere variation was restricted to the three main types discussed previously $N_2/10\%H$ (reducing), argon (inert reference) and air (oxidising), all used at a flow rate of 500 $ml.min^{-1}$. Air was included since the possibility of entrapping air within pressed compacts could not be discounted.

(d) Atmosphere flow rate. Investigation of the influence of flow rate on the decomposition characteristics of lubricants was restricted to one system only, zinc stearate in $N_2/10\%H_2$. This combination was found to exhibit two reactions, stearate radical decomposition/volatalisation and hydrogen

reduction of a metal oxide (figure 3-3). Thus a study could be made of both the ability of an atmosphere to remove decomposition products and its role in supplying at least one reactent. Flow rates of 200, 500 and 1100 ml.min^{-1} were used with a constant sample weight of 200mg.

(e) Sample weight. It was proposed that lubricant content would be one variable investigated when considering the decomposition of lubricants within compacts. It was therefore necessary to determine the influence of the amount of lubricant present on the basic decomposition reactions. The material used again was zinc stearate in $N_2/10\%H_2$ at a flow rate of 500 ml. min^{-1}. Sample weights were 50mg, 100mg and 300mg.

The resultant thermograms, weight loss as a percentage of initial weight versus actual temperature, are plotted in figures 3-3 to 3-12 inclusive in the results section(3).

2-1-5 Lubricant decomposition within compacts.

The basic decomposition characteristics exhibited by pure lubricants may be modified when the lubricant is contained within a pressed powder compact. Prediction of the behaviour of lubricants during the heating of a compact is hindered by the lack of previous data,but it is possible to outline areas where the introduction of the physical limitations of a compact could cause slight, or extensive, changes in decomposition behaviour.

(i) Basic decomposition reactions could be modified in terms of temperature, rate and extent, by compact properties such as pore space and dispersion of the lubricant. Particular significance may be given to the possibility of inhibited diffusion[35] conditions within pores, especially when considering the higher temperature reactions exhibited by lubricants in the previous section (2-1-4).

(ii) The possibility of lubricants or their decomposition products reacting with the matrix must be considered, particularly at internal surfaces.

(iii) Reactions attributable to loose pure lubricants may even be completely

changed by the physical limitations of a compact. The large specific surface area may act catalytically to cause different reactions or enhance the basic ones.

Weight changes recorded during thermogravimetric analysis were used again to enable lubricant reactions within compacts to be detected. Comparison with basic lubricant decomposition characteristics together with controlled variation of system properties should enable the modifications suggested in (i), (ii) and (iii) above to be identified and studied. Atmosphere variation was restricted to $N_2/10\%H_2$ and argon.

The iron powders used in this investigation were not pure and contained total oxygen and carbon contents of 0.3% and 0.07% respectively. These elements were not expected to remain inactive when heated to 1200°C in either atmosphere and would consequently cause weight changes characteristic of their own reactions. If total carbon and oxygen loss occurred a weight change of 37mg would be recorded from a compact weighing 10g (section 2-1-2). Typical additions of lubricant were 1% by weight or 100mg. The maximum weight change corresponding to complete removal of lubricant and combined elements would therefore be 137mg, C and O loss accounting for 27% of this total. Reactions producing a smaller weight change would be obscured and comparison with basic pure lubricant reactions would be difficult.

The weight losses due to combined carbon and oxygen were eliminated from the total weight loss curves by subtraction. Compacts were pressed to physical properties equivalent to those containing lubricants, but using no admixed lubricant. These were then thermogravimetrically treated in the same conditions as the corresponding lubricated compacts. Subtraction of the resultant thermograms from the total weight losses would leave a weight loss curve characteristic of:

(a) Decomposition of the lubricant within the compact.

(b) Reactions between the compact and the lubricant.

(c) Reactions between decomposition products and the compact.

(d) Reactions between elements combined with the matrix (C,O) and lubricants or decomposition products.

Compacts were generally formed from MP 32 iron powder in the as-received condition. However some early work was carried out using MP 32 sieved to a restricted particle size range (-104, +53μm). Initially it was felt desirable to restrict the particle size distribution in this way, this was found to be unnecessary later. The type of powder used is indicated on each figure and direct comparison between them is unnecessary.

The possibility of deterioration of the Pt/Pt.Rh thermocouple at high temperatures in atmospheres containing hydrogen was recognised. Direct comparison of thermograms, in terms of temperature, has therefore been limited to experimental groupings obtained over short time periods. This was also effective in eliminating the influence of variation within the iron powder batch.

Thermobalance operation was essentially the same as for pure lubricants (2-1-4) differing only in the necessity to counterbalance the heavier sample and thus keep the support rod upright. Cooling to ambient temperature was invariably carried out in the protective atmosphere to prevent oxidation.

The following sections of practical work are presented in a logical order, however some work was actually completed out of sequence, such as isothermal treatment, since it was felt that the data could have assisted the investigations involving mechanical properties, running concurrently. The aspects of lubricant decomposition within compacts investigated may be considered under the following headings.

(a) Reproducibility and matrix reactions.

Thermograms due to compacts containing no lubricant were obtained as necessary with each experimental group. Typical curves for MP32 in $N_2/10\%H_2$ and argon are shown in figures 3-13a and 3-13b respectively. Having

considered the possibility of the elements responsible for these weight losses contributing to lubricant reactions, it was considered desirable to establish their nature. Chemical analysis for carbon and oxygen was performed on compacts corresponding to figure 3.13a, thermogravimetrically treated in $N_2/10\%H_2$ to temperatures of 520, 680, 960, 1120 and 1200°C. Total oxygen was determined in a Balzer Exhalograph and carbon analysis was carried out by oxidation and carbon dioxide determination. Results are shown in table 3-2.*

Several curves are shown in figure 3-13a, [a1] and [a2] illustrate reproducibility and were plotted using temperature calibration curve (a) figure 2-2. Curve [b] is due to a different powder batch and was plotted using calibration (b). Comparison of [a1], [a2] and [b] in figure 3-13a, which are in chronological order, illustrates reproducibility in terms of reaction temperatures (a1 and a2), the comparability of curves plotted using temperature calibrations (a) and (b) (a1 and b) and the effect of powder batch changes in terms of weight changes.

Thermograms were also obtained from compacts of MP32 (-104, +53μm), 80% dense containing 1% zinc stearate, treated in an atmosphere of $N_2/10\%H_2$. These are shown in figure 3-14. Trace [a] was obtained early during this investigation and was plotted using calibration (a) of figure 2-2. Curve [b] was obtained during the final stages from a different powder batch and using calibration (b).

(b) The decomposition of lubricants within compacts of constant density and lubricant content.

The lubricants employed in this section included those of section 2-1-4 and also stearic acid applied to the iron powder as a coating by evaporation of a solvent. The method used was equivalent to that used for zinc stearate in part I. Diethyl ether was found to be a more environmentally suitable solvent for stearic acid than benzene. This material was specifically used to determine the effect of lubricant dispersion. Specimens were thermogravi-

* p 266

metrically treated to a maximum temperature of 1200°C in atmospheres of $N_2/10\%H_2$ and argon, at a constant flow-rate of 500 ml.min^{-1} and a linear heating rate of 6°C min^{-1}.

The basic parent thermograms, corrected for temperature, are shown in figures C-1 to C-6 in appendix C. These are grouped separately since no direct reference is made to them during discussion. Thermograms resulting from subtraction are shown in figures 3-15 to 3-20. It was found necessary to study other materials to assist interpretation and the results due to these are shown in figures at the appropriate points within the discussion (section 4). The use of cylindrical specimens enabled both radial and longitudinal dimensional change to be determined. These are recorded with final trace carbon analyses in table 3-3.

(c) Effect of atmosphere flow-rate.

The influence of atmosphere flow-rate, or velocity, on lubricant removal was investigated using compacts pressed from MP32 (-104, +53μm) to a density of 80% and containing 1% by weight admixed zinc stearate. These were thermogravimetrically treated to 1200°C in $N_2/10\%H_2$ at maximum and minimum flow-rates of 1100 ml.min^{-1} and 200 ml.min^{-1} (35.9 and 6.5mm.S^{-1} at NTP, table 2-1). Parent thermograms are shown in figure C-7, appendix C and subtracted thermograms are shown in figure 3-21.

This combination of lubricant and atmosphere was used again because of the two reactions it exhibits. It should be noted that atmosphere flow-rates refer only to gas passing the external surface of compacts and not passing through pores. In this system the atmosphere is flowing and not dynamic[35] and conditions within pores will be determined by the limits of inhibited diffusion imposed by the presence of a compact. This is discussed in more detail later (section 4).

(d) Effect of compact density, pore characteristics and lubricant content.

The initial work of this section was concerned only with the effect

of limiting pore space on decomposition of the stearate radical, which yields large quantities of vapour over a short temperature range, and on diffusion of gaseous reactents and products through pores. The system chosen was again zinc stearate in $N_2/10\%H_2$.

Lubricant content was maintained constant at 1% by weight whilst pore size was varied by pressing compacts of MP32 (-104, +53μm) to densities of 60%, 80% and 85%. Blanks containing no lubricant were also pressed for subtraction. Thermogravimetric analysis was carried out to 1200°C. The parent thermograms, matrix (blank) reactions and subtracted lubricant reactions are shown in figure 3-22.

Following this work it was decided to limit density variation to 60% and 85% and investigate the effect of pore size and lubricant content simultaneously. Variation of pore size was achieved by using fine and coarse sieved fractions of MP32 (-53μm and 104-180μm). Compacts at each density were pressed, containing 0, 0.5, 1.0 and 2.0% zinc stearate. Open pore space would not only be restricted by density but also by these lubricant additions.

These compacts were thermogravimetrically treated to 1200°C. in $N_2/10\%H_2$ at a flow-rate of 500 $ml.min^{-1}$. Parent thermograms are shown in figures C-8 and C-9 whilst the lubricant reactions are shown in figures 3-23 and 3-24, section 3. Radial and dimensional changes were determined on the compacts corresponding to the initial results (MP32 -104, +53μm). These are recorded in table 3-4. Those pertaining to the compacts formed from coarse and fine MP32 powder are recorded in table 3-5.

It was decided that it would be advantageous to determine the relative proportions of open and closed porosity in compacts pressed from coarse and fine MP32. Compacts containing no lubricant were pressed from these powders to densities between 60% and 92%. Die-wall lubrication was used to prevent damage to the toolset at high densities. Each compact was weighed as pressed and then vacuum impregnated with an oil of pre-determined specific gravity.

Impregnation was carried out repeatedly until constant weight was achieved. Densities were determined by Archimedes' principle, giving the total volume of porosity. The proportion of open porosity, filled with oil, was taken as the volume of impregnated oil (weight of oil/specific gravity). Closed porosity was the difference between total and open.

In this context the term closed implies that which oil of a specific gravity of 0.878 could not penetrate. It can only be assumed that gases and lubricant decomposition products would at least find difficulty in penetrating such porosity. The results are plotted as porosity, open or closed, versus density in figure 3-25.

Microspecimens were produced from fine and coarse compacts in the as-pressed condition at densities of 65% and 90%. Longitudinal and transverse sections of each specimen were mounted and vacuum impregnated with epoxy resin, then polished normally. It was found advantageous to etch with 2% Nital diluted to approximately 1% Nital with further alcohol additions, to prevent undue staining. The corresponding micrographs are shown in plates 3-1 to 3-4.

The effect of density on the decomposition of lithium stearate within compacts was also investigated although here the influence on higher temperature reactions was of major interest. Compacts of MP32 powder with 1% lithium stearate were pressed to densities of 60%, 80% and 85% and heat treated as before. Basic thermograms are shown in figure C-10 and the resultant lubricant reactions are shown in figure 3-26.

2-1-6 Isothermal thermogravimetry.

During the initial thermogravimetric work very high decomposition rates were observed as the stearate radical was removed in the temperature range 300 to 500°C. This could possibly lead to the build up of high pressures within compacts with unfortunate consequences. It was proposed that, if the imposed heating rate was encouraging a high decomposition rate, isothermal

treatments at temperatures within this range may be effective in reducing this decomposition rate. The use of isothermal temperatures below the terminal temperature indicated by normal thermogravimetric analysis should allow decomposition of the stearate radical to proceed at its own natural rate rather than that dictated by the imposed heating rate.

Compacts containing 1% zinc stearate, pressed to a density of 80% were used for this investigation. These were heated in the thermobalance at a linear heating rate of $6^{\circ}C.min^{-1}$ as in previous sections. Isothermal temperatures of 340, 380 and 500°C were chosen to correspond to the stages of initial decomposition, maximum decomposition rate and the end of decomposition for the stearate radical, as shown by the appropriate full thermogram figure 3-14 curve (a). When the isothermal temperature had been achieved the programme controller was isolated and the power input regulated such that isothermal conditions were attained. Maximum temperature variation was $\pm 5^{\circ}C$. Each test was terminated when the rate of weight loss had stopped. The resultant weight loss curves are shown in figure 3-27.

2-2 The removal of lubricants from compacts at high heating rates.

All previous investigations were carried out at a linear heating rate of $6^{\circ}C.min^{-1}$. Commercial sintering commonly employs heating rates of the order of $100^{\circ}C.min^{-1}$, far in excess of the maximum attainable in the thermobalance. In a thermobalance the heating rate is deliberately maintained at a low level to encourage equilibrium conditions to be approached. To achieve high heating rates it was necessary to use a conventional horizontal tube sintering furnace and isothermally heat-treat compacts.

This furnace, a diagram of which is shown in figure 3-28, had a 76mm diameter Inconel tube sealed at each end with a rubber stopper. There was provision for moving specimens from the hot zone to the cooling zone whilst maintaining the protective atmosphere. $N_2/10\%H_2$ was used as the protective

atmosphere throughout this study, at a flow-rate of 1000 $ml.min^{-1}$ to match the velocity of gas flowing through the thermobalance furnace sheath at 200 $ml.min^{-1}$.

With such a furnace arrangement it was difficult to include a thermocouple with specimens therefore heating curves were pre-determined. This was achieved by inserting a Chromel/Alumel thermocouple into a drilled compact. This compact was then placed in a furnace boat with a normal load of samples. The boat was drawn into the furnace hot zone at various preset temperatures and the temperature recorded against time. Cooling rates were also recorded, all results being shown in figure 2-3. With this thermocouple arrangement these times would correspond to temperatures at the centre of compacts not the surface.

It was decided to reheat individual compacts, in duplicate, to a series of temperatures between ambient and 1100°C to reduce experimental error and reduce the number of specimens required. These temperatures, heating times and corresponding preset temperatures taken from figure 2-3, and heating rates are shown in table 2-3. Combinations of preset temperature and desired temperature were chosen to give heating times between 2 and 3.5 minutes and as can be seen from table 2-3, this caused the heating rate to increase with temperature. However even the minimum was an order of magnitude higher than that of the thermobalance.

Compacts were of the same type as those used during thermogravimetric analysis. All were compacted from MP32 to a density of 80% and contained 1% by weight of the lubricants used in section 2-1-5. The influence of compact density was again studied with compacts containing 1% zinc stearate pressed to densities of 60% and 80%. Appropriate blanks containing no lubricant were treated in the same manner for subtraction as before. Results were plotted as weight loss (% of initial) versus temperature as shown in figures C-11 to C-13. These figures represent the total weight losses and are the means

Figure 2-3 .Heating calibration curves for high heating rate thermogravimetric specimens.

Furnace boatload ; 10, 12·5 mm dia. compacts.

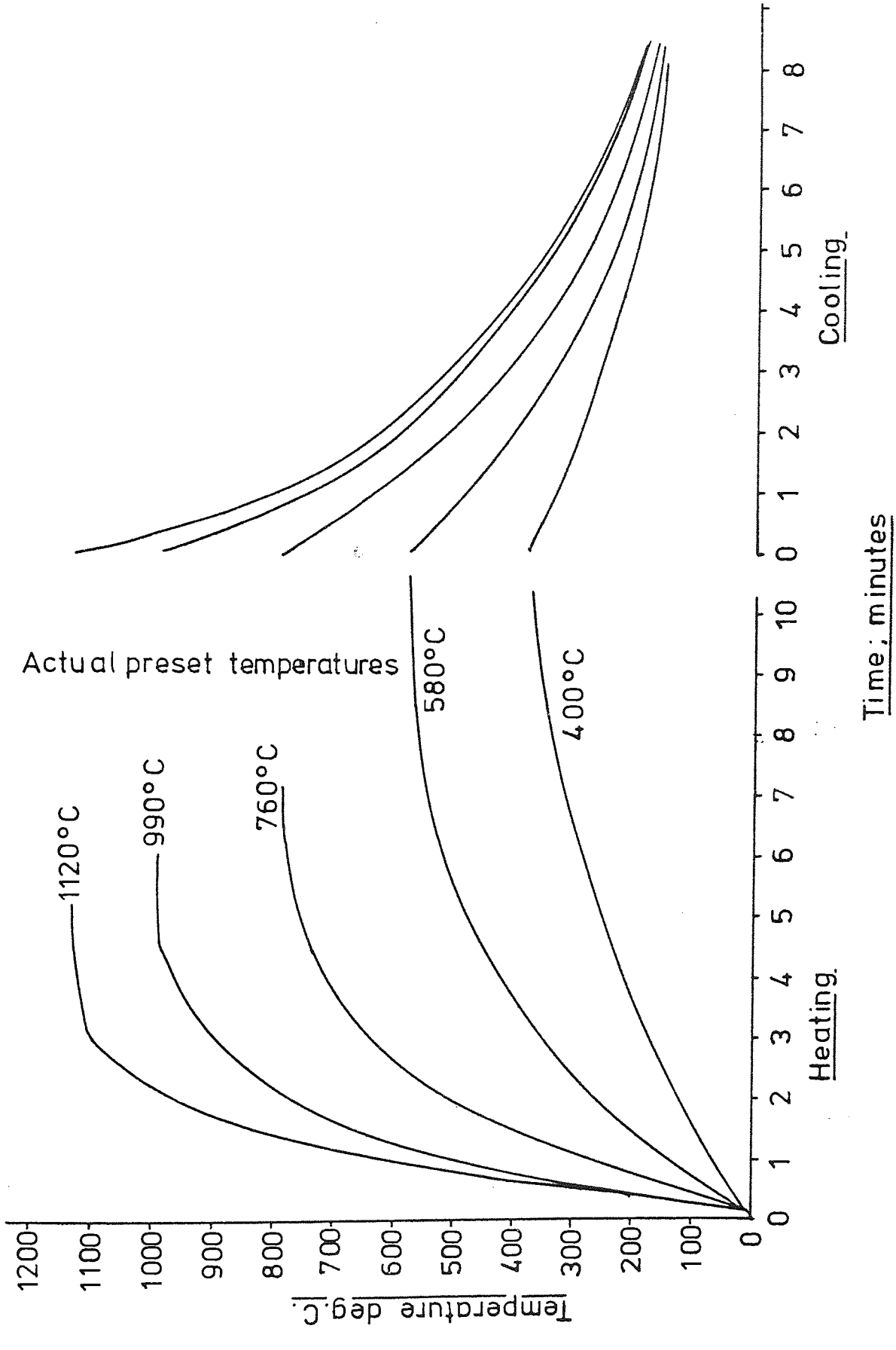

of duplicate specimens.

Table 2-3

Temperatures, furnace pre-set temperatures, heating times and heating rates for weight loss determinations at high heating rates.

Temperature °C	Furnace Pre-set Temperature °C	Time min	Heating rate $^{o}C.min^{-1}$ (overall)
150	400	2.5	60
200	400	3.5	57
260	580	2.0	130
310	580	2.5	120
350	580	3.0	117
400	580	3.5	111
450	760	1.8	250
500	760	2.0	250
580	760	2.5	232
690	760	3.5	197
780	990	2.0	390
900	990	3.0	300
1000	1120	2.3	435
1100	1120	3.0	366

Lubricant reactions were derived from these results by subtraction of blank weight losses, as with thermogravimetric samples. The results of subtraction are shown in figures 3-29 to 3-31. Typical duplicate results are shown for the matrix reactions of figure 3-29 only. Final radial and longitudinal dimensional changes were determined as before with trace carbon analysis. These results are recorded in table 3-6.

2-3 Direct observations of lubricant decomposition.

It was obvious from the previous work that decomposition of the stearate radical involved the rapid removal of at least 80% of the total addition.

However, although there was no doubt that rapid decomposition rates were experienced, there was no indication of the mode of decomposition. Decomposition may proceed by melting, with exudation of molten lubricant from pores onto the compact surface, followed by breakdown on this external surface. Alternatively decomposition may occur entirely within compacts. In the former large pressure increases are unlikely but with the latter the possibility of such pressure increases cannot be discounted.

Unfortunately, thermogravimetric analysis was unable to distinguish between the two possibilities. Surface markings (see plate 4-2) characteristic of spots of molten lubricant had been observed after thermogravimetric treatment of compacts, but only in those in excess of 85% dense. No surface markings were evident on other compacts and so the possibility of either mechanism operating still remained. It seemed that the answer could only be obtained by direct observation.

A simple apparatus, as shown in figure 2-4, was constructed. This consisted essentially of a silica glass tube, 50mm diameter, sealed at each end by bungs with atmosphere inlet and exhaust ports. The total cross-sectional area of the exhaust ports was less than that of the inlet to encourage the maintenance of a positive pressure within the system and thus discourage the ingress of air. A bunsen burner was used as a source of heat which would not obscure the sample. Temperature measurement was achieved with a Chromel-Alumel thermocouple and digital thermometer.

Specimens were either pure lubricants in a silica crucible or compacts pressed from MP32 containing lubricant. When using a crucible the thermocouple was allowed to remain exposed, when using a compact the thermocouple was inserted in the centre of a drilled compact as in section 2-2. Both samples and thermocouple were held on a mesh gauze to prevent contact with the glass tube with consequent uneven heating. $N_2/10\%H_2$ was used as protective atmosphere throughout these observations, at a flow-rate sufficient

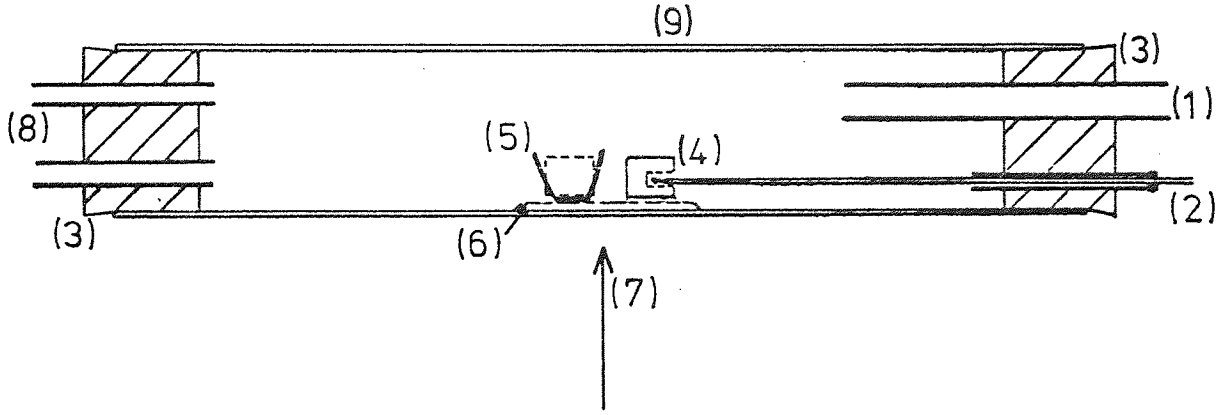

KEY Scale 1 : 25

1- atmosphere inlet

2- thermocouple

3- bungs

4- optional drilled compact for thermocouple

5- sample, compact or crucible

6- mesh support

7- heat

8- atmosphere outlet

9- glass tube

Figure 2-4 . Apparatus for direct observation of lubricant decomposition

to move decomposition products away from the vicinity of specimens.

The maximum temperature obtained was 530°C, a note was taken of the maximum temperature and corresponding time for each sample in order to calculate overall heating rates. Weight losses were recorded for all compacts.

Observations were made with the following specimens.

(a) Pure lubricants; zinc stearate, lithium stearate, stearic acid (fine, medium and coarse particle sizes), stearamide and Cosmic 64 wax.

(b) Compacts pressed from MP32 80% dense, containing 1% by weight of lubricants as in (a), and also 1% evaporated stearic acid.

(c) Compacts formed from MP32 containing 1% by weight zinc stearate at green densities of 60%, 80% and 85%.

(d) Compacts pressed to a density of 85% from fine (-53μm) and coarse (104-180μm) MP32, containing 0.5 and 2.0% by weight admixed zinc stearate.

Observations are recorded in note form in the results, section 3, page 300.

2-4 Influence of lubricants and their removal on mechanical properties of sintered compacts.

There is little data available on the influence of lubricants on sintered mechanical properties. Indeed it is not clear whether they have beneficial or deleterious effects. During the previous sections of this investigation it was found that lubricant decomposition was characterised by an initial reaction, breakdown of the stearate radical or its equivalent, involving the removal of a large quantity of material as vapour over a short temperature or time interval. The contribution by lubricants to observed reactions did not cease with this reaction. In all lubricants studied there was evidence of a residue. This residue was generally a sooty deposit of carbon on particle surfaces, but when a metal radical was present other compounds remained after the initial reaction, notably zinc oxide and lithium carbonate. The possibility of surface reactions between molten lubricant and the metal

particles of the compact was also noted.

Lubricants are deliberately encouraged to adhere to metal particle surfaces during mixing. Their decomposition occurs on this surface and residues are deposited on the same surfaces. There is also the possibility of lubricant not being completely eliminated from interparticle bonds during compaction, as indicated by reductions in green strength (Part I), by virtue of their lubricating properties.

It can be seen that ample opportunity exists for lubricants to influence the development of mechanical properties in sintering compacts, perhaps in the following ways.

(a) Pressure may increase markedly in pores during the initial stages of decomposition, producing a purely physical effect within the compact. This effect may be aggravated by the removal of lubricant trapped in interparticle bonds, perhaps even as a monomolecular layer.

(b) The surface of particles may be modified by reaction with the stearate radical or its decomposition products.

(c) Residues, especially if inert or temporarily so, may prevent reactions between the particle surface and sintering atmosphere. They may also modify surface diffusion characteristics particularly when this is a significant sintering mechanism.

(d) Residues may react with the matrix material or the sintering atmosphere. The products of these reactions may again modify surface properties of metal particles and if gaseous exclude the sintering atmosphere from pores.

Thus many combinations are possible and they may not be temporary or deleterious. The influence of some, particularly physical effects, may also be dependent on compact morphology.

The following parts of work were designed to determine some of the effects of decomposing lubricant on the development of mechanical properties. One was devoted to the physical effect, with emphasis on heating rate. The

second section was concerned with the influence of lubricant decomposition on the development of properties, in terms of temperature and time, and particularly the relative permanence of such effects.

2-4-1 Specimens and measured properties.

Tensile test pieces were pressed from MP32 iron powder, with additions as described later, to the standard 'dogbone' pattern (BS 2590) using floating die compaction. Densities were determined (as-pressed and sintered) from dimensions. Dimensional changes were measured after heat treatment along the tensile axis, perpendicular to the pressing direction.

All dewaxing and sintering was carried out in the horizontal tube furnace described in section 2-2. Calibration of temperature or heating times is described in the appropriate sections.

Ultimate tensile strengths were determined by using a motor driven Hounsfield tensometer with a constant strain rate of 3.18mm.min^{-1} (0.125in. min^{-1}). Elongations were not determined as these were considered unreliable particularly as many of the specimens would not even be approaching a fully sintered condition.

2-4-2 Effect of heating rate on mechanical properties of sintered compacts.

Stearate radical removal is associated with the rapid expulsion of gaseous decomposition products, as shown by direct observation, implying an increase in pressure occurs within compacts as decomposition proceeds. By making the assumptions listed below it is possible to calculate the maximum pressure increase within compacts at this stage. The data is based on the decomposition of 1% stearic acid in a compact of 10g weight. The results for various compact densities are given in table 2-4 below.

Table 2-4

Maximum possible pressure increases within compacts during decomposition of 1% stearic acid (10g compact).

Density %	Pressure Increase					
	20°C(NTP)		400°C		600°C	
	Atmos	Nmm^{-2}	Atmos	Nmm^{-2}	Atmos	Nmm^{-2}
90	560	57	1300	131	1680	170
80	247	25	566	57	735	74
60	94	9	215	22	280	28

The assumptions are;

(1) Breakdown to simple hydrocarbon gases CH_4, C_2H_4 and carbon dioxide.

(2) Perfect gases.

(3) Instantaneous decomposition of all the lubricant present with no escape of decomposition products to atmosphere.

(4) No back reaction.

Comparison of the pressures shown in table 2-4 with green strengths given in figure 4-13* section 4-6-1 reveals that, even allowing for more realistic conditions, pressures may exceed green strength. It is difficult to compare internal pressure increases with transverse rupture strength, as used for green strength determination. However transverse rupture strengths usually exceed the equivalent uniaxial tensile strength. If internal pressure increases are more comparable with tensile strength measured uniaxially the difference becomes even more significant.

Variation of decomposition rate was achieved by using two extreme heating rates, a high one approximately $110^{\circ}C\ min^{-1}$ overall, and a low one of $5.5^{\circ}C\ min^{-1}$. It was proposed to heat tensile specimens containing lubricants to 1100°C in $N_2/10\%H_2$ using these heating rates with no separate low temperature dewaxing treatment. It would be expected that physical

*(and fig. 3-33, part I)

effects due to lubricant decomposition would be most marked at the high heating rate where thermal conditions are probably changing faster than the natural decomposition rate of lubricants. It would be convenient to illustrate the physical effect by direct comparison of tensile strengths obtained with each heating rate. Unfortunately, this would not be valid since compacts subjected to the low heating rate would experience longer times at elevated temperatures, obviously producing a higher final tensile strength than at the high heating rate.

Comparison between heating rates was made on the basis of tensile strength relative to that of unlubricated compacts and also on the basis of the shape of tensile strength versus final density curves. At high densities pressure increases may be large but green strength is high. At low densities pressure increases are low but so are green strengths. A compromise may occur at an intermediate density. If a physical effect is present it may therefore manifest itself in a change in shape of tensile strength/density curves, perhaps even causing a reversal of the normal shape. Tensile compacts were pressed from MP32 with no admixed lubricant and containing 1% by weight of all the lubricants used in this investigation. Initial relative densities were approximately 70%, 80% and 85%. Duplicates were prepared for each heating condition, each duplicate compact being heat treated separately.

The high heating rate was achieved by introducing compacts directly into the furnace hot zone preset at 1100°C. The low heating rate was obtained by allowing compacts to heat up at the natural heating rate of the furnace started from ambient. Heating curves were obtained by inserting a thermocouple, contained within a compact, with a normal furnace load. The result is shown in figure 2-5. The broken form of the low heating rate curve was due to externally imposed changes in power input to the furnace elements which were of the crusilite type. Total heating times were chosen

Figure 2-5 Heating curves for sintering tensile testpieces, high and low heating rate

(furnace load 7 sample, measuring thermocouple set in test piece centre)

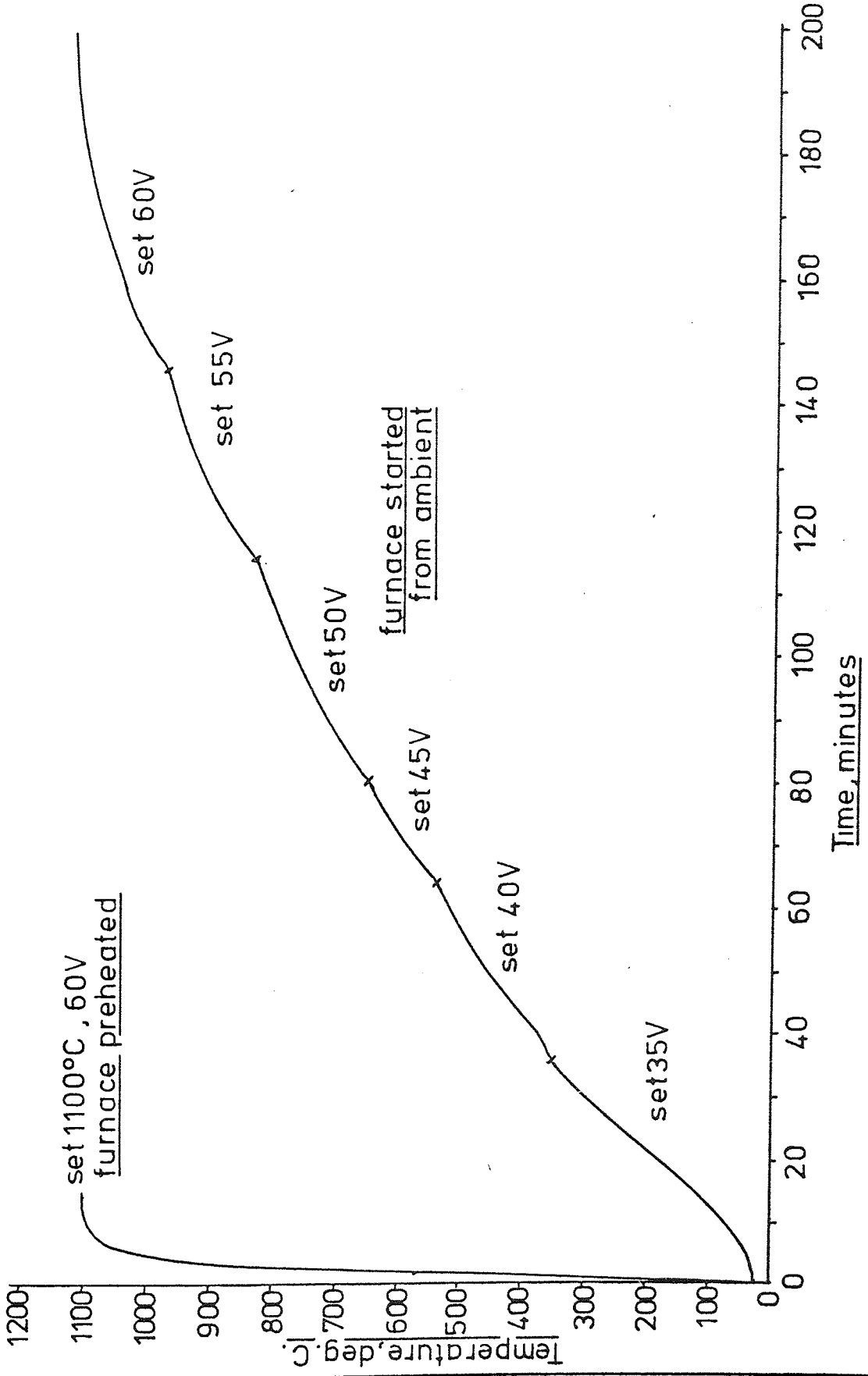

to give a maximum of two minutes at 1100°C to prevent elimination, by isothermal sintering, of damage caused by physical effects.

This time was obviously most critical for the high heating rate with the shortest overall heating time. With this consideration it was decided to investigate reproducibility at this heating rate. Two sets of duplicate compacts containing 1% Cosmic 64 wax were subjected to the high heating rate. The resultant tensile strength/density curves are shown in figure 3-32(a). The results for all materials are shown in figures 3-32 to 3-35. The results, including dimensional change and trace carbon analysis, are also recorded in table C-1 in appendix C.

2-4-3 The influence of residues and other decomposition products on sintering mechanisms.

Final sintered mechanical properties, particularly after prolonged isothermal heat treatment, may only partially reflect any influence that the presence of a lubricant may have had on the development of these properties. Differences in mechanical properties attributable to the presence of lubricants may be more apparent at short isothermal heat treatment times or even during heating up. It was therefore considered advantageous to study the development of properties (tensile strength and dimensional change) during a simulated heating up and sintering cycle. Study of the changes in tensile strength and dimensional change with varying temperature would also help identify the mechanisms whereby lubricants influence the development of sintered properties.

The lubricants used were all stearate based, zinc stearate, lithium stearate and stearic acid(admixed medium particle size and evaporated). Tensile specimens were pressed to a density of 80% from MP32 with 1% by weight of each lubricant. Tensile specimens were also pressed from MP32 containing no lubricant as the basic reference. Heat treatment was carried out in the horizontal tube furnace described previously, duplicate specimens

of each material being heat treated separately in atmospheres of $N_2/10\%H_2$ and argon.

All specimens were subjected to an isothermal dewaxing treatment at 500°C for a total time of 25 minutes in the appropriate atmosphere. The results are therefore more indicative of the effects of lubricant residues than the purely physical effects expected in section 2-4-2.

The furnace was again pre-calibrated using a Chromel-Alumel thermocouple inserted in a drilled compact which was included with a normal furnace boatload of samples. The resultant heating curves for various pre-set temperatures are shown in figure 2-6. The combinations of heating times and pre-set temperatures for isochronal treatment are also shown on this figure. During isochronal treatment (varying temperature) the time given at each temperature was effectively zero. However, as can be seen from figure 2-6, combinations of pre-set temperature and heating times were chosen such that the final heating rates were low and hence slight errors in time would not lead to significant changes in temperature.

Isothermal treatment was carried out at 1100°C for times between 0 and 40 minutes. As can be seen from figure 2-6 the heating up time at this temperature was 10 minutes.

For all conditions each specimen was heat treated separately from its duplicate to obtain a good indication of reproducibility. These duplicate results have been plotted for one material only to avoid confusion. All results are recorded in tables C-2 and C-3 in appendix C. The example given to illustrate reproducibility is shown in figure 3-36 and is the tensile strength curve for MP32 containing no lubricant, isochronally and isothermally heat treated in $N_2/10\%H_2$. It can be seen that variation was particularly high where the development of tensile strength was most rapid, that is in this case at 800°C.

The results of tensile strength determinations are shown in figures 3-

Figure 2-6 .Heating curves for tensile testpieces.

(Heating to centre of compacts, furnace load 7 samples)

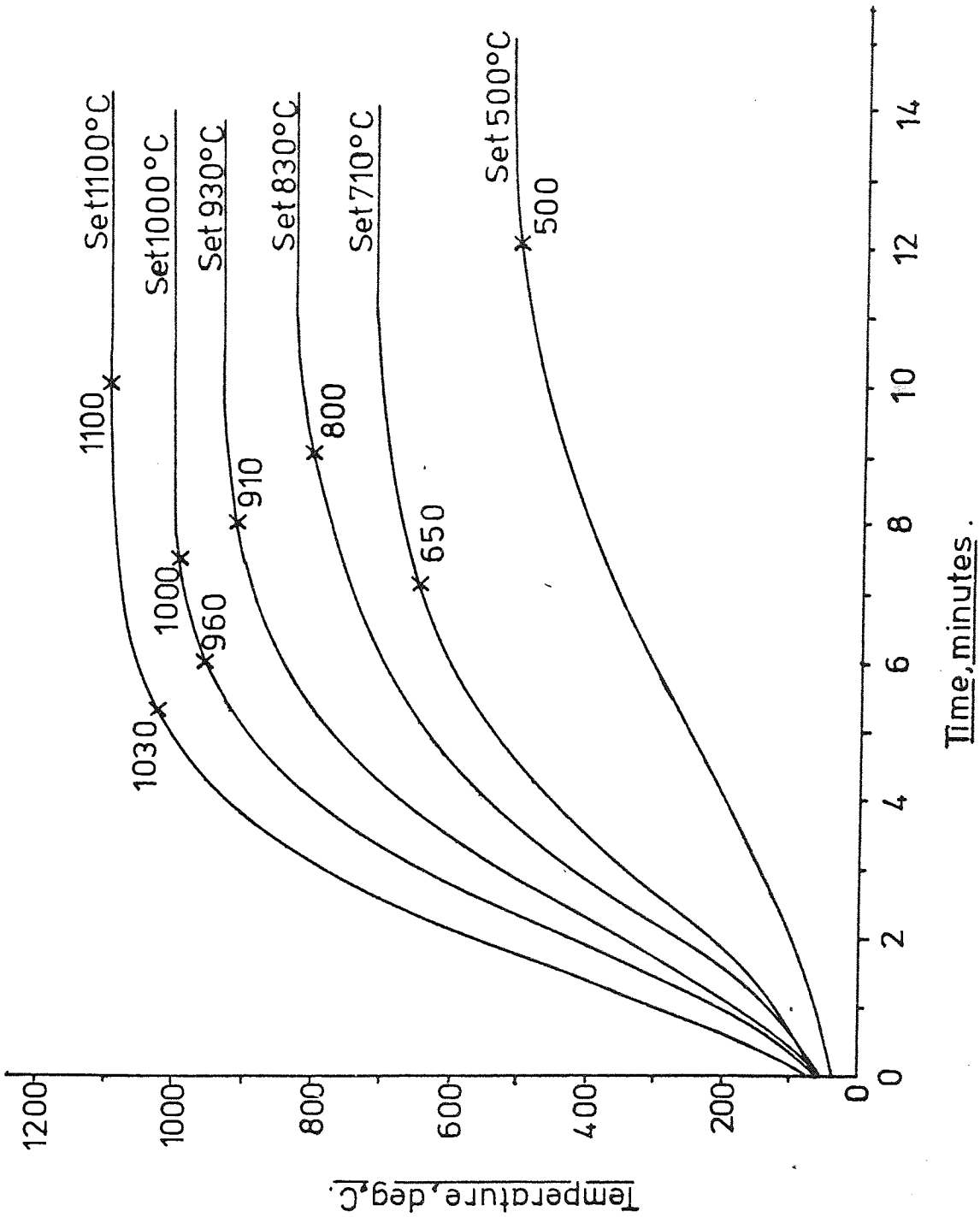

38 and 3-39, whilst the development of dimensional change is shown in figures 3-37, 3-40 and 3-41. Carbon analysis was carried out on selected specimens heat treated in $N_2/10\%H_2$, these are recorded in table C-2 in appendix C.

3 - RESULTS.

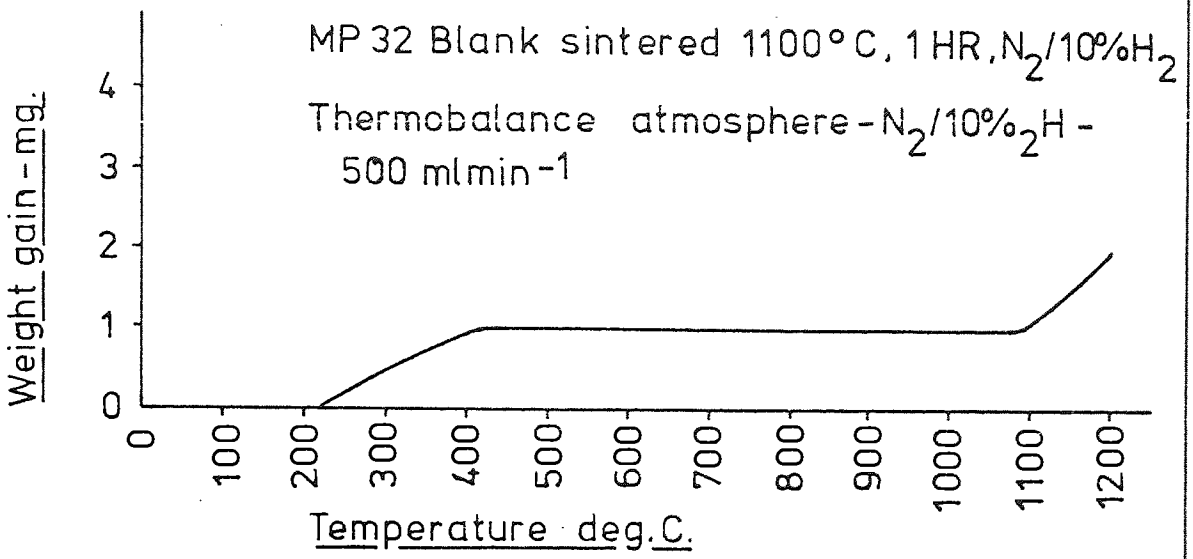

Figure 3-1 . Buoyancy - sintered blank.

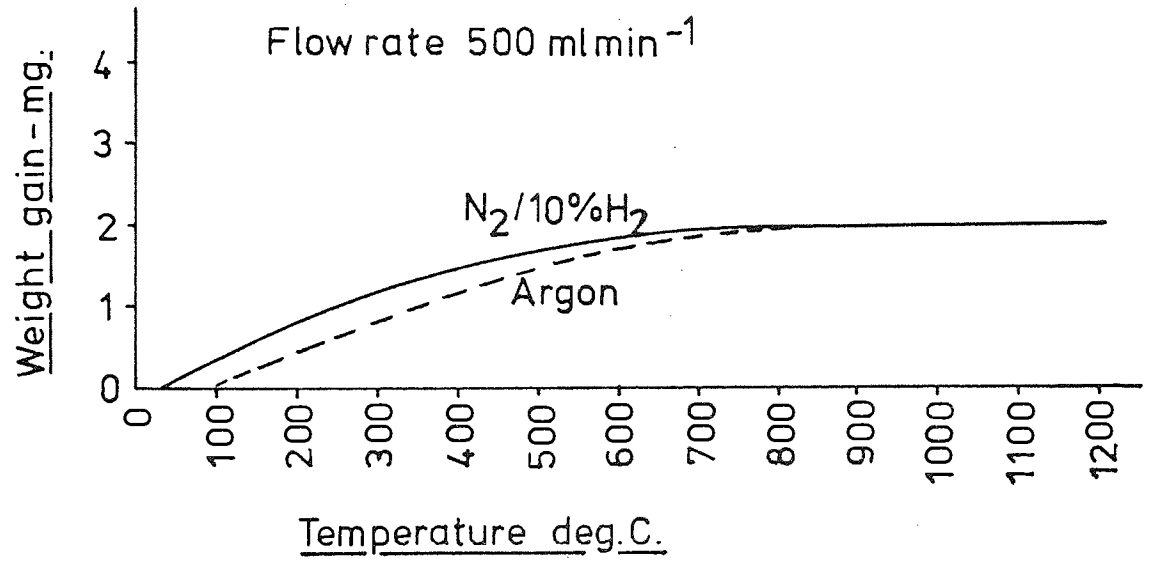

Figure 3-2 . Buoyancy - crucible

Table 3-1

Total carbon and oxygen analyses of compacts used for oxidation and buoyancy trials.

Material and Treatment	% by weight	
	Carbon	Oxygen
MP32 as-received	0.07	0.30
Compact sintered 1100°C 1 hour, $N_2/10\%H_2$	—	0.17
Pre-sintered compact, thermogravimetrically treated to 1300°C, $N_2/10\%H_2$	—	0.13
Compact pressed from as-received MP32, thermogravimetrically treated to 1200°C, $N_2/10\%H_2$	N/D*	0.10
As above Argon atmosphere	<0.01	0.21

*N/D - not detectable

Table 3-2

Total carbon and oxygen analyses for compacts containing no lubricant and thermogravimetrically treated in $N_2/10\%H_2$. (Second powder batch).

Element \ Temp. °C	Ambient	520	680	850	960	1120	1200
Oxygen	0.30	0.26	0.23	0.23	0.20	0.16	0.15
Carbon	0.07	0.07	0.07	0.05	0.04	<0.01	—

(Atmosphere $N_2/10\%H_2$, 500 ml.min^{-1}. Density - 80%).

Figure 3-3 . Pure lubricant reactions-Zinc Stearate.
(300 mg.)

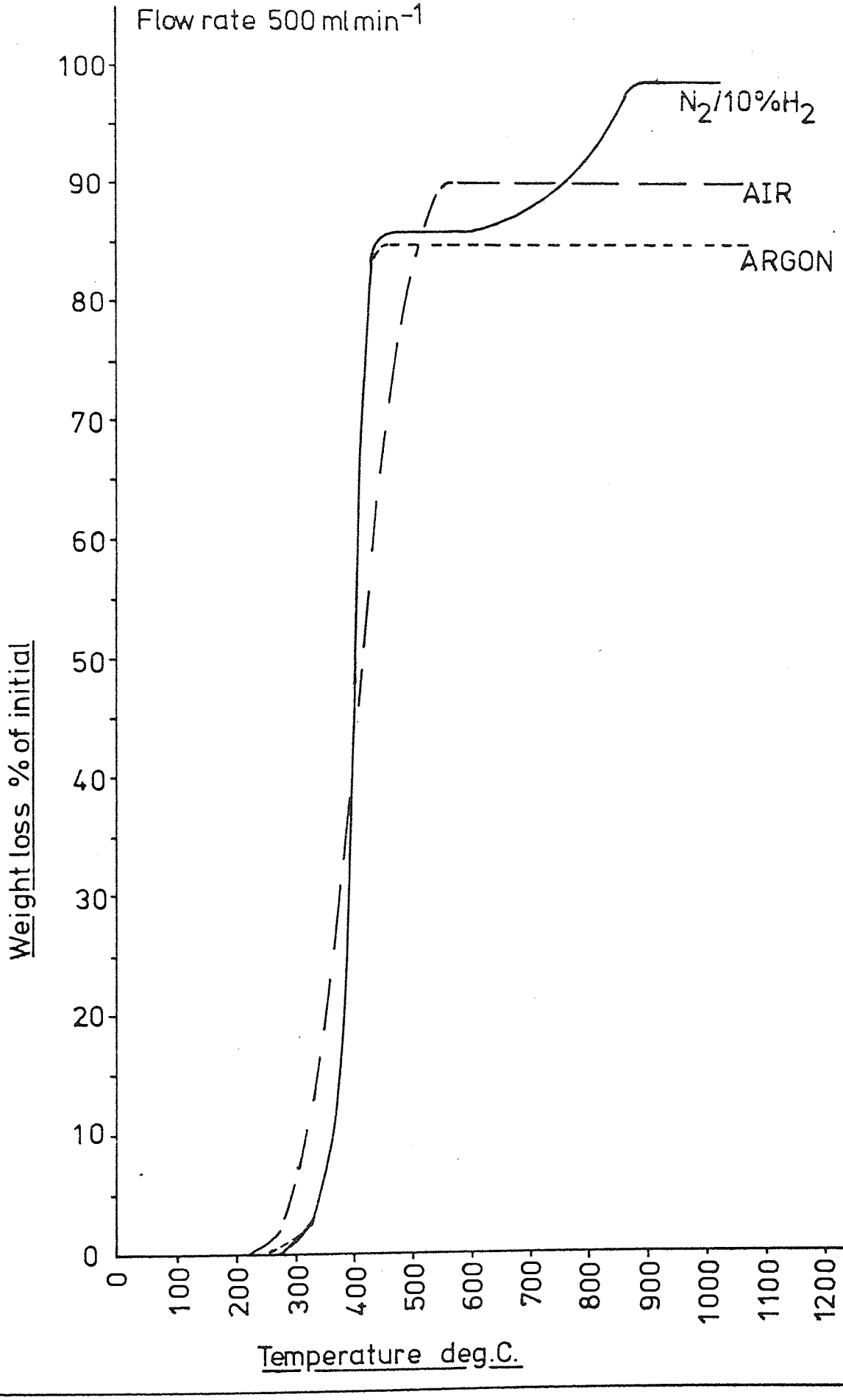

Figure 3-4 . Pure lubricant reactions - Lithium Stearate. (200mg)

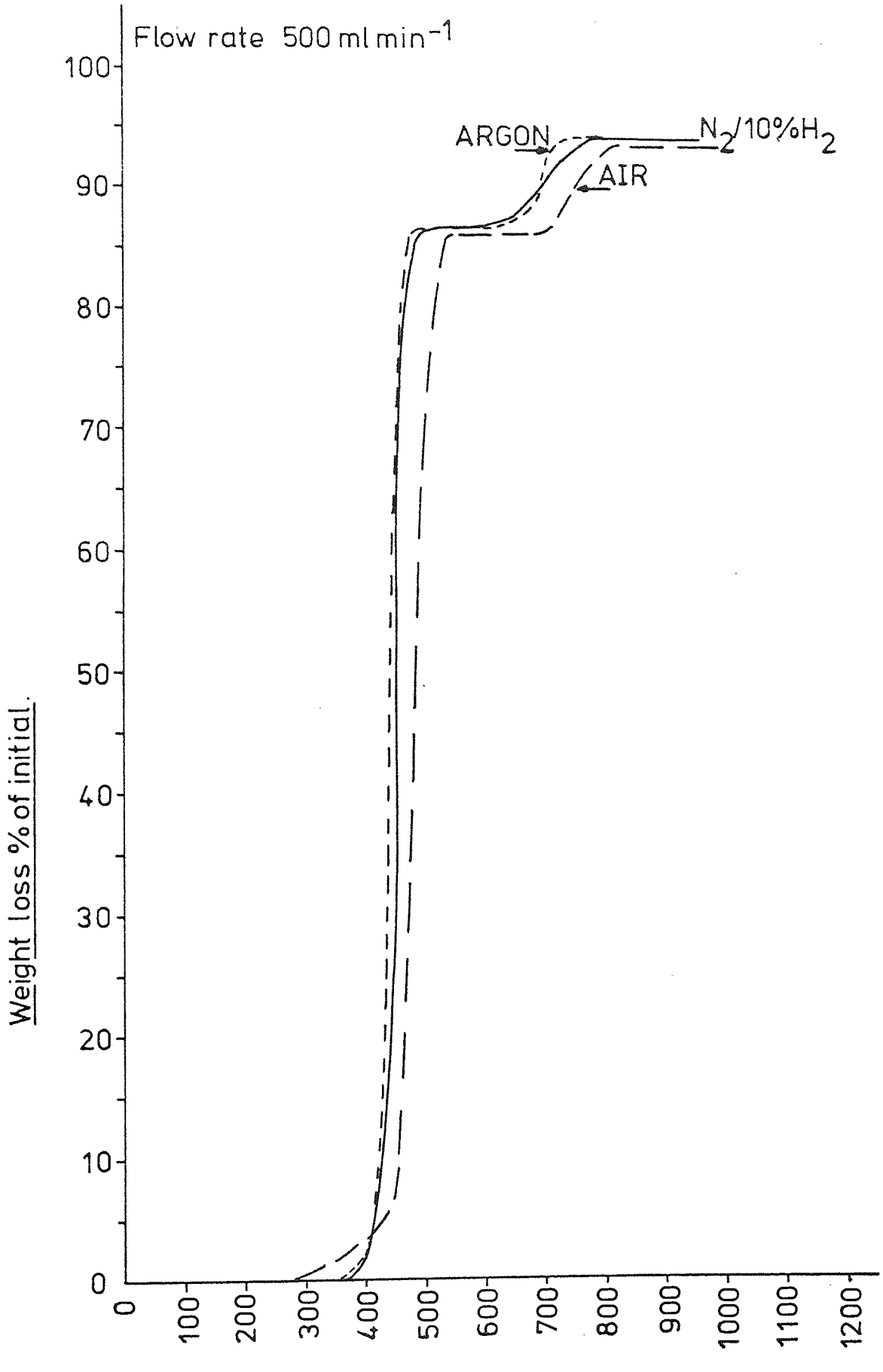

Pure lubricant reactions - Stearic Acid
(200 mg)

Figure 3-5 FINE

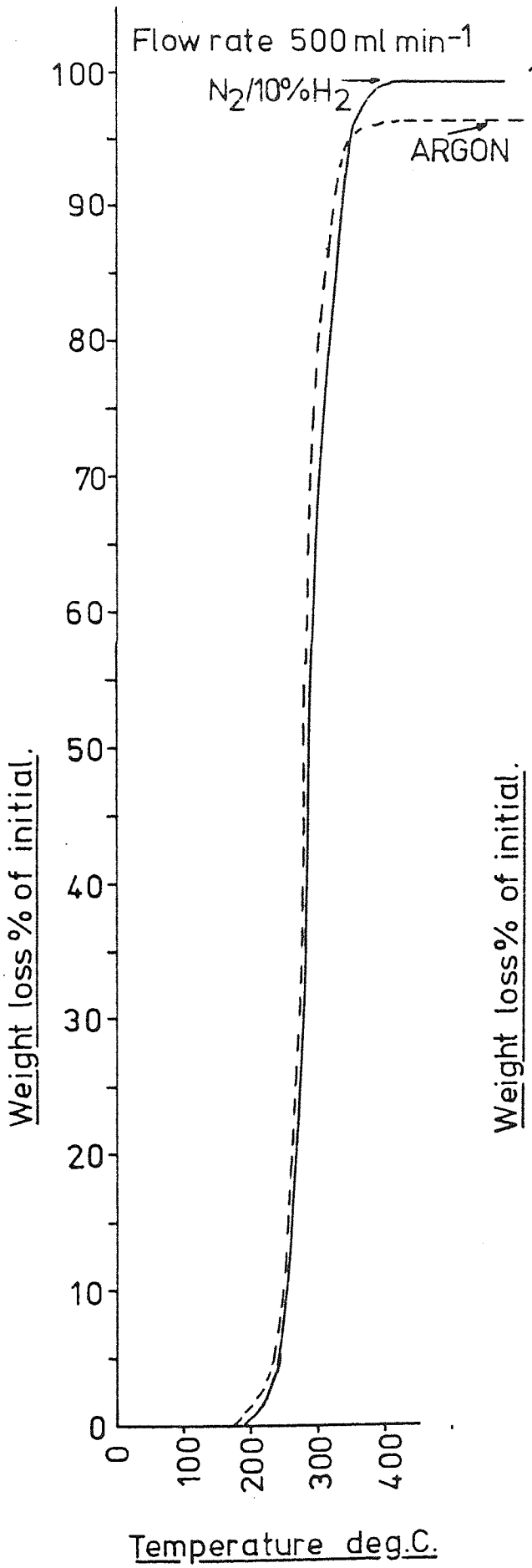

Figure 3-6 COARSE

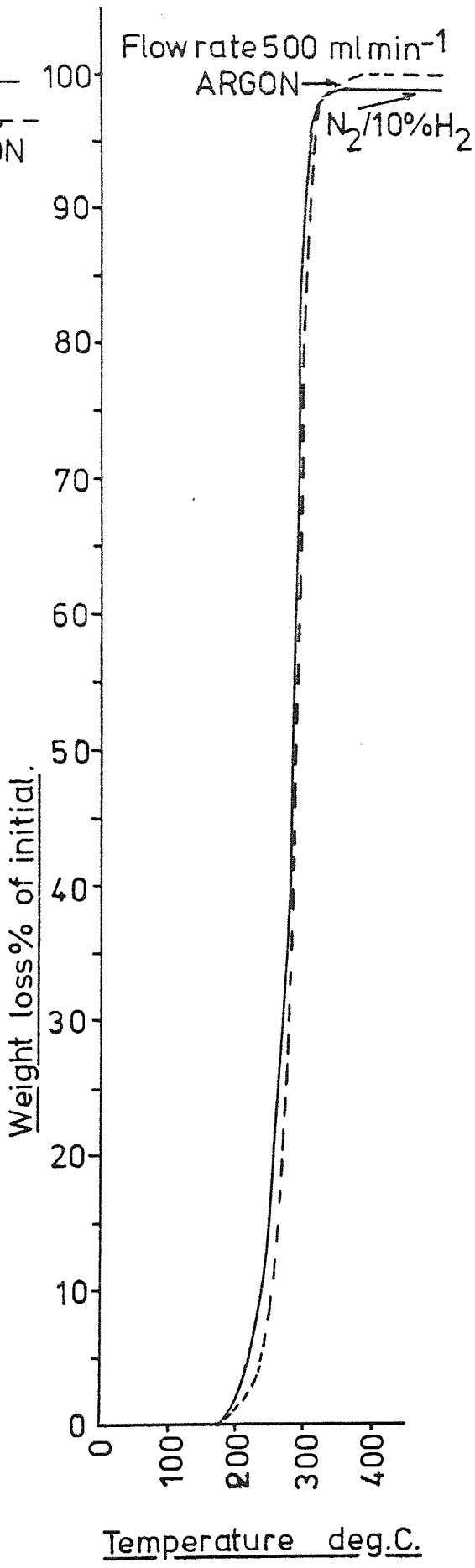

Figure 3-7 . Pure lubricant reactions - Stearic Acid medium. (200mg)

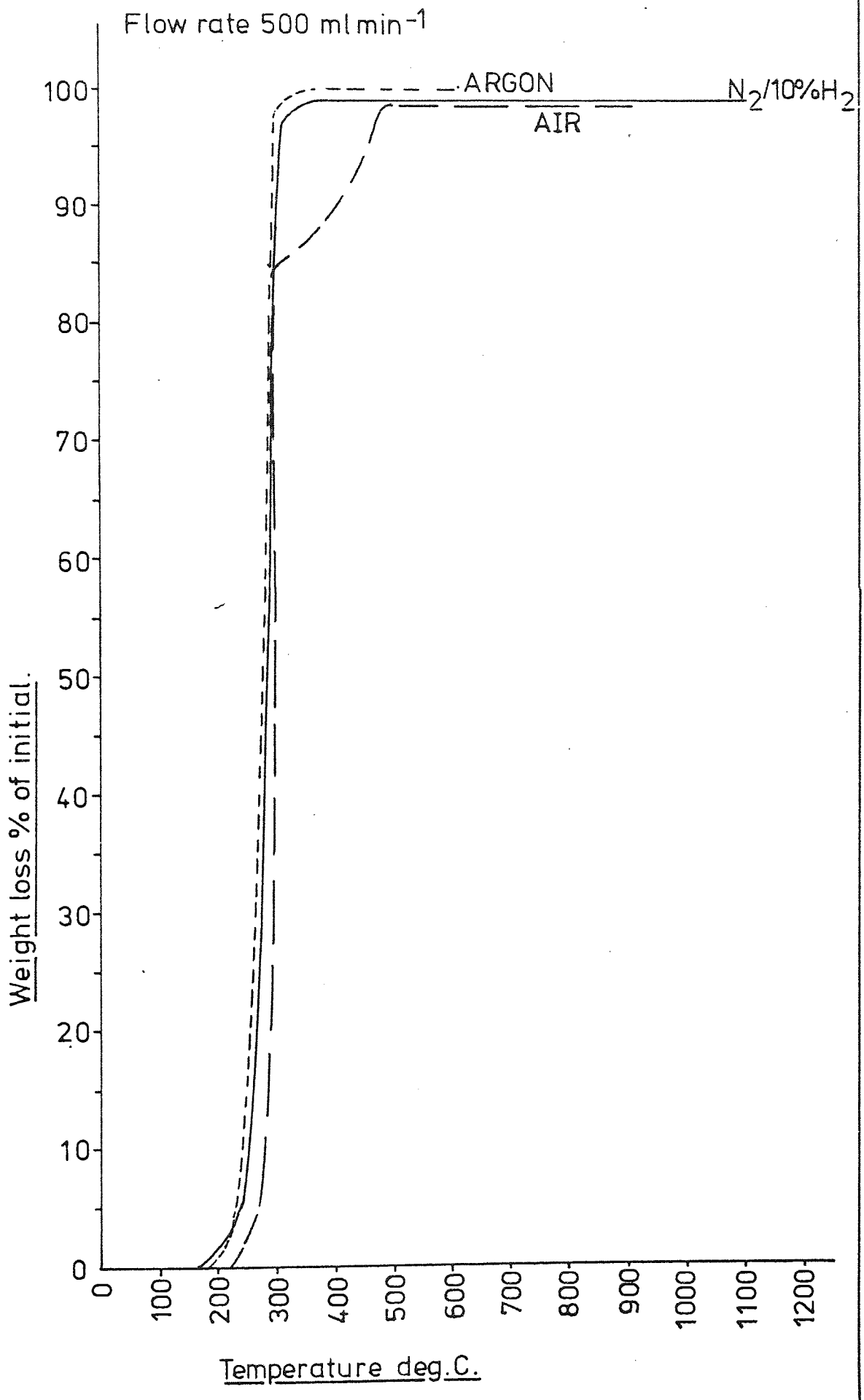

Figure 3-8 . Pure lubricant reactions - Stearamide. (200 mg)

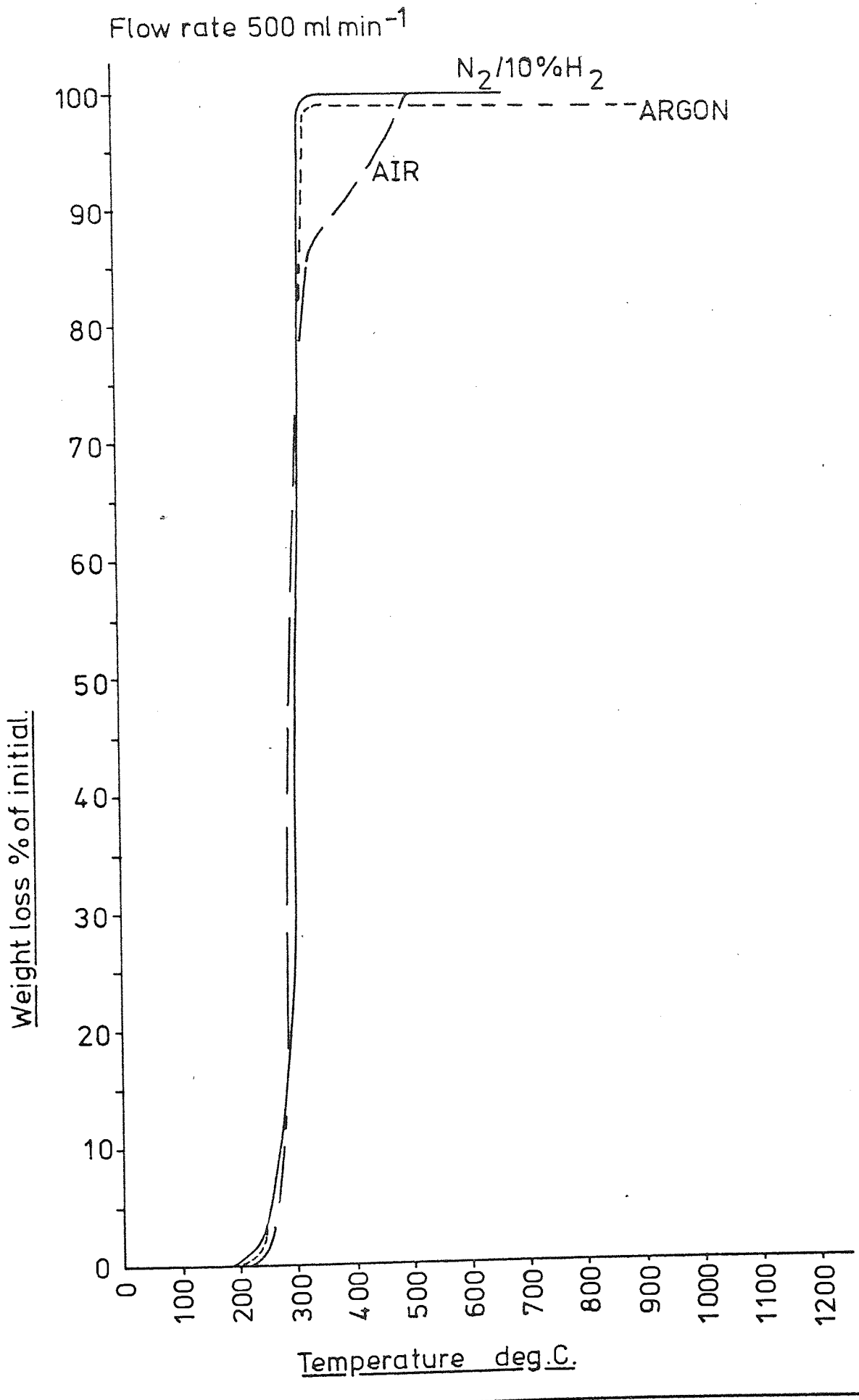

Figure 3-9 . Pure lubricant reactions-Cosmic 64 wax (200 mg)

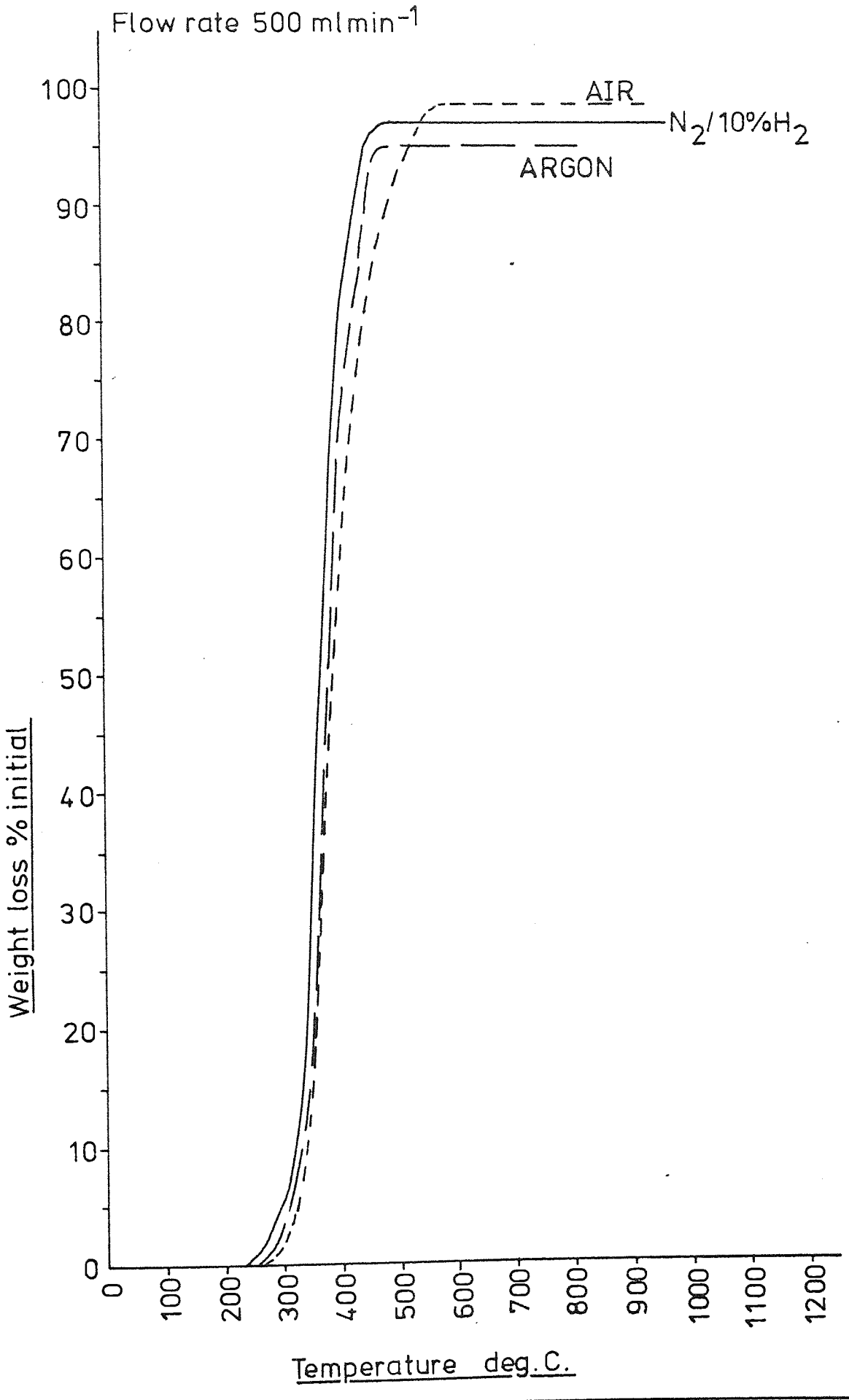

Figure 3-10 , Pure lubricant reactions - Effect of particle size

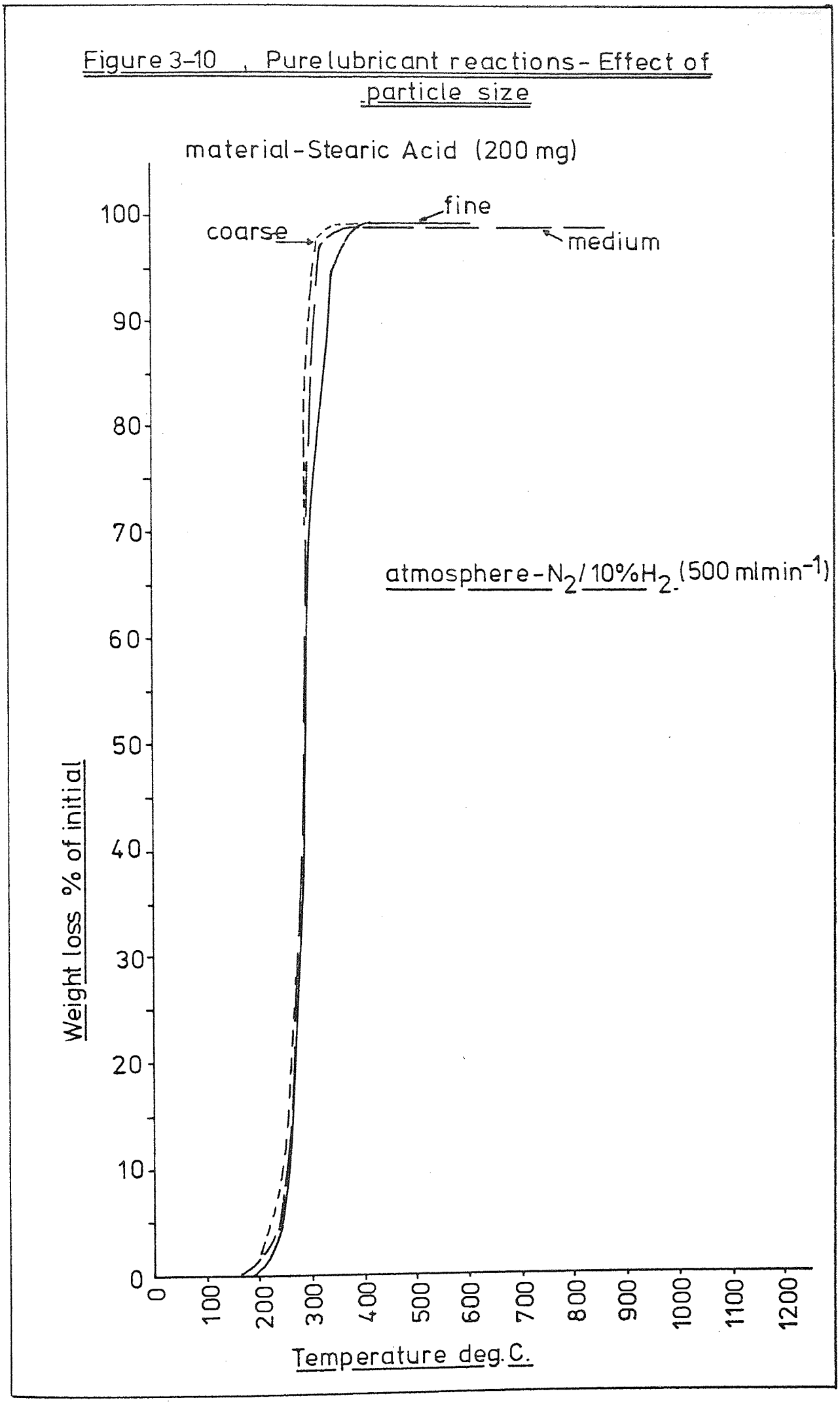

Figure 3-11 . Pure lubricant reactions- Effect of atmosphere flow rate.

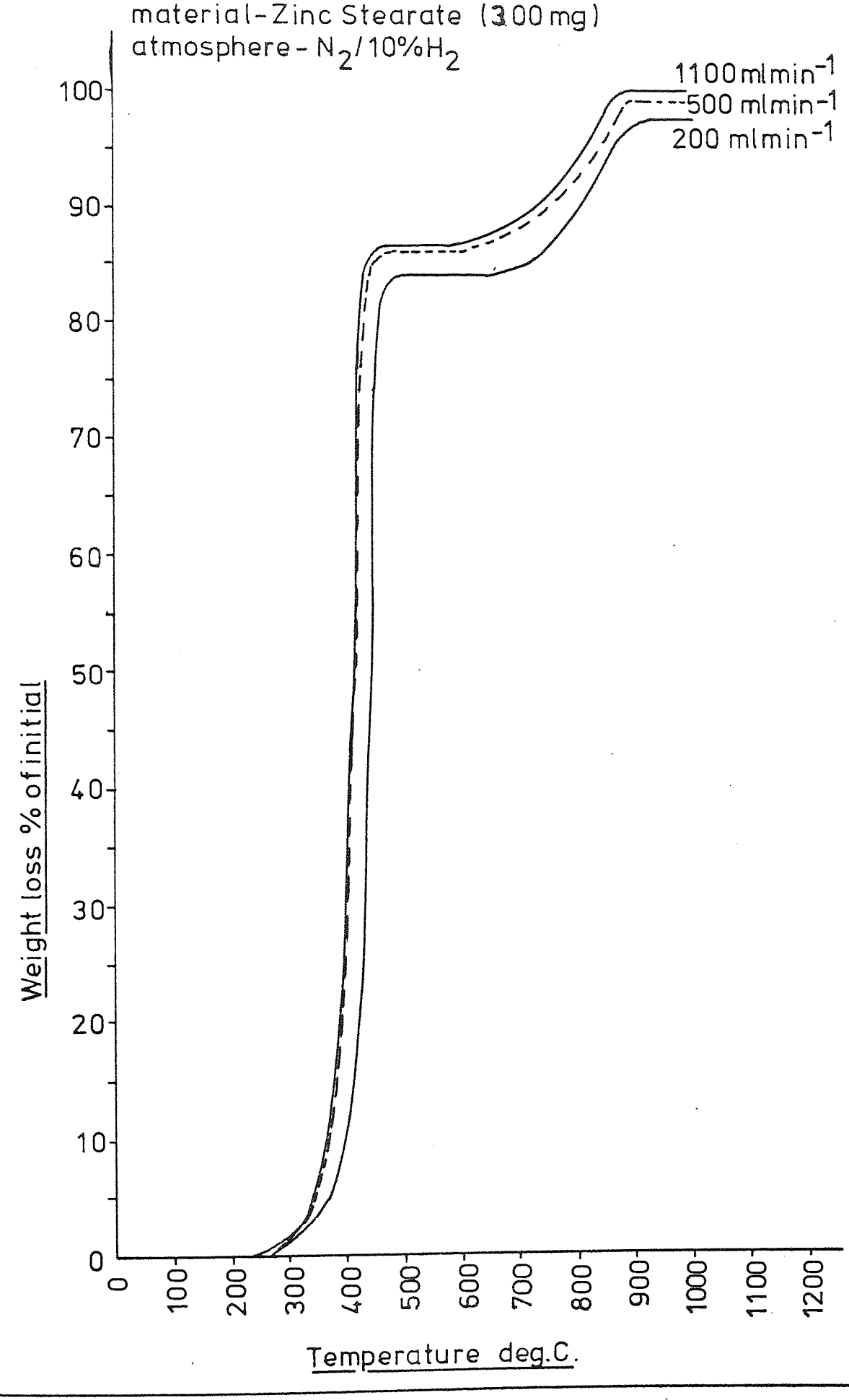

Figure 3-12 . Pure lubricant reactions-Effect of sample weight

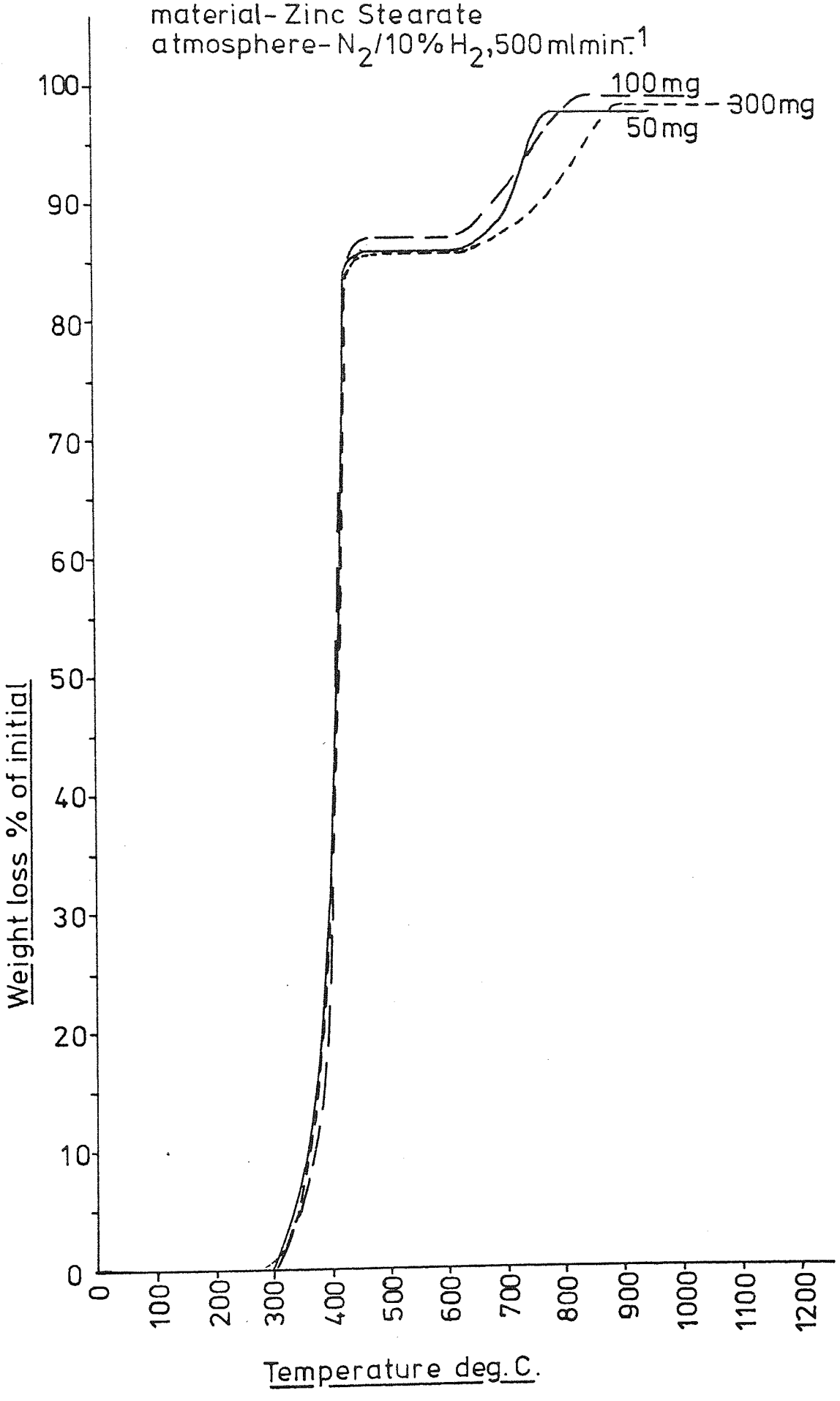

Figure 3-13 .Lubricant reactions within compacts - matrix reactions.

material - MP 32 80% dense. No lubricant.

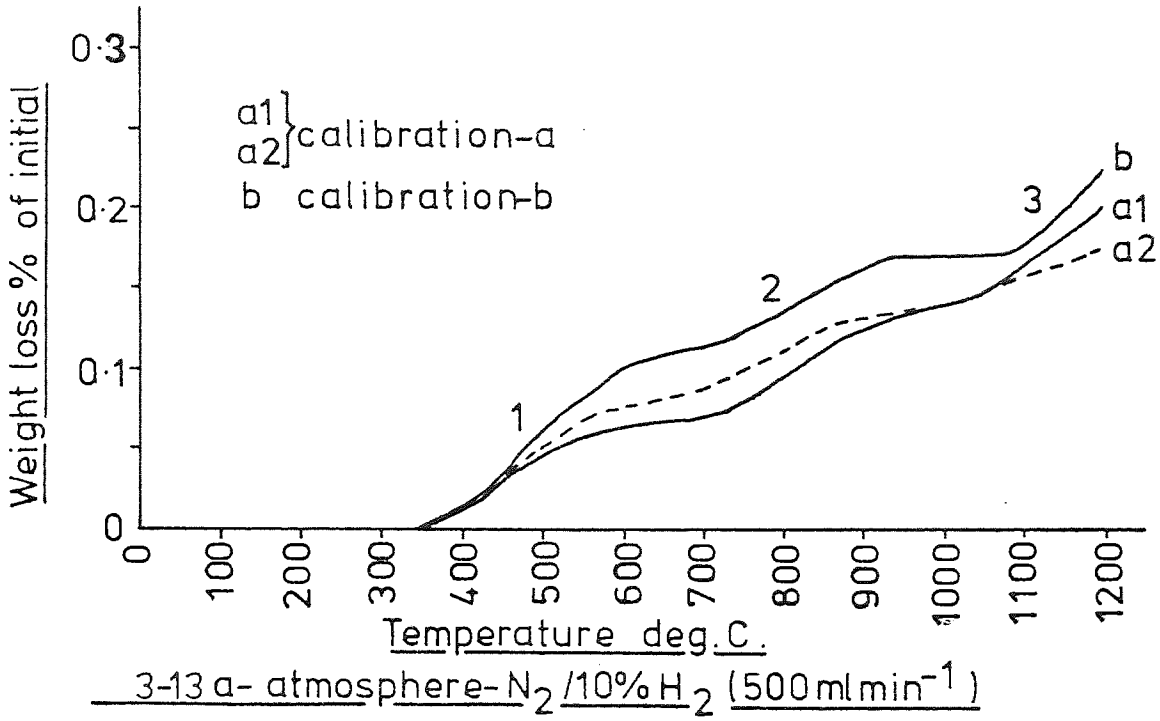

3-13 a- atmosphere- N_2 /10% H_2 (500 ml min^{-1})

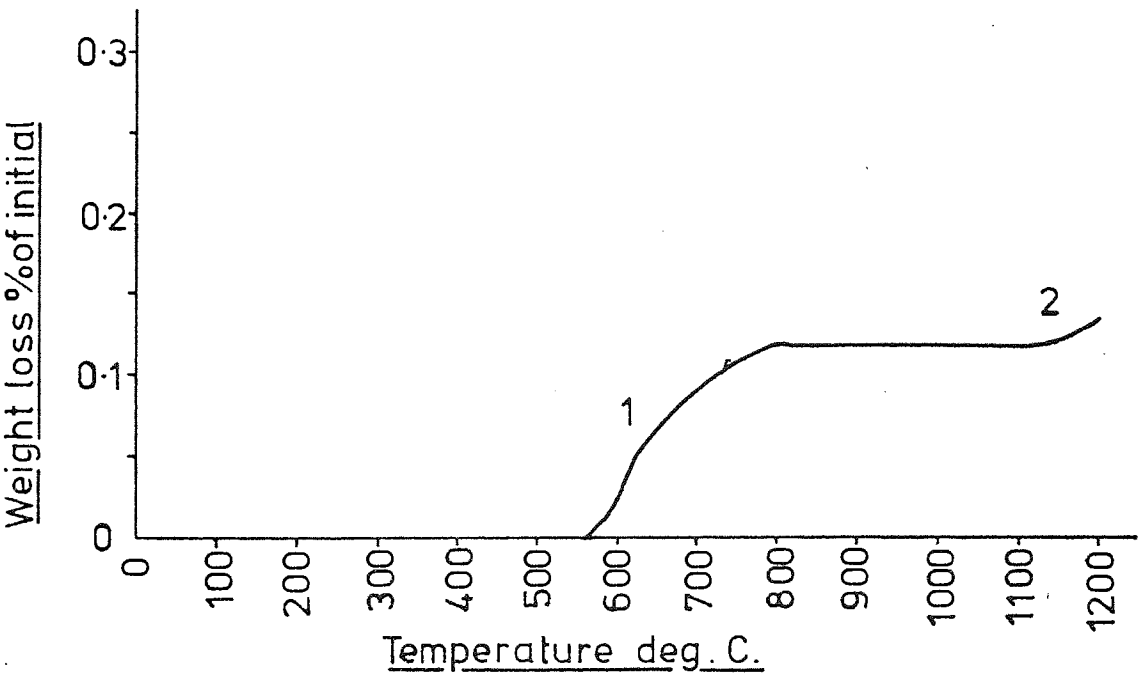

3-13 b - atmosphere - Argon (500 ml min^{-1})

Figure 3-14 . Lubricant reactions within compacts - reproducibility, total weight loss

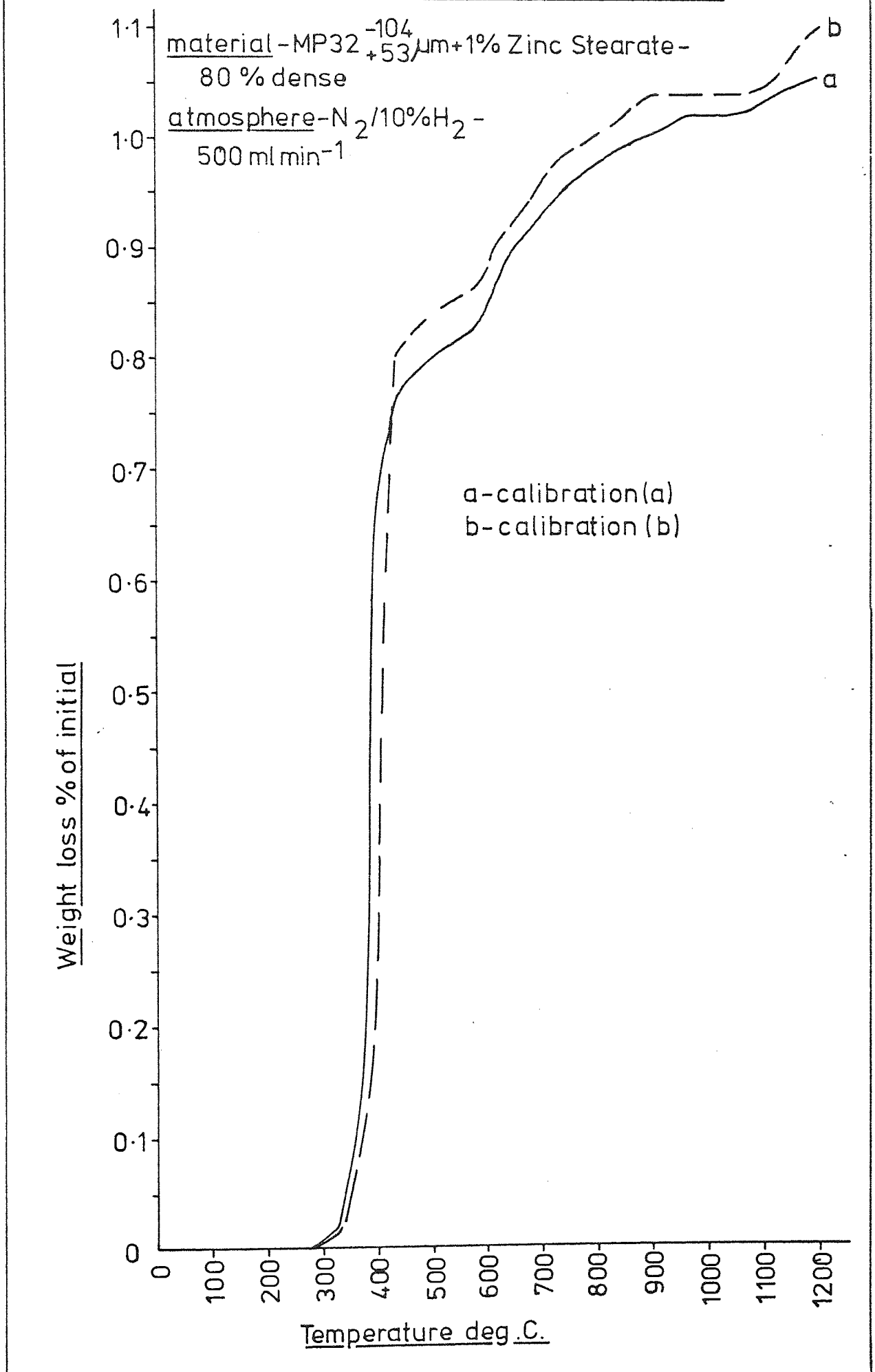

Figure 3-15 . Lubricant reactions within compacts - Zinc Stearate

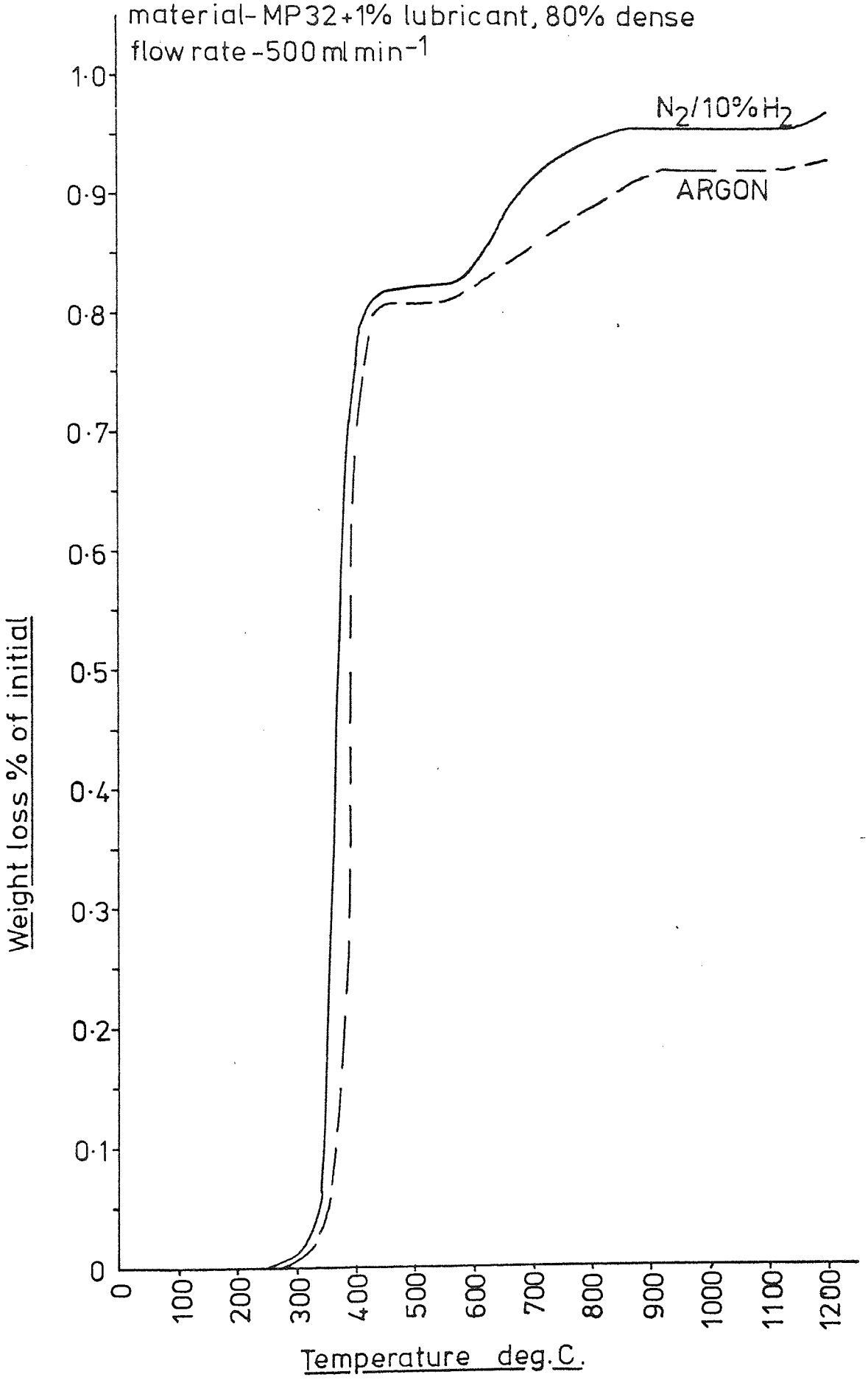

Figure 3-16 . Lubricant reactions within compacts - Lithium Stearate

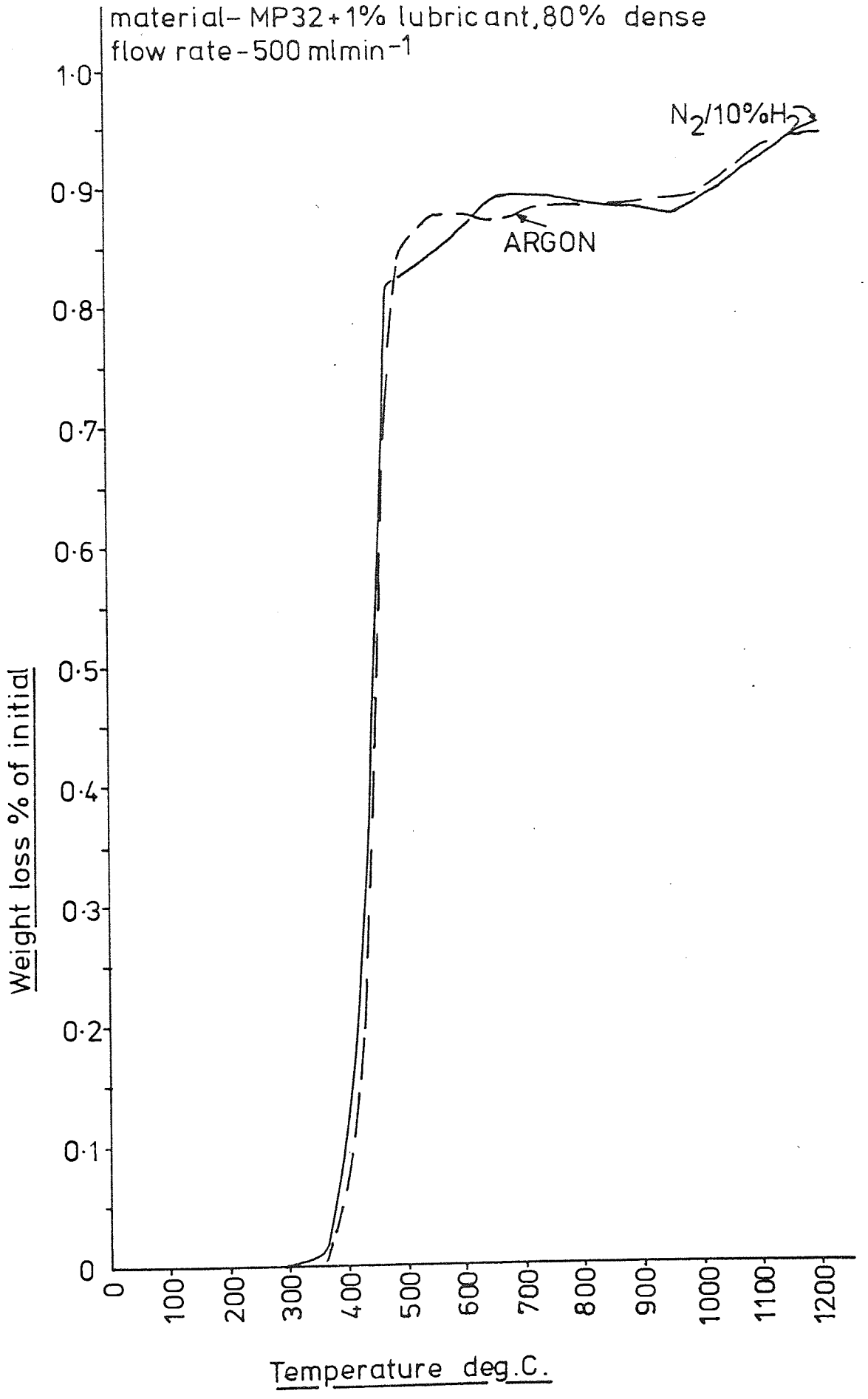

Figure 3-17 . Lubricant reactions within compacts - Stearic Acid

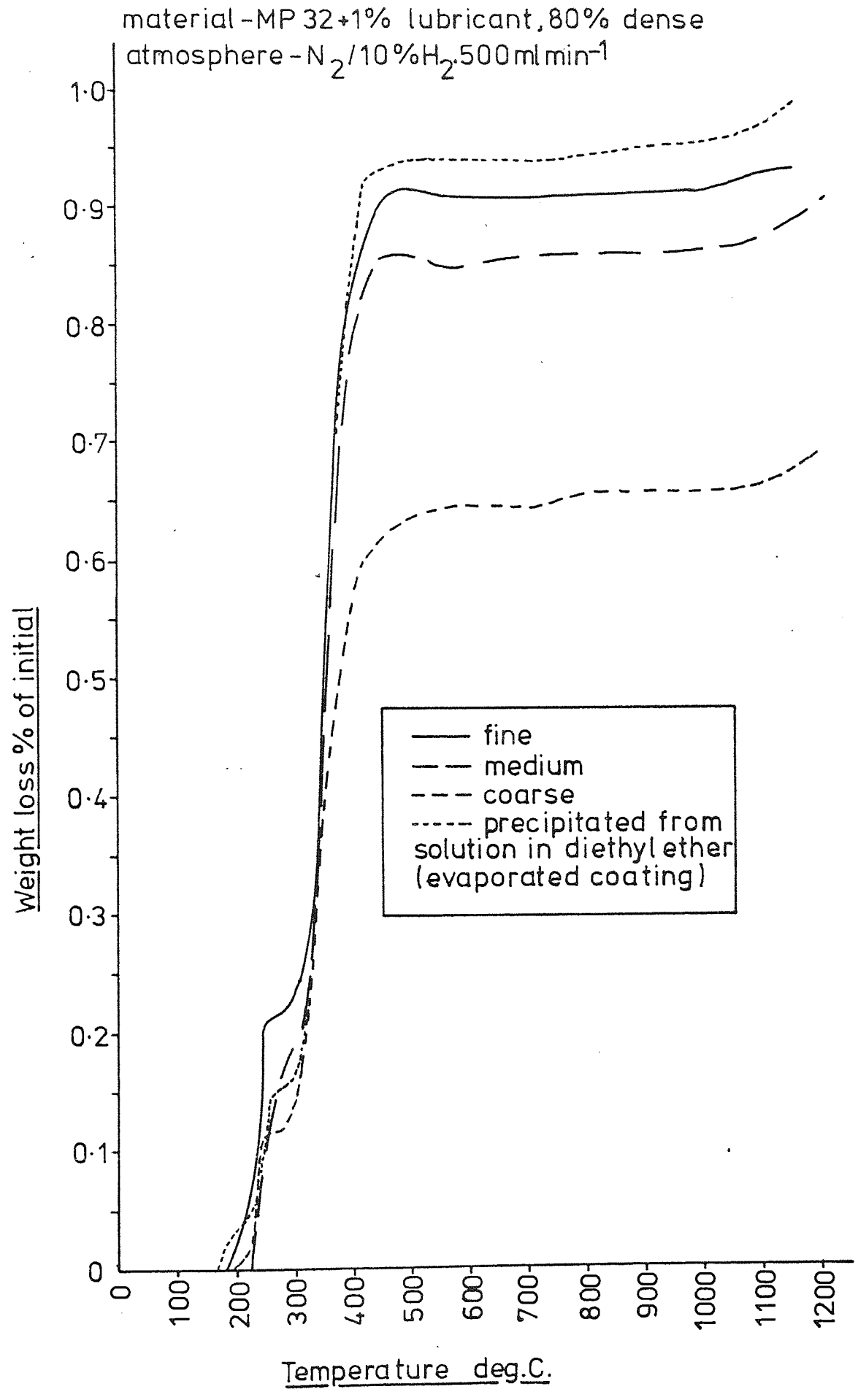

Figure 3-18 . Lubricant reactions within compacts - Stearic Acid

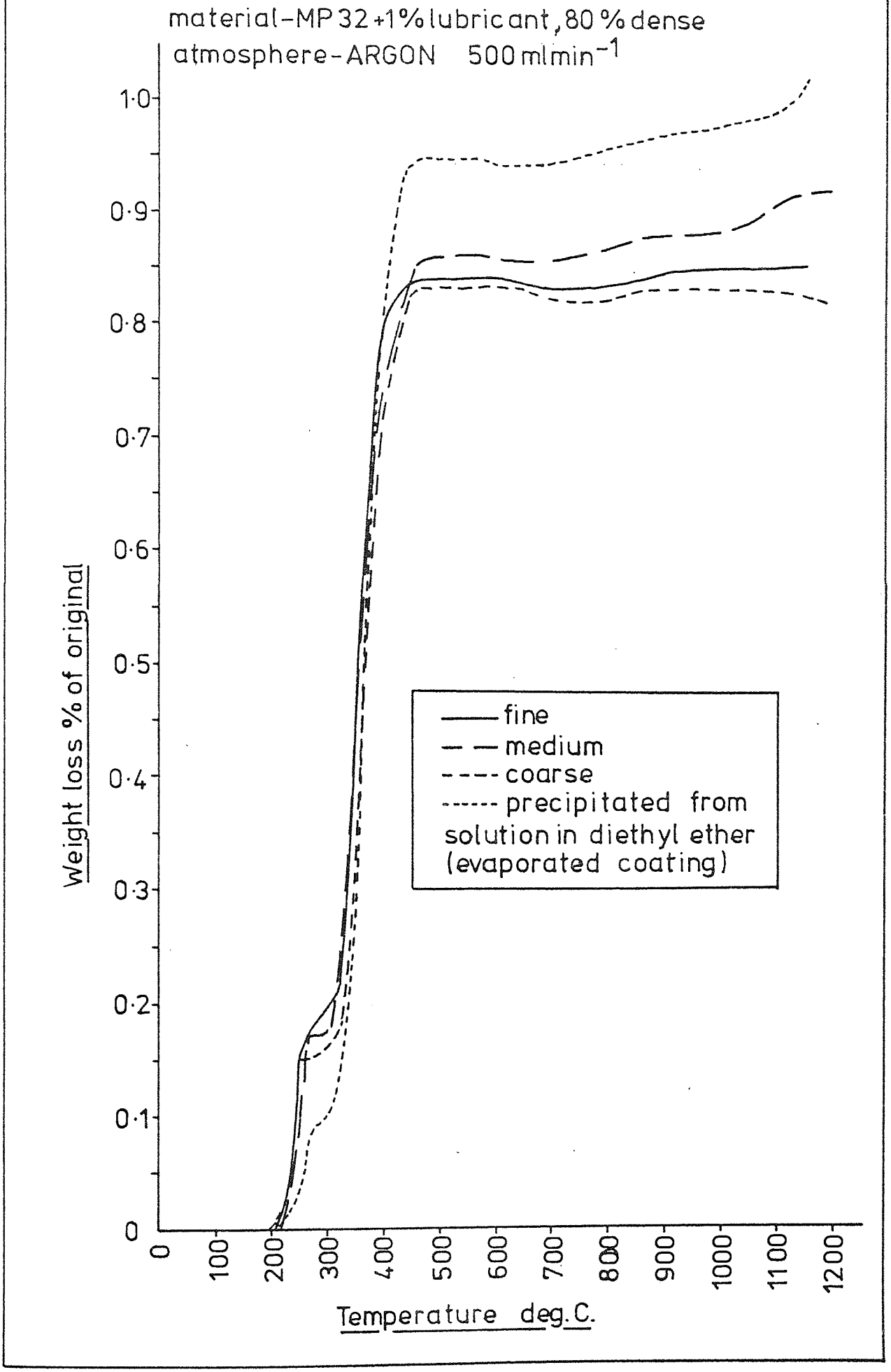

Figure 3-19 . Lubricant reactions within compacts - Stearamide

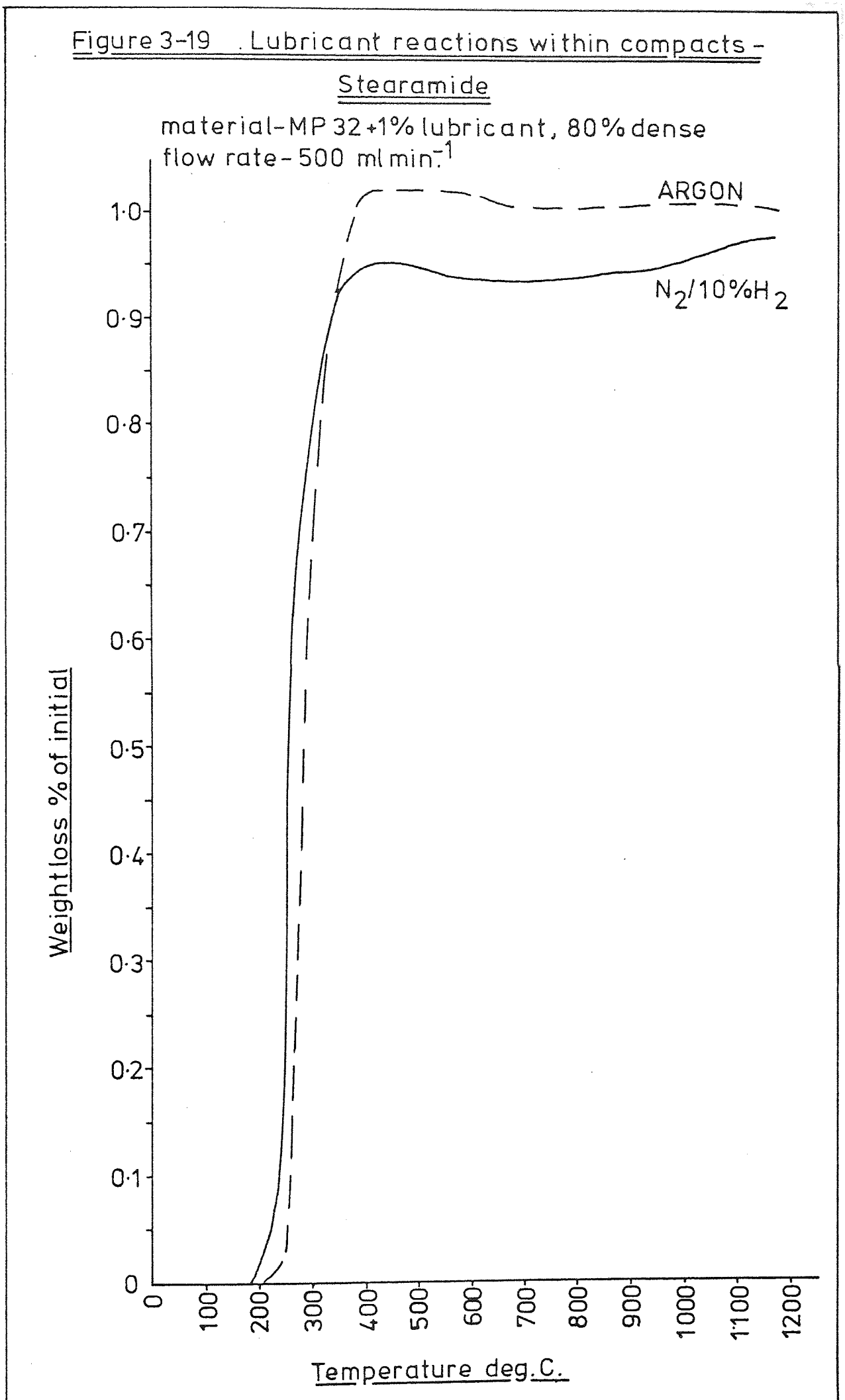

Figure 3-20 . Lubricant reactions within compacts - Cosmic 64 Wax

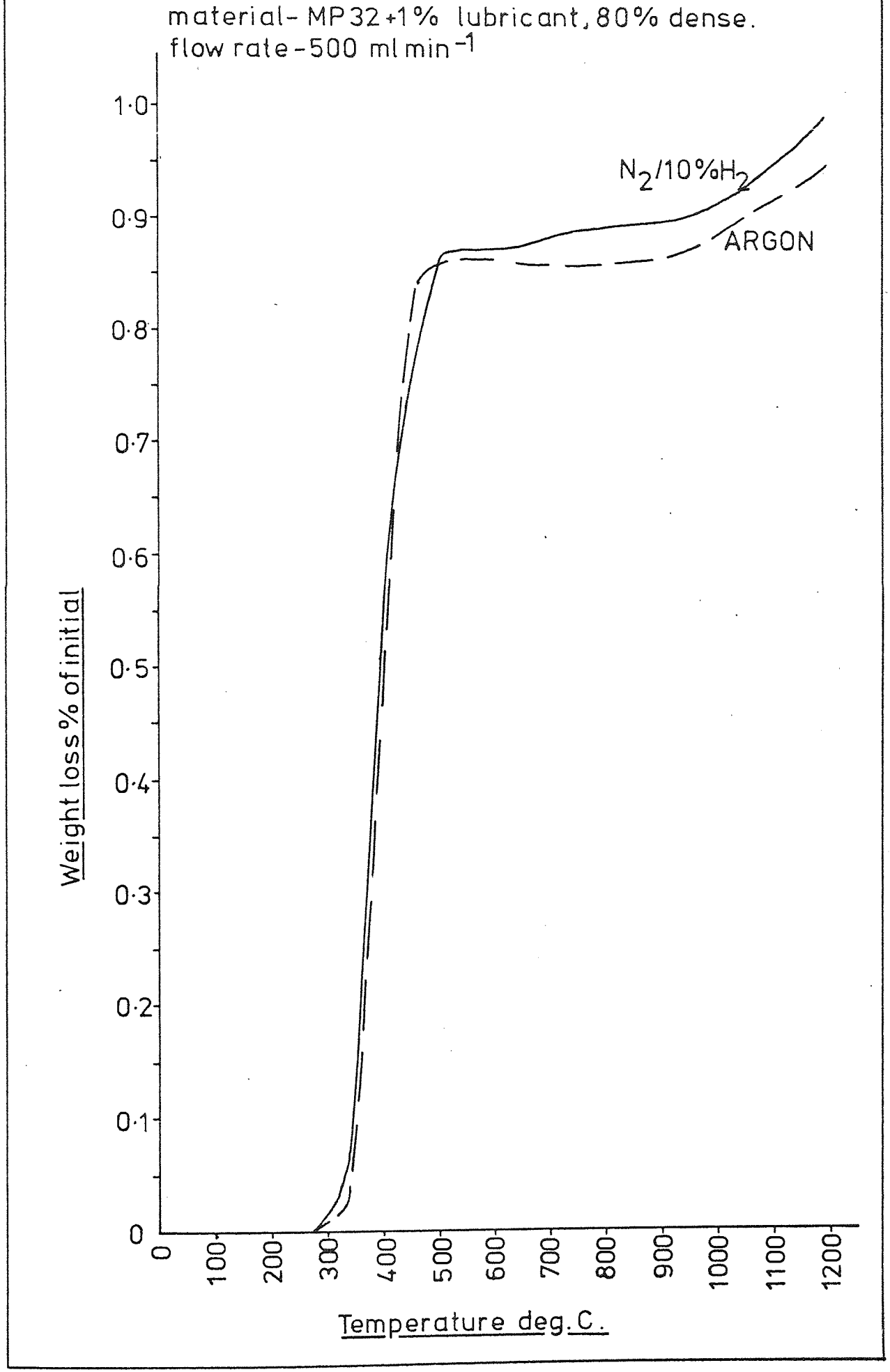

Table 3-3

Final dimensional change and trace carbon contents of compacts containing 1% lubricant, 80% dense, thermogravimetrically treated to 1200°C.

	Lubricant	Dimensional Change %		Carbon %
		Radial	Longitudinal	
$N_2/10\%H_2$	None	-0.39	-0.66	N/D
	Zinc stearate	-0.39	-0.67	N/D
	Lithium stearate	-0.55	-0.89	<0.01
	Stearic acid-Fine	-0.39	-0.76	<0.01
	--- Medium	-0.39	-0.75	<0.01
	--- Coarse	-0.39	-0.93	0.029
	-- Evaporated	-0.40	-0.74	0.039
	Stearamide	-0.39	-0.91	<0.01
	Cosmic 64 wax	-0.35	-0.85	0.058
Argon	None	-0.28	-0.55	<0.01
	Zinc stearate	-0.36	-0.78	0.024
	Lithium stearate	-0.47	-0.91	<0.01
	Stearic acid-Fine	-0.28	-0.71	N/D
	--- Medium	-0.39	-0.70	<0.01
	--- Coarse	-0.16	-0.85	N/D
	-- Evaporated	-0.43	-0.74	N/D
	Stearamide	-0.24	-0.82	<0.01
	Cosmic 64 wax	-0.24	-0.84	0.039

(atmosphere flow-rate - 500 $ml.min^{-1}$). N/D-not detectable.

Figure 3-21 . Lubricant reactions within compacts - Effect of atmosphere flowrate

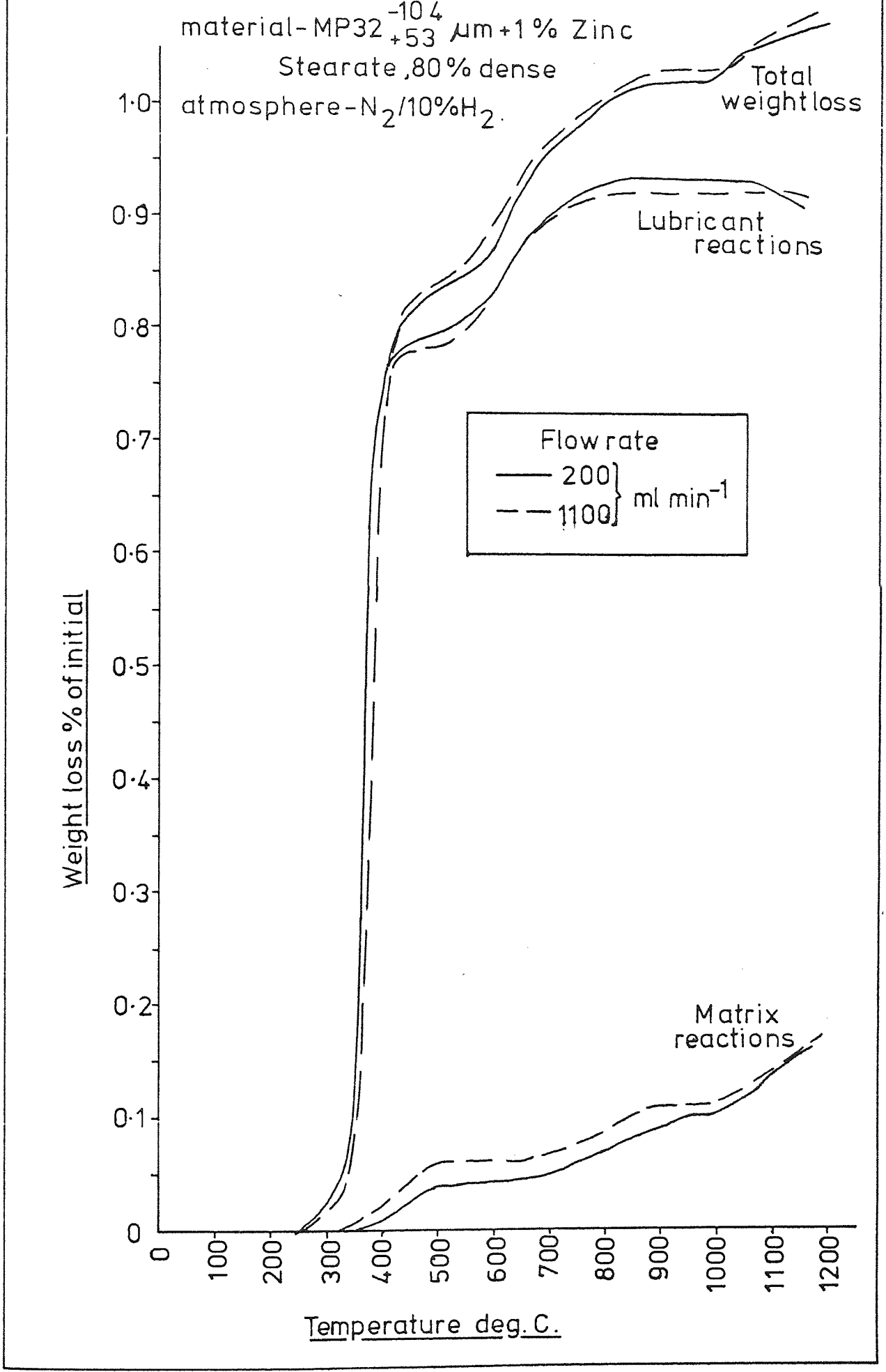

Figure 3-22 .Lubricant reactions within compacts - Effect of compact density

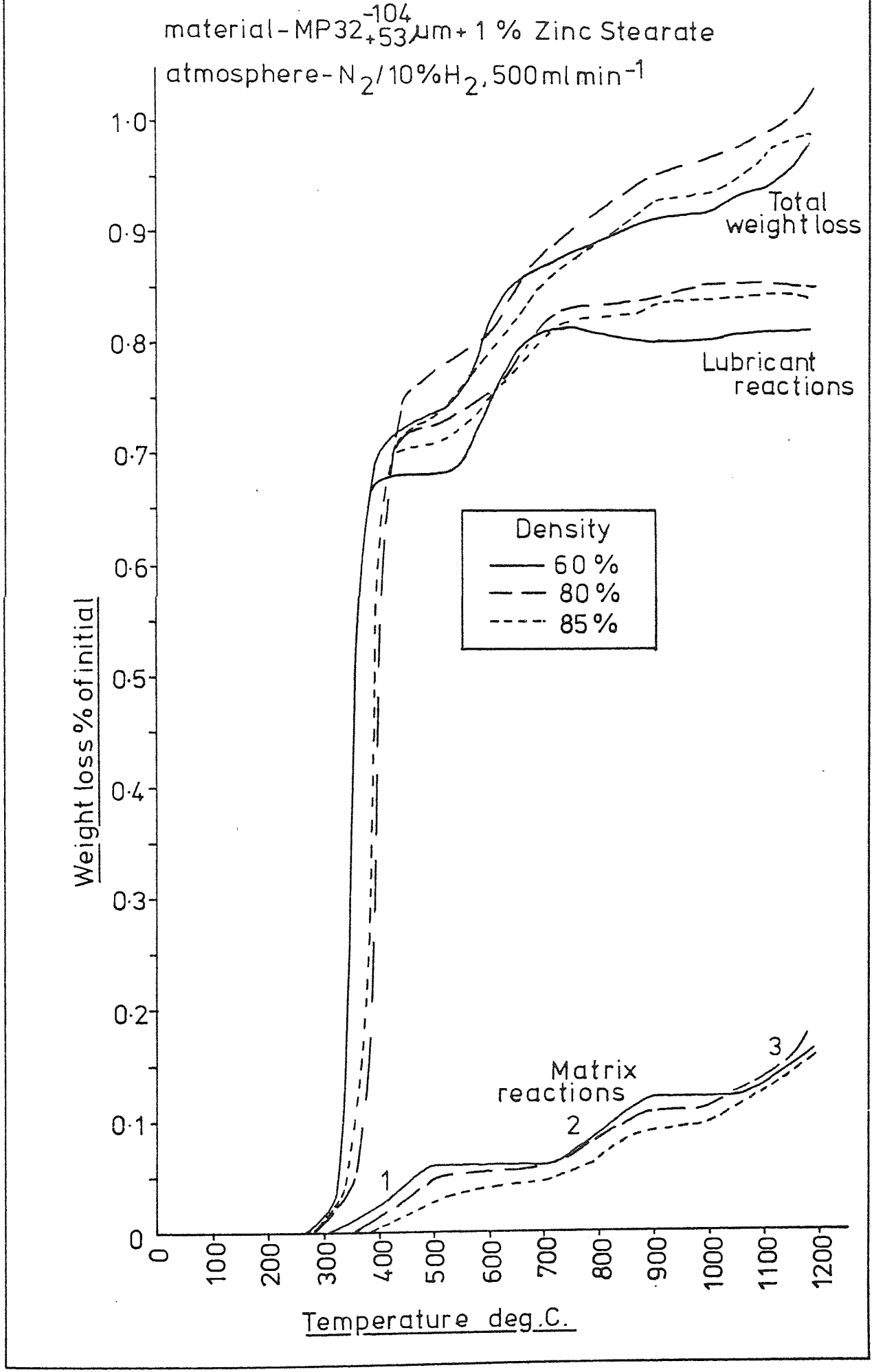

Figure 3-23 . Lubricant reactions within compacts- Effect of matrix particle size, lubricant content and density.

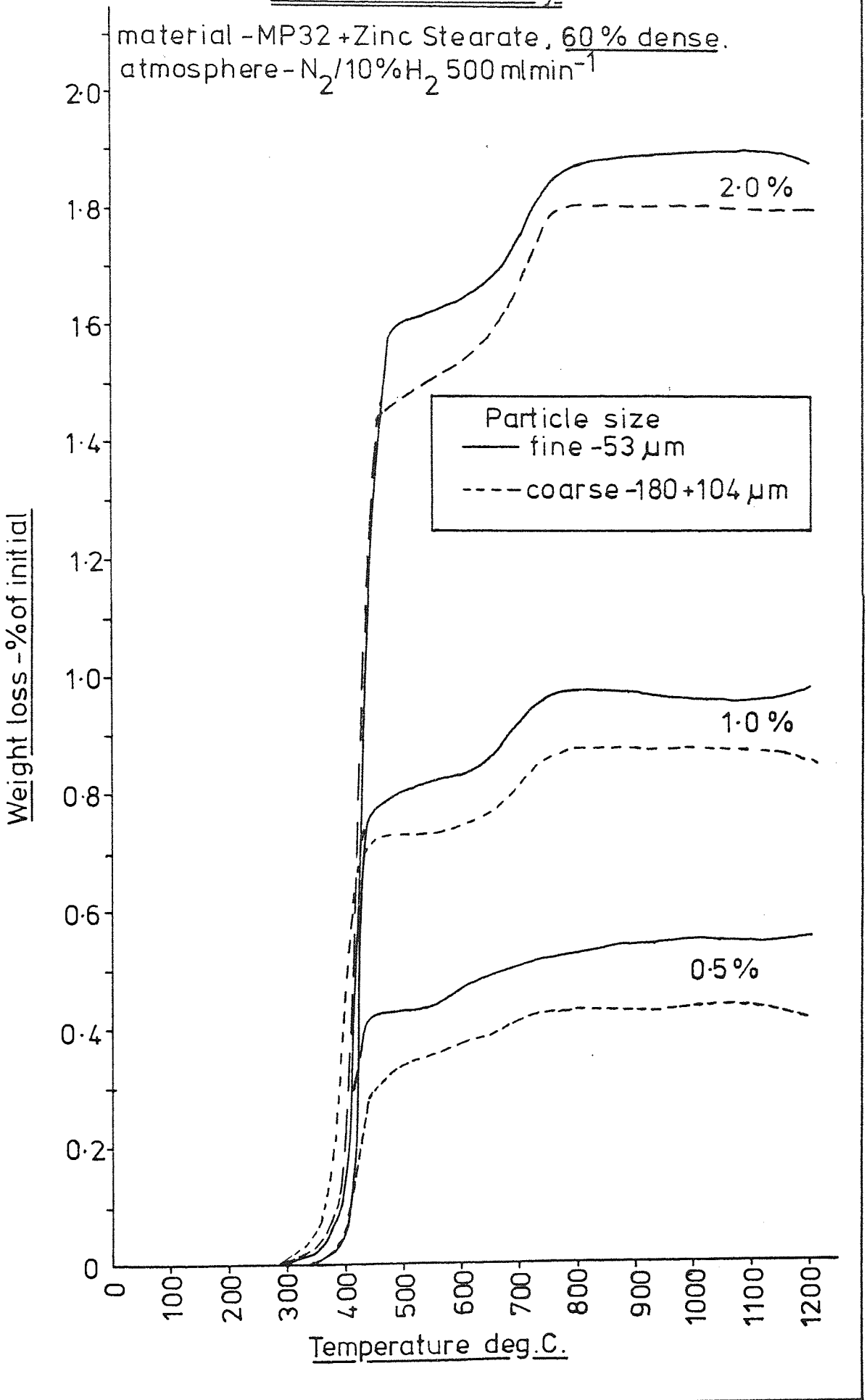

Figure 3-24. Lubricant reactions within compacts- Effect of matrix particle size, lubricant content and density

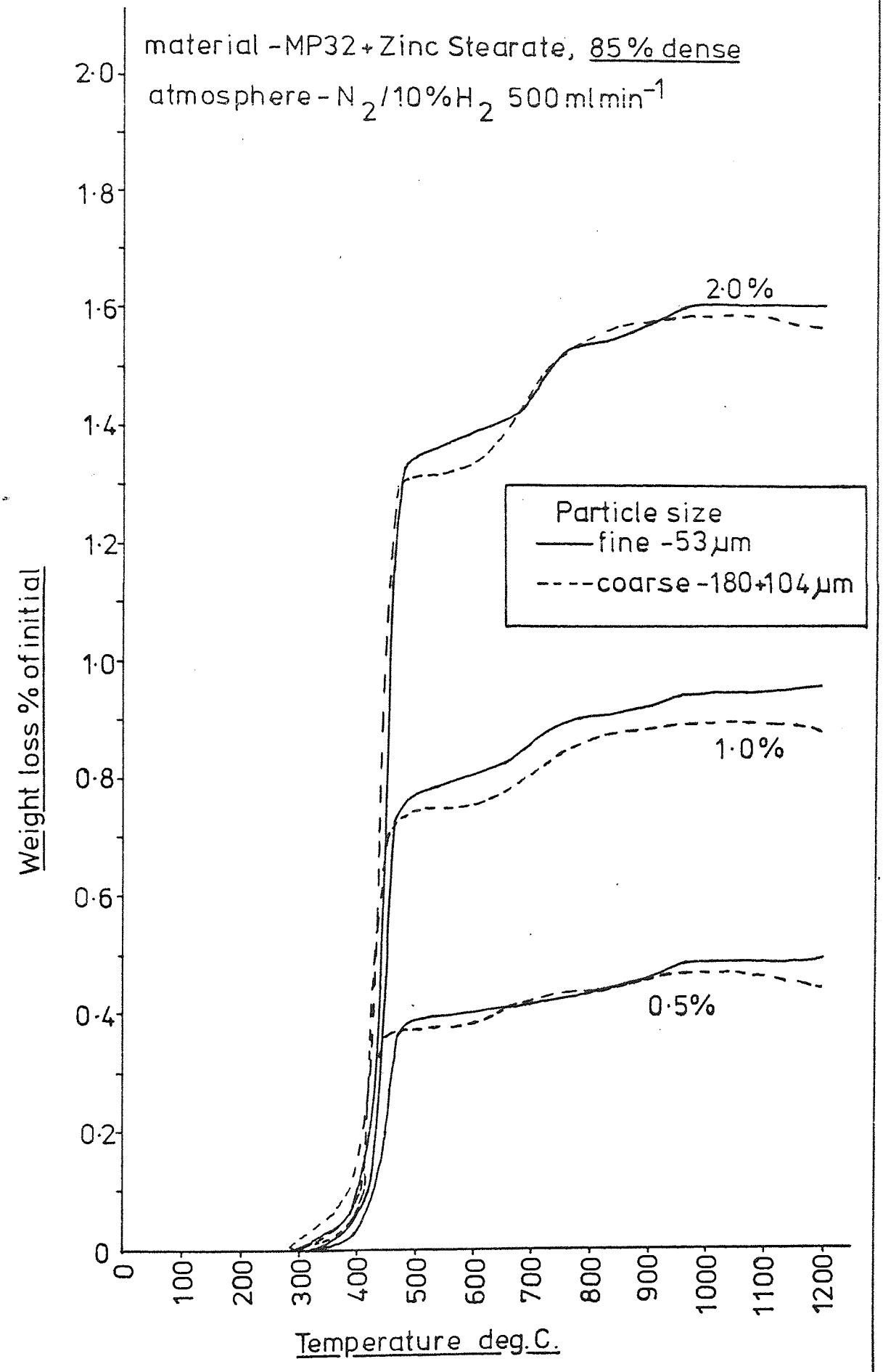

Table 3-4

Final dimensional change for compacts containing 1% zinc stearate thermogravimetrically treated to 1200°C. - Effect of Density.

Lubricant %	Density %	Dimensional Change %	
		Radial	Longitudinal
0	60	-0.47	-0.52
0	80	-0.39	-0.62
0	85	-0.39	-0.50
1	60	-0.40	-0.67
1	80	-0.32	-0.71
1	85	-0.39	-1.07

(Material-MP32 53-104μm. Atmosphere-N_2/10%H_2, 500 ml.min^{-1}).

Table 3-5

Final dimensional change of compacts containing zinc stearate, thermogravimetrically treated to 1200°C. - Effect of density, lubricant content and pore size.

Matrix	Density %	Lubricant Content %	Dimensional Change %	
			Radial	Longitudinal
MP32, -53μm	60	0	-0.83	-0.82
		0.5	-0.75	-0.76
		1.0	-0.95	-0.91
		2.0	-0.87	-0.79
	85	0	-0.39	-0.79
		0.5	-0.51	-1.26
		1.0	-0.55	-1.38
		2.0	-0.59	-1.91
MP32 -180 +104μm	60	0	-0.39	-0.46
		0.5	-0.43	-0.37
		1.0	-0.39	-0.51
		2.0	-0.43	-0.52
	85	0	-0.28	-0.54
		0.5	-0.32	-0.71
		1.0	-0.31	-0.87
		2.0	-0.35	-1.13

(Atmosphere - N_2/10%H_2 500 ml.min^{-1}).

Figure 3-25 .Open and closed porosity versus density for coarse and fine MP32

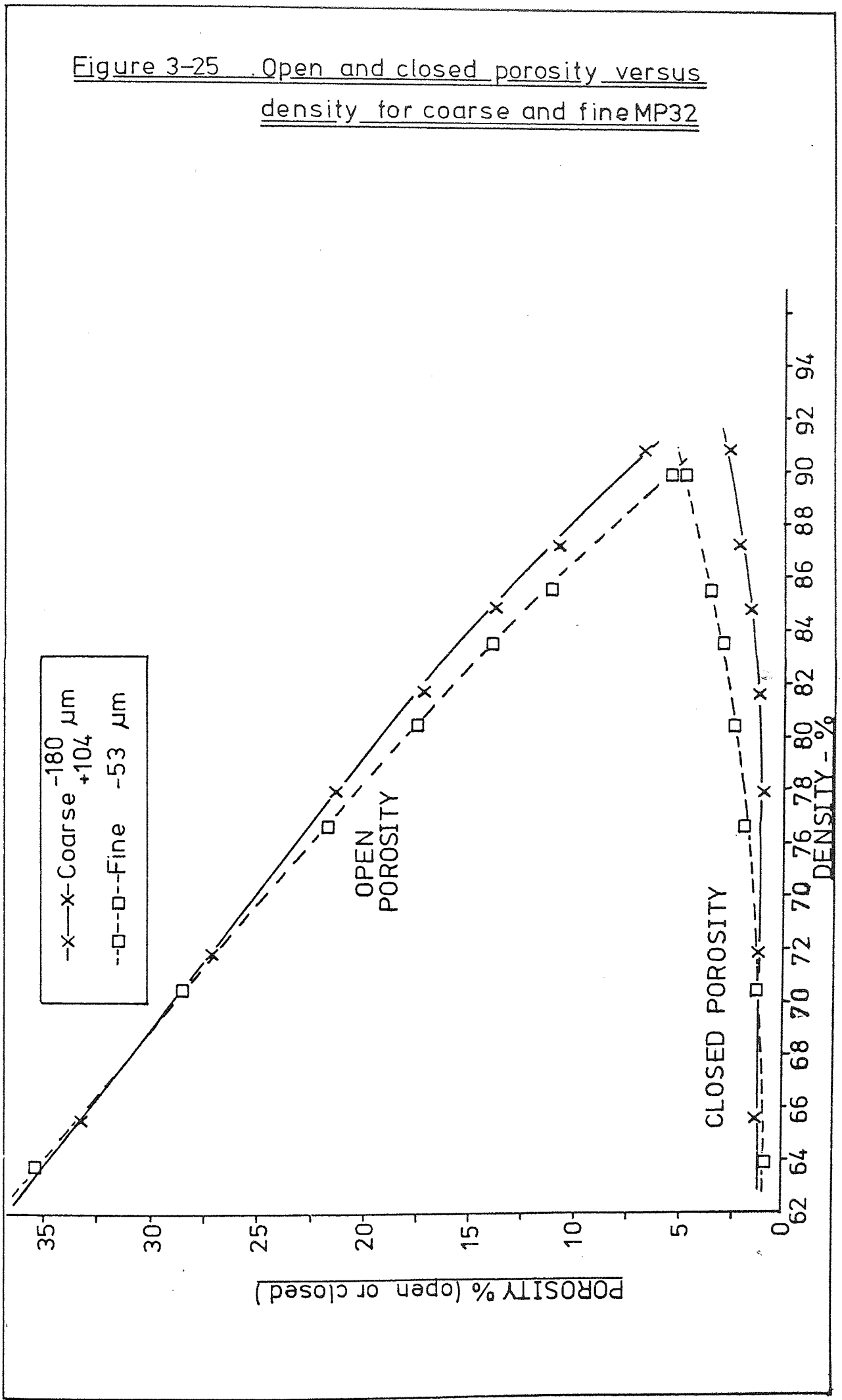

Plates 3-1, 2, 3 and 4.

The following plates are photo micrographs of sections of as-pressed compacts. All specimens were vacuum impregnated with epoxy resin before polishing and have been etched in 2% nital.
Sections were taken perpendicular to (transverse) and parallel with (longitudinal) the pressing directions. The specimens were uniaxially pressed cylindrical compacts, die wall lubricated.

Plate 3-1 Fine MP32 (-53μm). Relative density 64%.

Plate 3-2 Fine MP32 (-53μm). Relative density 90%.

Plate 3-3 Coarse MP32 (104-180μm). Relative density 66%.

Plate 3-4 Coarse MP32 (104-180μm). Relative density 91%.

These microspecimens were prepared to show particle flattening occurring, perpendicular to the pressing axis, as density increases.

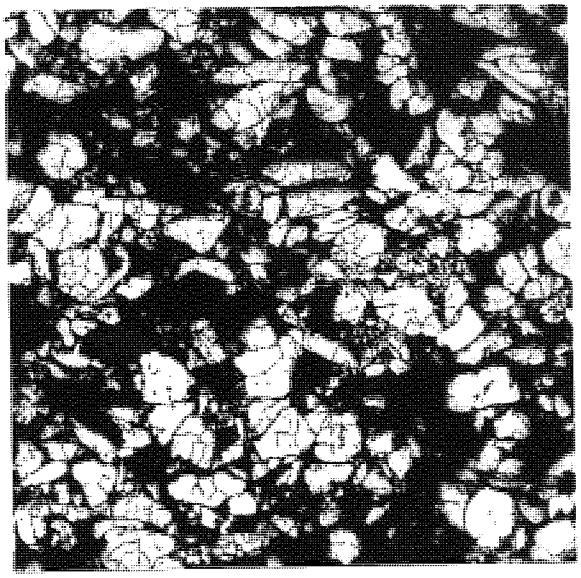

Longitudinal

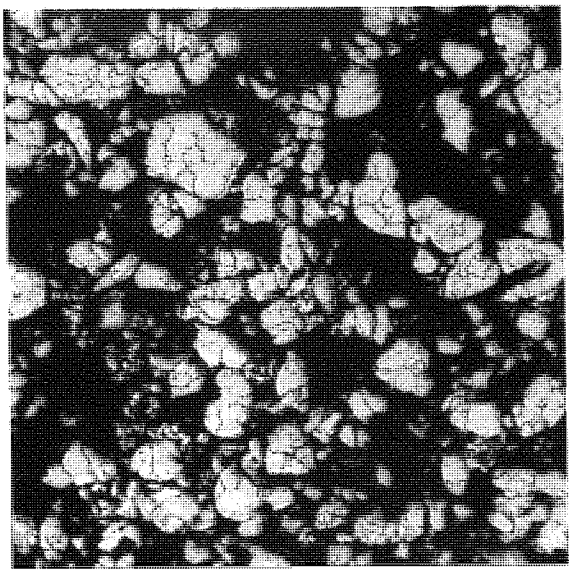

Transverse

3-1. Relative density 64 %

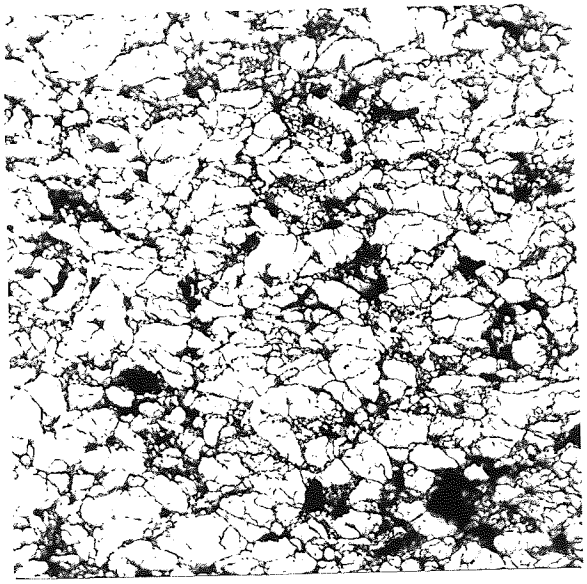

Longitudinal

↑ Pressing direction ⊙

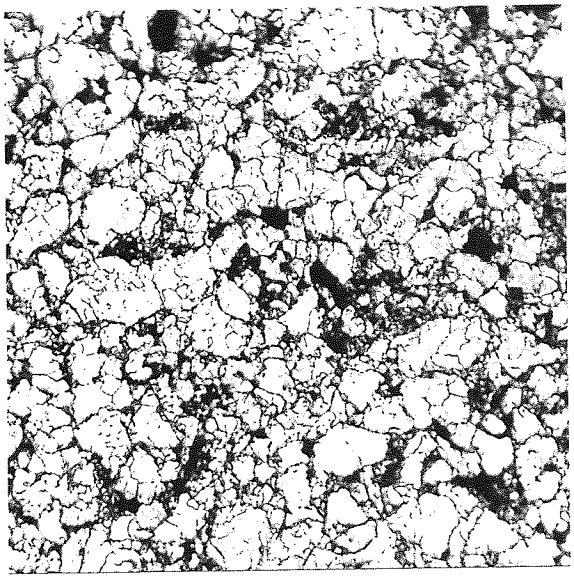

Transverse

3-2. Relative density 90 %

PLATES 3-1 and 3-2 Particle flattening in compacts pressed from fine MP 32 (x300)

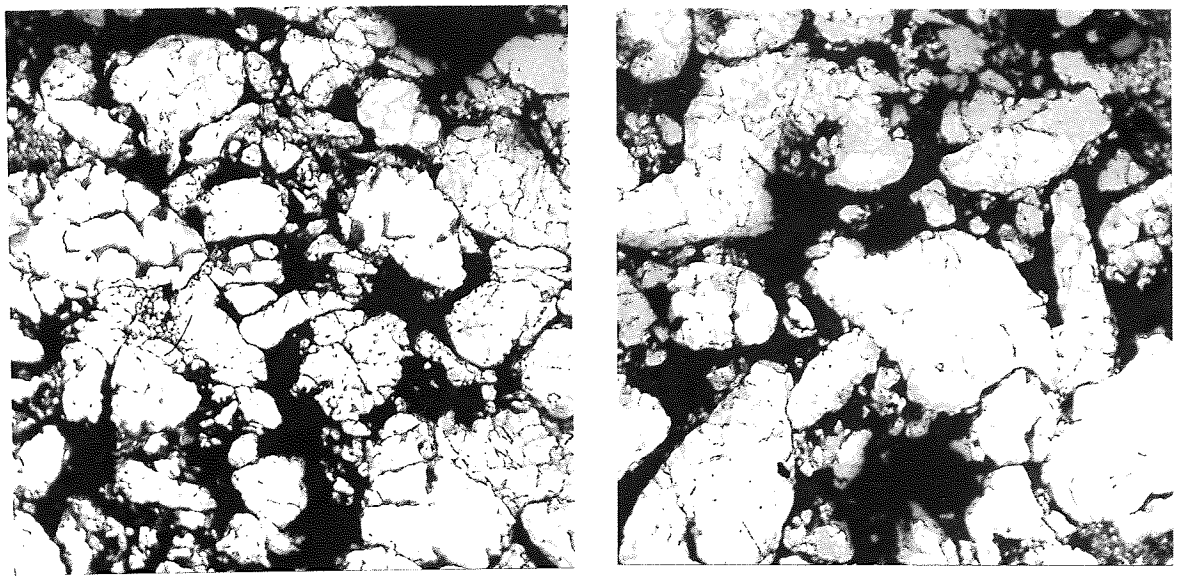

Longitudinal Transverse

3-3 Relative density 66%

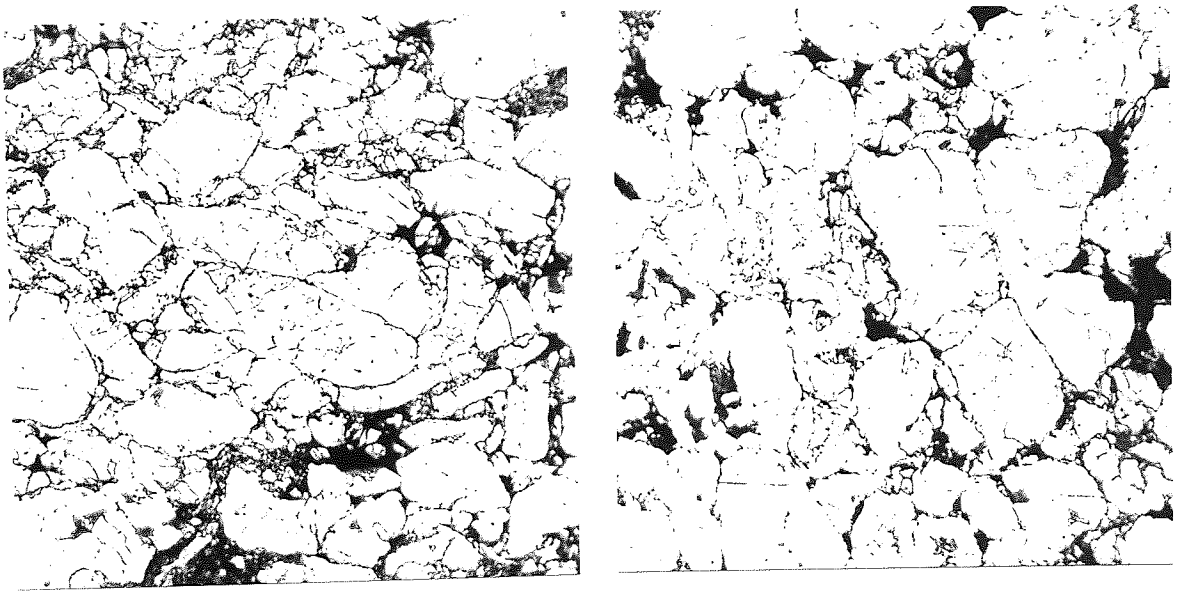

Longitudinal Pressing direction Transverse

3-4 Relative density 91%

PLATES 3-3 and 3-4 Particle flattening in compacts pressed from coarse MP 32 (x300)

Figure 3-26 .The effect of compact density on the decomposition characteristics of Lithium Stearate

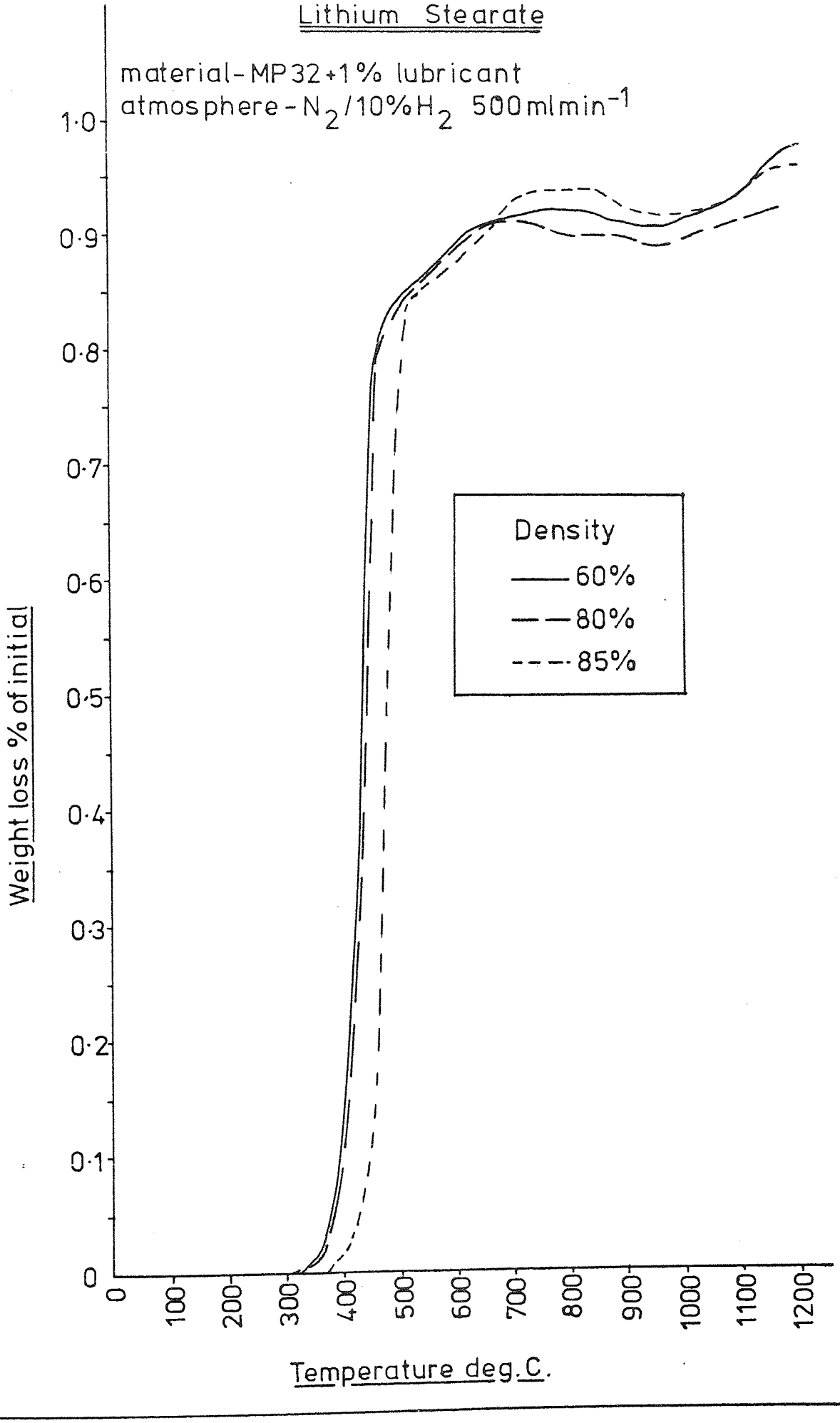

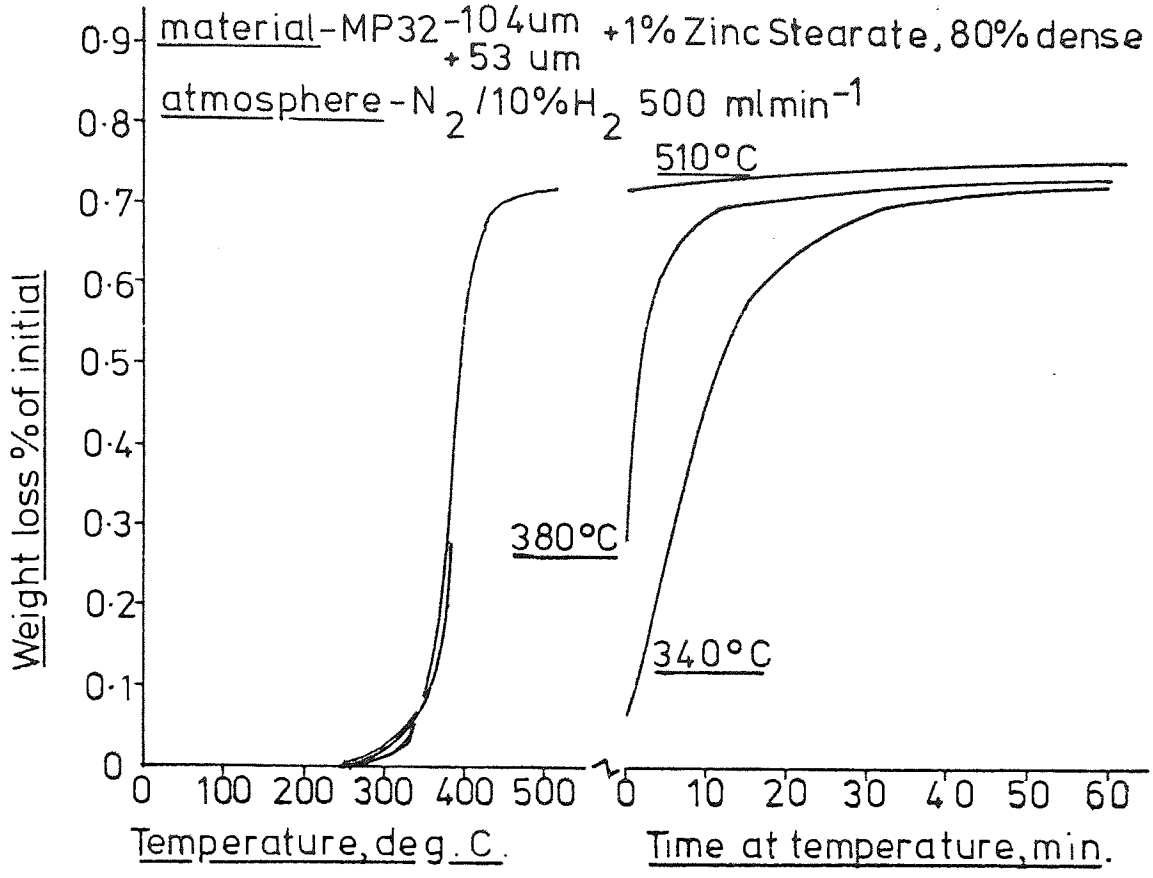

Figure 3-27 .The decomposition of Zinc Stearate under isothermal conditions

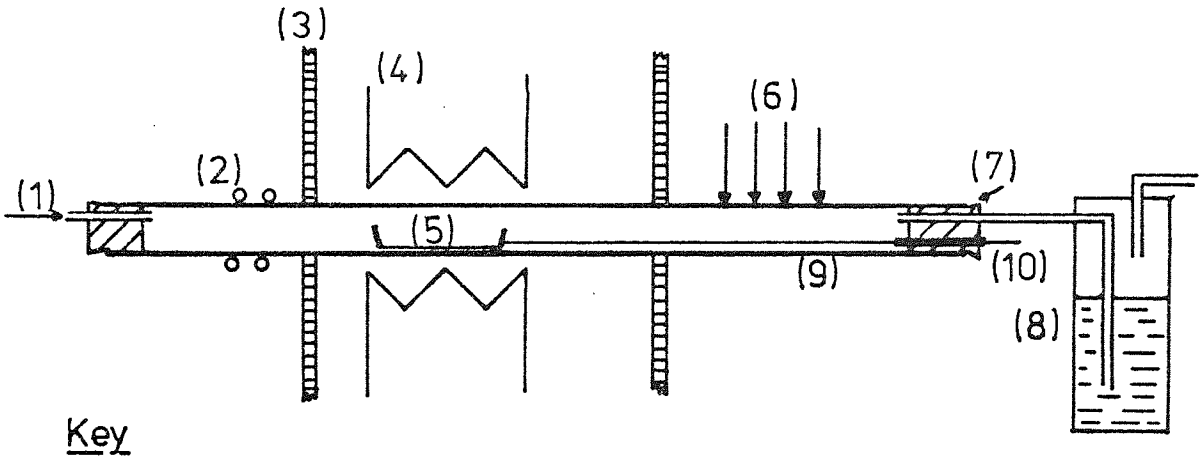

Key

1 - atmosphere inlet from dessicator and flowmeter.
2 - cooling coil.
3 - furnace box.
4 - elements; hot zone length 14cm over which temperature varies ± 5° C.
5 - specimen boat. 6 - water spray to aid specimen cooling.
7 - seal. 8 - water trap to maintain positive atmosphere pressure.
9 - Inconel furnace tube. 10 - boat withdrawal wire.

Figure 3-28 .Representation of the sintering furnace.

Figure 3-29 Lubricant reactions within compacts- high heating rate, effect of density on Zinc Stearate decomposition and matrix reactions.

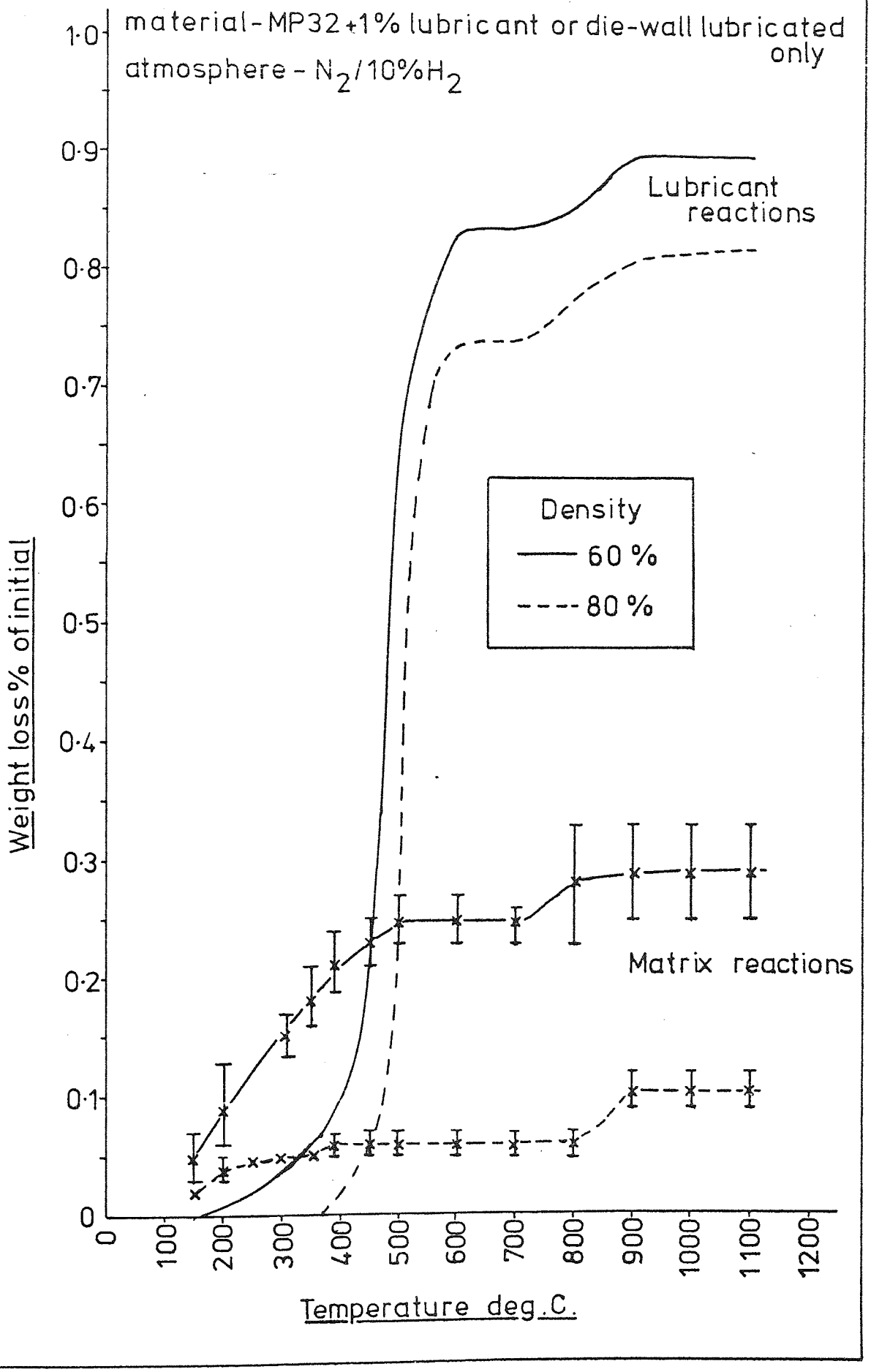

Figure 3-30 Lubricant reactions within compacts - high heating rate, Zinc Stearate, Lithium Stearate, Stearamide, Cosmic 64 Wax.

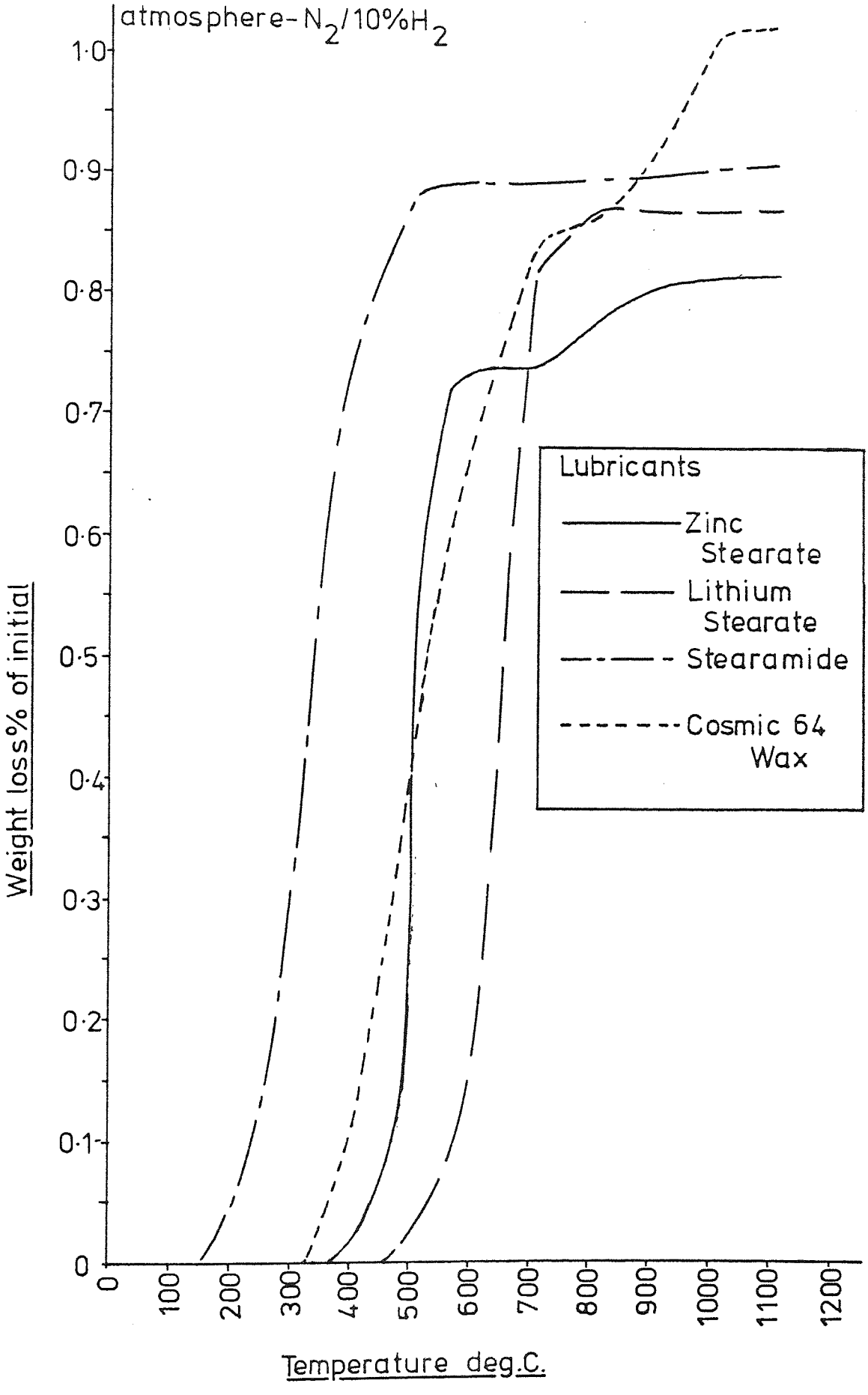

Figure 3-31 Lubricant reactions within compacts - high heating rate, Stearic Acid, effect of particle size and dispersion.

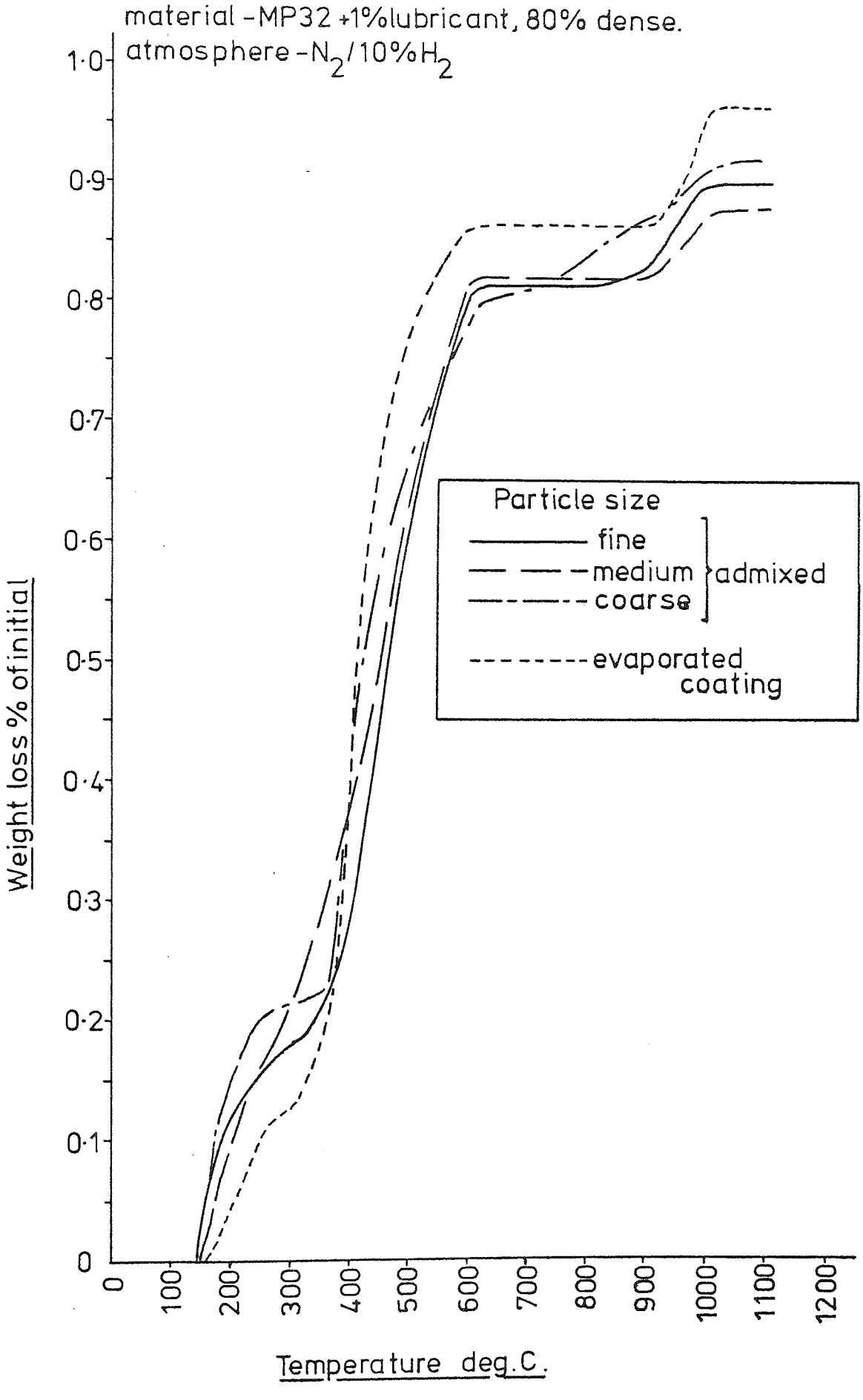

Table 3-6

Final dimensional change and carbon content of compacts containing 1% lubricant, heat-treated at a high heating rate.

Lubricant	Dimensional change %		Carbon %
	Radial	Longitudinal	
None	-0.08	-0.25	0.014
Zinc stearate	-0.16	-0.42	0.013
Lithium stearate	-0.18	-0.40	0.018
Stearic acid-Fine	-0.20	-0.52	<0.01
—— Medium	-0.14	-0.43	0.029
—— Coarse	-0.18	-0.75	0.017
—— Evaporated	-0.16	-0.44	N/D*
Stearamide	-0.18	-0.54	0.016
Cosmic 64 wax	-0.26	-0.67	0.018

*N/D- Not detectable

(Compacts - MP32, 80% dense. Atmosphere N_2/10%H_2.

Maximum temperature 1100°C).

Direct observation of lubricant removal.

The following are the observational notes obtained during direct observation, as described in section 2-3. Quoted temperatures are only approximate and are based on visual estimates of the start or finish of reactions. For all materials it was found that vapour in the immediate vicinity of samples was colourless and not detected until condensed by contact with the cold stream of $N_2/10\%H_2$.

Pure lubricants (Thermocouple exposed)

(a) Zinc stearate. $66^{\circ}C.min^{-1}$. maximum $530^{\circ}C$.

Melting observed $140^{\circ}C$, boiling at $235^{\circ}C$. Vapour became apparent at $305^{\circ}C$ but was not associated with any vigorous reaction until $320^{\circ}C$. $370^{\circ}C$ yellowing of the sample was observed with profuse volatilisation/decomposition at $390^{\circ}C$. Reactions appeared to cease by $430^{\circ}C$ and a sooty deposit developed at $470^{\circ}C$.

(b) Lithium stearate. Maximum $515^{\circ}C$.

Melting occurred at $230^{\circ}C$, with boiling at $370^{\circ}C$. Vapour appeared at $420^{\circ}C$ with vigorous boiling and decomposition observed at $475^{\circ}C$. The residue became thick and yellow at $495^{\circ}C$ and sooty at $515^{\circ}C$. No carbon deposit.

(c) Stearic acid - fine. $74^{\circ}C.min^{-1}$. maximum $480^{\circ}C$.

Melting occurred at $85^{\circ}C$, vapour at $220^{\circ}C$ becoming profuse at $315^{\circ}C$ to $375^{\circ}C$. Slight vapour was observed up to $405^{\circ}C$. A slight sooty residue remained.

(d) Stearic acid - medium. $67^{\circ}C.min^{-1}$. maximum $500^{\circ}C$.

Melting observed below $100^{\circ}C$, vapour at $235^{\circ}C$. There was no boiling apparent. Profuse vapour from $345^{\circ}C$ to $405^{\circ}C$, followed by slight vapour from a thick clear residue which continued to breakdown slowly to $465^{\circ}C$, leaving a slight dark residue.

(e) Stearic acid - coarse. $72^{\circ}C.min^{-1}$. maximum $430^{\circ}C$.

Melting at $95^{\circ}C$, vapour at $250^{\circ}C$ becoming profuse at $320^{\circ}C$. Boiling/vigorous

reaction at 380°C, slowing at 400°C. A slight vapour was observed up to 420°C.

(f) Stearamide. $62^{\circ}C.min^{-1}$. maximum 530°C.

Melting observed 115°C, boiling at 300°C. Boiling was associated with rapid breakdown, slowing at 390°C, and finishing at 405°C. A brown residue remained which decomposed further at 445°C. Decomposition ceased at 530°C leaving a sooty residue.

(g) Cosmic 64 wax. $72^{\circ}C.min^{-1}$. maximum 540°C.

Melting was observed at 135°C, boiling at 235°C and vapour at 290°C. Profuse vapour at 350°C with foaming above 380°C, slowing 440°C. A thick sooty residue remained which slowly decomposed, finishing at 540°C to leave soot.

Lubricants within compacts. (Thermocouple sheathed in compact).

(A) Effect of density. Compacts MP32 plus 1% admixed zinc stearate.

(a) 60% dense. $60^{\circ}C.min^{-1}$. maximum 480°C. Weight loss 0.90%. See (b).

(b) 80% dense. $60^{\circ}C.min^{-1}$. maximum 480°C. Weight loss 0.87%.
Vapour observed 300°C, profuse at 370°C. Reactions slowed at 440°C to finish at 470°C.

(c) 85% dense. $64^{\circ}C.min^{-1}$. maximum 480°C. Weight loss 0.89%.
Molten spots appeared on the compact surface at 190°C, profuse at 270°C. Exudation particularly from pores on the circumference of the compact, at the ends rather than the centre. Boiling/decomposition at 310°C, profuse at 380°C. Boiling continued up to 430°C leaving a surface deposit, but profuse vapour was observed to come from within the compact up to 450°C, slowing rapidly to finish at 470°C. Surface deposits became sooty.

(B) Effect of lubricant content and matrix particle size. Compacts; coarse (104-180μm) and fine (-53μm) MP32 powder, containing admixed zinc stearate, pressed to a density of 85%.

(a) Fine + 0.5% lubricant. 64°C.min^{-1}. maximum 480°C. Weight loss 0.43%. Vapour visible at 370°C, no noticeable melting, reactions ceased at 450°C.

(b) Fine + 2.0% lubricant. 69°C.min^{-1}. maximum 480°C. Weight loss 1.82%. Molten spots exuded from pores at 160°C, profuse at 180°C, and boiling became apparent at 210°C. Decomposition commenced at 250°C, becoming rapid at 355°C. There was further boiling apparent at 370°C with profuse vapour at 390°C. Surface deposits formed at 410°C, followed by normal profuse volatilisation/decomposition from within the compact. Reactions ceased 470°C-480°C leaving considerable sooty surface deposits.

(c) Coarse + 0.5% lubricant. 69°C.min^{-1}. maximum 480°C. Weight loss 0.41%. Vapour apparent at 380°C, increasing up to 430°C then decreasing to 450°C. Reactions ceased at 470°C.

(d) Coarse + 2.0% lubricant. 69°C.min^{-1}. maximum 480°C. Weight loss 1.75%. Molten spots appeared, exuding from pores on to the compact surface, at 180°C, becoming profuse at 210°C. Apparent boiling commenced 230°C with decomposition at 250°C. Vapour increased slowly whilst surface activity decreased. Vapour became profuse at 380°C with an increase in surface activity. Extreme reactions were observed at 405°C. Surface deposits formed at 425°C whilst vapour continued to come from within the compact. Reactions ceased at 480°C. Final surface deposits were less marked than with fine MP32 plus 2.0% lubricant.

(C) Decomposition of other lubricants. Compacts - MP32 plus 1% lubricant pressed to a density of 80%.

(a) Lithium stearate.- maximum 508°C. Weight loss 0.91%.
Vapour commenced at 410°C, increasing very slowly until profuse at 445°C. Vapour decreased at 480°C, reactions ceasing at 500°C.

(b) Stearic acid - fine. 65°C.min^{-1}. maximum 490°C. Weight loss 0.96%

Initial vapour appeared at 220°C, increased to 340°C then ceased. Slight vapour was observed between 370°C and 380°C, increasing steadily to become profuse at 430°C. Reactions decreased at 450°C and finished at 485°C.

(c) Stearic acid - medium. 64°C.min^{-1}. maximum 480°C. Weight loss 0.96%. Vapour commenced at 235°C, increasing rapidly at 280°C, profuse above 300°C. This decreased markedly at 330°C, increased again at 390°C and then maintained a steady rate finishing at 470°C.

(d) Stearic acid - coarse. 67°C.min^{-1}. maximum 500°C. Weight loss 0.92%. Vapour commenced at 235°C, lubricant particles clearly visible at the compact surface showing no indication of melting. Vapour steady to 340°C then arrested. At this stage the large particles in the surface had disappeared. Vapour recommenced at 370°C, increased to 400°C then remained steady to 450°C. Reactions ceased at 490°C.

(e) Evaporated stearic acid. 69°C.min^{-1}. maximum 480°C. Weight loss 1.0%. Vapour appeared at 220°C, increased to 310°C then ceased. Vapour re-appeared at 350°C becoming profuse at 400°C and then steady to 460°C. Reactions ceased at 470°C.

(f) Stearamide. 64°C.min^{-1}. maximum 480°C. Weight loss 1.02%.
A slight surface reaction was observed at 140°C followed by vapour at 220°C. No boiling was evident. The proportion of vapour increased rapidly, becoming profuse at 280°C and extreme between 310°C and 370°C. There was slight vapour up to 445°C.

(g) Cosmic 64 wax. maximum 500°C. Weight loss 0.95%.
Vapour was observed at 345°C, increasing to become profuse at 390°C. Slight sooting was observed on the glass tube. Vapour decreased from 450°C to finish at 495°C.

Figure 3-32 Effect of heating rate on the tensile strength of compacts containing lubricants - high heating rate

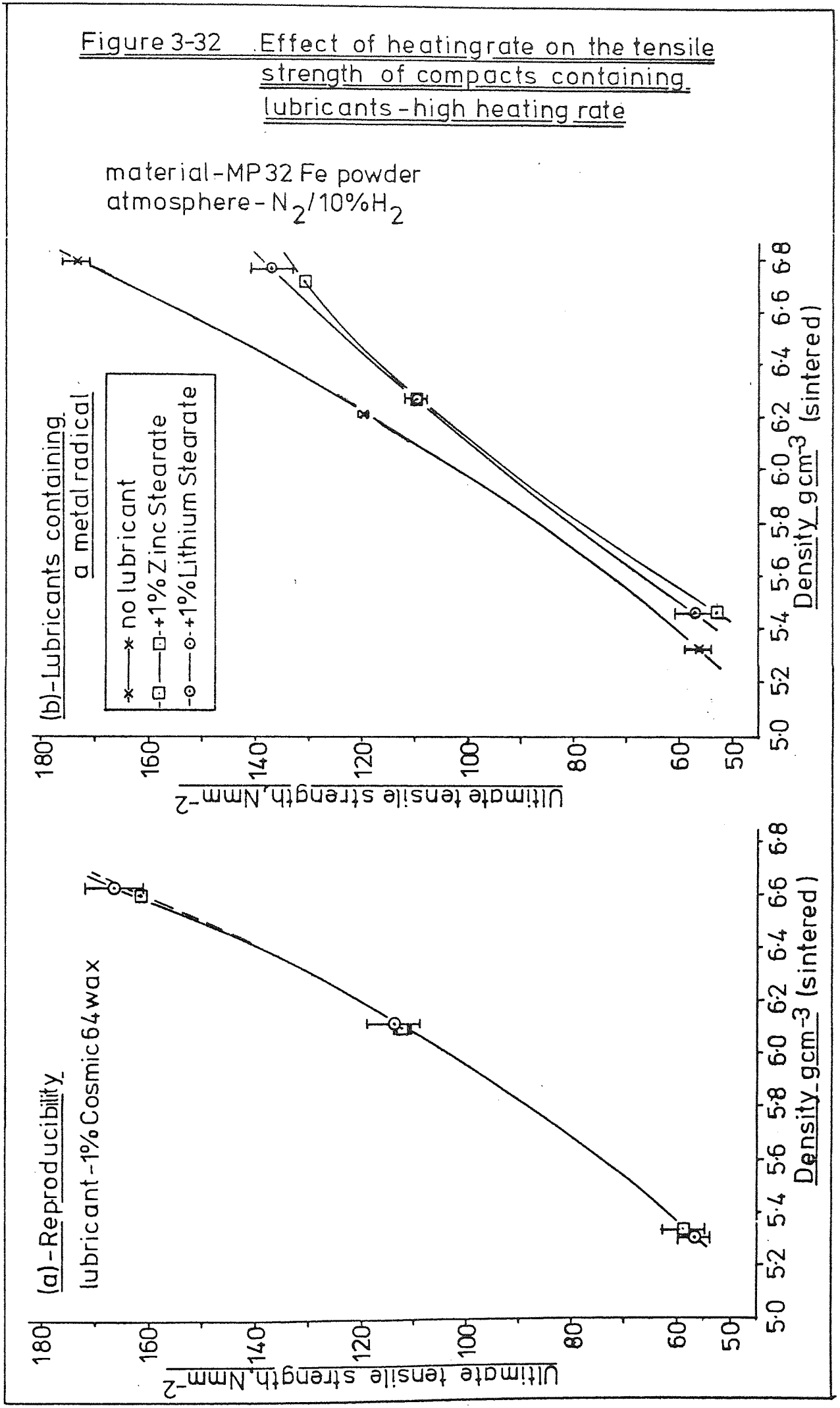

Figure 3-33 .Effect of heating rate on the tensile strength of compacts containing lubricants - high heating rate

material-MP32 Fe powder
atmosphere- N_2 /10% H_2

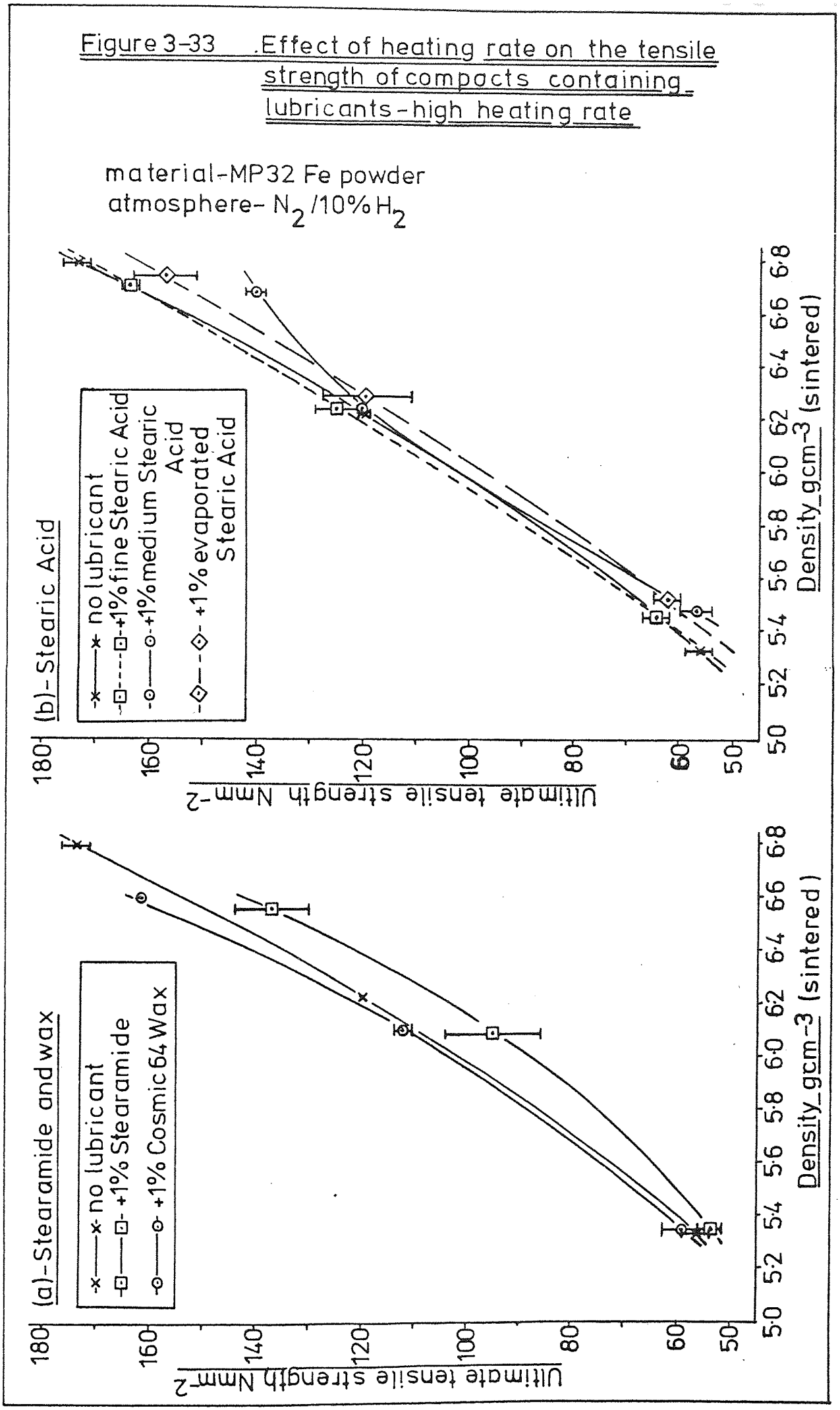

Figure 3-34 .Effect of heating rate on the tensile strength of compacts containing lubricants - low heating rate

material - MP32 Fe powder
atmosphere - N_2 / 10% H_2

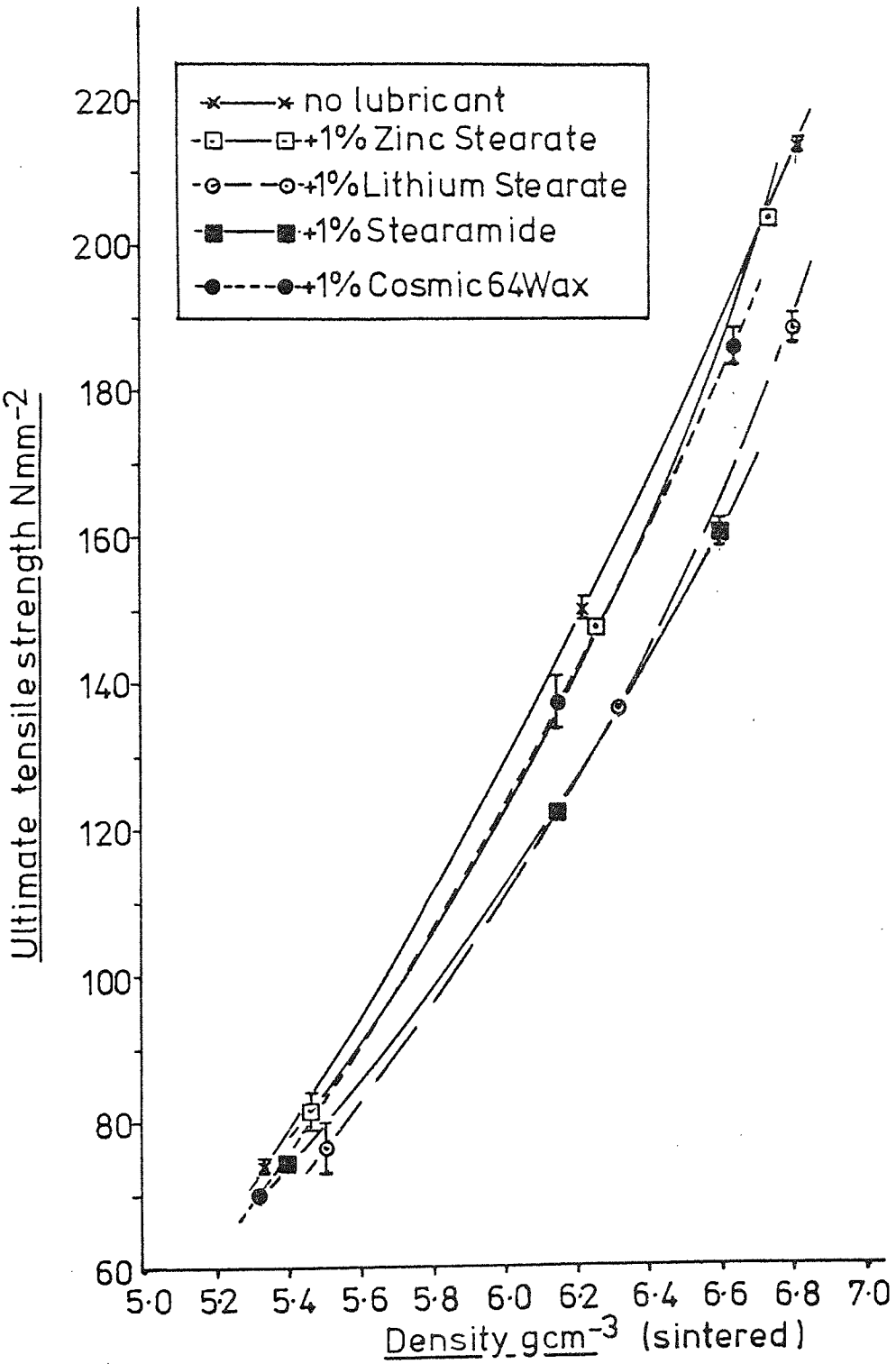

Figure 3-35 Effect of heating rate on the tensile strength of compacts containing lubricants - low heating rate

material - MP32 Fe powder
atmosphere - N_2/10%H_2

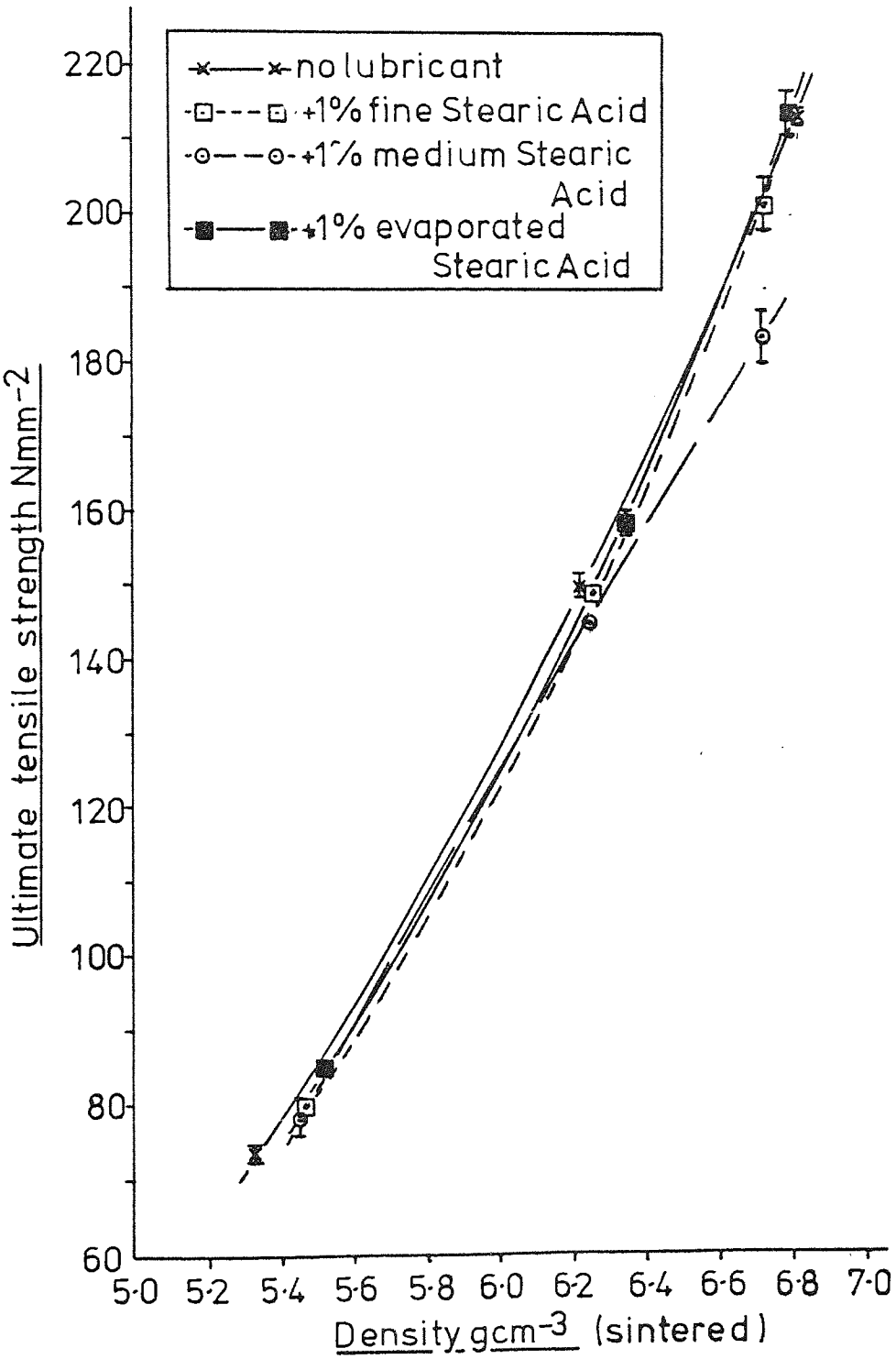

FIGURE 3-36. The effect of residues on the development of tensile strength. Compacts containing no lubricant.

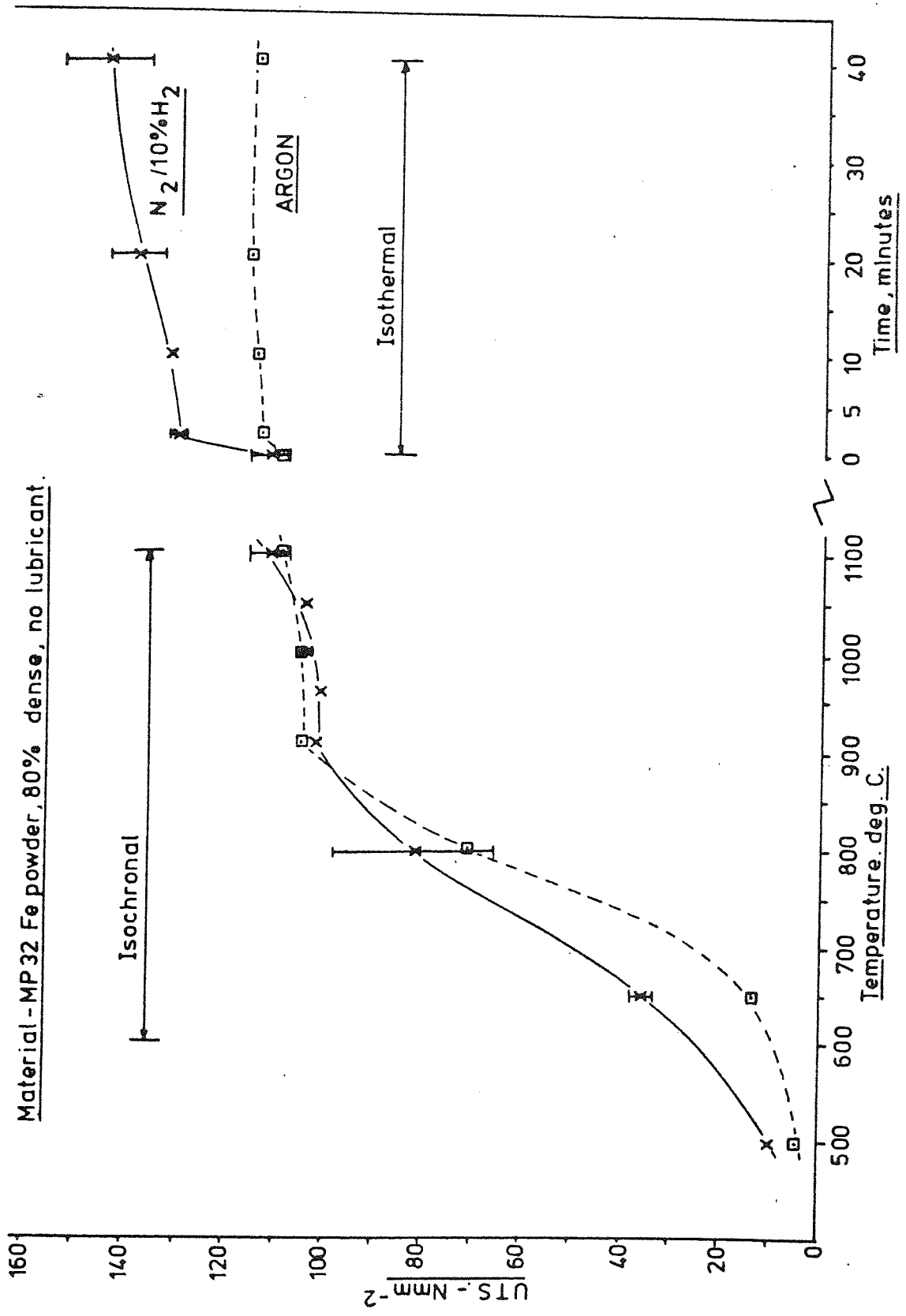

FIGURE 3-37. The effect of residues on dimensional change. Compacts containing no lubricant.

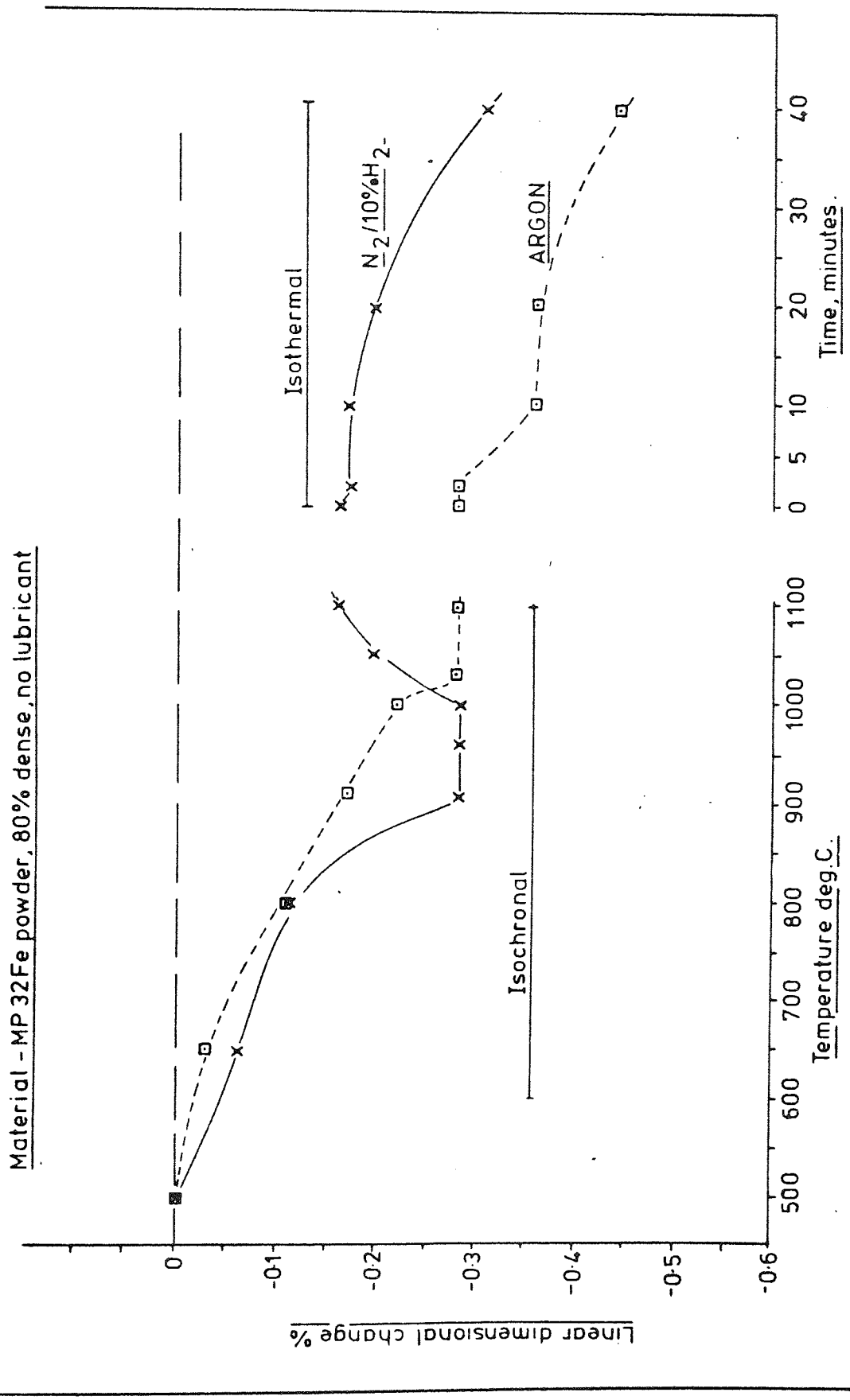

FIGURE 3-38. The effect of residues on the development of tensile strength. $N_2/10\%H_2$ atmosphere.

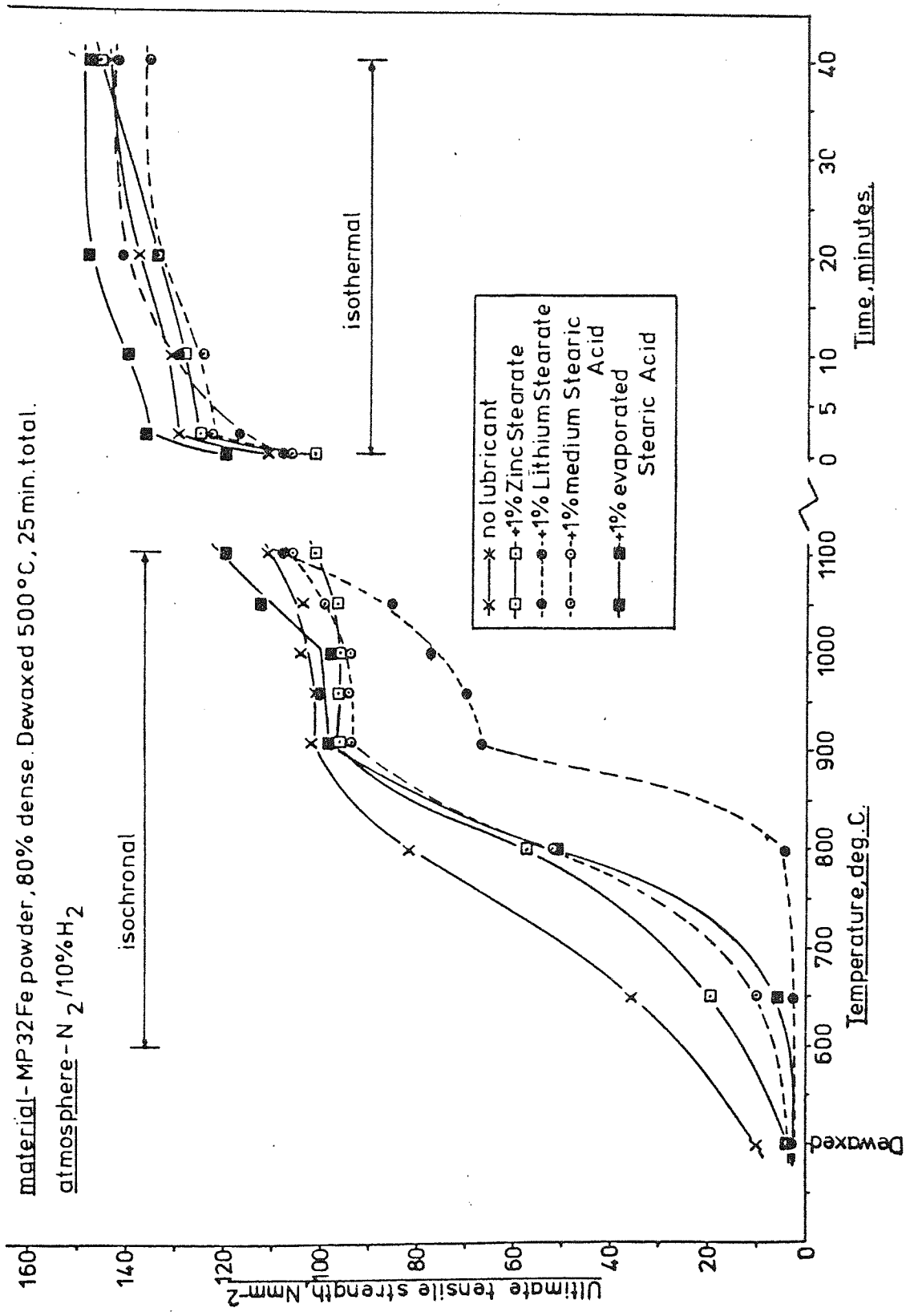

FIGURE 3-39. The effect of residues on the development of tensile strength. Argon atmosphere.

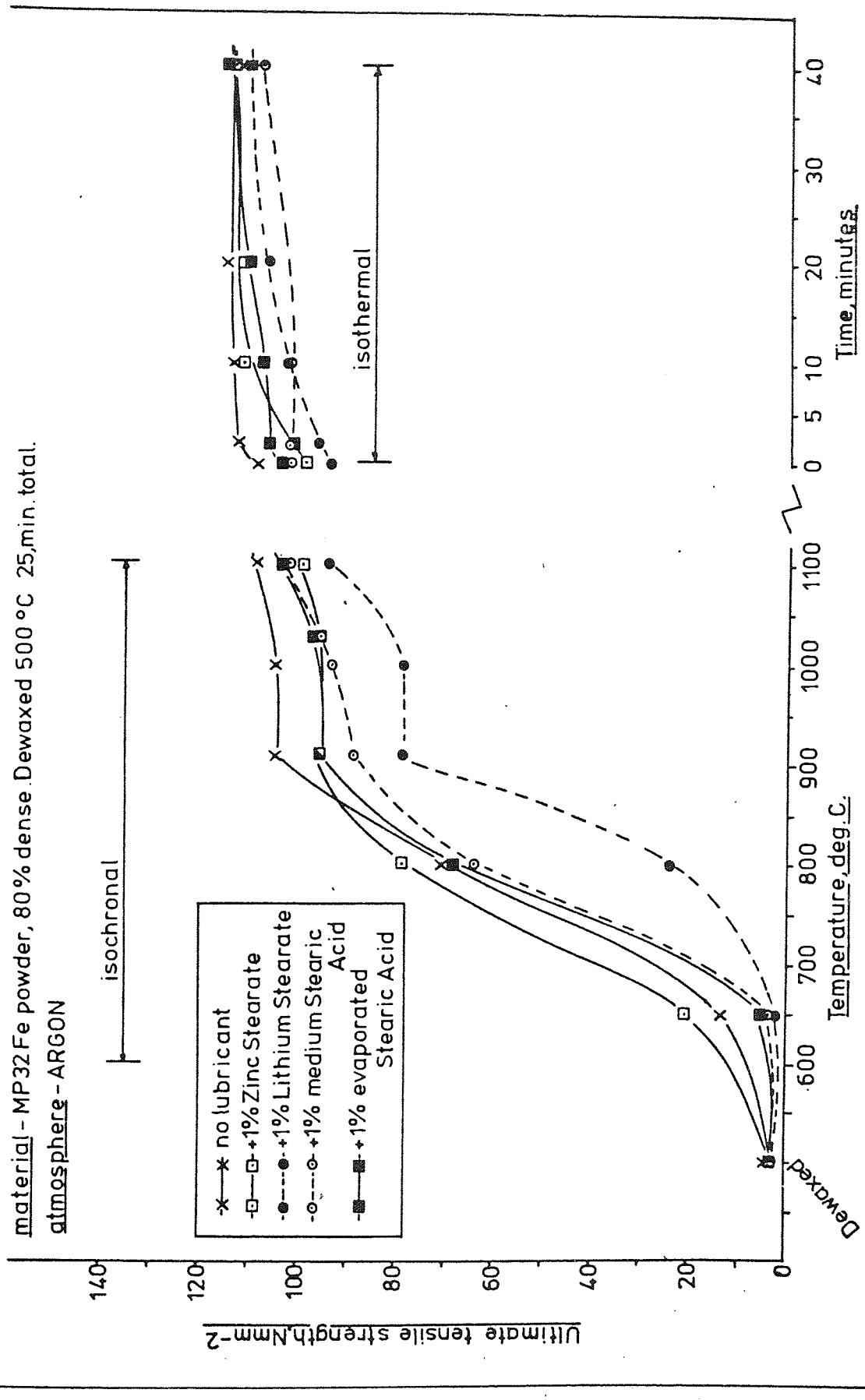

FIGURE 3-40, The effect of residues on dimensional change. $N_2/10\%H_2$ atmosphere.

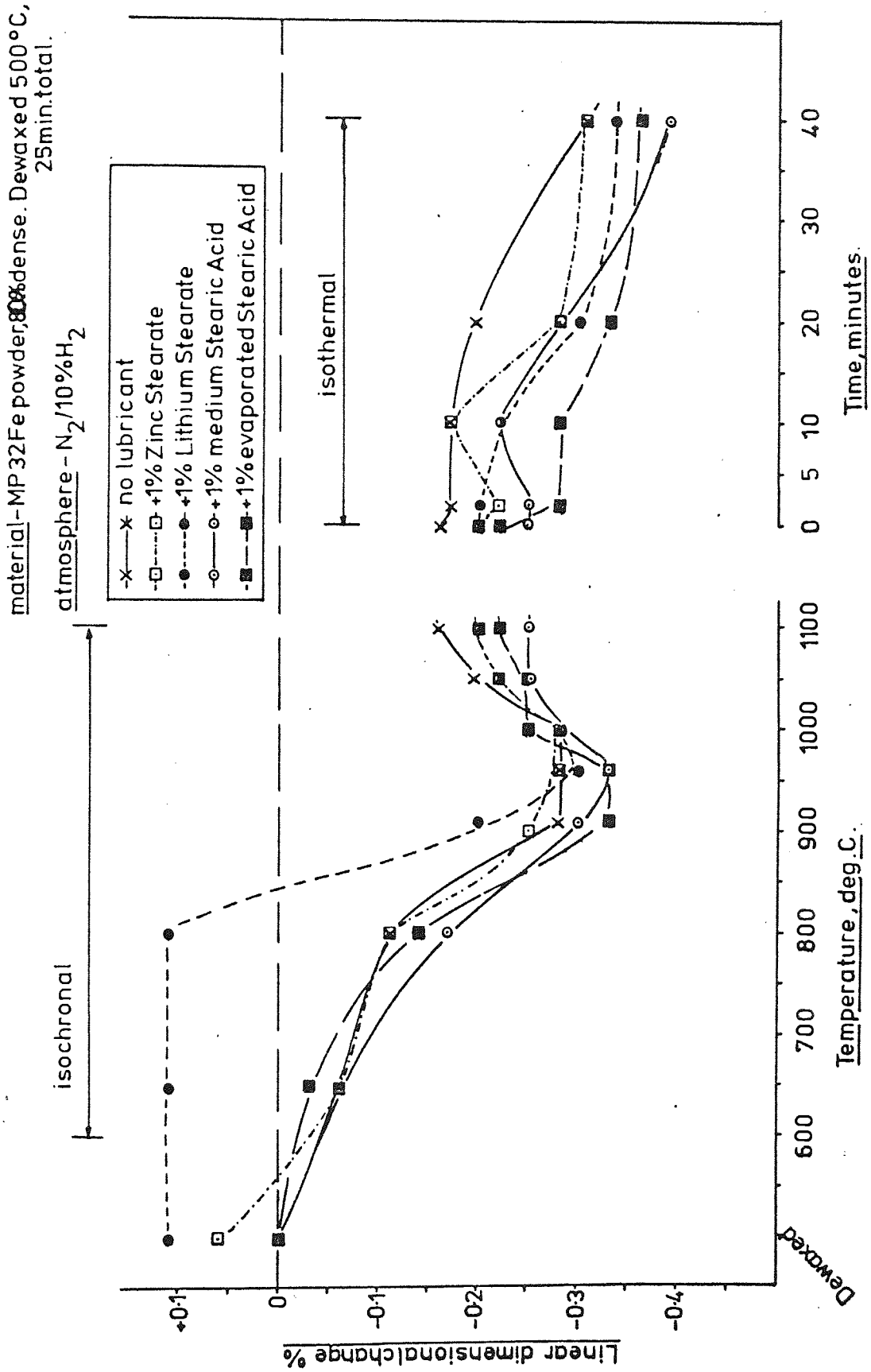

FIGURE 3-41. The effect of residues on dimensional change. Argon atmosphere.

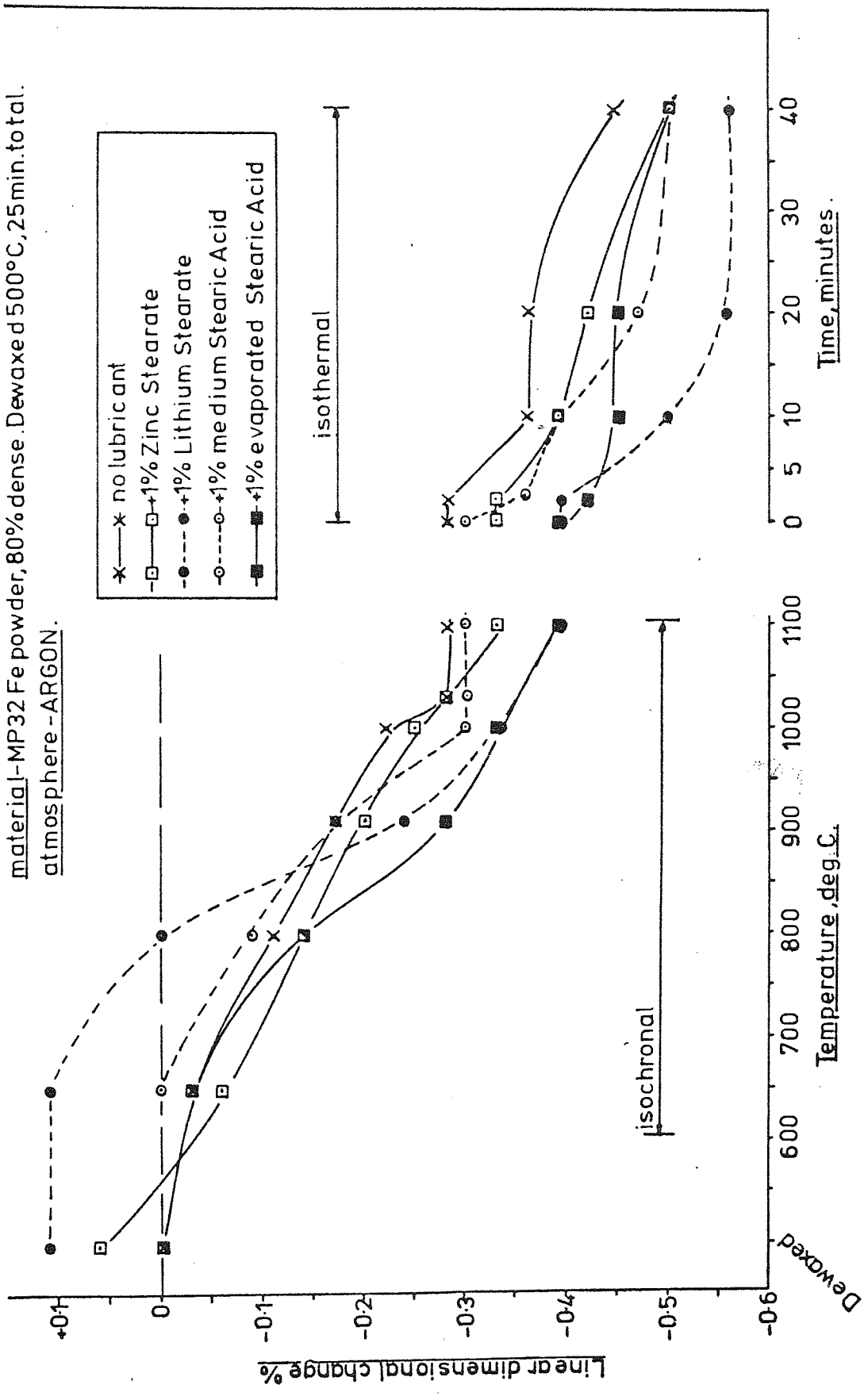

4 Discussion

In this discussion results have been dealt with in the same order as they were presented in the experimental procedure, section 2. Where discussion of one set of results necessitated reference to others which have not been discussed, sufficient information will be given to develop the argument fully with reference to the more complete discussion which occurs later.

Generally each subsequent section of work should be more dependent on previous results and discussion than its predecessor. Pure lubricant reactions are therefore placed first and mechanical properties last.

4-1 Temperature calibration, buoyancy and oxidation

The necessity for temperature calibration has already been discussed (2-1-3) and its justification as applied to the heat treatment of compacts will be discussed later. It can be seen clearly from the two calibration curves given in figure 2-2 that alterations in the system, such as change in thermocouple position, can markedly influence temperature measurement characteristics. As there was a considerable time lapse between these two calibrations it may be argued that the difference was due to deterioration of the Pt/Pt-Rh thermocouple, caused by operating at high temperatures in atmospheres containing hydrogen. This possibility was not overlooked and hence critical comparisons on the basis of reaction temperatures have been confined to sets of samples heat treated over short time periods. It will be shown later that variations in recorded weight changes due to metal powder batch or mix variation were more critical and noticeable than temperature variation caused by any thermocouple deterioration.

In any non-static non-equilibrium system, such as that used in this investigation, care must be taken in the interpretation of thermal and gravimetric data. Garn[35] described three atmosphere systems, static (no imposed flow), flowing (atmosphere flowing

past or over samples) and dynamic (atmosphere flow imposed through samples). Throughout this work a flowing atmosphere has been used and any flow through samples has been natural and not externally imposed.

Many ways have been indicated[35] in which apparent results may differ from true results, or erroneous phenomena may be introduced into thermoanalytical systems. Temperature lag between specimen and furnace was not a problem in this investigation due to pre-calibration. Buoyancy and gas flow were also sources of error in indicated weight changes during thermogravimetric analysis[35]. An apparent weight gain with temperature is often observed due to the decrease in weight of displaced gas, obviously dependent on the physical dimensions of the sample. The highest weight increase due to this effect is usually observed initially, at low temperatures. The sudden application of a higher voltage heats the furnace wall quicker than the sample since at low temperatures heat transfer is mainly by convection. The flow velocity at the furnace wall increases markedly and displaces cooler gas down the centre of the furnace tube, causing an apparent weight gain.

This phenomenon would be most noticeable in static systems where any gas flow would unbalance the system. In this present thermogravimetric work the use of an imposed gas flow has minimised these effects as shown by figures 3-1 and 3-2, the buoyancy curves for compacts and crucibles respectively. The greatest weight gain was obtained with crucibles (figure 3-2) since these occupied the largest cross-sectional area of the sheath. The weight change was largest at low temperatures accounting for a maximum gain of only 2mg (figure 3-2). This represented only 2% of the expected weight change for most of the specimens used (in fact only 1% of the pure lubricant sample weight) and has been ignored unless otherwise stated. Flow-rate was found to have very little effect on this buoyancy for crucibles. The use of an imposed gas flow therefore effectively eliminated buoyancy effects except at low temperatures.

Figure 3-1 is the buoyancy curve for a compact presintered at 1100°C. There was a small apparent weight gain at low temperatures. However, there was another weight gain at 1100°C which became a weight loss of 0.04% of the original weight at 1300°C. It is not clear why a weight gain was recorded at 1100°C, it would seem to indicate a chemical reaction with the atmosphere or diffusion of an atmosphere component such as nitrogen into the matrix. This weight gain did change to a weight loss beyond 1200°C and this can be accounted for by hydrogen reduction of oxides. Final oxygen analyses are given in table 3-1. As-sintered the oxygen content was 0.17%. That of the buoyancy specimen after treatment to 1300°C was 0.13%, a reduction of 0.04% by weight, matching the weight loss. It appeared therefore that the desiccating apparatus on the thermobalance was performing its function in drying the atmosphere. The exact match between indicated weight loss and oxygen loss is encouraging but it does not mean necessarily that such an exact correspondence was usual.

Figure 3-1 is further support for the validity of temperature calibration. The compact had been sintered in a furnace the temperature of which was easily checked. No further reaction between the specimen and a similar atmosphere was expected therefore during thermogravimetric analysis up to 1100°C. Above this temperature further reactions became possible. The temperature indicated in figure 3-1 for the start of the high temperature reactions was indeed 1100°C. This curve had been calibrated for actual temperature using the appropriate calibration curve in figure 2-2.

4-2.The decomposition of pure lubricants.

The determination of the thermal behaviour of pure lubricants, without the physical or chemical limitations of a compact, would seem to be a good starting point for a general study of lubricant decomposition. Samples were placed loosely in a crucible so that there would be no diffusion considerations like those of inhibited diffusion within compacts. The atmosphere used throughout was flowing, as in normal sintering practice. The decomposition of pure lubricants, where the term pure indicates the absence of a compact rather than chemical purity, discussed in this chapter represents a compromise between equilibrium and practical conditions.

Two main types of reaction were recognised, decomposition of the hydrocarbon radical or its equivalent in non stearate based lubricants, and higher temperature reactions involving decomposition residues. The importance of the latter becomes more apparent when discussing lubricant decomposition within compacts.

Where carbon deposits have been noted they have been observed directly within the crucible following each test. The presence of carbon has not been implied only by studying the weight loss curves. It can be seen that total weight losses did not reach 100% often, for example medium stearic acid in air, figure 3-7. It was found that with such a light sample, approximately 2g. total, the weighing unit varied slightly such that it could indicate between 98% and 102% for complete decomposition. The presence of residues was always confirmed visually.

4-2-1. Zinc stearate

Thermograms obtained for the decomposition of zinc stearate are shown in figure 3-3.The major weight loss occurred between 200°C and 550°C in all three atmospheres, $N_2/10\%H_2$, argon and air, accounting for 86%, 85% and 90% of the sample weight respectively. The decomposition ranges of this stage

in $N_2/10\%H_2$ and air were similar to those obtained by Meyer et al[11]. This initial stage was characterised by the profuse appearance of a white vapour which readily condensed in the cold trap.

The stearate radical accounts for some 87% by weight of zinc stearate and so this reaction corresponds to removal of the stearate radical by volatilisation or a similar process. Under oxidising conditions (air) this stage started approximately 50°C sooner than under reducing conditions ($N_2/10\%H_2$) but then proceeded over a wider temperature range with the removal of 90% of the sample. This weight loss suggested the removal of some extra material other than the stearate radical.

The residue at 1200°C in argon and air was a greyish powder, in $N_2/10\%H_2$ only soot remained. The greyish residue turned to yellow when heated, a characteristic of zinc oxide. A higher temperature reaction was recorded in $N_2/10\%H_2$ only, as can be seen in figure 3-3. This reaction caused a weight loss of 13% between 600°C and 900°C, and was more temperature dependent than the initial reaction, the rate of weight loss increasing with increasing temperature. Since 13% is the expected proportion of zinc oxide in zinc stearate and the unreduced residue displayed characteristics of zinc oxide, it seemed probable that this reaction in $N_2/10\%H_2$ was reduction of zinc oxide by hydrogen according to equation 4-1.

$$ZnO + H_2 \longrightarrow Zn\uparrow + H_2O\uparrow \qquad -(4\text{-}1)$$

The increasing rate of this reaction with temperature, as indicated by increasing rate of weight loss, may have been due to the loss of zinc as its vapour pressure became appreciable. It can be seen from table 4-1 that above its melting point the vapour pressure of zinc increases rapidly with temperature.

Table 4-1

Zinc vapour pressure as a function of temperature.

(after Smithells. - Metals reference book[39]).

Temperature °C	500	600	700	800	900
Vapour Pressure mmHg	1.3	11.2	58.9	240	741

A portion of the free energy diagram for oxides[40] is shown in figure 4-1. From this it can be seen that under equilibrium conditions zinc oxide reduction by hydrogen occurs at a temperature in excess of 1100°C. Equilibrium for equation 4-1 is determined by the balance between hydrogen and water vapour, although this is rather simplified since zinc will be present as vapour not the solid metal. At equilibrium this ratio (H_2/H_2O) is 1:1 for reduction above 1100°C. However, atmospheric conditions in the thermobalance did not equate to equilibrium. There was a copious replenishment of hydrogen so that pH_2 was constant, no water vapour was present at the start of reaction 4-1 and water vapour produced would be removed rapidly by the flowing atmosphere. Under such conditions the ratio H_2/H_2O would be expected to be considerably higher than 1:1.

For zinc oxide reduction by hydrogen at 600°C, as obtained in figure 3-3, it can be seen from figure 4-1 that the required H_2/H_2O ratio is 10^4:1. This was not unreasonable in this system, especially when only the local atmosphere around the sample is considered. As the temperature rises the tolerable level of water vapour, before zinc is oxidised, increases. At the end of this reaction, at 900°C, the tolerable H_2/H_2O ratio has decreased to 10^2:1 (figure 4-1).

Figure 4-2 is confirmation that this was indeed zinc oxide reduction by hydrogen and not by residual carbon. The weight loss curves shown in

Figure 4-1 .FREE ENERGY DIAGRAM FOR OXIDES

(after Mackowiak, ref.40)

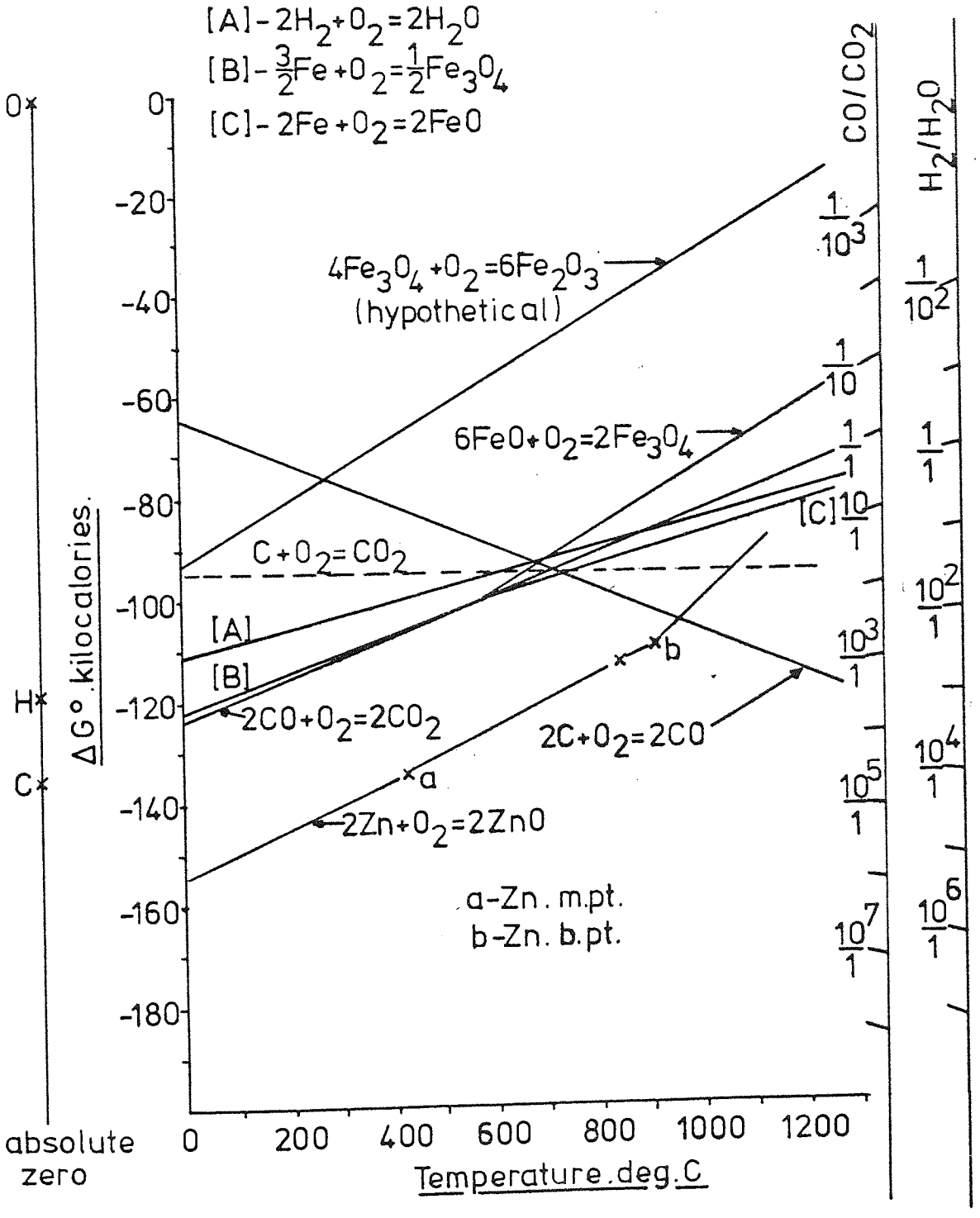

FIGURE 4-2 . The reduction of zinc oxide by hydrogen in N_2/10%H_2.

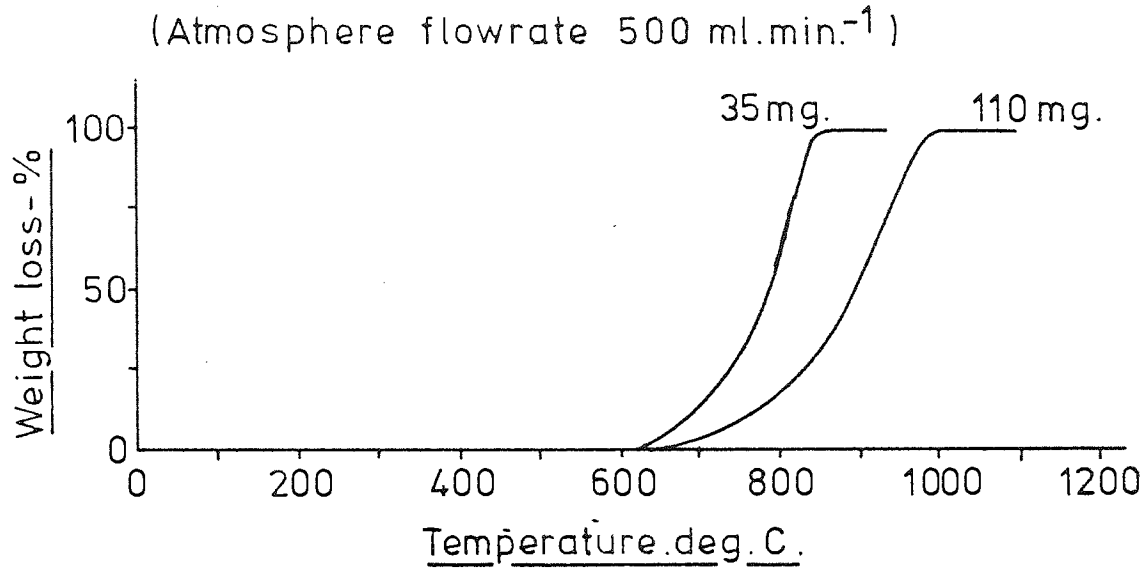

FIGURE 4-3 . The reduction of zinc oxide by carbon in argon

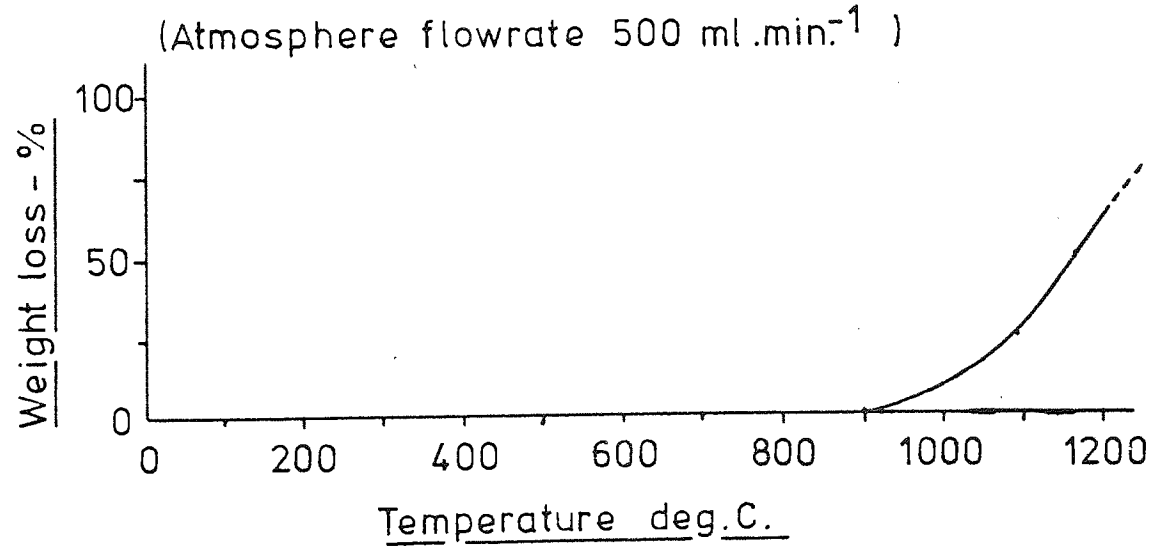

this figure are for two different sample weights of zinc oxide thermogravimetrically treated in $N_2/10\%H_2$. The factor controlling the decomposition range is obviously the amount of oxide to be reduced. When an intimate mixture of graphite and zinc oxide was thermogravimetrically treated in argon the weight loss curve shown in figure 4-3 was obtained. Reduction of zinc oxide by carbon in the absence of hydrogen occurs therefore, by reaction 4-2 at a temperature close to the equilibrium temperature indicated in the free energy diagram, figure 4-1.

$$ZnO + C \longrightarrow Zn + CO\uparrow \qquad -(4\text{-}2).$$

When the same ZnO/C mixture was heat-treated in $N_2/10\%H_2$, preferential reduction by hydrogen occurred leaving the carbon as a residue.

After lubricant decomposition at least part of the residue in $N_2/10\%H_2$ and argon was carbon. In $N_2/10\%H_2$ this was the only residue. In air there was only one reaction, corresponding to decomposition of the stearate radical. In such an oxidising atmosphere it would be expected that all the zinc oxide would remain, a residue of 13% of the initial weight. Since reduction is extremely unlikely under such conditions and no reduction reaction was indicated in figure 3-3, the only explanation at present for the low residue, 10%, lies in the possibility of zinc oxide being physically removed by a vigorous stearate radical reaction.

4-2-2 Lithium stearate

Thermograms obtained for lithium stearate are shown in figure 3-4. Comparison of stearate radical decomposition temperature ranges is discussed later, however comparison of figures 3-3 and 3-4 reveals that this reaction occurred at a higher temperature and rate in lithium stearate than in zinc stearate. As in the latter (figure 3-3) decomposition in air commenced sooner and finished later than in $N_2/10\%H_2$ and argon.

The difference in initial decomposition behaviour between these two metallic stearates was probably connected with their atomic bonding. This was also reflected in their melting points (zinc stearate - 122°C, lithium stearate - 205°C). Once stearate radical breakdown had been initiated in lithium stearate it proceeded at a faster rate than in zinc stearate due to the higher temperature favouring decomposition kinetics. Similar decomposition curves were obtained by Meyer et al[11] in atmospheres of hydrogen, nitrogen and air.

In all three atmospheres there was a further reaction following the initial decomposition, accounting for a weight loss of approximately 8%. Unlike zinc oxide reduction this reaction occurred independently of atmosphere and was characterised by an optimum rate of weight loss at an intermediate temperature. Temperature ranges were 600-770°C in $N_2/10\%H_2$, 600-720°C in argon and 680-800°C in air. In all cases the residue following stearate radical decomposition was a loose white powder.

The residue following this second reaction was glassy, pink and reacted readily with silica crucibles at high temperatures. This latter material seemed to be characteristic of lithia, Li_2O, and the final proportion of residue (5-6%) corresponded to the theoretical proportion of lithia present in lithium stearate.

The reaction producing this residual lithia was obviously not a reaction between the atmosphere and a compound, although its temperature range was particularly sensitive to the presence of air. This stage displayed the characteristics of thermal decomposition. The formation of lithium carbonate in compacts containing lithium stearate has been discussed theoretically elsewhere[41], although it was suggested that it was formed by chemical reaction rather than as a residue. The second reaction in figure 3-4 could therefore be the decomposition of Li_2CO_3 according to equation 4-3.

$$Li_2CO_3 \longrightarrow Li_2O + CO_2\uparrow \qquad \text{— (4-3).}$$

The lithium atom in lithium stearate is attached to the remains of the carboxyl group, consisting of C and O atoms. The theoretical weight loss of 60% for removal of CO_2 also corresponds to the actual weight losses of figure 3-4, when expressed as proportions of the residue remaining after the initial reaction.

Final confirmation that this was decomposition of lithium carbonate is given in figure 4-4. Samples of Li_2CO_3 were thermogravimetrically treated in $N_2/10\%H_2$ and argon. The weight losses, temperature ranges and final glassy residues matched the results of figure 3-4. It is possible that the presence of CO_2 in air was responsible for retarding this reaction, when using the latter as the thermogravimetric atmosphere. It should be noted that in neither atmosphere was carbon found as a residue.

4-2-3 Stearic acid

The thermograms obtained for fine, coarse and medium particle-sized stearic acid are shown in figures 3-5, 3-6 and 3-7 respectively. All were heat treated in $N_2/10\%H_2$ and argon, only the medium stearic acid was treated in air. A slight residue of soot was found for each lubricant in all atmospheres except air. As can be seen from the thermograms this varied from an amount beyond the sensitivity of the thermobalance to approximately 3% of the initial weight, independent of atmosphere. These were confirmed visually due to the variation in total weight losses indicated by the thermobalance, as discussed in 4-2.

Stearic acid decomposition occurred in a similar manner in both $N_2/10\%H_2$ and argon, but was modified again by the presence of air. Weight loss commenced at a higher temperature in this atmosphere, then proceeded at a higher rate to finish at the same temperature as $N_2/10\%H_2$ and argon. After a weight loss of 84% this reaction in air altered its characteristics as can be seen in figure 3-7. The remaining 15% of material was removed by a reaction

FIGURE 4-4 . The decomposition of lithium carbonate in N_2/10%H_2- and argon.

(Atmosphere flowrate 500 ml.min^{-1})

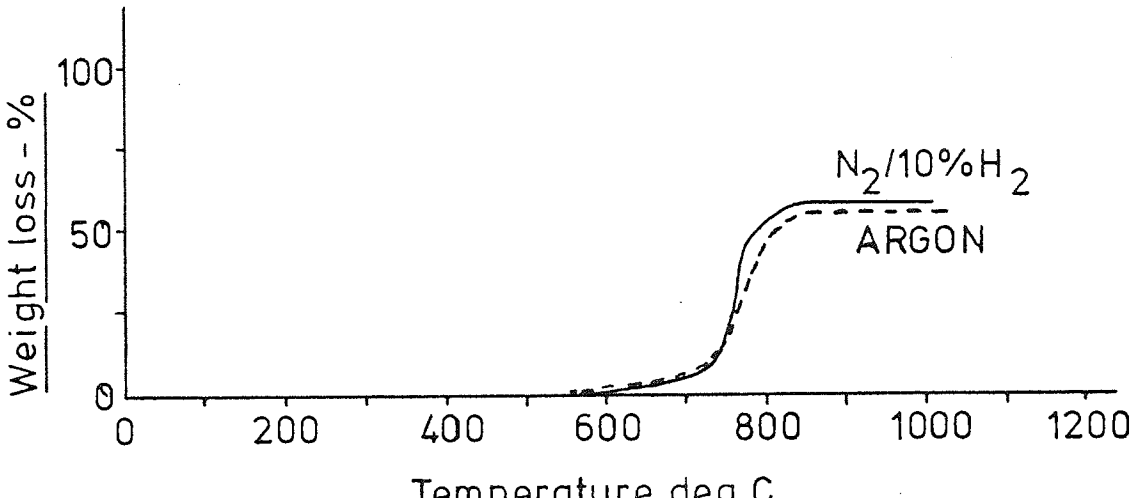

with a weight loss curve suggesting a temperature dependent reaction. It is interesting to note that this weight loss (15%) corresponded to the theoretical weight percentage of the carboxyl radical (- COOH) in stearic acid. If this group could remain stable in some form following removal of the aliphatic group, it would require only heat and a supply of oxygen to form carbon dioxide and water vapour, perhaps as indicated in equation 4-4.

$$4(\text{-}C\leq^{O}_{OH}) + O_2 \longrightarrow 4CO_2\uparrow + 2H_2O\uparrow \qquad \text{— (4-4).}$$

The obvious difference between air and the other atmospheres was the presence of copious oxygen.

In the metal stearates the carboxyl group is attached to the metal ions and undergoes reactions involving these, as discussed previously. However, despite the coincidence of weight loss it is difficult to envisage the carboxyl group alone remaining stable up to 300°C.

Only a small atmosphere dependence was indicated in figures 3-5 to 3-7 for stearic acid decomposition. However, Meyer et al[11] did find a strong dependence of decomposition temperature range on atmosphere. In H_2, air and N_2 the ranges were 125-325°C, 190-330°C and 220-360°C respectively.

4-2-4 Stearamide

The decomposition characteristics of stearamide (figure 3-8) were very similar to those of stearic acid. Atmosphere had little effect on the initiation or rate of decomposition and a sooty residue was obtained with all samples in N_2/10%H_2 and argon. In air a second reaction was noted, again very similar to that obtained with stearic acid, involving the removal of 15% of the total sample.

In this stearate the hydroxyl of the carboxyl group is replaced by NH_2 which also accounts for 15%-16% of the molecular weight of stearamide. If it is possible in some way that this group can remain stable to 330°C and oxidation is again responsible for the second reaction of figure 3-8, then it

may be the result of equation 4-5.

$$2(-C\overset{O}{\underset{NH_2}{<}}) + 2O_2 \longrightarrow 2CO_2\uparrow + 2H_2O\uparrow + N_2\uparrow \qquad -(4\text{-}5).$$

There is a more detailed description and comparison of the characteristics of stearate radical decomposition in the summary, section 4-2-9.

4-2-5. Cosmic 64 wax

The decomposition of Cosmic 64 wax, figure 3-9, was characterised by a more measurable carbonaceous residue in $N_2/10\%H_2$ and argon (3% and 5% by weight respectively) than that due to the previous stearates. Carbon deposition was least in air where the oxidising conditions encouraged complete decomposition. It is not surprising that more carbon should remain as a residue with this material since elemental analysis showed it to consist of 74% by weight carbon, a higher proportion than a stearate such as stearic acid (67%).

The overall decomposition range of this wax was larger than in the stearates and hence the overall reaction rate was lower. Atmosphere had little effect on decomposition, there were no secondary reactions (figure 3-9) but oxidising conditions did encourage a lower reaction rate, particularly during later stages.

4-2-6 Effect of particle size.

The thermograms obtained from stearic acid (figures 3-5 to 3-7) for decomposition in $N_2/10\%H_2$ were plotted in figure 3-10 to illustrate the influence of particle size on decomposition characteristics. It can be seen that there was very little difference in behaviour until the later stages of decomposition, where there was a tendency for decreasing particle size to cause a lag in the reaction.

Figure 3-10 does show that there was no difference in decomposition behaviour due to the methods of producing the different particle sizes. The

coarse and fine materials were produced by ball-milling, whilst the medium was produced by precipitation from solution in diethyl ether (see section 4, Materials).

4-2-7. Effect of atmosphere flow rate.

The effect of atmosphere flow rate on the decomposition of zinc stearate is shown in figure 3-11. As flow rate decreased decomposition of the stearate radical was retarded, occurred over a larger temperature range and became slightly less complete, leaving more carbonaceous residue.

This may simply have been a physical effect due to the inability of the atmosphere to carry away decomposition products, thus delaying weight loss. If decomposition products were not carried away this may also cause a true increase in reaction temperature. It appears that if lubricant or decomposition products are encouraged to remain to slightly higher temperatures than normal, then final decomposition to leave a carbon residue becomes more likely.

In $N_2/10\%H_2$ the atmosphere is responsible for supplying one of the reactants and removing both decomposition products during zinc oxide reduction. As can be seen from figure 3-11, a reduction in the supply of hydrogen retarded the start of this reaction. As flow rate decreased the final temperature and final reaction (or weight loss) rate decreased due to the reduced carrying capacity of the atmosphere. However, the intermediate reaction rate appeared to be higher at the low flow rate. If zinc oxide reduction is delayed to a higher temperature, as with a low flow rate, then when reduction commences the vapour pressure of zinc will be high and the corresponding rate of weight loss will be high, but the reaction rate need not be so high.

4-2-8 Effect of sample weight.

As can be seen from figure 3-12, sample weight had little effect on

removal of the stearate radical. It is possible that in most cases the rate of this stage in terms of weight loss had been dictated by the recording capability of the thermobalance.

As would be expected, the initiation of zinc oxide reduction was not sensitive to sample weight but the overall rate was, at least in terms of weight loss. The actual rate of weight loss was probably similar for all three samples as there were no diffusion considerations and this atmosphere flow rate was able to remove all decomposition products. However, the amount of material to be removed at a given rate will determine the overall reaction time and hence temperature interval. The overall % weight loss rate and apparent reaction rate decreased therefore with increasing sample weight.

4-2-9 Summary

This discussion on the decomposition characteristics of pure lubricants has been very detailed. The applicability of this data to real systems, lubricants within compacts, may be questioned perhaps, especially as the presence of a compact may well alter the system considerably (inhibited gaseous diffusion seems likely[35]). However, detection and identification of reactions obviously becomes easier as any system becomes simplified. There is little point investigating the effect of process variables on decomposition if the basic reactions are not known first. The effects of compact variables upon lubricant decomposition are not only important but it will be shown later that the products of decomposition may play an important role in the development of mechanical properties. A more generalised discussion of the decomposition characteristics of the stearate radical, or dewaxing to use the more convenient term, is therefore pertinent at this stage.

The main temperature ranges over which dewaxing occurred for pure lubricants are shown in table 4-2 together with the melting points obtained during this investigation. It can be seen that in $N_2/10\%H_2$ and argon, stearic acid and stearamide had the lowest decomposition temperatures and similar

ranges. Stearates containing metal ions had noticeably higher reaction start and finish temperatures, lithium stearate particularly, but exhibited temperature ranges similar to that of stearic acid (approximately 200°C). Cosmic 64 wax was notable in having an intermediate reaction initiation temperature with a wide decomposition temperature range. The similarity of the short temperature ranges obtained for stearate based lubricants may suggest that these ranges had been controlled by the maximum weight change response rate of the balance.

It can also be seen from table 4-2 that the initiation temperatures for stearate radical decomposition were proportional to the melting points of the stearates. The melting points of all lubricants were well exceeded before weight loss started. It should be noted here that where the terms reaction initiation or finish are used they refer more specifically to reactions causing weight changes only. The drawback with thermogravimetric analysis is that it may only detect reactions which cause a weight change.

Table 4-2

Decomposition temperature ranges and melting points of free (pure) lubricants

Material	Melting point °C	Decomposition reaction temperatures °C		
		$N_2/10\%H_2$	Argon	Air
Zinc stearate	122	270-460	260-450	220-550
Lithium stearate	205	360-490	350-480	280-530
Stearic acid-fine	67	190-400	170-400	—
— -medium	64	160-360	180-360	220-490
— -coarse	69	180-360	180-380	—
Stearamide	90	180-340	200-350	220-500
Cosmic 64 wax	138	230-480	250-480	260-570

(Atmosphere flow rate - 500 $ml.min^{-1}$).

Metal stearates produced high temperature reactions involving compounds formed from the metal ion and carboxyl radical. It would also seem that, from the results in air (figures 3-7 and 3-8), the carboxyl and amide groups of stearic acid and stearamide breakdown in the later stages of decomposition. This would seem to indicate that decomposition of free lubricants proceeds by the progressive removal of the hydrocarbon chain, leaving the carboxyl or modified carboxyl group to decompose last. One implication of this is that the oxygen bearing group of a stearate would remain within a compact at temperatures in excess of 400°C. There would also be no decomposing hydrocarbons to expel this oxygen.

The result of hydrocarbon decomposition was a white vapour which condensed easily at ambient temperature to form a white powder. The analysis of this condensate (obtained from zinc stearate) indicated carbon and oxygen contents of 82 and 14 percent by weight respectively. It was found to flash readily when heated in air over a bunsen burner, burning with a sooty flame. This treatment left a zinc oxide residue of approximately 2% by weight of the total.

If it is assumed that this condensate was a mixture of hydrocarbons and zinc oxide (it did in fact always appear damp, hence the balance may be water), then the chemical analysis suggests an alkane, either $C_{16}H_{34}$ or $C_{17}H_{36}$, hexadecane and heptadecane respectively. These are also close in composition to the aliphatic chain of the stearate group ($-C_{17}H_{35}$). One possible decomposition reaction for stearic acid could then be as in equation 4-6.

$$CH_3.(CH_2)_{16}.C\overset{O}{\underset{OH}{=}} \longrightarrow C_{16}H_{34} + H.C\overset{O}{\underset{OH}{=}} + C. \qquad \text{--- (4-6).}$$

Obviously the formic acid ($H.COOH$) would not be stable at such temperatures, in excess of 300°C, when separated from the hydrocarbon chain, and would eventually be removed by evaporation or decomposition to such compounds as

H_2O and CO_2. In air it would seem that this group was oxidised rather than simply decomposing thermally (figure 3-7).

The condensate was found to exhibit two melting points 58 and 67°C. Unfortunately the melting points of hexadecane and heptadecane are 18 and 23°C[46] respectively. However, it is possible that the presence of zinc oxide tended to increase the actual melting points of these compounds.

4-3 The decomposition of lubricants within compacts at a low heating rate.

All investigations of lubricant decomposition at a low heating rate have been carried out using the thermobalance at its maximum linear heating rate of $6^{o}C.min^{-1}$. As discussed previously this was chiefly due to convenience since many variables may be studied using single specimens. Decomposition temperatures may be dependent on heating rate[35] and so there will be discussion later of results obtained at a higher and more commercial heating rate, but not obtained thermogravimetrically.

Throughout this discussion quoted relative densities are $\pm$ 1% and it has been assumed that solid density was $7.87 g.cm^{-3}$.

4-3-1 Matrix reactions and reproducibility

Reactions due to MP32 iron powder, when compacted with only die wall lubrication, are shown in figure 3-13(a)and(b) for atmospheres of $N_2/10\%H_2$ and argon respectively. In figure 3-13(a)traces marked[a1]and[a2]have been obtained using temperature calibration curve(a)(figure 2-2) and one particular batch of powder. The trace marked[b]was obtained after the thermobalance refit from another powder batch and using temperature calibration(b) (figure 2-2). The effect of changing powder batch is discussed later with the aid of other results.

4-3-1-1. Matrix reactions

As can be seen from figure 3-13. there were clearly reactions between elements associated with the iron powder (argon, figure 3-13b) and reactions between the iron powder and the atmosphere ($N_2/10\%H_2$, figure 3-13a). Carbon and oxygen seemed probable candidates for reacting species since both were present in the as-received powder in considerable quantities (0.07%C, 0.30%O_2, table 3-1). Compacts of MP32, containing no lubricant and pressed to a density of 80%, were thermogravimetrically treated in $N_2/10\%H_2$

to temperatures between ambient and 1200°C. Residual carbon and oxygen analyses for these are shown in table 3-2. These correspond to the second batch of powder, curve[b]in figure 3-13a and it can be seen from the results of analysis that the total carbon and oxygen losses were indeed responsible for the total weight loss in $N_2/10\%H_2$.

Three reactions are indicated in either trace of figure 3-13(a) marked 1, 2 and 3 in order of temperature. Each reaction was separated from its neighbours by periods of only slight activity, as indicated by a very low rate of weight loss. The definition of these three reactions was found to be dependent on density, as shown by the matrix reactions for compacts of varying density in figure 3-22,page286. In a compact 60% dense the temperature intervals between reactions did become periods of inactivity. It is possible to identify the matrix reactions shown in figures 3-13(a)and(b) by comparison of these with the matrix thermograms of figures 3-22 and the data of table 3-2,and with reference to the free energy diagram for oxides, figure 4-1. In argon (figure 3-13b) only two reactions were observed the final one being similar to reaction 3 in $N_2/10\%H_2$.

The reactions obtained in $N_2/10\%H_2$ will be explained first as these have been investigated more fully than those in argon. Reaction 1 (figure 3-13a) was observed in $N_2/10\%H_2$ only. The initiation temperature and rate were both density dependent (figure 3-22) and the indicated weight loss was due to oxygen removal only, there was no carbon loss at this stage (table 3-2). This suggests reduction of oxygen in the sample by hydrogen from the protective atmosphere according to equation 4-7.

$$H_2 \rightarrow 2H \text{ (adsorbed on Fe surface)}$$
$$O_{[Fe]} + 2H \rightarrow H_2O \qquad \text{—— (4-7).}$$

This oxygen may have been adsorbed on the particle surfaces or in the form of Fe_3O_4. It is probable that only surface oxygen or oxides were involved,

as these would be the first exposed to a gaseous reducing agent diffusing into a compact through the pores.

The atmosphere was capable of reducing zinc oxide at 600°C (chapter 4-2-1) and, as can be seen from figure 4-1, it was theoretically capable of reducing Fe_3O_4 at any temperature above 100°C. It can be seen in figure 3-22 that both the initiation temperature and rate of this reaction were density dependent. The former could be associated with the ease with which hydrogen may diffuse into larger pores. Perhaps preferential diffusion into the inhibited diffusion space of pores occurred such that a local internal atmosphere of higher hydrogen content than the surrounding atmosphere was produced.

Where diffusion through pores was not a primary consideration, such as with loose powder, a high initiation temperature was recorded, as shown in figure 4-5. Both hydrogen and nitrogen were able to diffuse into pores with such loose packing. At high densities, for example 85%, physical limitations on the diffusion of all gases, especially at low temperatures, became significant and the high initiation temperature probably reflected the difficulty of displacing oxidising species such as entrapped air. It will be shown later that at such a density the proportion of closed pores becomes significant. It is possible therefore that the optimum density for minimising the initiation temperature of reaction 4-7 was a compromise between the inhibition of diffusion of all gases present and free diffusion of all gases.

As shown by figure 3-22, the rate of this reaction was reduced by increasing density. This was possibly caused by the difficulty of removing the reaction product, water vapour, from within pores as their size decreased.

The intermediate reaction (2) in $N_2/10\%H_2$ commenced at 700°C independent of density (figure 3-22) and involved the loss of equal proportions

FIGURE 4-5 Weight loss curve for loose MP 32 (53-104 μm) in N_2 / 10% H_2.

(Atmosphere flowrate 500 ml.min.$^{-1}$)

(Sample weight 4 mg.)

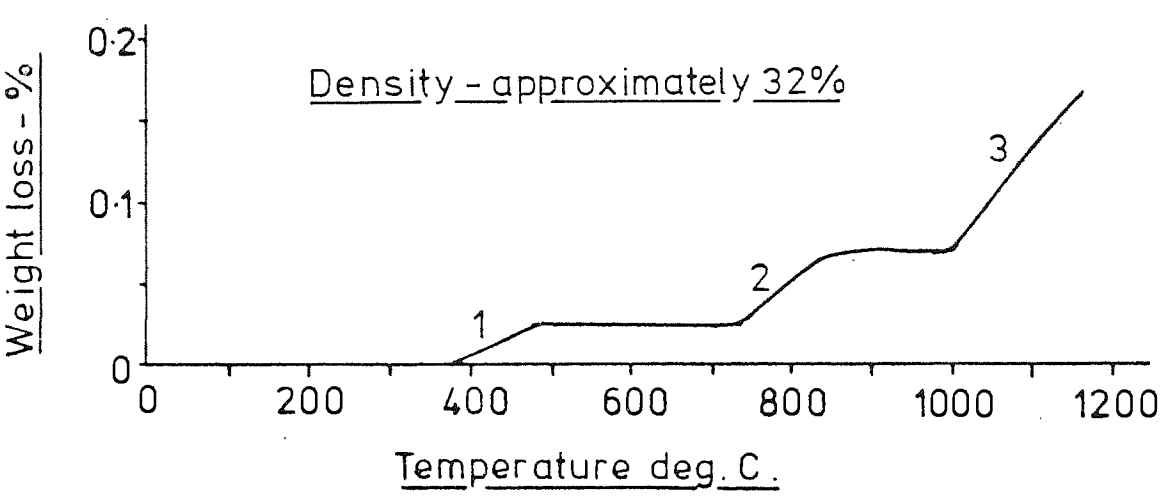

of carbon and oxygen (table 3-2). The rate of this reaction was observed to increase with decreasing density but not to such a marked degree as for reaction 1. Hydrogen was probably not the major reducing agent during this reaction since the initiation temperature was not density dependent; both oxygen and carbon losses were recorded (table 3-2) and carbon monoxide stabilises rapidly above 700°C (figure 4-1) relative to H_2O, FeO and Fe_3O_4. At 700°C FeO is more stable than Fe_3O_4 (shown in figure 4-1 and by the eutectoid reaction $4FeO \rightleftharpoons Fe + Fe_3O_4$ at 560°C in the iron/oxygen system). Reaction 2 was therefore most probably the reduction of FeO by carbon present within the matrix according to equation 4-8.

$$FeO + C_{Fe} \longrightarrow Fe + CO\uparrow \qquad \text{—— (4-8).}$$

The analysed carbon and oxygen losses corresponding to this stage were in the ratio 1:1 (table 3-2), approximating to the stoichiometric ratio of 3:4. The difficulty of removing carbon dioxide from within pores would explain the dependence of the rate of this reaction upon density. However, this density dependence was not so marked as for reaction 1 (fig. 3-22) due partly to the difference in diffusing species and partly to the increased thermal activity at these higher temperatures.

The final reaction (3) in $N_2/10\%H_2$ was also found to occur in argon (fig.3-13). Equal proportions of carbon and oxygen were removed again in $N_2/10\%H_2$ (table 3-2) but only up to 1120°C. At this point total carbon loss was achieved. However, as shown in figures 3-13a and 3-22 there was no check in the rate of weight loss and the reaction proceeded to the maximum testing temperature. There seemed to be no relationship between compact density and either reaction rate or initiation temperature (figure 3-22).

As carbon was the only known reducing agent present in an atmosphere of argon, and in $N_2/10\%H_2$ initial losses of carbon and oxygen approached the stoichiometric ratio for carbon reduction of iron oxides (table 3-2), at

least part of this final reaction must have been reduction by carbon. In $N_2/10\%H_2$ the continuance of oxygen loss suggests that hydrogen took over reduction as carbon was depleted. At such high temperatures diffusion of reactants and reaction products, particularly through pores, was probably not a problem, hence the lack of density dependence.

The oxides involved in this reaction were possibly complex, requiring a high reduction temperature or perhaps some degree of thermal decomposition prior to reduction. They may have been FeO originally within ferrite and inaccessible to carbon, the increased solubility of carbon in austenite would then have helped the small amount remaining after reaction (2) to reach the oxide.

In an atmosphere of argon only two reactions were recorded (fig.3-13b) and the final, high temperature, reaction has already been discussed. The initiation temperature of the first reaction, 560°C, corresponds to the temperature where Fe_3O_4 becomes unstable relative to FeO and CO_2 (fig.4-1), below 560°C CO_2 is only marginally more stable than Fe_3O_4. As carbon was the only known reducing agent in this system, it seems likely that initially this reaction was carbon reduction of Fe_3O_4 to Fe and FeO, with CO_2 as a gaseous reaction product. This would be aided by the eutectoid reaction in the Fe/O system ($Fe + Fe_3O_4 \rightleftharpoons 4FeO$ at 560°C). Above 700°C the reduction of FeO to produce CO becomes more probable (fig.4-1).

Final carbon and oxygen analyses for a compact thermogravimetrically treated to 1200°C in argon are recorded in table 3-1. The carbon and oxygen losses (0.07% and 0.09% respectively) were of the right order, but if the actual weight losses of figure 3-13b are matched to the stoichiometric ratios of carbon and oxygen (3:8 below 700°C, 3:4 above 700°C) a slightly higher oxygen loss would be expected.

Analysis of the weight loss curves of figure 3-13 has shown the importance of the local atmosphere within pores. This may be related to the

surrounding atmosphere but not necessarily of the same composition. Density variations within a compact may cause a given reaction to occur at different rates and over different temperature intervals within the same compact. The overall effect would be an extension of the time over which such reaction products as CO_2 and H_2O would be present within pores.

4-3-1-2 Reproducibility

Typical total weight loss curves for compacts containing 1% by weight zinc stearate are shown in figure 3-14. Curve(a) corresponds to a sample pressed from the initial powder batch and plotted using temperature calibration curve(a) (figure 2-2). Trace(b) represents the second powder batch and was plotted with calibration(b)(figure 2-2). It can be seen that the overall difference was in degree of weight loss not reaction temperatures (figure 3-14). This difference in weight loss was attributable to a corresponding difference in weight loss due to matrix reactions, as shown in figure 3-13a. The majority of oxygen analyses discussed in 4-3-1-1 were obtained from compacts pressed from the second powder batch which was found to have a total oxygen content of 0.30%. The first batch had an oxygen content of 0.25% so that the weight loss differences shown by figures 3-13a and 3-14 may be attributed to an increase in oxygen content. Consequently care has been taken to ensure that the matrix weight loss curves used for subtraction corresponded to the same powder batch as the appropriate total weight loss curve.

There was little difference in reaction initiation temperatures as obtained using the two calibration curves (a)and(b) (figure 2-2). This would seem to support the validity of using these calibrations. The major difference between curves(a1) and(a2) in figure 3-13a was in terms of weight loss, not reaction temperatures. The samples for these traces were pressed from the initial batch of powder and plotted using calibration(a). The difference between them was the time of testing,(a1) was obtained at an early

stage whilst (a2) was obtained after a lapse of approximately one year, with the thermobalance in frequent operation between. The coincidence of reaction temperatures would seem to indicate that thermocouple deterioration was not a problem. However, as stated previously, direct comparison of reaction temperatures has been confined to compacts thermogravimetrically treated in experimental groups over short time periods.

Appropriate matrix reaction thermograms, such as those of figure 3-13, have been used for subtraction from total weight loss curves as obtained by thermogravimetrically treating compacts containing lubricants. Only the subtracted weight loss curves are shown in section 3. However parent curves are shown in appendix C should a check on the method be required. It may be argued that the matrix reactions actually occurring in a compact containing lubricant may be modified by (i) the relative absence of air within the pores and (ii) by the reactions attributed to lubricants and their residues.

There has been no evidence to show that air has played a significant role in the matrix reactions discussed. It seems likely that sufficient time elapsed prior to the initiation of any reaction for almost complete elimination of air retained within pores. At the start of reaction 1 in $N_2/10\%H_2$ (figure 3-13a) a compact would have been in a flowing protective atmosphere within the thermobalance furnace for at least two hours. An important part of the object of subtraction was to reveal modifications to matrix reactions caused by lubricant reactions and so detection of the effects noted in (ii) above was actually desirable.

The relative insignificance of retained air and importance of these reactions may be put into perspective if the volume of gaseous reaction product of a typical reaction is considered. The volume of CO_2 produced by reaction 2 in $N_2/10\%H_2$ (figure 3-13a) would be sufficient to fill the available pore volume of a compact 80% dense ten times at N.T.P. and at least thirty times at 800°C.

4-3-2 Lubricant reactions - Low heating rate.

All the samples studied in this chapter were of constant physical properties (80% dense, as-received MP32) and treated in $N_2/10\%H_2$ and argon at a constant flow rate of 500 $ml.min^{-1}$. Lubricant content was maintained at 1% by weight.

The appropriate weight loss curves, obtained by subtraction as described previously, are shown in figures 3-15 to 3-20 inclusive. These should be representative of reactions due solely to lubricants, reactions between the matrix and lubricant or reaction products,and modifications to the matrix reactions caused by the presence of lubricant.

Final carbon analysis was made on all compacts thermogravimetrically treated to 1200°C and these results are tabulated in table 3-3 with longitudinal and radial dimensional changes.

4-3-2-1 Zinc stearate

Lubricant reactions for compacts containing zinc stearate in atmospheres of $N_2/10\%H_2$ and argon are shown in figure 3-15. The corresponding pure lubricant thermograms are shown in figure 3-3. It can be seen from figure 3-15 that stearate radical removal was again rapid despite the physical restraints of a compact. Comparison between pure lubricants and lubricants within compacts during this initial stage will be given further consideration in the summary (4-3-2-11).

In $N_2/10\%H_2$ (figure 3-15) the zinc oxide reduction reaction was again present, commencing at 560°C and terminating at 850°C. Residual zinc analysis was carried out on similar compacts heated to temperatures between 400°C and 1200°C, the results are given in table 4-3.

Table 4-3

Residual zinc analysis as a function of temperature for compacts containing 1% by weight zinc stearate.

Temperature°C	400	510	780	1180
Zinc %	0.09	0.08	0.02	0.01

(Atmosphere - $N_2/10\%H_2$, 500 $ml.min^{-1}$. Density - 80%)

The theoretical zinc addition corresponding to 1% by weight lubricant is 0.1% and it can be seen from table 4-3 that at 400°C, following expulsion of the stearate radical, the majority of this zinc remained. This residual zinc was not dispersed evenly over particle surfaces but was found to remain in discrete areas, as shown in plate 4-1. These areas may reflect original lubricant particles or may represent the extent of molten spots of lubricant.

It can be seen from table 4-3 that, although zinc oxide was not carried from the compact by the decomposing stearate radical, the zinc produced by reduction did not diffuse into the iron matrix. It is valid to question why this was so since the solubility of zinc in iron at 600°C is some 18% by weight[39]. It is unlikely that unreduced zinc oxide provided a physical barrier to freshly reduced zinc as the oxide has been shown to be discontinuous (plate 4-1).

The vapour pressure of zinc as a function of temperature is recorded in table 4-1. At the start of this reaction, at 560°C, the zinc vapour pressure would not have been significantly high. The weight loss, which reveals a reaction, would probably have been caused mainly by loss of oxygen as water vapour. Under these conditions some elemental zinc may have diffused into ferrite. Zinc vapour pressure rises rapidly with increasing

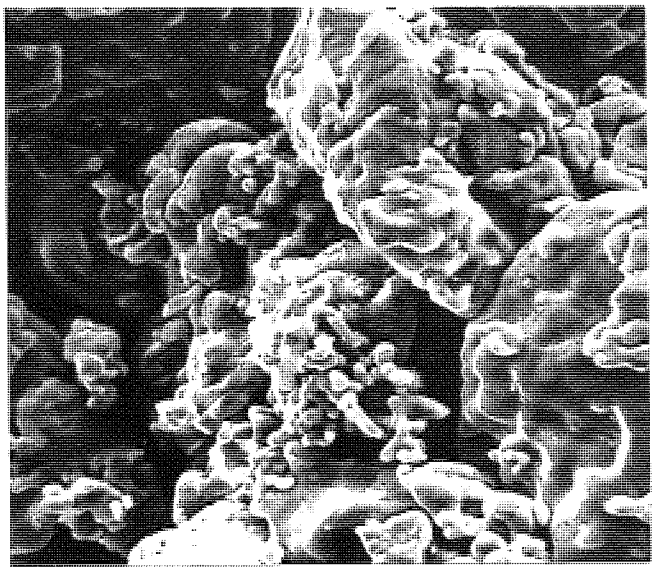

(a) Fracture surface

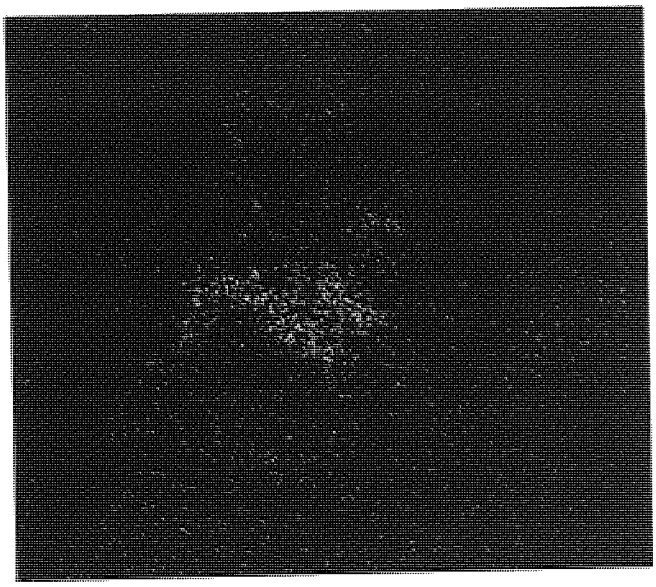

(b) Zn X-ray map

PLATE 4-1 The dispersion of ZnO on Fe particles after dewaxing at 500°C

(1% admixed zinc stearate.)

temperature so that later stages of the reaction were probably indicated by loss of zinc vapour. Solution of zinc in ferrite was therefore prevented by its high vapour pressure.

The validity of comparing pure lubricant decomposition with compacts is considered later (section 4-3-2-11) with particular reference to the thermal properties of the two types of sample (crucible and compact). At this stage a comparison will be made between the characteristics of the zinc oxide reduction reaction in $N_2/10\%H_2$ as a residue from pure lubricant decomposition and as a residue from decomposition within a compact. To equate actual lubricant weights the thermogram for a 100mg pure zinc stearate sample shown in figure 3-12 will be used.

It can be seen from figures 3-12 and 3-15 that the reduction of residual zinc oxide by atmospheric hydrogen commenced at a lower temperature in a compact, at 560°C, and at 600°C for pure lubricant. It has already been suggested that preferential diffusion of hydrogen into pores may occur, increasing the H_2/H_2O ratio locally. It seems unlikely that the temperature reduction could be explained by a catalytic effect due to the high surface area since the residual zinc oxide was not uniformly dispersed over all the available surface area. This may even have made contact between oxide and hydrogen more difficult.

The reduction of zinc oxide in the absence of a compact (figure 3-12) proceeded at an increasing rate as the temperature increased, to produce a maximum weight loss rate close to the terminal temperature. Zinc oxide reduction within a compact was characterised by a maximum rate at an intermediate temperature, followed by a reducing rate as temperature increased. It has been established that there was no problem initiating this reaction within a compact and that the weight loss at low temperatures was probably mainly due to the removal of oxygen as water vapour. The maximum weight loss rate probably corresponded to the optimum balance between diffusion of

hydrogen into pores, the actual reduction of zinc oxide and the diffusion of water and zinc vapour out of pores. As the reaction proceeded beyond this optimum point the vapour pressure of zinc within the pores increased, tending to exclude hydrogen,and the amount of residual zinc oxide was depleted. The inhibited diffusion conditions prevalent in pores,therefore, promoted initiation of zinc oxide reduction by hydrogen,but were also at least partially responsible for restricting the reaction as products built up.

No zinc oxide reduction was detected for pure lubricant in an atmosphere of argon, as shown by figure 3-3. However, it is obvious from figure 3-15 that an incomplete reaction has occurred. The initiation temperature of this reaction would seem to indicate hydrogen reduction,but the form of the weight loss curve suggests a purely internal reaction involving only reactants within the compact and no diffusion into pores from the external atmosphere. There was,therefore,only unidirectional diffusion out of the pores and the depletion of reactants as temperature increased was compensated by an increase in thermal activity, hence there was a tendency for the reaction rate to remain constant until one reactant was completely removed.

Carbon reduction was unlikely since this has been shown to occur typically at a temperature of 900°C (figure 4-3), but there was no obvious explanation for the presence of hydrogen in the argon atmosphere. The iron powder used in this investigation was based on reduced mill-scale and may have been hydrogen reduced or hydrogen annealed. This powder had considerable internal porosity and it is possible that during cooling, after reduction or annealing, atomic hydrogen diffused rapidly through the ferrite lattice to be retained in molecular form within internal pores. Increasing temperature during thermogravimetric analysis would then allow this hydrogen to diffuse again through the lattice in atomic form. In such a condition it would readily reduce the residual zinc oxide.

The proportion of hydrogen required to reduce the 0.12% zinc oxide involved in this reaction would be a minimum of 0.003% by weight. With a sample weight of 0.1g this proportion of hydrogen proved to be near the detectability of the Balzer Exhalograph. The presence of such large quantities of oxygen (0.25%-0.30%) completely obscured detection of the hydrogen and the use of a larger sample only compounded the problem. The presence of hydrogen within the powder, therefore, relies on circumstantial rather than analytical evidence.

It is reasonable to question why this hydrogen did not take part in the matrix reactions in argon, discussed in 4-3-1-1. If the oxygen removed (0.09%) in figure 3-13b were reduced solely by hydrogen the proportion required would be 0.01%. However it is possible that the small quantity believed to be present may have contributed to reduction, but not above 700°C when CO stabilisation becomes rapid.

It can be seen from figure 3-15 that there was a slight high temperature reaction, particularly in $N_2/10\%H_2$, similar to the final matrix reaction. Residual carbon was observed following the decomposition of pure lubricants (section 4-2) and so this could be an extension of the final matrix reaction caused by residual carbon. The deposition of carbon by lubricants decomposing within compacts is given further consideration in the summary (4-3-2-11).

4-3-2-2 Lithium stearate

The subtracted weight loss curves for the decomposition of lithium stearate within compacts are shown in figure 3-16. Stearate radical decomposition was insensitive to atmosphere composition again, but comparison with pure lubricant reactions (figure 3-4) shows that the higher temperature reactions differed considerably. Within compacts a reaction involving a weight loss was recorded as soon as removal of the stearate radical ceased (figure 3-16). In $N_2/10\%H_2$ the corresponding weight loss was 0.08%, in argon

an apparent loss of 0.04% was recorded but this may have been obscured by the initial reaction since total weight losses after this second reaction were similar in both atmospheres.

The weight loss of 0.08% recorded in $N_2/10\%H_2$ corresponded to that expected from decomposition of lithium carbonate. However, comparison with figure 3-4 will show that within a compact this reaction occurred at a temperature 100-150°C lower than with pure lubricant. This reaction involved only thermal decomposition of the carbonate and so may have been catalytically promoted by dispersion on the surface of the iron powder particles.

It can be seen from figure 3-16 that weight changes did not cease after Li_2CO_3 decomposition. Slight weight gains were recorded, particularly in $N_2/10\%H_2$, and there was a marked final weight loss corresponding to the final matrix reaction. The latter suggested an extension of the final reduction reaction or an increase in oxygen content at an earlier stage. The reduction of lithia was extremely unlikely as this is very stable and was found to be so during pure lubricant decomposition studies.

Carbon dioxide was a reaction product resulting from lithium carbonate decomposition. This carbon dioxide was free to escape to the surrounding atmosphere during pure lubricant breakdown but would fill the pores of a compact. This gas,retained in pores, could retard the matrix reduction reactions and possibly cause oxidation if retained above 700°C.

The temperature ranges over which weight gains were noted seem to approximate to those of reaction 2 in $N_2/10\%H_2$ (figure 3-13a) and reaction 1 in argon (figure 3-13b) and so retardation of matrix reactions was most probable. Figure 4-6 illustrates the effect of increasing the proportion of CO_2 present. The thermograms in this figure were obtained from a compact of MP32, 80% dense, containing an addition of 0.5% lithium carbonate. A weight gain due to oxidation was even recorded in the parent curve. Oxygen analyses were carried out on similar compacts heated to 850°C, 960°C and

FIGURE - 4-6

Decomposition of lithium carbonate within a compact

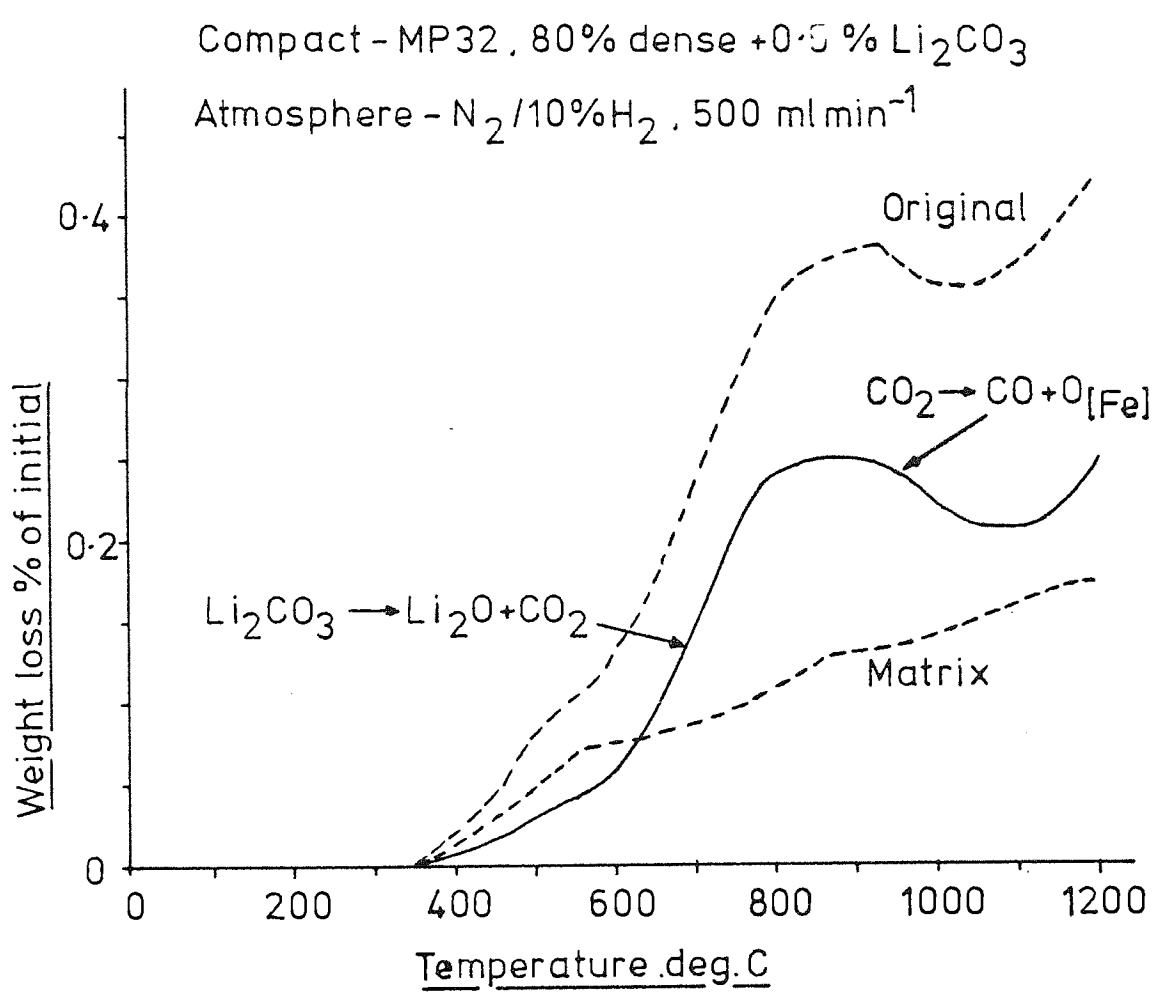

1200°C, the results are given in table 4-4.

Table 4-4

Oxygen determinations of compacts containing 0.5% lithium carbonate, thermogravimetrically treated in $N_2/10\%H_2$.

Temperature °C	850	960	1200
Oxygen % by weight	0.27	0.31	0.22

(Material - MP32, 80% dense. Flow rate 500 $ml.min^{-1}$).

It can be seen from comparison of figure 4-6 and table 4-4 that the weight gain did correspond to oxidation. In these latter results oxidation had been promoted artificially by increasing the quantity of carbon dioxide present. Some of the weight increase possibly being caused by oxidation of the external surface of compacts by carbon dioxide escaping from pores to the surrounding atmosphere. However, a similar effect would be expected if a smaller quantity of carbon dioxide were encouraged to remain within pores to higher temperatures. This may happen if density is increased, restriction of pore space would mean that a given quantity of CO_2 could achieve a higher partial pressure within pores or take longer to be removed due to inhibited diffusion and its ability to fill the smaller space to a greater degree. Further consideration is given to this in 4-3-2-10. High residual oxygen contents have been noted elsewhere[10] in compacts containing lithium stearate, this may have been due to residual lithia or oxidation as described above.

It will be noted that the lithium carbonate decomposition reaction as obtained in figure 4-6 corresponded to those of figure 3-16 in terms of temperature.

4-3-2-3 Stearic acid

The subtracted weight loss curves due to the decomposition of stearic acid within compacts are shown in figures 3-17 and 3-18 separated on the basis of atmosphere. Corresponding pure lubricant thermograms are shown in figures 3-5 to 3-7. The medium particle sized stearic acid and the evaporated coating were prepared in the same manner, by precipitation from a solvent, and so the pure lubricant reactions observed for the former (figure 3-7) will be taken as corresponding to the evaporated material.

There was very little effect attributable to atmosphere variation again, but comparison of figures 3-17 and 3-18 with the pure lubricant reactions reveals significant differences in decomposition characteristics caused by the presence of a compact.

The decomposition of all the stearic acid types was characterised by a step in the weight loss curves. This step was generally sharp and consisted of a temperature interval of approximately 50°C over which there was little or no weight loss. Decomposition recommenced after each step at a rate similar to the initial rate.

Of the lubricants studied stearic acid was the only one with an uncombined carboxylic radical. It was, therefore, at least theoretically capable of undergoing chemical reaction with the iron powder matrix. The steps observed in thermograms may then have been a reflection of molten stearic acid reacting with the surface of iron powder particles.

The surface dependence of this reaction is shown in figure 4-7. Compacts were pressed from coarse and fine MP32 (180-104μm, -53μm respectively) to a density of 80%. An evaporated coating of stearic acid was used to obtain maximum surface dispersion of lubricant and reduce the risk of weight loss variation caused by mix segregation. It can be seen from figure 4-7 that the proportion of stearic acid removed prior to the step was inversely proportional to the specific surface area of the matrix. This

FIGURE - 4-7

The dependence of stearic acid decomposition on matrix particle size

Compacts - MP32 + 1% stearic acid (evaporated)
Atmosphere - $N_2/10\%H_2$ 500 ml min^{-1}

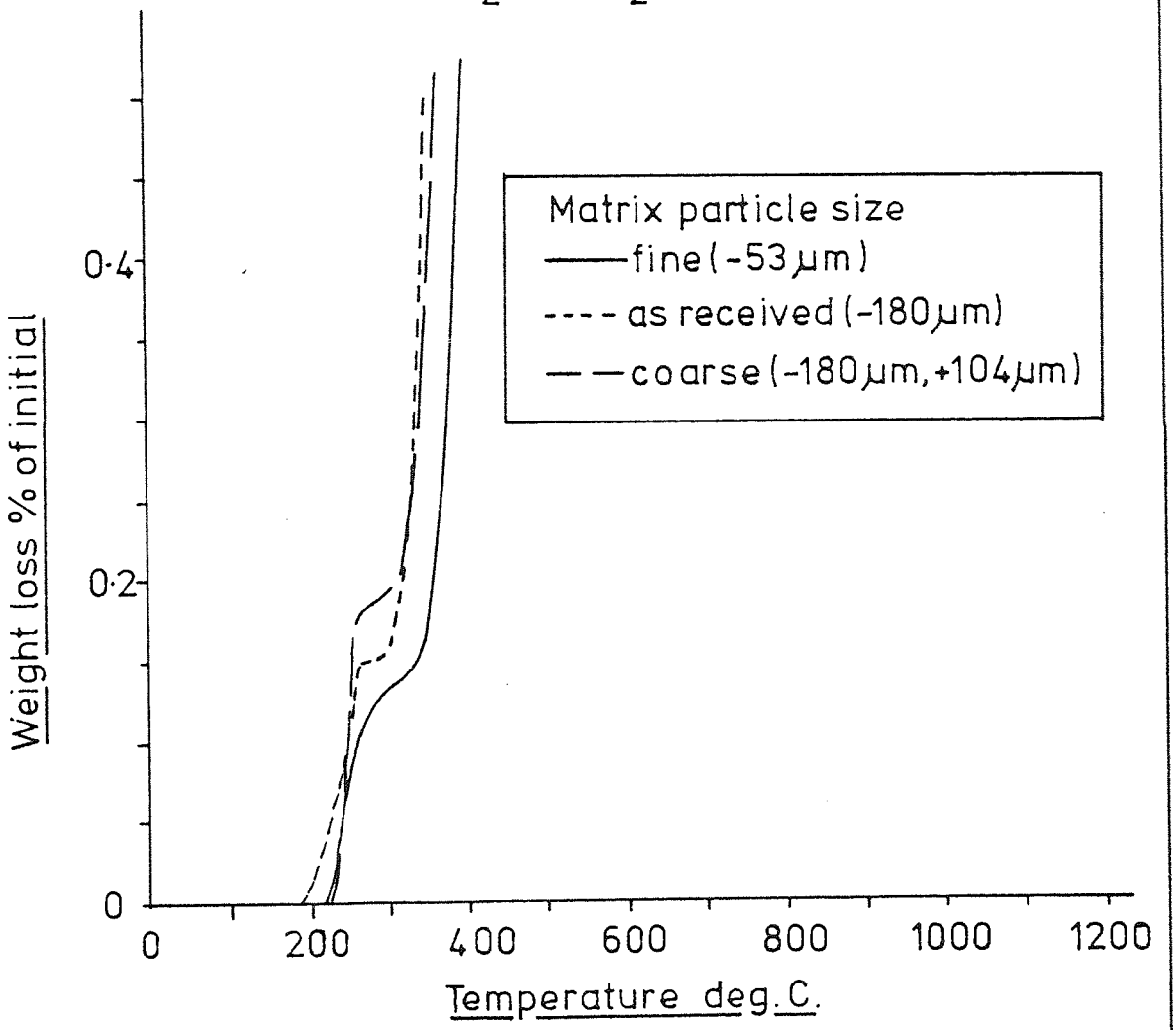

suggests that there was a chemical reaction between the iron powder and stearic acid, either soon after melting or over the temperature range of the step. The proportion of acid reacting would be proportional to the available surface area and the initial weight loss would be due to the decomposition of free uncombined stearic acid. The reaction temperature range of the combined acid was indeed similar to that of stearates containing metal radicals, particularly zinc stearate (figure 3-15).

Considerable variation in total weight losses occurred as shown in figures 3-17 and 3-18. The evaporated coating of stearic acid produced a consistantly high total weight loss, whilst the coarse grade was invariably low. Segregation due to the large particle size [6] was considered as the cause of this, it was observed clearly in the mix containing coarse material. The dispersion and deliberate precipitation onto the iron powder of the evaporated material minimised segregation.

The final high temperature reaction exhibited by the majority of curves in figures 3-17 and 3-18, particularly in $N_2/10\%H_2$, suggested that carbon deposited by stearic acid decomposition extended the final matrix reduction reaction. Total carbon and oxygen analyses were carried out on compacts, 80% dense, containing 1% stearic acid as an evaporated coating. These had been thermogravimetrically treated in $N_2/10\%H_2$ to temperatures of 500, 900, 1050 and 1200°C, and the results are shown in table 4-5. These conditions were chosen because the trace for evaporated stearic acid, shown in figure 3-17, had a clearly defined final reaction with no indication of intermediate reactions. The corresponding analyses for compacts containing no lubricant, treated in a similar manner, are shown in table 3-2.

Carbon deposition following the decomposition of all pure lubricants except lithium stearate has been discussed previously (4-2-9). Comparison of the analyses given in tables 3-2 and 4-5 reveals that carbon deposition (by 500°C) also occurred in compacts. The decomposition of stearic acid

increased the total carbon content by 40% of the original matrix level (table 4-5). There was a corresponding decrease in final oxygen due to the extension of the final matrix reaction.

Table 4-5

Final oxygen and carbon analysis of compacts containing 1% by weight evaporated stearic acid, thermogravimetrically treated in $N_2/10\%H_2$

Element \ Temp°C	500	900	1050	1200
Oxygen	0.26/0.27	0.20/.20	0.16/.16	0.13/.13
Carbon	0.10	0.05	0.03	N/D

N/D - Not detectable

(Flow rate - 500 ml.min^{-1}. Density - 80%).

Some of the curves shown in figures 3-17 exhibit a slight weight gain shortly after termination of the initial reaction at 500°C. If this was a real effect and not attributable to experimental error, then it may have been caused by reaction products such as water vapour retained in pores and producing oxidation. However, this is difficult to accept in an atmosphere containing hydrogen unless the H_2O content of pores was increased to such a proportion as to prevent reduction of oxides by hydrogen.

Retardation of the initial reduction reaction (reaction 1 in figure 3-13a involving hydrogen) rather than oxidation, seems more acceptable considering the diffusion behaviour of H_2O to be sluggish relative to hydrogen and its origin (stearic acid decomposition, not reduction of oxides). It is interesting to note that stearic acid was the simplest lubricant studied and yet its decomposition characteristics were the most extensively modified by the presence of a compact.

4-3-2-4 Stearamide

The subtracted lubricant reactions for stearamide in both $N_2/10\%H_2$ and argon are shown in figure 3-19. There was a difference in initial reaction temperatures, attributable to atmosphere type, but this was not consistently greater than that expected from reproducibility (4-3-1-2). The decomposition of stearamide was characterised by its general inactivity. In argon all the lubricant was removed by the initial reaction which ceased at 400°C, and then there was only a slight apparent weight gain between 400°C and the final temperature of 1200°C. Decomposition in $N_2/10\%H_2$ was similar but resulted in an apparently lower final weight loss.

It was thought possible that these slight weight gains may have been caused by nitriding of the iron powder matrix by the dissociated amide radical. This would not necessarily be detected as a weight gain since the amide radical would be weighed already as a gas within pores, as with carbon dioxide from lithium stearate. However nitriding may have suppressed the matrix reduction reactions, as suggested with lithium stearate decomposition.

It has been shown that decomposition of the carboxyl group of stearate based lubricants occurs in the later stages of the initial reaction (4-2). The decomposition of the amide group at this point, when there was no longer any decomposing hydrocarbons to physically remove reaction products, could possibly produce nascent nitrogen within pores capable of nitriding the matrix at temperatures around 500 to 600°C.

The difference in total weight losses, as shown in figure 3-19, was probably caused by physical segregation of stearamide in the mix prior to compaction. This lubricant had a coarse particle size (Chapter 4, Materials) and behaved similar to the coarse stearic acid in segregating visibly in the loose powder mix.

4-3-2-5 Cosmic 64 wax

The weight loss curves obtained for the decomposition of Cosmic 64 wax are shown in figure 3-20. It can be seen that atmosphere had little effect on reaction temperatures, even less so than for pure lubricant decomposition (fig.3-9). A noticeable effect caused by the presence of a compact was a reduction in weight loss due to initial decomposition, compared with the corresponding pure lubricant reactions. Elemental analysis has shown this lubricant to have a high carbon content (chapter 4, Materials) compared to a stearate based lubricant such as zinc stearate (74% and 67% respectively). A measurable quantity of carbon remained after decomposition of the pure lubricant (4-2-5) and carbon deposition was noted during direct observation (section 3). All the observations mentioned above suggest that the low initial weight loss was caused by deposition of carbon within a compact and, as can be seen from figure 3-20, this was reflected by marked extensions of the final reduction reaction.

The weight loss curves of figure 3-20 indicate that the extra carbon deposited by decomposition of Cosmic 64 wax may have been as high as 0.15% by weight, a significant quantity when carbon control and deoxidation in a sintering compact are considered. It can be seen from table 3-3 that even the final carbon contents of compacts containing this wax were consistently high.

The decomposition of Cosmic 64 wax was significantly modified, therefore, by the presence of a compact in that deposition of carbon was encouraged, possibly by dispersion of the lubricant on the surface of the iron powder or by increasing the decomposition temperature (see 4-3-2-11).

4-3-2-6 Dimensional change and residual carbon

Radial and longitudinal dimensional changes for the compacts used in section 4-3-2 are recorded in table 3-3. These are expressed as a percentage

of the original dimensions measured at ambient temperature. At a relative density of 80% the diameter and length of these compacts were approximately equal, hence measurement errors should have been equal for both directions.

It can be seen from table 3-3 that in all cases dimensional change was negative and generally more extensive in the longitudinal (pressing) direction than radially. Compacts were pressed using uniaxial floating die compaction similar to that used in Part I. Consequently, deformation of particles tended to be unidirectional, with flattening perpendicular to the longitudinal axis as compaction proceeded. This is illustrated in plates 3-1 to 3-4 for as-pressed compacts of coarse and fine MP32.

Flattening can be seen to develop as compaction progressed. After die-fill the number of particles or interparticle contacts per unit length would be similar along both axes. Densification is achieved by reducing the length since the die imposes physical restraints on radial changes, and so the number of particles or interparticle contacts/unit length increases along the pressing axis. If overall dimensional change is a cumulative measure of the shrinkage at each contact or particle then a greater dimensional change would be expected along the pressing axis, as recorded in table 3-3.

It is also obvious from table 3-3 that the presence of a lubricant generally increased the longitudinal dimensional change most notably. To consider only the physical effect of the removal of lubricant is at this stage probably an over simplification since it will be shown later that chemical effects attributable to lubricants also influence dimensional change. However, the results recorded in table 3-3 do seem to indicate that the removal of lubricant from interparticle contact areas, particularly where these areas are large and have a high number per unit length, does increase shrinkage. This could be due to a number of factors. Firstly, due to their lubricating properties it is unlikely that lubricants would be completely removed from interparticle contacts. Secondly, as density

increases they have been shown to actively interfere with compaction (part I) preventing the full development of green density. However, it is unlikely that molten lubricant would assist repacking of particles in pressed compacts,due to the degree of bonding between particles imparted by the applied compaction pressure and indicated by green strength. It will be shown later (4-3-2-9) that the presence of a lubricant tended to contribute more to longitudinal shrinkage as density increased.

For an evaporated coating of stearic acid carbon was deposited within a compact by decomposing lubricant (table 4-5). However, due to the extension of reduction reactions this may not have been reflected in final carbon analyses. Where a significant final carbon content was noted, such as with Cosmic 64 wax, this must be an indication that considerable carbon must have been deposited by the decomposing lubricant (table 3-3).

4-3-2-7 Effect of atmosphere flow rate on lubricant decomposition within compacts.

The subtracted weight loss curves for zinc stearate decomposing within compacts in varying flow rates of $N_2/10\%H_2$ are shown in figure 3-21. The thermograms due to matrix reactions are also shown in the same figure.

In the matrix reactions the effect of changing $N_2/10\%H_2$ flow rate was confined to changing the initiation temperature of the first reaction and encouraging it to proceed to a greater degree. This was probably caused by varying the supply of hydrogen, in terms of quantity per unit time, to the surface of the compact. This would seem to be further support for the nature of this reaction, as discussed in 4-3-1-1. Comparison with the matrix reactions for varying density, shown in figure 3-22 and also discussed in 4-3-1-1, shows that density variation influenced this reaction more than varying flow rate, emphasising the importance of pores as diffusion channels.

The influence of varying flow rate on zinc stearate decomposition (fig. 3-21) can be seen to have been only marginal. The removal of the stearate

radical was hardly affected and even a reduction reaction such as that involving zinc oxide was relatively unaffected. The main influence would seem to have been in terms of definition. At a low flow rate the transition between the end of stearate radical decomposition and the start of zinc oxide reduction was ill-defined compared to the higher flow rate. The influence of flow rate was certainly not so marked as for pure lubricant (fig.3-11). These results again confirm the overiding influence of pores where diffusion of gases is involved.

The apparent tendency to show a weight gain at high temperatures in a flow rate of 200 $ml.min^{-1}$ (fig.3-21) may have been due to experimental error. However, it may be an indication of the inability of the reduced atmosphere supply to totally prevent oxidation at such temperatures. The removal of reaction products such as water vapour may perhaps have been incomplete, suppressing the final matrix reaction.

4-3-2-8 The effect of compact variables on lubricant decomposition.

The influence of compact density and iron powder particle size on the decomposition of zinc stearate within compacts in $N_2/10\%H_2$ is illustrated in figures 3-22 to 3-24. Figure 3-22 represents an early study confined to the effect of density on the removal of 1% by weight zinc stearate from compacts pressed from MP32 (53-104μm) iron powder. The matrix reactions in figure 3-22 have already been discussed in 4-3-1-1.

As can be seen from figure 3-22, the initiation of stearate radical decomposition occurred at the same temperature independent of density. However, as density increased further weight loss was delayed. This delay, in terms of reaction temperature, was maintained until the end of the initial reaction, suggesting that it represented an increase in pressure within the higher density compacts necessary to overcome the restricted pore space. It will be shown later that the initiation temperature may also be increased by increasing density. It should be noted that thermogravimetry will only detect

a reaction if a weight change occurs. If decomposition characteristics change, but there is still a resultant weight loss, then thermogravimetry will not necessarily indicate the change in decomposition mechanisms. Surface markings indicative of the presence of molten lubricant were observed on the external surface of compacts 85% dense following heat treatment. This will be referred to again later.

Increasing compact density decreased the definition between the end of stearate radical removal and the start of zinc oxide reduction (fig.3-22). Only at a density of 60% was there an apparent period of inactivity between the initial reaction and the latter. It appears therefore that increasing compact density, and consequently decreasing pore space, inhibited the diffusion out of a compact of the products from stearate radical decomposition, delaying the end of this reaction.

Increasing density also inhibited the reduction of zinc oxide by initially restricting the diffusion of hydrogen into pores, possibly reducing the proportion of compact involved at any given temperature and hence decreasing the detectability. The rate of reaction, as indicated by rate of weight loss, was also decreased due to the inhibitive effect of reduced pore space upon diffusion of reaction products (water and zinc vapour) outwards. It will be shown later that apparent pore closure during compaction became significant in this material at densities exceeding 80%.

It is not clear why the total weight losses shown in figure 3-22 were so low compared with those expected from other work (figure 3-15). It is also not obvious why a compact of only 60% relative density should have exhibited the lowest weight loss. A possible explanation is the presence of substantial segregation within the original powder mix, or perhaps operator (the author) inexperience at this early stage.

The results shown in figures 3-23 and 3-24 illustrate the effect of varying pore size at constant density or constant pore volume. The variation

of lubricant additions would mean that the proportion of pore space occupied by lubricant would also vary from 10% (0.5% lubricant, 60% dense compact) to 100% (2.0% lubricant, 85% dense compact).

Several points may be noted from comparison of figures 3-23 and 3-24;

(a) At a density of 60% the overall weight loss in compacts pressed from coarse powder was consistently lower than in those pressed from fine powder (fig.3-23). There was little difference at a density of 85% (fig.3-24).

(b) Initiation of stearate radical decomposition appeared to occur at a lower temperature in coarse powder compacts.

(c) There was a marked difference in weight loss betweem the two densities at a lubricant content of 2% only.

(d) At lubricant levels of 1% and 2% zinc oxide reduction was well defined for both iron powder particle sizes at a density of 60%, but only for the coarse powder at 85% dense. At the latter density this reaction tended to assume two stages in compacts formed from the fine powder (fig.3-24).

At a given density the total volume of pore space was constant for each matrix particle size but the size and hence number of pores was controlled by the iron powder particle size. This is illustrated in plates 3-1 to 3-4 which are photomicrographs of sections through as-pressed compacts of various densities. The proportion of open and closed porosity in such compacts is shown in figure 3-25. It should be noted here that in this context use of the term closed implies the inability for oil to penetrate such pores even with repeated vacuum impregnation. However, they may not have been completely closed to gaseous elements.

It can be seen from figure 3-25 that beyond a relative density of 72% the proportion of closed porosity in compacts pressed from the fine powder increased more rapidly than in the coarse powder.

This is illustrated more clearly in figure 4-8 which is a plot of overall relative density versus the ratio of closed to open pores. If a

FIGURE 4-8 .The ratio closed:open porosity as a function of as-pressed density for compacts pressed from coarse and fine MP 32.

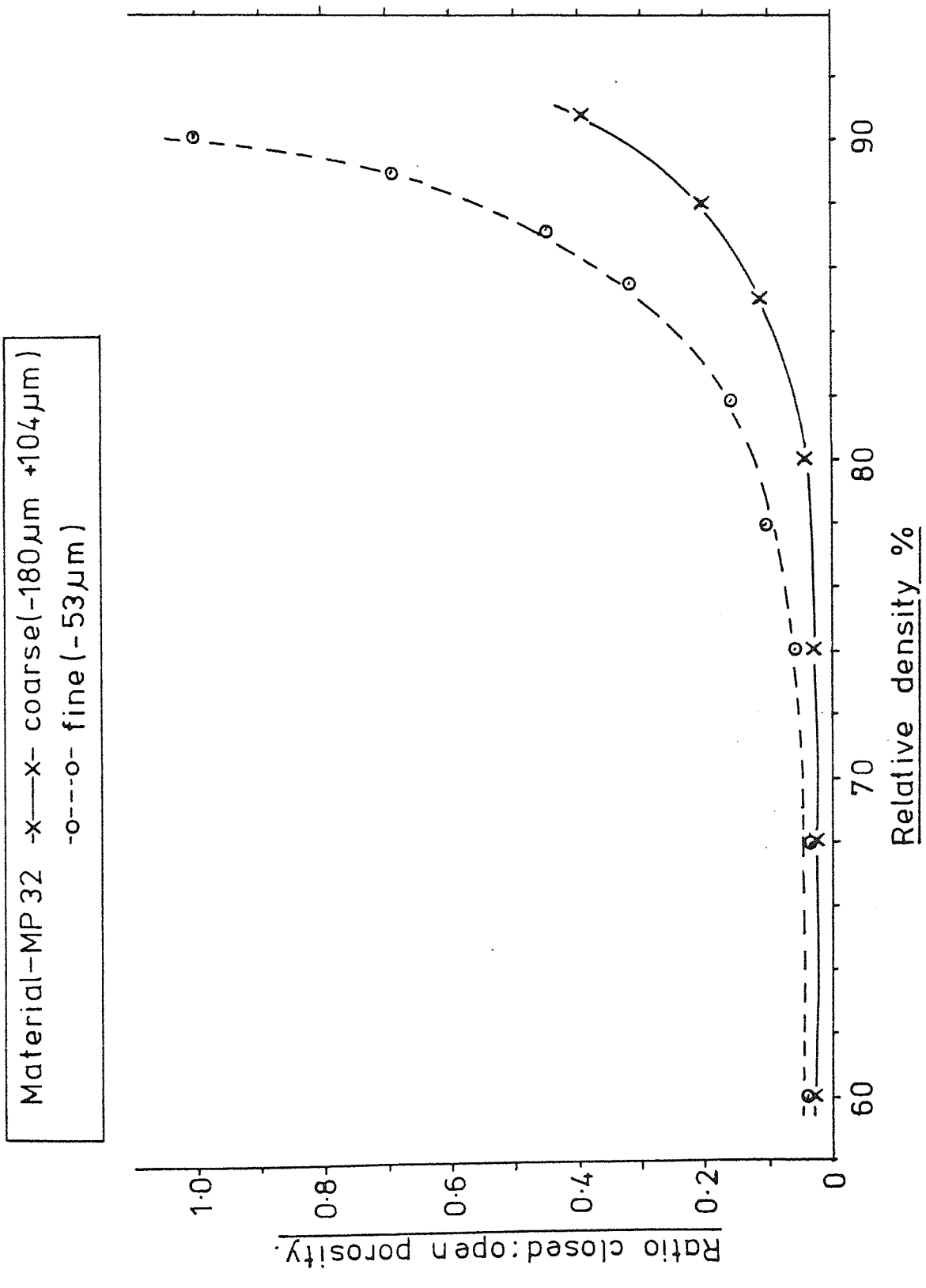

ratio of 0.1 is chosen arbitrarily as a significant proportion of closed porosity then it can be seen that this occurred at a density of 78% for fine powder and 85% for coarse.

The compacts used to establish the results of figure 3-25, and hence figure 4-8, were pressed with no admixed lubricants. It is possible that compaction inhibition by admixed lubricants, as discussed in part I, could prevent the development of closed porosity. However, the results of figures 3-25 and 4-8 do indicate the equilibrium conditions compacts would like to achieve during pressing.

It is now possible to return to the observations made earlier concerning figures 3-23 and 3-24. It has been shown that the presence of a compact influenced the decomposition of zinc stearate to a greater extent as density increased (fig.3-22). At a density of 60% the compact appeared to have the least effect. The total weight losses shown in figure 3-23 for compacts 60% dense, therefore, seemed to indicate a surface effect rather than a pore size effect. The relative high surface area of compacts pressed from the fine powder had encouraged the decomposition of the stearate radical, whilst at this density pore size was too large to influence decomposition characteristics. Indeed, the weight loss difference was established at the end of the initial reaction, zinc oxide reduction did not contribute . It has been shown in 4-3-2-3 that the extent of stearic acid removal was assisted by increasing its dispersion and utilising available surface area more fully.

Unfortunately, with this interpretation it would have been expected from previous results that the residue of incomplete removal of the stearate radical would be carbon. This would have caused an extension of the final matrix reaction, as noted for stearic acid (4-3-2-3) and Cosmic 64 wax (4-3-2-5). This was not observed for the coarse powder in figure 3-23. Segregation within the mix or differences between the two mixes must

be discounted as the cause of the difference in weight losses since they were so consistent at a density of 60% and were not observed at a density of 85%.

At a density of 85% (fig.3-24) the restriction of pore volume had a stronger influence than surface area and the weight loss difference between the two powder particle sizes was eliminated. If catalysis due to surface area was responsible for the phenomenon, as discussed previously, then the encouragement of the initiation of the first reaction would seem to be an anomaly. This may be due to a physical effect, initiation may have occurred earlier in compacts pressed from the fine powder, but weight loss was delayed due to the necessity of producing sufficient pressure within pores to overcome their restricted size. This was suggested previously and it can be seen from figures 3-23 and 3-24 that initiation appeared to be delayed as lubricant content decreased, again probably due to the inability of thermogravimetry to detect reactions until a sufficiently high proportion of reactants was involved.

The notable reduction in total weight loss observed for compacts containing 2.0% zinc stearate, 85% dense (fig.3-24) may be at least partly connected with the use of lubricant during ejection. Under these conditions there was sufficient volume of lubricant to completely fill the available pore space (compaction inhibition, discussed in part I). If it is assumed that entrapped air cannot be avoided then there would be an excess of lubricant. A higher compaction pressure must also be employed to achieve this density with 2.0% lubricant present compared to lower contents, due to compaction inhibition. The possibility of forcing more lubricant from the compact, particularly during ejection, cannot therefore be discounted as contributing to the apparently low weight loss. It seems unlikely that there could be such a high residue (approximately 0.4%) of carbon.

A more noticeable effect of restricting pore size is shown by the

zinc oxide reduction reactions in figure 3-24, again particularly at the high lubricant content. Where pore size was small, in compacts pressed from the fine powder, this reaction tended to exhibit two stages. This could have been caused by a build-up of reaction products, unable to diffuse from the compact at a sufficiently high rate, temporarily halting the reaction. However, an overall reduction of reaction rate would be more likely due to such a build-up. A more probable explanation could be that the initial weight loss reflected the removal of water vapour,whilst the second reaction indicated the loss of zinc vapour. It is possible that a higher zinc vapour pressure, and hence higher temperature, was required to remove zinc from the smaller pores compared to compacts pressed from the coarse powder. Even where only a single reaction was indicated (fig.3-23) the rate of this reaction was higher in large pores.

4-3-2-9 Effect of compact variables on dimensional change.

The radial and longitudinal dimensional changes of compacts of varying density used in the previous section are recorded in tables 3-4 and 3-5. The difference between longitudinal and radial shrinkages and the influence of lubricants on each have already been discussed (4-3-2-6). It is also clear from the tables that longitudinal shrinkage was more dependent than radial on the presence of a lubricant, radial shrinkage possibly only reflected sintering conditions.

The effect of compact density on dimensional change is best shown in table 3-4 for a constant matrix particle size, both in the presence and absence of lubricant. There was a tendency for radial shrinkage to be highest at a density of 60%, possibly due to the relative ease with which particle centres could approach at such a low density. Also the rate of densification during sintering probably would have been higher at low densities. This radial shrinkage was not affected significantly by the addition of 1% zinc stearate at either density. However, longitudinal

shrinkage was increased markedly, especially at the highest density (85%) where particle flattening became most pronounced and much of the pore space was filled with lubricant.

The influence of a further variable, matrix particle size, is shown in table 3-5. Generally less shrinkage occurred with the coarse powder than with the fine, probably due to the higher number of interparticle contacts, or particles, per unit length in the latter. In the absence of lubricant shrinkage would be determined by growth of these contact points and the consequent change in morphology of the associated pores.

At low densities (60%) and in the absence of lubricant radial and longitudinal changes were similar, as can be seen from both tables 3-4 and 3-5. At such densities the number of particles per unit length was probably similar along each axis. There was indeed no apparent difference between transverse and longitudinal sections of compacts at low densities, as shown by plates 3-1 and 3-3.

As density increased, in the absence of lubricant radial shrinkage decreased, most noticeably for the fine powder (table 3-5). This was probably caused by the increasing physical restraint imposed by higher densities on any further change. When sintering pure materials shrinkage is a measure of the degree of densification. For given sintering conditions a driving force for densification is the difference between the compact density and solid density. The higher the initial compact density the lower the driving force, with a consequently small shrinkage.

In the absence of lubricant longitudinal shrinkage seemed to be largely independent of density. However, it can be seen from both table 3-4 and 3-5 that it was significantly increased at the higher densities by lubricant additions. At low densities longitudinal shrinkage was barely influenced by the presence of lubricant, behaving similar to radial shrinkage.

The data of table 3-5 illustrates the influence of increasing lubricant content on the longitudinal shrinkage of compacts 85% dense. These results are also plotted in figure 4-9, which shows the strong relationship between lubricant content and longitudinal shrinkage. In this figure the shrinkage for zero lubricant (characteristic of sintering only) has been subtracted from the shrinkage obtained with lubricant additions to leave the dimensional change largely attributable to the removal of lubricant .

As discussed previously, in uniaxial compaction the number of contact points per unit length will only change appreciably along the pressing axis as compaction proceeds. Due to their lubricating properties it seems possible that stearate based lubricants cannot be entirely removed from interparticle contacts, particularly with irregular shaped particles where considerable material could be trapped between particles. If it is arbitrarily assumed that the average compressed size of particles of the fine MP32, compacted to a density of 85%, was 10μm, then it is possible to calculate that the contribution (0.6%) to longitudinal shrinkage of a 1% addition could be produced by a thickness of 0.05μm lubricant in each interparticle contact. This would seem to be a large amount of lubricant, considering the properties of such materials.

The slope of the relationship between lubricant content and dimensional change for the fine powder was -0.6 (fig.4-9). This would seem to indicate a direct relationship between lubricant content and longitudinal dimensional change, possibly caused by entrapped lubricant as discussed above. However, the possibility of compaction inhibition caused by lubricant cannot be discounted as contributing to shrinkage.

Figure 4-10 shows the compaction curves for coarse and fine MP32 with no addition and with 0.5% and 2.0% zinc stearate. These were obtained by continuous compaction as described in part I. It can be seen from figure 4-10 that inhibition occurred at lower densities in the fine powder. At a

FIGURE 4-9

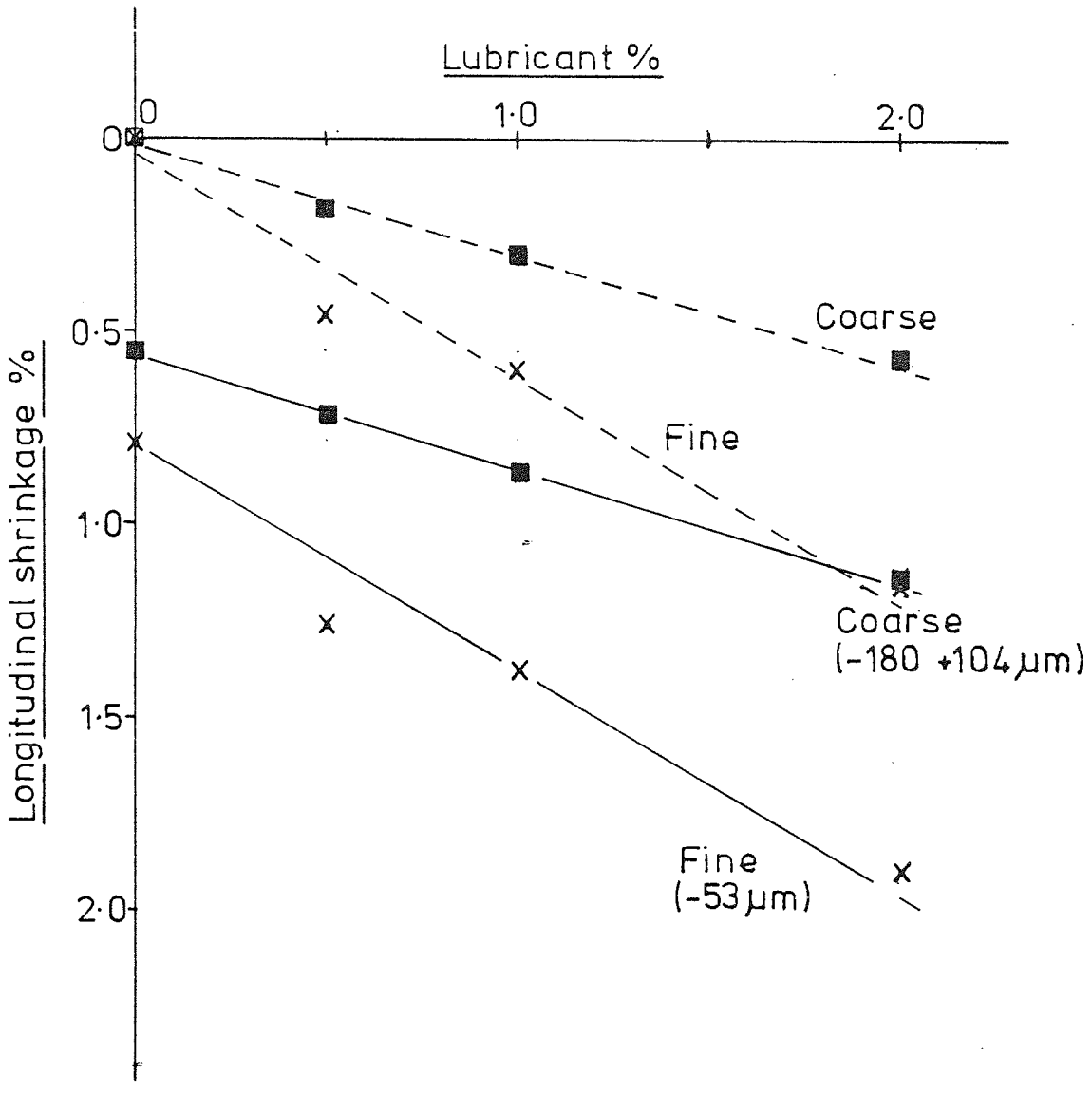

The contribution of zinc stearate additions to longitudinal shrinkage in iron powder compacts of 85% relative density

Overall shrinkage.

Overall minus shrinkage at 0% lubricant.

FIGURE 4-10 .The compressibility of coarse and fine MP 32 plus admixed zinc stearate.

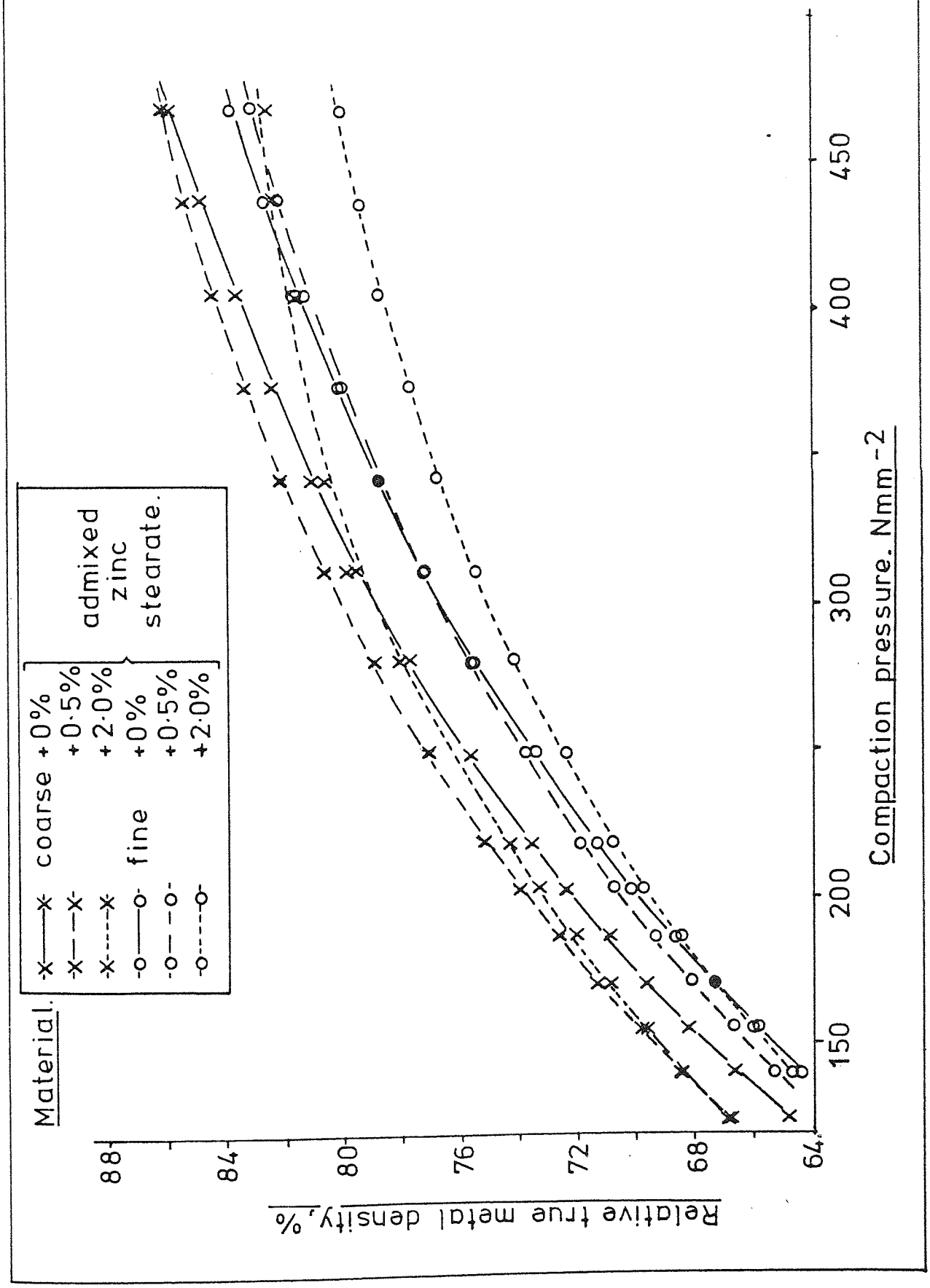

density of 85% considerable inhibition must have been experienced by compacts formed from the latter , such that high applied loads were necessary to achieve this density. (The compaction curves were obtained with a 28.6mm diameter cylindrical die having a maximum load rating of $3x10^5$N. Thermogravimetric specimens were compacted in a 12.7mm diameter die with a much higher relative load rating).

Inhibition is a measure of the degree to which lubricant holds particles apart. As the compaction forces were largely unidirectional this reaction against them would also be expected to be unidirectional, parallel to the pressing axis. It is possible, therefore, that when considerable compaction inhibition occurred, as with the fine powder, the removal of lubricant during sintering allowed particles to approach the positions they would have occupied in the absence of lubricant at the equivalent pressure.

The strong relationship between longitudinal dimensional change and lubricant content (fig.4-9) may therefore be attributable to lubricant trapped in interparticle contacts and to compaction inhibition. The latter would be particularly active at high levels of addition and would resist the removal of lubricant from within contacts during compaction.

4-3-2-10 Effect of density on the decomposition of lithium stearate within compacts.

The subtracted weight loss curves for the decomposition of lithium stearate in compacts of varying density are shown in figure 3-26. As observed previously (fig.3-16) lithium carbonate decomposition was delayed only by the removal of the stearate radical. Stearate radical decomposition (fig.3-26) was again density dependent so that the carbonate reaction was also delayed in the highest density compact. At each density the weight loss corresponding to this reaction was similar.

Weight gains due to oxidation or suppression of reduction by carbon dioxide above 700°C were recorded (fig.3-26). This gain increased from

0.015% at 60% dense and 0.020% at 80% dense, to 0.025% at 85% dense. This may seem a small change but it should be noted that it increased consistently with density despite the reduction in available surface area which must have accompanied densification.

The theoretical weight percentage of carbon dioxide associated with lithium stearate is 8%. A 0.1g addition of lubricant (1% in a 10g compact) would therefore produce $4.8 \times 10^{3} mm^{3}$ of gaseous CO_2 at N.T.P. The theoretical volumes of pore space in compacts 60% and 85% dense were $8.5 \times 10^{2} mm^{3}$ and $2.2 \times 10^{2} mm^{3}$ respectively. The volume of this gas produced was therefore more than sufficient to fill the available pore space.

At the end of lithium carbonate decomposition the pores must have been entirely filled with carbon dioxide, physically excluding hydrogen. There would seem to be more opportunity for oxidation to occur as compact density increased (fig.3-26) since the consequent reduction of pore size would increase diffusion inhibition. This would not only restrict hydrogen diffusion inwards but also carbon dioxide outwards.

The overall reaction during such oxidation above 700°C would probably be as in equation 4-9,

$$Fe + CO_2 \longrightarrow FeO + CO. \quad K = \frac{P_{CO} \cdot a_{FeO}}{P_{CO_2} \cdot a_{Fe}} \qquad \text{--- (4-9)}$$

The driving force for reaction 4-9 was the decomposition of carbon dioxide to carbon monoxide and oxygen, equation 4-10,

$$2CO_2 \xrightarrow{>700^{\circ}C} 2CO + O_2. \quad K = \frac{P^2_{CO} \cdot P_{O_2}}{P^2 CO_2} \qquad \text{--- (4-10)}$$

It can be seen that the overall controlling factor, in conditions of inhibited diffusion through pores, would be the ratio CO/CO_2. This would initially be low, causing oxidation.

After completion of lithium carbonate decomposition there would be no further supply of CO_2. During oxidation, therefore, the proportion of CO_2 within pores would be decreased continuously by thermal expansion, diffusion exchange with atmosphere components and usage in reaction 4-9. A temperature must be reached where the CO/CO_2 ratio is sufficiently high to reverse reaction 4-9 such that a weight loss would consequently be recorded. This would also be assisted by the reduction of FeO by carbon from within the matrix (equation 4-8) which is known to occur from studies of matrix reactions. The point at which this occurred would probably be influenced by the quantity of CO_2 initially present within pores, or by the ease of diffusion of CO_2 out from the compact.

It is difficult to draw conclusions about a reaction which exhibits such indefinite weight change traces, but it does seem from figure 3-26 that the final weight loss due to a reduction reaction did commence at a lower temperature in the compact 60% dense than in that of 85%. This suggested that diffusion of CO_2 through pores was the controlling factor in this reaction.

The final oxygen analysis for the compact 80% dense used in this investigation was 0.22% by weight. The corresponding matrix oxygen content under these conditions was 0.15% (table 3-2). The residual Li_2O content of 0.05% could provide only 0.03% O_2 for analysis hence it appears that oxygen had been retained and not fully reduced. Meyer et al[10] also noted the oxygen affinity of compacts containing lithium stearate.

It has been shown that radial shrinkage of uniaxially pressed compacts is characteristic of the sintering process and matrix material rather than the presence of lubricant (4-3-2-6). In both $N_2/10\%H_2$ and argon the radial shrinkage of compacts containing lithium stearate was rather high, as can be seen from table 3-3. This was the only lubricant which deposited a residue other than carbon, Li_2O. It is possible that a glass formed from

combination of Li_2O and FeO may explain this shrinkage and hence the high residual oxygen discussed above.

4-3-2-11 Summary

Comparison of weight loss curves for pure lubricants (fig.3-3 to 3-9) and those for lubricants within compacts (fig.3-15 to 3-20) shows that in the presence of a compact, all stearate based lubricants achieved a high initial reaction rate at lower temperatures than pure lubricants. As this reaction proceeded the reaction rate reduced such that thermograms obtained from the two different conditions became coincident, or crossed to terminate at a higher temperature. Comparison will perhaps be easier if the tables of stearate radical decomposition temperature ranges are used (tables 4-2 and 4-6).

It seems unlikely that this was due to any difference in thermal properties of the two types of sample (crucible or compact) since Cosmic 64 wax was found to be a consistent exception. Within a compact wax decomposition initiated and the entire reaction proceeded at a higher temperature than that recorded for free wax.

Free lubricants were contained within silica crucibles. This imposed a poor thermal conductor between the decomposing material and the source of heat, the furnace wall. However, the large outside diameter of crucibles, compared with compacts, would place them closer to the furnace wall. The low heating rate, $6^{o}C\ min^{-1}$, would have produced a shallow thermal gradient and probably allowed thermal conditions to approach equilibrium irrespective of the differing thermal characteristics of the samples.

It appears, therefore, that the decomposition of stearate based lubricants was encouraged to initiate at lower temperatures by dispersion on a medium of high surface area. As decomposition proceeded reactions occurred between the matrix and the lubricant such that the breakdown of the stearate

radical was inhibited. This was most strongly indicated by the decomposition of stearic acid within compacts (4-3-2-3). At high densities, where the restriction of pore space becomes significant, this behaviour was modified. The restriction of pore space tended to delay stearate radical decomposition.

Table 4-6

	Decomposition temperature range °C	
ATMOSPHERE / LUBRICANT	$N_2/10\%H_2$	Argon
Zinc stearate	250-450	270-460
Lithium stearate	300-470	350-490
Stearic acid - fine	180-470	210-450
medium	220-450	220-480
coarse	190-550	200-460
evaporated	160-470	210-460
Stearamide	180-420	210-410
Cosmic 64 wax	270-510	270-520

(Atmosphere flow rate - 500 $ml.min^{-1}$. Compacts - MP32, 80% dense plus 1% lubricant).

It has been shown that higher temperature reactions may be controlled by varying the pore space, for example the reduction of zinc oxide. They may be promoted by increasing the surface area upon which the reactants are dispersed, as with the decomposition of lithium carbonate during lithium stearate removal. Reactions between lubricant decomposition products and the matrix have been observed, these included oxidation by carbon dioxide and oxide reduction by residual carbon. If the underlying reactions between elements within the matrix material and the atmosphere are also considered

then the nature of reactions occurring within compacts becomes very complex indeed.

In most of these reactions the local atmosphere, determined by the restrictions of porosity, was found to be more important than the external atmosphere, at least over short time periods. The inhibition or preferential diffusion of atmosphere components through pores was proposed, mainly from circumstantial evidence.

It has been shown that for commercial densities (the high densities of this investigation, 80%-85%, 6.3-6.7g cm^{-3}) the presence of lubricant can increase the linear shrinkage along the pressing axis markedly. Consequently, due solely to the presence of a lubricant and in the absence of further complicating factors, uneven dimensional changes may be produced along the different axes of a sintered component. The contribution of a lubricant to shrinkage was also found to be density dependent so that variation of density within powder components may also produce uneven shrinkage.

4-3-3 The isothermal decomposition of zinc stearate within compacts.

The initial decomposition of zinc stearate within a compact under isothermal conditions is shown in figure 3-27. It can be seen that when the temperature was maintained between the start and end of stearate radical decomposition, the reaction proceeded almost to completion if given sufficient time. Stearate radical decomposition, therefore, would proceed isothermally once the initial critical temperature was exceeded.

The implication of this is that there was no real terminal temperature to this reaction as indicated by the previous thermogravimetric results. This was probably more a function of the system than the reaction type. It can be seen from figure 3-27 that the rate of this reaction was sensitive to temperature. A temperature increase of only 40°C was able to produce maximum weight loss some 20 minutes sooner.

This work was carried out early in the project and lacked purpose, other than showing that control of the normally vigorous stearate radical decomposition was possible by using isothermal treatments. The significance of this work became apparent during discussions with a representative of an industrial powder metallurgy concern. Problems had been encountered during the dewaxing of some high density ferrous compacts (>90% dense). The extreme effect was explosive breakdown of some components.

The dewaxing temperature being used was well above the theoretical terminal temperature of the initial reaction. Even 500°C may be too high, as can be seen from figure 3-27. If dewaxing was carried out at a temperature in excess of 500°C then cold, as-pressed compacts were introduced to thermal conditions where the stearate radical should no longer be present. The consequent high heating and decomposition rates produced high pressures within compacts, particularly at high densities. This reaction has been shown to be self perpetuating under isothermal conditions and was not retarded significantly by restricted pore space (4-3-2-8). It will be shown later that the rapid expulsion of lubricant can reduce the dewaxed tensile strength of a compact, and the catastrophic industrial example of this was an extreme case.

It was suggested that the problem could be alleviated by subjecting compacts to a low temperature isothermal dewaxing treatment, using a temperature such that perhaps 80% to 85% of the stearate (hydrocarbon) radical was removed in a reasonable time. The remaining stearate could be harmlessly removed at a high heating rate. Thermogravimetric analysis was carried out on two zinc stearate based lubricants provided by the industrial concern, and their decomposition characteristics and suitable isothermal dewaxing treatments were determined. A copy of the report supplied to them is included in appendix D.

It is obviously not sufficient to assume that the terminal temperature

of stearate radical decomposition, as indicated by the thermogravimetric analysis, should be exceeded to achieve efficient and economic dewaxing. There are advantages in removing a large proportion, but not necessarily all, of the stearate at a lower isothermal temperature. Furnace time could subsequently be regained by using high heating rates up to sintering temperature.

4-4 The decomposition of lubricants within compacts at high heating rates.

Weight loss curves for the decomposition of lubricants within compacts at high heating rates are shown in figures 3-29 to 3-31 inclusive. Typical reproducibility bars are given for the matrix reactions only. As the weight loss curves for lubricants in these figures were the results of subtraction no individual points have been plotted. Dimensional changes and residual carbon contents of these compacts are recorded in table 3-6. Comparison with the dimensional changes obtained at the low heating rate (table 3-3) will show that the latter were consistently greater. This was not surprising since compacts subjected to high heating rates attained a maximum temperature of 1100°C and were maintained at an elevated temperature for only 3 minutes.

It is possible to make some general observations on the conditions used during this investigation in comparison to thermogravimetry. Higher reaction temperatures were expected to accompany the high heating rates[35]. However, as described in the experimental method (2-2), the thermocouple was placed in the centre of a compact during temperature measurement. High heating rates would produce a steep thermal gradient across the section of a compact. The surface temperature of compacts could thus be considerably higher than that indicated by the central thermocouple. Reactions were expected to initiate in the regions of highest temperature, that is, the surface, and proceed into the compact following the thermal gradient. Therefore the indicated temperature, as measured in the core of a compact, will be lower than the actual reaction temperature. Overall the two effects should have tended to cancel each other out.

It was possible that the size of the zone within a compact undergoing a particular reaction was restricted also by a steep thermal gradient. A particular reaction temperature range was then partly dependent on a zone

moving through the compact. At the low heating rate of the thermobalance ($6^{o}C.min^{-1}$) it is possible that large proportions of a sample were simultaneously involved in any reaction. Reaction temperature ranges therefore may have been more dependent on diffusion of reactants and products through pores, than on the movement of reaction zones.

In the thermobalance it has been assumed that the low heating rate and consequent long times involved would allow thermal conditions and gaseous diffusion through pores to approach equilibrium. With the high heating rates used during this part of the project only very short times were involved. Consequently, it cannot be assumed that gaseous diffusion through pores or lattice diffusion through the iron powder matrix approached equilibrium. Under these conditions reactions involving the surface of iron powder particles and the contents of pores might have assumed greater importance.

The samples used in this section were removed from the protective atmosphere repeatedly for weight determinations. Long delays between heat treatments were unavoidable hence it was inevitable that air could have displaced the atmosphere retained with pores. It seems unlikely that the short times at elevated temperatures would have allowed complete displacement of this air. Compacts were given at least 15 minutes soak in the protective atmosphere prior to insertion into the furnace hot zone. However, this soak was at ambient temperature and the possibility of retained air participating in high temperature reactions could not be discounted.

4-4-1 Matrix reactions.

The weight loss curves due to compacts of MP32 containing no lubricant, pressed to relative densities of 60% and 80%, are shown in figure 3-29. The matrix reactions obtained from compacts 80% dense by thermogravimetry are shown in figure 3-13a. Comparison of these two diagrams shows that reactions corresponding to (1) and (2) of figure 3-13a were also present at a high heating

rate. It can be seen that at a density of 80% the overall weight loss was considerably lower than that obtained at the low heating rate (fig.3-13a). This was probably a reflection of the short heat treatment times involved and the retardation of reduction reactions by retained air.

Reaction(2)in a compact 80% dense was retarded by approximately 100°C at the high heating rate, but occurred at its expected temperature of 700°C in the low density compact (fig.3-29). This was possibly an indication that the temperatures obtained in this section were directly comparable with those obtained by thermogravimetry. Therefore the delay of reaction(2)at a density of 80% could be attributed to the presence of retained air and the difficulty of displacing it when the pore size was restricted.

The inordinately high weight loss obtained at a relative density of 60% may be associated with the physical loss of iron powder from the compact. It was noted that due to the inherent low green strength of such compacts it was initially very easy to remove material, particularly from the corners, during handling. This has been reflected by the high initial weight loss where development of bond strength was slow due to the low temperatures.

A noticeable difference between the matrix weight loss curves of figures 3-29 and 3-13a was the existence of a low temperature reaction in the former. This reaction commenced at approximately 150°C. If the curves of figure 3-13a were corrected for buoyancy (fig.3-1) they would also exhibit an initial low temperature reaction, commencing at approximately 200°C. This weight loss was possibly due to the removal of volatile material and perhaps some surface adsorbed gases.

4-4-2 The effect of compact density on the decomposition of zinc stearate

The subtracted weight loss curves for the decomposition of 1% by weight zinc stearate within compacts 60% and 80% dense are shown in figure 3-29. Similar features to those obtained at the low heating rate (fig.3-22) were recorded. Stearate radical decomposition was retarded again by increasing

density.

It is not safe to conclude that the difference in total weight loss in figure 3-29 was due to more extreme decomposition at a density of 60%. The extra weight loss can be accounted for by taking the weight loss between the initiation of stearate radical decomposition at 60% dense (160°C) and the temperature corresponding to the start of weight loss at a density of 80% (360°C). A compact 60% dense containing lubricant was found to be particularly sensitive to handling. The physical removal of material during handling would seem to be the most likely explanation of this weight loss difference. The presence of zinc stearate has been shown to reduce green strength (part I).

The reduction of zinc oxide in these specimens commenced at a temperature of 660°C, 100°C higher than under thermogravimetric conditions. Zinc oxide reduction was also incomplete, only 50% of the total residue was removed. The retention of air may explain the extent and retardation of this reaction. However, the high initiation temperature may also be attributable to the increased heating rate[35]. There was no indication in either the matrix reactions, or those concerning zinc stearate, of a final high temperature reduction reaction (fig.3-29).

4-4-3 Lubricant reactions within compacts.

Subtracted weight loss curves for the metal stearates, stearamide and Cosmic 64 wax are shown in figure 3-30. It can be seen from the trace for lithium stearate (fig.3-30) that lithium carbonate decomposition within a compact once again waited only for completion of the hydrocarbon radical decomposition. The weight loss corresponding to this reaction was 0.05% compared to the theoretical expected weight loss of 0.08%.

The form of the weight loss curve for stearamide was similar to that obtained thermogravimetrically (fig.3-19). The highest weight loss of the stearic acids (fig.3-31) was attributable again to the most evenly dispersed

lubricant, evaporated stearic acid. The weight losses corresponding to the steps of the stearic acid samples were also present. These steps were thought to correspond to the decomposition of free lubricant, uncombined with the matrix. In figure 3-31 it can be seen that the largest step weight loss was obtained with coarse stearic acid, whilst the smallest was associated with the evaporated coating. This again suggested that combination with the matrix was the cause of these steps, the large particle size of the coarse stearic acid allowing more decomposition before reactions with the matrix occurred.

The temperature ranges for hydrocarbon radical and wax decomposition reactions are given in table 4-7. These may be compared with those obtained at a low heating rate in the thermobalance (table 4-6).

Table 4-7

Temperature ranges for hydrocarbon radical and wax decomposition within compacts at high heating rates.

LUBRICANT	TEMPERATURE RANGE. °C
Zinc stearate	360-610
Lithium stearate	450-700
Stearic acid - fine	140-620
medium	150-610
coarse	140-610
evaporated	160-600
Stearamide	150-510
Cosmic 64 wax	330-720

(Compacts - MP32 + 1% lubricant, 80% dense. Atmosphere - $N_2/10\%H_2$).

The temperature range of hydrocarbon radical decomposition was extended in comparison to thermogravimetrically treated compacts. This was probably

caused by the narrow reaction zone in such compacts as discussed previously (4-4).

Decomposition commenced at a higher temperature, relative to the low heating rate, for both metal stearates and the wax. Initiation occurred at lower temperatures for the stearic acids and stearamide. The effect of increasing heating rate was, therefore, dependent on lubricant composition.

High temperature reactions of the types associated with reduction of oxides by carbon deposited by hydrocarbon decomposition, were observed only with Cosmic 64 wax (fig.3-30) and the stearic acids (fig.3-31). Final carbon analyses for all compacts corresponding to these figures are recorded in table 3-6. It can be seen that these were generally higher than those for low heating rate compacts (table 3-3), probably due to the much shorter time involved. None of them were markedly high.

Final oxygen analyses for some compacts are given in table 4-8.

Table 4-8.

Final oxygen contents of compacts containing lubricants heat-treated at high heating rates.

LUBRICANT	OXYGEN CONTENT %
None	0.32/.33
Zinc stearate	0.31/.32
Stearamide	0.29/.32
Cosmic 64 wax	0.22/.21

(Compacts - MP32 + 1% lubricant, 80% dense. Atmosphere - $N_2/10\%H_2$).

It can be seen that despite the removal of considerable carbon associated with the matrix (originally 0.07%) oxygen contents have remained at the

original level (0.3%) or were slightly higher. The exception in table 4-8 was the compact containing wax, in which reduction did occur. This carbon must have been oxidised by a source other than oxygen associated with the matrix. The retention of air within pores is suggested, as discussed previously.

Where high temperature carbon reduction reactions were exhibited, as with stearic acid and wax, sufficient carbon must have been deposited by initial decomposition to effectively deal with retained air and reduce some of the oxides associated with the matrix. Therefore, the reactions recorded in figures 3-30 and 3-31 have been modified, relative to those obtained by thermogravimetry, by increasing heating rate and by the method employed.

This method (reheating and weighing) was used because it was considered that the number of specimens necessary for separate duplicate compacts at each temperature was prohibitive. However, it has provided further confirmation of the importance of the local atmosphere within pores. It has also shown that the decomposition behaviour of some lubricants may be beneficial in dealing with the problem of retained air.

4-4-4 Dimensional change

Final dimensional changes are recorded in table 3-6. These were generally lower than those of thermogravimetrically treated compacts (table 3-3) due to the shorter heating times and lower final temperature (1100°C). Longitudinal shrinkages were again increased most markedly by the presence, or removal, of lubricants.

4-4-5 The removal of lubricants at high heating rates, summary.

The overall effect of subjecting compacts containing lubricants to high heating rates has been shown to be dependent on the composition of the lubricant. The decomposition temperatures of metal stearates and Cosmic 64 wax were increased by increasing heating rate whilst those of stearic acid

and stearamide were decreased. The decomposition temperature ranges of all lubricants were increased by increasing heating rate.

Due to the short times involved equilibrium conditions were not achieved and reactions consequently became characteristic of the contents of pores. This was notably so when the retention of air within pores was considered. This was found to retard all high temperature reduction reactions.

The limitations of the experimental method have been noted. This enabled the supply of air within pores to be repeatedly renewed after hydrocarbon radical decomposition. This is certainly not an acceptable industrial practice. However, it has served to accentuate the importance of the non-equilibrium conditions characteristic of high heating rates.

4-5 Direct observations of lubricant decomposition.

The results of direct observations of lubricant decomposition have been presented in section 3*. They have helped the interpretation of thermogravimetric data, but it is not intended to restate the observations here in relationship to each characteristic weight loss curve. However it is proposed to relate the observations to some specific thermograms, as examples, particularly where a feature of interest was revealed.

4-5-1 Zinc stearate.

Figure 4-11 is the weight loss curve for pure zinc stearate in N_2/ 10%H_2, as originally presented in figure 3-3. Observational points have been superimposed on this thermogram and the corresponding notes from section 3 are listed below.

1- Melting observed at 140°C (melting point as recorded in table 4-2 - 122°C).

2- Boiling observed at 235°C.

3- Vapour becomes apparent at 305°C, condensed by the cold stream of N_2/ 10%H_2.

4- Vapour associated with a vigorous reaction at 320°C.

5- The sample appeared to change colour to yellow, due to zinc oxide, at 370°C.

6- Profuse decomposition at 390°C.

7- Reactions appeared to cease by 430°C.

8- A sooty deposit developed by 470°C.

It can be seen that the observed features seemed to match the weight loss curve well. There was no suggestion of decomposition upon melting, but once boiling was established breakdown followed quickly. Profuse vapour was observed at a temperature corresponding to the maximum rate of weight loss.

Comparison of figures 3-3 to 3-9, thermograms for pure lubricants, and

* p300

FIGURE 4-11 .Weight loss curve for free zinc stearate in N_2/10%H_2 with direct observation points.

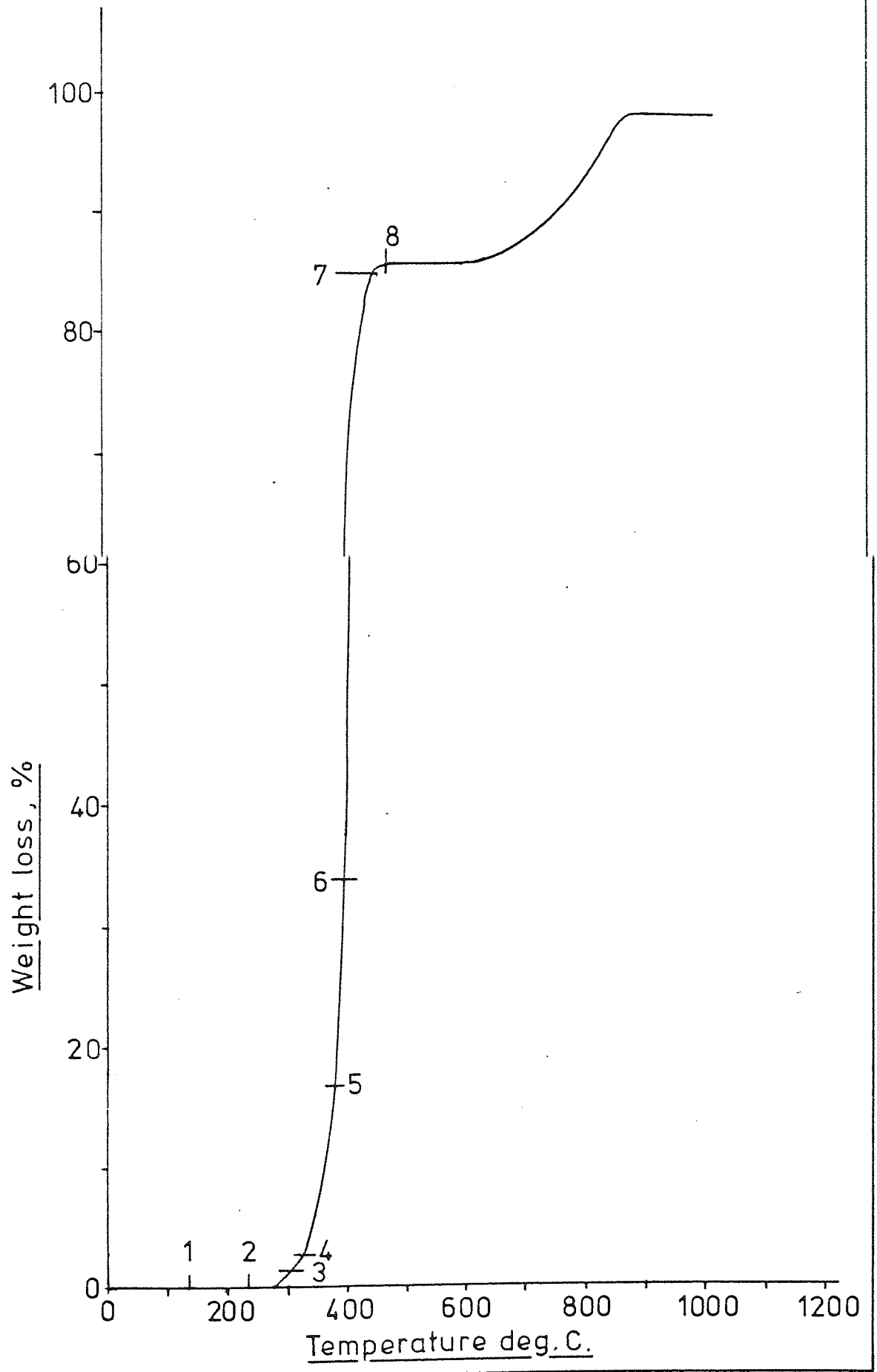

the observations noted in section 3 suggested that the lubricants may be divided into two groups. Those containing a metal radical and the wax, where boiling was established prior to decomposition; and stearic acid and stearamide where decomposition commenced before boiling was observed. The presence of a metal radical tended to stabilise the stearate.

4-5-2 Zinc stearate within compacts.

1% by weight zinc stearate within compacts 60% and 85% dense were taken as examples of lubricant decomposition within compacts. These were chosen to help explain the difference in weight loss characteristics as shown in figure 3-22.

Weight loss curves for these compacts in $N_2/10\%H_2$ are reproduced in figure 4-12 with superimposed observation points. These thermograms were taken from figure 3-22 and were obtained at the low heating rate of $6^{o}C.\ min^{-1}$, since these seemed to match the observations well. It was suggested in the experimental procedure (section 2-3) that the observations would equate with the high heating rate weight loss curves, this was not found to be so.

The observational points taken from the notes in section 3 and superimposed on figure 4-12 were as follows.

On the 60% dense curve;

1- Initial vapour observed at $280^{o}C$.

2- Profuse vapour at $350^{o}C$.

3- Reactions slowed by $420^{o}C$.

4- No further reaction beyond $450^{o}C$.

On the 85% dense curve;

1- Molten spots of lubricant appeared on the compact surface at $190^{o}C$.

2- Surface spotting became profuse by $270^{o}C$, with lubricant exuding from pores.

3- Boiling associated with decomposition at $310^{o}C$.

FIGURE 4-12 Weight loss curves for zinc stearate decomposition within compacts, with direct observation points.

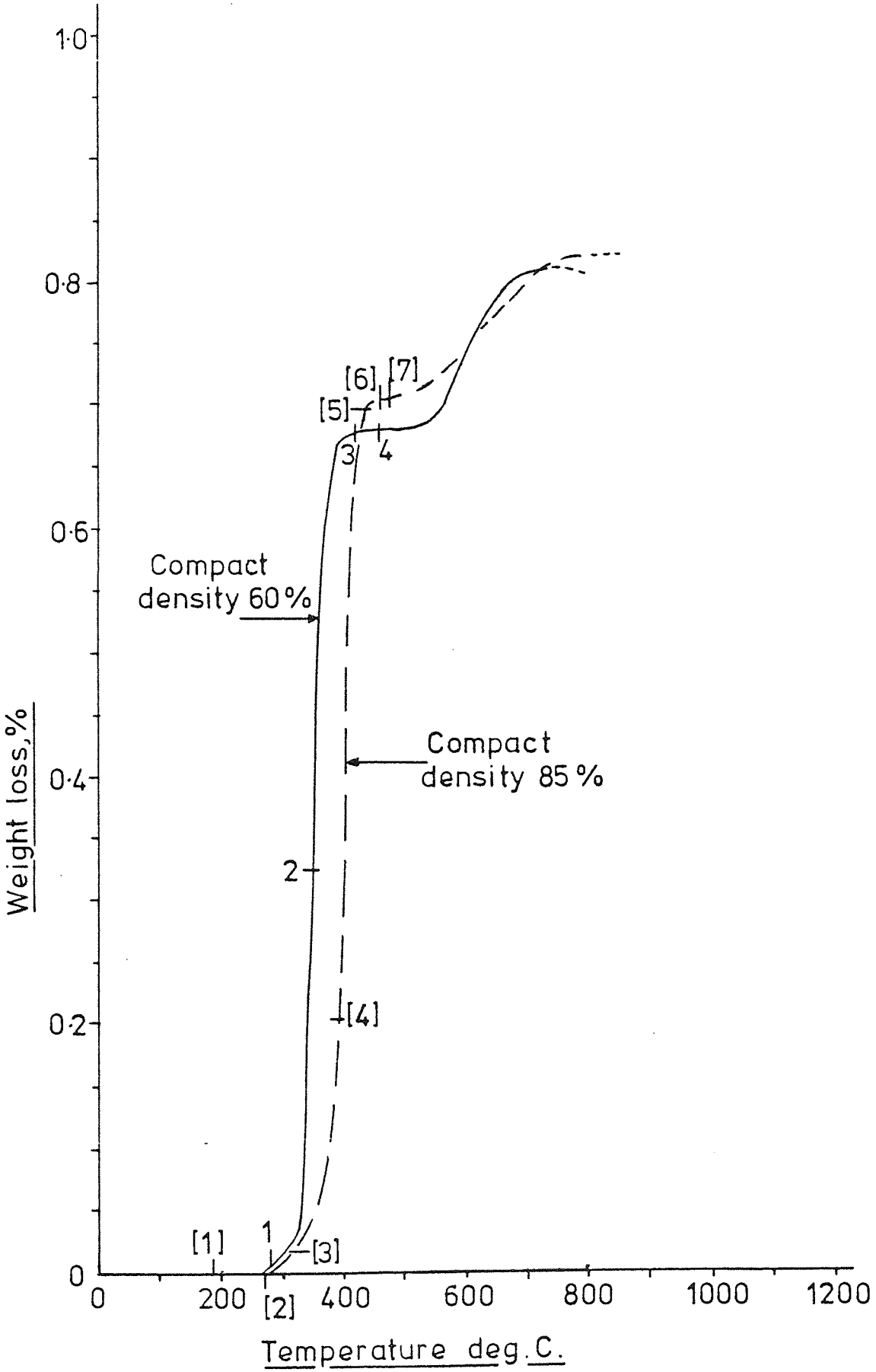

4- Profuse boiling and decomposition by 380°C.

5- Boiling continued up to 430°C leaving a surface deposit.

6- Profuse vapour was observed to come from within the compact up to 450°C.

7- Reactions ceased leaving sooty surface deposits at 470°C.

In low density compacts, therefore, decomposition occurred entirely within the compact. As density increased, and the open space within a compact decreased, lubricant exuded from pores after melting. This would have been aided by the expansion of entrapped air initially and later by boiling. It is possible that decomposition would not occur until sufficient space was produced within high density compacts. This would account for the difference in decomposition behaviour of zinc stearate in compacts of varying density (4-3-2-8). If the pressure increase due to stearate radical decomposition within high density compacts was the sole cause of the delay noted in figure 3-22, it would not explain why an earlier weight loss was not recorded due to the free lubricant exuded onto the surface decomposing.

Plate 4-2 shows compacts of 60%, 80% and 85% relative density, similar to those used to produce figure 3-22. These compacts contained 1% by weight zinc stearate and were thermogravimetrically treated to 500°C in $N_2/10\%H_2$. The surface spotting can be seen on the 85% dense compact.

PLATE 4-2 The effect of density on the development of surface deposits on compacts containing zinc stearate, heated to 450°C in N_2/10%H_2.

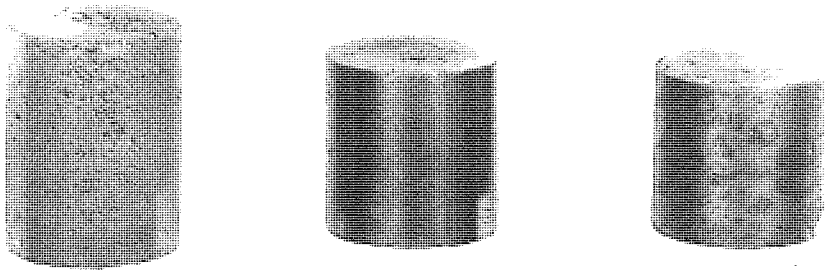

Density — 60% 80% 85%

10 mm

4-6 The effect of lubricant expulsion on the mechanical properties of compacts.

The measurement of tensile strangth was chosen as a convenient method of assessing the overall influence on sintering compacts of the reactions detected and discussed in the previous chapters. The development of tensile strength will not only be an indication of the development of interparticle bonds but also of chemical reactions occurring within compacts. It is because of this that detailed discussion of sintering mechanisms will be largely avoided.

It was intended that the measurement of tensile strength should reflect the total effect of all those factors influencing sintering, particularly reactions attributable to lubricants. Where it is necessary to discuss sintering mechanisms it will be found that it will be generalised and largely based on circumstantial evidence.

4-6-1 The effect of heating rate on the mechanical properties of sintered compacts containing lubricants.

The results of reproducibility are shown in figure 3-32a. It can be seen that there was little difference between the mean tensile strengths of duplicates belonging to the two separate experiments. At the high heating rate (figures 3-32 and 3-33) a reversal of the tensile strength/density curve has been obtained with some lubricants. At the low heating rate (figures 3-34 and 3-35) this relationship was normal for all lubricants except medium admixed stearic acid. The appropriate green strength/density curves used to assist this discussion were determined as described in part I and reproduced here as figure 4-13 for convenience.

With the high heating rate inversion of the tensile strength/density curve only occurred where there was a significant reduction in green strength relative to the unlubricated condition. This was so for medium stearic acid (figure 3-33b) and metal stearates (figure 3-32b). It appears therefore that

FIGURE 4-13 .Green strength versus density for compacts containing lubricants.

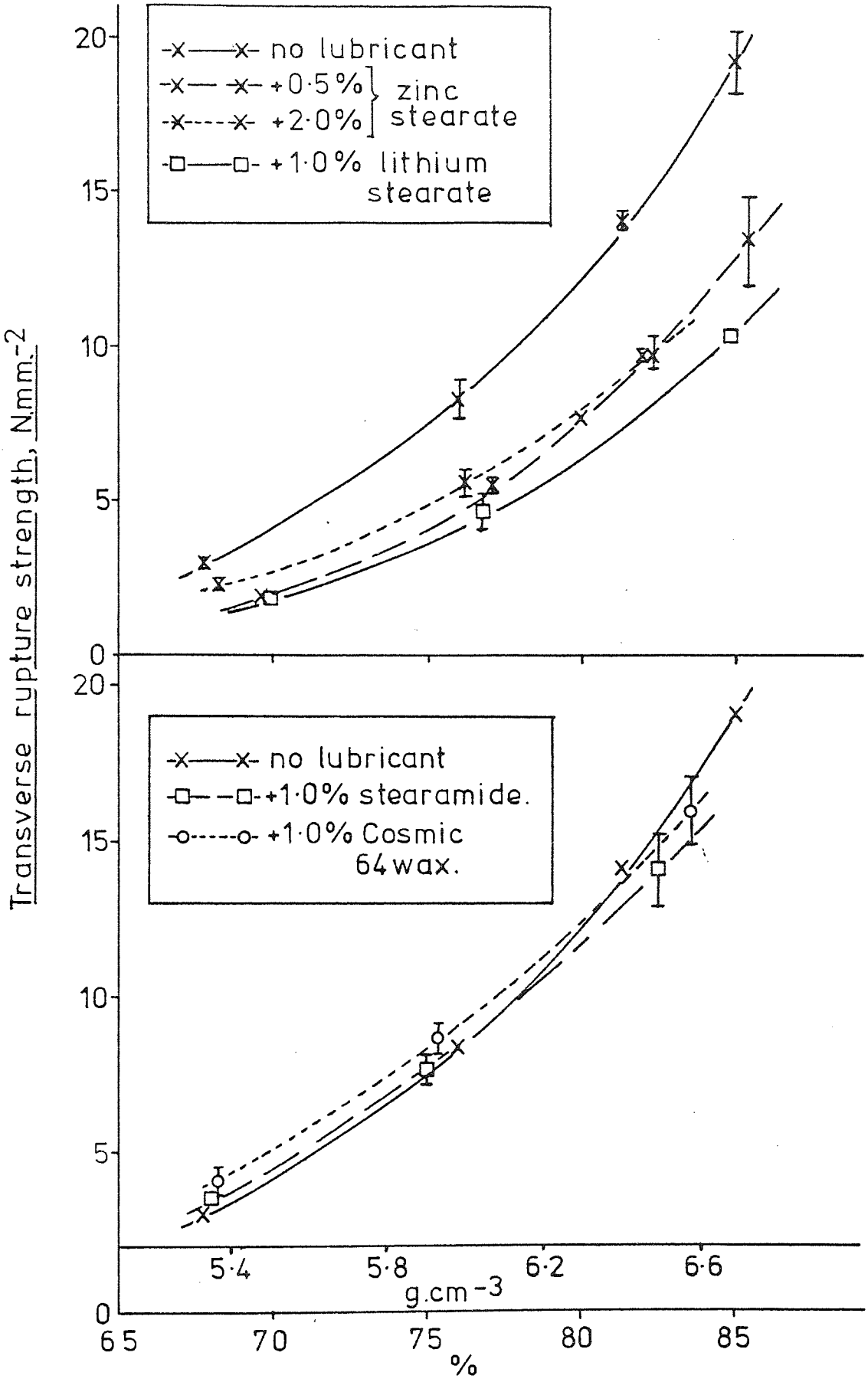

FIGURE 4-13 continued.

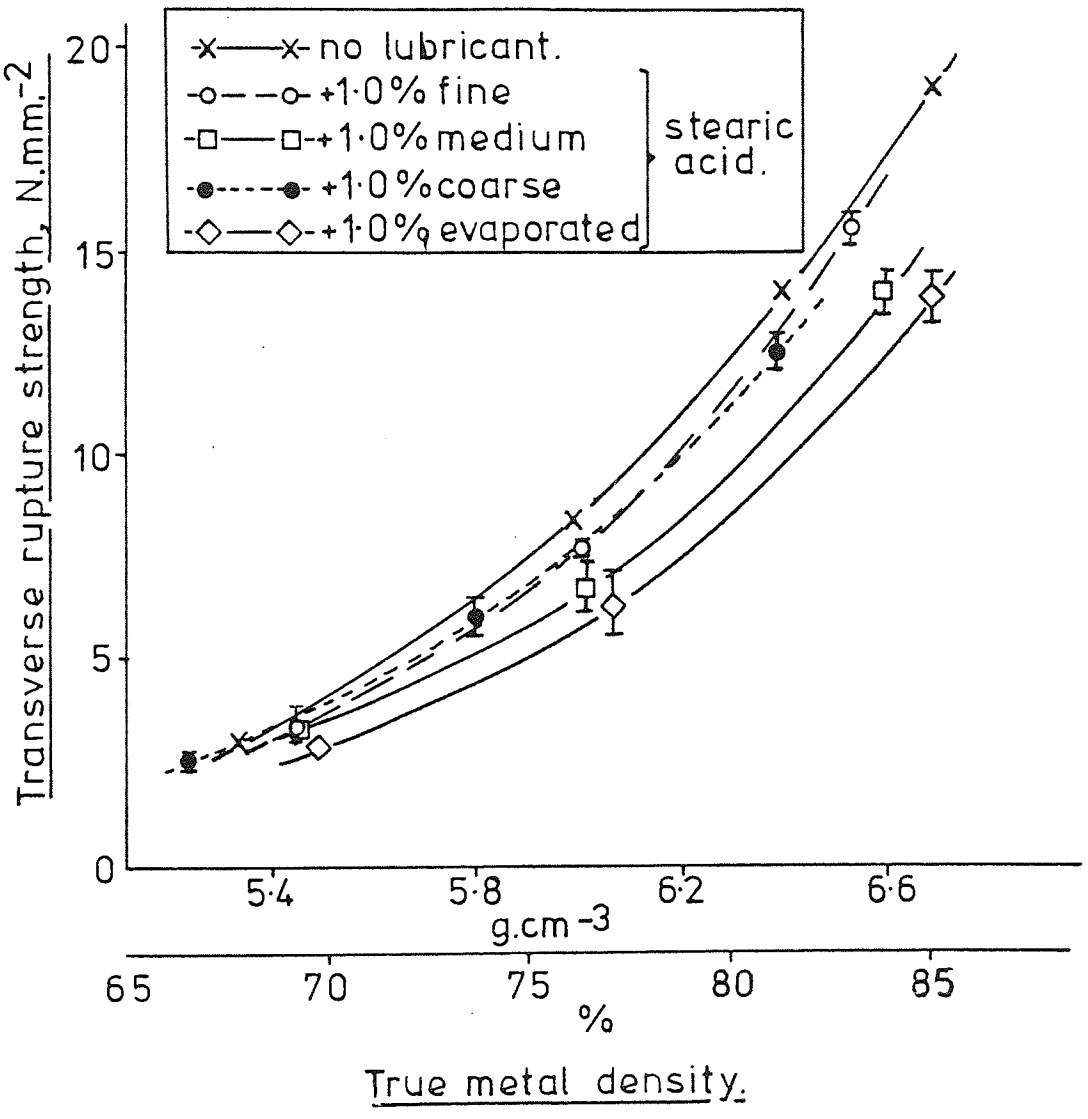

the rapid expulsion of any lubricant which also reduces green strength can have serious effects on the tensile strength of sintered compacts. When subjected to a low heating rate zinc stearate (figure 3-34) neither reduced tensile strength nor caused an inversion. However, the presence of lithium stearate did cause a significant decrease, but again no inversion. This was probably due to the presence of carbon dioxide, resulting from lithium carbonate decomposition, which would retard sintering. Such a chemical effect, rather than physical, was suggested by the absence of inversion (figure 3-34).

The influence of lubricant particle size and dispersion was illustrated by stearic acid (figures 3-33b and 3-35). When a particle size increase was accompanied by a reduction in green strength (figure 4-13), as with medium stearic acid, a high decomposition rate caused a reduction of tensile strength and an inversion of the tensile strength/density relationship. This was shown by the medium stearic acid even at a low heating rate.

The evaporated stearic acid reduced green strength significantly (fig. 4-13) due to its dispersion and yet its effect was limited to a slight reduction of tensile strength at the high heating rate (fig.3-33b). There has been no evidence presented to suggest that this lubricant decomposed at a slower rate than others. It must therefore be assumed that pressure differences within compacts containing stearic acid were not responsible for the variations in tensile strength shown in figure 3-33b. It will be shown later (4-6-2) that the extension of final reduction reactions, due to carbon deposited by this lubricant (sections 4-3-23 and 4-4-3),led to rapid development of tensile strength during heating between 1000 and 1100°C.

The presence of fine stearic acid in a compact did not significantly reduce green strength (fig.4-13) and consequently its rapid expulsion did not reduce sintered tensile strength. Evaporated stearic acid did reduce green strength, as discussed above, but extension of oxide reduction reactions by deposited carbon would seem to have rapidly repaired any damage due to the

rapid expulsion of this lubricant. The slight decrease in tensile strength shown in figure 3-33b could be attributable to the removal of lubricant from within interparticle bonds. It is possible that the influence of the medium particle sized stearic acid, causing an inversion at both heating rates, was connected with its particle shape. This was flat and plate-like (section 4, Materials) and it is possible that the removal of such particles from within interparticle contacts caused damage which was slow to heal.

Cosmic 64 wax was consistent in not affecting tensile strength at either heating rate (figs.3-33a and 3-34). Green strength was similarly unaffected and it seems probable that this was sufficient to withstand pressure increases during the expulsion of this lubricant. Relatively high residual carbon contents were obtained from compacts containing wax, at both heating rates, as recorded in table C-1. This may have aided sintering during the later stages of heating[25] as discussed above for evaporated stearic acid.

Stearamide was somewhat of an anomaly. There was no significant reduction of green strength due to addition of stearamide (fig.4-13), however the expulsion of this lubricant did reduce tensile strength consistently at both heating rates (figs.3-33a and 3-34). There was no inversion of the tensile strength density curve, indicating that the factor responsible for reducing strength was not dependent on density. It was, therefore, probably not due to the physical forces of decomposition. It has been suggested that nitriding may occur in compacts containing decomposing stearamide (4-3-2-4). This nitriding may have retarded sintering processes whilst it was occurring.

Compacts containing no lubricant, 1% zinc stearate and 1% Cosmic 64 wax were heat-treated to 1100°C at the high heating rate and given 3 minutes at temperature. The results are shown in figure 4-14 as tensile strength versus density, together with the original results taken from figure 3-32 obtained after a maximum of 2 minutes at 1100°C.

FIGURE 4-14 .Repeated results for tensile specimens treated at a high heating rate in $N_2/10\%H_2$.

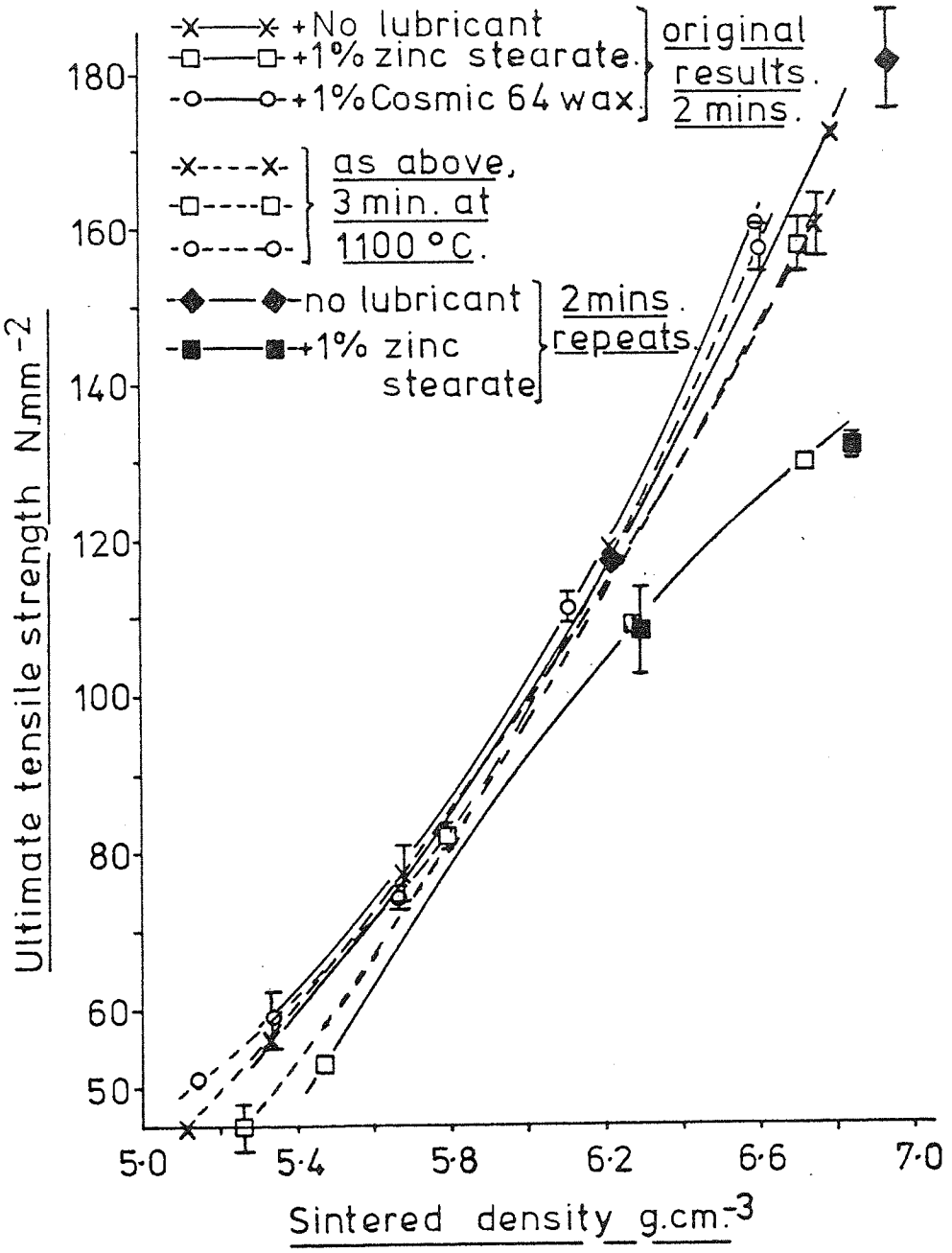

It can be seen that the purely physical pressure effect of decomposing zinc stearate may be eliminated by an extremely short isothermal heat treatment. It seems that,if interparticle bonds were partially forced apart,the spaces involved must be of the order of only a few atomic diameters. It is possible that such narrow defects could be repaired by short high temperature heat treatments. It will also be shown in section 4-6-2 that in $N_2/10\%H_2$, rapid development of tensile strength does occur during the initial stages of isothermal sintering at 1100°C. In all cases final dimensional change was a shrinkage, with no relationship with density, as can be seen from table C-1. It seems unlikely that the production of such small spaces at interparticle bonds would cause a measurable expansion of a compact,particularly if the considerations given to the influence of the removal of interposed lubricant (4-3-2-9) are noted.

The original results obtained for compacts containing no lubricant and 1% zinc stearate (fig.3-32b) were rechecked by heat treating medium and high density compacts in the same manner. These results are superimposed on the original results in figure 4-14 and confirm that the pressure effect was not eliminated by a heat treatment of 2 minutes maximum at 1100°C.

It has been shown that there are three possible effects that a decomposing lubricant may have on the development of mechanical properties of sintering compacts;

A- Physical - (a) due to the increase of pressure within compacts caused by decomposing lubricants.

(b) due to the removal of lubricant interposed within interparticle bonds[28].

B- Chemical - residues and decomposition products may influence sintering mechanisms.

Further consideration is given to chemical effects in the next section, however it has been shown that these may have a more permanent influence

than physical effects. During this investigation the latter have been detected by using conditions which were definitely not commercial, but effects were observed on a compact axis shown to be the least sensitive to the presence of a lubricant, the radial axis.

There is no doubt that the pressure effect may be much more permanent under commercial conditions, as indicated by the report reproduced in appendix D, discussed previously in section 4-3-3. In the case of compacts which crack or explode the effect is obviously permanent.

4-6-2 The influence of residues and other decomposition products on sintering mechanisms.

The results of isochronal and isothermal heat treatment of compacts containing lubricants are shown in figures 3-36 to 3-41. The points plotted in these figures are the mean results of separately heat treated duplicate specimens. Reproducibility bars have been shown for tensile strength in N_2/ 10%H_2 only, to avoid unnecessary confusion. However full results are recorded in tables C-2 and C-3 (appendix C) for reference.

It can be seen from these tables that final densities varied slightly between the different materials. However, it was generally found that the lowest densities were associated with the higher tensile strengths. It was therefore unlikely that density variation was responsible for the differences in tensile strength curves of figures 3-36, 3-38 and 3-39.

It will be most convenient initially to consider the behaviour of unlubricated compacts before discussing the influence of decomposing lubricants. The results of tensile strength in both atmospheres are presented in figure 3-36 and dimensional change in figure 3-37.

It can be seen from figure 3-36 that the sintering of ferrite was characterised by rapid development of strength associated with considerable shrinkage (fig.3-37). In both atmospheres sintering, when measured in terms of tensile strength, effectively ceased immediately following ferrite-

austenite transformation. This was also reflected by dimensional change in $N_2/10\%H_2$ (fig.3-37).

Sintering appeared to recommence at temperatures around 1000°C in $N_2/10\%H_2$ as indicated by a small increase of tensile strength (figure 3-36). This increase was associated with a reduction in final shrinkage between 1000 and 1100°C (fig.3-37). The most significant difference between the two atmospheres was established during isothermal sintering at 1100°C (fig.3-36). This was characterised by a rapid initial increase of tensile strength in $N_2/10\%H_2$, with only a slight corresponding increase in argon. The increase of tensile strength in $N_2/10\%H_2$ was associated with a low shrinkage compared with argon, as can be seen in figure 3-37.

It is not possible to isolate sintering mechanisms completely, in such a system, using only two parameters (mechanical strength and dimensional change). However, by assuming the major contributors to be volume, surface and grain boundary diffusion, it should be possible to suggest the probable influence of each mechanism.

It seems possible that all sintering mechanisms were able to contribute to the sintering of ferrite. This is indicated by the rapid development of tensile strength at low temperatures, reflecting the consolidation of bonds. All three diffusion mechanisms are capable of causing kneck growth [43]. The sintering of ferrite has been shown to be dependent on surface diffusion[37] and the high surface areas of such commercial powders could be expected to encourage surface diffusion. The development of tensile strength was found to be atmosphere dependent during this stage (fig.3-36) and the activation energy for surface diffusion in ferrite is also lower than that for volume diffusion[37, 39].

Rapid sintering rates relative to austenite, in terms of densification, have been observed when sintering ferrite[44]. This was attributed to a fine grain size in ferrite allowing grain boundary diffusion to play a

decisive role. Photomicrographs of specimens isochronally heat treated in $N_2/10\%H_2$ are shown in plate 4-3. It is evident that the ferritic grain size was finer than that of austenite and changed little until transformation occurred.

The rapid shrinkage observed at this stage in both atmospheres (fig. 3-37) suggested a significant contribution by volume diffusion. Surface and grain boundary diffusion are capable of producing kneck growth, hence improving mechanical properties, but are not believed[43] capable of causing shrinkage. It seems possible that volume diffusion could also be encouraged by the preferential production of point defects at interparticle contacts during compaction. A vacancy concentration gradient could therefore exist between these contacts and the interior of adjoining particles. However, all compacts were subjected to a dewaxing treatment at 500°C, close to the recrystallisation temperature of ferrite. This pretreatment may, therefore, have caused recrystallisation of deformed ferrite with the subsequent annealing out of point defects.

The relatively fine grain size would also provide short diffusion paths to vacancy sinks (particle surfaces and grain boundaries). The sintering of this iron powder as ferrite would, therefore, seem to have involved significant contributions from all three diffusion mechanisms.

Extensive grain growth following the ferrite/austenite transformation has been observed to cause a marked reduction in sintering rate[45]. Rapid grain growth was also observed in these compacts (plate 4-3). The self diffusion rate of austenite immediately following transformation is also lower than ferrite just before, by a factor of 10 to 10^2 [39]. The combination of low diffusion rate, long diffusion paths and a reduction of vacancy sinks such as grain boundaries, has produced a decrease in sintering rate.

As the temperature approached 1100°C, strength development recommenced with a marked atmosphere dependence, particularly during the initial stage

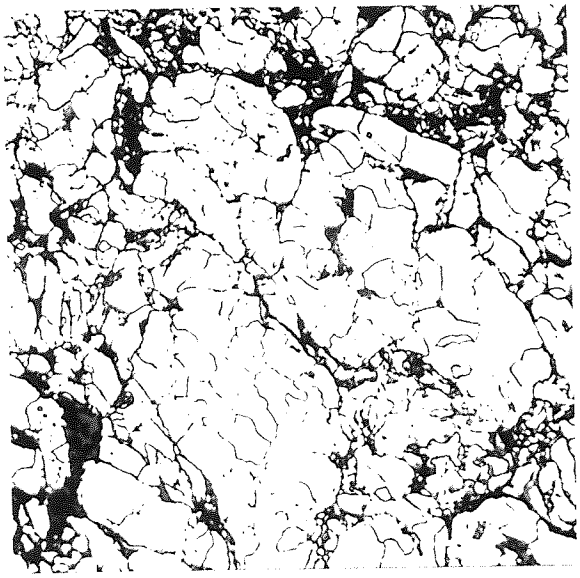

(a) 650°C

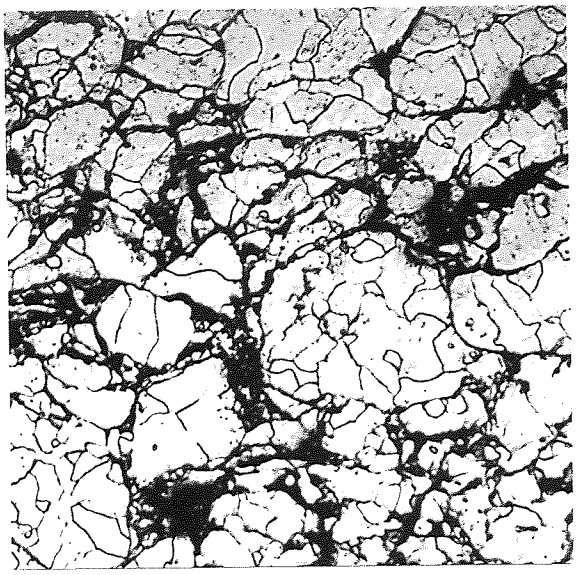

(b) 800°C

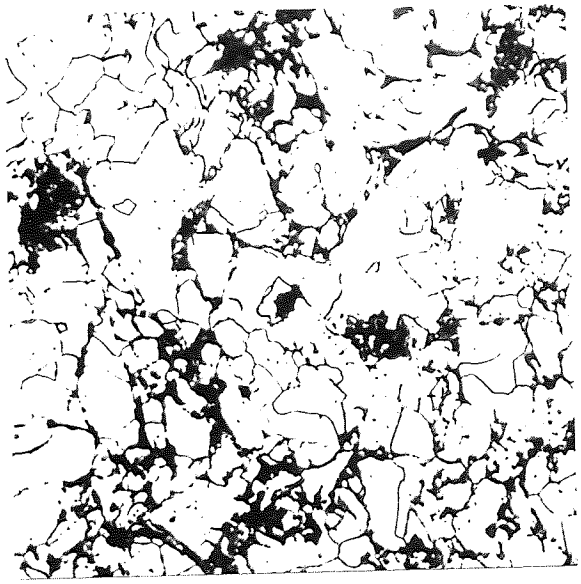

(c) 910°C

PLATE 4-3 The effect of temperature on grain size in unlubricated compacts isochronally sintered in N_2/10%H_2-

(Etched 1% Nital x400)

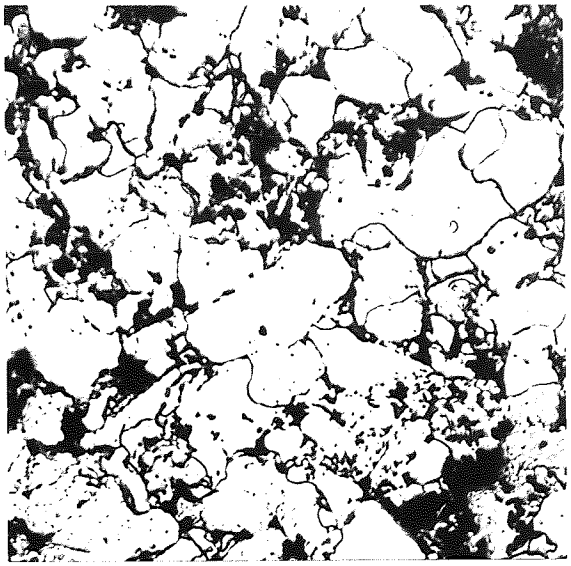

(d) 1000°C

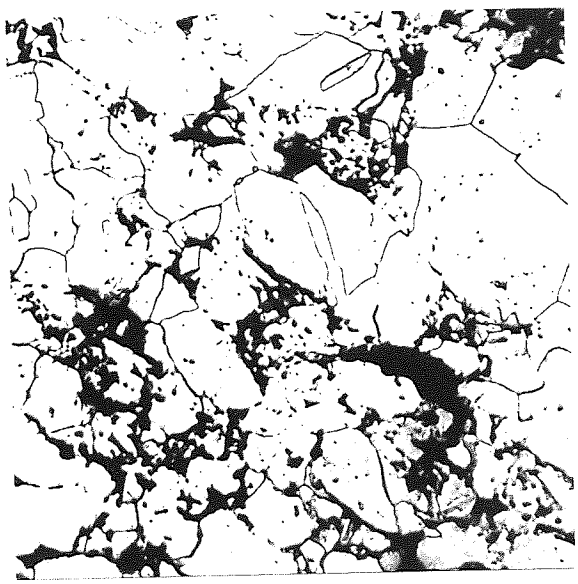

(e) 1100°C

PLATE 4-3 continued

of isothermal sintering at 1100°C (fig.3-36). The rapid increase of tensile strength at this stage in $N_2/10\%H_2$ was matched by a reduction in the degree of shrinkage relative to argon (figures 3-36 and 3-37). As discussed above, grain size and boundary area at this stage differed considerably from those of ferrite. However, the irregularity of the pores and particles, shown in plate 4-3, seem to indicate that the material possessed a high specific surface area at all stages.

This rapid development of tensile strength in $N_2/10\%H_2$, associated with the lack of shrinkage and high surface area, suggested that surface diffusion may have assumed a predominant role at this stage. The diffusion rates of both hydrogen and nitrogen in iron are very much faster than the self diffusion rate of iron at these temperatures[39]. It is possible that a similar effect occurs with surface diffusion. Carbon diffusion seems an unlikely contributor to sintering at this stage since its removal was found to be complete by the end of isochronal treatment, as indicated by the analysis results recorded in table C-2.

All compacts were subjected to a dewaxing treatment at 500°C to remove the hydrocarbon group of the lubricants and leave only residues. These were carbon from the stearic acid, zinc oxide and carbon from zinc stearate and lithium carbonate from lithium stearate. It was hoped that the low heating rate up to 500°C, $4°C.min^{-1}$ overall, would avoid the pressure effect discussed in the previous section. There is some indication from figure 3-38 that in $N_2/10\%H_2$ the expulsion of lubricants did cause a slight reduction in tensile strength. In argon, figure 3-39, no such effect was apparent. Therefore the former may be attributable to experimental error. However, slight expansions at 500°C were obtained for compacts containing zinc and lithium stearate , shown in figures 3-40 and 3-41.

It seems possible that this apparent reduction in strength following dewaxing in $N_2/10\%H_2$ (fig.3-38) was not in fact due to the pressure effect.

It may be recalled that reduction of oxides by hydrogen was observed to occur in compacts containing no lubricants in the temperature range 340-500°C (4-3-1-1). It is suggested, therefore, that this was responsible for improving the tensile strength of unlubricated compacts dewaxed in $N_2/10\%H_2$. The residues from lubricant decomposition present on particle surfaces in other compacts could possibly have inhibited this initial reduction reaction.

The sintering of ferrite and austenite will again be considered separately for convenience. It can be seen from figure 3-38 that as ferrite the specimens may be divided into three groups.

(a) Those containing no lubricant.

(b) Compacts containing stearic acid or zinc stearate.

(c) Compacts containing lithium stearate.

These are in order of decreasing tensile strength at any given temperature up to 900°C.

Shrinkage in $N_2/10\%H_2$ (fig.3-40) was only retarded for compacts containing lithium stearate, all others being similar to compacts containing no lubricant. The tensile strengths of group (b) shown in figure 3-38 were similar to those obtained for group (a) in argon, figures 3-36 and 3-39. In argon (fig.3-39) groups (a) and (b) behaved in a similar manner.

This evidence suggests that surface diffusion had been inhibited by the presence of surface deposits. An extreme effect is shown by compacts containing lithium stearate. The production of carbon dioxide and resultant oxidation (4-3-2-2) seriously retarded sintering until reduction by atmospheric hydrogen or carbon within the matrix allowed diffusion to proceed.

It can be seen from figure 3-39 that in argon there was an apparent tendency for sintering to be enhanced in compacts containing zinc stearate. This may have been due to the reduction of zinc oxide by hydrogen from within the iron powder, as discussed in 4-3-2-1. Greatly increased surface self diffusion rates have been observed to occur in metals when heated in

the presence of the vapour of another metal[36]. There is perhaps a possibility of this occurring for iron in zinc vapour. The increase shown in figure 3-39 was small however, and may have been attributable to experimental error only.

All compacts containing lubricants showed a marked reduction in sintering rate following the ferrite/austenite transformation, as observed for unlubricated compacts. When tensile strength development recommenced in $N_2/10\%H_2$ (fig.2-38) it was most rapid in compacts containing precipitated/evaporated stearic acid or lithium stearate.

Previous investigations (4-3-2) have shown that this stage corresponded to oxide reduction at high temperatures by carbon deposited from decomposing precipitated stearic acid. Generally, higher carbon contents were obtained from compacts containing lubricants, as recorded in table C-2. In the case of precipitated stearic acid the improvement in strength may have been caused by this carbon enhancing sintering.

In compacts containing lithium stearate this stage corresponded to reduction of surface oxide, caused by carbon dioxide, by atmospheric hydrogen or carbon associated with the matrix. The reduction of this oxide may then have allowed sintering mechanisms to develop a degree of sintering approaching those expected under equilibrium conditions.

It can be seen from table C-2 that, contrary to the indications of thermogravimetric work, carbon deposition did occur with this lubricant. However, it appears that this was utilised in trying to reduce the carbon dioxide produced by lithium carbonate decomposition.

These effects were much less pronounced in argon (fig.3-39). In this atmosphere the only bulk reducing agent was carbon associated with the matrix or deposited by decomposing lubricant. Due to the experimental procedure air was initially carried into the system within pores, and there was no hydrogen to help remove the associated oxygen. Carbon was also employed at

an early stage to reduce oxides, as observed during thermogravimetric work on matrix reactions (4-3-1-1). It seems possible that in argon, carbon was depleted by the austenitic stage and hence there was a trend for all materials to behave similarly. This was reflected in the final isothermal tensile strengths where there was little difference between the materials.

In $N_2/10\%H_2$ (figure 3-38) the rapid initial strength increase at 1100°C was present in all materials to the same degree, with the exception of compacts containing lithium stearate. In the latter tensile strength development was more leisurely. The order of final isothermal tensile strengths in this atmosphere reflected the results obtained in the previous section at the low heating rate, figures 3-34 and 3-35. However it can be seen that, as in argon, increasing time tended to eliminate effects attributable to the presence of residues. This was also illustrated by the tendency for final shrinkages to approach a similar value (fig.3-40).

4-6-3 The effect of decomposing lubricants on mechanical properties, summary.

The results of the previous two sections have shown that decomposing lubricants can influence the development of mechanical properties in sintering compacts. The extent of these physical or chemical effects has been found to depend primarily on the type of lubricant. However, predictions of mechanical property behaviour must also consider factors such as as-pressed strength, compact density and the stage of sintering. Overall reactions are therefore somewhat complex.

Many of the deleterious effects were removed as sintering proceeded. However, the influence of lubricants on mechanical properties was determined along the longitudinal axis of tensile compacts. This axis is equivalent to the radial axis of cylindrical compacts, perpendicular to the pressing axis, and has been shown to be the least sensitive to the presence of lubricant. The compacts used were also of simple shape with a maximum section thickness

of approximately 5mm along the gauge length.

Commercial compacts are usually of much more complex shape and higher mass, with the possibility of density variation within each component. The influence of decomposing lubricant may vary throughout the section of a complex part. It can be seen, therefore, that a geometrical effect must also be considered when discussing the possible influence of decomposing lubricants. Physical effects have certainly been found to be permanent in commercial compacts, as discussed in 4-6-1.

PART III General discussion and conclusions

1 General discussion.

In comparison to the application of lubricant directly to the die-wall, the overall influence of admixed lubricant on the production of iron powder compacts must be considered as deleterious since many of its advantages are matched by disadvantages. The choice of an ideal addition of a given lubricant would be difficult since the optimum content was found to vary with each production stage and therefore it would be necessary to decide which stage was the most important. As an example, additions chosen to reduce particle/die-wall friction would decrease the die-wear rate and energy expenditure during compaction and ejection but would also adversely affect loose packing and inhibit densification.

Lubricant is added primarily to reduce friction, however it is utilised throughout the entire bulk of a compact only when reducing inter-particle friction and even this involves mainly the small proportion actually adhering to the metal particles. Friction at the die-wall is reduced by that lubricant only actually within the compact/die interface or just within the compact. The bulk, which must be removed prior to or during sintering, remains within the compact and is encouraged to remain there by the form of the density distribution produced during uniaxial compaction.

The exclusion of air by lubricant during compaction or its expulsion during dewaxing may be considered as advantageous. However the oxygen bearing radical of most stearate based lubricants decomposes during the later stages of dewaxing and thus replaces atmospheric oxygen as a possible oxidising agent. Stearates contain a high proportion of carbon and some is often deposited during decomposition to assist oxide reduction in the matrix, but again only a small proportion of the total carbon is involved, most is expelled at an early stage. Some reductions in the mechanical properties of compacts during dewaxing or sintering are associated with

physical and chemical influences which are caused by decomposing lubricants. If carbon deposition is also considered as undesirable, for example in stainless steels, then all the lubricants used in this investigation are undesirable in some respect. One of the most important considerations may be that they reduce the degree of atmosphere control during sintering.

Simple cylindrical or tensile compacts have been used to detect the deleterious or beneficial effects of lubricants during this investigation, but the extent of many effects may depend on compact geometry. This could determine the relative significance of phenomena such as interparticle friction and particle/die-wall friction, whilst during sintering, shrinkage and pressure effects would be dependent on changes of section and density variation within compacts of complex shape. In this investigation the reduction of mechanical properties by pressure increases in tensile compacts during dewaxing were generally temporary but permanent effects have been observed in commercial shapes (appendix D).

When all the variables are considered the specific effect of a particular lubricant on the production of a commercial component can only be assessed precisely by comparing the properties of the compact in the lubricated and unlubricated conditions. However, generally it would seem that undesirable influences observed in simple compacts could become even more evident as the complexity of shape increases.

The present advantage of using internal lubricant is expediency. During mass production the rapid application of lubricant directly to the die-wall is difficult and it is more convenient to admix lubricant powder with the other materials prior to production. The reduction of particle/die-wall friction, particularly during ejection, seems to be the most important factor to control. Die-wear will reduce the control of dimensional tolerance and excessive friction can cause seizure, breakage of tools and compacts and at least produce a poor surface finish. The

resultant blockage of pores (see plate 3-4,part I) would be undesirable in components such as oil-retaining bearings. Friction at the die-wall can be reduced effectively by the direct application of lubricant and if a suitable method was developed, this would be more desirable than admixing. The problems associated with internal lubricant would be removed and the bulk of the lubricant better utilised. It may even be provident to admix small proportions of lubricant, with simultaneous die-wall lubrication, to take advantage of the resultant reduction of interparticle friction, thus improving loose packed density and densification by particle rearrangement.

In this investigation it was found that large additions of zinc stearate were apparently more effective at reducing ejection forces than die-wall lubrication. Yarnton and Prosser[26] have shown that the lubricating properties improve with increasing molecular size, which they measured in terms of the carbon chain length. During the present investigation stearic acid (C_{18}) was applied to the die-wall and zinc stearate (C_{36}) was admixed, hence die-wall friction could probably be reduced further by applying a lubricant of long molecular chain length to the die.

2 Conclusions

1. Small additions of admixed zinc stearate form thin coatings on irregular iron powder particles and improve loose packed density by reducing interparticle friction. The degree of improvement increases with mix duration but at a decreasing rate. Large additions are associated with thick coatings and the presence of free lubricant which reduce density.

2. A linear pressure/density relationship can be applied to the closed-die compaction of iron powder, but its ability to describe the influence of variables such as the addition of lubricant may be very limited.

3. Small additions of zinc stearate reduce interparticle friction during compaction but do not reduce particle/die-wall friction to the level obtained with lubricant applied directly to the die-wall.

4. Large additions of zinc stearate reduce particle/die-wall friction to the level of die-wall lubrication. They also reduce interparticle friction at low densities or applied pressures but inhibit densification at higher densities. The reduction of particle/die-wall friction by internal lubricant is associated with the formation of a film in the compact/die interface, assisted by this inhibition.

5. Compaction inhibition is experienced before the available pore space is completely filled with lubricant, due to the presence of entrapped air.

6. Relative to die-wall lubrication, particle/die-wall friction during ejection is reduced by internal lubricant only at high contents where it is forced from compacts by inhibition.

7. The optimum lubricant content required to minimise friction increases as the lubricating requirements become more arduous with each subsequent production stage.

8. The presence of thin films of lubricant within interparticle contacts reduces green strength relative to the unlubricated condition. Precipitated and fine admixed lubricants are able to produce such films, coarse materials are not.

9. The decomposition of free stearates consists of two stages. The first corresponds to the rapid removal of the hydrocarbon radical. The second occurs at higher temperatures and is associated with carbon deposition in simple stearates and reactions involving the metal ions in metal stearates.

10. The basic decomposition reactions of lubricants occur in compacts during dewaxing but are modified by restricted pore space and reaction with the matrix. The latter is associated particularly with residual carbon.

11. Over short time intervals the local atmosphere within pores is important in deciding the nature of the reactions which will occur. Under certain conditions hydrogen may diffuse through pores in preference to other atmosphere components.

12. During sintering lubricant can markedly increase shrinkage in compacts produced by unidirectional pressing. This effect occurs particularly when density and content cause compaction inhibition and is confined mainly to the pressing axis.

13. The decomposition rate of the hydrocarbon radical may be reduced by isothermal treatment at intermediate temperatures in its decomposition range.

14. Lubricants and their decomposition products generally have undesirable physical and chemical effects on the development of tensile strength during dewaxing and sintering. In compacts of simple shape the deleterious effects of both may be temporary and removed by isothermal sintering.

15. Physical effects are caused by the removal of lubricant from inter-particle contacts to leave a space and by pressure increases in pores during decomposition of the hydrocarbon radical. The pressure effect is dependent on density.

16. Chemical effects are associated with the influence of residues and gaseous decomposition products on sintering mechanisms. These may be beneficial or deleterious depending on the stage of sintering and the chemical species involved.

3 Further work

1. Die-wall lubrication.

There would probably be engineering problems associated with the complexity of commercial forming tools but there is obviously scope for work on developing a method of applying lubricant directly onto the tools, to replace the use of admixed lubricant. The method developed would be required to reliably produce a consistent lubricant coating on all the surfaces of tools where sliding of the compact occurs during compaction and ejection. This may involve the surfaces of several punches or core rods. It must also accomodate the high forming rates necessary in commercial production. These considerations may require also that an alternative lubricant to the usual solid stearate powders be chosen or formulated.

2. Reactions between metal powder surfaces and sintering atmospheres.

In this investigation it was noted that reactions between the iron powder and the atmosphere during heat-treatment were characteristic of the local atmosphere within pores. This local atmosphere is related to, but not necessarily the same composition as, the surrounding atmosphere. It would be constructive to undertake further investigations concerned with the nature of reactions between metal powder surfaces and gaseous sintering atmospheres. Some emphasis should be placed on the diffusion of atmosphere components through the pores of compacts.

Thermogravimetry has been shown to be capable of detecting such reactions and would also be useful for determining reaction rates. Such a study would involve the use of the surface area apparatus also. Preliminary results from this have been encouraging but further work is required to establish a reproducible operational procedure.

Acknowledgements

The author would like to thank all the members of the Department of Metallurgy and Materials for their help, advice and moral support, particularly Dr.J.C.Billington for his encouragement.

He would also like to offer special thanks to all friends within and outside the department who have helped, in particular Miss J.F.A. Cockram for her excellent proof reading.

The Science Research Council are gratefully acknowledged for their financial support.

APPENDIX A

APPENDIX A. The determination of density distribution diagrams.

The use of cylindrical compacts has enabled density distributions representative of the bulk density to be determined on vertical radial sections (fig.A1). Such sections were used to produce the particle micro-hardness/density relationships of section 2-2-2-3, part I. This appendix is concerned with the determination of density distributions and the influence of the compaction method on them.

A-1 Method

Sections were taken through appropriate as-pressed compacts (28.6mm diameter, 60g, as used in section 2-2-1, part I), shown in figure A-1.

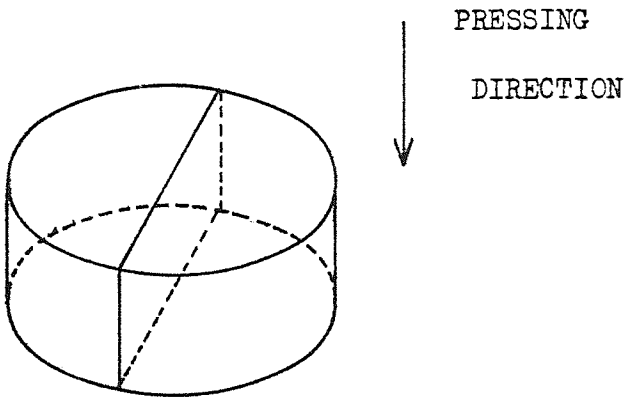

Figure A-1 The vertical section taken through compacts.

The section face was coarsely ground and then vacuum infiltrated with epoxy resin, as fully as possible. Several attempts were required to ensure the complete infiltration of high density compacts due to their restricted pore size.

The resin was allowed to harden. The specimens were then ground and polished as normal. Some samples were etched in 2% Nital to assist polishing but all were finally examined in the unetched condition. Polishing

was carried out until porosity was well defined. If pore edges bevelled the specimen was reground and polished. If there was any indication of the removal of particles the sample was reimpregnated.

Area percentages of porosity were determined on the polished face of each specimen using a Quantimet Image analysing computer. Specimens were regarded as consisting of horizontal layers of 1mm thickness and readings were taken at 1mm intervals along each layer. Each Quantimet determination covered $0.8mm^2$ in a spacing on the specimen of $1mm^2$, hence 80% of the total surface area was scanned. The results were recorded such that their positions corresponded to those on the specimen.

Area readings were converted to density (100-area%) and averaged into $4mm^2$ blocks (fig.A-2(A)).Specimens were now regarded as consisting of 2mm thick horizontal layers. Density was plotted against radial distance (fig.A-2(B)) to produce smoothing curves. Density contours were then drawn from these curves at 2% relative density intervals (fig.A-2(C)).

The density contours represent imaginary boundaries separating adjacent areas of differing density ranges. During their construction it has been assumed that the densities along any section must form a continuous range. This means that narrow regions beyond the resolution of the method may have been drawn in between areas which do not have a common boundary. An example is shown by the line x-x in figure A-2(C). The narrow regions of C dividing B and D are beyond the resolution of the system. However, they must exist since B (78-80%) and D (82-84%) have no common boundary.

Density distribution diagrams were determined on compacts pressed to 47, 156 and $470Nmm^{-2}$ from materials B, E and F, and 47, 78, 156, 311 and $470Nmm^{-2}$ from K (B with no die-wall lubrication). These were used primarily for the determination of the particle microhardness/density relationships (figs.3-10 to 3-13,part I). Only those for B and K, pressed to 47, 156 and

470Nmm^{-2}, are reproduced here, figures A-3 and A-4.

A copy of a diagram for B (470Nmm^{-2}, fig.A-3) was divided into separate areas and the mean density calculated gravimetrically. The result was a relative density of 86%. The actual density of the compact was 86%, an encouraging correlation between area % and actual volume %.

A-2 Discussion

It is possible to make some useful comments on the compaction conditions from the diagrams of figures A-3 and A-4. At low pressures (47 Nmm^{-2}) the lowest density region was close to the top of each compact and moved towards the centre as the compaction pressure increased. It was observed that during the initial stages of compaction the die tended to remain stationary with respect to the top punch. This was due to the force of gravity. The bottom punch moved up with the press ram effectively producing single end compaction.

Particle/die-wall friction increased as the density of the bottom portion of the compact increased. Therefore the die started to move up with the bottom punch. This caused densification of the top of the compact until the density distribution equalised. Beyond this point, densification by normal floating die compaction produced more regular density distributions (figs.A-3, A-4, 470Nmm^{-2}).

The regions of highest density were produced in the top and bottom circumference of each compact (the corners of distribution diagrams). In these areas restraint on particle movement was highest and pressure transmission most efficient. With die-wall lubrication (fig.A-3), these areas moved in from the corners towards the compact centre as pressure increased.

As density increased (fig.A-3, 470Nmm^{-2}) the total density range decreased. Compacts are short at high densities so that pressure transmission is improved. Pressure/density curves also become asymptotic to the pressure axis ($\frac{dD}{dP}$ tending to zero) so that the available range of densities

becomes restricted.

The effect of particle/die-wall friction is illustrated by comparison of figures A-3 and A-4. With no die-wall lubrication (fig.A-4, 470Nmm^{-2}) discrete low density regions have been retained at the mid-points of the die-wall contact face. This reflects the high resistance to the movement of particles in contact with the die-wall which is experienced in the absence of a lubricant film.

The highest range recorded was equal for both B and K (88-90%, 470 Nmm^{-2}). Therefore the difference in the overall densities of these compacts (86 and 83% respectively) was largely due to the presence of these low density regions in the unlubricated compact (fig.A-4, 470Nmm^{-2}).

Diameter, mm. ⟶ TOP

Length, mm.	0	2	4	6	8	10	12	14	16	18	20	22	24	26	28
1	90	89	88	86	85	83	80	80	83	85	86	88	89	90	
2	89	88	87	85	84	81	78	78	81	84	85	87	88	89	
3	85	84	84	83	83	79	76	76	79	83	83	84	84	85	
4	82	82	80	79	78	78	76	76	78	78	79	80	82	82	
5	85	84	84	83	83	79	76	76	79	83	83	84	84	85	
6	89	88	87	85	84	81	78	78	81	84	85	87	88	89	
7	90	89	88	86	85	83	80	80	83	85	86	88	89	90	

BOTTOM

(A) Actual area readings averaged into 4mm^2 blocks and converted to relative density.

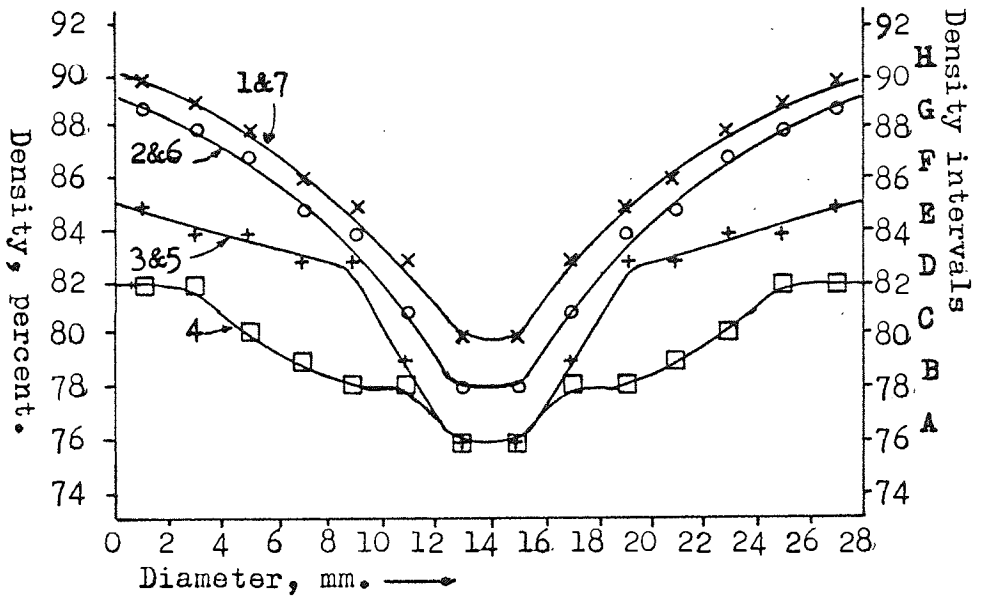

(B) Smoothing curves.

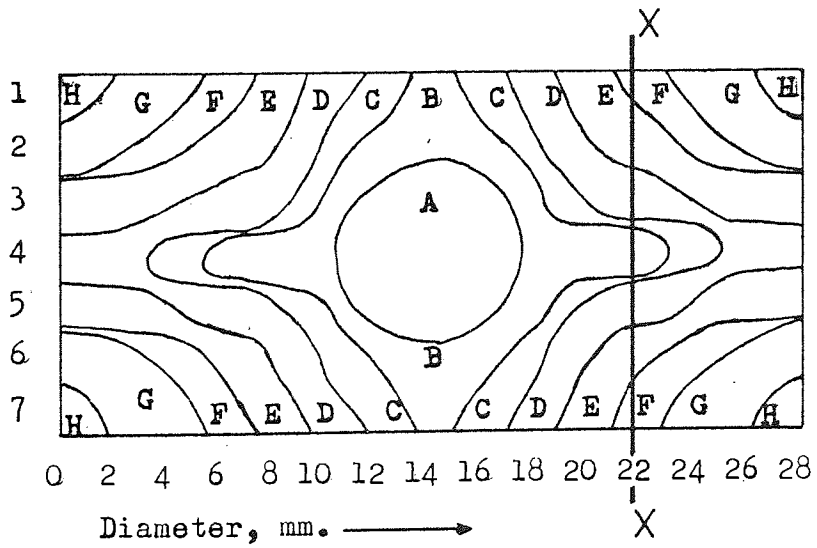

(C) Final density distribution.

FIGURE A-2. The construction of density distribution contours.

FIGURE A-3. Density distribution diagrams for material B - (die-wall lubricated).

All diagrams - scale 5:1

Densities are given as relative density - %

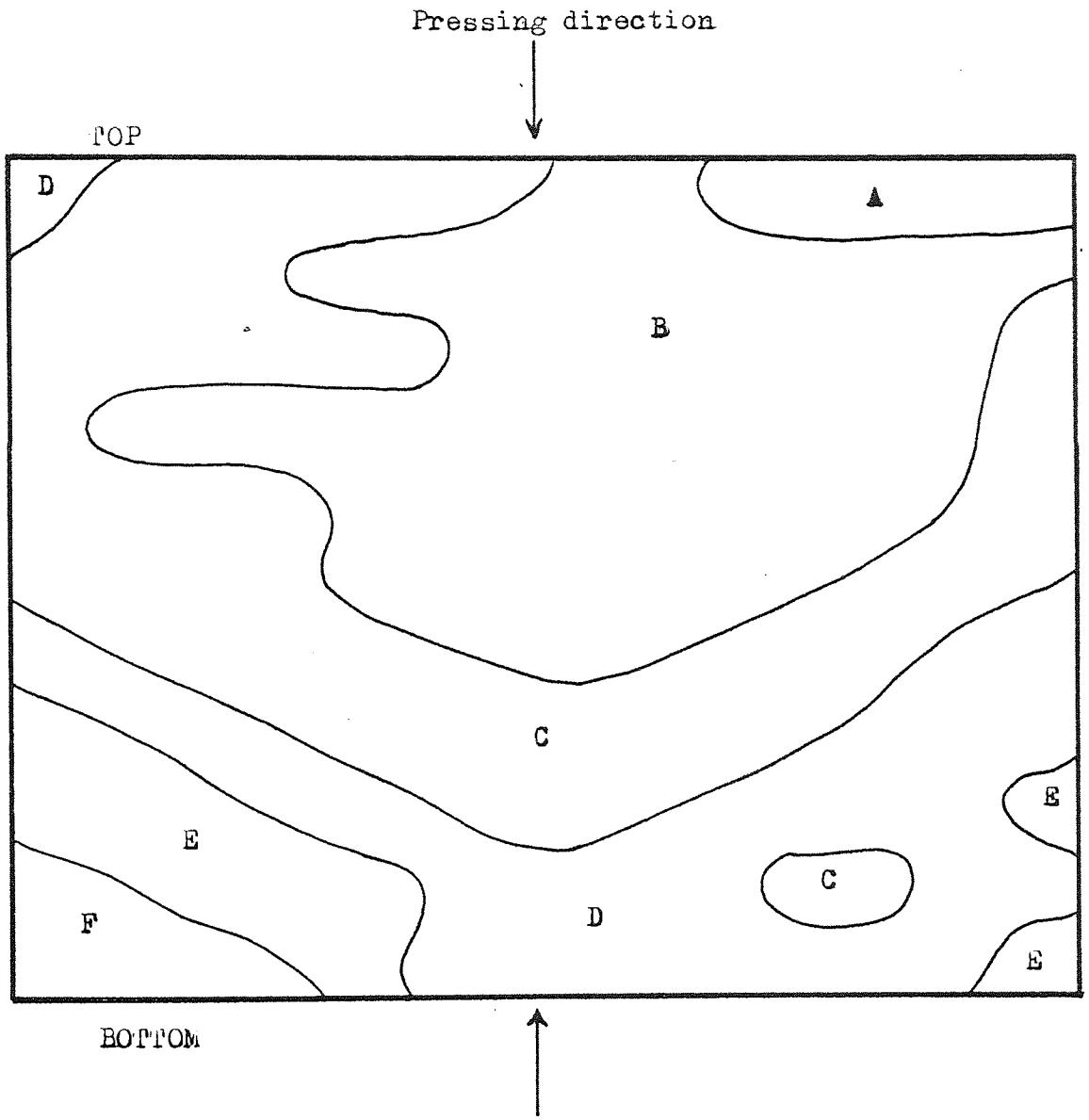

A= 48-50
B= 50-52
C= 52-54
D= 54-56
E= 56-58
F= 58-60

$P = 47\ Nmm^{-2}$

FIGURE A-3, continued.

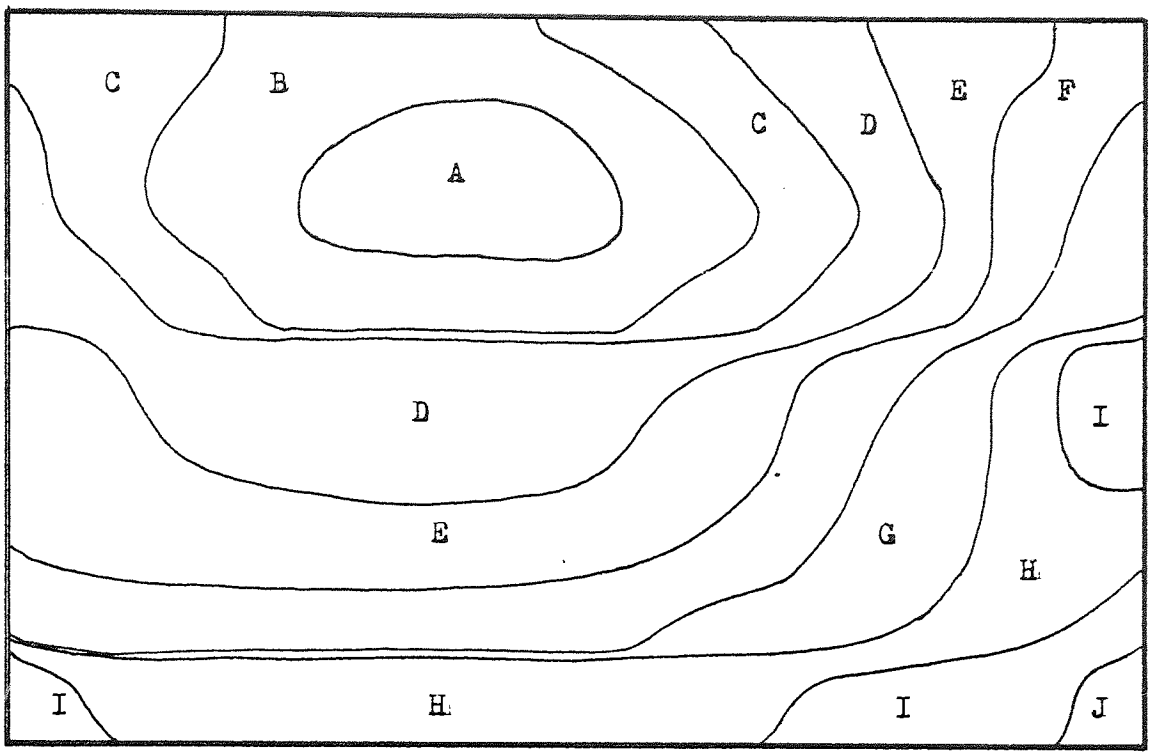

A= 58–60
B= 60–62
C= 62–64
D= 64–66
E= 66–68
F= 68–70
G= 70–72
H= 72–74
I= 74–76
J= 76–78

P = 156 Nmm^{-2}

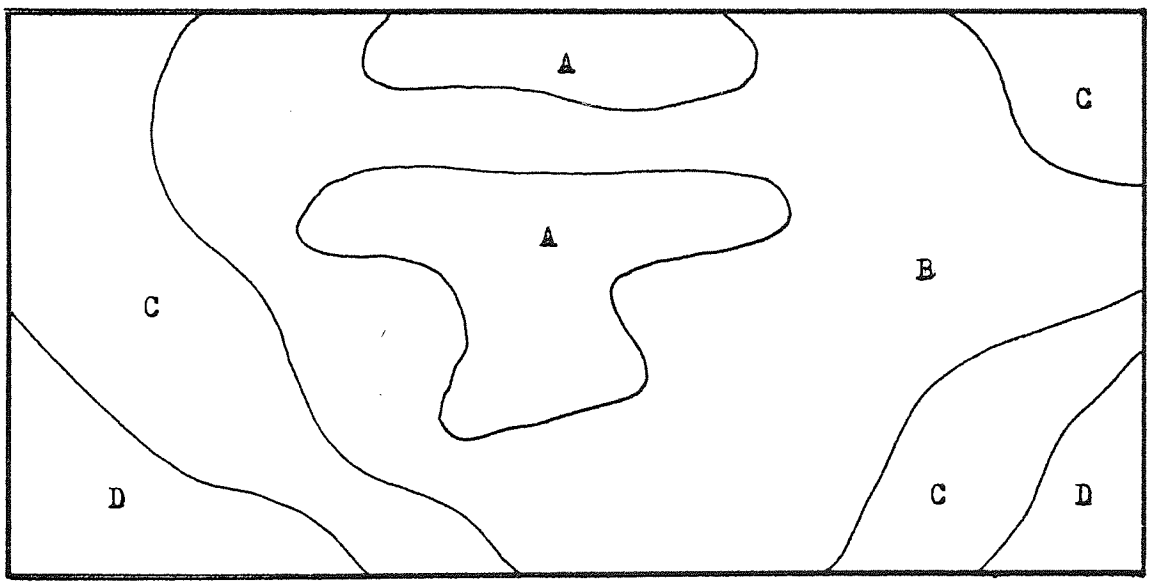

A= 82–84
B= 84–86
C= 86–88
D= 88–90

P = 470 Nmm^{-2}

FIGURE A-4. Density distribution diagrams for material K - (no die-wall lubrication) .

All diagrams - scale 5:1

Densities are given as relative density - %

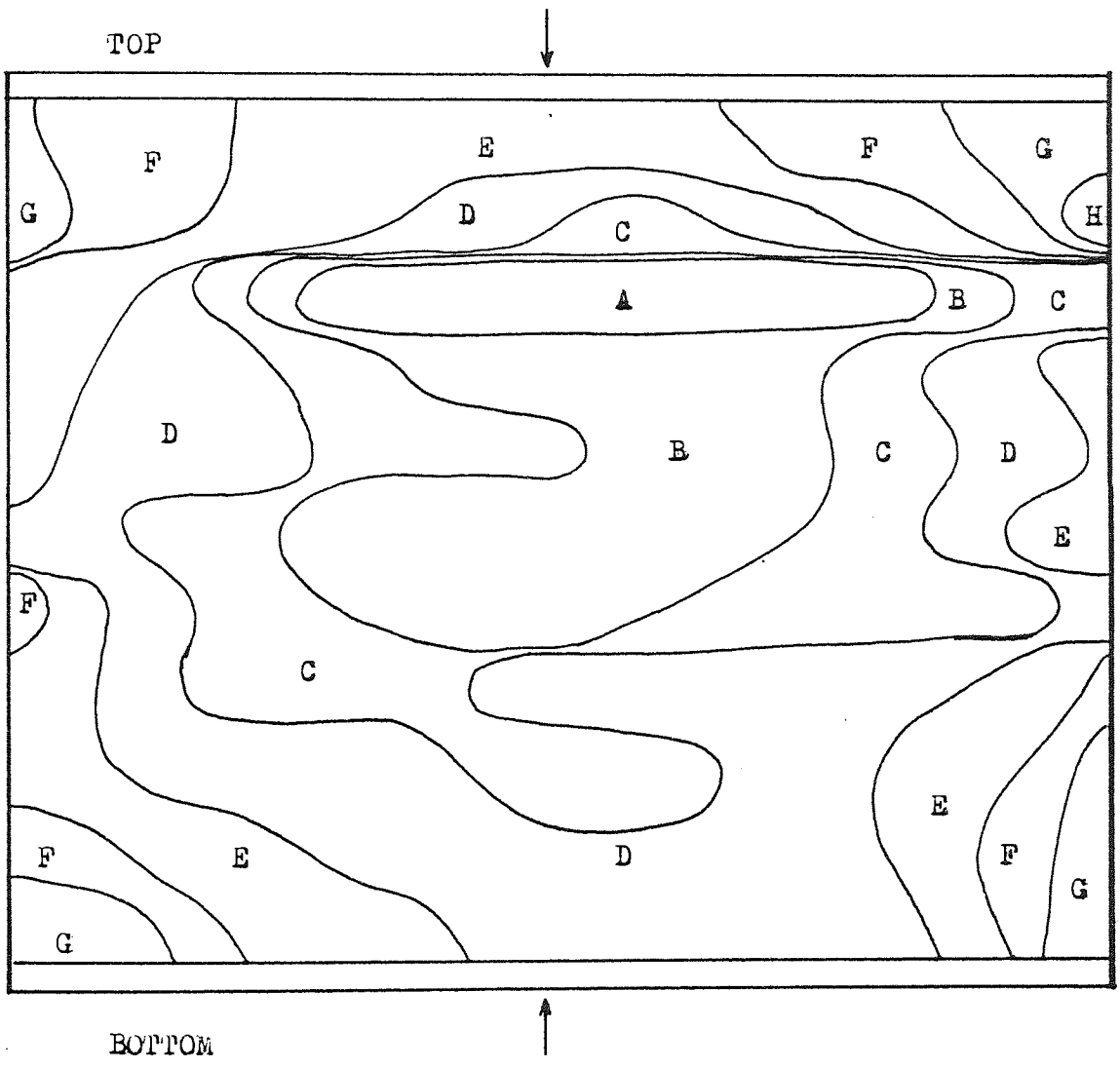

A= 42-44 E= 50-52

B= 44-46 F= 52-54

C= 46-48 G= 54-56

D= 48-50 H= 56-58

$P = 47\ Nmm^{-2}$

FIGURE A-4 continued.

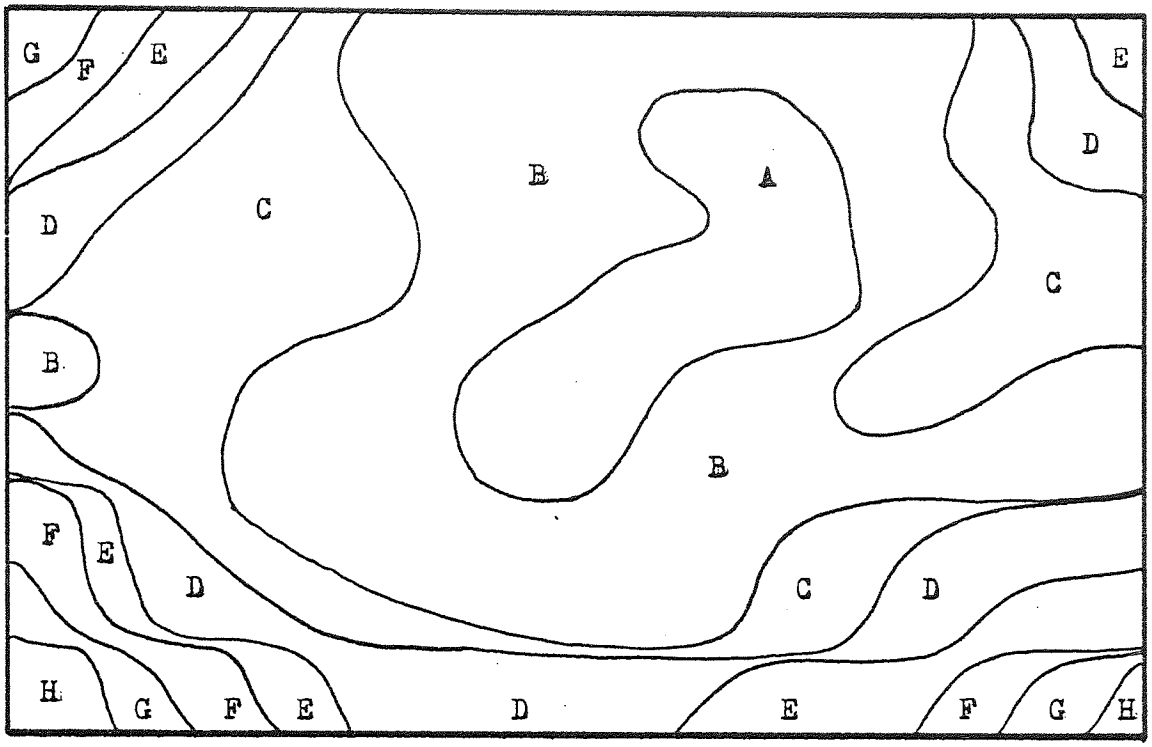

A= 60-62
B= 62-64
C= 64-66
D= 66-68
E= 68-70
F= 70-72
G= 72-74
H= 74-76

$P = 156\ Nmm^{-2}$

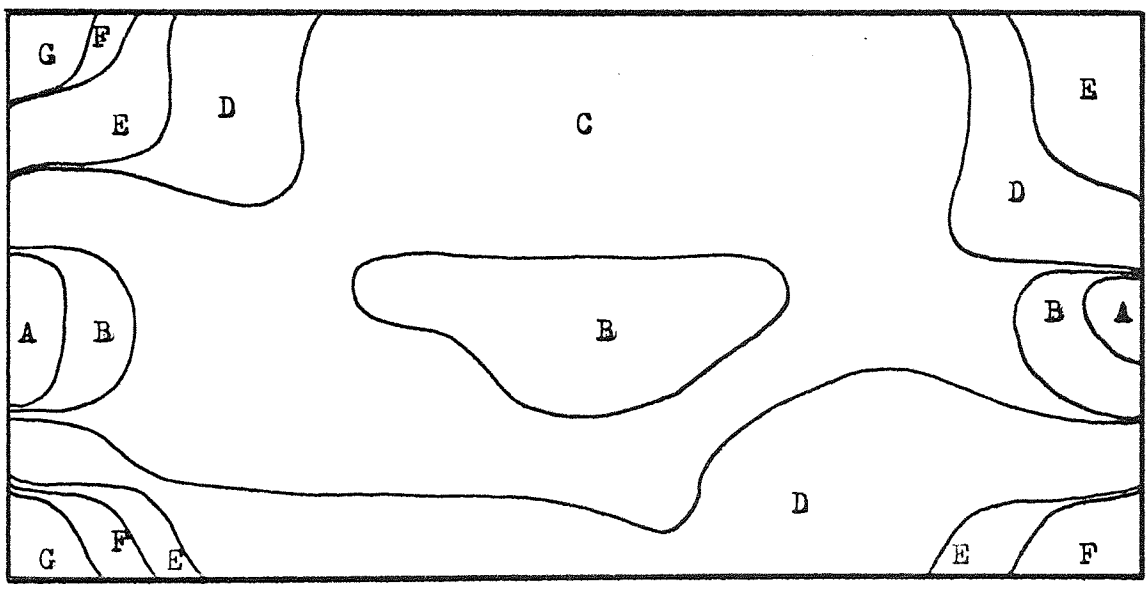

A= 76-78
B= 78-80
C= 80-82
D= 82-84
E= 84-86
F= 86-88
G= 88-90

$P = 470\ Nmm^{-2}$

APPENDIX B

APPENDIX B

Specific surface area determination by gas adsorption techniques.

B-1 Principles of gas adsorption

The atoms in the surface layer of a solid are bound on one side only, to their inner neighbours, and are incompletely attached on the outer surface. Under favourable conditions these surface atoms may attract free atoms or molecules of other materials such as gases to satisfy the balance of atomic forces. If this attachment of gas molecules is reversible, for example by applying a vacuum, the mechanism of attachment is physical adsorption. Physical adsorption of a gas onto a metallic surface will continue under suitable conditions until a multimolecular layer is produced[47] and cracks, capillaries and pores are progressively filled.

A typical complete adsorption/desorption isotherm is shown in figure B-1[47]. P_o is the saturation vapour pressure of the adsorbate gas at the operating temperature and P is the equilibrium pressure of the adsorbate in contact with the adsorbent sample. Such S-shaped isotherms have been obtained[47] for adsorption of a variety of gases onto many metallic and non-metallic surfaces.

The low pressure region of the isotherm is associated with the progressive formation of a monomolecular layer of adsorbate. If a monomolecular layer of gas is produced on a surface and the volume of gas in this layer and its molecular cross-sectional area are known, then it is possible to calculate the surface area of the adsorbent material. The surface areas of materials of non-geometric shape, including particles with open internal pores and involutes, may be determined in this way.

The B.E.T volumetric method for the determination of surface areas by gas adsorption has been pioneered by Brunauer, Emmett and Teller[47], after whom it is named. It has since been confirmed by many other workers [48-51] and accepted as a standard test procedure by the British Standards

Institution[52]. Ideal conditions for inducing the formation of an adsorbed monomolecular layer of gas have been found to be low temperature (liquid nitrogen) and low pressure ($0.05-0.30P_o$)[52].

B-2 Volumetric B.E.T method.

Brunauer et al[47] have derived the following equation (B-1) to describe adsorption isotherms when P is much less than P_o.

$$V = \left(\frac{V_m C}{P_o} P\right) / \left(1 + \frac{C}{P_o} P\right) \qquad \ldots.(B-1)$$

where - V is the total volume of adsorbed gas,

V_m is the volume of gas in a monomolecular layer,

C is a constant related to the system,

P is the equilibrium pressure of adsorbate gas in contact with the adsorbent material,

P_o is the saturation vapour pressure of the adsorbate gas at the temperature of test.

If $P/V(P-P_o)$ is plotted against P/P_o it can be seen that the result should be a straight line of slope $(C-1)/V_m C$ and intercept $1/V_m C$, enabling V_m and C to be evaluated.

Equation B-1 has been applied successfully by Brunauer et al[47] using various gases including nitrogen at 77.3°K. They found it to be valid between the limits P/P_o = 0.05-0.30. (these are now the limits of linearity suggested by the British Standards Institution[52]). Investigations by other workers[48-51] have confirmed the B.E.T method and the customary values of atomic cross-sectional area of various gaseous adsorbates.

The measurement of metal powder specific surface areas by volumetric gas adsorption is described in BS 4359 (part 1)[52] and by Haertlein and Sachse[48]. This involves preparation of the sample by outgassing at an

elevated temperature and in a vacuum lower than 10^{-5}mm Hg. This removes material adsorbed on to the surface naturally, such as oxygen and water. Outgassing is followed by the introduction of known volumes of adsorbate gas to the sample which is maintained at 77.3°K by immersing the reaction vessel into liquid nitrogen.

The volume of gas adsorbed (V_a) is obtained as the difference between the volume of gas required to fill the free space at the equilibrium pressure and the volume admitted. The former, termed 'dead space', may be found by repeating the experiment with a gas whose adsorption is negligible, V_a is then corrected to N.T.P. The gas pressure at each stage must be measured to enable true volumes to be calculated.

Nitrogen has been used widely for the determination of specific surface areas in excess of $2m^2g^{-1}$, however metal powders have typical surface areas closer to $0.05m^2g^{-1}$. If nitrogen is used as adsorbate for such powders then, without using extremely large samples, the ratio of unadsorbed to adsorbed gas ($V_u:V_a$) is extremely high. The use of nitrogen as an adsorbate limits the lower level of measurable surface area due to its high vapour pressure at its boiling point (741mm Hg at 77.3°K).

It has been found possible to use krypton for materials of low specific surface area[49,50]. At 77.3°K krypton has a saturated vapour pressure of only 2.2mm Hg and so for a given unadsorbed volume there will be many fewer molecules of krypton than nitrogen. The molecular cross-sectional area of krypton is only slightly greater than that of nitrogen (customary values 19.5×10^{-20} and $16.2 \times 10^{-20}m^2$ respectively) so that V_a will be similar for both gases. Using krypton at 77.3°K reduces $V_u:V_a$ sufficiently to extend the useful range of volumetric B.E.T. analysis to include surface areas appreciably lower than $0.05m^2g^{-1}$. The validity of using krypton has been confirmed by Beebe et al[50].

B-3 The gravimetric adsorption method

The number of molecules required to form a mono-molecular layer on an adsorbent sample is determined as a volume (V_m) in the normal B.E.T. method. It would be equally valid to determine the weight of adsorbate (W_m) required. If the weight of gas adsorbed is measured directly then the need to measure gas volumes and to correct for deviations from ideal would be eliminated. The volume of gas admitted would become significant only in determining the equilibrium pressure. A gravimetric method should therefore be simpler in operation than the volumetric method.

If V_m is replaced by the weight of adsorbate in a monomolecular layer, W_m, the B.E.T. equation (B-1) becomes,

$$W_A = (W_m C P/P_o) / (1 + \frac{C}{P_o} P) \qquad \ldots.(B-2)$$

where W_A is the weight of gas adsorbed at the equilibrium pressure P. W_A may be measured directly and W_m calculated as 1/(slope + intercept) of a plot of $P/W_A(P_o - P)$ versus P/P_o.

The operation may be outlined as consisting of outgassing, as with the B.E.T. method, followed by the introduction of controlled amounts of adsorbate to vary P between $0.05P_o$ and $0.3P_o$. W_A and P would be the only direct measurements necessary. Correction for adsorption onto the weighing apparatus could be obtained by repeating the operation with no sample or a blank.

The sensitivity of a gravimetric system would be improved by using an adsorbate gas of high atomic weight. Krypton has a higher atomic weight than nitrogen (84 and 14 respectively) and only a slightly higher cross-sectional area (19.5 and 16.2 x $10^{-20} m^2$ respectively). Therefore for a given sample it would provide a weight change approximately 2.5 times that of nitrogen.

Table B-1 gives examples of theoretical weights of monomolecular layers (W_m) of krypton and nitrogen for various specific surface areas.

TABLE B-1

Specific surface area m^2g^{-1}	Krypton			Nitrogen		
	W_m g	P_o at 77.3°K mm Hg	P $(0.05P_o-0.3P_o)$ mm Hg	W_m	P_o at 77.3°K mm Hg	P $(0.05P_o-0.3P_o)$ mm Hg
0.05	3.6×10^{-5}	2.2	0.11 - 0.66	1.44×10^{-5}	741	37 - 223
5.0	3.6×10^{-3}	2.2	0.11 - 0.66	1.44×10^{-3}	741	37 - 223
50.0	3.6×10^{-2}	2.2	0.11 - 0.66	1.44×10^{-2}	741	37 - 223

(W_m calculated for a 1g sample).

B-4 Construction of gravimetric apparatus

The apparatus was based on a Perkin-Elmer AR-2 microbalance and is shown in plate B-1 and schematically in figure B-2. The balance was theoretically capable of recording weight changes of 10^{-7}g. However, it was envisaged that a sensitivity of 10^{-6}g would be quite sufficient for the present work. Construction materials were confined to stainless steel and glass as far as possible.

The vacuum was produced by a rotary backing pump and a 2 inch diameter oil diffusion pump (figure B-2). The backing and ultimate (approximately 10^{-6}mm Hg) pressures were monitored with Pirani and Penning gauges respectively. Samples were stored in a vacuum desiccator which was included in the backing system.

The sample and tare pans of the balance were enclosed by removable glass hangdown tubes. During adsorption the sample tube (left hand) was immersed in liquid nitrogen held in a Dewar flask (fig.B-2).

The adsorbate was research grade krypton (99.995% purity) which

was drawn from a cylinder and stored in the reservoir at an approximate pressure of 10mm Hg. This pressure was monitored with the mercury manometer. Krypton input during adsorption was made more controllable by using this low supply pressure and by using the capillary supply tube between valves 2 and 3 (fig.B-2).

Equilibrium adsorption pressures were determined with a McLeod type of mercury gauge. Initially problems were encountered with mercury vapour from this gauge condensing on the cold sample during adsorption. This was overcome by inserting a cold trap cooled with liquid nitrogen between the gauge and the remainder of the system.

B-5 Operation

Due to delays in delivery and available time restrictions it was possible only to construct the apparatus and determine one surface area using an arbitrary method. Time was required to cure some operational problems such as mercury condensation and static.

B-5-1 Outgassing

The balance was calibrated according to the manufacturers instructions. A preweighed sample, powder in this case, was then placed in the sample pan and tared. Calibration and specimen replacement necessitated admitting air into the balance system and this was achieved via valve 5 (fig.B-2). Incoming air was dried to reduce the outgassing time by passing through silica gel.

Sample outgassing was necessary to provide a fresh surface for adsorption and remove molecules already adsorbed onto the surface. It was carried out at the ultimate pressure (10^{-6}mm Hg) and was assisted by baking the specimen at approximately 70°C. A heating tape was placed around the sample hangdown tube which was adjusted so that the specimen actually touched the glass tube. This ensured heating of the sample by conduction.

The same heating tape was used to bake the balance chamber ensuring that the ultimate pressure could be obtained. Further work is required to determine optimum outgassing conditions.

B-5-2 Adsorption

The following procedure is outlined only briefly since it cannot be regarded as a definite reproducible method.

The sample used was Höganäs NC100 iron powder sieved to 74-104μm. A specific surface area of $8 \times 10^{-2} m^2 g^{-1}$ had been determined on this powder by Coulter Electronics Ltd. using volumetric apparatus constructed by Micrometrics Ltd.

The same adsorption procedure was used to determine weight changes with a 1g nickel blank in place of the sample. These weight changes were attributed to buoyancy and adsorption onto the weighing mechanism. They were subtracted from the total weight changes obtained with the sample to leave the weight of krypton adsorbed (W_A).

To avoid damage to the balance control mechanism it was always shorted whenever changes were made in the system, such as specimen heating/cooling and admission of krypton.

The procedure after outgassing was as follows;

(a) The sample Dewar and McLeod cold trap were filled with liquid nitrogen. It was possible then to open valve 4 (fig.B-2) to the McLeod gauge. At this stage the ultimate pressure usually improved as the liquid nitrogen encouraged molecules to adsorb onto the glassware.

(b) When the pressure stabilised (to approximately 10^{-6}mm Hg) the sample tube was moved slightly until the sample touched the glass enabling it to cool by conduction. The system was left to equilibrate in this condition for at least 1 hour.

(c) The Penning gauge and pumping system were isolated (valve 1) and the balance system was allowed to equilibrate for 30 minutes. The specimen

was freed and the balance control unit adjusted to an appropriate scale. A steady weight reading maintained for more than 5 minutes was taken as zero.

(d) The balance was shorted, the sample cooled by contact with the hang-down tube and a small charge of Kr. was admitted via valves 2 and 3 (fig. B-2).

(e) The sample was freed and the weight recorded for 2 minutes. If this was constant the sample was cooled for a further minute. The weight was then recorded again and if this corresponded to the previous reading the weight gain was noted and the equilibrium pressure determined with the McLeod gauge. The process was then repeated from step (d) over the appropriate pressure range.

The first admission of krypton initially caused a large apparent weight loss due to a buoyancy effect. Cooled gas in the sample tube would have been denser than that in the tare tube causing an apparent decrease in the weight of the sample. This first charge of Kr. also represented a large pressure change from the ultimate pressure, from a pressure lower than 10^{-5}mm Hg to approximately 10^{-2}mm Hg.

As adsorption proceeded and the system equilibrated this apparent weight loss became a gain and equilibrium occurred more rapidly for subsequent pressure changes.

The weight changes obtained for the nickel blank (W_B) are shown in figure B-3 as a function of the equilibrium pressure (P). The recorded weight changes (W_R) obtained from the sample of NC100 iron powder are noted in table B-2.

B-5-3 Calculation

Appropriate blank weight gains (W_B) taken from figure B-3 were subtracted from the recorded weight gains (W_R) to obtain the gains due to adsorption alone (W_A). The results are noted in table B-2 and the adsorp-

Table B-2

Results obtained from the adsorption of krypton onto NC100 iron powder at 77.3°K

P mm Hg	W_R $gx10^{-6}$	$W_A=W_R-W_B$ $gx10^{-6}$	P/P_o	$\frac{P}{W_A(P_o-P)}$ $(gx10^{-6})^{-1}$
0.03	52	15	0.014	0.00093
0.12	58	18	0.055	0.0032
0.15	59	21	0.068	0.0035
0.22	56	26	0.10	0.0043
0.28	57	30	0.127	0.0049
0.39	58	36	0.177	0.0060
0.57	61	46	0.259	0.0076
0.68	64	52	0.309	0.0086

P = equilibrium pressure

W_R = recorded weight gain

W_B = blank weight gain

W_A = actual weight adsorbed

P_o = saturated vapour pressure of the adsorbate at 77.3°K.

tion isotherm for this sample is shown in figure B-4. It can be seen that krypton was adsorbed to a degree directly proportional to the pressure.

The surface area of the sample was calculated as outlined in section B-3. A good linear relationship was obtained between $P[W_A(P_o-P)]^{-1}$ and P/P_o as shown in figure B-5. The slope and intercept of this relationship were calculated as 0.0215 and 0.0021 respectively enabling the weight of krypton in a monomolecular adsorbed layer (W_m) to be determined.

$$W_m = (\text{slope} + \text{intercept})^{-1}$$

$$= \underline{42.4 \times 10^{-6} g}$$

$$\text{weight per atom krypton} = \frac{83.8}{6.02 \times 10^{23}} \quad g$$

The number of atoms of Kr. in a monomolecular layer,

$$N = \frac{42.4 \times 6.02 \times 10^{23}}{83.8 \times 10^{6}}$$

The customary value for the molecular cross-sectional area of krypton is $19.5 \times 10^{-2} m^2$, therefore the total surface area

$$S_T = N \times 19.5 \times 10^{-2} m^2$$

$$= \underline{0.06 m^2}$$

The sample weight was 1g therefore the specific surface area S_W was $0.06 m^2 g^{-1}$.

B-6 Conclusions

This result ($0.06 m^2 g^{-1}$) was encouragingly close to the value obtained by volumetric analysis ($0.08 m^2 g^{-1}$) and a good linear relationship was obtained over the recommended pressure range[52] (fig.B-5). Therefore, the method and apparatus did show promise although further work is required to establish a reproducible method.

Incomplete outgassing was one factor which would have reduced W_A and further work is also required to determine optimum outgassing conditions.

There was no guarantee of the accuracy of the surface area which was determined by volumetric analysis. It would be preferable to undertake future trials with standard samples of known surface area.

FIGURE B-1. Adsorption isotherm for nitrogen adsorbed onto an $Fe-Al_2O_3$ catalyst at 77·3 °K. (after Brunauer et al[47])

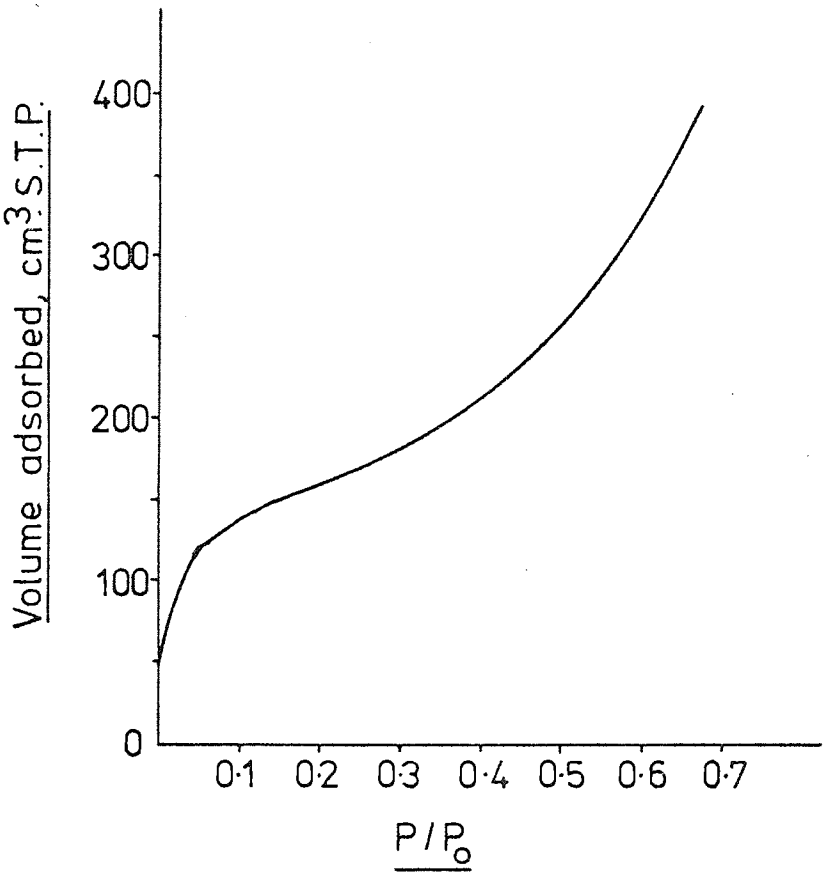

PLATE B-1 General view of the surface area apparatus

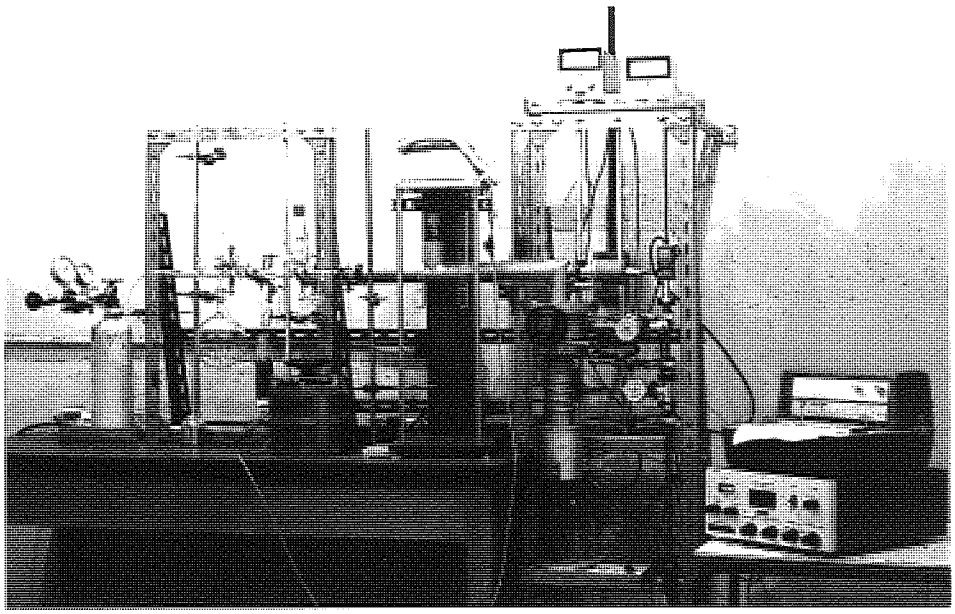

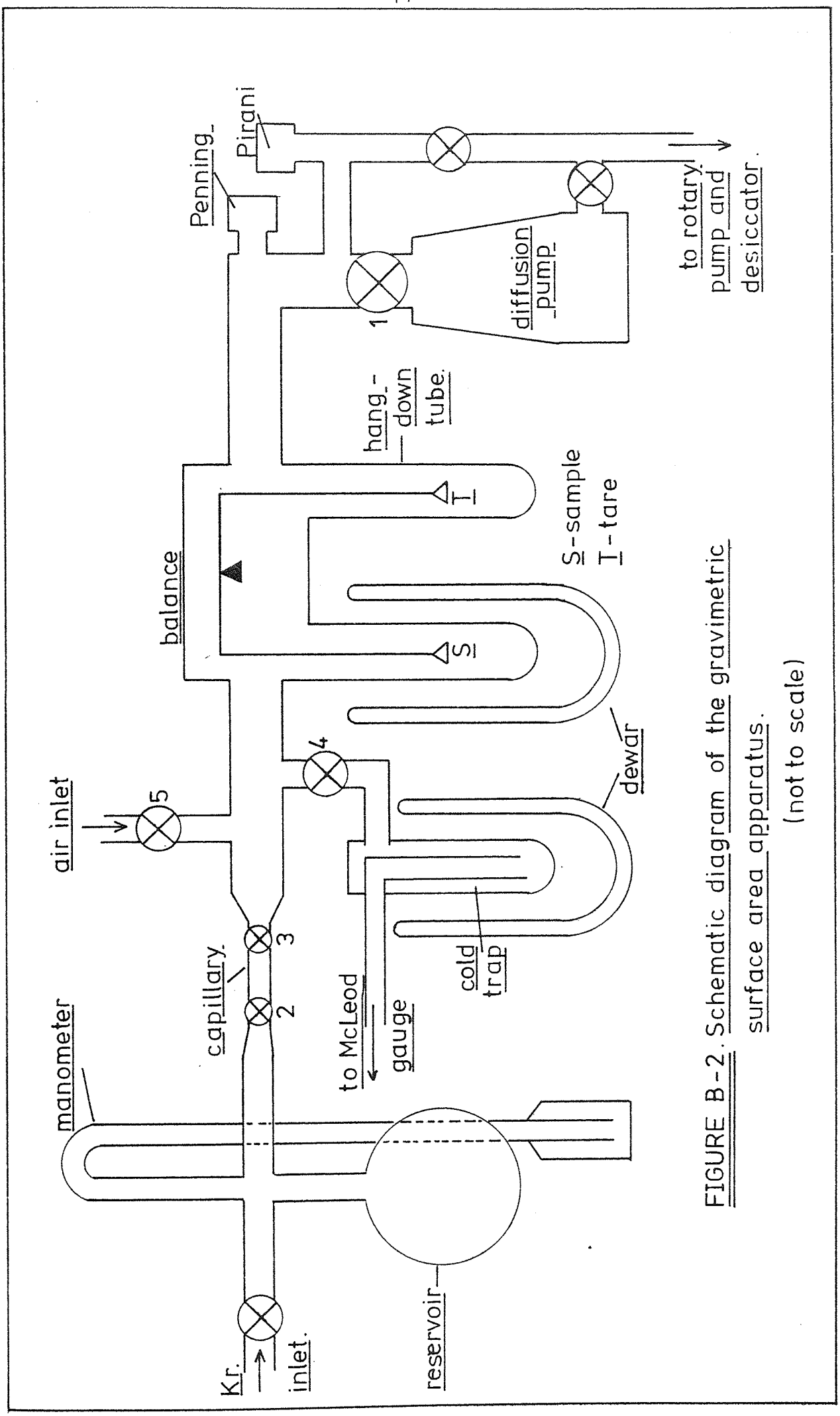

FIGURE B-2. Schematic diagram of the gravimetric surface area apparatus.

(not to scale)

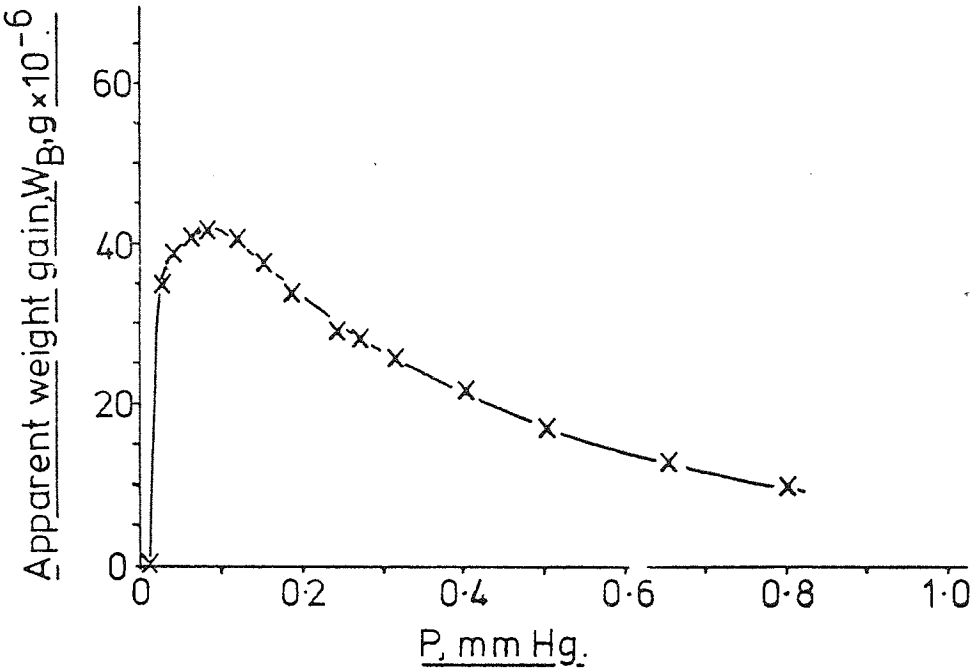

FIGURE B-3. Weight gain (W_B) for a nickel blank, as a function of equilibrium pressure. (P).

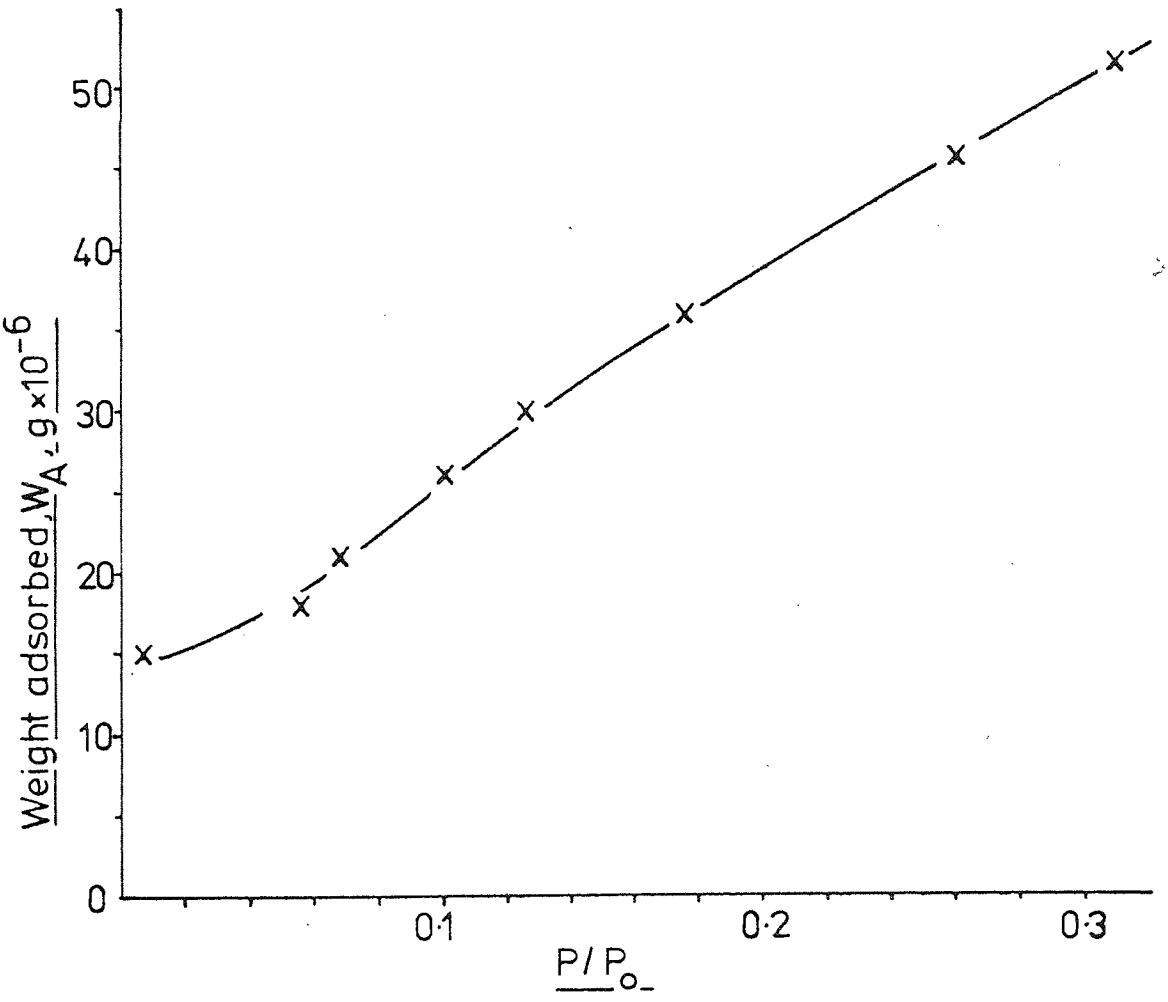

FIGURE B-4. Adsorption isotherm for krypton adsorbed onto NC100 iron powder at 77°K.

FIGURE B-5. $P/[W_A(P_o-P)]$ versus P/P_o for krypton adsorbed onto NC100 iron powder.

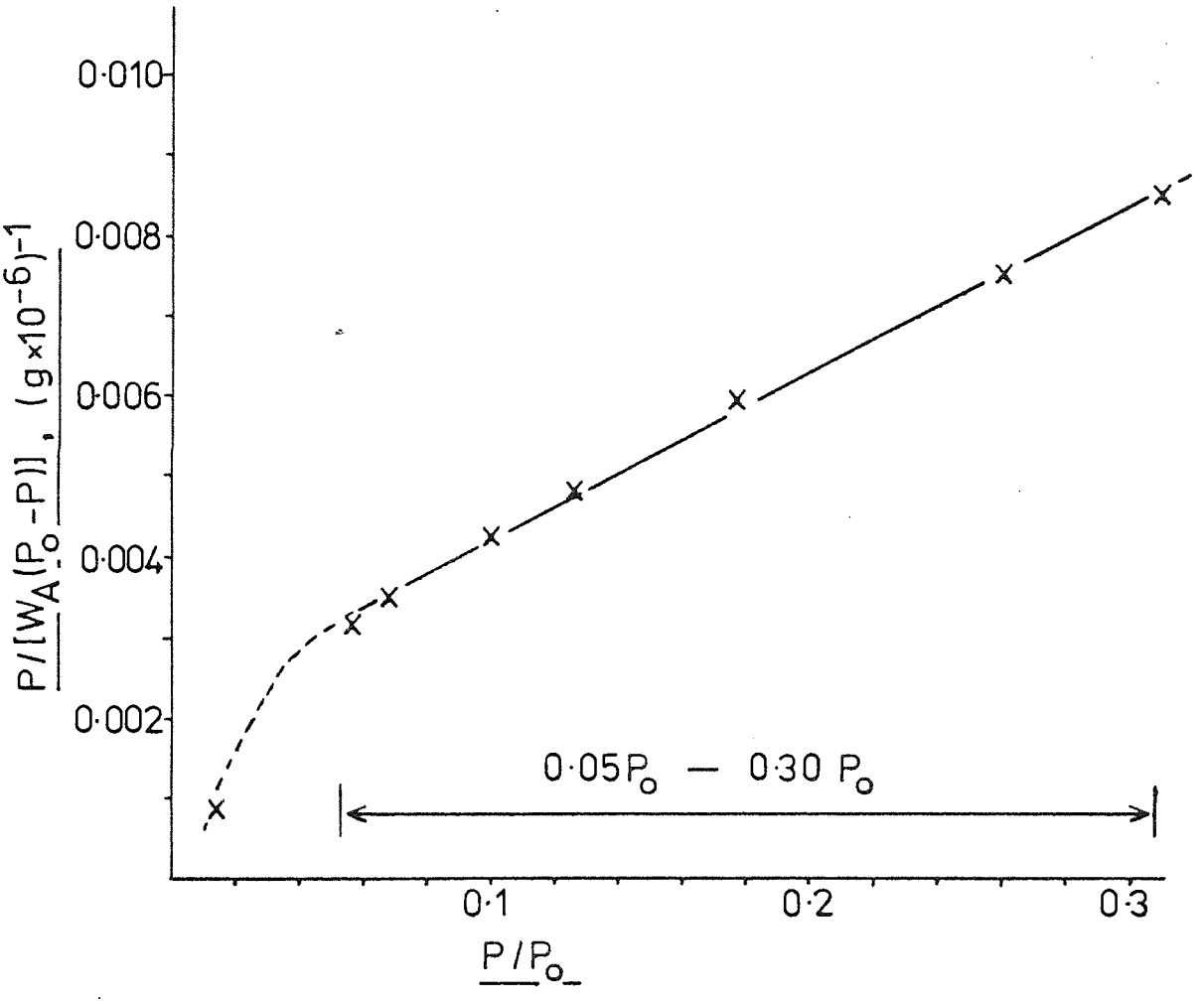

APPENDIX C

Figures C-1 to C-7

These figures show the total weight loss curves (parent curves) for compacts containing lubricants, thermogravimetrically treated at a heating rate of $6^{\circ}C.min^{-1}$. Atmosphere flow rate was 500 $ml.min^{-1}$, unless otherwise stated (figure C-7). The matrix material was as-received MP32, except for the results of figure C-7 which were obtained using MP32 (53-104μm). Compact relative density was 80% for all figures.

C-1 Zinc and lithium stearate.

C-2 Stearic acid - fine admixed.

C-3 Stearic acid - medium admixed

C-4 Stearic acid - coarse admixed.

C-5 Stearic acid - evaporated/precipitated.

C-6 Stearamide and cosmic 64 wax.

C-7 Effect of $N_2/10\%H_2$ flow rate on the decomposition of zinc stearate within compacts.

FIGURE C-1 .Zinc stearate and lithium stearate.

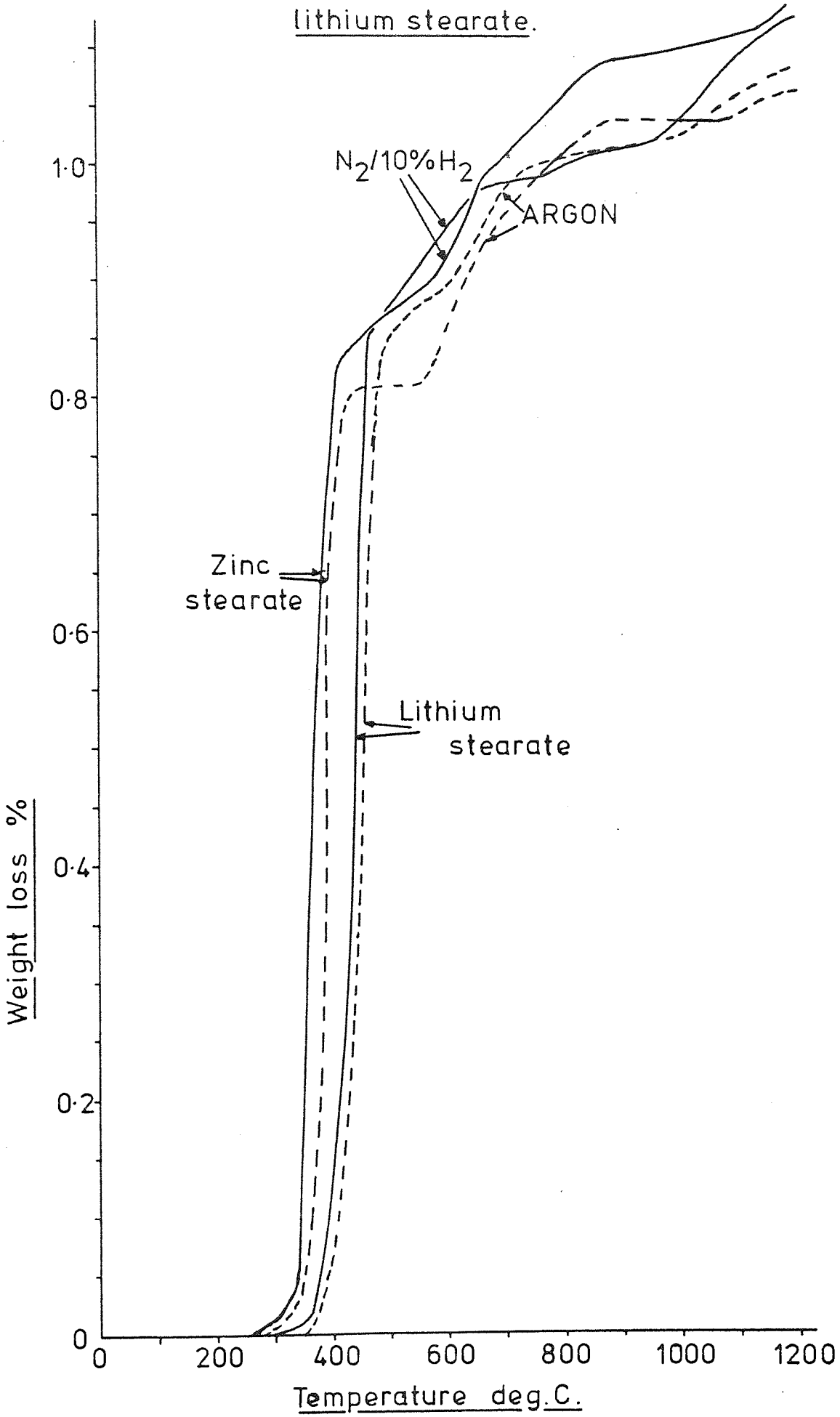

FIGURE C-2 .Fine admixed stearic acid.

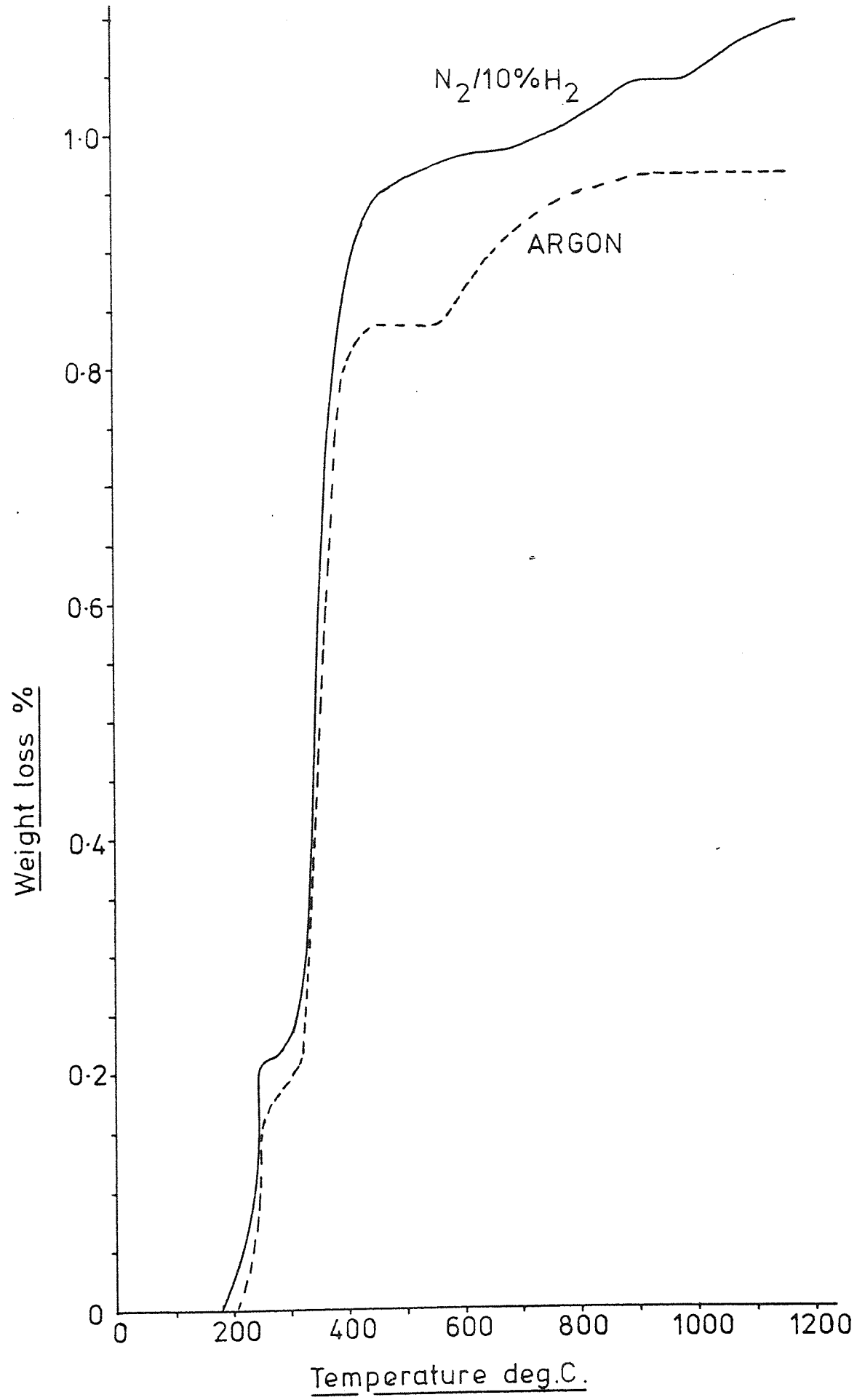

FIGURE C-3 . Medium admixed stearic acid.

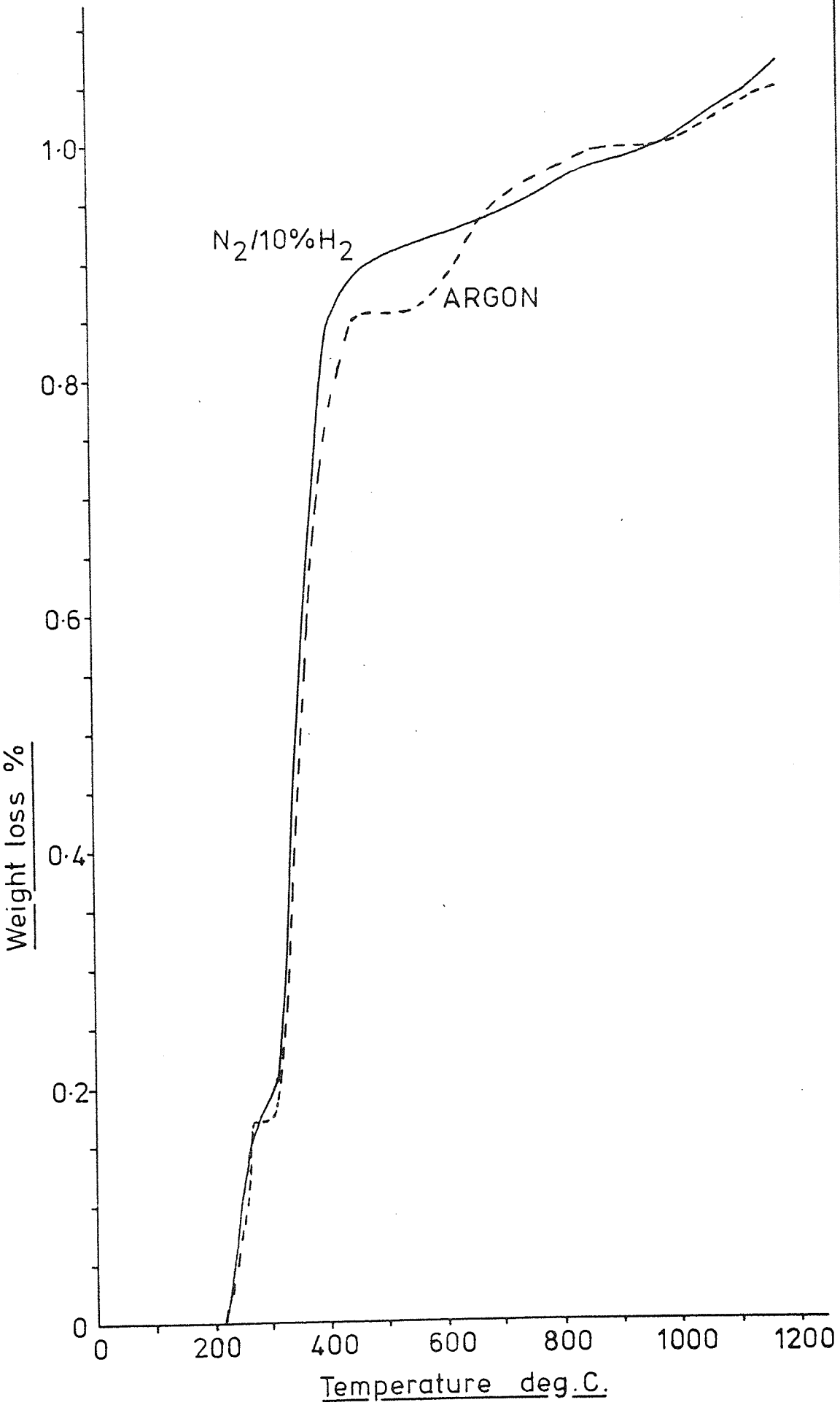

FIGURE C-4 .Coarse admixed stearic acid.

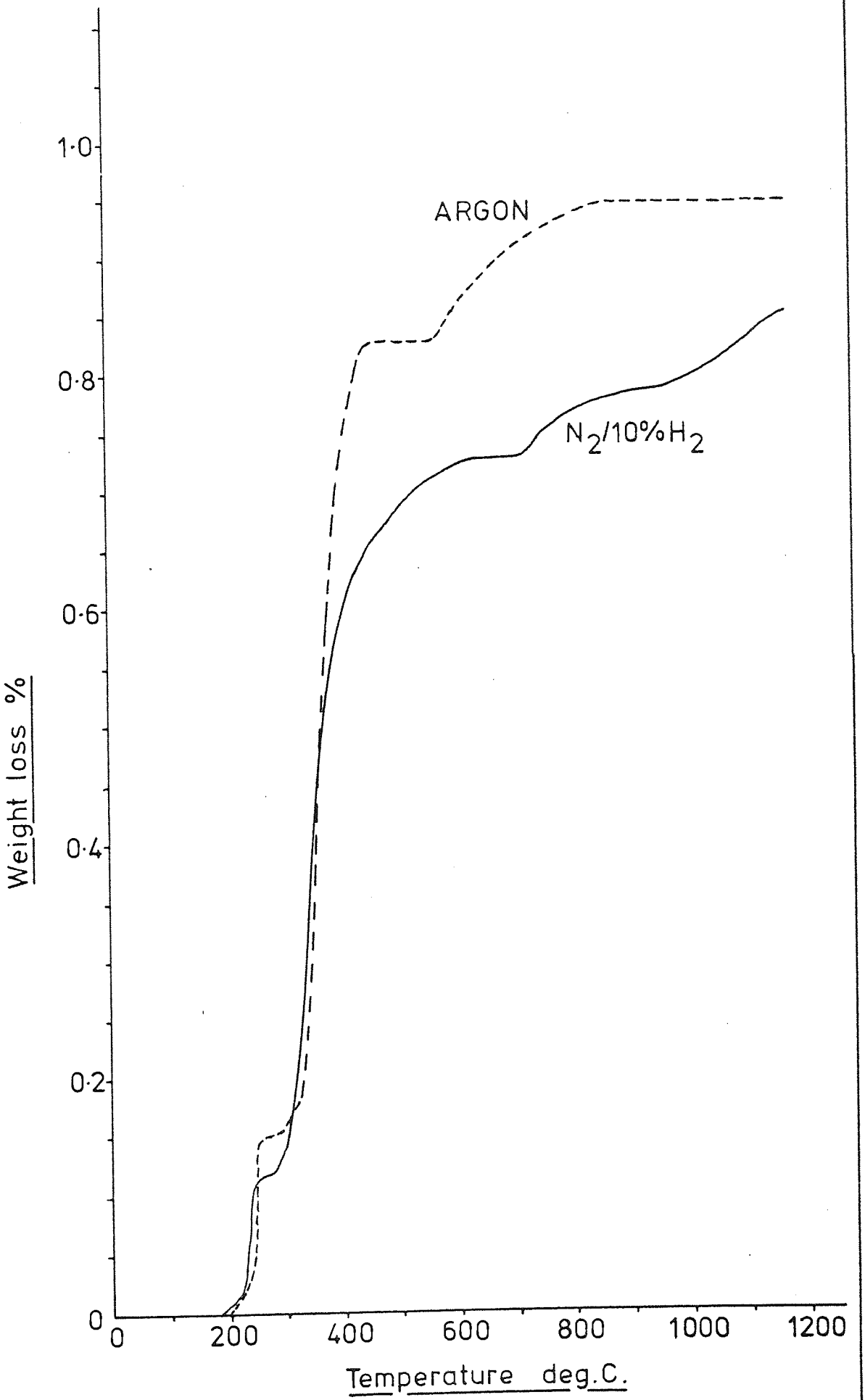

FIGURE C-5 . Stearic acid, evaporated coating.

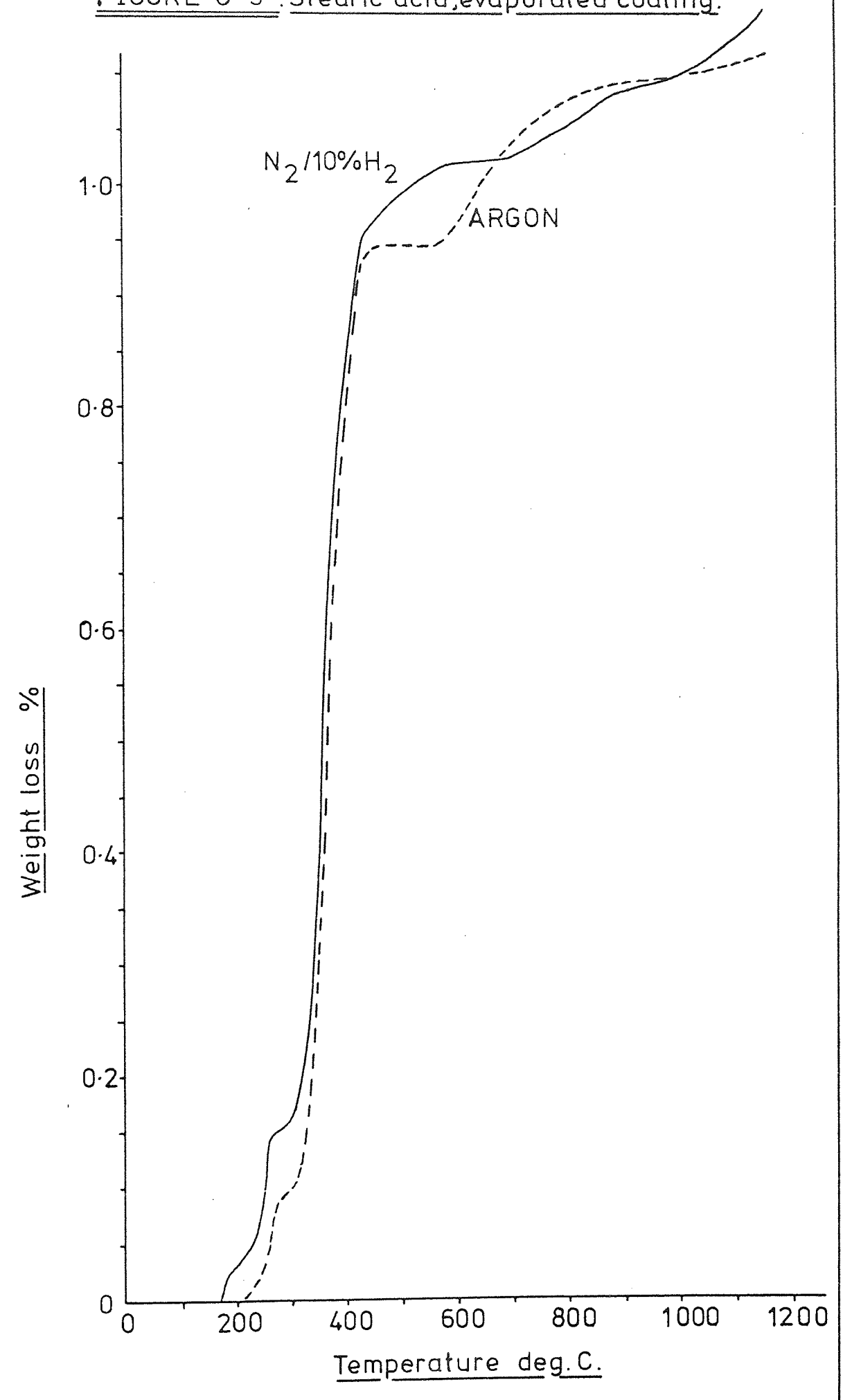

FIGURE C-6 .Stearamide and Cosmic 64 wax.

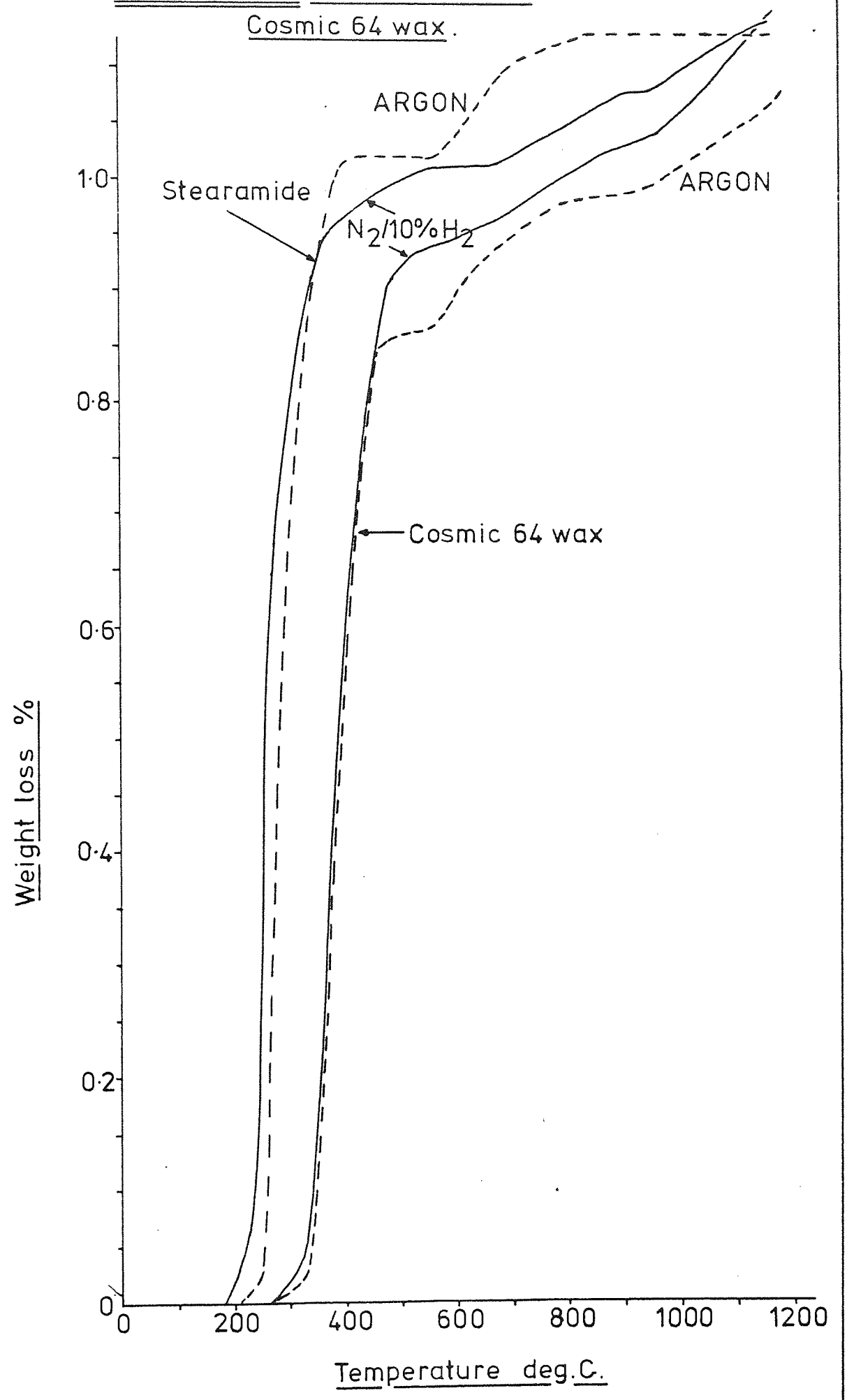

FIGURE C-7 The decomposition of zinc stearate in compacts. Atmosphere of N_2/10%H_2 with varying flowrates.

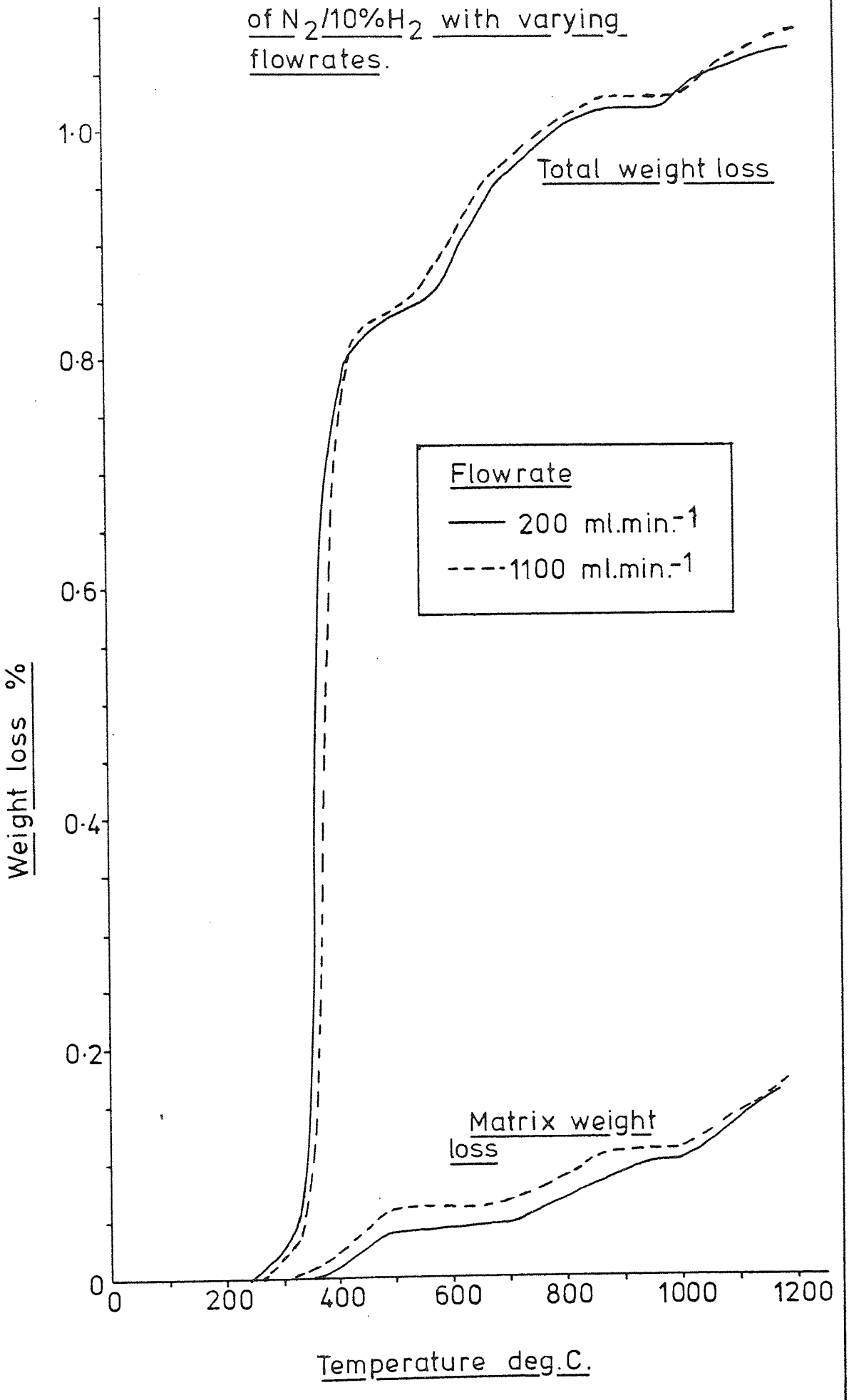

Figures C-8, C-9 and C-10.

Figures C-8 and C-9 are the parent and matrix thermograms for compacts of MP32 containing varying additions of zinc stearate. $N_2/10\%H_2$ at a flow rate of 500 $ml.min^{-1}$ was used as protective atmosphere throughout.

C-8 The effect of pore size and lubricant content on the decomposition of zinc stearate within compacts of 60% relative density.

C-9 The effect of pore size and lubricant content on the decomposition of zinc stearate within compacts of 85% relative density.

Figure C-10 shows the total and matrix weight loss curves for the decomposition of 1% lithium stearate in compacts of as-received MP32 pressed to relative densities of 60%, 80% and 85%. The protective atmosphere was $N_2/10\%H_2$ at a flow rate of 500 $ml.min^{-1}$.

All specimens in figures C-8 to C-10 were thermogravimetrically treated at a heating rate of $6^{\circ}C.min^{-1}$.

FIGURE C-8 .Matrix and total weight loss curves- the effect of density and pore size on zinc stearate decomposition within compacts.

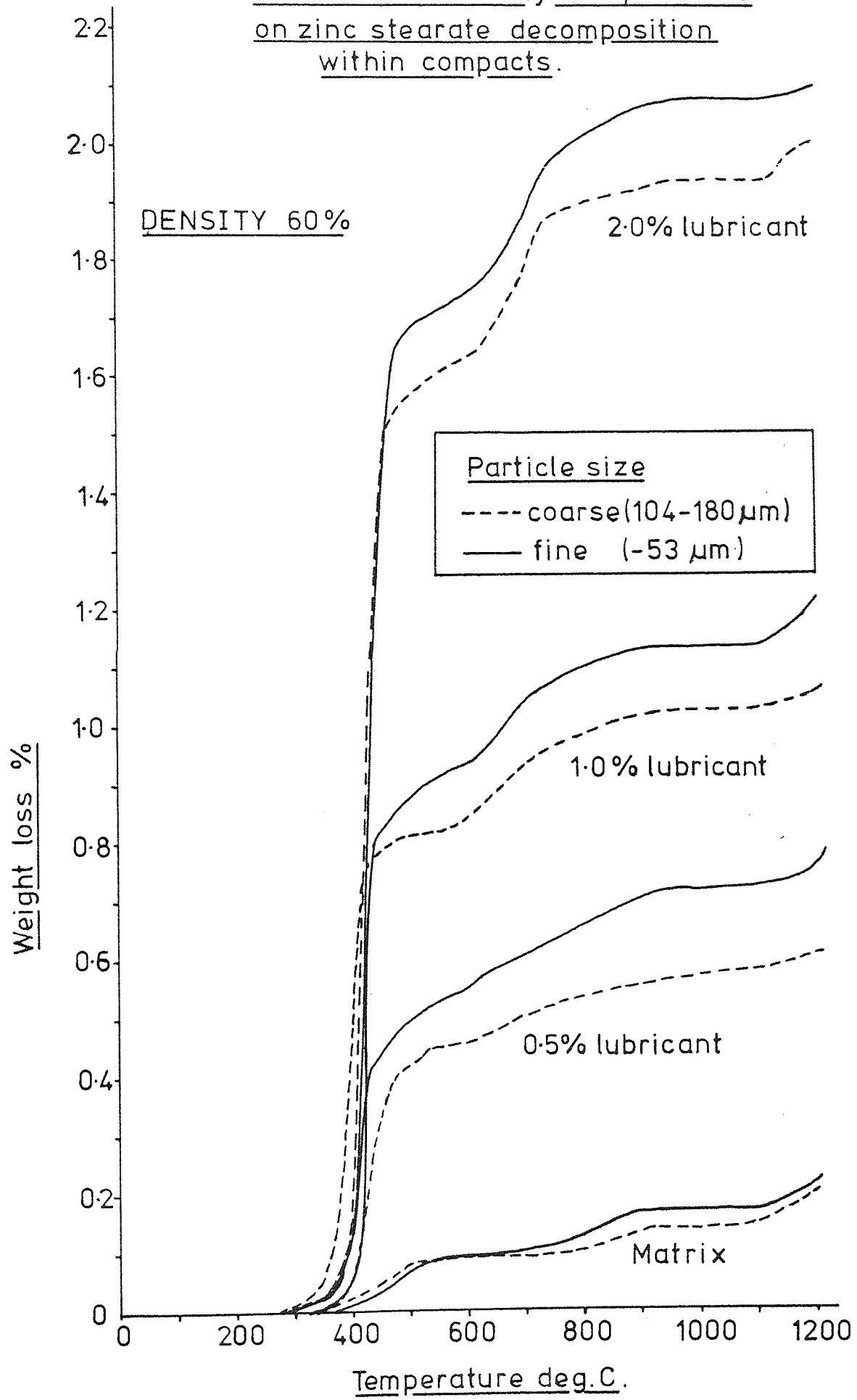

FIGURE C-9 Matrix and total weight loss curves - the effect of density and pore size on zinc stearate decomposition within compacts.

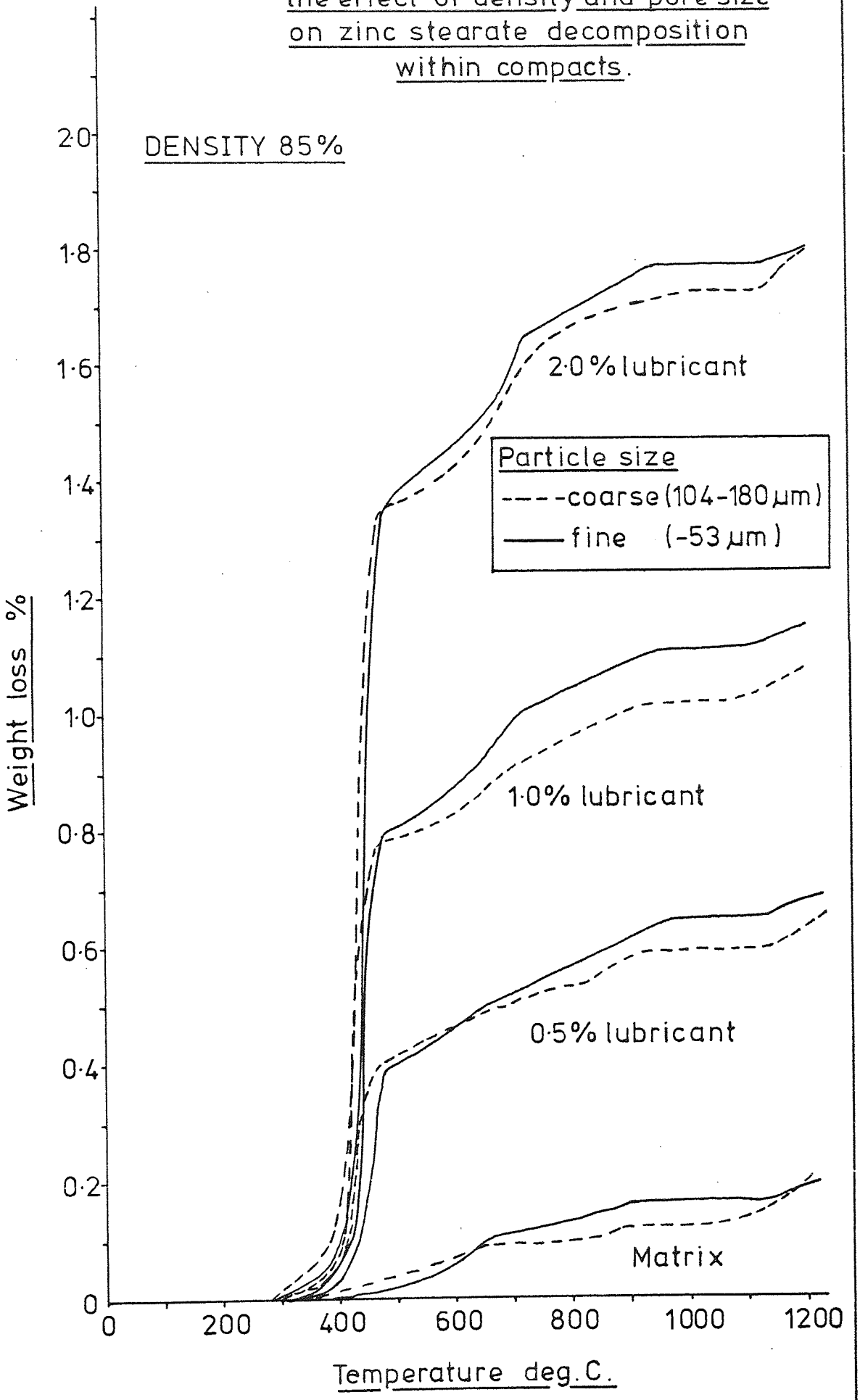

FIGURE C-10 .Total and matrix weight loss curves for lithium stearate within compacts.

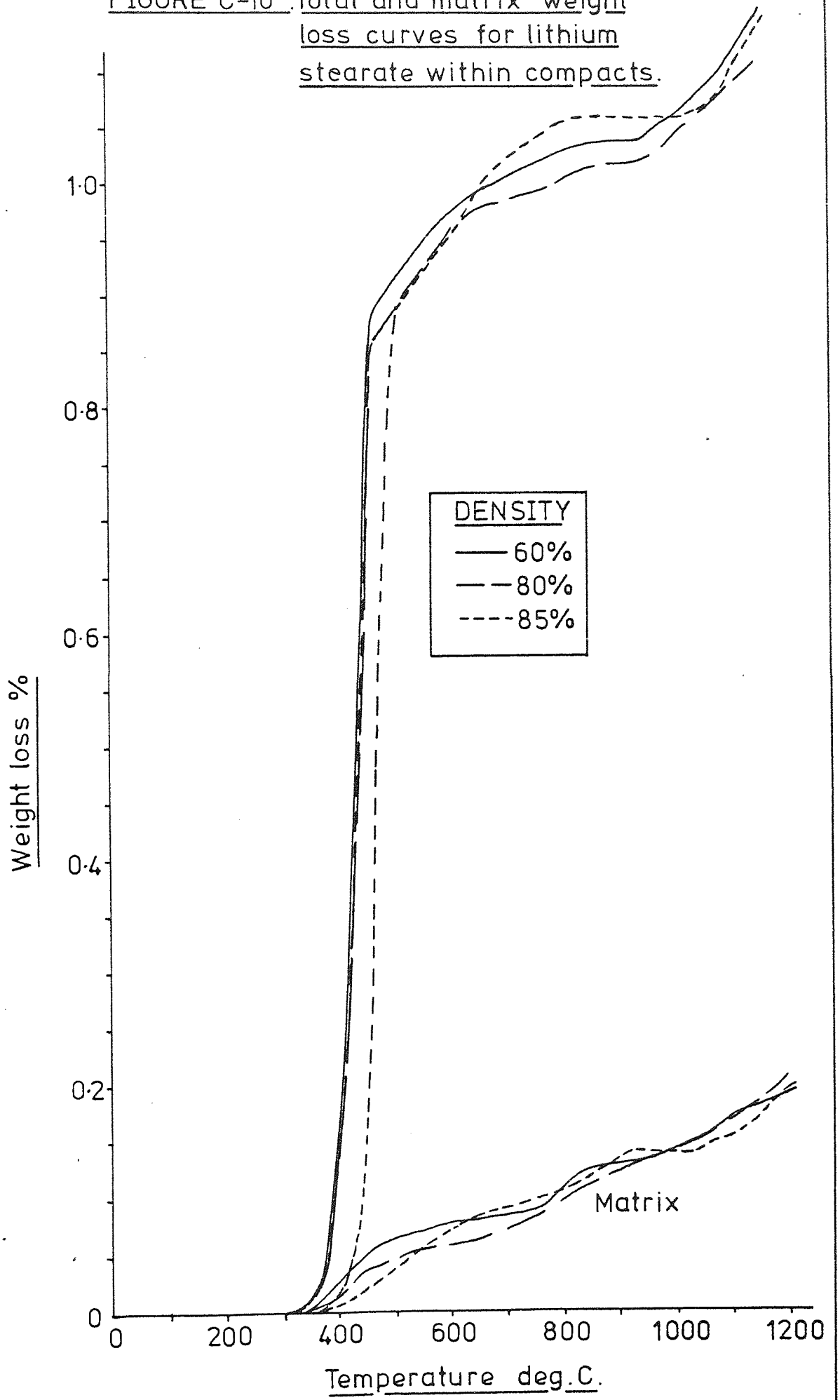

Figures C-11, C-12 and C-13.

Figures C-11 to C-13 show the parent and matrix thermograms obtained for the decomposition of 1% lubricant in compacts of MP32 (as-received) in an atmosphere of $N_2/10\%H_2$ at a high heating rate. The relative density of compacts in figures C-12 and C-13 was 80%.

C-11 The effect of compact density on the decomposition of zinc stearate, at a high heating rate.

C-12 The decomposition of zinc stearate, lithium stearate, stearamide and cosmic 64 wax within compacts at a high heating rate.

C-13 The decomposition of stearic acid within compacts at a high heating rate.

FIGURE C-11 Effect of density

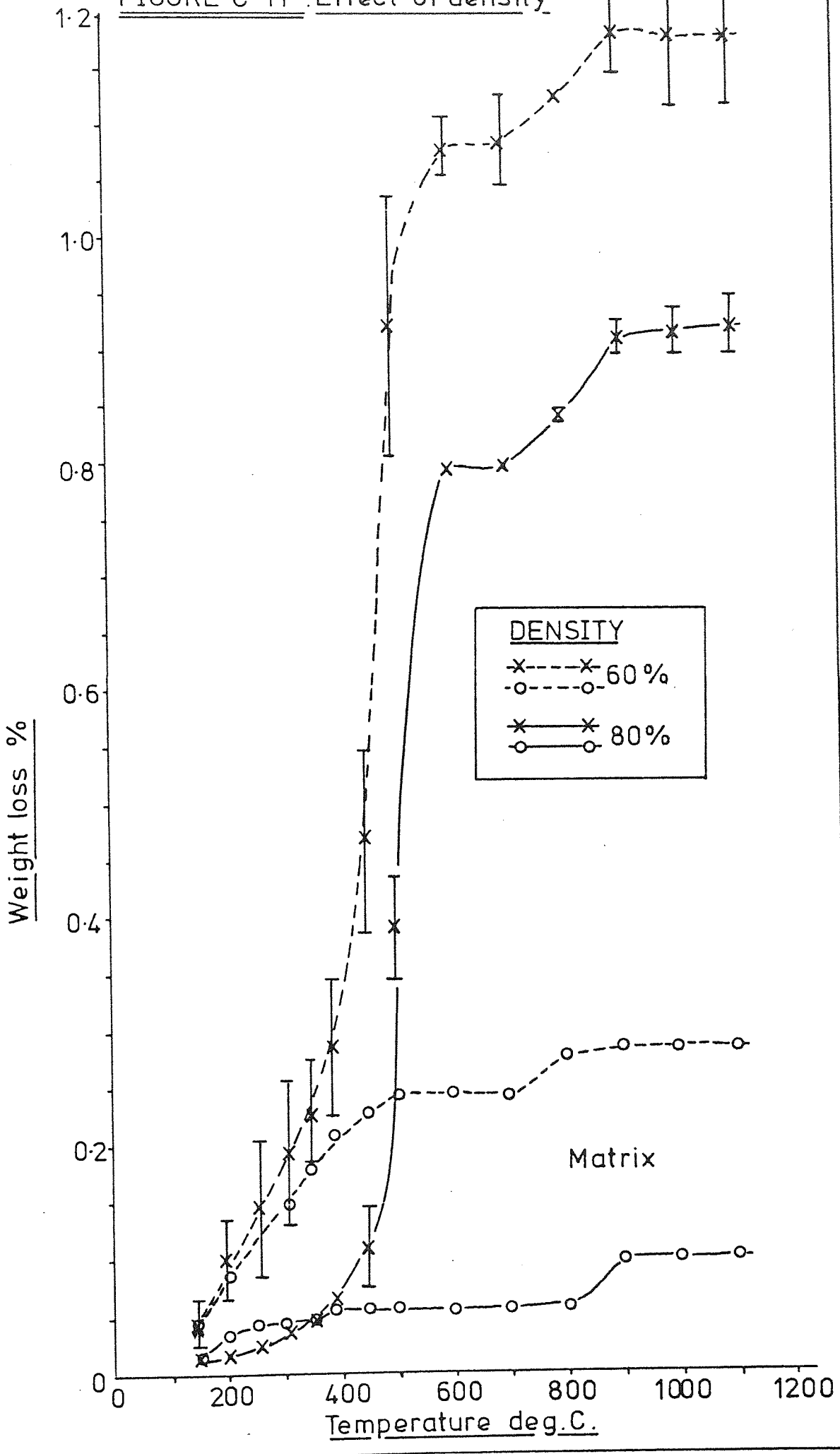

FIGURE C-12 High heating rate, total weight loss curves

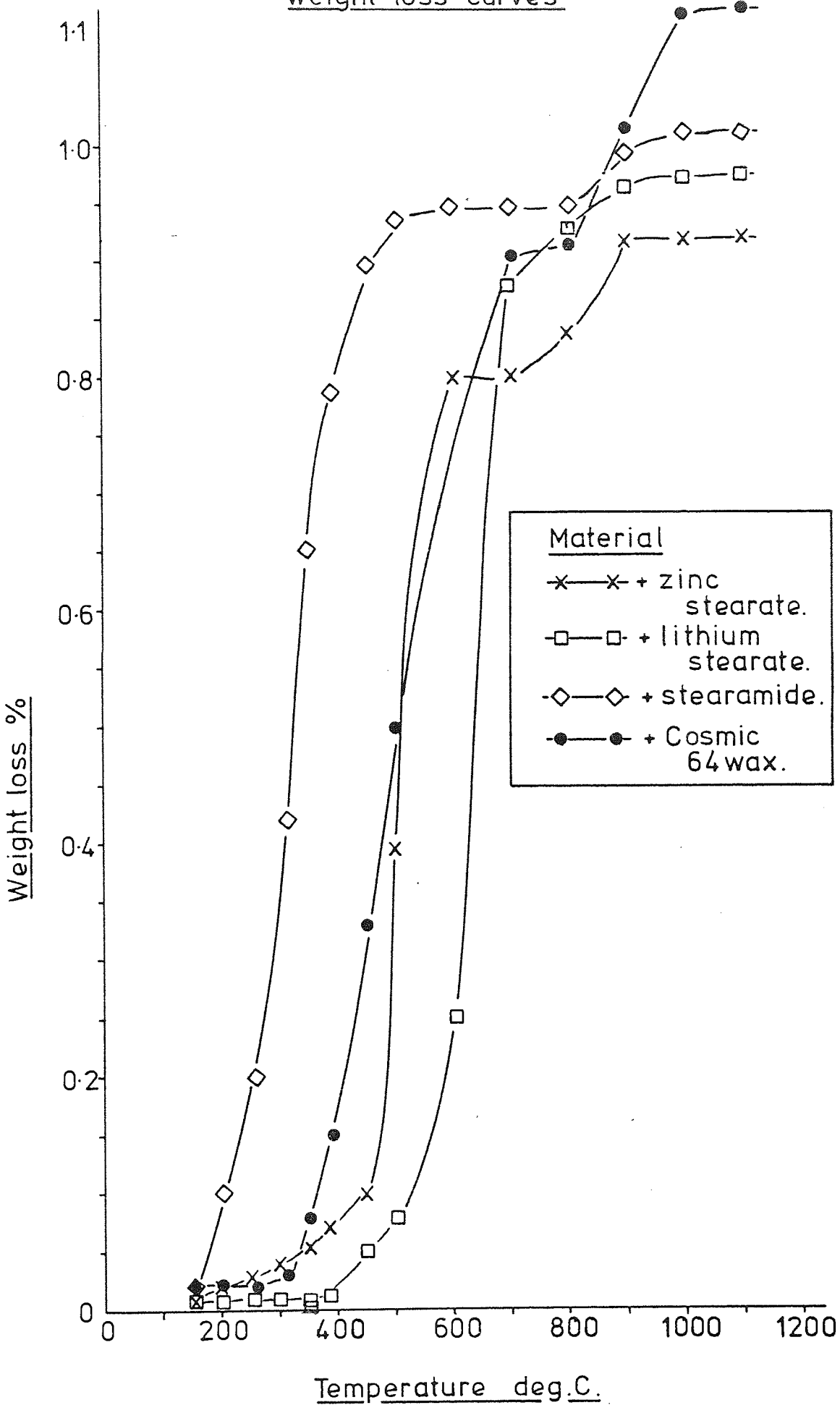

FIGURE C-13 High heating rate, total weight loss curves.

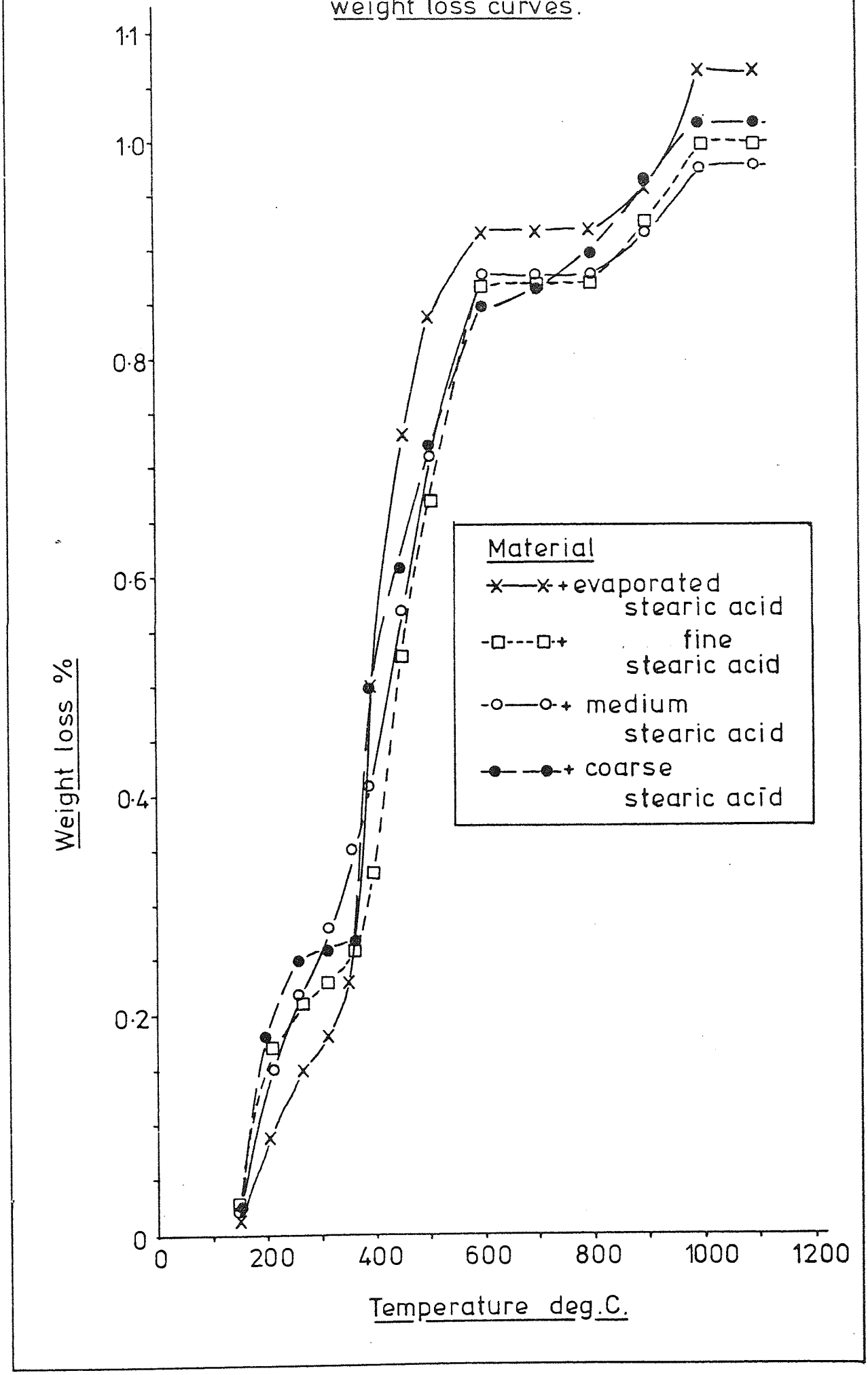

APPENDIX C

Table C-1 .The effect of heating rate on the development of mechanical properties of compacts containing lubricants.

Material and condition		Initial density $g.cm^{-3}$	Dimensional change percent.	U.T.S $N.mm^{-2}$	Final density $g.cm^{-3}$	Final carbon content percent.
No lubricant	High heating rate	5.32 6.20 6.76	-0.17 -0.17 -0.11/0.17	54/59 119/121 171/176	5.33 6.23 6.80	0.01 - 0.01
	Low heating rate	5.31 6.19 6.78	-0.33 -0.28 -0.28	73/75 149/152 213/215	5.33 6.21 6.81	0.03 - 0.01
1% zinc stearate	High heating rate	5.48 6.30 6.75	-0.28 -0.28 -0.22	52/54 108/112 130/132	5.47 6.27 6.73	N/D - 0.01
	Low heating rate	5.48 6.27 6.75	-0.39 -0.33 -0.33	84/79 147/149 203/205	5.46 6.25 6.73	0.01 - 0.01
1% lithium stearate	High heating rate	5.50 6.30 6.78	-0.28/-0.17 -0.17/-0.33 -0.17	61/53 108/112 141/133	5.47 6.27 6.77	0.01 - N/D
	Low heating rate	5.53 6.33 6.77	-0.39 -0.33/-0.39 -0.33/-0.33	80/73 137 191/187	5.50 6.31 6.80	0.01 - N/D
1% fine stearic acid	High heating rate	5.48 6.27 6.71	-0.22 -0.22 -0.22	62/67 129/121 162/165	5.45 6.23 6.70	0.01 - 0.03
	Low heating rate	5.48 6.27 6.70	-0.39/-0.45 -0.39 -0.39/-0.33	80 150/148 205/198	5.47 6.25 6.72	0.01 - 0.03
1% medium stearic acid	High heating rate	5.50 6.27 6.68	-0.28 -0.28 -0.22/-0.28	60/54 119/121 142/138	5.47 6.23 6.67	0.02 - N/D
	Low heating rate	5.48 6.25 6.70	-0.39/-0.45 -0.33 -0.28/-0.33	76/81 145 180/187	5.45 6.24 6.71	0.02 - 0.02
1% coarse stearic acid	High heating rate	5.19 5.95 6.41	-0.28 -0.28/-0.22 -0.22	48 96/90 127/130	5.16 5.92 6.37	0.02 - 0.01
	Low heating rate	5.20 6.05 6.44	-0.45 -0.33/-0.39 -0.33	59/44 110/111 158/150	5.17 6.06 6.47	0.02 - 0.01
1% evaporated stearic acid	High heating rate	5.56 6.32 6.74	-0.28 -0.28 -0.28	60/65 111/128 163/151	5.52 6.28 6.73	N/D - 0.01
	Low heating rate	5.55 6.34 6.78	-0.45/-0.39 -0.39 -0.39	85/86 160/157 211/217	5.52 6.34 6.79	0.02 - 0.01

APPENDIX C

Table C-1, continued

Material and condition		Initial density $g.cm^{-3}$	Dimensional change Percent	U.T.S $N.mm^{-2}$	Final density $g.cm^{-3}$	Final carbon content Percent
1% stearamide	High heating rate	5.39 6.13 6.59	-0.28 -0.22 -0.22	52/56 86/104 144/130	5.35 6.09 6.56	0.01 - N/D
	Low heating rate	5.42 6.16 6.59	-0.39/-0.45 -0.39 -0.33	74/75 122/123 163/159	5.39 6.14 6.59	0.02 - 0.01
1% Cosmic 64 wax	High heating rate	5.36 6.11 6.61	-0.45/-0.39 -0.33 -0.33	55/63 111/114 161/162	5.35 6.10 6.60	0.03 - 0.02
	Low heating rate	5.34 6.15 6.62	-0.45 -0.45/-0.39 -0.39	70 141/134 184/189	5.31 6.14 6.63	0.04 - 0.05
	High heating rate	5.34 6.15 6.63	-0.33/-0.39 -0.33 -0.28	54/60 118/109 172/161	5.31 6.13 6.63	- - -

N/D - not detectable.

TABLE C-2. The effect of lubricant decomposition residues on the mechanical properties of sintering compacts. $N_2/10\%\ H_2$ atmosphere.

Material	Initial Density $g.cm^{-3}$	Dimensional Change %	Final Density $g.cm^{-3}$	U.T.S. $N.mm^{-2}$	Temperature ^oC	Time min	Residual Carbon %
No Lubricant	6.24	0	6.23	9.6/10.8	500	25	0.07
	6.24	-0.06	6.24	34/38	650	0	——
	6.26	-0.11	6.28	66/98	800	0	0.03
	6.25	-0.28	6.27	102	910	0	0.02
	6.25	-0.28	6.27	101	960	0	——
	6.25	-0.28	6.27	103/105	1000	0	<0.01
	6.29	-0.20	6.30	95/112	1050	0	——
	6.27	-0.16	6.28	107/115	1100	0	<0.01
	6.27	-0.17	6.29	128/131	1100	2	<0.01
	6.25	-0.17	6.28	130/131	1100	10	——
	6.27	-0.20	6.29	132/143	1100	20	——
	6.24	-0.33/.28	6.27	135/152	1100	40	<0.01

Table C-2 continued

* N/D - not detectable

Material	Initial Density $g.cm^{-3}$	Dimensional Change %	Final Density $g.cm^{-3}$	U.T.S. $N.mm^{-2}$	Temperature ^{o}C	Time min	Residual Carbon %
1% Zinc stearate	6.31	+0.06	6.25	3.7	500	25	0.09
	6.33	-0.06	6.27	19/20	650	0	——
	6.32	-0.11	6.29	54/61	800	0	0.03
	6.32	-0.25	6.29	96/97	910	0	<0.01
	6.32	-0.28	6.29	96/97	960	0	——
	6.31	-0.28	6.29	95/97	1000	0	<0.01
	6.33	-0.22	6.30	90/103	1050	0	——
	6.33	-0.20	6.30	109/114	1100	0	<0.01
	6.31	-0.22	6.29	120/130	1100	2	N/D*
	6.31	-0.17	6.29	125/131	1100	10	——
	6.31	-0.28	6.31	131/136	1100	20	——
	6.29	-0.33/.28	6.28	145/146	1100	40	<0.01

Table C-2 continued

Material	Initial Density $g.cm^{-3}$	Dimensional Change %	Final Density $g.cm^{-3}$	U.T.S. $N.mm^{-2}$	Temperature ^{o}C	Time min	Residual Carbon %
1% lithium stearate	6.36	+0.11	6.27	3.0	500	25	0.11
	6.36	+0.11	6.27	2.7	650	0	——
	6.34	+0.11	6.27	3.5/5.3	800	0	0.06
	6.36	-0.20	6.30	67	910	0	0.03
	6.35	-0.30	6.29	70	960	0	——
	6.36	-0.28	6.30	76/79	1000	0	<0.01
	6.35	-0.22	6.31	76/95	1050	0	——
	6.34	-0.20	6.31	101/115	1100	0	<0.01
	6.35	-0.20	6.31	115/119	1100	2	N/D
	6.36	-0.22	6.33	128/129	1100	10	——
	6.35	-0.30	6.33	140/142	1100	20	——
	6.30	-0.28/.39	6.30	142/143	1100	40	<0.01

Table C-2 continued

Material	Initial Density $g.cm^{-3}$	Dimensional Change %	Final Density $g.cm^{-3}$	U.T.S. $N.mm^{-2}$	Temperature ^{o}C	Time min	Residual Carbon %
1% medium admixed stearic acid	6.30	0	6.24	3.7/4.6	500	25	0.06
	6.30	-0.06	6.24	8.5/12	650	0	——
	6.29	-0.17	6.25	46/58	800	0	0.04
	6.31	-0.30	6.27	92/96	910	0	0.02
	6.30	-0.33	6.28	95	960	0	——
	6.30	-0.28	6.27	89/99	1000	0	0.02
	6.30	-0.25	6.27	95/104	1050	0	——
	6.30	-0.25	6.27	111/121	1100	0	< 0.01
	6.30	-0.25	6.28	121/124	1100	2	< 0.01
	6.30	-0.22	6.27	121/128	1100	10	——
	6.30	-0.28	6.28	131/136	1100	20	——
	6.26	-0.39/.39	6.26	132/139	1100	40	< 0.01

Table C-2 continued

Material	Initial Density $g.cm^{-3}$	Dimensional Change %	Final Density $g.cm^{-3}$	U.T.S. $N.mm^{-2}$	Temperature ^{o}C	Time min	Residual Carbon %
1% stearic acid. Evaporated/Precipitated.	6.41	0	6.34	3.4	500	25	0.10
	6.41	-0.03	6.33	5.1/6.8	650	0	——
	6.38	-0.14	6.33	34/68	800	0	0.03
	6.42	-0.33	6.37	96/101	910	0	0.03
	6.41	-0.33	6.37	101/102	960	0	——
	6.41	-0.25	6.37	94/102	1000	0	0.02
	6.39	-0.25	6.35	110/114	1050	0	——
	6.37	-0.23	6.34	114/125	1100	0	<0.01
	6.41	-0.28	6.37	132/140	1100	2	0.02
	6.37	-0.28	6.35	138/142	1100	10	——
	6.39	-0.33	6.37	148/149	1100	20	——
	6.28	-0.33/.39	6.27	145/151	1100	40	<0.01

APPENDIX C

TABLE C-3 The effect of lubricant decomposition residues on the mechanical properties of sintering compacts. Argon atmosphere

Material	Initial Density $g.cm^{-3}$	Dimensional Change %	Final Density $g.cm^{-3}$	U.T.S. $N.mm^{-2}$	Temperature ^{o}C	Time min.
No Lubricant	6.30	0	6.30	4.5/5.2	500	25
	6.29	0/-0.06	6.29	12.5/15.1	650	0
	6.30	-0.11	6.32	65/77	800	0
	6.27	-0.17	6.27	105/106	910	0
	6.28	-0.17	6.30	108/112	910	0
	6.29	-0.22	6.33	104/106	1000	0
	6.31	-0.28	6.34	105/113	1100	0
	6.31	-0.28	6.35	113	1100	2
	6.30	-0.39/.33	6.34	111/117	1100	10
	6.31	-0.39/.33	6.35	113/118	1100	20
	6.25	-0.39/.50	6.29	112	1100	40

Table C-3 continued

Material	Initial Density $g.cm^{-3}$	Dimensional Change %	Final Density $g.cm^{-3}$	U.T.S. $N.mm^{-2}$	Temperature ^{o}C	Time min.
1% zinc stearate	6.30	+0.06	6.25	3.1/3.5	500	25
	6.30	-0.06	6.26	13/31	650	0
	6.30	-0.11/.17	6.27	78/80	800	0
	6.30	—	6.28	96/97	910	0
	6.28	-0.17/.22	6.27	95	910	0
	6.29	-0.28	6.26	96	1030	0
	6.30	-0.33/.33	6.28	95/102	1100	0
	6.31	-0.33	6.28	98/105	1100	2
	6.30	-0.39	6.29	111/112	1100	10
	6.33	-0.39/.45	6.30	111/113	1100	20
	6.28	-0.50	6.27	113/115	1100	40

Table C-3 continued

Material	Initial Density $g.cm^{-3}$	Dimensional Change %	Final Density $g.cm^{-3}$	U.T.S. $N.mm^{-2}$	Temperature ^{o}C	Time min.
1% lithium stearate	6.28	+0.11	6.23	3.1/3.5	500	25
	6.28	+0.11	6.23	3.1	650	0
	6.28	+0.06/-.06	6.24	5/43	800	0
	6.30	-0.22/.28	6.26	81/77	910	0
	6.28	-0.33	6.25	77/80	1000	0
	6.29	-0.39	6.26	94	1100	0
	6.28	-0.39	6.26	95/98	1100	2
	6.27	-0.50	6.28	101/104	1100	10
	6.28	-0.56	6.28	102/112	1100	20
	6.29	-0.56	6.30	108/113	1100	40

Table C-3 continued

Material	Initial Density $g.cm^{-3}$	Dimensional Change %	Final Density $g.cm^{-3}$	U.T.S. $N.mm^{-2}$	Temperature ^{o}C	Time min
1% admixed medium stearic acid	6.27	0	6.23	3.5/3.8	500	25
	6.27	0	6.24	4.1/3.7	650	0
	6.27	-0.06/.11	6.25	36/92	800	0
	6.27	-0.17	6.26	86/91	910	0
	6.27	-0.28/.33	6.25	93/94	1000	0
	6.27	-0.28/.33	6.24	91/100	1030	0
	6.29	-0.28/.33	6.27	97/107	1100	0
	6.27	-0.33/.39	6.27	98/106	1100	2
	6.27	-0.33/45	6.27	101/103	1100	10
	6.27	-0.50	6.27	108/108	1100	40

Table C-3 continued

Material	Initial Density $g.cm^{-3}$	Dimensional Change %	Final Density $g.cm^{-3}$	U.T.S. $N.mm^{-2}$	Temperature ^{o}C	Time min.
1% stearic acid. Evaporated/ precipitated.	6.29	0	6.26	3.5	500	25
	6.31	0/-0.06	6.27	3.8/7.0	650	0
	6.30	-0.11/.17	6.28	59/78	800	0
	6.30	-0.28	6.28	95/97	910	0
	6.30	-0.28/.39	6.29	92/94	1000	0
	6.31	-0.28/.33	6.27	96/98	1030	0
	6.31	-0.39	6.28	101/107	1100	0
	6.30	-0.39/.45	6.28	104/109	1100	2
	6.30	-0.45	6.29	104/112	1100	10
	6.30	-0.39/.50	6.29	110/113	1100	20
	6.30	-0.50	6.29	115	1100	40

APPENDIX D

The decomposition characteristics of Metalub and Durham zinc stearate 'A'.

Introduction

The decomposition characteristics of two commercial lubricants (Ex. B.S.A. Ltd.), Swedish Metalub and Durham Zinc Stearate A (fused and ground), have been established by thermogravimetric analysis. All thermogravimetric tests were carried out in a modified Stanton thermobalance using an atmosphere of dry $N_2/10\%H_2$, flow rate 500 $ml.min^{-1}$ and a heating rate of $6^{o}C$ min^{-1}. Compacts 12.7mm diameter, 10g weight were pressed from MP32 iron powder, the tool set used allowed a maximum density of 87% (6.8g cm^{-3}) to be achieved with mixes containing 1% lubricant. Compressibility and ejection stress ($\frac{\text{maximum ejection Load}}{\text{friction surface area}}$) were determined for 1% lubricant mixes for comparison with a technical grade of zinc stearate. Compacts 28.6mm diameter and 60g weight were used.

Results and Discussion.

Figure D-1 shows the thermogravimetric curves for the pure lubricants. There is little difference at this heating rate between Metalub and the zinc stearate in terms of stearate removal however, Metalub does appear to contain less zinc with a corresponding increase in the proportion of the stearate radical. Metalub also has a tendency to leave a sooty residue after high temperature decomposition and a larger ZnO reduction temperature range, as can be seen from the thermogravimetric curve.

Lubricant reactions within compacts are shown in figure D-2. The main difference between the two lubricants is again the degree of removal, no difference in the decomposition characteristics of the stearate radical are apparent. Lubricant removal is more complete for the zinc stearate. It may be noted that the proportion of zinc oxide in the lubricants as indicated in figure D-2 compare favourably with those indicated by figure D-1 (Metalub

11% and 0.11%, zinc stearate 14% and 0.14%). This would suggest that the lower weight loss exhibited by Metalub in figure D-2 is due to a residue of carbon.

The results of isothermal dewaxing are shown in figures D-3 and D-4 for Metalub and Zinc Stearate A respectively. The rate and extent of stearate removal are obviously critically dependent on isothermal temperature, both increase rapidly with increasing temperature. The dewaxing characteristics of a compact have also been observed to depend on compact density. At low/ medium densities and lubricant contents, such that the total volume of lubricant is less than the total pore volume, lubricants are observed to decompose within the compact and are removed directly as vapour which recondenses on a cooler part of the sintering apparatus. No melting or surface reaction is observed. In this case there is sufficient space within pores for melting and decomposition to occur. At high densities and lubricant contents, such that the lubricant volume is equal to or theoretically greater than the pore volume, molten lubricant exudes from surface pores prior to decomposition until there is sufficient space for melting and decomposition to occur within the compact. Exudation of molten lubricant is probably also aided by expansion of entrapped gases. Decomposition then proceeds by simultaneous breakdown of lubricant within pores and that on the surface, the latter results in carbonaceous surface deposits the effects of which may often be seen on the surface of a fully sintered compact (fig. D-5).

Compacts 87% dense with 1% lubricant, as used in this investigation, probably exhibit similar behaviour to compacts with a higher density and lower lubricant content. The surface deposits on the isothermal specimens resulting from the second process of stearate removal are shown in the photomacrographs of figure D-5(c). At 60% and 80% dense no surface deposits are formed, but at 85% dense deposits are produced.

It is possible to calculate the maximum pressure increase within a

compact due to stearate decomposition, assuming instantaneous breakdown to simple hydrocarbon gases such as ethylene (C_2H_4) and sealed pores. For a 1% addition of stearate in a compact 90% dense (7.1g cm^{-3}) the pressure increase is of the order of 1300 atmospheres at 400°C. This figure is probably grossly overestimated since decomposition always occurs over a temperature range, the removal of a stearate is more akin to volatilisation than breakdown to simple hydrocarbons, pores are rarely entirely closed and any back reaction has been ignored. However, assuming only 10% decomposes at any instant the possible pressure increase could still be in excess of 100 atmospheres and hence greater than the green strength of a compact.

The consequences of this pressure build up are shown in figure D-6 Tensiles containing no lubricant, 1% zinc stearate and 1% Cosmic 64 wax, were formed over a range of densities from 5.0g cm^{-3} to 6.9g cm^{-3}. These were dewaxed and partially sintered in $N_2/10\%H_2$ by placing them directly into a furnace hot zone at 1100°C. The overall heating rate was 110°C min^{-1}, maximum 284°C min^{-1}, the specimens were left in the furnace to give an effective 2 minutes at 1100°C.

Two effects are evident from these curves:-

(a) tensiles with no lubricant and wax exhibit a normal density/U.T.S. relationship, whilst addition of zinc stearate produces an inverted relationship,

(b) there is a slight increase in strength with a wax addition but a marked decrease for an addition of zinc stearate.

Under slow heating rates these effects were not observed.

The inversion caused by zinc stearate may be explained by the pressure increase caused by stearate decomposition. Optimum strength is developed at an intermediate density, at low densities the pressure increase is low but so is the green strength. An intermediate density is a compromise between green strength and pressure. There was found to be slightly more residual

carbon in the tensiles containing wax and, although this was insufficient to cause the strength increase shown in figure D6, it does suggest that break-down of the wax caused carbon deposition at an earlier stage. This would have aided sintering and consequently faster repair of the pressure damage. The latter comment assumes that the damage due to the pressure increase is temporary. That this is so has been demonstrated by some tests that were carried out to give an effective 3 minutes at 1100°C, as shown by the curves in figure D-6. Tensiles containing no lubricant or wax were basically unchanged but tensiles containing zinc stearate assumed a normal density/U.T.S. relationship. Unfortunately these tests were carried out some 12 months after the initial investigation and there is an apparent strength decrease for a longer sintering time. This is probably due to variations in powder batch properties. Rechecks have also been carried out at 2 minutes effective at 1100°C (fig. D6) and these confirm the earlier results. This effect is obviously very temporary in a simple shaped compact such as a tensile. However, the effects may be more serious and permanent in a complex shape, especially one in which changes in section are associated with changes in density.

It can be seen from this discussion that care must be taken in choosing the correct dewaxing temperature for a given compact. Stearate radical removal is generally complete when the compact reaches a temperature of the order of 450°C, figure D-2. At this temperature all the stearate radical should have decomposed, so that if a compact containing a stearate is introduced into a sintering zone in excess of 450°C a high heating rate is imposed on the compact which provides a large driving force for stearate decomposition, resulting in a large pressure increase. With a slow heating rate, such as that used in the thermobalance ($6^{\circ}C\ min^{-1}$), pressure build up is not a problem since the heating rate imposed by the furnace is the driving force for the reaction. It can be seen from figures D-3 and D-4 that

stearate decomposition will proceed isothermally at temperatures such as 300°C and 350°C at a rate strongly dependent on the temperature. Low heating rates are probably not commercially viable, but an isothermal treatment at a temperature less than 450°C would be, the object being the removal of most but not necessarily all of the stearate radical with a minimum pressure increase.

As can be seen from figures D-3 and D-4, as the isothermal temperature approaches 410°C-420°C stearate radical decomposition becomes more rapid and more complete. However, much of the stearate is removed during the heating stage, with high commercial heating rates this would be undesirable. At 350°C much, although not all, of the stearate radical is removed at a gentle rate with very little being removed during heating up. The zinc stearate would require 50-60min at 350°C for maximum removal and Metalub would require 80-90min at the same temperature. These may be rather long so that a temperature in the region of 370°C-380°C would probably be the ideal compromise. Metalub would require the higher temperature.

Figures D-7 and D-8 are comparisons of Metalub, zinc stearate A and technical zinc stearate in terms of compressibility and ejection stress respectively. It can be seen that Metalub is the poorest on both counts despite its high stearate content. For compressibility the difference is well in excess of the experimental reproducibility error, for ejection stress the difference is not so marked. This effect may be caused by a difference in particle size. It was not possible to determine particle sizes but the Metalub does appear to be coarser.

Conclusions

Isothermal dewaxing treatments should be beneficial in the removal of lubricants, particularly from high density compacts. An isothermal temperature of 370°C is suggested for Durham zinc stearate A and 380°C for Metalub,

the optimum time at temperature would depend on compact geometry, as would the heating up time.

FIGURE D-1. Thermogravimetric curves - pure lubricants.

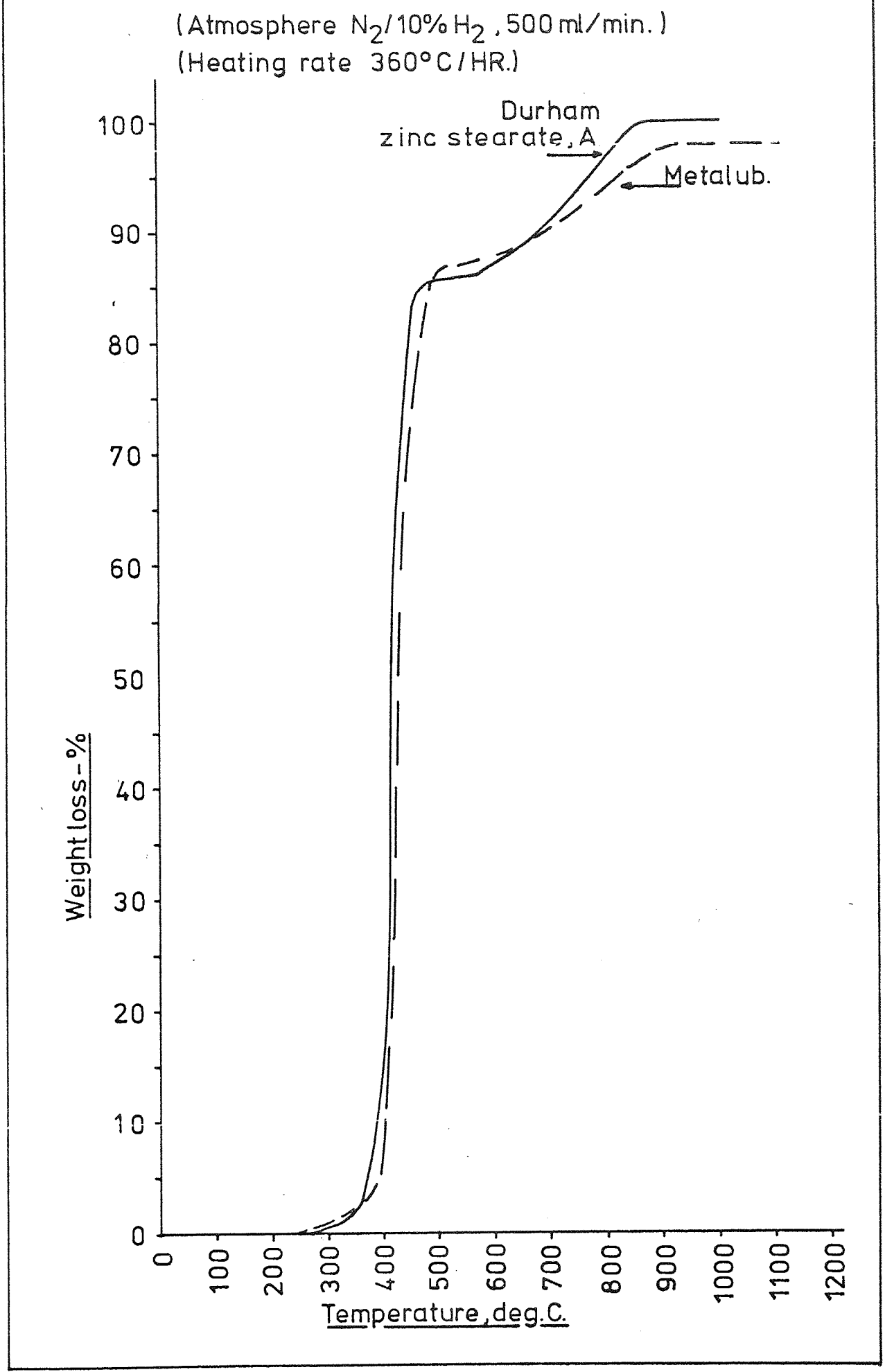

FIGURE D-2 Thermogravimetric curves - compacts containing 1·0 % lubricant.

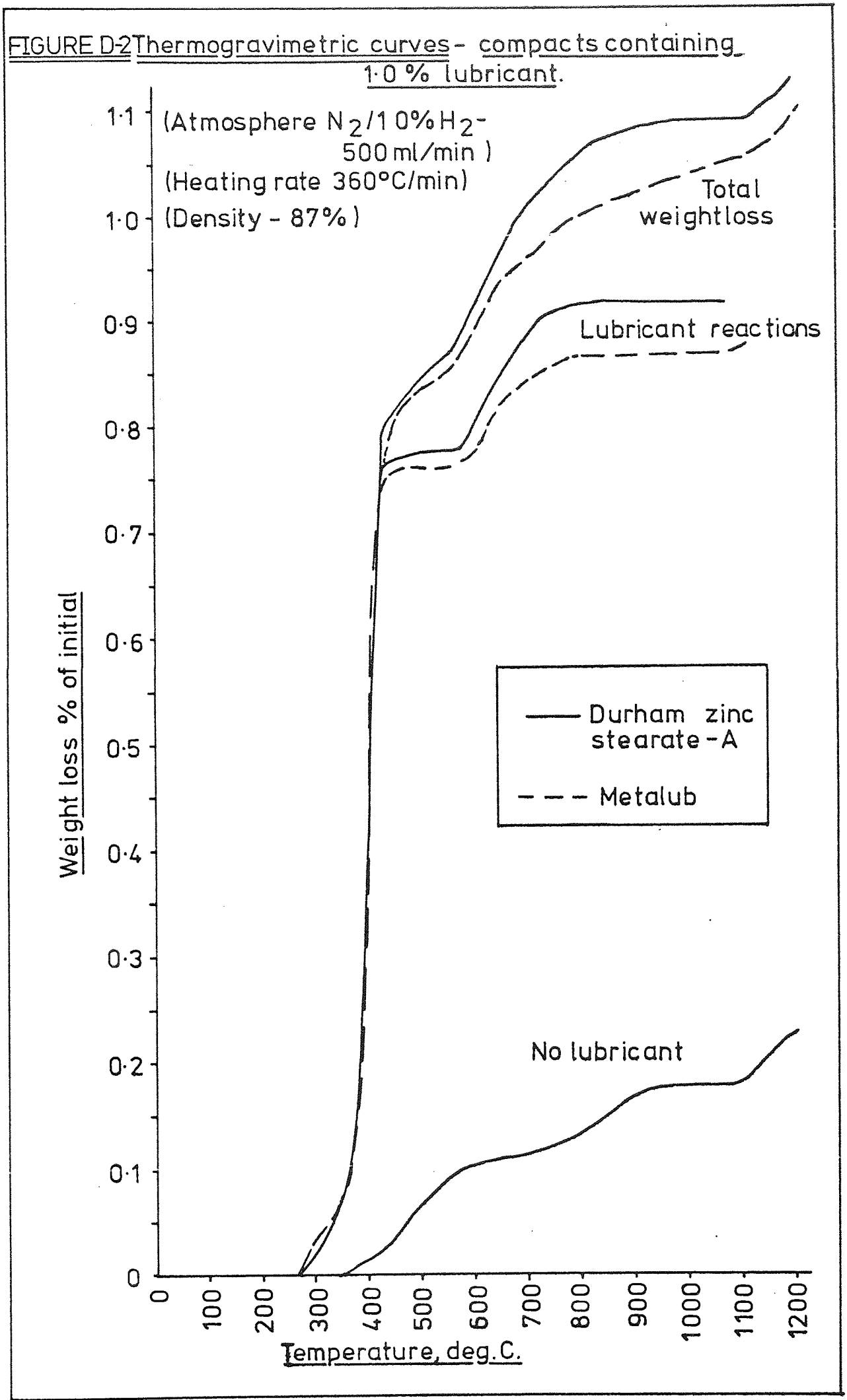

FIGURE D-3

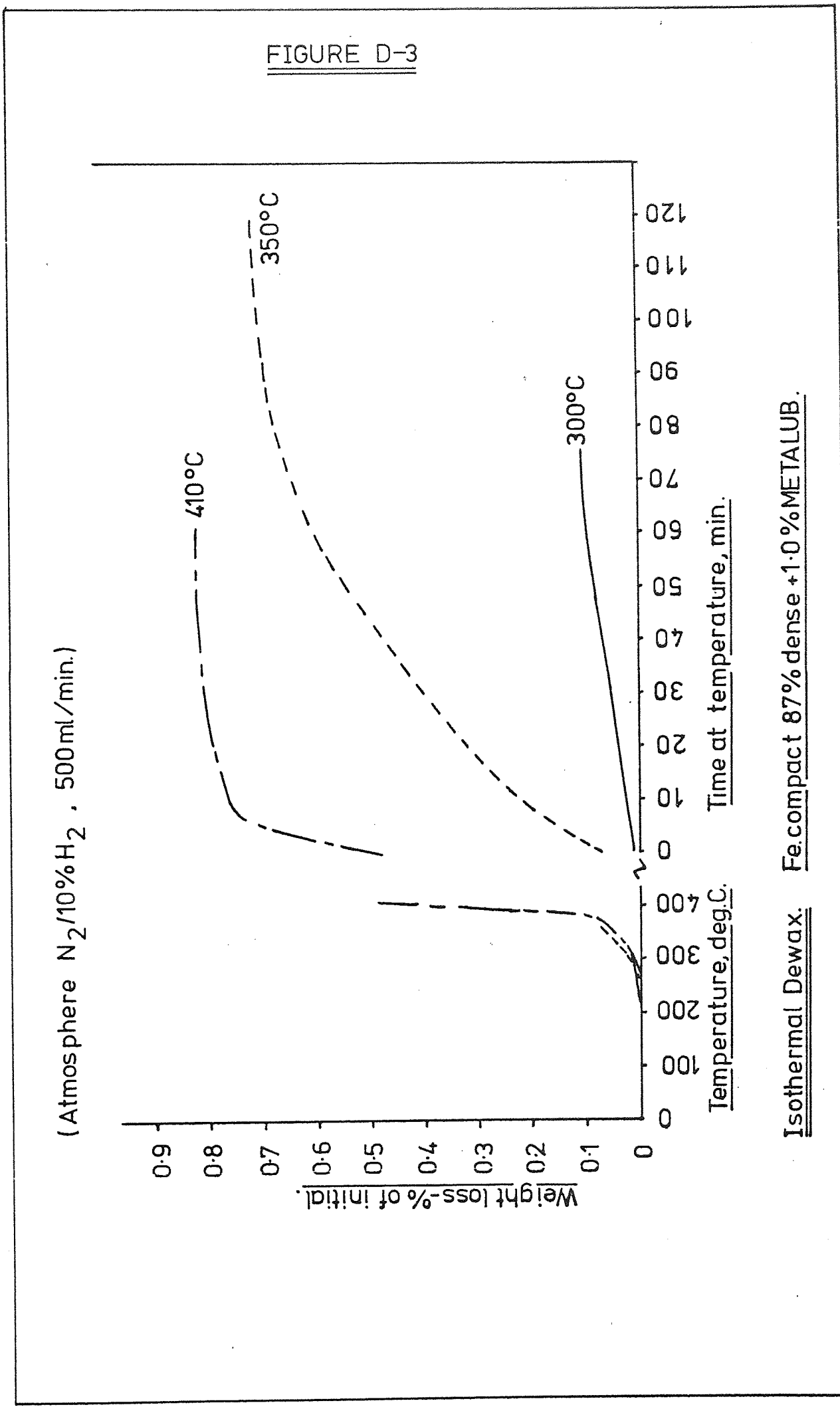
Isothermal Dewax. Fe.compact 87% dense +1·0% METALUB.
(Atmosphere N_2/10% H_2 , 500ml/min.)
Weight loss-% of initial.
0·9
0·8
0·7
0·6
0·5
0·4
0·3
0·2
0·1
0
Temperature, deg.C.
0
100
200
300
400
Time at temperature, min.
0
10
20
30
40
50
60
70
80
90
100
110
120
410°C
350°C
300°C

FIGURE D-4

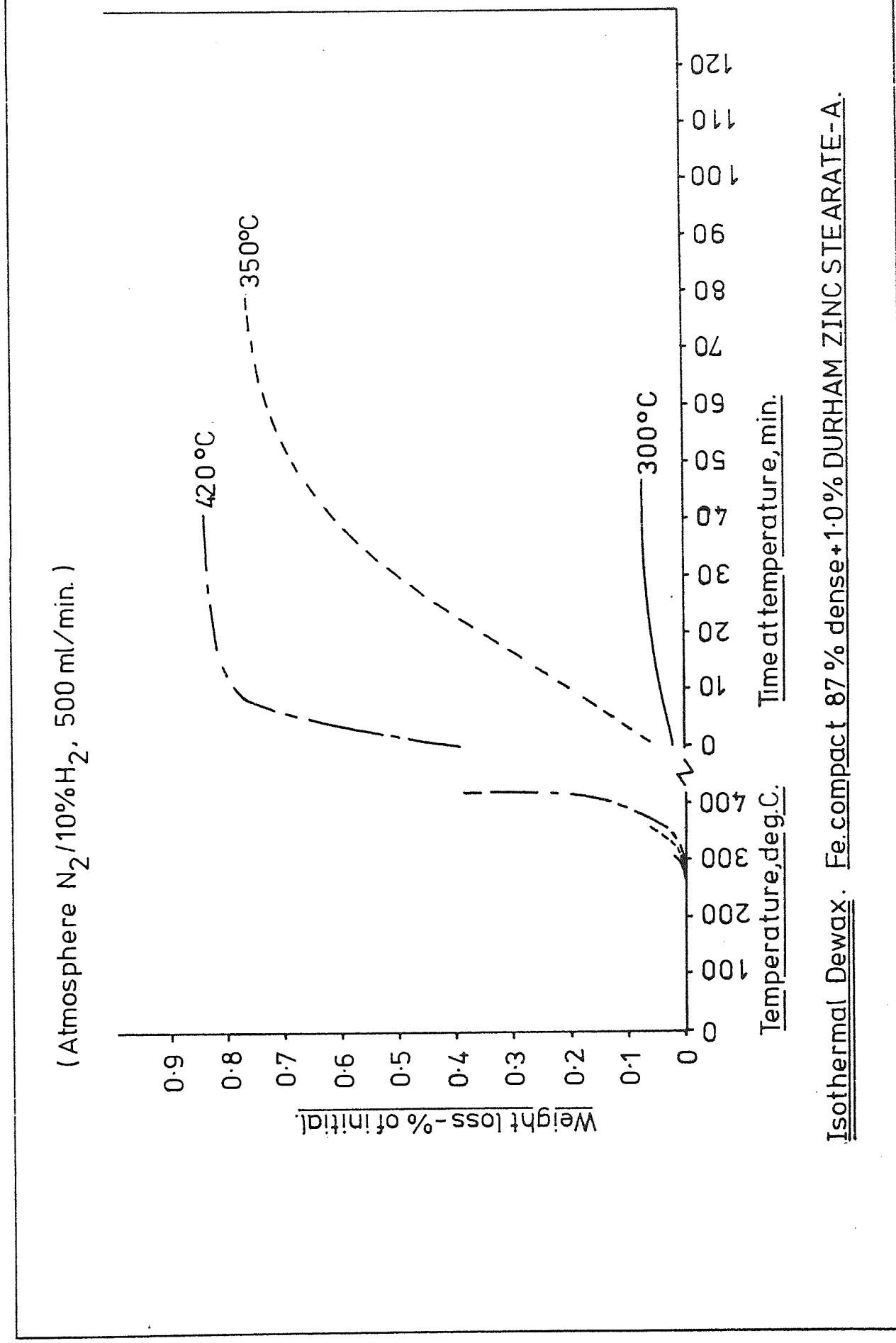

Isothermal Dewax. Fe. compact 87 % dense + 1·0 % DURHAM ZINC STEARATE-A.

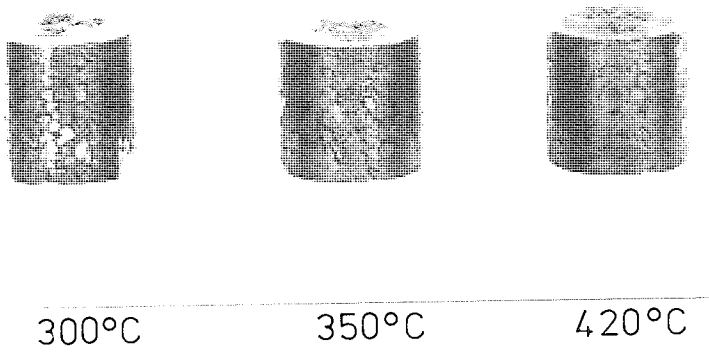

300°C 350°C 420°C

(a) Durham zinc stearate A 87% dense. 1% lubricant.

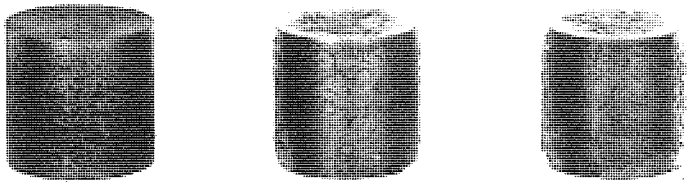

300°C 350°C 410°C

(b) Metalub. 87% dense. 1% lubricant

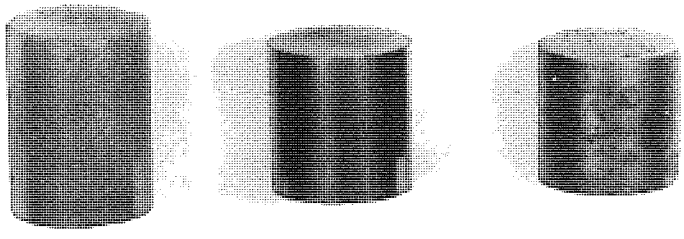

60% 80% 85% density

(c) Effect of density. (max. 450°C. 1% zinc stearate)

10mm

FIGURE D-5 Surface deposits after dewaxing.

(N_2/10% H_2 500 ml min^{-1} Material MP32)

FIGURE D-6 .Repeated results for tensile specimens treated at a high heating rate in N_2/10% H_2.

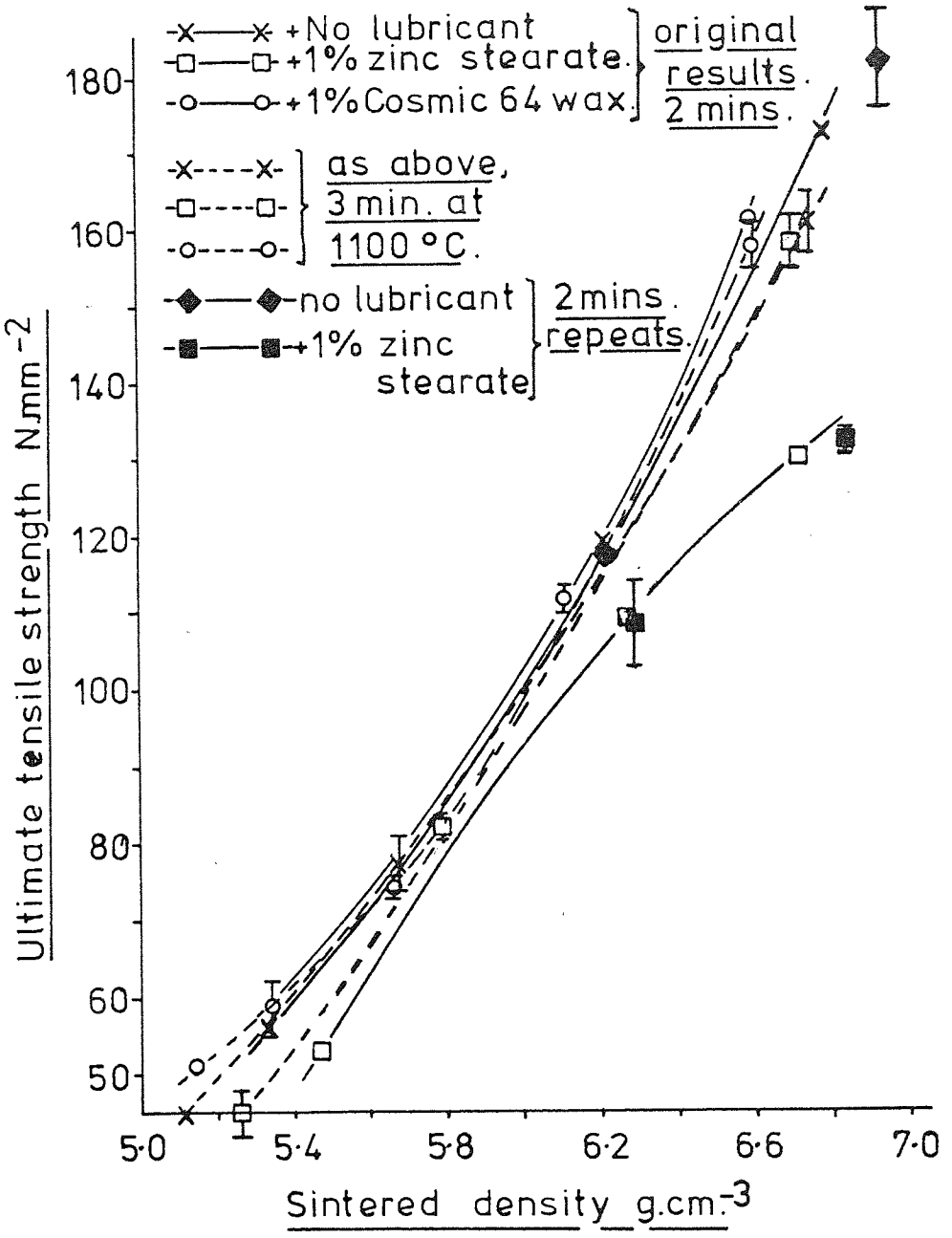

FIGURE D-7. COMPRESSIBILITY

Compacts - MP 32 +1% lubricant.

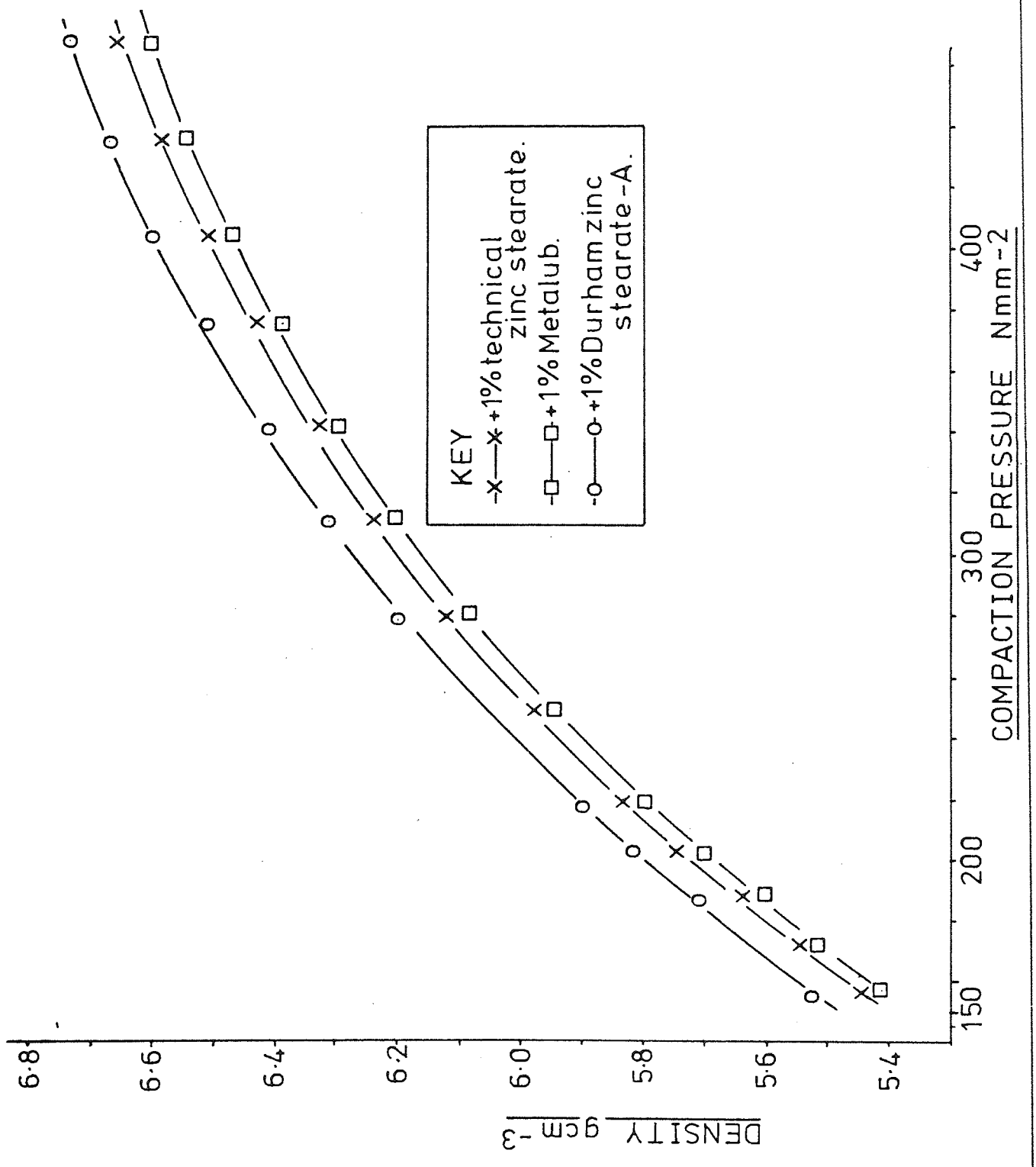

FIGURE D-8. EJECTION STRESS VERSUS DENSITY

Compacts - MP 32 + 1% lubricant.

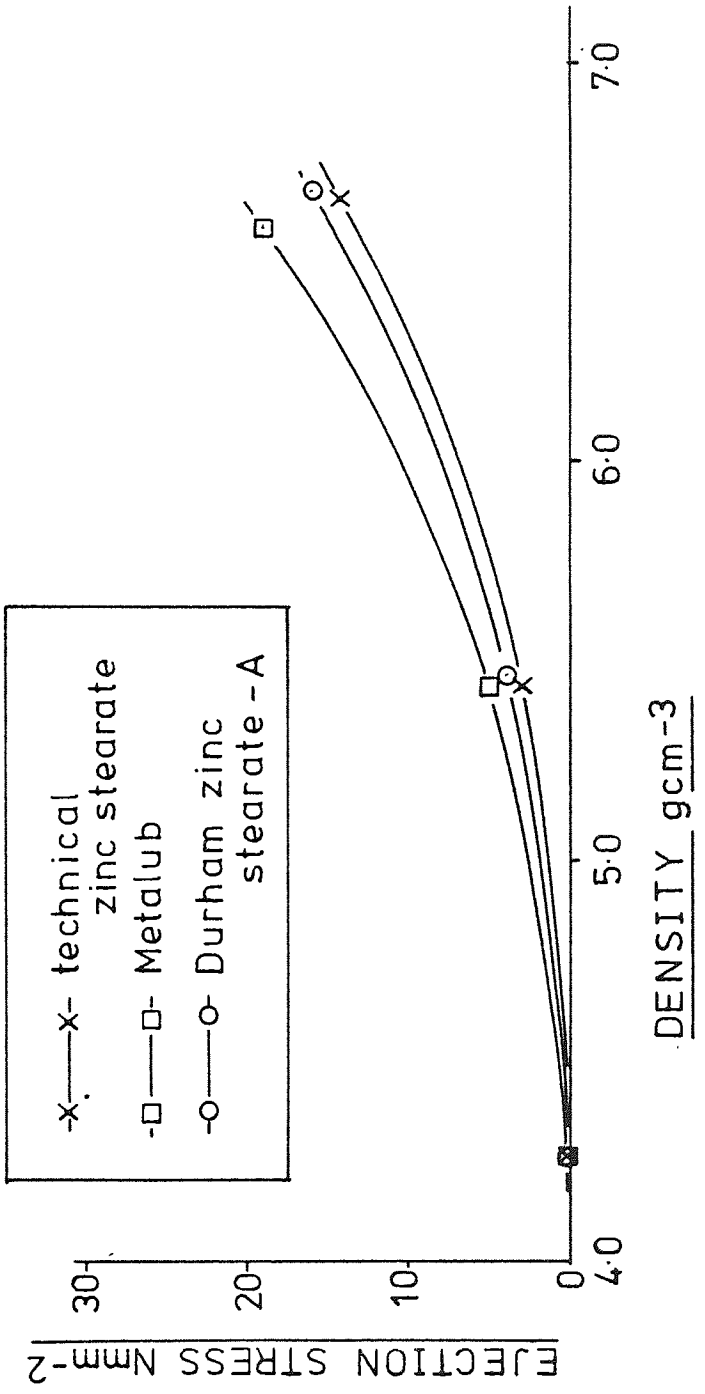

REFERENCES

1. I.L.JUNGBERG and P.G.ARBSTEDT. Proceedings of the 12th Annual Meeting of the Metal Powder Association. 1956. 78.

2. G.BOCKSTIEGEL and O.SVENSSON. Modern developments in powder metallurgy. 1971. 4. 'Processes'. 87. Ed. H.H.Hausner. Plenum Press.

3. D.YARNTON and T.J.DAVIES. Engineering Materials and Design. Sept.1970. 13. (9). 1103.

4. P.M.LEOPOLD and R.C.NELSON. International Journal of Powder Metallurgy.

Part 1. Effect of lubricant on powder compaction. 1965. 1. (3). 37.

Part 2. Effect of lubricant on ejection pressure. 1965. 1. (4). 37.

5. G.W.CULL. Private communication. Formerly with G.K.N. Bound Brook Ltd.

6. J.CARR and J.KEARNS. Precision Metal Molding. 1967. 25. (4). 61.

7. S.Å.KVIST, H.ZETTERSTRÖM and P.LINDSKOG. Experiences with different types of lubricant at Höganas A.B. Contribution to a symposium on lubrication held at Loughborough University of Technology. June 1973.

8. N.A.LANGE. Handbook of Chemistry. 10th Edition. McGraw-Hill.

9. The Durham Chemical Group. Birtley, Co.Durham.

10. K.H.MOYER. International Journal of Powder Metallurgy. 1971. 7. (3). 33-43.

11. R.MEYER, J.PILLOT and H.PASTOR. Powder Metallurgy. 1969. 12. (24). 298-304 (Including unpublished thermograms).

12. R.J.SAJDAK, R.P.McNALLY, M.D.NASTA and J.K.BEDDOW. International Journal of Powder Metallurgy. 1970. 6. (2). 13.

13. D.YARNTON and T.J.DAVIES. Metallurgia. 1962. 66. (10). 153.

14. H.H.HAUSNER. 'Friction as a characteristic of metal powders. Contribution to the 2nd. European Symposium on Powder Metallurgy. Stuttgart. May 1968.

15. R.E.RILEY and H.H.HAUSNER. International Journal of Powder Metallurgy. 1970. 6. (1). 17-22.

16. F.THÜMMLER and W.THOMMA. The sintering process. Metallurgical Reviews June 1967. Nº 115.

17. R.W.HECKEL. Transactions of the A.I.M.E. 221. 1001-1008.

18. R.W.HECKEL. Progress in Powder Metallurgy. 1961. 17. 66.

19. R.L.HEWITT, W.WALLACE and M.C.de MALHERBE. Powder Metallurgy. 17. (33). 1-12.

20. J.L.BRACKPOOL. Modern developments in Powder Metallurgy. 5 'Materials and properties.' Ed. H.H.Hausner. Plenum Press.

21. J.K.BEDDOW. International Journal of Powder Metallurgy. 9. (4). 127

22. M.J.DONACHIE, Jr . and M.F.BURR. Journal of Metals. 1963. 15. 849.

23. W.R.MORGAN and R.L.SANDS. Metallurgical Reviews. 1969. 14. Nº 134. 85.

24. D.YARNTON and T.J.DAVIES. Powder Metallurgy 1963. (11). 1

25. D.YARNTON and T.J.DAVIES. International Journal of Powder Metallurgy 8. (2). 51.

26. D.YARNTON and D.R.PROSSER. International Journal of Powder Metallurgy. 11 (1). 43.

27. R.F.MALLENDER, C.J.DANGERFIELD and D.S.COLEMAN. Powder Metallurgy. 15. (30). 130-152.

28. S.D.ELWAKIL and R.DAVIES. Powder Metallurgy. 1973. 16. (31). 72.

29. R.F.MALLENDER, C.J.DANGERFIELD and D.S.COLEMAN. Powder Metallurgy. 17. (34). 288.

30. K.E.EASTERLING and A.R.THÖLEN. Powder Metallurgy. 16. (31). 112.

31. J.C.BILLINGTON, C.FLETCHER and P.SMITH. Powder Metallurgy. 16. (32). 327.

32. D.TABOR. 'Friction mechanisms, effect of lubricants.' Tribology Handbook. ED.M.J.Neale. 1973. Butterworths.

33. D.A.SMITH. Analytical Chemistry. 1963. 35. 1306.

34. J.BASSETT and J.W.BETTS. Analyst. 1967. 92. 653.

35. P.D.GARN. Thermoanalytical Methods of Investigation. 1965. Academic Press.

36. J.HENRION and G.E.RHEAD. 'On high surface diffusivities of solid metals in the presence of adsorbed metallic vapours.' Diffusion processes. Ed. J.N.Sherwood. 1971. Gordon and Breach.

37. H.F.FISCHMEISTER and R.ZAHN. 'The mechanism of sintering in α-iron.' Modern developments in Powder Metallurgy. 2. Applications. Ed. H.H.Hausner. Plenum Press.

38. P.LENNY. M.Sc. Thesis. University of Aston. 1974.

39. C.J.SMITHELLS. Metals reference book. Butterworths.

40. J.MACKOWIACK. Physical Chemistry for Metallurgists. Institution of Metallurgists, Modern Metallurgical Texts. George Allen and Unwin Ltd.

41. P.BARKER, M.Sc. Thesis. University of Aston. 1975.

42. J.D.FAST. Interaction of metals and gases. Vol.1. Thermodynamics and phase relationships. 1965. Philips technical library.

43. F.THÜMMLER and W.THOMMA. The sintering process. Metallurgical Reviews. June 1967. N°.115.

44. A.R.POSTER and H.H.HAUSNER. 'α and γ phase sintering of carbonyl and other iron powders.' Modern developments in Powder Metallurgy. 2 'Applications' Ed. H.H.Hausner. Plenum Press.

45. S.L.FORSS. Some aspects of the sintering of iron powder. ibid.

46. Handbook of Chemistry and Physics. Ed. R.C.Weast. C.R.C. Press. 1972-1973. 53rd. edition.

47. S.BRUNAUER, P.H.EMMETT and E.TELLER. Journal of the American Chemical Society. 1938. 60. (2). 309-319.

48. J.B.HAERTLEIN and J.F.SACHSE. 'Some experiences in specific surface area measurement of metal powders by low temperature gas adsorption'. Contribution to a symposium on metal powders. A.S.T.M. Special technical publication. 140. 1952. 57-84.

49. Jan.MEDEMA and J.P.W.HOUTMAN. Analytical Chemistry 1969. 41. (1). 209

50. R.A.BEEBE, J.B.BECKWITH and J.M.HONIG. Journal of the American Chemical Society. 1945. 67. 1554.

51. W.D.HARKINS and G.JURA. Journal of the American Chemical Society. 1944. 66. 1362 and 1366.

52. British Standards Institution. The determination of specific surface of powders. BS. 4359. part 1. 1969.

53. Handbook of tables for probability and statistics. Ed. W.H.Beyer. C.R.C. Press. 1968. 2nd. edition.